Synthesis and Biological Evaluation of Truncated Sarganaphthoquinoic Acid Derivatives as Hsp90 Inhibitors

A Thesis Submitted in Fulfillment of the Requirements

for the Degree of

DOCTOR OF PHILOSOPHY (PHARMACY)

of

RHODES UNIVERSITY

By

Maynard T. Chiwakata

February 2015

Acknowledgements

My sincere gratitude goes to my supervisor, Assoc. Prof D. Beukes, for his guidance, assistance, patience and advice throughout my project. He made these three years enjoyable and fun. Thank You BOSS, you are simply the best.

I would like to thank Dr A. Edkins for a job well-done with the biological activity aspects of this project. Everything worked out beautifully, and to Dr C. Veale for his great expertise in molecular modelling. I wouldn't have managed without you, and thank you so much for sharing your knowledge with me. It was indeed a pleasure.

I would also want to thank the following people who also contributed to the success of my work: Dr E. Antunes for her assistance with the STD NMR studies, Dr Marietjie Stander from Stellenbosch University for her help with ESI-MS, Professor John Bolton from University of Cape Town for the collection and identification of algae, Dr Jo-Anne de la Mare for assistance in biological activity assays, Mr and Mrs Morley for technical support and Pharmaceutical Chemistry lectures: Dr Tandlich and Dr Goosen for advice and contributions to my work

And to my great colleagues and friends: Jameel Fakee (the most amazing guy I will ever know), Mohammed Adams and Tafadzwa Mutsvairo, the best people anyone can share a lab with. Thank you guys for the fun times. I will surely miss our crazy chats in G3 and all those talks to and fro Cape Town.

Special thanks to my best friends; Natasha Mutasa, Tendai Mafuma, Eldinah Hwengwere, Anthonia Afolayan and Safeeya Ally. Your company, support and motivation is greatly appreciated. And to my selected few friends, Nabeela Sader, Taherah Moola, Sonal Patel, Archibald Svogie, Ashmita Ramanah, Byron Mubaiwa, Nicole Naidoo, my gratitude to you guys for making my stay at Rhodes University an amazing one.

A special mention goes to my parents (**Samson** and **Smolly Chiwakata**), my two amazing brothers, **Marlon** and **Allen Chiwakata,** my sister-in-law **Susan Chiwakata** and my adorable little nephew, **Akudzweishe Riley Chiwakata**. Thank you for the undying love, support, encouragement and belief in me. I love you guys may God be with you always.

Finally, my gratitude goes to the man who made all this possible from the very beginning, Luan Schutte, thank you for your belief in me and making my dreams come true.

Lastly but not the least, THANK YOU LORD JESUS for seeing me through all.

Abstract

Hsp90 inhibition has been at the centre of attention in current research due to the possibility of "cracking down" on the entire process leading to the development of malignant cancers. Small underlying principles common in all types of cancers have been determined that govern the transformation of normal human cells into cancerous cells, with all relying on the ATPase activity of Hsp90 protein. Hsp90 protein is therefore an attractive drug target that if successfully inhibited can result in the remission of cancer tumours by one form of treatment. To date, no Hsp90 inhibitor has been sanctioned for cancer treatment as most are still in clinical development.

Our research was therefore inspired by reports that indicated the potential of quinones / naphthoquinones to act as Hsp90 inhibitors. Preliminary results of a few selected marine natural product quinone systems i.e. sargaquinoic acid (SQA) (**2.47**) and lapachol (**3.6**) showed moderate cytotoxicity and weak interactions with the Hsp90 molecular chaperone, and evidence suggested C-terminal binding of these molecules. No correlation has been determined yet between cytotoxicity and Hsp90 inhibition, hence we aimed to develop natural product inspired molecules that exhibit both cytotoxic and Hsp90 inhibition properties.

Due to limited amounts of the natural product that can be acquired from natural sources, synthetic analogues were opted for. Isolation of a few selected quinones was conducted to have material that could be used in biological assays. For structural modifications, a series of truncated naphthoquinone systems were prepared adopting the sarganaphthoquinoic acid (**3.5**) scaffold. The naphthoquinones were prepared *via* Diels-Alder reactions of relevant benzoquinones with myrcene, followed by aromatization reactions using MnO_2. Various alkyl and aryl amines were then coupled to the C-2/3 position of the naphthoquinone using Michael's addition reactions. Tricyclic naphthoquinones were also synthesized from reactions with hypotaurine and citral. Design of the analogues incorporated functionalities from known Hsp90 inhibitors e.g. geldanamycin (**2.28**) and its analogues.

Preliminary results obtained showed that coupling of naphthoquinones with aryl-amines resulted in the most cytotoxic compounds (**4.14-4.19**) with IC_{50} values as low as 0.3 µM against Hs578T breast cancer carcinoma (triple negative). Most of the alkyl amines (**4.20-4.25**) had IC_{50} values greater than 50 µM except for **4.20** and **4.21** that showed IC_{50} values of 7.6 µM and 2.6 µM respectively. Tricyclic naphthoquinones (**4.28-4.29**) showed moderate cytotoxic activity of approximately 10 µM.

Hsp90 inhibition was assessed by client protein degradation assays, of which SQA (**2.47**), showed the best Hsp90 inhibition properties, followed by compound **4.20**. The most cytotoxic arylamino-naphthoquinone (**4.16**) and tricyclic naphthoquinones (**4.28-4.29**) showed only moderate inhibition. None of the compounds led to Hsp70 induction, suggesting possible binding to the C-terminus of Hsp90.

Interactions at the binding site were assessed by molecular docking studies and saturation transfer difference (STD) NMR. Docking studies were conducted on the N-terminus of Hsp90 and better binding was observed for arylamino naphthoquinones (**4.14-4.19**) than for other series of compounds. Unfortunately, the co-crystal structure for the C-terminus of Hsp90 is unavailable, hence docking study comparisons on both domains could not be conducted. However, STD NMR offered a platform to assess binding interactions between the naphthoquinones and the N- or C-terminal domains of Hsp90. However no interactions were observed at both the N- and C- termini of Hsp90 due to either weak binding of ligands to the protein or poor water solubility of the ligands.

From these preliminary results, naphthoquinones bind to Hsp90 protein but conclusive remarks to which terminal domain they bind to could not be made. The best candidate from amongst the series of naphthoquinones prepared that showed moderate cytotoxicity and promising Hsp90 inhibition was compound **4.20**. We therefore succeeded in developing a new series of naphthoquinones that possess moderate cytotoxicity and show Hsp90 inhibition.

Table of Contents

List of Figures

List of Schemes

List of Tables

List of abbreviations

ºC	Degrees Celsius
COSY	^{1}H-^{1}H Homonuclear Correlation Spectroscopy
d	Doublet
dd	Doublet of doublets
eV	Electron Volt
DCM	Dichloromethane
DEPT	Distortionless Enhancement by Polarization Transfer
ESI-MS	Electronspray Ionization-Mass spectrometry
EtOAc	Ethyl Acetate
FDA	Food and Drug Administration
GC-MS	Gas chromatography-Mass spectrometry
HMBC	Heteronuclear Multiple Bond Correlation
HMT	Halogenated Monoterpenes
HPLC	High Performance Liquid Chromatography
HSQC	Heteronuclear Single Quantum Coherence
Hsp90	Heat shock protein (90 kDa)
HREI-MS	High Resolution Electron Impact Mass Spectrometry
Hz	Hertz
IC_{50}	Inhibitory Concentration 50 %
IR	Infrared
J	Spin-Spin Coupling constant (Hz)
MeOH	Methanol
m	Multiplet
m/z	Mass to charge ratio
NCI	National Cancer Institute
NMR	Nuclear Magnetic Resonance Spectroscopy

ppm	Parts per million
q	Quartet
ROS	Reactive oxygen species
s	Singlet
SAR	Structural activity relationships
SHQA	Sargahydroquinoic acid
SNQA	Sarganaphthoquinoic acid
SQA	Sargaquinoic acid
t	Triplet
TLC	Thin Layer Chromatography
UV	Ultra violet

CHAPTER ONE

Natural products in the treatment of cancer

Abstract

Numerous cytotoxic molecules have been isolated from natural sources in search of new anticancer drug leads. Halaven®, Yondelis® and Adcetris® are a few examples of successful drugs derived from marine origin that are discussed in this chapter. They highlight the process of drug design and development, and indicate the importance of the marine environment as a source of cytotoxic compounds.

1.1 Introduction

The use of natural products as lead compounds in the discovery and design of new drugs has continued unabated over the past century (Cragg and Newman, 2013). They offer a rich and unexplored source of bioactive molecules (Corson and Crews, 2007) compared to combinatorial chemistry and high-through put screening methods (Molinari, 2009; Cragg and Newman, 2013). The key element responsible for the success of natural products in drug discovery is accredited to the vast structural diversity of these compounds. Advances in technology, including the ability to synthesize highly complex natural products in the laboratory, has aided the exploration of compounds from natural sources and allowed their potential to be realized (Lahlou, 2013).

Until recently, the marine environment has been the least explored compared to terrestrial and microbial environments for potential lead compounds. The ocean was regarded as a hostile and inhospitable place, not fit for exploration. An advancement in technologies involving snorkelling, use of self-contained underwater breathing apparatus (SCUBA diving), manned submersibles, and use of remotely operated vehicles (ROVs) has enabled vast bodies of water to be explored in search of new drug molecules. To date, six marine drugs have been registered by the Food and Drug administration board (FDA), one by the European Union (EU) and approximately 25 natural products are in different stages of clinical trials (Mayer, 2014).

1.2 Eribulin mesylate (Halaven®)

Halichondrin B (**1.1**) is a macrocyclic polyether first isolated from the sponge *Halichondria okadai* (Uemura, *et al*., 1985). It exhibited cytotoxic activity by inhibiting cell division of cancerous cells which led to its inclusion in pre-clinical studies by the National Cancer Institute (NCI) in 1992. Under these studies it demonstrated great potency against blood cancer cell lines i.e., leukaemia. However further developments were hindered by difficulties in collecting sufficient material and the lengthy processes in the synthesis of the natural compound. Discovery of the C1-C38 moiety as the pharmacophoric element in the macrocyclic lactone led to the development and synthesis of ER-086526 (**1.2**) (Towle, *et al*., 2001) which is also known as E7389, NSC 707389 (Perez, 2009) and ER-076349 (**1.3**).

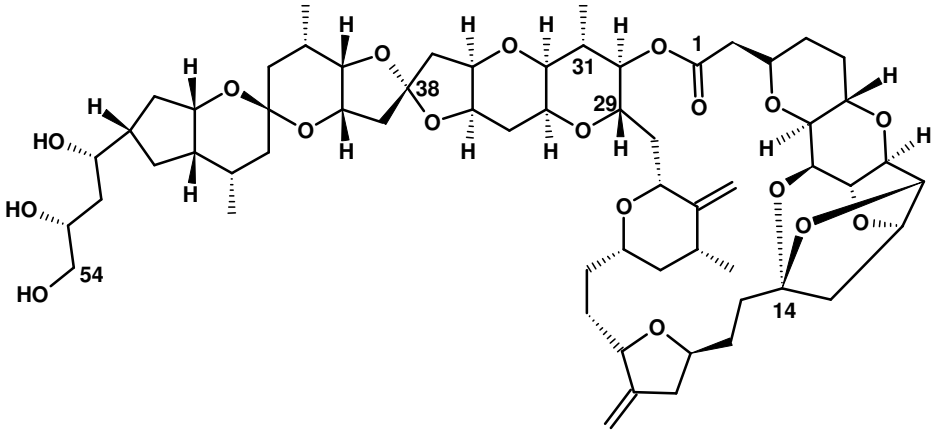

1.1

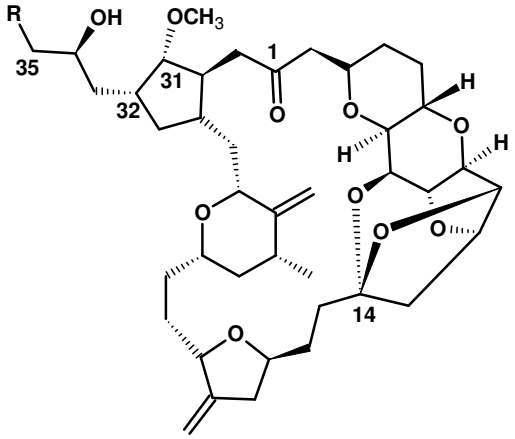

1.2 R = NH_2
1.3 R = OH

Assessment of more than 180 macrocyclic ketones resulted in the development of the above mentioned analogues, their structural difference being the substituent at C-35 which is either an alcohol or amine functionality. The analogues differed in structure to halichondrin B (**1.1**) by replacing a lactone ester at C-1, a methyl functionality at C-31 and a tricyclic system C29-C38 on halichondrin B (**1.1**) with a ketone, methoxy group and a five-membered ring respectively.

These compounds (**1.1-1.3**) have been identified as tubulin-based antimitotic agents. They disrupt microtubule formation during mitosis of rapidly dividing cells i.e., cancer cells. However, their interaction with tubulin is somehow different and specific in comparison to other tubulin depolymerizers e.g., Vinca alkaloids, dolastatins etc. A different interaction to the known mechanism may aid in unique tumour specificities and other desirable clinical outcomes (Bai, *et al*., 1991), hence the interest in this natural product.

ER-086526 (**1.3**), now known as Eribulin has been pursued further due to better efficacy in *in-vivo* studies, and was approved by the FDA for the treatment of metastatic breast cancer in 2010 (Scarpace, 2012). The drug is metabolized by cytochrome P450 and was shown not to influence metabolism of other drugs (McBride and Butler, 2012; Zhang, *et al*., 2008). Eribulin has promising drug outcomes when used as a single agent in patients with locally advanced disease and in those with metastatic breast cancer that has become resistant to taxanes and anthracyclines (Cortes, *et al*., 2011).

1.3 Trabectedin (Yondelis®)

Trabectedin (**1.4**) is a novel marine antineoplastic alkaloid that was initially isolated from the marine ascidian *Ecteinascidia turbinata* (D'Incalci and Galmarini, 2010). It consists of three tetrahydroisoquinoline rings, two fused together and linked *via* a benzylic sulphide bond to a ten carbon lactone bridge, and the other connected *via* a spiro ring.

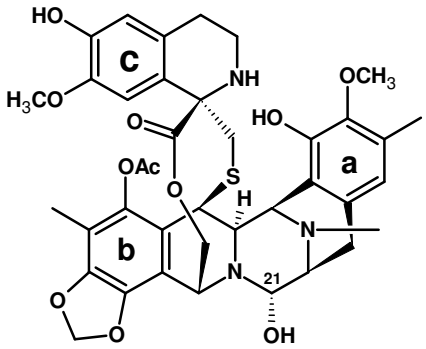

1.4

Six ecteinascidins [(ET's) 729, 743, 745, 759A, 759B, and 770] were first described and characterized from a tunicate found in the Caribbean Sea, of which ET 743 (Trabectedin (**1.4**) was the most abundant (Rinehart, *et al*., 1991). Preliminary structure activity relationships conducted showed that the carbinolamine of C-21 and the presence of the aromatic C subunit were crucial for potency in cytotoxicity assays done against murine leukaemia cells L1210 (Cuevas and Francesch, 2009).

Trabectedin (**1.4**) was selected for clinical development due to its large relative abundance in the crude extracts and novel chemical structure. In 2007, it was registered for use in the treatment of advanced soft tissue sarcoma in patients showing resistance to anthracyclines and ifosfamide treatments. Concomitant use with pegylated liposomal doxorubicin was approved in 2009 for treatment of platinum-sensitive ovarian cancer in patients that had a relapse of the disease (Monk, *et al*., 2012). Its mode of action was determined to be related to DNA alkylation but not in a similar way to traditional alkylating agents. It binds to the exocyclic N2 amino group of guanines in the DNA minor groove compared to known guanine N7 or O6 positions in the major groove where other alkylating agents bind. Such alkylation results in DNA damage, thus inhibiting cancer growth and division, and leading to death of cancer cells (D'Incalci and Galmarini, 2010).

As with most natural products, supply of the active metabolite had to be addressed. Trabectedin (**1.4**), currently marketed as Yondelis®, was initially manufactured by total synthesis using a

multi-step enantio-controlled process developed by Corey and colleagues (1996). Improvement in synthetic strategies led to the preparation of trabectedin (**1.4**) *via* semi-synthesis from cyanosafracin B (**1.5**). Cyanosafracin B (**1.5**) is a derivative of safracin B, an antibiotic obtained by fermentation of *Pseudomonas fluorescens.* Optimization of the fermentation process yields kilogram quantities of cyanosafracin B (**1.5**) that is used as the starting material for the synthesis of trabectedin (**1.4**) (Cuevas, *et al*., 2000; Cuevas and Francesch, 2009).

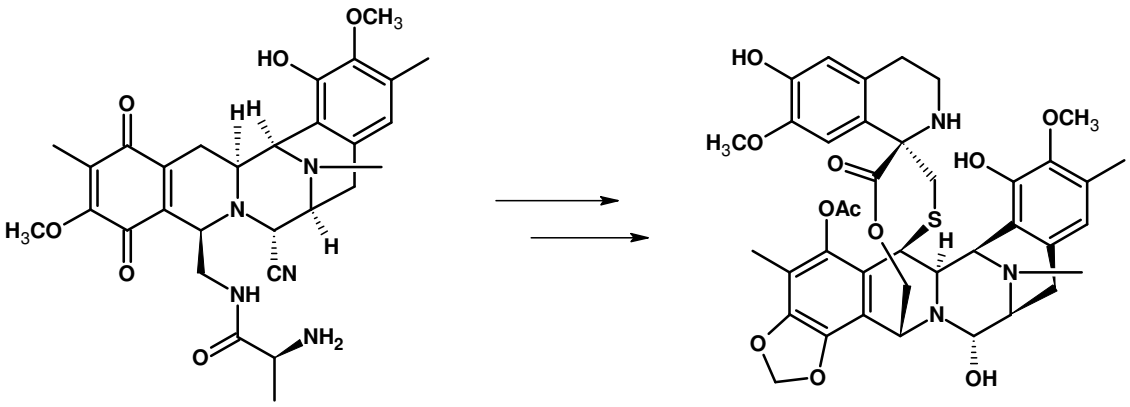

1.5 **1.4**

Scheme 1.1: Scheme showing cyanosafracin B (**1.5**) as the starting material for the preparation of trabectedin (**1.4**) (Cuevas, *et al*., 2000)

Trabectedin (**1.4**) is licensed by the Spanish pharmaceutical drug company PharmaMar, and was co-developed by Johnson & Johnson Pharmaceutical Research and Development group. Induced toxicities related to trabectedin (**1.4**) are mainly haematological and hepatic. Current efforts are focusing on the development of new trabectedin-based combinations.

1.4 Dolastatin-10

Dolastatins are naturally occurring cytotoxic pseudo peptides that display antineoplastic, bactericidal and antifungal properties (Pettit, *et al*., 1998). They were first isolated from the marine shell-less mollusc *Dolabella auricularia*, and dolastatin-10 (**1.6**) and dolastatin-15 stood out as the most promising anti-proliferative natural products (Pettit, *et al*., 1987).

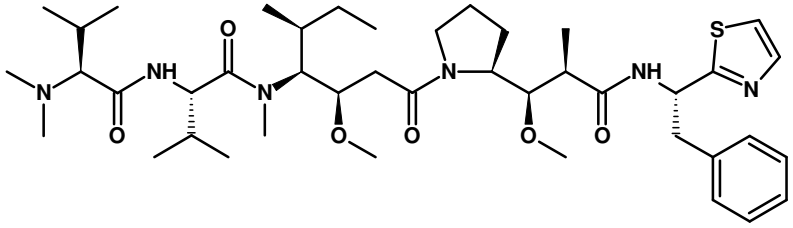

1.6

Their mode of action involves inhibition of microtubule assemblies and inducing apoptosis in several malignant cell lines (Gajula, *et al*., 2013). Activity has been noticed mainly in human prostate cancer models, both in *in vitro* and *in vivo* assays. Complete growth inhibition was determined at concentrations as low as 1 nM of dolastain-10 (**1.6**) in *in vitro* studies (Turner, *et al*., 1998). Cell cycle arrest in G_2-M phase and α-tubulin depolymerisation mechanisms are believed to be the main causes of inhibition. *In vivo* studies demonstrated a decrease in the number and size of tumours in the diaphragm of mice and prevented invasion of musculature (Vaishampayan, *et al*., 2000). Such promising results of dolastatin-10 (**1.6**) led to its introduction in Phase II clinical trials together with several of its synthetic analogues.

Recently a dolastatin analogue, brentuximab vedotin was approved by the FDA for use in the treatment of relapsed Hodgkin lymphoma and systemic anaplastic large cell lymphoma. The drug is marketed as Adcetris® and contains a very potent auristatin derivative monomethyl auristatin E (MMAE) (**1.7**) which is highly toxic.

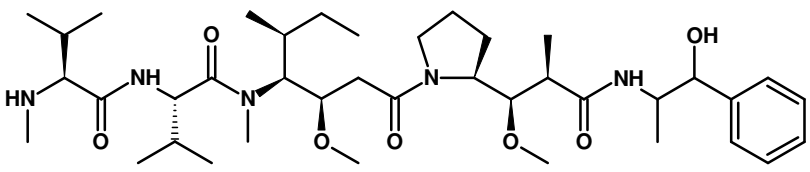

1.7

To circumvent its toxicity, an antibody-drug conjugate (ADC) of the drug was developed. MMAE is linked to a tumour-seeking monoclonal antibody that directs it to cancer cells, sparing normal cells. Research is under way to extend the applications of brentuximab vedotin

and to advance the field by developing other ADCs with new linker and conjugation strategies (Senter and Sievers, 2012).

1.5 Previous studies on cytotoxic marine prenylated quinones

Successful stories of marine natural products mentioned above inspired us to explore this untapped source of the ocean for cytotoxic lead compounds. Our major focus was aimed at molecules that have the potential to disrupt the six Hallmarks of cancer *via* Hsp90 inhibition. There is some evidence that suggests marine quinones have the potential to inhibit Hsp90 molecular chaperone (Hadden, *et al*., 2009), in addition to the cytotoxic properties they exert *via* generation of reactive oxygen species (ROS) and by DNA alkylation mechanisms (Castro, *et al*., 2008; Rahmoun, *et al*., 2013). We were determined to explore this aspect further and of interest were meroterpenoids isolated from marine brown algae collected along the south-western coastlines of South Africa. *Sargassum incisifolium* is available in relative abundance on the South African sea shores and isolated meroterpenoids from this brown alga display cytotoxic and antiplasmodial activities (Afolayan, *et al*., 2008) while preliminary evidence also suggests that selected metabolites may inhibit Hsp90 (Moyo, 2013).

The main aim of the research was thus to explore the cytotoxicity and Hsp90 inhibition of selected naturally occurring terpenyl quinones and their derivatives.

Specific objectives included:

- Exploring the cytotoxic properties of marine quinones (meroterpenoids, lapachol and derivatives)
- Synthesizing natural product inspired analogues to improve cytotoxicity and Hsp90 inhibition
- Conducting client protein degradation assays related to Hsp90 inhibition
- Assessing Hsp90 inhibition by use of computational methods, i.e., molecular modelling
- Assessing binding to Hsp90 protein *via* Saturation Transfer Difference NMR studies

1.6 Thesis summary

Chapter one provides a general introduction to marine natural product based anticancer drug discovery while chapter two reviews the potential of Hsp90 protein as a drug target for cancer treatment. Known natural product inhibitors of Hsp90 are also reviewed in chapter two, with chapter three describing the isolation and characterization of selected natural product quinones that have the potential to inhibit Hsp90. Chapter four focuses on the synthesis of natural product analogues to enhance cytotoxicity and Hsp90 inhibition properties, and these activities are assessed in chapter five in *in vitro* assays. Possible binding interactions to the active site of Hsp90 by test compounds is presented in chapter six using molecular docking and saturation transfer difference (STD) NMR, and chapter seven contains the summary of set goals, results obtained and conclusions drawn with regards to the development of cytotoxic Hsp90 inhibitors.

References

Afolayan, A., Bolton, J., Lategan, C., Smith, P., & Beukes, D. (2008). Fucoxanthin, tetraprenylated toluquinone and toluhydroquinone metabolites from Sargassum heterophyllum inhibit the in vitro growth of the malaria parasite Plasmodium falciparum. *Zeitschrift für Naturforschung, 63c*, 848-852.

Bai, R., Paull, K., Herald, C., Malspeis, L., Pettit, G., & Hamel, E. (1991). Halichondrin B and homohalichondrin B, marine natural products binding in the vinca domain of tubulin. Discovery of tubulin-based mechanism of action by analysis of differential cytotoxicity data. *Journal of Biological Chemistry, 266*, 15882-15889.

Castro, F., Mariani, D., Panek, A., Eleutherio, E., & Pereira, M. (2008). Cytotoxicity mechanism of two naphthoquinones (Menadione and Plumbagin) in Saccharomyces cerevisiae. *PLoS ONE, 3*, 1-6.

Corey, E., Gin, D., & Kania, R. (1996). Enantioselective total synthesis of ecteinascidin 743. *Journal of American Chemical Society, 118*, 9202–9203.

Corson, T., & Crews, C. (2007). Molecular understanding and modern application of traditional medicines: triumphs and trials. *Cells, 130*, 769-774.

Cortes, J., Montero, A., & Gluck, S. (2011). Eribulin mesylate, a novel microtubule inhibitor in the treatment of breast cancer. *Cancer Treatment Reviews, 38*, 143-151.

Cragg, G., & Newman, D. (2013). Natural products: a continuing source of novel drug leads. *Biochimica et Biophysica Acta, 1830*, 3670–3695.

Cuevas, C., & Francesch, A. (2009). Development of Yondelis (Trabectedin, ET-743): a semisynthetic process solves supply problem. *Natural Product Reports, 26*, 322–337.

Cuevas, C., Perez, M., Martin, M., Chicharro, J., Fernandez-Rivas, C., Flores, M., Francesch, A., Gallego, P., Zarzuelo, M., de La Calle, F., García, J., Polanco, C., Rodríguez, I., & Manzanares, I. (2000). Synthesis of ecteinascidin ET-743 and phthalascidin Pt-650 from cyanosafracin B. *Organic Letters, 2*, 2545-2548.

D'Incalci, M., & Galmarini, C. (2010). A review of trabectedin (ET-743): a unique mechanism of action. *Molecular Cancer Therapeutics, 9*, 2157-2163.

Gajula, P., Asthana, J., Panda, D., & Chakraborty, T. (2013). A Synthetic dolastatin 10 analogue suppresses microtubule dynamics, inhibits cell proliferation, and induces apoptotic cell death. *Journal of Medicinal Chemistry, 56*, 2235−2245.

Hadden, M., Hill, S., Davenport, J., Matts, R., & Blagg, B. (2009). Synthesis and evaluation of Hsp90 inhibitors that contain the 1,4- naphthoquinone scaffold. *Bioorganic and Medicinal Chemistry, 17*, 634–640.

Lahlou, M. (2013). The Success of natural products in drug discovery. *Pharmacology & Pharmacy, 4*, 17-31.

Mayer, A. (2014). *Marine pharmaceuticals: The clinical pipeline*. Retrieved from Marine Pharmacology: http://marinepharmacology.midwestern.edu/clinPipeline.htm

McBride, A., & Butler, S. (2012). Eribulin mesylate: a novel halichondrin B analogue for the treatment of metastatic breast cancer. *American Journal of Health-System Pharmacy, 69*, 745-755.

Molinari, G. (2009). Natural products in drug discovery: present status and perspectives pharmaceutical biotechnology. *Guzmaín, C.A., Feuerstein, G.Z. (Eds.), Springer New York,*, 13-27.

Monk, B., Dalton, H., Benjamin , I., & Tanovic, A. (2012). Trabectedin as a new chemotherapy option in the treatment of relapsed platinum sensitive ovarian cancer. *Current Pharmaceutical Design, 18*, 3754-3769.

Moyo, B. (2013). *The screening and characterisation of compounds for modulators of heat shock protein (Hsp90) in a breast cancer cell model.* (PhD) Rhodes University.

Perez, E. (2009). Microtubule inhibitors: Differentiating tubulin-inhibiting agents based on mechanisms of action, clinical activity, and resistance. *Molecular Cancer Therapeutics, 8*, 2086-2095.

Pettit, G., Kamano, Y., Herald, C., Tuinman, A., Boettner, F., Kizu, H., Schmidt, J., Baczynskyj, L., Tomer, K., & Bontems, R. (1987). The isolation and structure of a remarkable marine animal antineoplastic constituent: dolastatin 10. *Journal of American Chemical Society, 109*, 6883–6885.

Pettit, R., Pettit, G., & Hazen, K. (1998). Specific activities of dolastatin 10 and peptide derivatives against Cryptococcus neoformans. *Antimicrobial Agents and Chemotherapy, 42*, 2961–2965.

Rahmoun, N., Atmani, Z., Benabdallah, M., Boucherit, K., Villemin, D., & Braham, N. (2013). Antimicrobial activities of the henna extract and some synthetic naphthoquinones derivatives. *American Journal of Medical and Biological Research, 1*, 16-22.

Rinehart, K., Holt, T., Fregeau, N., Stroh, J., Keifer, P., Sun, F., Li, H., Martin, D. (1991). Ecteinascidins 729, 743, 745, 759A, 759B, and 770: potent antitumor agents from the Caribbean tunicate Ecteinascidia turbinata. *Journal of Organic Chemistry*, *56,* 1676–1676.

Scarpace, S. (2012). Eribulin mesylate (E7389): review of efficacy and tolerability in breast, pancreatic, head and neck and non–small cell lung cancer. *Clinical Therapeutics, 34*, 1467–1473.

Senter, P., & Sievers, E. (2012). The discovery and development of brentuximab vedotin for use in relapsed Hodgkin lymphoma and systemic anaplastic large cell lymphoma. *Nature Biotechnology, 30*, 631–637.

Towle, M., Salvato, K., Budrow, J., Wels, Wels, B., Kuznetsov, G. (2001). *In vitro* and *in vivo* anti-cancer activities of synthetic macrocyclic ketone analogues of halichondrin B. *Cancer Research, 61*, 1013-1021.

Turner, T., Jackson, W., Pettit, G., Wells, A., & Kraft, A. (1998). Treatment of human prostate cancer cells with dolastatin-10, a peptide isolated from a marine shell-less mollusc. *Prostate, 34*, 175–181.

Uemura, D., Takahashi, K., Yamamoto, T., Katayama, C., Tanaka, J., Okumura, Y., & Hirata, Y. (1985). Norhalichondrin A: an antitumor polyether macrolide from a marine sponge. *Journal of the American Chemistry Society, 107*, 4796-4798.

Vaishampayan, U., Glode, M., Du, W., Kraft, A., Hudes, G., Wright, J., & Hussain, M. (2000). Phase II study of dolastatin-10 in patients with hormone-refractory metastatic prostate adenocarcinoma. *Clinical Cancer Research, 6*, 4205–4208.

Zhang, Z., King, B., Pelletier, R., & Wong, Y. (2008). Delineation of the interactions between the chemotherapeutic agent eribulin mesylate (E7389) and human CYP3A4. *Cancer Chemotherapy and Pharmacology, 62*, 707-716.

CHAPTER TWO

The hallmarks of cancer

Abstract

Six hallmarks of cancer have been identified as essential for the propagation of tumours to malignant cancers, and are related to regulatory mechanisms that deal with cell proliferation and homeostasis. The engine that drives these aspects of cancer has been discovered to be the Hsp90 molecular chaperone. Drug leads that target this chaperone are being designed and developed so as to combat all stages of cancer with one form of treatment. This chapter gives a general overview of the hallmarks of cancer, the structural features of Hsp90 protein and examples of known Hsp90 inhibitors.

2.1 Introduction

Advances in cancer knowledge over the last century have indicated the disease to comprise of dynamic changes in the genome (Bishop and Weinberg, 1996). Several research studies are focused on discovering mutations that lead to activation of oncogenes, with the aim of a more targeted approach to drug design. Despite the complexity of the disease, small underlying principles have been identified that govern the transformation of normal human cells into cancerous ones. Such principles involving molecular, biochemical and cellular traits are common in all types of cancer, providing a potential drug target that can cripple the entire process leading to the development of malignant cancers (Hanahan and Weinberg, 2000; Hanahan and Weinberg, 2011).

Six essential alterations in cell physiology are responsible for malignant cancer growth, related to regulatory mechanisms that deal with cell proliferation and homeostasis. These six alterations are commonly known as the hallmarks of cancer (**Figure 2.1**) and include: self-sufficiency in growth signals, insensitivity to growth-inhibitory signals, evasion of programmed cell death (apoptosis), limitless replicative potential, sustained angiogenesis, and tissue invasion and metastasis (Hanahan and Weinberg, 2000).

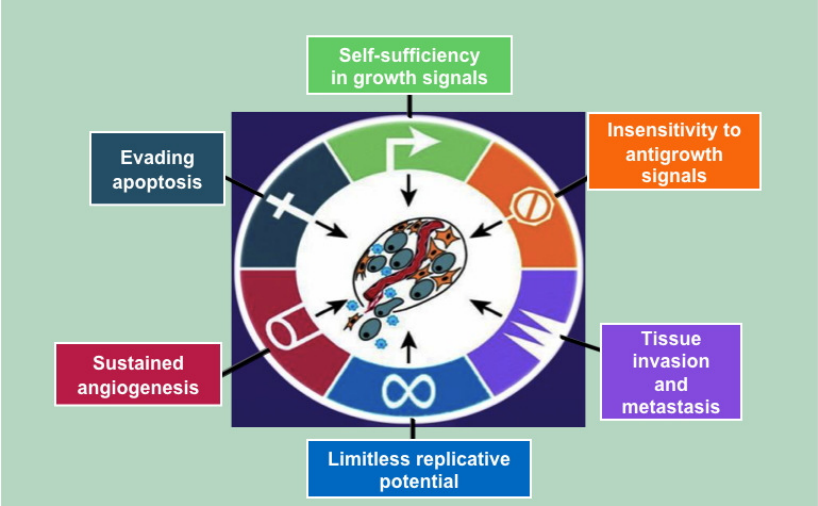

Figure 2.1: The six hallmarks of cancer (Hanahan and Weinberg, 2000; Hanahan and Weinberg, 2011).

Two additional hallmarks of cancer have been identified. One involves the capability to modify cellular metabolism such that neoplastic proliferation is adequately supported and the second allows cancer cells to evade immunological destruction, mainly by T and B lymphocytes. (Hanahan and Weinberg, 2011). These hallmarks have not been fully validated and are considered as emerging hallmarks. The first six hallmarks will be discussed in this chapter.

2.1.1 Self-sufficiency in growth signals

One of the trademark signatures of cancer cells is the ability to proliferate uncontrollably. Normal cells are regulated by mitogenic growth promoting signals that are transmitted into the cell by transmembrane receptors containing intracellular tyrosine kinase domains. Cell proliferation is conducted *via* diffusible growth factors, extracellular matrix components and cell adhesion molecules bound to surface receptors that activate the cell to enter cell cycle. With mutated cells, such signals are deregulated and cell cycles are uncontrolled leading to massive aggregations of cell growths (Hanahan and Weinberg, 2011). Certain oncogenes in tumour cells mimic growth signalling pathways of normal cells by producing their own growth factor ligands or by stimulating neighbouring normal cells within the supporting tumour-associated stroma to provide them with various growth factors (Cheng, *et al*., 2008).

Other ways in which deregulation of growth signals can occur in malignant cells is by overexpression of oncogenic growth factor receptor proteins on the cell surface of cancer cells. This renders such cells hyper-responsive to an otherwise limiting amount of growth factor ligand resulting in excessive growth. Structural alterations to the receptor proteins can also occur which allows growth stimulation of cells without the ligand bound to it (Hanahan and Weinberg, 2011). Such independence from normal signal factors disrupts important homeostatic functions played by a particular tissue, resulting in loss of control of a set of cells embedded in the tissue.

2.1.2 Insensitivity to growth-inhibitory signals

Under normal circumstances, the extracellular matrix and nearby cells contain growth inhibitors (soluble and immobilized inhibitors) that associate with transmembrane receptor proteins and intracellular signalling circuits to initiate the end of the proliferation cycle. Anti-proliferative signals are channelled through one of the most important factors, retinoblastoma protein (pRb), which alters the function of E2F transcription factors responsible for cell proliferation. Disruption of pRb in malignant cells allows the function of E2F transcription factors to continue, and thereby making such cells insensitive to antigrowth signals (Weinberg, 1995). pRb is inactivated by phosphorylation reactions and is therefore protected by TGFβ in normal cells to allow its function. In tumour cells, TGFβ receptors are down regulated or lose responsiveness, promoting pRb inactivation and E2F function (Fynan and Reiss, 1993). In other cases, pRb function may be lost due to mutation of its gene, hence a mutated protein is

produced which cannot inhibit cell proliferation. This is one strategy that is used by tumour cells for continuous cell division, although other mechanisms do exist.

2.1.3 Evasion of programmed cell death (apoptosis)

Apoptosis is a complex process that involves a series of events in tissue homeostasis. Once triggered, cell membranes are disrupted, and cytoplasmic and nuclear components are broken down within 30-120 min. All broken down components are engulfed by neighbouring cells in the tissue (Wyllie, *et al*., 1980). This process is governed by sensors and effectors. Sensors monitor extracellular and intracellular environments of cells for any abnormalities, and the effectors are responsible for the actual apoptotic death process when triggered to act by sensors. Cell death signals are channelled by FAS ligand binding to FAS receptor and by TNFα binding to TNF-R1 (Ashkenazi and Dixit, 1999). The signals may emanate from the extracellular environment *via* cell surface receptors (extrinsic), primarily leading to activation of caspases or *via* the intrinsic pathway which initiates in the mitochondria and involves the BCL family of proteins, which in turn activate the caspase effectors (Green and Reed, 1998). Caspase enzymes are responsible for the destruction of cells (Thornberry and Lazebnik, 1998; Fulda and Debatin, 2006).

Tumour cells upregulate *bcl-2* and *myc* oncogenes that possess anti-apoptotic properties. Such a phenomenon was observed in follicular lymphomas *via* chromosomal translocation (Korsmeyer, 1992). In addition, the p53 tumour suppression gene loses its function *via* mutation in malignant cells, resulting in a defective p53 protein that cannot initiate apoptosis.

2.1.4 Limitless replicative potential

Disruption mechanisms described above do not necessarily result in the growth of cancer cells into tumours. All mammalian cells contain programs that limit cell replication and are independent of cell-to-cell signalling (Hayflick, 1997). These programs are distorted in cancer cells which results in life threatening masses emerging. Immortalization, as it is called, is an acquired phenomenon after several replications of cancer cells. Initially, the fast growing cells enter into a crisis state that is characterized by massive cell death and from it a variant cell (1 in 10^7 cells) emerges with the ability to multiply without limit (Wright, et al., 1989). Under normal circumstance, rapid growth results in the loss of DNA telomere ends, and unprotected chromosomal ends fuse together yielding a karyotypic disarray associated with cell death. Immortalization is obtained by maintenance of telomere ends of chromosomes *via* upregulation of telomerase enzymes that add hexanucleotide ends, inhibiting chromosomal fusion (Shay and

Bacchetti,, 1997; Bryan and Cech, 1999). Such enzymes are almost non-existent in normal cells but are expressed in levels as high as 90 % in malignant cells. They are the main cause for cell survival in tumours, giving them limitless replicative potentials (Hanahan and Weinberg, 2011).

2.1.5 Sustained angiogenesis

All cells in a tissue are located within 100 µm of a capillary blood vessel so as to receive oxygen and nutrients for its survival. Angiogenesis is carefully regulated once a tissue is formed and cancer cells in their initial stages lack angiogenic ability. They only acquire this ability prior to appearance of a full blown tumour (Hanahan and Folkman, 1996). Angiogenesis is initiated by overexpression of vascular endothelial growth factor (VEGF), and acidic and basic fibroblast growth factors (FGF1/2), with the down regulation of angiogenesis inhibiting factors, thrombospondin-1 or β-interferon (Volpert, *et al.*, 1997).

2.1.6 Tissue invasion and metastasis

Human cancer deaths are mainly as a result of cancer cells breaking off from the parent tumour and invading new tissues in a process known as metastasis (Sporn, 1996). They inhabit new tissues or organs where space and nutrients are not a limiting factor for their growth. As with the primary tumour, invading cancer cells also need to acquire the five mechanisms discussed above for them to survive in a new territory. Though the process is complex and more understanding is required, there is no question that several classes of proteins that are involved in tethering cells to their environment in a tissue are altered (Hanahan and Weinberg, 2000). One important protein whose function is eliminated to allow tissue invasion and metastasis is E-cadherin (Christofor and Semb, 1999). Changes to cell-to-cell adhesion molecules in addition to E-cadherin are also noticed which are believed to play a role in tissue invasion and metastasis.

It should be noted that the discussed aspects are common within most cancer types and other alternative pathways are being discovered that assist in propagation of this disease. It is no surprise that a lot of research is being conducted in this area, with new drug molecules being sought to combat the different complexity stages of cancer. Marine natural sources offer great diversity in chemical structures that can be explored for anticancer activity. Of particular interest are cytotoxic prenylated quinones and related compounds, of which a few will be discussed in the next section.

2.2 Cytotoxic marine natural products

2.2.1 Sesquiterpene quinones and hydroquinones

Marine natural products with a 1, 4-benzoquinone moiety have received a fair amount of attention due to their cytotoxic and anti-proliferative properties (Gordaliza, 2010). Promising opportunities for the development of new drug molecules are offered by quinones, naphthoquinones and hydroquinones of marine origin, and have been used to understand chemically induced toxicity in cellular mechanisms (Sunassee and Davies-Coleman, 2012). Of interest are the sesquiterpene quinones and hydroquinones isolated from sponges. The order Dictyoceratida is well-known for producing cytotoxic quinones that include avarone (**2.1**), avarol (**2.2**), bolinaquinone (**2.3**), nakijiquinone (**2.4**) and illimaquinone (**2.5**). They have been shown to be cytotoxic against several tumour cell lines, hence offer the promise of new structures that can be used in drug development (Gordaliza, 2010).

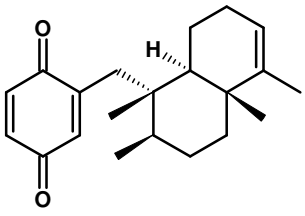

avarone (2.1)

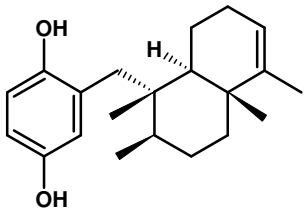

avarol (2.2)

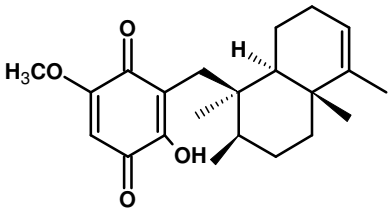

bolinaquinone (2.3)

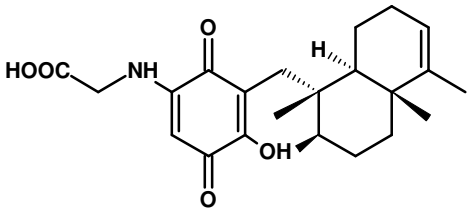

nakijiquinone A (2.4)

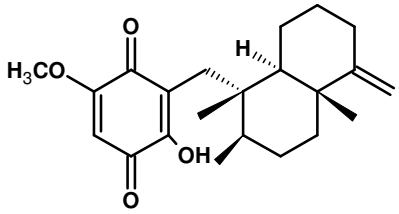

illimaquinone (2.5)

Avarone (**2.1**) and its hydroquinone avarol (**2.2**) are isolated from marine sponge *Dysidea avara* and have shown cytotoxic activity against leukaemia in both *in vitro* and *in vivo* studies, though they were determined to be more cytostatic rather than cytotoxic (Cozzolino, *et al*., 1990). Bolinaquinone (**2.3**), on the other hand causes DNA damage and its cytotoxic activity has been noticed in HCT-116 human colon carcinoma cell line with an IC_{50} value of 1.9 µg/mL (Guzmán, *et al*., 1998). As for the nakijiquinones (**2.4**), cytotoxic activity has been observed against L-1210 and KB cell lines, with IC_{50} values ranging between 2.8 - 8.1 µg/mL and 1.2 - 7.6 µg/mL, respectively (Gordaliza, 2010), whilst illimaquinone (**2.5**) exhibited cytotoxicity against P-388 leukaemia cells and in several solid tumours A-549, HT-29 and B16/F10 with

IC_{50} values of 0.9 µg/mL, 3.4 µg/mL and 1.1 µg/mL, respectively (Rodriguez, *et al*., 1992). Further developments are underway to improve these molecules as drug candidates as potency for some of these metabolites has only been three times less than that of doxorubicin (Laube, *et al*., 2009).

2.2.2 Isoquinoline quinones and iminoquinones

Several isoquinoline quinones have been isolated from marine sponges *Cribrochalina* and *Petrosia* (Hawas, *et al*., 2009) and from sponge related microbes such as *Streptomyces* and *Calothrix* (Milanowski, *et al*., 2004). Antimicrobial and antitumour activities have been demonstrated with this class of compounds and a few are displayed below:

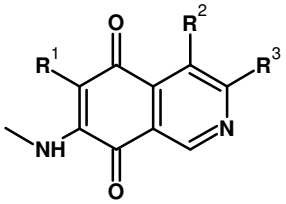

2.6 R^1 = H, R^2 = H, R^3 = $COOCH_3$

2.7 R^1 = Cl, R^2 = H, R^3 = CH_3

2.8 R^1 = H, R^2 = H, R^3 = CH_3

2.9 R^1 = H, R^2 = CH_3, R^3 = CH_3

2.10 R^1 = H, R^2 = H, R^3 = 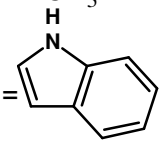

In monolayer cell proliferation assays conducted with these metabolites, mansouramycin C (**2.6**) was the most active with an overall potency of 0.1 µM across a panel of 36 human tumour cells, of which 14 were different solid tumour types. It showed great selectivity towards 10 of these tumours i.e., bladder cancer (T-24), glioblastoma (SF-268), lung cancer (LXFA 629L), mammary cancer (MCF-7), melanoma (MEXF 276L, MEXF 514L, MEXF 520L), ovarian cancer (OVCAR-3), renal cancer (RXF 944L), and uterus cancer (UXF 1138L (Hawas, et al., 2009). With regards to the other isoquinolines, mansouramycin B **(2.7**) and 3-methyl-7-(methyl amino)-5, 8-isoquinolinedione (**2.8**) had second highest activities with average cytotoxic IC_{50} values of 2.7 µM and 3.5 µM, respectively. They also showed some degree of selective cytotoxicity to some cancers but to a lesser extent than **2.6**.

Different substitution patterns on mansouramycins mapped some SARs with chlorination (R^1) influencing cytotoxic activity. R^2 and R^3 substitution also influenced cytotoxicity as observed in compounds **2.9** and **2.6** (Hawas, *et al*., 2009)**.** Related compounds to mansouramycins, caulibugulones A-F (**2.11-2.16**), also possess cytotoxic properties. They have been isolated from extracts of the marine bryozoan *Caulibugula intermis* and tested by the U.S. National Cancer Institute (NCI) on their 60 tumour cell lines (Milanowski, *et al*., 2004).

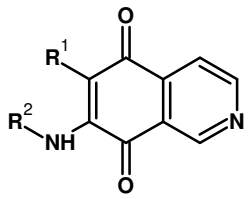

2.11 R^1 = H, R^2 = CH_3
2.12 R^1 = Br, R^2 = CH_3
2.13 R^1 = Cl, R^2 = CH_3
2.14 R^1 = H, R^2 = CH_2CH_2OH

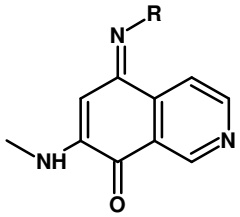

2.15 R = H
2.16 R = CH_2CH_2OH

The biological data for caulibugulones A-F (**2.11-2.16**) encompasses cytotoxic activities obtained against a murine IC-2WT cell line. Halogenation at R^1 was determined to be unimportant for cytotoxicity as compounds **2.11-2.13** had similar IC_{50} values. However the iminoquinone **2.15** was more potent than its counterpart **2.11** and substitutions with the ethyl alcohol at R^2 and R on both compound classes resulted in the more active metabolites (Milanowski, *et al*., 2004). Comparable activities were noticed for caulibugulones, cribrostatins and related isoquinoline quinones (Pettit, *et al*., 2000).

2.2.3 Prenylated quinones and hydroquinones

Over 600 prenylated quinone-type metabolites have been isolated from marine organisms, and approximately a third of these metabolites have demonstrated cytotoxic behaviours, with some possessing antioxidant properties (Sunassee and Davies-Coleman, 2012). Brown algae and sponges account for 60 % of prenylated systems produced by marine species. Their chemical structures usually contain a benzoquinone or hydroquinone moiety with a prenyl side chain attached to the C-2 position relative to the ketone. The length of the side chain and substitution patterns along this chain vary from species to species, which results in different metabolites being produced.

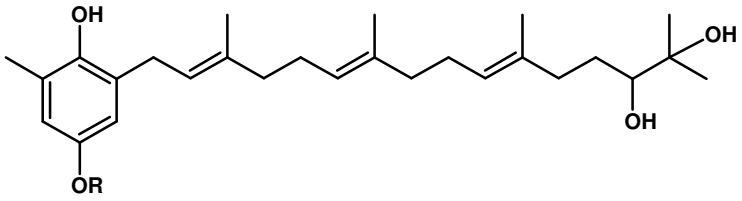

2.17 R = H

2.18 R =

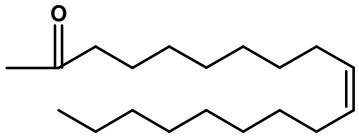

2.19 R =

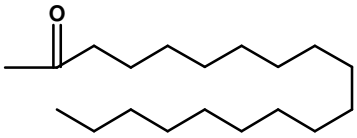

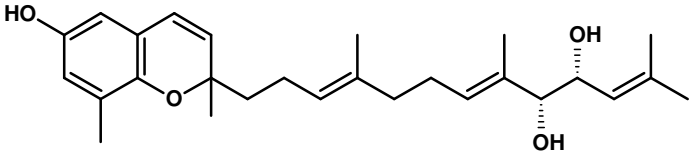

2.20

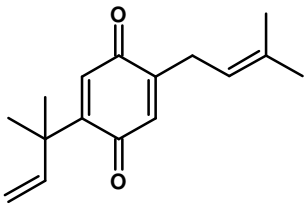

2.21

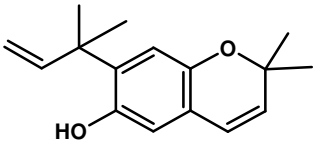

2.22

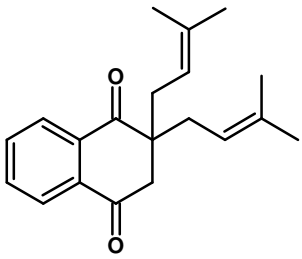

2.23

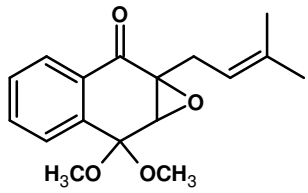

2.24

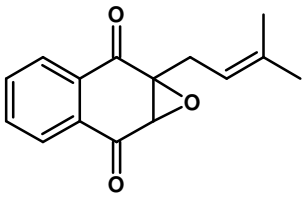

2.25

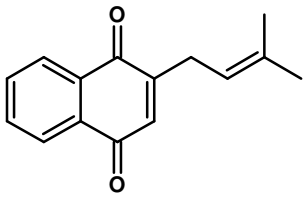

2.26

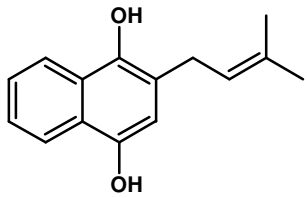

2.27

Plastoquinones **2.17-2.19** were obtained from crude extracts of *Sargassum micracanthum* and have been shown to be cytotoxic against a colon 26–L5 cancer cell line. *In vitro* assays indicated **2.17** and **2.18** as strongly cytotoxic with **2.19** showing moderate cytotoxicity (Mori, *et al*., 2005). The sargachromanol **2.20** induces apoptosis in human leukaemia HL-60 cells *via* caspase-3 signalling activation (Heo, *et al*., 2011), a phenomenon essential in one of the hallmarks of cancer described above. Smaller prenylated quinones, **2.21** and **2.22** isolated from the brown alga *Perithalia capillaris* found in New Zealand also exhibited cytotoxicity against human leukaemia HL-60 cell lines. Compound **2.21** was more cytotoxic with an IC_{50} of 0.3 μM compared to compound **2.22** that had an IC_{50} value of 5.6 μM (Sansom, et al., 2007). An addition to these unusual smaller prenylated systems are the naphthoquinones **2.23-2.27.** These metabolites are isolated from the brown algae *Landsburgia quercifolia*. They are quite similar to those found in higher plants and exhibit cytotoxic activity against P-388 leukaemia cells, compound **2.26** showing the greatest activity (Perry, *et al*., 1991)

Cytotoxic activities of marine quinones from sponges and brown algae discussed above have sparked interest in the chemical composition and cytotoxicity of a large number of marine species that contain metabolites with hybrid structures related to quinones / hydroquinones / naphthoquinones. More selective drug candidates are needed, that exert their action with little to no side effect profiles. An ideal anticancer drug should result in the disruption of all six hallmarks of cancer, and Hsp90 inhibition has been linked to such a disruption (Miyata, *et al*., 2013). Detailed mechanistic analysis have suggested that Hsp90 is a promising target for anticancer therapy.

2.3 Heat shock proteins (Hsp90)

Molecular chaperones are a diverse set of enzymes that are responsible for proper folding and assembly of proteins in eukaryotic cells. Three major molecular chaperone systems have been reported in literature which include Hsp70, Hsp90 and TRiC/CCT (Frydman, 2001). Although their roles in biological systems are thought not to overlap, they function in a coordinated way that brings about survival of that particular cellular system (Li, *et al*., 2012).

The 90 kDa heat shock proteins (Hsp90) have been intensely studied and are involved in fundamental processes related to cell cycle control, cell survival, hormone signalling and response to cellular stress (Donnelly and Blagg, 2008; Li, *et al*., 2012). Four human Hsp90 isoforms have been identified with the 2 major cytosolic forms being Hsp90α and Hsp90β (Donnelly and Blagg, 2008). Hsp90 interacts as part of a multiprotein complex with other sets of proteins known as co-chaperones that assist it in its function (Pratt and Toft, 2003). Cancer cells are exposed to numerous cellular stresses, including nutrient deprivation, oxidative stress and high growth rates, hence such chaperones play an important role in maintaining multiple mutated and over-expressed signalling proteins that promote cancer cell growth and survival. In normal cells, Hsp90 accounts for 1-2% of all cellular proteins (Csermely, *et al*., 1998). In stressed cells the concentrations of certain Hso90 isoforms are upregulated in an effort to preserve protein homeostasis. In so doing, they provide tumour cells with the means to survive in harsh conditions by stabilizing oncogenic proteins that would otherwise be degraded (Sreedhar, *et al*., 2004).

The main goal for Hsp90 inhibition is centred on prohibiting proper functioning of several “client proteins” that are key regulators of cellular growth, differentiation, stress-response and apoptotic pathways in cancer cells. These include mutated signalling proteins (p53, Bcr-Abl, Raf-1, Akt), HER2/Neu (ErbB2), nNos, HIF-1α, epidermal growth factor receptors (EGFRs) and growth factor receptors (IGF-1Rs), Cdk4 (Kamal, *et al*., 2004). Hsp90 inhibition results in client protein degradation and subsequently leads to cell death. To effectively synthesize molecules that inhibit such a big chaperone, an understanding of its crystal structure and function is essential.

2.3.1 Hsp90 crystal structure

Hsp90 is a homodimeric protein, with each protomer consisting of three main structural domains i.e., N-terminal domain, middle domain and C-terminal domain (**Figure 2.2**) (Li, *et al*., 2012). The N-terminal domain contains an ATP binding site and most inhibitors that have been designed thus far bind to this pocket of Hsp90 e.g., analogues of the natural occurring Hsp90 inhibitor, geldanamycin (Kamal, *et al*., 2003). The middle domain is connected to the N-terminus by a charged linker and is a site for binding for most client proteins and co-chaperones (Street, *et al*., 2011). Tetratricopeptide repeat (TPR) domain-containing co-chaperones are anchored at the C-terminus with its C-terminal MEEVD motif (Scheufler, *et al*., 2000). A few molecules e.g., novobiocin have been demonstrated to bind to an alternative site in the C-terminus of Hsp90 (Hadden, *et al*., 2009).

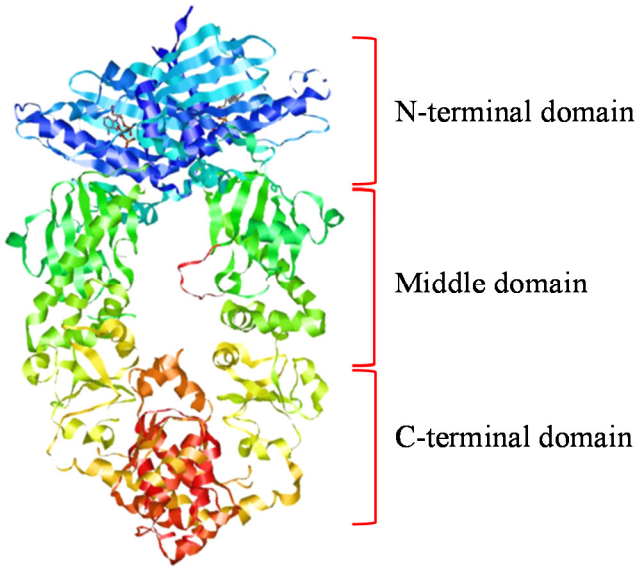

Figure 2.2: N-terminal, middle and C-terminal domains of Hsp90 protein (adapted from http://www.ucl.ac.uk/~zcbtfi4/domainm.html. accessed on 01.01 2015).

Hsp90 protein is a flexible macromolecule, and therefore can assume different conformations effected by ATP binding to the N-terminal domain, and interactions with co-chaperones. In its *apo* state, Hsp90 acquires the V-shaped open conformation due to constitutive dimerization at the C-terminus. This V shape closes up when bound to ATP, dimerizing the N-terminal domains and bringing them closer together to the middle domain. After ATP hydrolysis, ADP is released and an open conformation is restored (**Figure 2.3**). Progress through these different stages of the ATP cycle of Hsp90 also relies on interactions with a cohort of co-chaperones that influence ATP hydrolysis, post-translational modifications or client protein interactions of Hsp90 (not shown) (Li, *et al*., 2012).

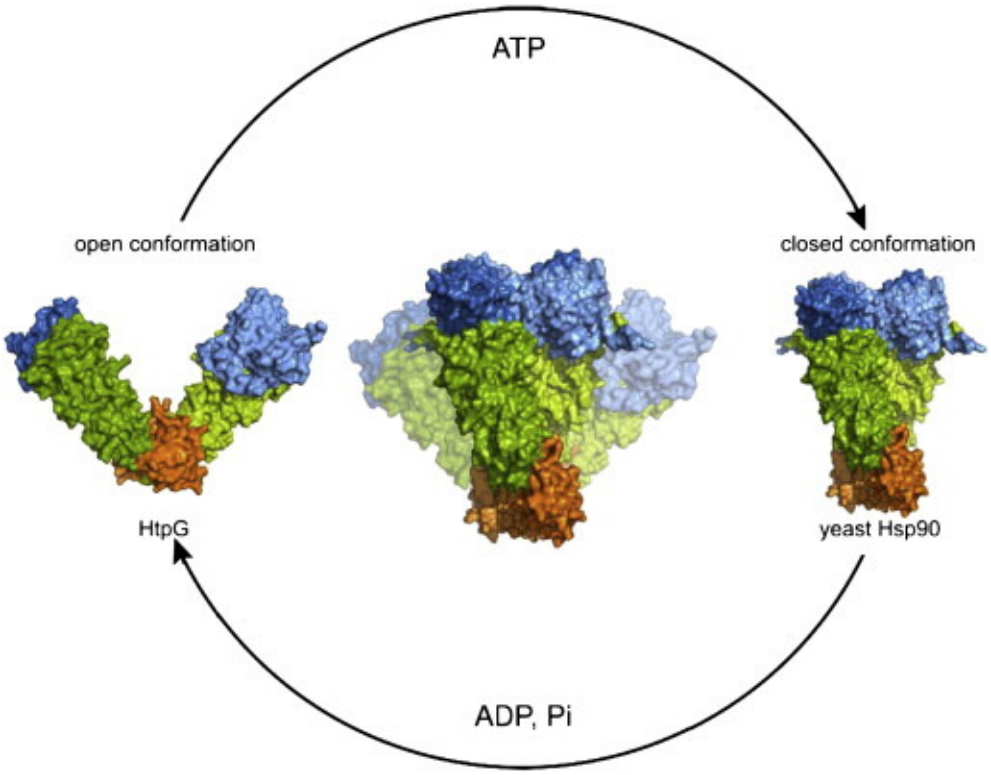

Figure 2.3: Hsp90 from *E. coli* (HtpG).

Open conformation and nucleotide-bound yeast Hsp90 in the closed conformation. The N-domain is depicted in blue, the M-domain in green and the C-domain in orange (Li, *et al*., 2012)

Due to such flexibility of the Hsp90 chaperone system, it is most likely that it can conform to various molecules binding to its domains, therefore favouring design of several classes of lead molecules that can be used as inhibitors.

2.3.2 N-terminal Hsp90 inhibitors

(Geldanamycin, resorcinol and purine related compounds)

Hsp90 in tumour cells has been demonstrated to be in its highly active state and has a higher affinity for geldanamycin (**2.28**) and its analogues (**2.29-2.30**) (Kamal, *et al*., 2003).

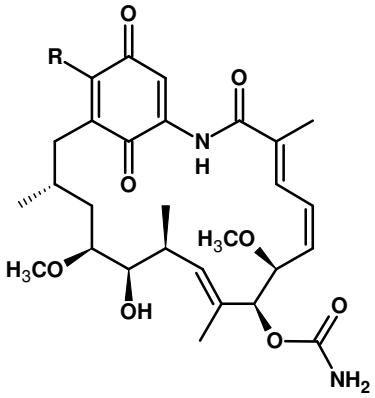

2.28 R = OCH_3 : Geldanamycin
2.29 R = $NHCH_2CH{=}CH_2$: 17 AAG
2.30 R = $NHCH_2CH_2N(CH_3)_2$: 17 DMAG
2.31 R = NH_2: IPI-493
2.32 R = $CH_3CH_2CH_2NH_2^+CI^-$: IPI-504

Differences in active states between tumour cells' Hsp90 and normal cell Hsp90 favours selectivity for drug design and development. Such an observation has triggered enormous attention to Hsp90 as a potential target for cancer therapy. Client proteins require ATPase activity of Hsp90 for their activation and stabilization which is non-existent in the presence of Hsp90 inhibitors (Kamal, *et al*., 2003). Molecules such as benzoquinones, ansamycins, radicicols and purine analogues have been shown to compete for the N-terminal binding site of Hsp90, thereby inhibiting its activity. Loss of ATPase activity results in loss of signal transduction pathways that promote growth signals of cancerous cells, and eventual death. However, one negative aspect of many N-terminal Hsp90 inhibitors is that they also induce the stress response that leads to the upregulation of other stress related proteins, like Hsp70 and Hsp27, which can partially compensate for the loss of Hsp90 function. Several Hsp90 inhibitors are in clinical trial phases and are shown below:

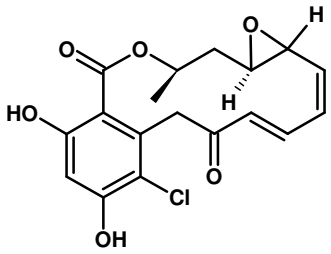

Radicicol (2.33)

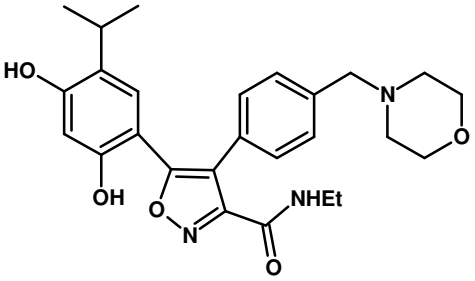

NVP-AUY922 (2.34)

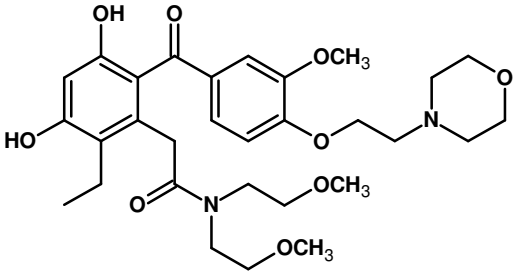

KW-2478 (2.35)

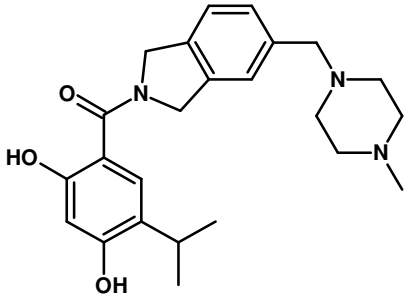

AT13387 (2.36)

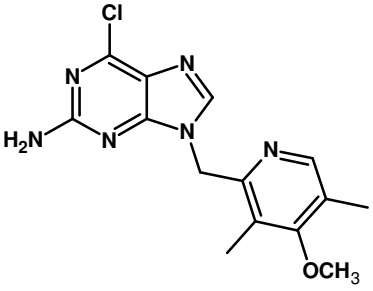

BIIB021 (2.37)

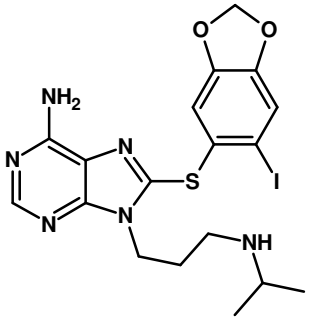

PU-H71 (2.38)

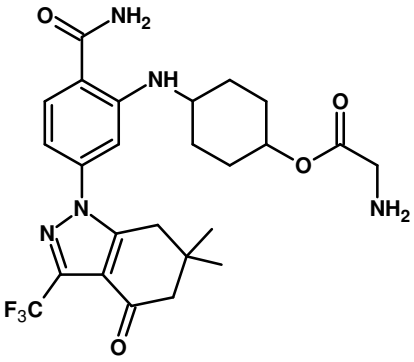

SNX-5422 (2.39)

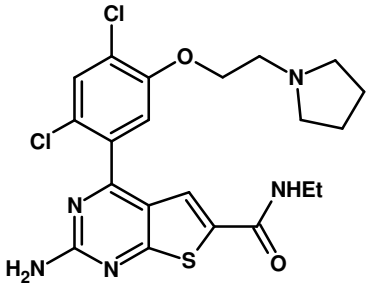

NVP-BEP800 (2.40)

Geldanamycin (**2.28**) and radicicol (**2.33**) were the first two natural products that were discovered to be Hsp90 inhibitors (Neckers and Workman, 2012). Although they were too toxic and unstable for clinical use, they paved the way for other derivatives that have entered clinical trials. 17-AAG (**2.29**), known as tanespimycin was the first geldanamycin (**2.28**) analogue to enter clinical studies, and it showed promising activity against several malignant cancers (Banerji, *et al*., 2005). However further studies were discontinued due to suboptimal inhibition of targeted client proteins by this drug. No tumour regression was observed but rather a form of cytostatic arrest of cancer cells was noticed (Neckers and Workman, 2012). Drug metabolism of tanespimycin also yielded products that resulted in liver toxicity and further advocated its discontinued use (Kelland, *et al*., 1999). 17-DMAG (**2.30**) (alvespimycin), was introduced which possessed better metabolism and pharmacokinetic profiles but its further development together with IPI-493 (**2.31**) was halted. IP1-504 (**2.32**) development was also discontinued due to hepatotoxicity when tested against gastrointestinal stromal tumour. Liver toxicity of geldanamycin (**2.28**) and its analogues (**2.39-2.32**) was linked to the presence of the quinone moiety and its metabolized products (Janin, 2010). .

With the assistance of virtual screening, new sets of compounds were discovered with resorcinol and purine scaffolds. BIIB021 (**2.37**) and PU-H71 (**2.38**) containing the purine skeleton are now in Phase 1 clinical trials, together with NVP-AUY922 (**2.34**), KW-2478 (**2.35)** and AT13387 (**2.36**) of resorcinol origin which are going further development (Neckers and Workman, 2012). Other chemotypes being investigated are SNX-5422 (**2.39**) and NVP-BEP800 (**2.40**), currently in clinical trials (Fadden, *et al*., 2010; Brough, *et al*., 2009).

2.3.3 C-terminal Hsp90 inhibitors

A second ATP binding pocket has been located in the C-terminus of Hsp90 protein. Several compounds have been identified that bind to this active site, which results in Hsp90 inhibition (Donnelly and Blagg, 2008).

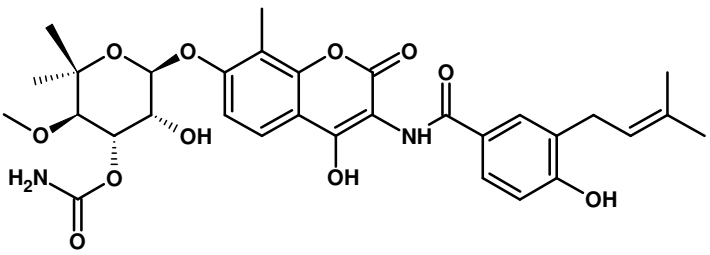

novobiocin (2.41)

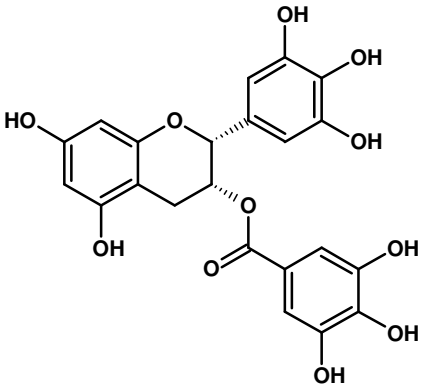

EGCG (2.42)

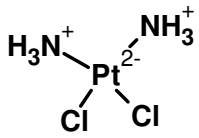

cisplatin (2.43)

Novobiocin (**2.41**) weakly interacts with Hsp90 at a concentration of 700 μM in SkBr3 cells, consequently leading to client protein degradation and cell death. A form of competitive inhibition with ATP has been demonstrated on the C terminus which results in the association of Hsp90 and its co-chaperones Hsc70 and p23 being disrupted (Marcu, *et al*., 2000). Cisplatin (**2.43**) on the other hand has a higher binding affinity for Hsp90, with its binding site located close to the C-terminal ATP binding site. It affects nucleotide binding and Hsp90 chaperone activity. However resistance has been noticed with this drug which could be a limiting factor for it to act as a potential Hsp90 inhibitor. (Donnelly and Blagg, 2008). Epigallocatechin-3-gallate (EGCG) (**2.42**) inhibits telomerases and kinases enzymes that are related to client proteins. It has been shown to also bind to the C-terminus of Hsp90 protein but in a different way to novobiocin (**2.41**) (Palermo, *et al*., 2005).

Unfortunately the co-crystal structure of the C-terminus is unknown, therefore there is limited knowledge about the nature of the binding pocket. However it has been proposed that the C terminus is only available for binding once the N-terminus is occupied (Csermely, *et al*., 1998).

Although this second ATP binding site does not possess ATPase activity, it is involved in the correct conformation of the entire Hsp90 protein upon ATP binding on the N-terminus. One of its functions is to trap the nucleotide in the ATPase cycle, which is altered when novobiocin (**2.41**) or any other inhibitor is bound to the C-terminus (Donnelly and Blagg, 2008). Further studies are still underway using novobiocin (**2.41**) and its analogues to fully understand the structure and role played by the C-terminal domain in Hsp90 functions (Marcu, *et al*., 2000).

2.3.4 Hsp90 inhibitors containing the naphthoquinone/quinone core

Exploration of a quinone moiety as a pharmacophoric element in Hsp90 inhibition has been continued by investigating the effect of having a naphthoquinone functionality on drug lead molecules. High through-put screening of small molecules has identified naphthoquinone containing molecules as potential inhibitors of Hsp90 protein.

HTS1-HTS3 scaffolds (**2.44-2.46**) were determined to possess Hsp90 inhibition properties. Preliminary studies indicated that they bind to the C-terminal domain in a similar way to novobiocin (**2.41**) though this is still to be fully ascertained. Anti-proliferative assays conducted for these compounds also showed their tendency to be effective in treating oestrogen dependent cancers, making them useful in breast cancer treatment (Hadden, *et al*., 2009).

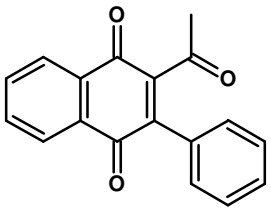

HTS1 (2.44)

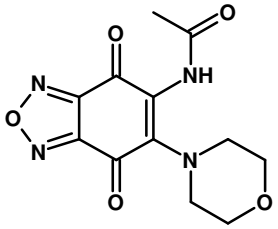

HTS2 (2.45)

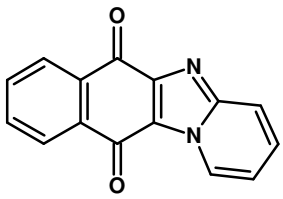

HTS3 (2.46)

From amongst the meroterpenoids, sargaquinonic acid (SQA) (**2.47**) has demonstrated some degree of interaction with Hsp90 protein (Moyo, 2013).

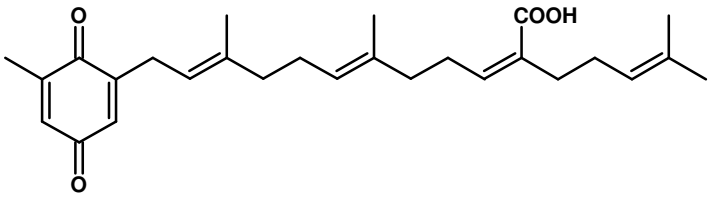

2.47

The potential of SQA (**2.47**) acting as a potential Hsp90 inhibitor inspired our research on meroterpenoids. SQA (**2.47**) as indicated in the previous chapter, is isolated from *S. incisifolium* with several other meroterpenoids (Afolayan, *et al*., 2008). Since hepatoxicity

reports have been published with regards to benzoquinones, modifications of SQA (**2.47**) to sarganaphthoquinoic acid (SNQA) as a potential Hsp90 inhibitor were targeted and comparison made to lapachol derivatives and known inhibitors belonging to the ansamycin class of compounds e.g., geldanamycin (**2.28**). Isolation and characterization of these natural quinones is therefore discussed in the following chapter.

References

Afolayan, A., Bolton, J., Lategan, C., Smith, P., & Beukes, D. (2008). Fucoxanthin, tetraprenylated toluquinone and toluhydroquinone metabolites from Sargassum heterophyllum inhibit the *in vitro* growth of the malaria parasite Plasmodium falciparum. *Zeitschrift für Naturforschung, 63c*, 848-852.

Ashkenazi, A., & Dixit, V. (1999). Apoptosis control by death and decoy receptors. *Current Opinion in Cell Biology, 11*, 255–260.

Banerji, U., O'Donnell, A., Scurr, M., Pacey, S., Stapleton, S., Asad, Y., Simmons, L., Maloney, A., Raynaud, F., Campbell, M., Walton, M., Lakhani, S., Kaye, S., Workman, P., Judson, I. (2005). Phase I pharmacokinetic and pharmacodynamic study of 17-allylamino, 17-demethoxygeldanamycin in patients with advanced malignancies. *Journal of Clinical Oncology, 11*, 7023–32.

Bishop, J., & Weinberg, R. (1996). *Molecular Oncology.* New York: Scientific American, Inc.

Brough P.A., Barril, X., Borgognoni, J., Chene, P., Davies, N.G., Davis, B., Drysdale, M.J., Dymock, B., Eccles, S.A., Garcia-Echeverria, C., Fromont, C., Hayes, A., Hubbard, R.E., Jordan, A.M., Jensen, M.R., Massey, A., Merrett, A., Padfield, A., Parsons, R., Radimerski, T., Raynaud, F.I., Robertson, A., Roughley, S.D., Schoepfer, J., Simmonite, H., Sharp, S.Y., Surgenor, A., Valenti, M., Walls, S., Webb, P., Wood, M., Workman, P., Wright, L. (2009). Combining hit identification strategies: fragment-based and in silico approaches to orally active 2-aminothieno[2,3-d]pyrimidine inhibitors of the Hsp90 molecular chaperone. *Journal of Medicinal Chemistry, 52*, 4794–809.

Bryan, T., & Cech, T. (1999). Telomerase and the maintenance of chromosome ends. *Current Opinion in Cell Biology, 11*, 318–324.

Cheng, N., Chytil, A., Shyr, Y., Joly, A., & Moses, H. (2008). Transforming growth factor-beta signaling-deficient fibroblasts enhance hepatocyte growth factor signaling in mammary carcinoma cells to promote scattering and invasion. *Molecular Cancer Research, 6*, 1521–1533.

Christofor, G., & Semb, H. (1999). The role of the cell-adhesion molecule E-cadherin as a tumour-suppressor gene. *Trends in Biochemical Sciences , 24*, 73–76.

Cozzolino, R., De Giulio, A., De Rosa, S., Strazzullo, G., Gašič, M., Sladić, D., & Zlatović, M. (1990). Biological activities of avarol derivatives, 1. Amino derivatives. *Journal of Natural Products, 53*, 699–702.

Csermely, P., Schnaider, T., So˜ ti, C., Proha´szka, Z., & Nardai, G. (1998). The 90-kDa molecular chaperone family: structure, function, and clinical applications. A comprehensive review. *Pharmacology & Therapeutics, 79*, 129– 168.

Donnelly, A., & Blagg, B. (2008). Novobiocin and additional inhibitors of the Hsp90 C-terminal nucleotide-binding pocket. *Current Medicinal Chemistry, 15*, 2702–2717.

Fadden P., Huang K.H., Veal J.M., Steed P.M., Barabasz A.F., Foley B., Hu M., Partridge J.M., Rice J., Scott A., Dubois L.G., Freed T.A., Silinski M.A., Barta T.E., Hughes P.F.,Ommen A., Ma W., Smith E.D., Spangenberg A.W., Eaves J., Hanson G.J., Hinkley L., Jenks M., Lewis M., Otto J., Pronk G.J., Verleysen K., Haystead T.A., & Hall S.E. (2010). Application of chemoproteomics to drug discovery: identification of a clinical candidate targeting Hsp90. *Chemical Biology, 17*, 686–94.

Frydman, J. (2001). Folding of newly translated proteins in vivo: the role of molecular chaperones. *Annual Review of Biochemistry, 70*, 603–647.

Fulda, S., & Debatin, K. (2006). Extrinsic versus intrinsic apoptosis pathways in anticancer chemotherapy. *Oncogene, 25*, 4798-4811.

Fynan, T., & Reiss, M. (1993). Resistance to inhibition of cell growth by transforming growth factor-b and its role in oncogenesis. *Critical Reviews in Oncogenesis, 4*, 493–540.

Gordaliza, M. (2010). Cytotoxic terpene quinones from marine sponges. *Marine Drugs, 8*, 2849-2870.

Green, D., & Reed, J. (1998). Mitochondria and apoptosis. *Science, 281*, 1309–1312.

Guzmán, F., Copp, B., Mayne, C., Concepcion, G., Mangalindan, G., Barrows, L., & Ireland, C. (1998). Bolinaquinone: a novel cytotoxic sesquiterpene hydroquinone from Philippine Dysidea sponge. *Journal of Organic Chemistry, 63*, 8042–8044.

Hadden, M., Hill, S., Davenport, J., Matts, R., & Blagg, B. (2009). Synthesis and evaluation of Hsp90 inhibitors that contain the 1,4- naphthoquinone scaffold. *Bioorganic and Medicinal Chemistry, 17*, 634–640.

Hanahan, D., & Folkman, J. (1996). Patterns and emerging mechanisms of the angiogenic switch during tumorigenesis. *Cell, 86*, 353–364.

Hanahan, D., & Weinberg, R. (2000). The hallmarks of cancer. *Cell, 100*, 57–70.

Hanahan, D., & Weinberg, R. (2011). Hallmarks of cancer: the next generation. *Cell, 144*, 646-674.

Hawas, U., Shaaban, M., Shaaban, K., Speitling, M., Maier, A., Kelter, G., Fiebig, H.H., Meiners, M., Helmke, E., & Laatsch, H. (2009). Mansouramycins A-D, cytotoxic isoquinolinequinones from a marine Streptomycete. *Journal of Natural Products, 72*, 2120–2124.

Hayflick, L. (1997). Mortality and immortality at the cellular level. A review. *Biochemistry, 62*, 1180–1190.

Heo, S., Kim, K., Yoon, W., Oh, C., Choi, Y., Affan, A., Lee, Y.J., Lee, H.S., & Kang, D. (2011). Chromene induces apoptosis via caspase-3 activation in human leukemia HL-60 cells. *Food and Chemical Toxicology, 49*, 1998–2004.

Janin, Y. (2010). ATPase inhibitors of heat-shock protein 90, second season. *Drug Discovery Today, 15*, 342–53.

Kamal, A., Boehm, M., & Burrows , F. (2004). Therapeutic and diagnostic implications of Hsp90 activation. *Trends in Molecular Medicine, 10*, 283–90.

Kamal, A., Thao, L., Sensintaffar, J., Zhang, L., Boehm, M., Fritz, L., & Burrows, F. (2003). A high-affinity conformation of Hsp90 confers tumour selectivity on Hsp90 inhibitors. *Nature, 425*, 407-410.

Kelland L.R,. Sharp, S.Y., Rogers, P.M., Myers, T.G., & Workman, P. (1999). DT-Diaphorase expression and tumor cell sensitivity to 17-allylamino17-demethoxygeldanamycin, an inhibitor of heat shock protein 90. *Journal of the National Cancer Institute, 91*, 1940–9.

Korsmeyer, S. (1992). Chromosomal translocations in lymphoid malignancies reveal novel proto-oncogenes. *Annual Review of Immunology, 10*, 785–807.

Laube, T., Bernet, A., Dahse, H., Jacobsen, I., & Seifert, K. (2009). Synthesis and pharmacological activities of some sesquiterpene quinones and hydroquinones. *Bioorganic & Medicinal Chemistry, 17*, 1422–1427.

Li, J., Soroka, J., & Buchner, J. (2012). The Hsp90 chaperone machinery: conformational dynamics and regulation by co-chaperones. *Biochimica et Biophysica Acta*, *1823*, 624–635.

Marcu M.G., Chadli, A., Bohouche, I., Catelli, B., & Neckers, L.M. (2000). The heat shock protein 90 antagonist novobiocin interacts with a previously unrecognized ATP-binding domain in the carboxyl terminus of the chaperone. *The Journal of Biological Chemistry, 275*, 37181–37186.

Marcu, M.G., Schulte, T.W., & Neckers, L. (2000). Novobiocin and related coumarins and depletion of heat shock protein 90-dependent signaling proteins. *Journal of the National Cancer Institute, 92*, 242–248.

Milanowski, D., Gustafson, K., Kelley, J., & McMahon, J. (2004). Caulibugulones A-F, novel cytotoxic isoquinoline quinones and iminoquinones from the marine Bryozoan Caulibugula intermis. *Journal of Natural Products, 67*, 70-73.

Miyata, Y., Nakamoto, H., & Neckers, L. (2013). The therapeutic target Hsp90 and cancer hallmarks. *Current Pharmaceutical Design, 19*, 347-365.

Mori, J., Iwashima, M., Wakasugi, H., Saito, H., Matsunaga, T., Ogasawara, M., Takahashi, S., Suzuki, H., & Hayashi, T. (2005). New plastoquinones isolated from the brown alga, Sargassum micracanthum. *Chemical and Pharmaceutical Bulletin, 53*, 1159–1163.

Moyo, B. (2013). *The screening and characterisation of compounds for modulators of Heat shock protein (Hsp90) in a breast cancer cell model.* (PhD) Rhodes University.

Neckers, L., & Workman, P. (2012). Hsp90 molecular chaperone inhibitors: are we there yet? *Clinical Cancer Research, 18*, 64-76.

Palermo, C.M., Westlake, C.A., & Gasiewicz, T.A. (2005). Epigallocatechin gallate inhibits aryl hydrocarbon receptor gene transcription through an indirect mechanism involving binding to a 90 kDa heat shock protein. *Biochemistry, 44*, 5041–5052.

Perry, N., Blunt , J., & Munro, M. (1991). A cytotoxic and antifungal 1,4-naphthoquinone and related compounds from a New Zealand brown alga, Landsburgia quercifolia. *Journal of Natural Products, 54*, 978–985.

Pettit, G. R., Knight, J. C., Collins, J. C., Herald, D. L., Pettit, R. K., Boyd, M. R., & Young, V. G. (2000). Antineoplastic agents 430. Isolation and structure of cribrostatins 3, 4, and 5 from the republic of Maldives Cribrochalina Species. *Journal of Natural Products, 63*, 793-798.

Pratt, W., & Toft, D. (2003). Regulation of signaling protein function and trafficking by the Hsp90/hsp70-based chaperone machinery. *Experimental Biology and Medicine*, *228*, 111–133.

Rodriguez, J., Quiñoá, E., Riguera, R., Peters, B., Abrell, L., & Crews, P. (1992). The structures and stereochemistry of cytotoxic sesquiterpene quinones from Dactylospongia elegans. *Tetrahedron, 48*, 6667–6680.

Sansom, C., Larsen, L., Perry, N., Berridge, M., Chia, E., Harper, J., & Webb, V. (2007). An Antiproliferative bis-prenylated quinone from the New Zealand brown alga Perithalia capillaris. *Journal of Natural Products, 70*, 2042–2044.

Scheufler, C., Brinker, A., Bourenkov, G., Pegoraro, S., Moroder, L., Bartunik, H., Hartl, F.U., & Moaref, I. (2000). Structure of TPR domain–peptide complexes: critical elements in the assembly of the Hsp70-Hsp90 multichaperone machine. *Cell*, *101*, 199–210.

Shay, J., & Bacchetti., S. (1997). A survey of telomerase activity in human cancer. *European Journal of Cancer, 33*, 787–791.

Sporn, M. (1996). The war on cancer. *Lancet , 347*, 1377–1381.

Sreedhar, A., Kalmar, E., Csermely, P., & Shen, Y. (2004). Hsp90 isoforms: functions, expression and clinical importance. *FEBS Letters*, *562*, 11– 15.

Street, T., Lavery, L., & Agard, D. (2011). Substrate binding drives large-scale conformational changes in the Hsp90 molecular chaperone. *Molecular Cell, 42*, 96–105.

Sunassee, S., & Davies-Coleman, M. (2012). Cytotoxic and antioxidant marine prenylated quinones and hydroquinones. *Natural Product Reports, 29*, 513–535.

Thornberry, N., & Lazebnik, Y. (1998). Caspases: enemies within. *Science, 281*, 1312–1316.

Volpert, O., Dameron, K., & Bouck, N. (1997). Sequential development of an angiogenic phenotype by human fibroblasts progressing to tumorigenicity. *Oncogene, 14*, 1495–1502.

Weinberg, R. (1995). The retinoblastoma protein and cell cycle control. *Cell, 81*, 323–330.

Wright, W., Pereira-Smith, O., & Shay, J. (1989). Reversible cellular senescence: implications for immortalization of normal human diploid fibroblasts. *Molecular and Cellular Biology, 9*, 3088–3092.

Wyllie, A., Kerr, J., & Currie, A. (1980). Cell death: the significance of apoptosis. *International Review of Cytology, 68*, 251–306.

CHAPTER THREE

Isolation and characterization of quinone natural products

Abstract

The isolation of cytotoxic prenylated quinones from *Sargassum incisifolium* was conducted in an effort to acquire starting material for further studies. We aimed to explore the potential of these metabolites to inhibit Hsp90 function in the treatment of cancer. Five metabolites were isolated and characterized from *Sargassum incisfolium.* Additional compounds were obtained from a natural product library that included lapachol and its semi-synthesized derivatives. Isolation and characterization of these natural products is discussed in this chapter.

3.1 Introduction

Prenylated quinones are particularly abundant in the brown algal genera *Sargassum* and *Cystoseria* (Reddy and Urban, 2009). Various biological activities have been associated with these types of compounds, and we were particularly interested in meroterpenoids isolated from *Sargassum incisifolium.* Previous work conducted on this species has afforded five secondary metabolites shown below. Sargahydroquinoic acid (SHQA) (**3.1**), sargaquinoic acid (SQA) (**2.47**), sargaquinal (**3.2**), sargachromenol (**3.3**) and fucoxanthin (**3.4**) demonstrate antiplasmodial and cytotoxic activities against a chloroquine sensitive strain of *Plasmodium falciparum* (Afolayan, *et al*., 2008) and MDA-MB-231 breast cancer cell line, respectively (de la Mare, *et al*., 2012; Munedzimwe, 2012).

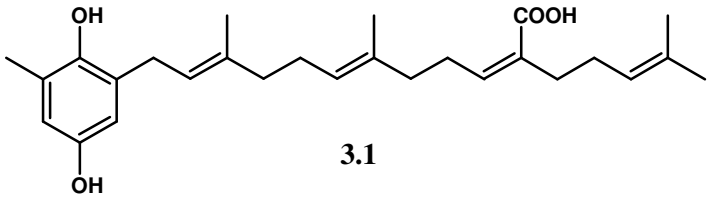

3.1

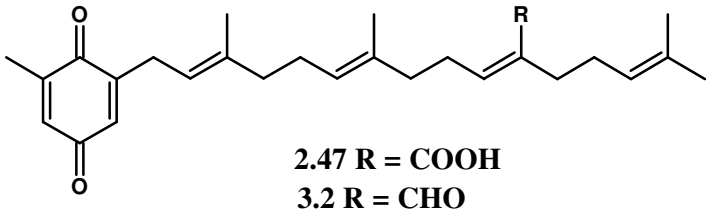

2.47 R = COOH
3.2 R = CHO

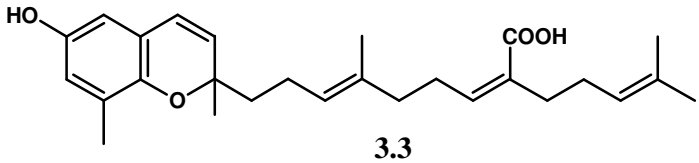

3.3

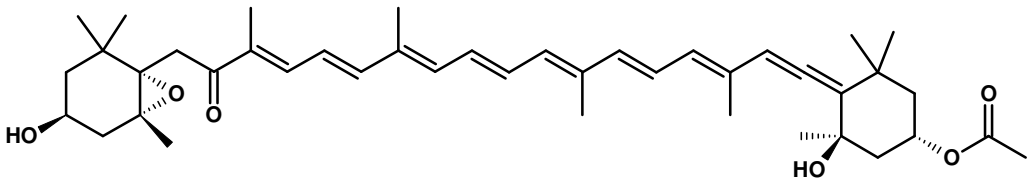

3.4

3.1.1 Aim of the study

Sargaquinoic acid (SQA) (**2.47**) and related compounds have been shown to be cytotoxic and potentially inhibit Hsp90 function (de la Mare, *et al*., 2012; Moyo, 2013). The main aim of this part of the project was to isolate and fully characterize natural products from *S. incisifolium* (**Figure 3.1**) for further studies. Previous studies had also indicated the potential of lapachol and its synthetic analogues to inhibit Hsp90 protein (Moyo, 2013), therefore they were incorporated in our search for cytotoxic Hsp90 inhibitors.

Figure 3.1: Photograph of *S. incisifolium*

(Photographs adapted from: http://oceanexplorer.noaa.gov/explorations/04etta/logs/aug25/media/sargassum.html. Web accessed: 07 Dec 2014)

3.2 Results and discussion

3.2.1 Extraction and isolation of secondary metabolites from *S. incisifolium*

S. incisifolium (NDK100213-1) was collected from Noordhoek (Port Elizabeth, South Africa) and extracted in DCM: MeOH (2:1) after soaking in MeOH for an hour. The DCM crude ^{1}H NMR spectrum obtained (**Figure 3.2**) showed the presence of one major metabolite, compound **3.1**. Further fractionation of the crude extract by column chromatography using solvents of increasing polarity (Hexane/EtOAc) gave eight fractions A-H (**Scheme 3.1**). Fraction B yielded compound **3.2**. Compound **2.47** was obtained from fraction C and fraction D gave compound **3.1** in great yields and in its pure form, together with compound **3.3** in minute quantities. Compound **3.4** was eluted in fraction E. The different metabolites were identified by comparing their ^{1}H and ^{13}C NMR spectra to those reported in literature. It is important to note how the presence of other metabolites was masked in the ^{1}H NMR crude extract and appear with further fractionation of the extract with relative purity, demonstrating the efficiency of the increasing polarity approach.

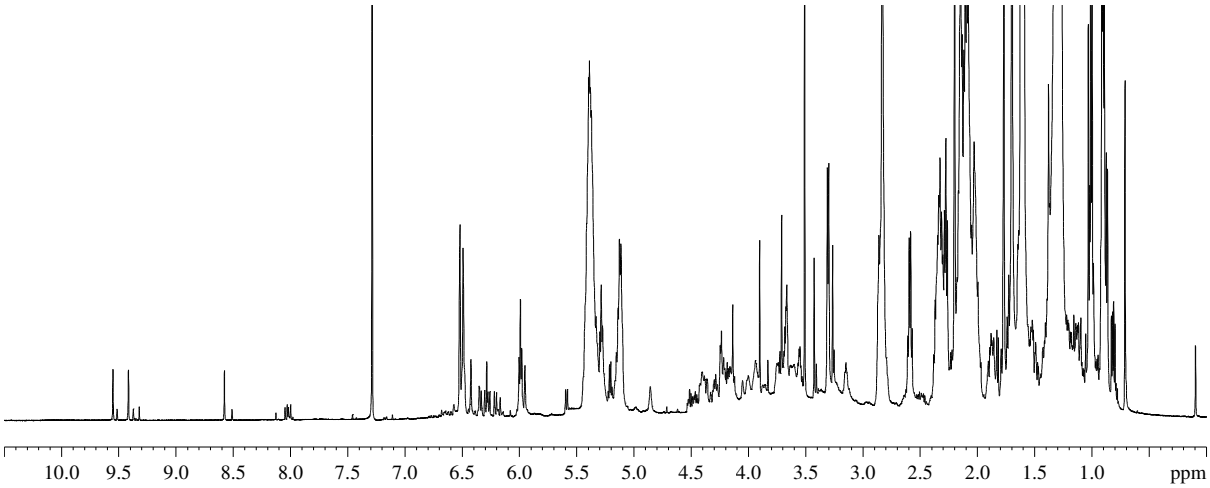

Figure 3.2: ^{1}H NMR spectrum (600 MHz, $CDCl_3$) of the crude extract of *S. incisifolium* collected from Noordhoek, Port Elizabeth (South Africa)

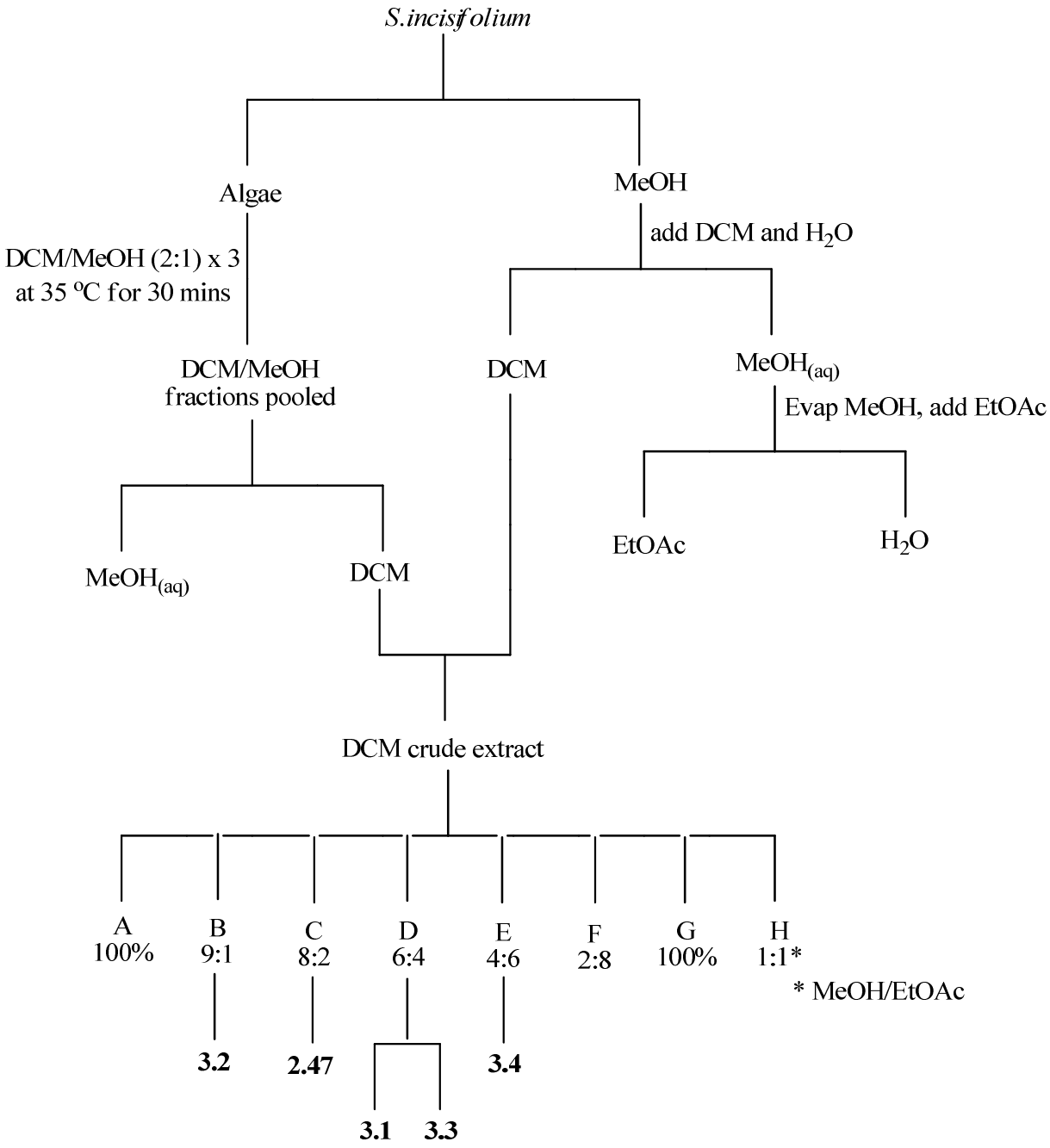

Scheme 3.1 Extraction and isolation of secondary metabolites from *S.incisifolium*[1,2]

[1] MeOH (aq) fractions were also pooled and extracted using EtOAc as shown above.

[2] Step gradient solvents systems are in the ratio of Hexane: EtOAc

3.2.2 Characterization of *S. incisifolium* metabolites

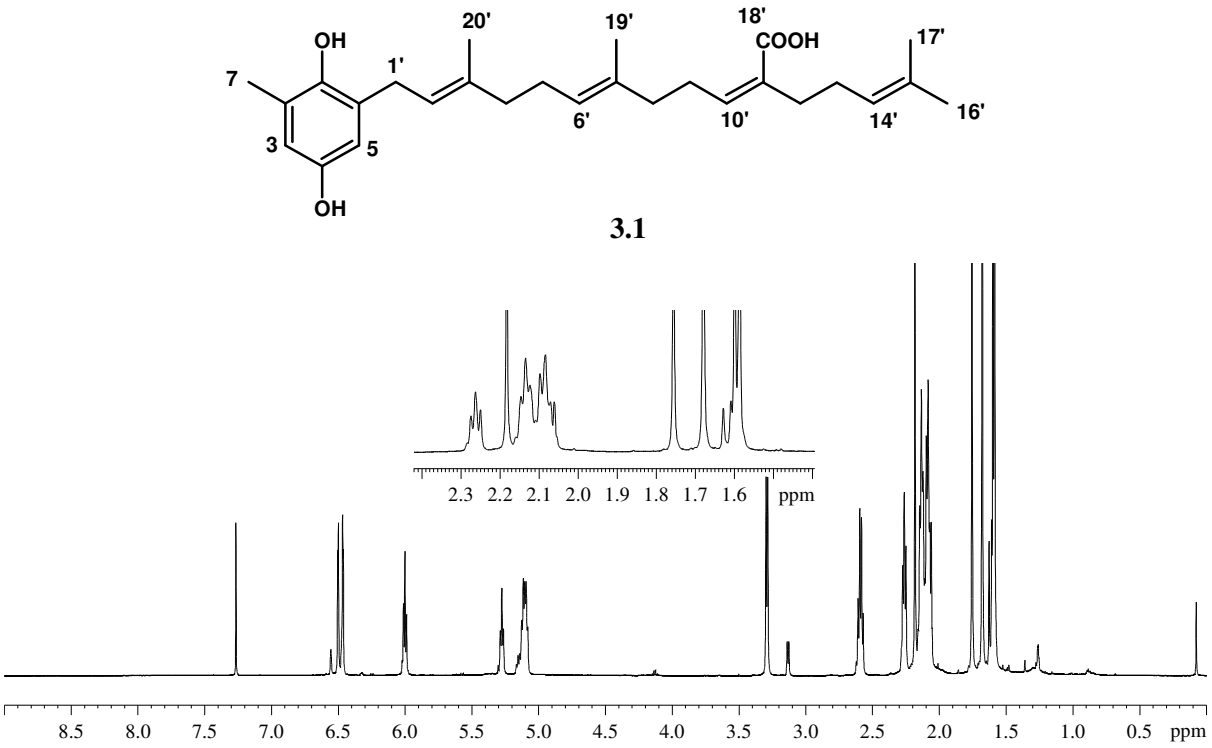

3.1

Figure 3.3: ^{1}H NMR spectrum (600 MHz, $CDCl_3$) of compound **3.1**

Compound **3.1** exists in abundance in DCM crude extracts of *S. incisifolium*. Characteristic features of its ^{1}H NMR spectrum (**Figure 3.3**) include two aromatic singlets at δ 6.49 (H-3) and δ 6.46 (H-5), along with three sets of olefinic protons at δ 5.99 (t, *J* = 7.0 Hz, H-10'), δ 5.27 (t, *J* = 7.2 Hz, H-2') and δ 5.10 (m, H-6' and H-14'). Three methylene signals for the prenyl chain are observed at δ 3.29 (d, *J* = 7.3 Hz, H-1'), δ 2.58 (q, *J* = 7.5 Hz, *J* = 7.7 Hz, H-9') and δ 2.26 (t, *J* = 7.2 Hz, H-12'). The other methylene signals appear as clusters at δ 2.13 (m) and δ 2.08 (m). Signals at δ 2.18 (s), δ 1.75 (s), δ 1.67 (s) and δ 1.59 (s) clearly show the methyl groups on the molecule. All chemical shifts were consistent with previously reported values (**Table 3.1**) (Afolayan, *et al*., 2008).

Compound **2.47** was obtained in minute quantities from *S. incisifolium*. The ^{1}H NMR spectrum of compound **2.47** shown in **Figure 3.4** showed two major differences to that of compound **3.1** in **Figure 3.3**. The aromatic proton at δ 6.54 (H-3) appears slightly more deshielded compared to the δ 6.49 (H-3) shown for compound **3.1**. The ^{13}C NMR spectrum of compound **2.47** (**Figure 3.5)** shows three carbonyl signals at δ 188.5 (C-1), δ 188.0 (C-4) and δ 172.8 (C-18'). The more deshielded signals correspond to the benzoquinone moiety, whilst in compound **3.1**,

those signals are absent. All other spectroscopic data matched those published in literature (**Table 3.1**) (Afolayan, *et al*., 2008)

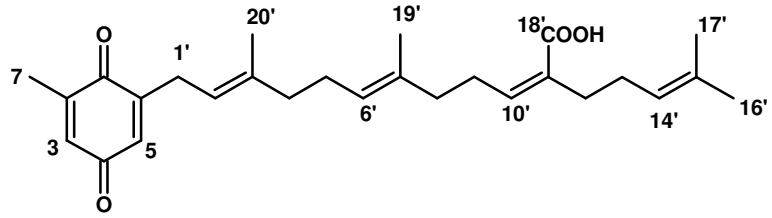

2.47

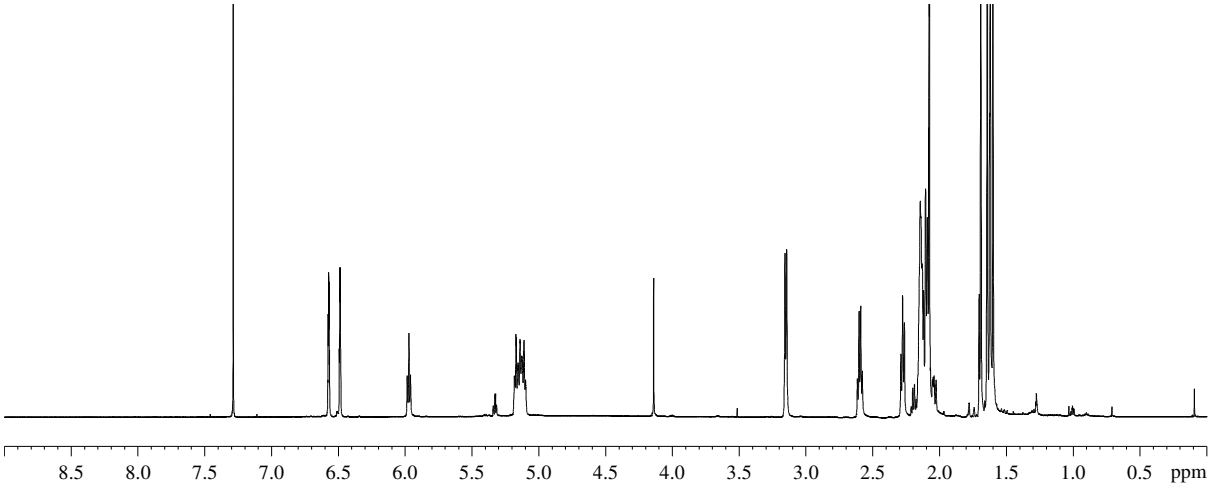

Figure 3.4: ^{1}H NMR spectrum (600 MHz, $CDCl_3$) of compound **2.47**

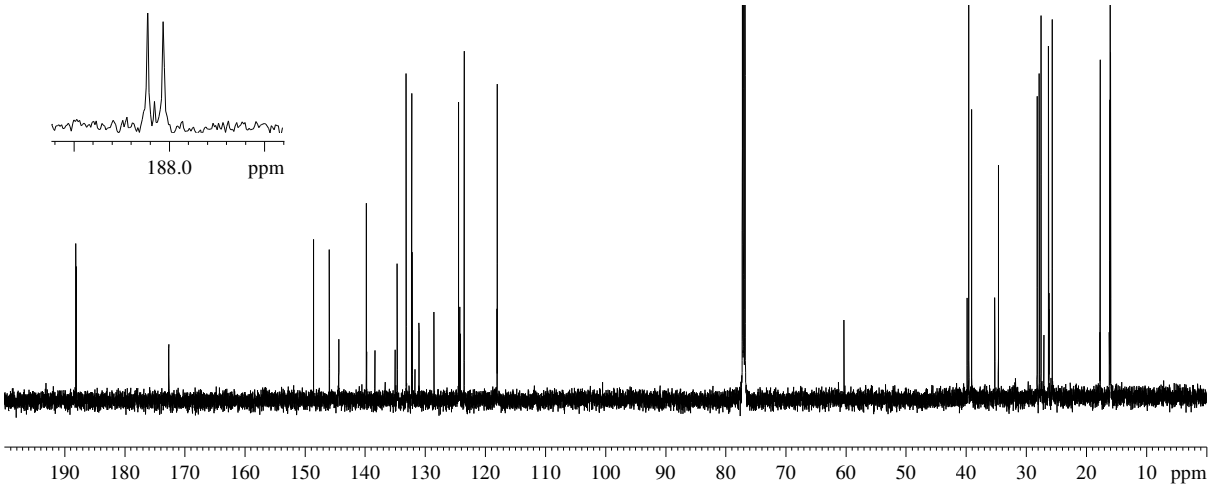

Figure 3.5: ^{13}C NMR spectrum (150 MHz, $CDCl_3$) of compound **2.47**

Compound **2.47** can also be prepared *via* semi-synthesis by oxidation of compound **3.1** using Ag_2O or MnO_2 in a mixture of solvents ($CHCl_3$/MeOH), if needed in larger quantities. In the same reaction, cyclization of sargahydroquinoic acid (**3.1**) can occur to form very minute quantities of sarganaphthoquinoic acid (**3.5**). We hypothesize that the reaction follows some type of Diels-Alder reaction, whereby the quinone moiety acts as the dienophile and the C1'-C3' portion of the prenyl chain system acts as the diene, or undergo a 6-π electron electrocyclic ring closure with subsequent re-aromatization (**Scheme 3.2**).

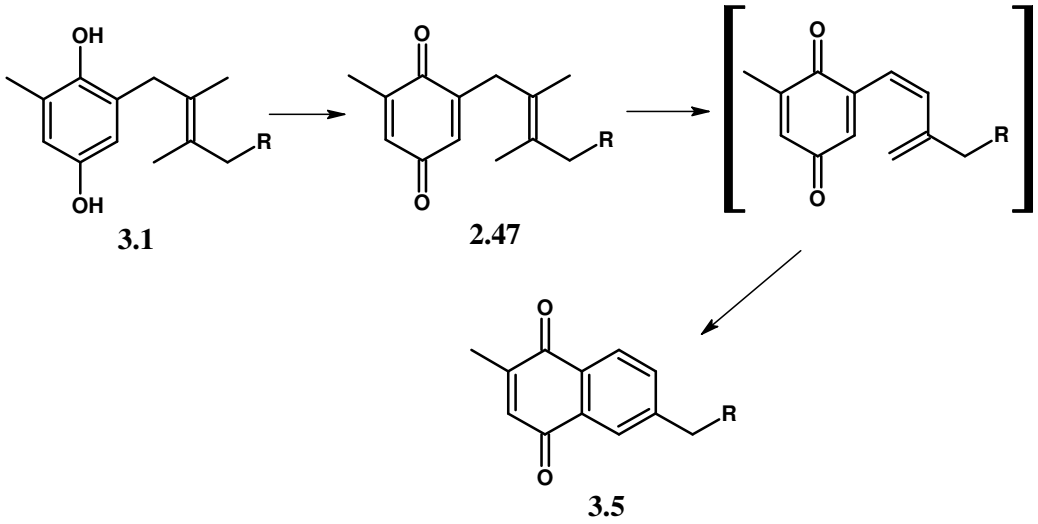

Scheme 3.2: Semi-synthesis of sarganaphthoquinoic acid (**3.5**) from sargahydroquinoic acid (**3.1**)

However, the reaction is unpredictable and yields vary with each attempt (Munedzimwe, 2012). Further research is underway to fully understand the dynamics of this reaction and to improve the yield of sarganaphthoquinoic acid (**3.5**) that is formed.

The ^{1}H NMR spectrum of compound **3.2** (**Figure 3.6**) was very similar to that of compound **2.47**. However it comprised of a characteristic aldehyde signal at δ 9.55 (s, H-18') indicative of sargaquinal (**3.2**), which was further confirmed by the carbonyl signal at δ 204.9 on the ^{13}C NMR spectrum. All other signals matched perfectly with reported values and confirmed compound **3.2** to be sargaquinal (**Table 3.1**) (Afolayan, *et al*., 2008).

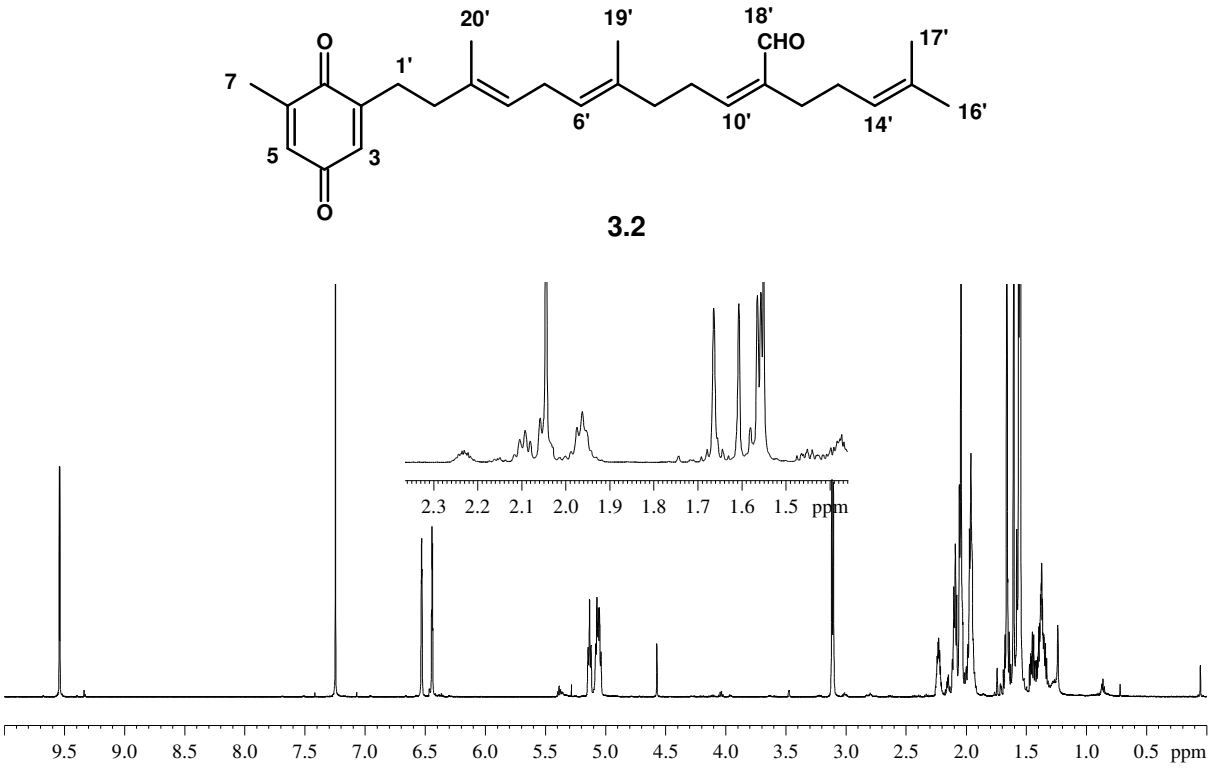

Figure 3.6: ^{1}H NMR spectrum (600 MHz, $CDCl_3$) of compound **3.2**

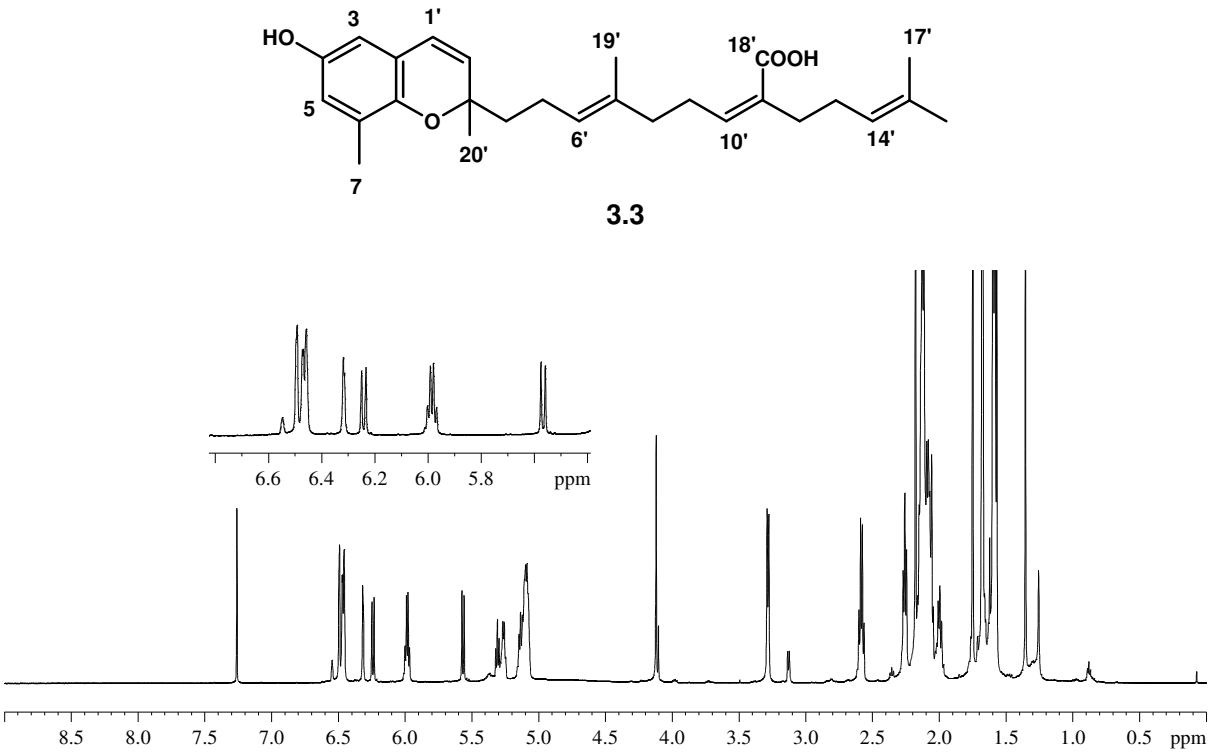

Figure 3.7: ^{1}H NMR spectrum (600 MHz, $CDCl_3$) of compound **3.3**

The ^{1}H NMR spectrum (**Figure 3.7**) for compound **3.3** also contained two aromatic protons as observed in other secondary metabolites, at δ 6.49 (s, H-5) and δ 6.31 (s, H-3). Of interest was the appearance of two new olefinic protons coupled to each other at δ 6.24 (d, J = 9.8 Hz, H-1') and δ 5.56 (d, J = 9.8 Hz, H-2'), and the disappearance of one of the olefinic triplets and benzylic methylene signal at δ 3.29 (d, J = 7.3 Hz). A comparison with published data of chromenols confirmed compound **3.3** to be sargachromenol, that was previously isolated from *S. micracanthum* (Ham, *et al*., 2010) (**Table 3.1**).

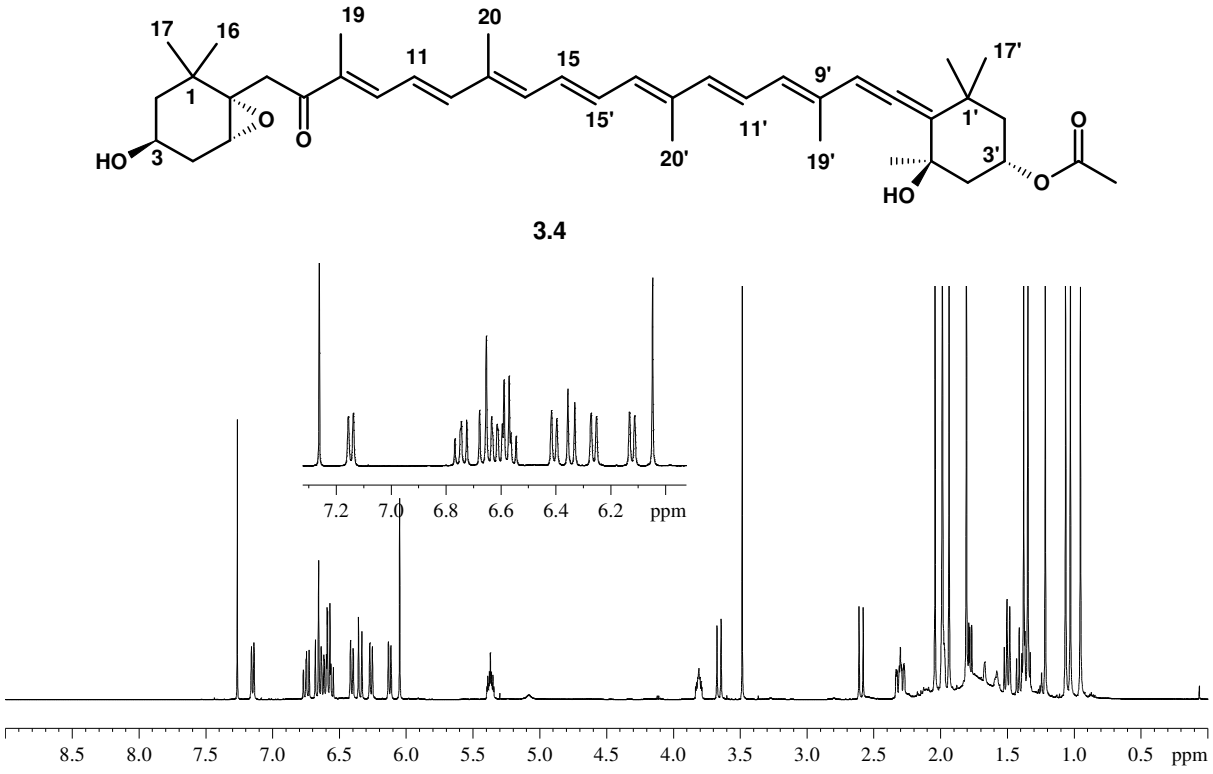

3.4

Figure 3.8: ^{1}H NMR spectrum (600 MHz, $CDCl_3$) of compound **3.4**

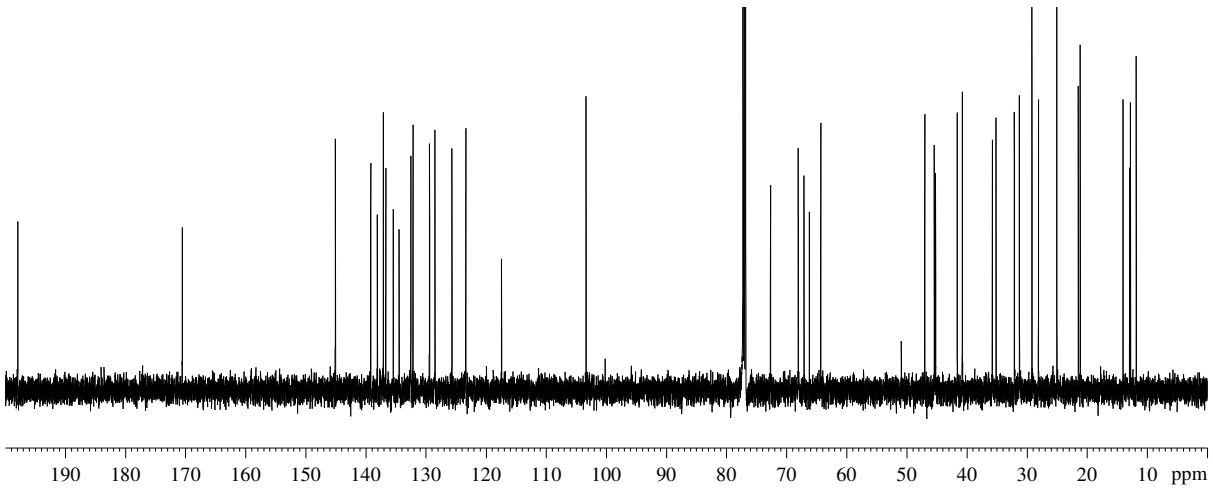

Figure 3.9: ^{13}C NMR spectrum (150 MHz, $CDCl_3$) of compound **3.4**

^{1}H and ^{13}C NMR spectra (**Figure 3.8** and **Figure 3.9**) for compound **3.4** were completely different from the other isolated metabolites. Overlapping signals were observed in the region between δ 6.00 and δ 7.00 indicative of a highly conjugated double bond system. This was confirmed in the ^{13}C NMR spectrum which showed a large number of resonances between δ110-150. In total, 42 resonances were noted and it was most likely that compound **3.4** belonged to a class of carotenoids. With careful analysis of the ^{1}H and ^{13}C NMR data published

of similar compounds isolated from *Sargassum*, compound **3.4** was identified as fucoxanthin (Afolayan, *et al*., 2008) (**Table 3.2**).

The ^{13}C NMR spectra for isolated metabolites from *S. incisifolium* not shown in this chapter are present in the supplementary section (**Figure S3.1 – S3.3)**

Table 3.1: ^{1}H and ^{13}C NMR chemical shifts of secondary metabolites from *S. incisifolium*

	2.47		**3.1**		**3.2**		**3.3**	
Carbon no.	δ_C	δ_H, mult, *J*(Hz)	δ_C	δ_H, mult, *J*(Hz)	δ_C	δ_H, mult, *J*(Hz)	δ_C	δ_H, mult, *J*(Hz)
1	188.1	-	146.5	-	188.0	-	145.7	-
2	145.9	-	125.5	-	145.9	-	121.0	-
3	133.1	6.54, br, s	115.3	6.49, br, s	132.3	6.53, s	110.3	6.31, m
4	188.0	-	148.7	-	187.9	-	148.7	-
5	131.0	6.45, s	114.0	6.46, br, s	132.2	6.44, s	117.2	6.49, m
6	148.5	-	127.6	-	148.4	-	126.4	-
7	17.7	2.04, m	16.1	2.18, s	16.1	1.66, s	15.8	2.12, s
1'	27.5	3.12, d, 7.3	29.9	3.29, d, 7.0	27.4	3.11, d, 7.3	123.0	6.24, d, 9.7
2'	118.0	5.11, m	121.6	5.27, t, 7.1	118.2	5.06, m	130.5	5.56, d, 9.8
3'	139.8	-	138.2	-	139.9	-	78.0	-
4'	39.5	2.07, m	39.5	2.08, m	39.6	2.05, m	40.5	1.99, m
5'	26.2	2.11, m	26.1	2.13, m	26.4	2.05, m	22.6	2.05, m
6'	124.4	5.11, m	124.4	5.10, m	125.2	5.06, m	125.0	5.13, m
7'	134.6	-	134.6	-	133.7	-	134.2	-
8'	39.0	2.07, m	39.1	2.08, m	39.0	2.23, m	40.0	2.05, m
9'	28.1	2.56, q, 7.3	28.3	2.58, q, 7.5	27.3	2.05, m	28.2	2.58, q, 7.3
10'	145.9	5.94, t, 7.2	145.5	5.99, t, 7.0	155.0	5.38, m	144.9	5.98, t, 7.0
11'	130.6	-	130.5	-	132.3	-	130.5	-
12'	34.6	2.24, t, 7.1	34.5	2.26, t, 7.2	27.5	2.05, m	34.6	2.25, t, 7.3
13'	28.1	2.11, m	27.8	2.13, m	25.6	2.09, m	27.8	2.12, s
14'	123.5	5.11, m	123.5	5.10, m	123.6	5.13, t, 7.7	123.4	5.13, m
15'	132.2	-	132.3	-	133.2	-	132.3	-
16'	25.6	1.66, s	25.7	1.67, s	25.0	1.66, s	25.6	1.67, m
17'	17.7	1.57, s	17.7	1.58, s	17.8	1.55, s	17.8	1.58, m
18'	172.6	-	172.3	-	204.9	9.55, d, 3.2	172.8	-
19'	15.9	1.59, s	16.0	1.59, br, s	16.0	1.60, s	15.6	1.58, m
20'	16.0	1.61, s	16.1	1.75, s	16.1	1.60, s	26.0	1.67, m

Table 3.2: ^{1}H and ^{13}C NMR chemical shifts of compound **3.4**

Carbon no.	δ_C	δ_H	Carbon no.	δ_C	δ_H
1	35.8	-	11	123.4	6.54
1'	35.1	-	11'	125.7	6.58
2	47.0	-	12	145.1	6.67
2'	45.4	1.48	12'	137.1	6.33
3	64.3	3.80	13	135.4	-
3'	68.1	5.36	13'	138.1	-
4	41.6	1.76	14	136.7	6.39
4'	45.2	1.50	14'	132.2	6.25
5	66.2	-	15	129.4	6.63
5'	72.7	-	15'	132.5	6.74
6	67.1	-	16	25.0	1.02
6'	117.4	-	16'	21.5	1.80
7	40.8	2.57	17	28.1	0.95
7'	202.4	3.64	17'	32.1	1.06
8	197.9	-	18	21.2	1.21
8'	103.4	6.04	18'	31.3	1.34
9	134.5	-	19	11.8	1.93
9'	132.5	-	19'	14.0	1.80
10	139.2	7.13	20	12.8	1.98
10'	128.5	6.11	20'	12.9	1.98

3.2.3 Lapachol and its derivatives

Compounds **3.6-3.11** were a gift from Professor Davies-Coleman, University of the Western Cape, South Africa. The natural naphthoquinone, lapachol (**3.6**) has been isolated from many species of *Bignoniaceae* family, particularly from those of the genus *Tabebuia* (*T. aurea, T. impetiginosa, T. ochracea* and *T. avellanedae*) (Hussain, *et al*., 2007). It comprises of an amylene hydroxy-naphthoquinone moiety, with both substituents attached to the quinone ring. Compound **3.6** has been intensely studied for various biological properties including anti-tumour properties, and was once registered by the NCI for clinical trials (de Almeida, 2009). Its antitumour properties led to the synthesis of a wide range of naphthoquinone (Sunassee, *et al*., 2013) derivatives and has been demonstrated to show Hsp90 inhibition, hence our interest in this molecule and its derivatives.

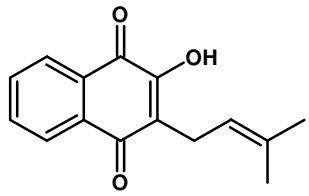

3.6

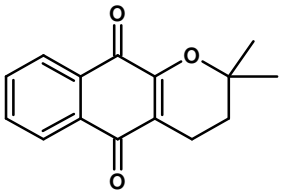

3.7

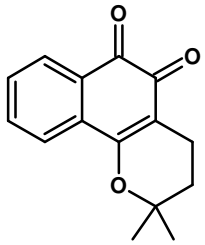

3.8

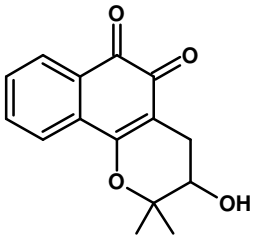

3.9

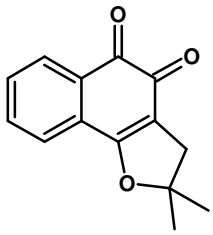

3.10

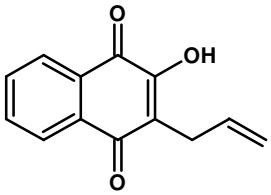

3.11

3.2.4 Synthetic strategies for lapachol and related compounds

Various methods have been employed to synthesize lapachol (**3.6**) in the laboratory, with relative success using silver salts, lithium salts and palladium as catalysts (Hussain, *et al*., 2007). Attempts to increase its cytotoxic nature have yielded semi-synthetic derivatives (**3.7-3.11**). α-Lapachone (**3.7**) and β-lapachone (**3.8**) are obtained by treating lapachol (**3.6**) with H_2SO_4 and HCl respectively (Salas, *et al*., 2008), which results in the cyclization of its isoprenyl chain by nucleophilic attack of the hydroxyl group (da Silva Junior, *et al*., 2008). β-OH-lapachone (**3.9**) is a hydroxylated analogue of β-lapachone (**3.8**), effected by use of

MCPBA in CH_2Cl_2 (Salas, *et al*., 2008; Sun, *et al*., 1998). The synthesis of β-nor-lapachone (**3.10**) requires an alternative precursor molecule and is conducted by C-allylation of lawsone and then cyclization by conc H_2SO_4 (Kongkathip, *et al*., 2003). C-allyl lawsone (**3.11**) is prepared by alkylation of lawsone with allyl bromide of the sodium salt (Silva, et al., 2006). All of these reactions are depicted in **Scheme 3.3**.

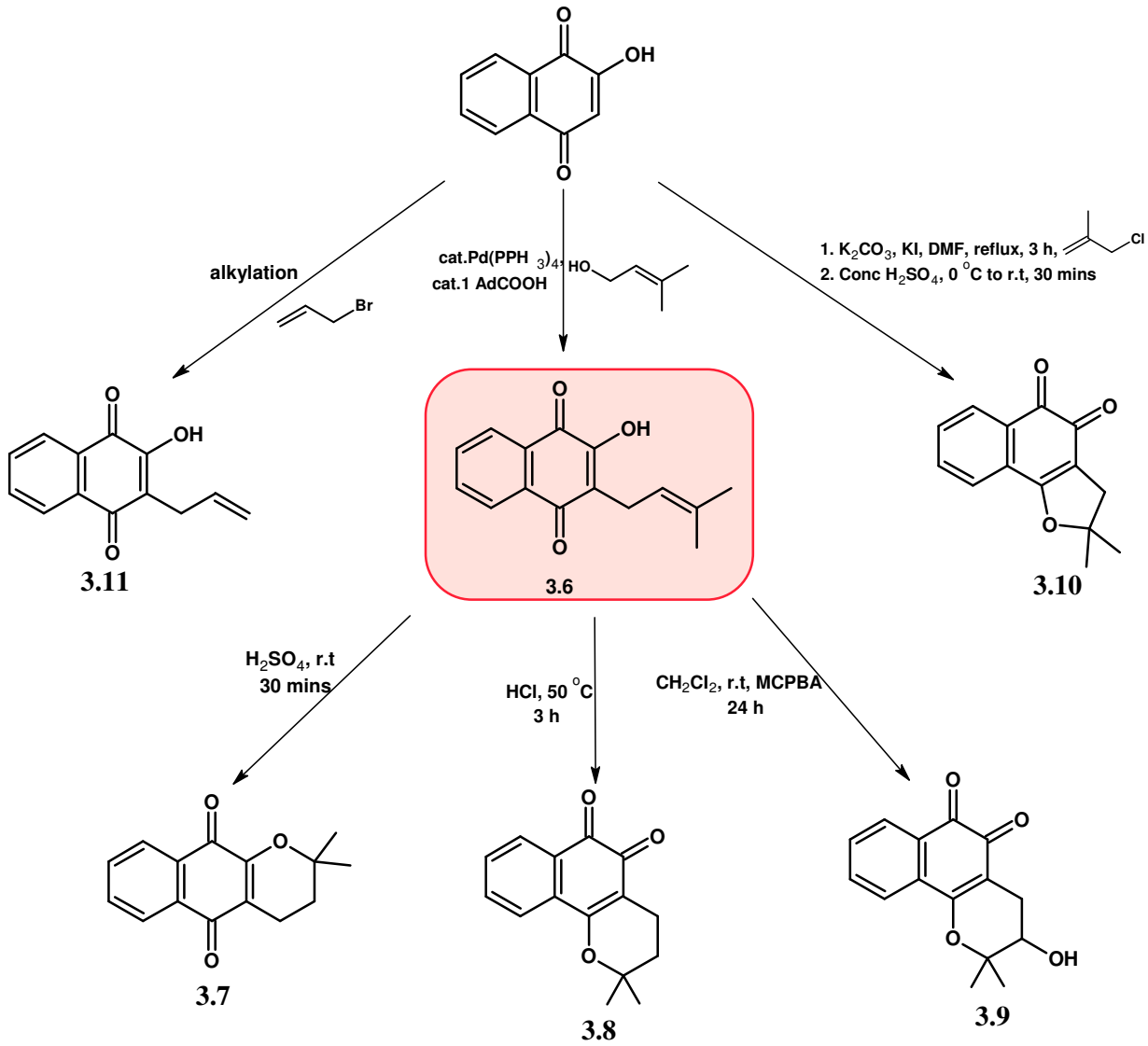

Scheme 3.3: Synthesis of lapachol (**3.6**) and derivatives

3.2.5 Characterization of lapachol and semi-synthetic derivatives

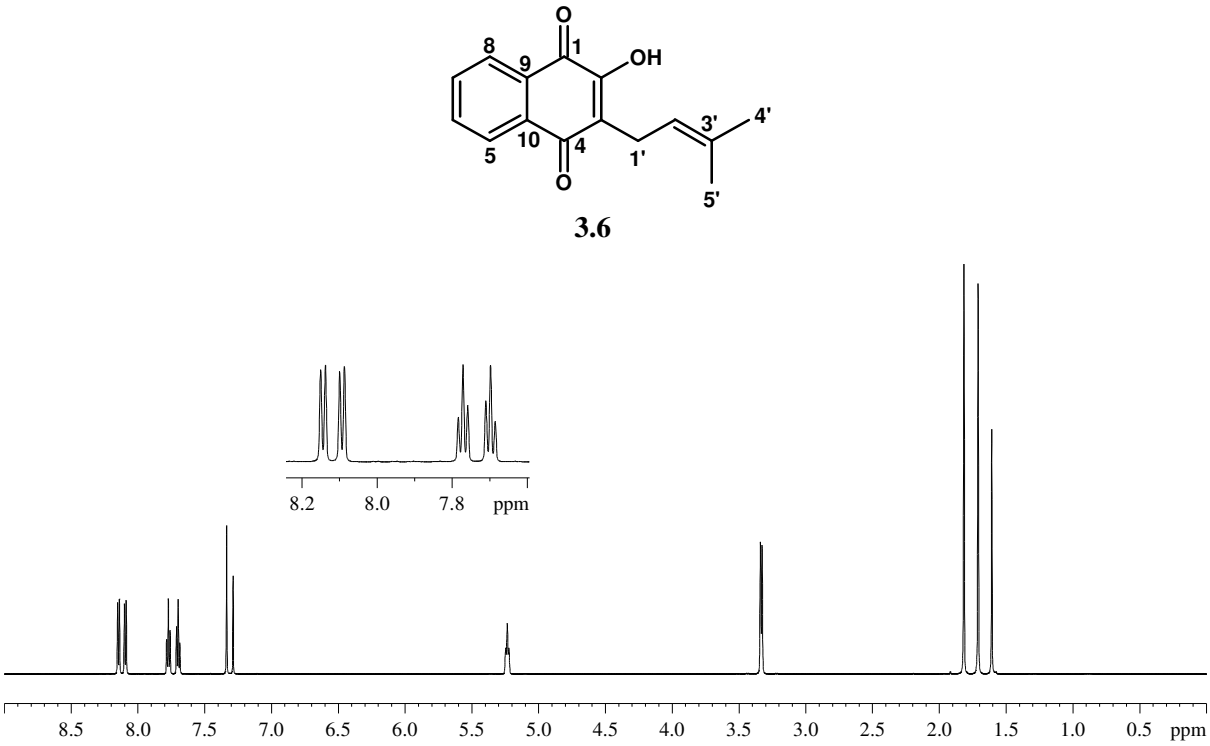

3.6

Figure 3.10: ^{1}H NMR spectrum (600 MHz, $CDCl_3$) of compound **3.6**

The ^{1}H NMR spectrum of lapachol (**3.6**) depicted in **Figure 3.10** shows four aromatic protons at δ 8.19 (d, *J* = 7.8 Hz, H-8) , δ 8.06 (d, *J* = 7.8 Hz, H-5), δ 7.74 (t, *J* = 7.5 Hz, H-7) and δ 7.67 (t, *J* = 7.5 Hz, H-6) indicative of the naphthoquinone system. The two C=O functionalities of the naphthoquinone are evident on the ^{13}C NMR spectrum at δ 181.7 (C-4) and δ 184.6 (C-1). A methylene group at δ 3.30 (d, *J* = 7.6 Hz, H-1') coupled to an olefinic methine proton at δ 5.21 (t, *J* = 7.6 Hz, H-2) was also observed, with two terminal methyl signals at δ 1.78 (s, H-4') and δ 1.68 (s, H-5'). All other ^{1}H and ^{13}C spectral data were consistent with reported literature values (**Table 3.3**) (Oliveira, *et al*., 2002).

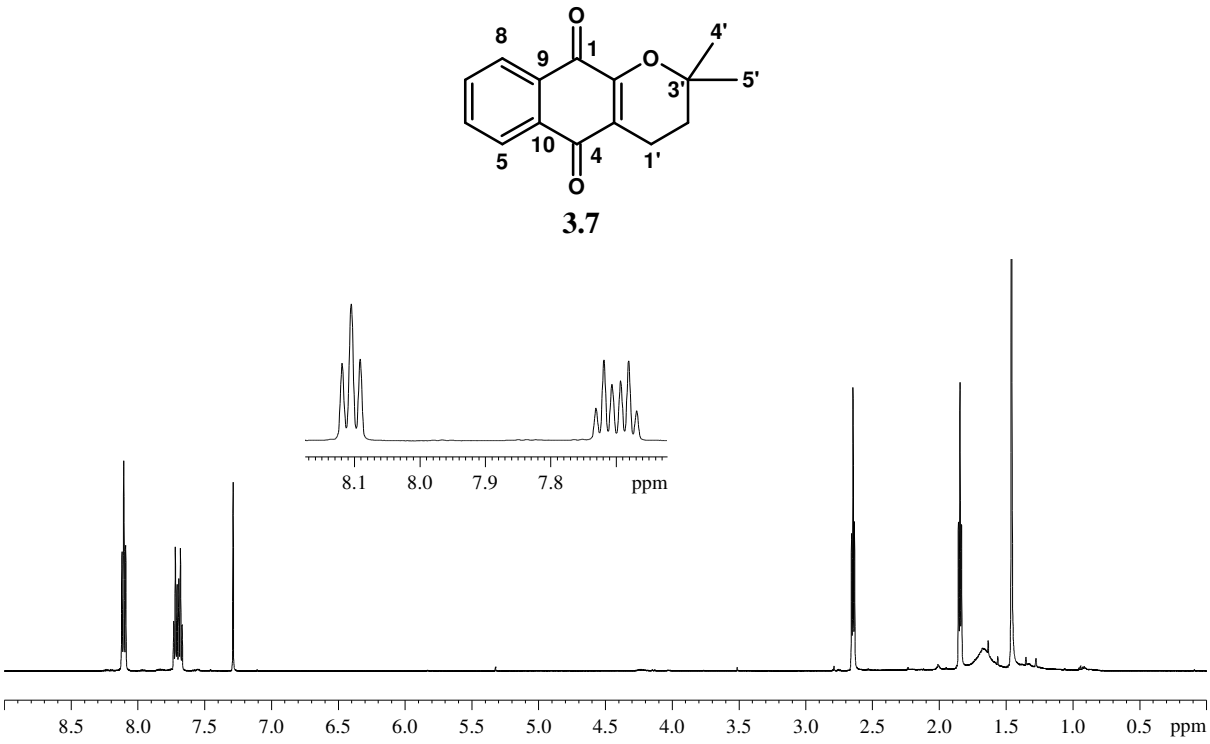

3.7

Figure 3.11: ^{1}H NMR spectrum (600 MHz, $CDCl_3$) of compound **3.7**

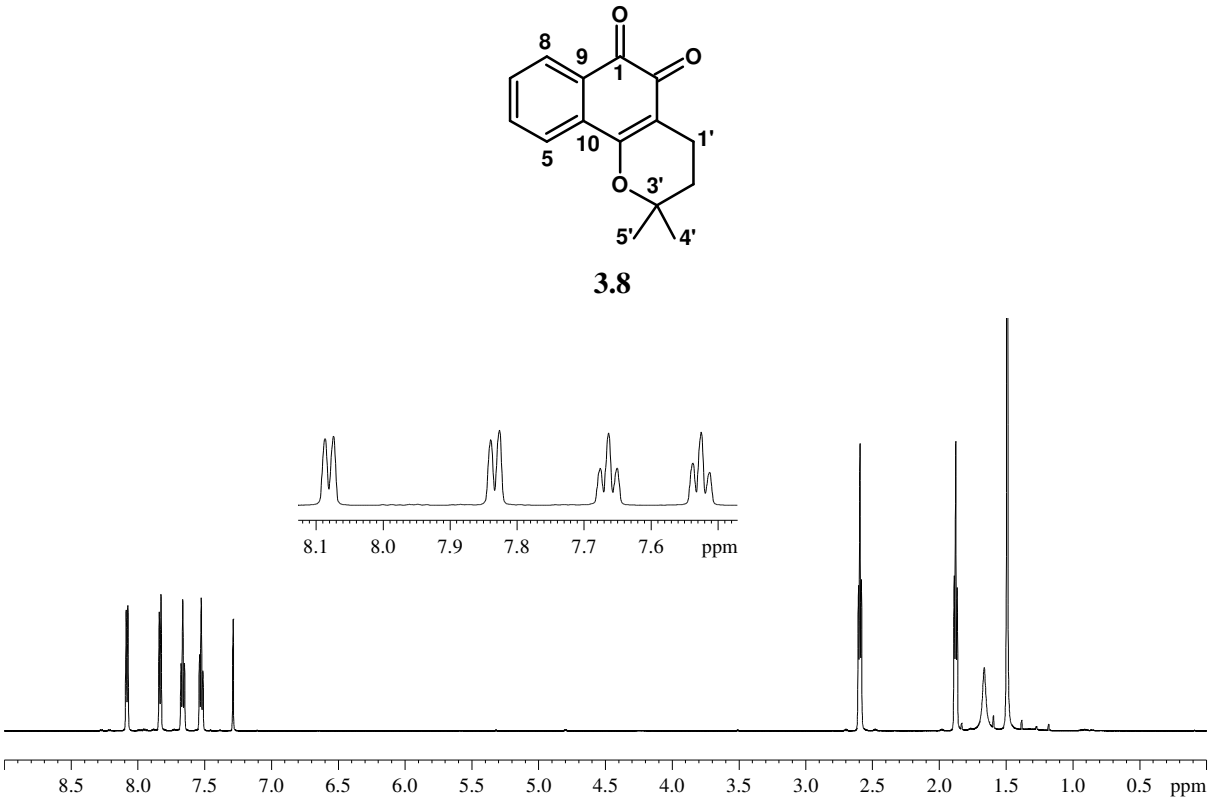

3.8

Figure 3.12: ^{1}H NMR spectrum (600 MHz, $CDCl_3$) of compound **3.8**

A distinguishing feature of the ^{1}H NMR spectra for both α-lapachone (**3.7**) and β-lapachone (**3.8**) is the disappearance of the olefinic methine proton at δ 5.21 (t, *J* = 7.6 Hz,) noticeable in lapachol (**3.6**), which clearly indicates the absence of an alkene functionality. Cyclization is evident by the appearance of two sets of methylene protons at δ 1.81 (t, *J* = 6.7 Hz, H-2') and δ 2.61 (t, *J* = 6.6 Hz, H-1') for α-lapachone (**3.7**), and at δ 1.84 (t, *J* = 6.7 Hz, H-2') and δ 2.56 (t, *J* = 6.5 Hz, H-1') for β-lapachone (**3.8**). The difference between the two natural products is noticeable in their aromatic regions of the ^{1}H NMR spectra. The aromatic protons in α-lapachone (**3.7**) are somehow more clustered due to the manner in which the cyclization has occurred, where by in β-lapachone (**3.8**), one sided cyclization occurs and results in aromatic protons (H-5 and H-6) being less deshielded due to absence of the carbonyl on C-4. Further confirmation of the structure was conducted by ^{13}C NMR spectroscopy and by comparison to the published NMR data (Salas, *et al*., 2008).

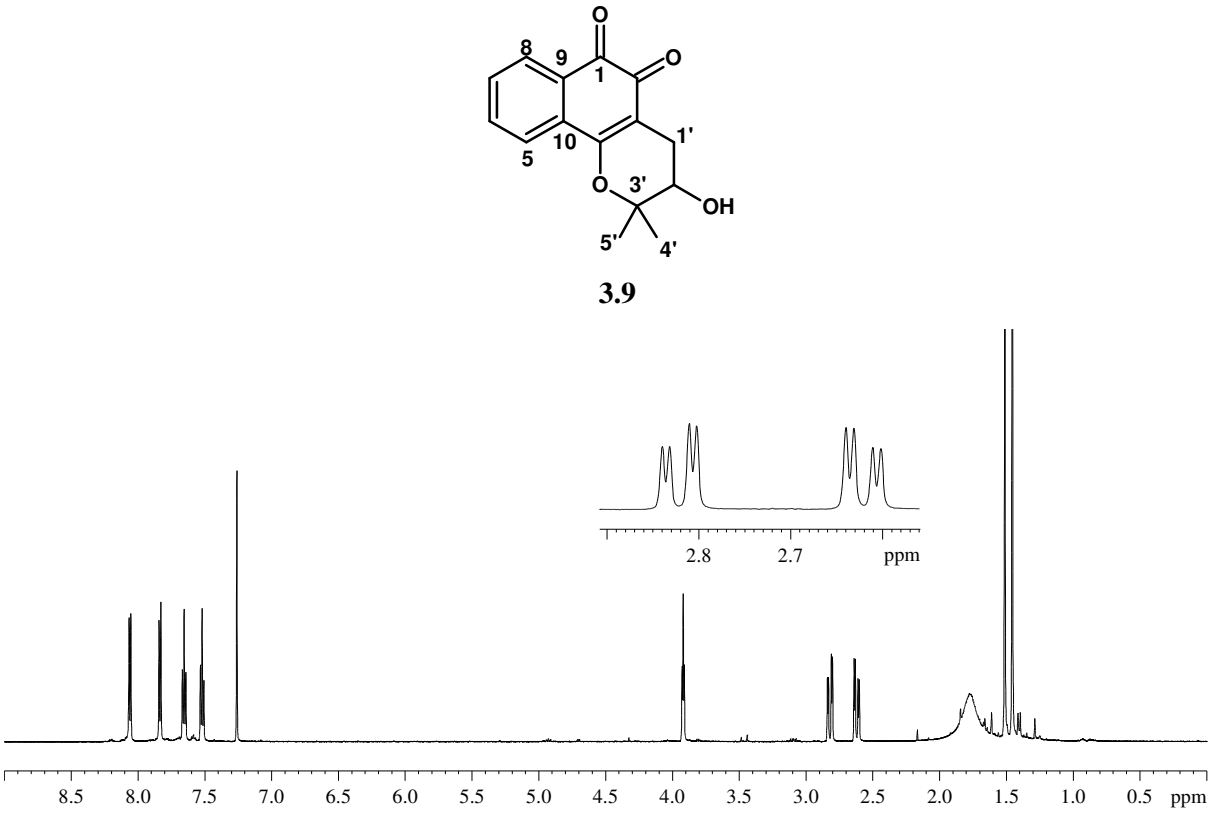

3.9

Figure 3.13: ^{1}H NMR spectrum (600 MHz, $CDCl_3$) of compound **3.9**

The ^{1}H NMR spectrum of β-OH-lapachone (**3.9**) shares similarities to that of β-lapachone (**3.8**) especially in the aromatic region. Differences are noted with the appearance of a single triplet signal of a methine proton at δ 3.91 (t, *J* = 5.2 Hz, H-2') bonded to the hydroxyl functionality. The one set of methylene protons of the cyclized isoprenyl chain is observed at δ 2.63 (dd, *J* =

17.8 and *J* = 5.3 Hz, H-1a') and δ 2.83 (dd, *J* = 17.8 Hz and *J* = 5.3 Hz, H-1b'). The C-OH signal was noted on the ^{13}C NMR spectrum at δ 68.5 (C-2'). All other chemical shifts were consistent with literature values and are displayed in **Table 3.4** (Salas, *et al*., 2008).

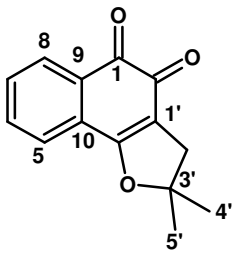

3.10

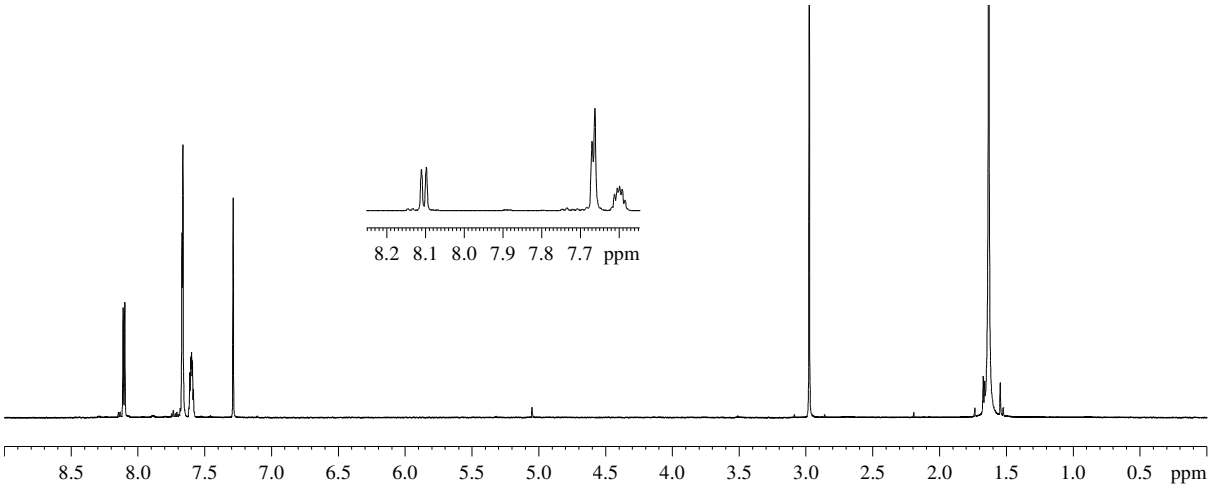

Figure 3.14: ^{1}H NMR spectrum (600 MHz, $CDCl_3$) of compound **3.10**

β-nor-lapachone (**3.10**) structural difference from β-lapachone (**3.8**) is the presence of a tetrahydrofuran moiety rather than a tetrahydro-*2H*-pyran. Cyclized part of the molecule is one carbon short and the ^{1}H NMR spectrum contains a characteristic methylene signal at δ 2.94 (s, H-2') uncoupled to any other proton. All other chemical shifts are consistent with published spectroscopic data (Kongkathip, *et al*., 2003).

A related compound to lapachol (**3.6**), C-allyl lawsone (**3.11**) consists of a similar hydroxynaphthoquinone system and a prenyl side chain that contains a terminal double bond. Its structure and spectroscopic data is depicted in **Figure 3.15**

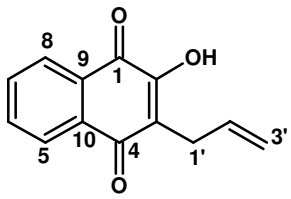

3.11

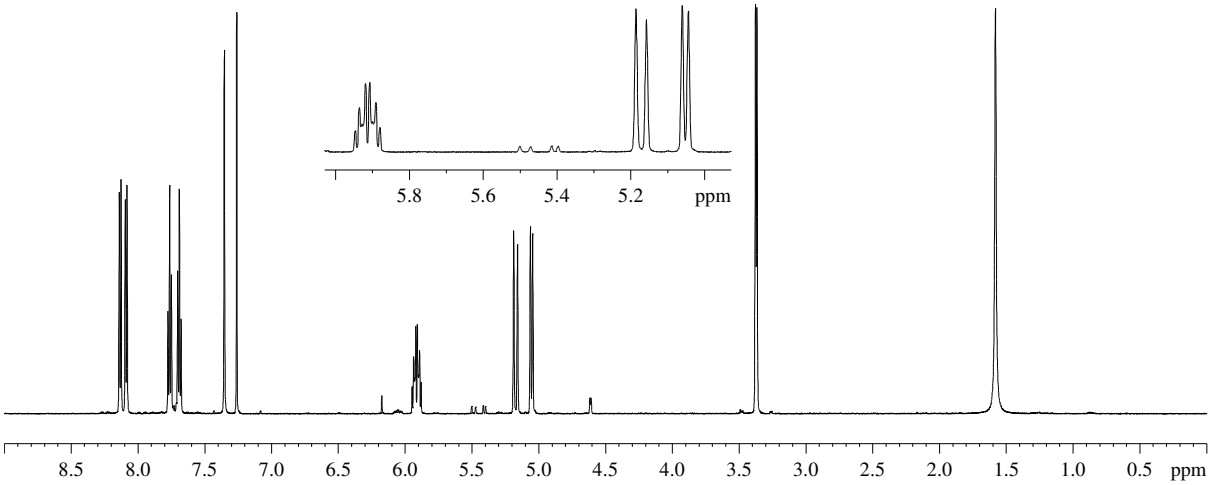

Figure 3.15: ^{1}H NMR spectrum (600 MHz, $CDCl_3$) of compound **3.11**

The ^{1}H NMR spectrum of **3.11** displays two terminal methylene protons indicated by doublets at δ 5.05 (d, *J* = 10.6 Hz, H-3a') and δ 5.17 (d, *J* = 17.2 Hz, H-3b'). These two protons are coupled to a methine proton at δ 5.91 (m, H-2') giving a -CH=CH_2 structural motif, and in turn the methine coupled to methylene protons at δ 3.37 (d, *J* = 6.9 Hz. H-1'), completing the prenyl system attached to the naphthoquinone. The ^{13}C NMR spectrum of **3.11** displays the absence of methyl carbons normally observed at δ 17.9 and δ 22.7 in lapachol (**3.6**). All other chemical shifts were similar to those of lapachol (**3.5**) and are shown in **Table 3.4** (Silva, *et al*., 2006).

The ^{13}C NMR spectra of lapachol and its related compounds have been compiled in the supplementary section (**Figure S3.4 – S3.8)**

Table 3.3: ^{1}H and ^{13}C NMR chemical shifts of compounds **3.6-3.8**

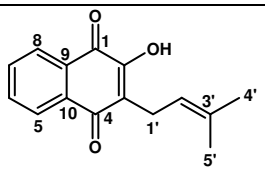

3.6

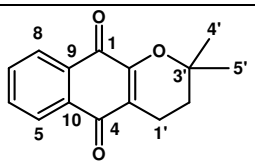

3.7

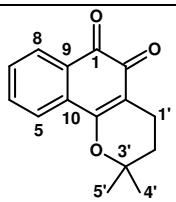

3.8

Carbon No.	δ_C	δ_H, mult, *J*(Hz)	δ_C	δ_H, mult, *J*(Hz)	δ_C	δ_H, mult, *J*(Hz)
1	181.7	-	180.0	-	179.8	-
2	152.6	-	154.6	-	178.5	-
3	123.4	-	120.1	-	112.7	-
4	184.5	-	184.4	-	162.1	-
5	126.7	8.06, d, 7.8	126.3	8.07, m, 2H	124.1	7.80, d, 7.6
6	134.8	7.67, t, 7.5	133.9	7.67. m, 2H	134.8	7.49, t, 7.8
7	132.8	7.74, t, 7.5	132.9	7.67, m, 2H	130.9	7.63, t, 7.8
8	126.0	8.19, d, 7.8	125.9	8.07, m, 2H	128.5	8.05, d, 7.6
9	129.4	-	131.1	-	130.1	-
10	132.9	-	132.0	-	132.6	-
1'	22.6	3.30, d, 7.6	16.7	2.61, t, 6.6	16.1	2.56, t, 6.5
2'	119.6	5.21, t, 7.6	31.4	1.81, t, 6.7	31.5	1,84, t, 6.7
3'	133.8	-	78.1	-	79.3	-
4'	25.7	1.68, s	26.5	1.43, s	26.7	1.46, s
5'	17.8	1.78, s	26.5	1.43, s	26.7	1.46, s

Table 3.4: ^{1}H and ^{13}C NMR chemical shifts of compounds **3.9-3.11**

	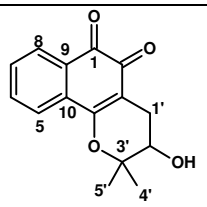 **3.9**		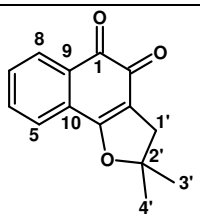 **3.10**		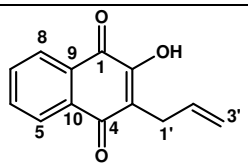 **3.11**	
Carbon No.	δ_C	δ_H, mult, *J*(Hz)	δ_C	δ_H, mult, *J*(Hz)	δ_C	δ_H, mult, *J*(Hz)
1	179.5	-	180.1	-	184.2	-
2	178.5	-	176.2	-	153.1	-
3	110.3	-	114.3	-	121.8	-
4	161.5	-	168.8	-	181.5	-
5	124.4	7.83, d, 7.6	124.1	7.57, m, 1H	126.9	8.08, d, 7.7
6	134.9	7.51, t, 7.6	133.5	7.63, m, 2H	133.7	7.68, t, 7.6
7	130.9	7.65, t, 7.8	129.2	7.63, m, 2H	133.0	7.76, t, 7.7
8	128.8	8.06, d, 7.6	128.3	8.07, d, 7.6	126.1	8.13, d, 7.8
9	130.0	-	131.1	-	129.3	-
10	132.0	-	133.4	-	132.8	-
1'	22.1	1a': 2.82, dd, 17.8 and 5.3 1b' :2.62, dd, 17.8 and 5.3	40.1	2.94, s	27.5	3.36, d, 6.6
2'	68.2	3.91, t, 5.2	94.1	-	135.0	5.91, m, 1H
3'	81.4	-	29.5	1.60, s	116.4	3a': 5.17, d, 17.3 3b': 5.05, d, 10.2
4'	25.0	1.45, s	29.5	1.60, s	N/A	-
5'	25.4	1.51, s	N/A	N/A	N/A	-

3.3 Conclusion

Five secondary metabolites (**2.47, 3.1-3.4**) were isolated from *S. incisifolium*. Six additional compounds i.e., lapachol and its related compounds (**3.6-3.11**), were added in the search for cytotoxic Hsp90 inhibitors. Structural modifications of the natural product skeleton are limited by quantities obtained from natural sources, therefore synthetic analogues inspired by natural product structures were opted for.

Our interest was in the natural product sarganaphthoquinoic acid (**3.5**) due to its naphthoquinone moiety that has been identified as a potential structural feature that imparts Hsp90 inhibition on lead molecules. Due to difficulties in preparing sarganaphthoquinoic acid (**3.5**) in sufficient amount for further research, truncated sarganaphthoquinoic acid derivatives were prepared in an attempt to modify its structure for improved cytotoxicity and Hsp90 inhibition properties. The different analogues prepared are discussed in the next chapter.

3.4 Experimental

3.4.1 General experimental

Solvents

All solvents used for extractions and chromatography were of HPLC grade (Chromasolv®) acquired from Merck, South Africa.

Chromatography

Column chromatography was conducted using silica gel 60 (0.040-0.063 mm), from ASTM Merck. Thin layer chromatography experiments were run on TLC silica gel $60F_{254}$ 20 x 20 aluminium sheets and visualized using a Syngene UV lamp 230 V, 50 Hz with dual wavelengths 365 nm and 254 nm.

High Performance Liquid Chromatography

HPLC separations were done on an instrument consisting of a Waters® 1515 isocratic HPLC pump connected to a Waters® 2414 refractive index detector. A Whatman Partisil® 10 (1 x 50 cm) normal phase column was used for purification.

Nuclear magnetic resonance (NMR)

NMR data (1D and 2D experiments) were acquired on a Bruker Avance 600 MHz spectrometer. Chemical shifts are recorded in ppm and referenced to residual non-deuterated solvent ($CDCl_3$ δ_H 7.26, δ_C 77.0). All coupling constants are reported in Hz.

Plant material

Specimens of *S. incisifolium* were collected at low tide at Kelly's Beach, Port Alfred and from Noordhoek near Port Elizabeth. Identification of algae collected were done by Prof John J. Bolton of the department of Botany, University of Cape Town, South Africa. Voucher specimens are kept in our repository at Rhodes University, South Africa. Crude and pure extracts isolated were stored in vials at -20 ºC, covered with a thin film of hexane and flushed with argon/nitrogen.

3.4.2. Isolation and purification of secondary metabolites from *S. incisifolium*

Protocols adopted for extraction, isolation and purification of metabolites are represented by the flow chart in **Scheme 3.1.**

Extraction and Isolation

Sufficient methanol was used to completely submerge the algae (45.7 g, dry weight) in a 1 L conical flask for 1 h. The solvent was decanted and the algae re-extracted three times with a 2:1 DCM/MeOH mixture at 35 ºC for 30 min. Appropriate volumes of DCM and H_2O were added to the decanted MeOH fraction, and H_2O to the DCM/MeOH fraction to allow phase separation. The DCM layers were collected and concentrated *in vacuo* to give the DCM crude extract.

The DCM crude extract (~ 1 g) was chromatographed on a silica column (10 g) using a step gradient protocol of increasing polarity from 100% hexane to 100% EtOAc, and the column was finally washed with EtOAc-MeOH. Further column chromatography (silica, 10 g, hexane-EtOAc, 95:5) of the hexane-EtOAc (9:1) fraction (120 mg) yielded compound **3.2** (23 mg). Compound **2.47** (9.8 mg) was obtained from fraction C (100 mg) of hexane-EtOAc (8:2) by column chromatography (silica-10 g, Hex/EtOAc 85:15). Fraction D of Hex/EtOAc (6:4) gave compound **3.1** in greatest yield (382 mg) and in its pure form, together with compound **3.3** (3 mg) in minute quantities. Compound **3.3** was purified by column chromatography (Hex/EtOAc 7:3). Compound **3.4** (37 mg) was eluted in fraction E of Hex/EtOAc (4:6). Dry weight of the algae after extraction was 45.7g.

^{1}H and ^{13}C NMR spectroscopy was used to characterize extracts obtained at each stage of the procedure. Fractions to further purify were chosen according to the NMR data acquired. All relevant chemical shifts for the natural product metabolites are in **Tables 3.1-3.4** and also complied below:

Isolated metabolites from *S. incisifolium*

Compound **3.1**

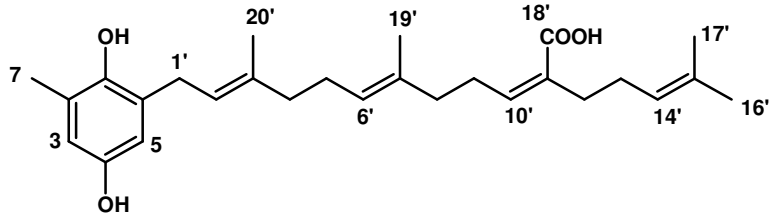

Orange-yellow oil; ^{1}H NMR ($CDCl_3$): δ 6.49 (br, s, H-3), 6.46 (br, s, H-5), 2.18 (s, H-7), 3.29 (d, 7.0 Hz, H-1'), 5.24 (t, 7.1 Hz, H-2'), 2.08 (m, H-4'), 2.13 (m, H-5'), 5.10 (m, H-6'), 2.08 (m, H-8'), 2.58 (q, 7.5 Hz, H-9'), 5.99 (t, 7.0 Hz, H-10'), 2.26 (t, 7.2 Hz, H-12'), 2.13(m, H-13'), 5.10 (m, H-14'), 1.67 (s, H-16'), 1.58 (s, H-17'), 1.59 (br s, H-19'), 1.75 (s, H-20')

^{13}C NMR ($CDCl_3$): δ 146.5 (C-1), 125.5 (C-2), 115.3 (C-3), 148.7 (C-4), 114.0 (C-5), 127.6 (C-6), 16.1 (C-7), 29.9 (C-1'), 121.6 (C-2'), 138.2 (C-3'), 39.5 (C-4'), 26.1 (C-5'), 124.4 (C-6'), 134.6 (C-7'), 39.1 (C-8'), 28.3 (C-9'), 145.5 (C-10'), 130.5 (C-11'), 34.5 (C-12'), 27.8 (C-13'), 123.5 (C-14'), 132.3 (C-15'), 25.7 (C-16'), 17.7 (C-17'), 173.2 (C-18'), 16.0 (C-19'), 16.1 (C-20') (Afolayan, *et al*., 2008).

Compound **2.47**

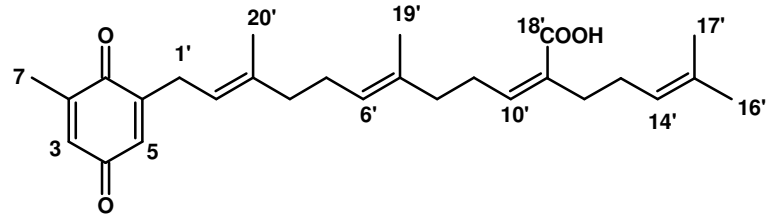

Orange-yellow oil; ^{1}H NMR ($CDCl_3$): δ 6.54 (br, s, H-3), 6.45 (br, s, H-5), 2.04 (s, H-7), 3.12 (d, 7.3 Hz, H-1'), 5.11 (m, H-2'), 2.07 (m, H-4'), 2.11 (m, H-5'), 5.11 (m, H-6'), 2.07 (m, H-8'), 2.56 (q, 7.3 Hz, H-9'), 5.94 (t, 7.3 Hz, H-10'), 2.24 (t, 7.1 Hz, H-12'), 2.11 (m, H-13'), 5.11 (m, H-14'), 1.66 (s, H-16'), 1.57 (s, H-17'), 1.59 (s, H-19'), 1.61 (s, H-20')

^{13}C NMR ($CDCl_3$): δ 188.1 (C-1), 145.9 (C-2), 133.1 (C-3), 188.0 (C-4), 131.0 (C-5), 148.5 (C-6), 17.7 (C-7), 27.5 (C-1'), 118.0 (C-2'), 139.8 (C-3'), 39.5 (C-4'), 26.2 (C-5'), 124.4 (C-6'), 134.6 (C-7'), 39.0 (C-8'), 28.1 (C-9'), 145.9 (C-10'), 130.6 (C-11'), 34.6 (C-12'), 28.1 (C-13'), 123.5 (C-14'), 132.2 (C-15'), 25.6 (C-16'), 17.7 (C-17'), 172.6 (C-18'), 15.9 (C-19'), 16.0 (C-20') (Afolayan, *et al*., 2008).

Compound **3.2**

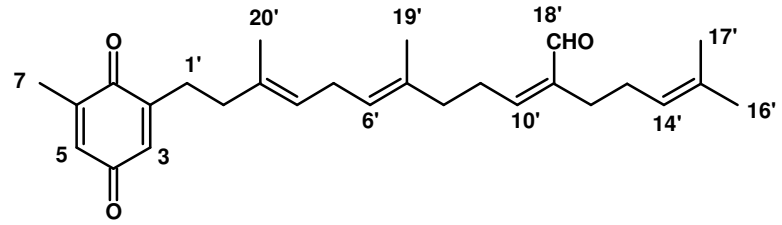

Orange-yellow oil; ^{1}H NMR ($CDCl_3$): δ 6.53 (br, s, H-3), 6.44 (s, H-5), 1.66 (s, H-7), 3.11 (d, 7.3 Hz, H-1'), 5.06 (m, H-2'), 2.05 (m, H-4'), 2.05 (m, H-5'), 5.06 (m, H-6'), 2.23 (m, H-8'), 2.05 (m, H-9'), 5.38 (m, H-10'), 2.05 (m, H-12'), 2.09 (m, H-13'), 5.13 (t, 7.7 Hz, H-14'), 1.66 (s, H-16'), 1.55 (s, H-17'), 9.54 (d, 3.2 Hz, H-18'), 1.60 (s, H-19'), 1.60 (s, H-20')

^{13}C NMR ($CDCl_3$): δ 188.0 (C-1), 145.9 (C-2), 132.3 (C-3), 187.9 (C-4), 132.2 (C-5), 148.4 (C-6), 16.1 (C-7), 27.4 (C-1'), 118.2 (C-2'), 139.9 (C-3'), 39.6 (C-4'), 26.4 (C-5'), 125.2 (C-6'), 133.7 (C-7'), 39.0 (C-8'), 27.3 (C-9'), 155.0 (C-10'), 132.3 (C-11'), 27.5 (C-12'), 25.6 (C-13'), 123.6 (C-14'), 133.2 (C-15'), 25.0 (C-16'), 17.8 (C-17'), 204.9 (C-18'), 16.0 (C-19'), 16.1 (C-20') (Afolayan, *et al*., 2008).

Compound **3.3**

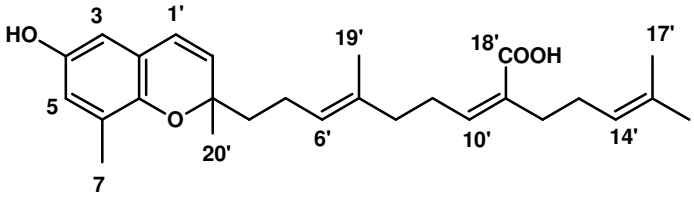

Orange-yellow oil; ^{1}H NMR ($CDCl_3$): δ 6.31 (m, H-3), 6.49 (m, H-5), 2.12 (s, H-7), 6.24 (d, 9.7 Hz, H-1'), 5.56 (d, 9.8 Hz, H-2'), 1.99 (m, H-4'), 2.05 (m, H-5'), 5.13 (m, H-6'), 2.05 (m, H-8'), 2.58 (q, 7.3 Hz, H-9'), 5.34 (t, 7.0 Hz, H-10'), 2.25 (t, 7.3 Hz, H-12'), 2.12 (s, H-13'), 5.13 (m, H-14'), 1.67 (m, H-16'), 1.58 (m, H-17'), 1.58 (m, H-19'), 1.67 (m, H-20')

^{13}C NMR ($CDCl_3$): δ 145.7 (C-1), 121.0 (C-2), 110.3 (C-3), 148.7 (C-4), 117.2 (C-5), 126.4 (C-6), 15.8 (C-7), 123.0 (C-1'), 130.5 (C-2'), 78.0 (C-3'), 40.5 (C-4'), 22.6 (C-5'), 125.0 (C-6'), 134.2 (C-7'), 40.0 (C-8'), 28.2 (C-9'), 144.9 (C-10'), 130.5 (C-11'), 34.6 (C-12'), 27.8 (C-13'), 123.4 (C-14'), 132.3 (C-15'), 25.6 (C-16'), 17.8 (C-17'), 172.8 (C-18'), 15.6 (C-19'), 26.0 (C-20') (Ham, *et al*., 2010).

Compound **3.4**

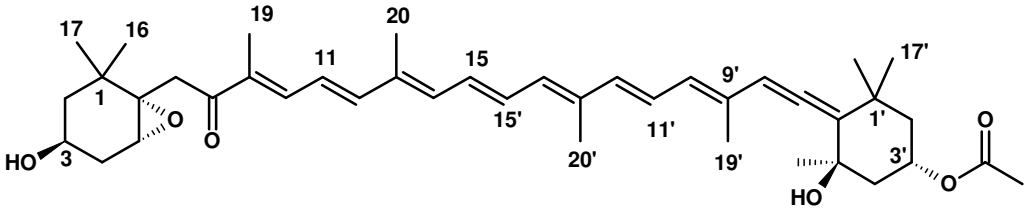

Red-Orange oil: ^{1}H NMR ($CDCl_3$): δ 1.48 (H-2'), 3.80 (H-3), 5.36 (H-3'), 1.76 (H-4), 1.50 (H-4'), 2.57 (H-7), 3.64 (H-7'), 6.04 (H-8'), 7.10 (H-10), 6.11 (H-10'), 6.54 (H-11), 6.58 (H-11'), 6.67 (H-12), 6.33 (H-12'), 6.39 (H-14), 6.25 (H-14'), 6.63 (H-15), 6.74 (H-15'), 1.02 (H-16), 1.80 (H-16'), 0.95 (H-17), 1.06 (H-17'), 1.21 (H-18), 1.34 (H-18'), 1.93 (H-19), 1.80 (H-19'), 1.98 (H-20), 1.98 (H-20')

^{13}C NMR ($CDCl_3$): δ 35.7 (C-1), 35.1 (C-1'), 47.0 (C-2), 45.4 (C-2'), 64.3 (C-3), 68.0 (C-3'), 41.6 (C-4), 45.2 (C-4'), 66.2 (C-5), 72.6 (C-5'), 67.1 (C-6), 117.4 (C-6'), 40.7 (C-7), 202.3 (C-7'), 197.8 (C-8), 103.3 (C-8'), 134.4 (C-9), 132.5 (C-9'), 139.2 (C-10), 128.5 (C-10'), 123.3 (C-11), 125.6 (C-11'), 145.0 (C-12), 137.1 (C-12'), 135.4 (C-13), 138.0 (C-13'), 136.6 (C-14), 132.1 (C-14'), 129.4 (C-15), 132.5 (C-15'), 25.0 (C-16), 21.4 (C-16'), 28.1 (C-17), 32.0 (C-17'), 21.5 (C-18), 31.6 (C-18'), 11.8 (C-19), 14.0 (C-19'), 12.7 (C-20), 12.9 (C-20') (Afolayan, *et al*., 2008).

Lapachol and its related compound

Compound **3.6**

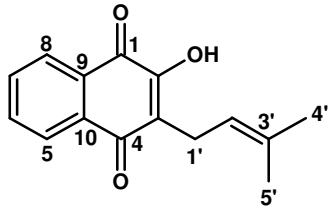

Yellow crystals; ^{1}H NMR ($CDCl_3$): δ 8.06 (d, 7.8 Hz, H-5), 7.67 (t, 7.5 Hz, H-6), 7.74 (t, 7.5 Hz, H-7), 8.19 (d, 7.8 Hz, H-8), 3.30 (d, 7.6 Hz, H-1'), 5.21 (t, 7.6 Hz, H-2'), 1.68 (s, H-4'), 1.78 (s, H-5'). ^{13}C NMR ($CDCl_3$): δ 181.7 (C-1), 152.6 (C-2), 123.4 (C-3), 184.5 (C-4), 126.7 (C-5), 134.8 (C-6), 132.8 (C-7), 126.0 (C-8), 129.4 (C-9), 132.9 (C-10), 22.6 (C-1'), 119.6 (C-2'), 133.8 (C-3'), 25.7 (C-4'), 17.8 (C-5') (Oliveira, *et al*., 2002).

Compound **3.7**

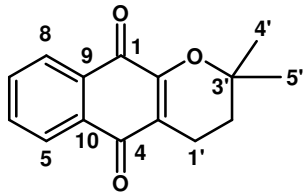

^{1}H NMR ($CDCl_3$): δ 8.07 (m, H-5), 7.67 (m, H-6), 7.67 (m, H-7), 8.07 (m, H-8), 2.61 (t, 6.6 Hz, H-1'), 1.81 (t, 6.7 Hz, H-2'), 1.43 (s, H-4'), 1.43 (s, H-5'). ^{13}C NMR ($CDCl_3$): δ 180.0 (C-1), 154.6 (C-2), 120.1 (C-3), 184.4 (C-4), 126.3 (C-5), 133. (C-6), 132.9 (C-7), 125.9 (C-8), 131.1 (C-9), 132.0 (C-10), 16.7 (C-1'), 31.4 (C-2'), 78.1 (C-3'), 26.5 (C-4'), 26.5 (C-5') (Salas, *et al*., 2008).

Compound **3.8**

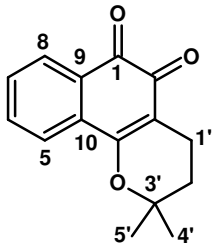

^{1}H NMR ($CDCl_3$): δ 7.80 (d, 7.6 Hz, H-5), 7.49 (t, 7.8 Hz, H-6), 7.63 (t, 7.8 Hz, H-7), 8.05 (d, 7.6 Hz, H-8), 2.56 (t, 6.5 Hz, H-1'), 1.82 (t, 6.7 Hz, H-2'), 1.46 (s, H-4'), 1.46 (s, H-5'). ^{13}C NMR ($CDCl_3$): δ 179.8 (C-1), 178.5 (C-2), 112.7 (C-3), 162.1 (C-4), 124.1 (C-5), 134.8 (C-6), 130.9 (C-7), 128.5 (C-8), 130.1 (C-9), 132.6 (C-10), 16.1 (C-1'), 31.5 (C-2'), 79.3 (C-3'), 26.7 (C-4'), 26.7 (C-5') (Salas, *et al*., 2008).

Compound **3.9**

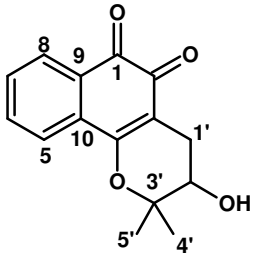

^{1}H NMR ($CDCl_3$): δ 7.83 (d, 7.6 Hz, H-5), 7.51 (t, 7.6 Hz, H-6), 7.65 (t, 7.8 Hz, H-7), 8.06 (d, 7.6 Hz, H-8), 2.82 (dd, 17.8 Hz, 5.3 Hz H-1a'), 2.62 (dd, 17.8 Hz, 5.6 Hz, H-1b'), 3.91 (t, 5.2 Hz, H-2'), 1.45 (s, H-4'), 1.51 (s, H-5'). ^{13}C NMR ($CDCl_3$): δ 179.5 (C-1), 178.5 (C-2), 110.3

(C-3), 161.5 (C-4), 124.4 (C-5), 134.9 (C-6), 130.9 (C-7), 128.8 (C-8), 130.0 (C-9), 132.0 (C-10), 22.1 (C-1'), 68.2 (C-2'), 81.4 (C-3'), 25.0 (C-4'), 25.4 (C-5') (Salas, *et al*., 2008).

Compound **3.10**

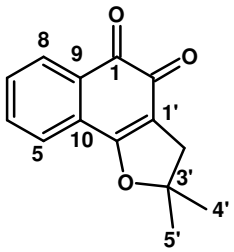

^{1}H NMR ($CDCl_3$): δ 7.57 (m, H-5), 7.63 (m, H-6), 7.63 (m, H-7), 8.07 (m, H-8), 2.94 (s, H-1'), 1.60 (s, H-3'), 1.60 (s, H-4'). ^{13}C NMR ($CDCl_3$): δ 180.1 (C-1), 176.2 (C-2), 114.3 (C-3), 168.8 (C-4), 124.1 (C-5), 133.5 (C-6), 129.2 (C-7), 128.3 (C-8), 131.1 (C-9), 133.4 (C-10), 40.1 (C-1'), 94.1 (C-2'), 29.5 (C-3'), 29.5 (C-4') (Kongkathip, *et al*., 2003).

Compound **3.11**

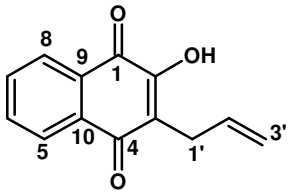

^{1}H NMR ($CDCl_3$): δ 8.08 (d, 7.7 Hz, H-5), 7.68 (t, 7.6 Hz, H-6), 7.76 (t, 7.7 Hz, H-7), 8.13 (d, 7.8 Hz, H-8), 3.36 (d, 6.6 Hz, H-1'), 5.91 (m, H-2'), 5.91 (m, H-3a'), 5.05 (m, H-3b'). ^{13}C NMR ($CDCl_3$): δ 184.2 (C-1), 153.1 (C-2), 121.8 (C-3), 181.5 (C-4), 126.9 (C-5), 133.7 (C-6), 133.0 (C-7), 126.1 (C-8), 129.3 (C-9), 132.8 (C-10), 27.5 (C-1'), 135.0 (C-2'), 116.4 (C-3') (Silva, *et al*., 2006)

References

Afolayan, A., Bolton, J., Lategan, C., Smith, P., & Beukes, D. (2008). Fucoxanthin, tetraprenylated toluquinone and toluhydroquinone metabolites from Sargassum heterophyllum inhibit the *in vitro* growth of the malaria parasite Plasmodium falciparum. *Zeitschrift für Naturforschung, 63c*, 848-852.

da Silva Junior, E.N., de Souza, M.C., Fernandes, M.C., Menna-Barreto, R.T., Pinto Mdo, C., de Assis Lopes, F., de Simone, C.A., Andrade, C.K., Pinto, A.V., Ferreira, V.F., & de Castro, S.L. (2008). "Synthesis and anti-trypanosoma cruzi activity of derivatives from nor-lapachones and lapachones." *Bioorganic & Medicinal Chemistry, 16,* 5030–5038.

de Almeida, E.R. (2009). "Preclinical and clinical studies of lapachol and beta-lapachone." *The Open Natural Product Journal, 2,* 42-47.

de la Mare, J.A., Lawson, J.C., Chiwakata, M.T., Beukes, D.R., Edkins, A.L., & Blatch, G.L. (2012). "Quinones and halogenated monoterpenes of algal origin show anti-proliferative effects against breast cancer cells in vitro." *Investigational New Drugs, 30,* 2187-2200.

Ham, Y.M, Kim, K.N., Lee, W.J., Lee, N.H., & Hyun, C.G., (2010). "Chemical constituents of Sargassum micracanthum and antioxidant activity." *International Journal of Pharmacology, 6,* 147-151.

Hussain, H., Krohn, K., Ahmad, V.U., Miana, G.A., & Green, I.R. (2007). "Lapachol: an overview." *ARKIVOC* ii: 145-171.

Kongkathip, N., Kongkathip, B., Siripong, P., Sangma, C., Luangkamin, S., Niyomdecha, M., Pattanapa, S., Piyaviriyagul, S., & Kongsaeree, P. (2003). "Potent antitumor activity of synthetic 1, 2-naphthoquinones and 1, 4-naphthoquinones." *Bioorganic & Medicinal Chemistry, 11,* 3179–3191.

Moyo, B. 2013. *The screening and characterisation of compounds for modulators of Heat shock protein (Hsp90) in a breast cancer cell model.* (PhD) Rhodes University.

Munedzimwe, T.C. (2012). *The Isolation, quantification and synthetic modification of antiplasmodial natural products from Sargassum heterophyllum.* MSc; Rhodes University.

Oliveira, M.F., Lemos, T.G., de Mattos, M.C., Segundo, T.A., Santiago, G.M., & Braz-Filho, R. (2002). "New enamine derivatives of lapachol and biological activity." *Annals of the Brazilian Academy of Sciences, 74,* 211-221.

Reddy, P., & Urban, S. (2009). "Meroditerpenoids from the southern Australian marine brown alga Sargassum fallax." *Phytochemistry, 70,* 250-255.

Salas, C., Tapia, R.A., Ciudad, K., Armstrong, V., Orellana, M., Kemmerling, U., Ferreira, J., Maya, J.D., & Morello, A. (2008). "Trypanosoma cruzi: activities of lapachol and α- and β-lapachone derivatives against epimastigote and trypomastigote forms." *Bioorganic & Medicinal Chemistry, 16,* 668–674.

Silva, R.S., Costa, E.M., Trindade, U.L., Teixeira, D.V., Pinto Mde, C., Santos, G.L., Malta, V.R., De Simone, C.A., Pinto, A.V., & de Castro, S.L. (2006). "Synthesis of naphthofuranquinones with activity against Trypanosoma cruzi." *European Journal of Medicinal Chemistry, 41,* 526–530.

Sun, J.S, Geiser, A.H., & Frydman, B. (1998). "A preparative synthesis of lapachol and related naphthoquinones." *Tetrahedron letters, 39,* 8221-8224.

Sunassee, S.N., Veale, C.G., Shunmoogam-Gounden, N., Osoniyi, O., Hendricks, D.T., Caira, M.R., de la Mare, J.A, Edkins, A.L., Pinto, A.V., da Silva Júnior, E.N., & Davies-Coleman, M.T. (2013). "Cytotoxicity of lapachol, β-lapachone and related synthetic 1, 4-naphthoquinones against oesophageal cancer cells." *European Journal of Medicinal Chemistry, 62,* 98-110.

CHAPTER FOUR

Synthesis of truncated sarganaphthoquinoic acid (SNQA) derivatives

Abstract

The quinone moiety was identified as the active component of secondary metabolites isolated from *Sargassum incisifolium* and *Tabebuia avellanedae.* Due to limited amounts of the natural products, prenylated naphthoquinone derivatives were designed and synthesized to improve the cytotoxicity of these compounds, and to develop them as potential Hsp90 inhibitors. The naphthoquinone moiety was constructed *via* Diels-Alder reactions of a range of benzoquinone analogues and myrcene, followed by MnO_2 catalyzed aromatization. Various aryl and alkyl amines were then coupled to the quinone in the presence of $Cu(OAc)_2$ to prepare a small library of compounds. The synthesized compounds were prepared in yields varying from 55-95% and characterized by Nuclear Magnetic Resonance (NMR) spectroscopy and mass spectrometry.

4.1 Introduction

Naphthoquinones are a class of compounds that possess a wide spectrum of biological activities that include anti-bacterial, anti-inflammatory, anti-parasitic, anti-tumour and cytotoxic activities (Chung, *et al*., 2007). The quinone moiety is an essential component of these molecules and several drugs that are used in current treatments have the quinone nucleus as the core pharmacophoric element (Rahmoun, et al., 2013) e.g. atovaquone (**4.1**) for the treatment and prevention of malaria (Ramirez, *et al*., 2014), mitomycin C (**4.2**) and doxorubicin (**4.3**) for treatment of cancer (Dubowchik, *et al*., 1998). In relation to cancer, quinones have been discovered to be effective inducers of apoptosis rather than the less preferred necrosis, which makes them ideal candidates for further investigation in cancer treatment (Ramirez, *et al*., 2014).

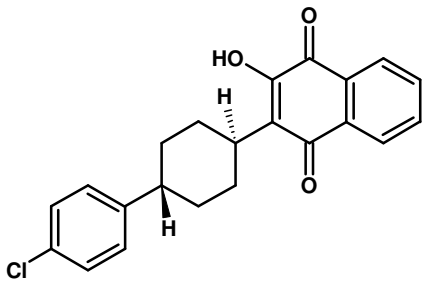

4.1

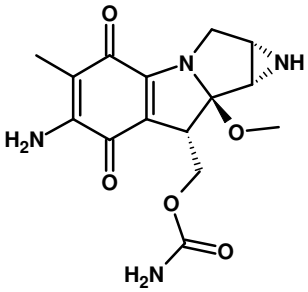

4.2

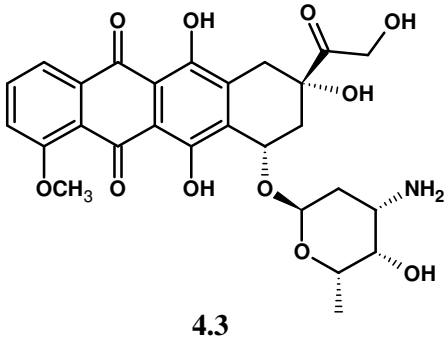

4.3

4.1.1 Mechanism of action of cytotoxic naphthoquinones / quinones

Two major mechanisms have been proposed for the cytotoxic action of quinones and naphthoquinones. Firstly, they possess the ability to undergo redox cycling effected by microsomal NADPH-cytochrome P-450 reductase or mitochondrial NADH ubiquinone oxidoreductase, thereby generating reactive oxygen species (ROS) that cause oxidative stress in cancer cells (Castro, *et al*., 2008). Secondly, quinones are susceptible to attack by nucleophiles e.g. thiol groups of proteins and reduced glutathione (GSH). Depletion of GSH

due to the formation of GS-conjugates catalysed by glutathione transferase isoforms has been the major cause of cytotoxicity and oxidative stress in cells (Seung, *et al*., 1998). Oxidative stress causes damage to proteins, cell membranes and DNA of cancer cells resulting in apoptosis. An example is presented below (**Scheme 4.1**) involving menadione and how ROS are generated and quenched in a biological system.

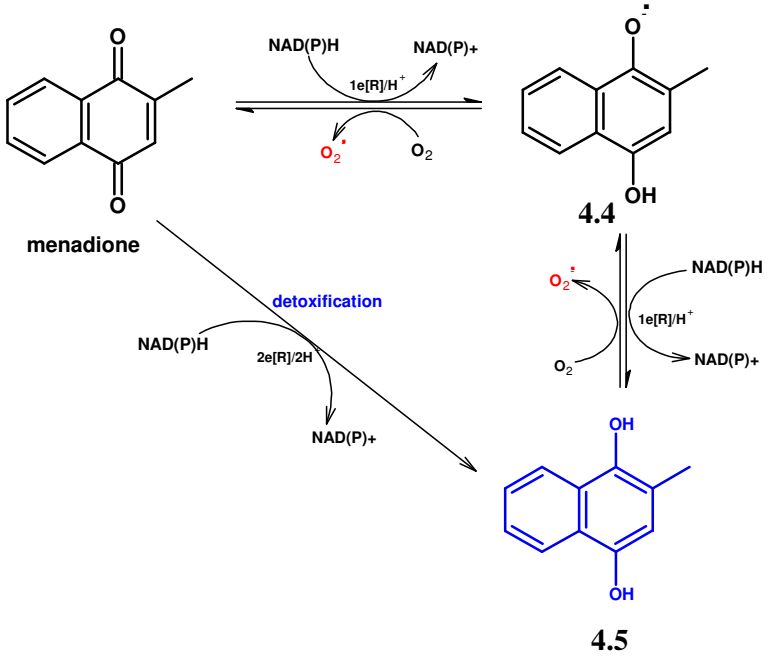

Scheme 4.1: Redox cycling reaction of menadione in cancer cells (Criddle, *et al*., 2006).

Quinones undergo one electron reduction reactions to produce unstable semi-quinones (**4.4**). In the presence of molecular oxygen, semi-quinones enter into a redox cycle to regenerate the quinone but in the process generate ROS (Criddle, *et al*., 2006). NAD(P)H is used as the electron donor and its concentration in cells decrease as more ROS are formed. Another route that occurs concomitantly to the one described above involves transfer of two electrons in the reduction process by use of NAD(P)H:quinone oxidoreductase 1 to produce the more stable hydroquinone (**4.5**). This route is seen as a detoxifying mechanism and NAD(P)H:quinone oxidoreductase 1 concentrations have been observed to be elevated in cancer cells during chemotherapy (Dinkova-Kostova and Talalay, 2000).

Other minor mechanisms highlighted for the quinones include DNA intercalation, alkylation, DNA strand breaks induction and inhibition of topoisomerase enzymes (Rahmoun, *et al*., 2013). Their binding properties can occur in three different oxidation states, i.e. i) in the quinone form ii) semi-quinone form (one electron reduced form) and iii) catechol form (two

electron reduced form), allowing them to interact with biological systems at different levels (Pierpont, 2001).

The following table (**Table 4.1**) gives examples of cytotoxic mechanisms of action of naphthoquinones as reported in literature.

Table 4.1: Examples of naphthoquinones and their cytotoxic mode of action.

Compound	Structure	Mode of Action	Reference
menadione	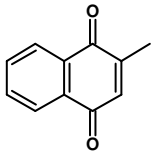	Generates ROS and cause oxidative stress	(Seung, *et al*., 1998)
diospyrin	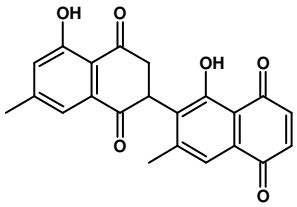	Inhibits action of topoisomerase I enzymes. Inhibits electron transport chain	(Sagar, *et al*., 2010)
isodiospyrin	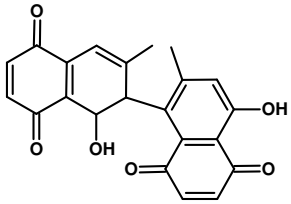	Inhibits action of topoisomerase I enzymes	(Ting, *et al*., 2003)
juglone	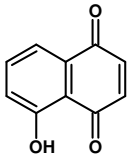	DNA damage and inhibition of transcription enzymes	(Paulsen and Ljungman, 2005)
plumbagin	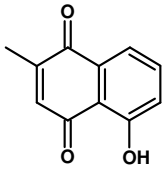	Generates ROS and causes oxidative stress	(Lee, *et al*., 2012)

4.1.2 Synthetic methodologies for the construction of naphthoquinones

Due to naphthoquinone's diversity in biological activity, vast attention has been given to develop methods that can be employed to synthesize these molecules. One of the most common methods used is the Diels-Alder reaction (Witayakran and Ragauskas, 2007). In this reaction, benzoquinones act as dienophiles that react with dienes to form a Diels-Alder adduct (**Scheme 4.2**), followed by aromatization to the naphthoquinone.

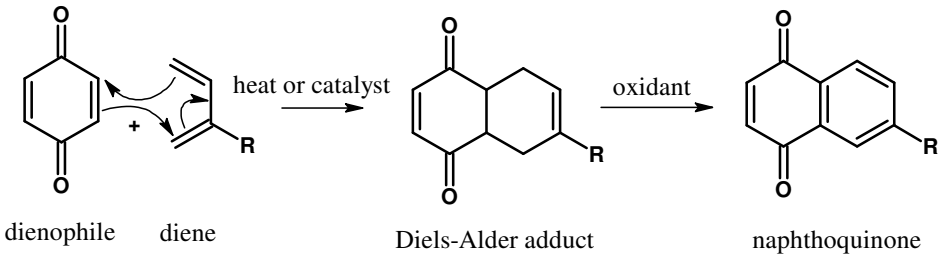

Scheme 4.2: General Diels-Alder and aromatization reactions

Various catalysts have been used to improve the outcome of the Diels-Alder reaction i.e. $BF_3 \cdot Et_2O$, Lewis acids etc., together with ultrasonic or microwave irradiation (Miguel del Corral, *et al*., 2002). In older methods, only heat was employed to form the Diels-Alder adduct, followed by aromatization to the naphthoquinone. Use of oxidants such as Ag_2O, CAN and DDQ have been investigated in aromatization reactions but they give rise to complex mixtures that are difficult to isolate and purify. Only MnO_2 yields fairly distinct cyclized adducts and has been the most preferred in aromatizing Diels-Alders adducts (Miguel del Corral, *et al*., 2002).

Other methods that have been employed to synthesize naphthoquinones involve oxidation of naphthols from benzenoid precursors e.g. *o*-allyl-*p*-cresol (Achari, *et al*., 1985) and methoxy-allylbenzamides, (Sibi, *et al*., 1986) or through rearrangement of hydroxycyclobutenones (**Scheme 4.3**). Presently, the Diels-Alder reaction is superior in preparing naphthoquinones and a similar method was adapted for the synthesis of our series of analogues discussed in this chapter.

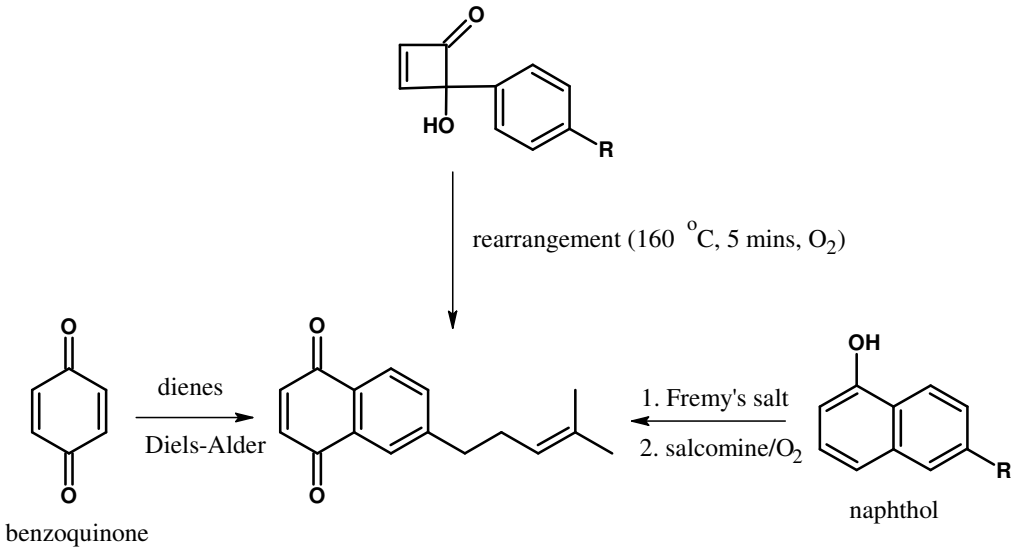

Scheme 4.3: Summary of naphthoquinone syntheses

4.1.3 Aim of this study

Investigation into the cytotoxic properties and Hsp90 inhibition of sarganaphthoquinoic acid (SNQA) (**3.5**) was limited due to the quantities of natural product we obtained. Semi-synthetic routes developed by our group to prepare **3.5** from sargahydroquinoic acid (**3.1**) only yielded minute quantities and the reaction was unpredictable and fell short of reproducibility. Optimization of the reaction is essential and warrants further investigation. However for this part of the project, we resorted to truncated sarganaphthoquinoic acid derivatives, with modifications targeted at increasing cytotoxic nature of these molecules. Their Hsp90 inhibition properties were then assessed.

Therefore, the aim of the project was to design and synthesize prenylated naphthoquinone analogues with improved cytotoxic activity and Hsp90 binding properties.

4.2 Results and discussion

4.2.1 Rationale for the design of prenylated naphthoquinone derivatives

Our design strategy was centred on incorporating moieties from known Hsp90 inhibitors onto our naphthoquinone scaffold, with the anticipation of enhancing their properties towards Hsp90 binding and also maintaining their cytotoxic properties. **Scheme 4.4** briefly highlights targeted compounds that were synthesized for this project.

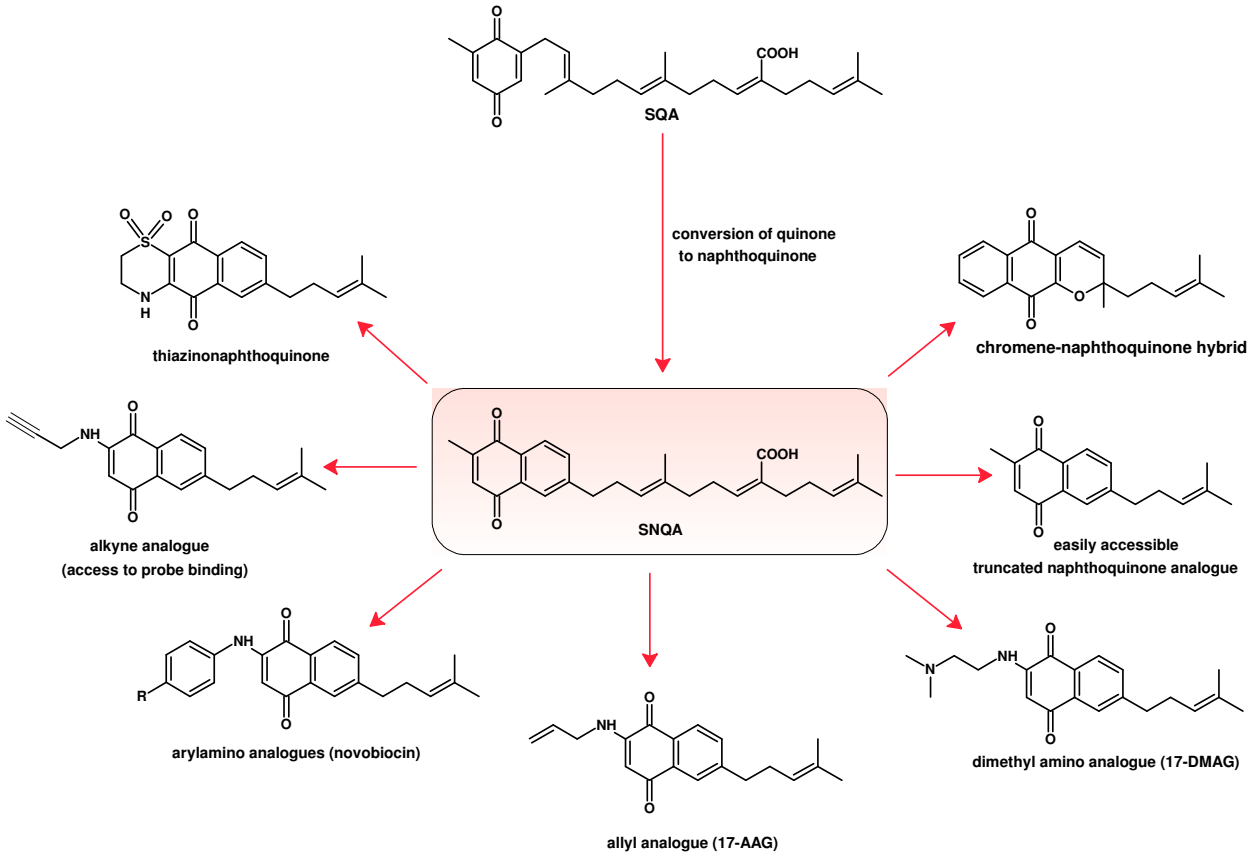

Scheme 4.4: Analogue design strategy

4.2.2 Synthesis of the naphthoquinone scaffold by the Diels-Alder reaction

The first series constituted simple naphthoquinone derivatives bearing H, CH_3, OCH_3 and Cl substituents at the C-2 or C-3 position of the quinone moiety. The aim was to evaluate the importance of position 2 and 3 in cytotoxicity and Hsp90 inhibition of naphthoquinones. Substituents were chosen based on their electron withdrawing and electron donating properties.

Benzoquinones **4.7** and **4.9** are commercially available while 2-methoxybenzoquinone (**4.8**) was prepared *via* oxidation of 2-methoxyhydroquinone by MnO_2. Reactions of *p*-benzoquinones **4.7-4.9** with myrcene in refluxing EtOH gave isomeric mixtures of the 2- and 3- substituted Diels-Alder products. This product was immediately oxidized to the naphthoquinone derivative with MnO_2 under reflux for four hours in C_6H_6 (**Scheme 4.5**). Other aromatization reactions explored included reactions with KOH and DDQ. The former yielded mainly 2- and 3- hydroxylated products while the latter yielded complex mixtures (Miguel del Corral, *et al*., 2002). MnO_2 was thus the preferred oxidant to use in all naphthoquinone syntheses conducted for this research. Final purification of naphthoquinones **4.11-4.13** was achieved by column chromatography and normal phase HPLC.

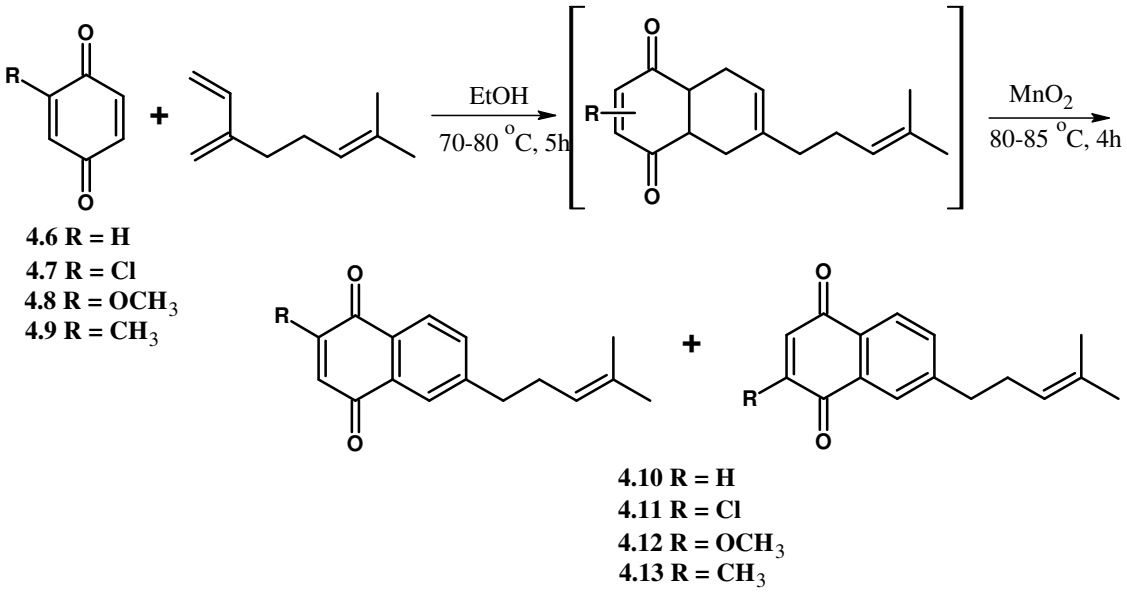

Scheme 4.5: Preparation of naphthoquinones *via* Diels-Alder and aromatization reactions

The synthesized naphthoquinones were characterized by 1D and 2D NMR spectroscopy. Representative ^{1}H and ^{13}C NMR spectra for naphthoquinones (**4.10-4.13**) are presented in Figure **4.1** and Figure **4.2** respectively for compound **4.10.**

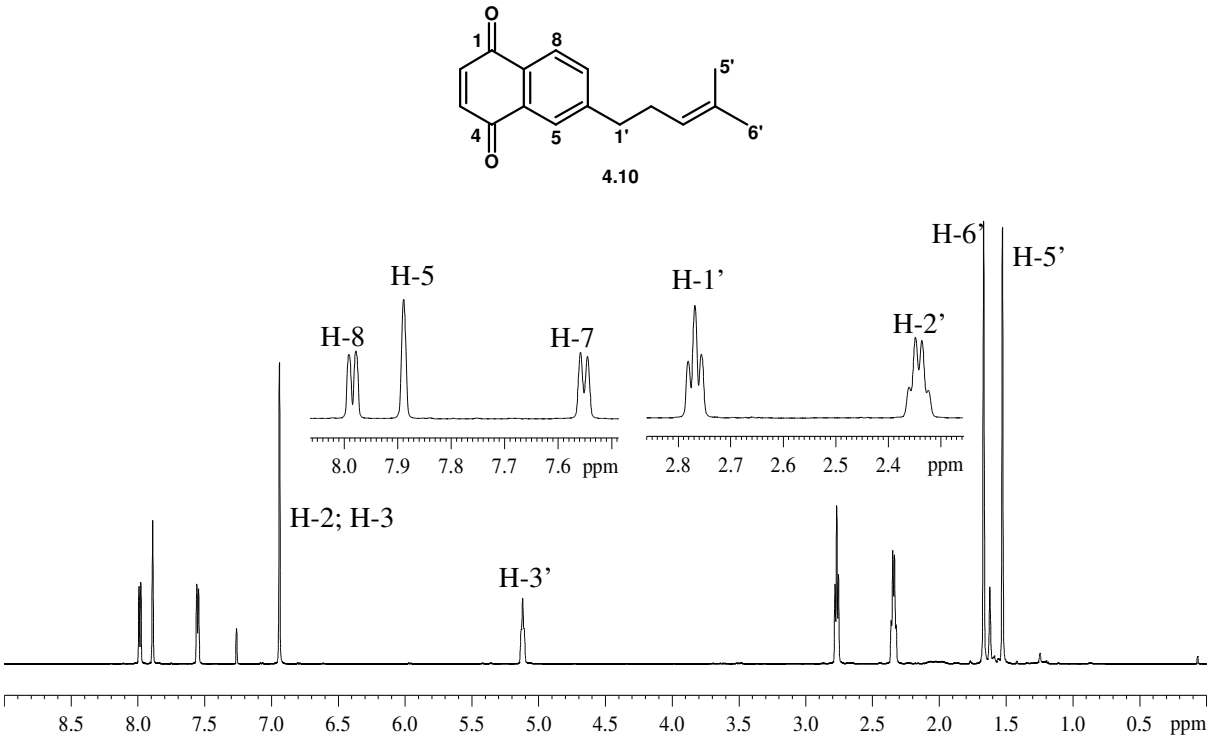

Figure 4.1: ^{1}H NMR spectrum (600 MHz, $CDCl_3$) of compound **4.10**

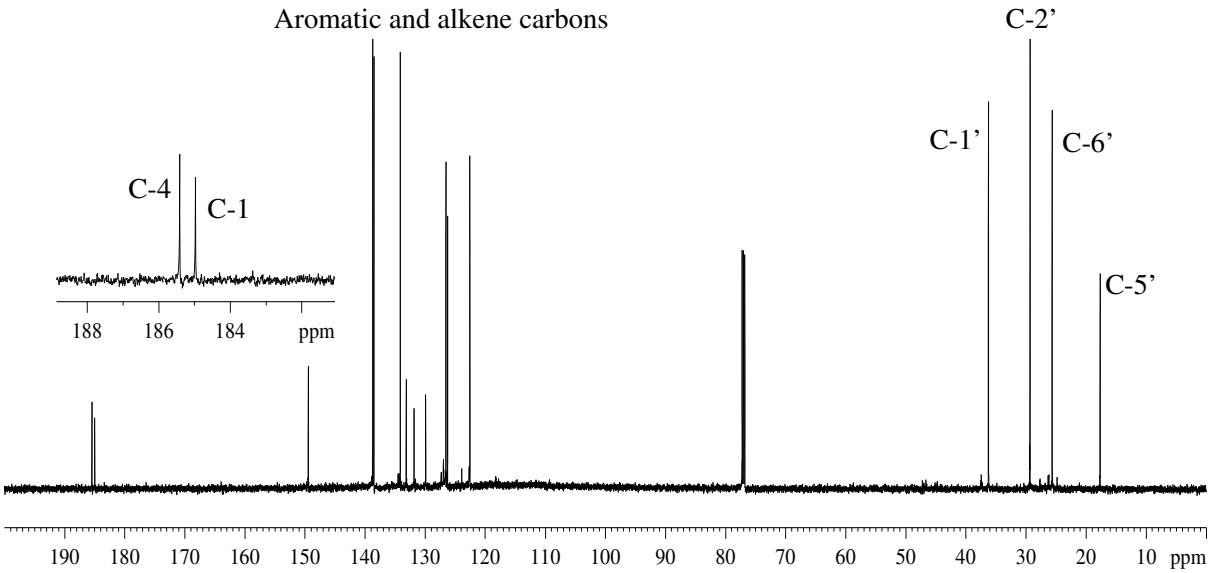

Figure 4.2: ^{13}C NMR spectrum (150 MHz, $CDCl_3$) of compound **4.10**

In the ^{1}H NMR spectrum (**Figure 4.1**), the naphthoquinone moiety was characterized by a set of mutually coupled aromatic doublets at δ 7.98 (d, *J* = 7.8 Hz, H-8) and δ 7.55 (d, *J* = 7.8 Hz, H-7), a methine singlet at δ 7.88 (s, H-5) and a benzoquinone methine proton at δ 6.93 (s, H-2 and H-3). The presence of C-1 and C-4 carbonyl carbons was observed in the ^{13}C NMR spectrum at δ 185.4 and δ 184.9 respectively. The prenyl side chain was represented by a triplet at δ 2.76 (t, *J* = 7.8 Hz, H-1') coupled to a quartet at δ 2.34 (q, *J* = 7.5 Hz, H-2'), which in turn was coupled to an olefinic methine at δ 5.11 (t, *J* = 7.1 Hz, H-3'). Two methyl signals observed at δ 1.66 (s, H-6') and δ 1.52 (s, H-5') completed the side chain. In total, the ^{13}C NMR spectrum showed the presence of four methyl and methylene carbons in the region δ 16-40, four quaternary carbons and six methine carbons consistent with compound **4.10**. The spectroscopic data matched literature values (Miguel del Corral, *et al*., 2002) and is shown in **Table 4.3**.

The ^{1}H and ^{13}C NMR spectra of compounds **4.11, 4.12, 4.13** were similar to that of compound **4.10** apart from signals corresponding to the -OCH_3 at δ 3.89 (s) and -CH_3 at δ 2.18 (s) appearing for compounds **4.12** and **4.13,** respectively. The integration of the aromatic protons to the benzoquinone signal reduced from two to one, indicative of a substituted molecule at position 2 or 3. Due to two possible substitution patterns that can occur on the molecule, the initial ^{1}H NMR spectra for compounds **4.11- 4.13** had duplicated signals in the aromatic region. The regioisomers were separated by normal phase HPLC (Hex/EtOAc) and a representative chromatogram obtained for compound **4.11** is shown in **Figure 4.3**.

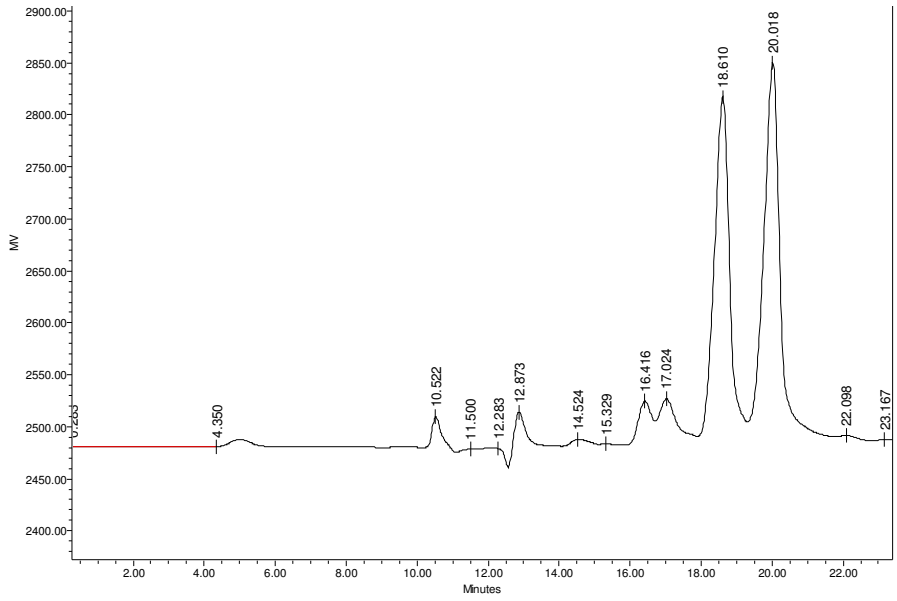

Figure 4.3: Normal phase HPLC chromatogram showing separation of the two regioisomers, eluting at different retention times of 18 min and 20 min.

The ratios of the individual isomers in the mixture were calculated relative to peak heights on the HPLC chromatograms, and the retention times were noted (**Table 4.2**). Isomer A appeared to elute first from the HPLC, followed by isomer B.

Table 4.2: Percentage yields and HPLC fractions obtained

Compound	% yield	Ratio of isomers		Retention times (mins)	
		A (%)	**B (%)**	**A**	**B**
4.11	83.3	49.8	50.2	18.6	20.0
4.12	84.6	49.6	50.4	34.1	35.7
4.13	98.4	50.0	50.0	23.9	25.0

The two regioisomers were identified based on their HMBC correlations which are shown in **Figure 4.4** and **Figure 4.5** for compounds **4.11A** and **4.11B** respectively. Several aspects are essential to note with these correlations:

i) The two carbonyl carbons were distinguished based on their HMBC correlations to H-5 and H-8

ii) Aromatic protons mainly correlate to carbonyl carbons that are three bonds away; two bond correlations are often missing in these systems.

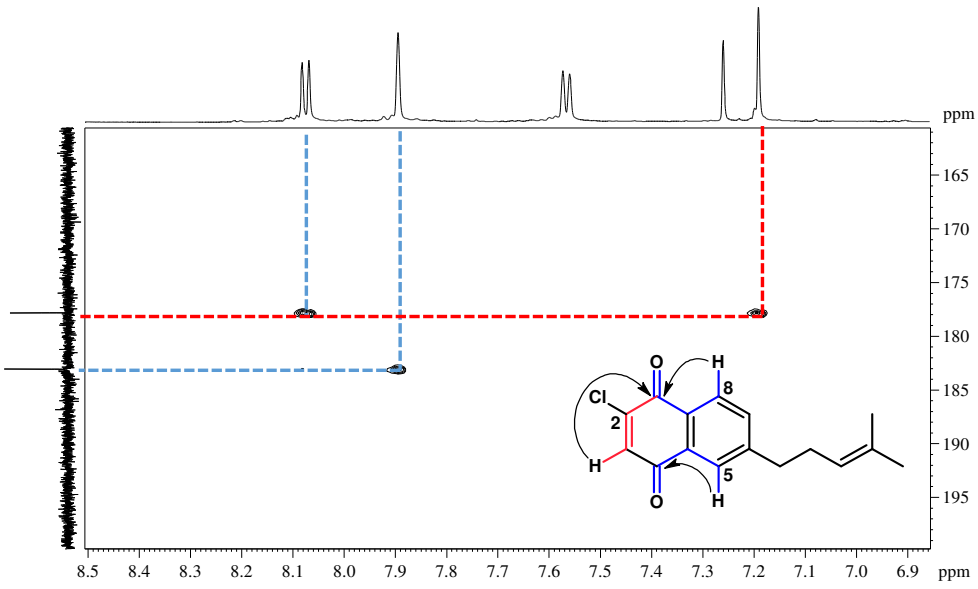

Figure 4.4: HMBC corrections of compound **4.11A**

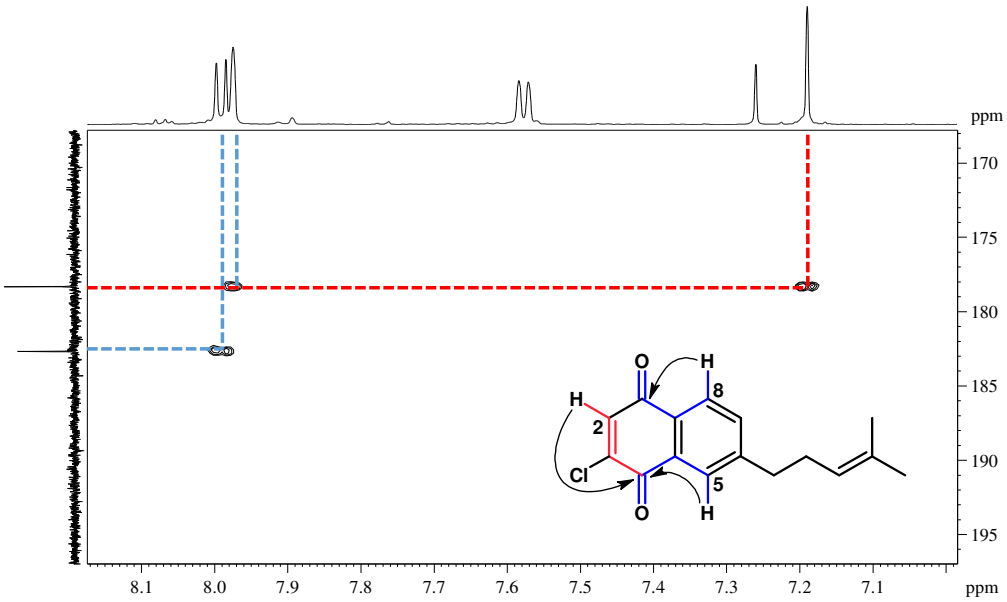

Figure 4.5: HMBC corrections of compound **4.11B**

Based on these aspects, a correlation of H-8 to the same carbonyl (C-1) as the benzoquinone signal indicates substitution at C-2. Correlation of H-5 and the benzoquinone signal to the same carbonyl (C-4) suggests substitution at C-3. Isomers **4.11A** and **4.11B** were therefore determined as having the halogen at C-2 and C-3, respectively. Such analysis is consistent with work published by Miguel del Corral and colleagues (2006).

Comparisons were also done between the acquired ^{1}H NMR spectra, before and after separation of the regioisomers (**Figure 4.6** and **4.7**) and it was noticed that C-3 substitution resulted in a more deshielded H-5 signal compared to C-2 substitution, which potentially could be used to distinguish the isomers. Similar patterns were observed in other substituted naphthoquinone derivatives, **4.12** and **4.13. Table 4.3** contains a list of all ^{1}H and ^{13} C chemical shifts of isomers belonging to compounds **4.10**-**4.13**.

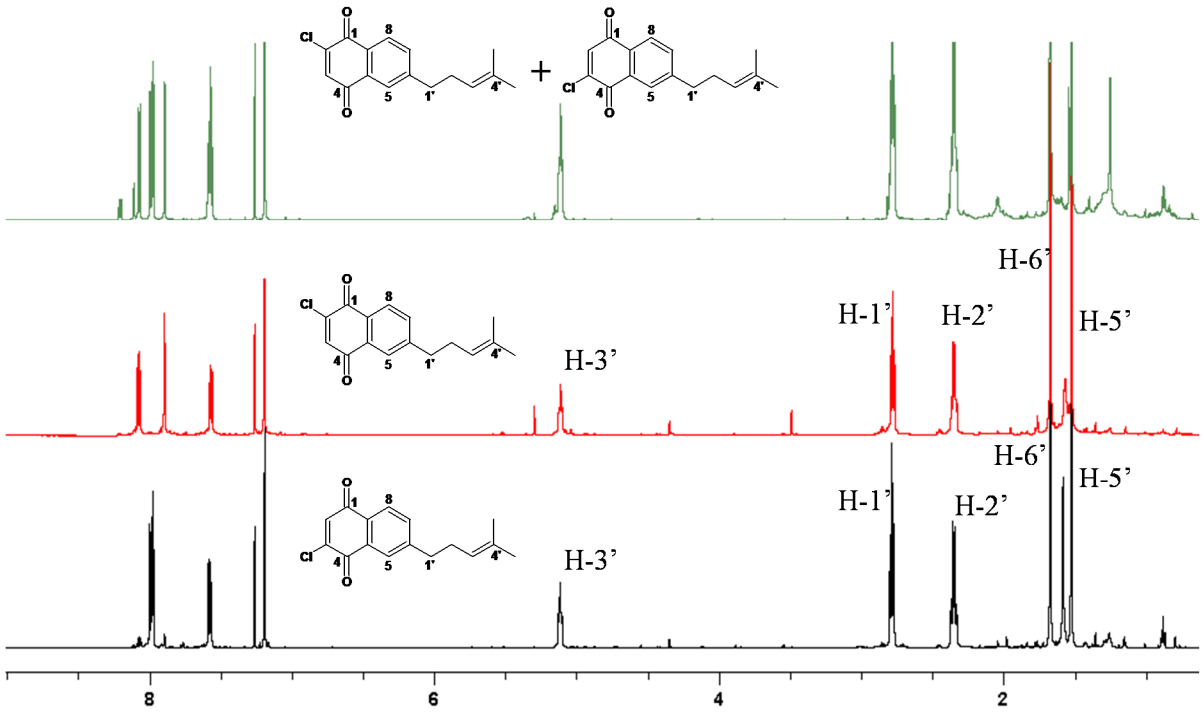

Figure 4.6: ^{1}H NMR spectra (600 MHz, $CDCl_3$) of compound **4.11** as a mixture and of the individual isomers after separation by normal phase HPLC.

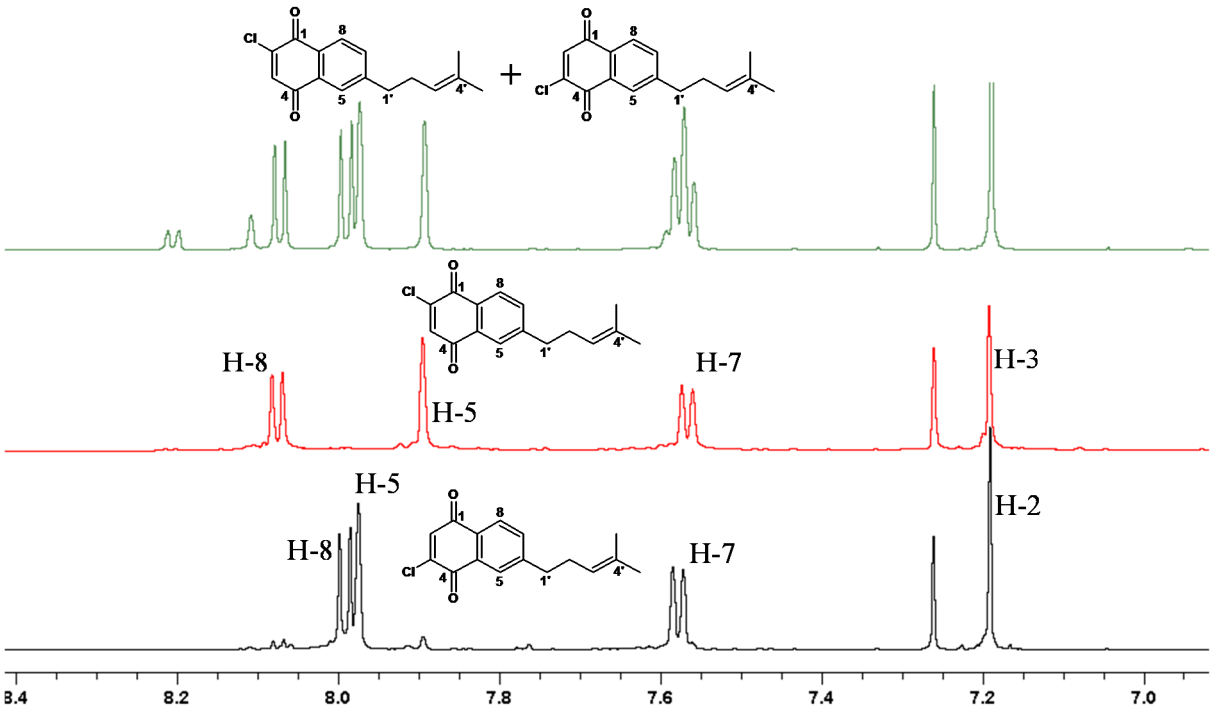

Figure 4.7: Expansion of the aromatic region of the ^{1}H NMR spectra (600 MHz, $CDCl_3$) of compound **4.11** regioisomers.

Table 4.3: ^{1}H and ^{13}C NMR chemical shifts of compounds **4.10-4.13**

	4.10		**4.11A**		**4.11B**		**4.12A**		**4.12B**		**4.13A**		**4.13B**	
C no.	δ_H, mult, *J*(Hz)	δ_C	δ_H, mult, *J*(Hz)	δ_C	δ_H, mult, *J*(Hz)	δ_C	δ_H, mult, *J*(Hz)	δ_C	δ_H, mult, *J*(Hz)	δ_C	δ_H, mult, *J*(Hz)	δ_C	δ_H, mult, *J*(Hz)	δ_C
1	-	184.9	-	177.8	-	182.6	-	180.2	-	182.9	-	185.5	-	185.9
2	6.93, s	138.5	-	146.4	7.18, s	135.9	-	155.3	6.13, s	113.2	-	148.2	6.80, s	133.9
3	6.93, s	138.7	7.19, s	135.7	-	146.1	6.14, s	113.4	-	155.6	6.80, s	133.8	-	147.9
4	-	185.4	-	183.0	-	178.3	-	183.1	-	181.1	-	185.6	-	185.0
5	7.88, s	126.5	7.89, s	126.6	7.97, s	127.4	7.89, s	127.1	7.93, s	127.9	7.86, s	126.7	7.90, s	126.4
6	-	149.4	-	150.2	-	149.8	-	149.5	-	149.9	-	149.2	-	149.0
7	7.55, dd, 7.8; 1.7	134.1	7.56, d, 7.9	134.3	7.57, d, 7.7	134.7	7.51, d, 7.8	135.6	7.53, d, 7.9	135.8	7.52, dd, 7.8, 1.7	135.5	7.52, dd, 7.8; 1.7	135.7
8	7.98, d, 7.8	126.2	8.07, d, 7.8	127.7	7.99, d, 7.7	126.8	8.03, d 7.8	126.7	7.98, d 7.9	126.8	8.00, d, 7.8	125.9	7.95, d, 7.8	126.2
9	-	129.9	-	129.2	-	129.7	-	131.5	-	131.7	-	130.1	-	130.2
10	-	133.1	-	133.3	-	133.3	-	133.8	-	132.0	-	133.1	-	133.1
1'	2.76, t, 7.8	36.2	2.78, t, 7.7	36.2	2.78, t, 7.7	36.1	2.76, t, 7.6	36.3	2.75, t, 7.6	36.2	2.75, t, 7.5	36.2	2.76, t, 7.6	36.2
2'	2.34, q, 7.5	29.3	2.34, q, 7.6	29.2	2.34, q, 7.4	29.2	2.34, q, 7.4	29.4	2.34, q, 7.6	29.5	2.34, q, 7.2	29.3	2.33, q, 7.5	29.4
3'	5.11, t, 7.1	122.5	5.11, t, 7.1	122.4	5.11, t, 7.0	122.4	5.12, t, 7.1	122.5	5.12, t, 7.2	122.6	5.12, t, 7.1	122.6	5.12, t, 7.3	122.6
4'	-	131.8	-	131.7	-	131.2	-	132.0	-	131.9	-	132.2	-	132.0
5'	1.54, s	17.6	1.52, s	17.6	1.52	17.7	1.53, s	17.6	1.52, s	17.7	1.52, s	17.7	1.52, s	17.7
6'	1.66, s	25.6	1.66, s	25.6	1.67	25.6	1.67, s	25.6	1.66, s	25.6	1.66, s	25.6	1.66, s	25.7
7'	-	-	-	-	-	-	3.89, s	58.8	3.89, s	58.9	2.18, s	16.5	2.18, s	16.5

NB. C-2 substituted naphthoquinones are presented as isomer A and C-3 substituted ones as isomer B

4.2.3 Synthesis of arylamino-naphthoquinones (second series)

2-Amino-1, 4-naphthoquinone moieties have been found to possess cytotoxic properties. They are known to take part in enzyme inhibition, DNA cross linking, as well as interfering with electron transport and oxidative phosphorylation systems (Miguel del Corral, *et al*., 2005; Ryu, *et al*., 2000). Two major methods have been developed to synthesize these molecules, and involve either oxidative coupling reactions of amines to unsubstituted naphthoquinones on C-2/3 position or *via* nucleophilic substitution of 2-halonaphthoquinones (Lisboa, *et al*., 2011). For this part of the project, the former method was used to prepare our second series of naphthoquinones.

Several anilines were coupled to compound **4.10**. Under normal conditions the reaction can be carried out in EtOH at room temperature with no catalyst, but longer reaction times of approximately 72 hours are required. A quicker and more efficient method has been developed which requires use of $Cu(OAc)_2$ as a catalyst in AcOH, at a temperature range of 60-70 °C. The reaction is complete within 30-40 min with stirring under atmospheric O_2 (Lisboa, *et al*., 2011). 4-*Para* substituted anilines were selected and a general reaction scheme is shown below for their preparation (**Scheme 4.6**).

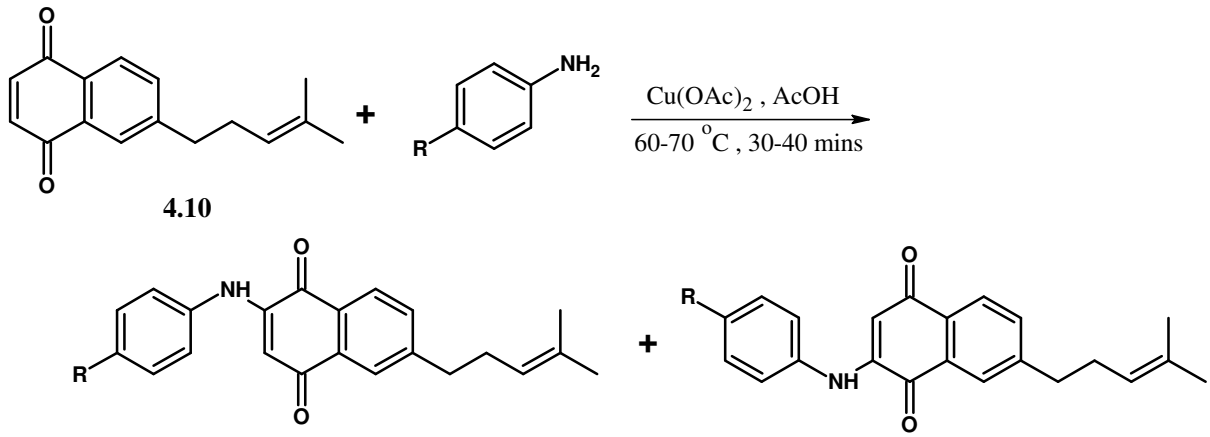

4.14 R = H
4.15 R = CH_3
4.16 R = OCH_3
4.17 R = Cl
4.18 R = CF_3

Scheme 4.6: Oxidative coupling of amines and naphthoquinones using $Cu(OAc)_2$ as a catalyst

Choice of substituents was based on electron donating and electron withdrawing properties, on the *para*-position to the amine functionality. A general reaction mechanism proposed by Lisboa, *et al*. is shown in **Scheme 4.7**, indicating the role of Cu (II) in this reaction.

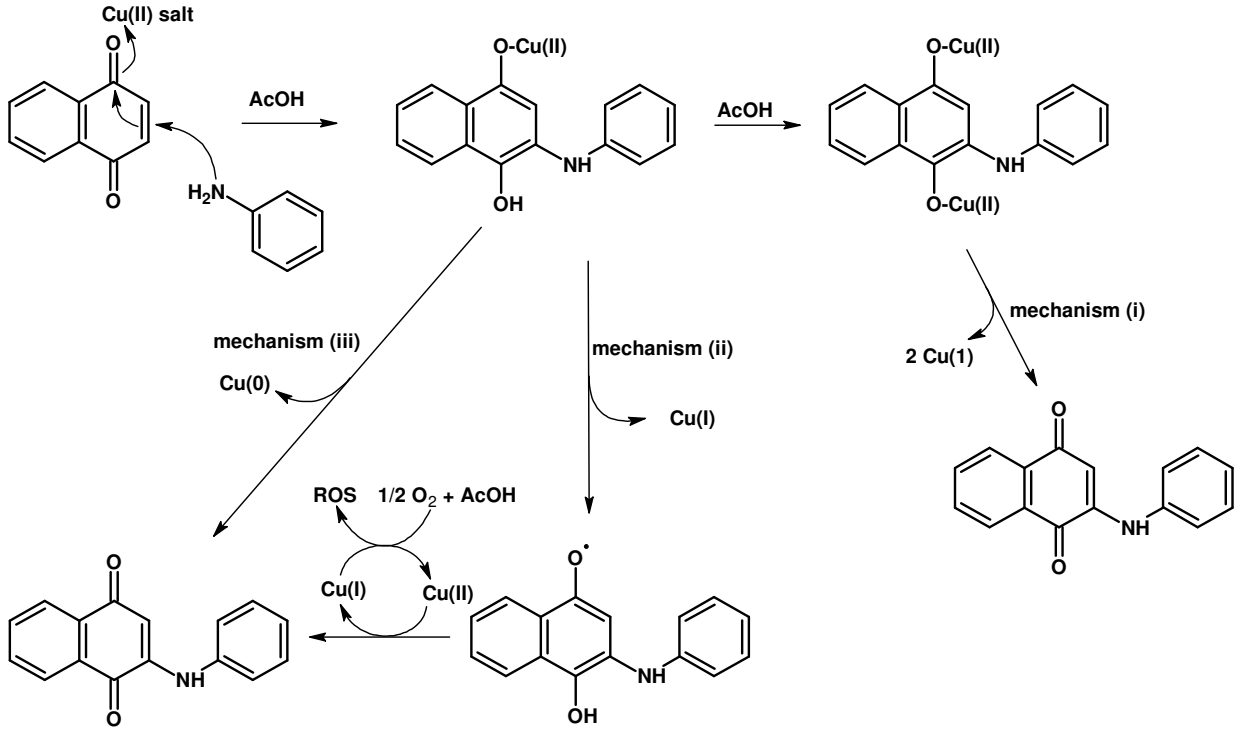

Scheme 4.7: Role of $Cu(OAc)_2$ in oxidative coupling of anilines and 1, 4-naphthoquinone (Lisboa, *et al*., 2011)

The addition-oxidation reaction to C-2 or C-3 position *via* nucleophilic attack by the amine is facilitated by formation of a complex between the quinone and Cu (II). Either one or both of the carbonyl groups can be involved in the complexation reaction, followed by direct interaction with atmospheric O_2 to yield back the quinone functionality. Conversion to the quinone can occur by a one electron oxidation step that produces Cu (I) and is oxidized back to Cu (II) by O_2, but in the process generating ROS. ROS in the presence of Cu(I) or Cu(0) and AcOH eventually take part in the regeneration of $Cu(OAc)_2$ and H_2O. Any copper salts at the end of the reaction are easily removed by solubilizing the product in CH_2Cl_2 and passing it through a plug of silica gel, eluting with CH_2Cl_2 (Lisboa, *et al*., 2011). High percentage yields have been reported by this method with the formation of fewer side products (Lisboa, *et al*., 2011)

Regioisomers were also obtained with this series of naphthoquinones due to the amination of quinones occurring either at the C-2 or C-3 position. The two isomers were separated by normal phase HPLC and calculated ratios of the isomers in the mixtures showed an approximate ratio of 1:1. As was with the case with the first series of compounds, the A isomer was eluted first, followed by the B isomer (**Table 4.4**).

Table 4.4: Percentage yields and HPLC fractions obtained

Compound	% yield	Ratio of isomers		Retention times (mins)	
		A (%)	**B (%)**	**A**	**B**
4.14	96.2	50.0	50.0	23.8	26.8
4.15	79.5	50.6	49.4	23.5	27.1
4.16	89.3	49.7	50.3	22.3	25.3
4.17	84.3	49.9	50.1	23.5	23.9
4.18	72.1	49.5	50.5	21.0	23.4
4.19	81.9	50.3	49.7	19.6	21.3

The separated isomers were characterized by 1D and 2D NMR spectroscopy. The naphthoquinone and prenyl side chain signals were clearly visible in the ^{1}H and ^{13}C NMR spectra as described above. Additional signals were noticed between δ 6.90 - δ 7.70, and between δ 120 - δ 140 in the ^{1}H and ^{13}C NMR spectra, representing the methine protons and methine carbons of the aniline moiety, respectively. **Table 4.5** and **Table 4.6** display the ^{1}H and ^{13}C NMR chemical shifts of compounds **4.14-4.19.**

The ^{1}H NMR chemical shift for H-7 and the ^{13}C NMR chemical shift for C-6 were used to distinguish between the isomers. This was consistent with the analysis conducted in literature on similar types of compounds in which C-2 substitution resulted is a less deshielded H-7 signal but with a more deshielded C-6 signal compared to C-3 substituted compounds (Miguel del Corral, *et al*., 2005).

For compounds **4.17, 4.18** and **4.19**, high resolution mass spectroscopy data was also obtained to fully ascertain the presence of the Cl, CF_3 and methylenedioxy moieties. Compounds **4.17**, **4.18** and **4.19** had adduct ions at 366.1249, 400.1592 and 376.1534, corresponding to molecular formulae of $C_{22}H_{21}NO_2Cl+H$, $C_{23}H_{21}NO_2F_3+H$ and $C_{23}H_{22}NO_4+H$, respectively for the A isomer. The relevant spectroscopic data is displayed in the supplementary section (**Figures S4.29-S4.57**)

Table 4.5: ^{1}H and ^{13}C NMR chemical shifts of compound **4.14-4.16**

	4.14A		**4.14B**		**4.15A**		**4.15B**		**4.16A**		**4.16B**	
Carbon no.	δ_H, mult, *J*(Hz)	δ_C	δ_H, mult, *J*(Hz)	δ_C	δ_H, mult, *J*(Hz)	δ_C	δ_H, mult, *J*(Hz)	δ_C	δ_H, mult, *J*(Hz)	δ_C	δ_H, mult, *J*(Hz)	δ_C
1	-	181.8	-	184.3	-	181.9	-	184.1	-	181.9	-	183.9
2	-	144.8	6.39, s	103.4	-	145.1	6.32, s	102.9	-	145.8	6.19, s	102.7
3	6.40, s	103.2	-	144.6	6.33, s	102.8	-	144.9	6.20. s	102.3	-	145.6
4	-	184.4	-	182.5	-	184.3	-	182.5	-	184.1	-	182.4
5	7.92, s	126.2	7.93, s	126.4	7.92, s	126.2	7.92, s	126.4	7.92, s	126.2	7.92, s	126.3
6	-	150.7	-	147.6	-	150.7	-	147.5	-	150.6	-	147.4
7	7.46, dd, 7.6; 1.5	132.5	7.56, dd, 7.8; 1.8	135.0	7.45, d, 7.9	132.4	7.55, d, 7.9	135.1	7.44, d, 7.8	132.3	7.55, d, 7.8	135.0
8	8.03, d, 7.6	126.8	8.01, d, 7.8	126.1	8.02, d, 7.9	126.7	8.00, d, 7.9	126.2	8.01, d, 7.8	126.7	7.99, d, 7.8	126.2
9	-	128.2	-	131.2	-	133.3	-	131.2	-	133.4	-	131.3
10	-	133.2	-	130.4	-	128.3	-	128.8	-	128.3	-	130.3
11	-	137.5	-	137.4	-	135.5	-	135.5	-	130.1	-	130.1
12	7.27, d, 7.9	122.5	7.27, d, 7.7	122.5	7.21, d, 8.2	130.2	7.21, d, 8.3	130.2	7.19, d, 8.9	124.8	7.20, d, 8.9	124.7
13	7.42, t, 7.6	129.6	7.42, t, 7.6	129.7	7.16, d, 8.2	122.7	7.16. d, 8.3	122.6	6.94, d, 8.9	114.9	6.94, d, 8.9	114.8
14	7.21, t, 7.4	125.5	7.21, t, 7.5	125.6	-	134.8	-	134.8	-	157.7	-	157.7
15	7.42, t, 7.6	129.6	7.42, t, 7.6	129.7	7.16, d, 8.2	122.7	7.16, d, 8.3	122.6	6.94, d, 8.9	114.9	6.94, d, 8.9	114.8
16	7.27, d, 7.9	122.5	7.27, d, 7.7	122.5	7.21, d, 8.2	130.2	7.21, d, 8.3	130.2	7.19, d, 8.9	124.8	7.20, d, 8.9	124.7
1'	2.76, t, 7.6	36.5	2.76, t, 7.6	36.1	2.76, t, 7.5	36.5	2.76, t, 7.6	36.0	2.76, t, 7.5	36.5	2.76, t, 7.5	36.0
2'	2.34, q, 7.6	29.3	2.35, q, 7.6	29.4	2.34, q, 7.5	29.4	2.34, q, 7.4	29.4	2.34, q, 7.6	29.4	2.35, q, 7.6	29.4
3'	5.13, t, 7.1	122.6	5.14, t, 7.1	122.6	5.13, t, 7.1	122.7	5.13, t, 7.2	122.6	5.13, t, 7.2	122.7	5.14, t, 7.1	122.7
4'	-	133.1	-	133.1	-	133.1	-	133.1	-	133.0	-	133.1
5'	1.53, s	17.7	1.54, s	17.6	1.53, s	17.7	1.53, s	17.7	1.54, s	17.6	1.54, s	17.7
6'	1.67, s	25.7	1.68. s	25.7	1.67, s	25.7	1.68, s	25.7	1.67, s	25.6	1.68, s	25.7
7'	**-**	**-**	**-**	**-**	2.36, s	21.0	2.36, s	21.0	3.83, s	55.6	3.83, s	55.6

NB. C-2 substituted naphthoquinones are presented as isomer A and C-3 substituted ones as isomer B

Table 4.6: ^{1}H and ^{13}C NMR chemical shifts of compound **4.17-4.19**

	4.17A		**4.17B**		**4.18A**		**4.18B**		**4.19A**		**4.19B**	
Carbon no.	δ_H, mult, *J*(Hz)	δ_C	δ_H, mult, *J*(Hz)	δ_C	δ_H, mult, *J*(Hz)	δ_C	δ_H, mult, *J*(Hz)	δ_C	δ_H, mult, *J*(Hz)	δ_C	δ_H, mult, *J*(Hz)	δ_C
1	-	183.2	-	184.1	-	181.4	-	184.2	-	181.8	-	184.0
2	-	144.5	6.33, s	103.7	-	143.7	6.50, s	104.9	-	133.3	6.20, s	102.7
3	6.33, s	103.5	-	144.3	6.50, s	104.7	-	143.5	6.21, s	101.7	-	131.2
4	-	184.3	-	182.1	-	184.4	-	182.0	-	184.1	-	182.3
5	7.92, s	126.2	7.92, s	126.5	7.93, s	126.3	7.94, s	126.3	7.91, d, 1.7	126.2	7.91, d, 1.7	126.3
6	-	150.9	-	147.7	-	151.0	-	148.0	-	150.6	-	148.4
7	7.47, d, 7.8	132.6	7.56, d, 7.9	135.2	7.49, d, 7.9	132.9	7.58, d, 7.9	135.4	7.45, dd, 7.8; 1.8	132.6	7.55, dd, 7.9; 1.8	135.0
8	8.03, d, 7.9	126.8	8.00, d, 7.8	126.3	8.04, d, 7.9	126.6	8.01, d, 7.9	126.4	8.01, d, 7.8	126.7	7.99, d, 7.9	126.2
9	-	133.2	-	131.0	-	133.2	-	130.8	-	131.3	-	131.3
10	-	128.2	-	130.7	-	128.1	-	130.1	-	128.7	-	130.3
11	-	130.1	-	130.1	-	140.7	-	140.7	-	148.5	-	145.5
12	7.21, d, 8.8	123.7	7.22, d, 8.7	123.7	7.38, d, 8.5	126.9	7.38, d, 8.4	126.9	6.77, d, 2.2	104.9	6.78, d, 2.2	104.8
13	7.33, d, 8.8	129.8	7.38, d, 8.7	129.8	7.67, d, 8.5	121.5	7.67, d, 8.5	121.5	-	145.6	-	147.5
14	-	136.1	-	136.1	-	141.0	-	141.0	-	145.7	-	147.7
15	7.33, d, 8.8	129.8	7.38, d, 8.7	129.8	7.67,d, 8.5	121.5	7.67, d, 8.5	121.5	6.83, d, 8.2	108.7	6.83, d, 8.2	108.6
16	7.21, d, 8.8	123.7	7.22, d, 8.7	123.7	7.38, d, 8.5	126.9	7.38, d, 8.4	126.9	6.71, dd, 8.2; 2.7	116.9	6.72, dd, 8.3; 2.1	116.1
1'	2.77, t, 7.5	36.5	2.76, t, 7.5	36.0	2.77, t, 7.5	36.5	2.77, t, 7.5	36.0	2.76, t, 7.5	36.5	2.76, t, 7.5	36.0
2'	2.35, q, 7.5	29.4	2.34, q, 7.5	29.4	2.35, q, 7.5	29.3	2.35, q, 7.5	29.4	2.34, q, 7.5	29.3	2.35, q, 7.5	29.4
3'	5.13, t, 7.2	122.6	5.13, t, 7.1	122.6	5.13, t, 7.1	122.6	5.13, t, 7.2	122.6	5.13, t, 7.2	122.7	5.13, t, 7.2	122.5
4'	-	133.0	-	133.2	-	132.8	-	133.2	-	133.1	-	133.1
5'	1.54, s	17.6	1.53, s	17.6	1.53, s	17.6	1.53, s	17.6	1.53, s	17.7	1.54, s	17.7
6'	1.67, s	25.7	1.68, s	25.7	1.67, s	25.7	1.67, s	25.7	1.67, s	25.6	1.68, s	25.6
7'	**-**	**-**	**-**	**-**	-	124.7	-	124.7	6.01, s	101.7	6.01, s	101.5

NB. C-2 substituted naphthoquinones are presented as isomer A and C-3 substituted ones as isomer B

4.2.4 Synthesis of alkylamino-naphthoquinones (third series)

The design of this series was centred on incorporating features of known Hsp90 inhibitors into the naphthoquinone scaffold. Firstly, allylamine and *N, N*-dimethylethyleneamine moieties, that are present on 17-AAG and 17-DMAG, were incorporated on the naphthoquinone scaffold to afford compounds **4.20** and **4.21** respectively. Additional functionalities were introduced to increase aqueous solubility and to allow for further manipulation of the alkyl amine side chain. Increasing reactivity by introducing epoxide functionalities (**4.25-4.26**) was also attempted and the synthesized derivatives are shown below[1].

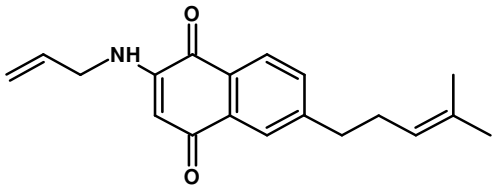

4.20

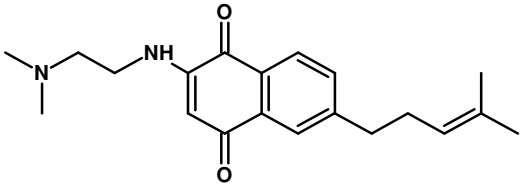

4.21

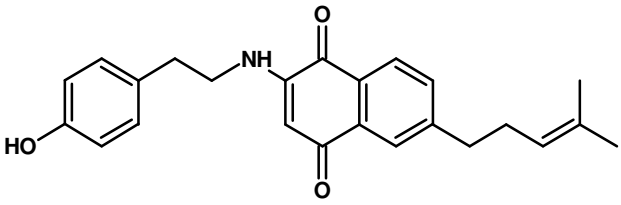

4.22

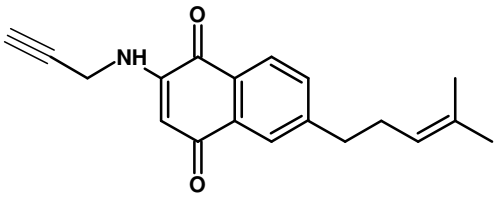

4.23

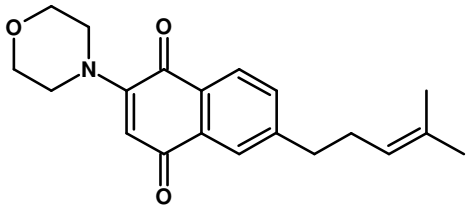

4.24

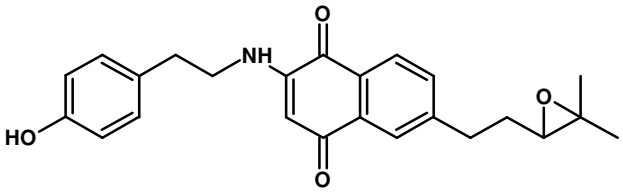

4.25

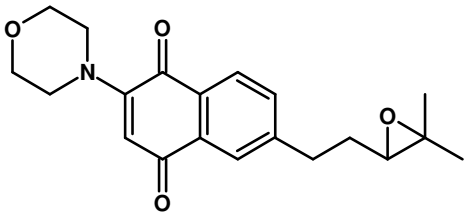

4.26

[1] NB: 2-subsituted products are shown but both 2- and 3-substituted products were isolated

Preparation of alkylamino-naphthoquinones **4.20-4.23** was conducted without the use of a catalyst. The amine and naphthoquinone were stirred in MeOH at room temperature for 48 hours under atmospheric O_2, with a simple workup protocol that involved evaporating the solvent and purifying the product by column chromatography. Published reports with regards to use of catalytic amounts of Cu(II)OAc for this reaction had shown that several side products may result in the presence of copper ions including cyclization reactions of alkylamines (Lisboa, *et al*., 2011). In order to avoid any side products forming, the catalyst was excluded with regards to alkylamines.

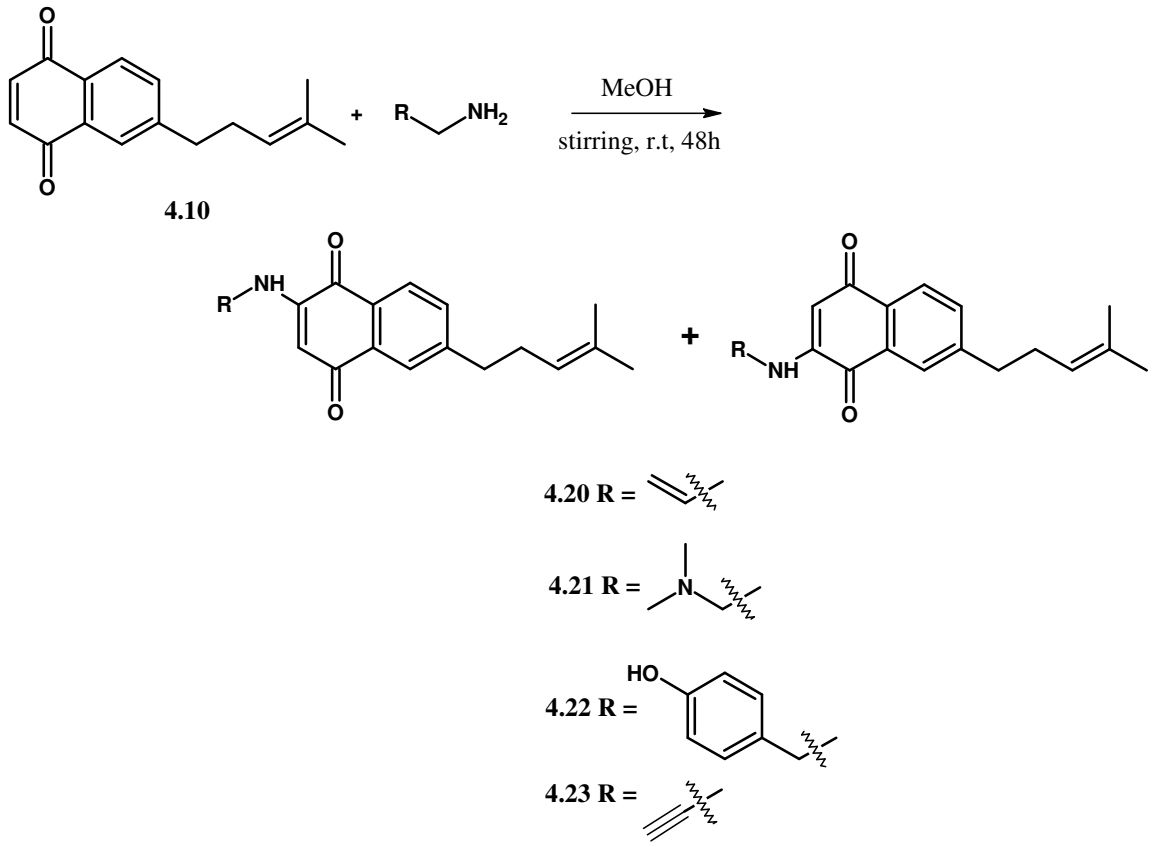

Scheme 4.8: General scheme for the preparation of alkyl amino-naphthoquinones **4.20-4.23**

The desired products were acquired in fairly good yields as indicated below (**Table 4.7**). The regioisomers were also isolated by normal phase HPLC and the calculated ratio of isomers in the mixture also indicated a 1:1 proportion of each isomer.

Table 4.7: Percentage yields and HPLC fractions obtained

Compound	% yield	Ratio of isomers		Retention times (mins)	
		A (%)	**B (%)**	**A**	**B**
4.20	71.8	50.3	49.7	24.0	27.2
4.22	71.7	49.8	50.2	19.3	21.6
4.23	73.5	50.0	50.0	25.7	28.1

Characterization of the individual isomers by 1D NMR showed the presence of the described signals for the naphthoquinone and prenyl side chain in the ^{1}H and ^{13}C NMR spectra of compounds **4.20-4.23**. Additional signals displayed belonged to the substituents attached to the C-2 or C-3 position of the quinone moiety. For compound **4.20**, of importance was a methylene triplet observed at δ 3.83 (t, *J* = 5.7 Hz, H-11) coupled to an olefinic methine at δ 5.87 (m, H-12), and two terminal methylene protons appearing as a multiplet at δ 5.28 (m, H-13) coupled to H-8' giving a -CH=CH_2 structural motif. The carbon shift values for the allylamine chain were observed at δ 44.8 (C-11), δ 131.5 (C-12) and δ 118.1 (C-13) on the ^{13}C NMR spectrum.

Compound **4.22A** had additional signals at δ 2.90 (t, *J* = 7.2 Hz, H-12) and δ 3.39 (q, *J* = 7.0 Hz, H-11) representing two mutually coupled methylene protons, and more deshielded doublets at δ 6.80 (d, *J* = 8.5 Hz, H-14) and δ 7.08 (d, *J* = 8.5 Hz, H-15) belonging to the aryl moiety. The ^{13}C NMR spectrum had two additional methylene signals displayed at δ 43.8 (C-11) and δ 33.4 (C-12), and two additional aromatic carbons at δ 115.7 (C-14, C-18) and δ 129.8 (C-15, C-17).

The substituent on compound **4.23A** was represented by a methylene singlet at δ 3.99 (s, H-11) and a methine signal overlapping with a quartet at δ 2.34 (m, H-2'). The terminal alkyne C-H signal was observed at δ 73.1 (C-13), its quaternary carbon at δ 88.0 (C-12) and the methylene carbon at δ 32.2 (C-11). The descriptions given were for the A isomers of compounds **4.20-4.23**. The other ^{1}H and ^{13}C NMR chemical shifts are presented in **Table 4.8.**

Compound **4.21** was successfully synthesized but separation of the respective isomers by the HPLC method used was unsuccessful. It showed characteristic signals at δ 3.20 (q, *J* = 5.8 Hz, H-11) and δ 2.62 (t, *J* = 5.8 Hz, H-12) representing two mutually coupled sets of methylene

protons, and two methyl groups observed as one signal at δ 2.29 (s, H-13a and H-13b). C-2 or C-3 substitution resulted in a less deshielded benzoquinone methine signal observed at δ 5.68 or δ 5.67 (s, H-2 or H-3). Additional carbons were noticed on the ^{13}C NMR spectrum at δ 39.5 (C-11), δ 56.4 (C-12) and δ 45.0 (C-13a & 13b). The ^{1}H and ^{13}C NMR spectrum for compound **4.21** are shown in the supplementary section (**Figure S4.140-S4.141**). ^{1}H and ^{13}C NMR data obtained for compounds **4.20-4.23** were as expected and matched the theoretically calculated values (**Table 4.8**)

Table 4.8: ^{1}H and ^{13}C NMR chemical shifts of compound **4.20 – 4.23**

	4.20A		**4.20B**		**4.22A**		**4.22B**		**4.23A**		**4.23B**	
Carbon no.	δ_H, mult, *J*(Hz)	δ_C	δ_H, mult, *J*(Hz)	δ_C	δ_H, mult, *J*(Hz)	δ_C	δ_H, mult, *J*(Hz)	δ_C	δ_H, mult, *J*(Hz)	δ_C	δ_H, mult, *J*(Hz)	δ_C
1	-	181.6	-	183.3	-	181.5	-	183.2	-	181.3	-	183.3
2	-	148.0	5.70, s	101.4	-	147.9	5.73, s	100.8	-	147.1	5.80, s	102.5
3	5.71, s	101.3	-	147.7	5.74, s	101.1	-	147.7	5.81, s	102.4	-	147.4
4	-	183.4	-	182.1	-	183.4	-	182.1	-	183.5	-	181.8
5	7.91, s	126.5	7.86, s	126.3	7.93, s	126.5	7.83, s	126.3	7.92, s	126.5	7.86, s	126.4
6	-	150.5	-	147.1	-	150.6	-	147.1	-	150.8	-	147.0
7	7.41, d, 7.9	132.1	7.52, d, 7.9	135.0	7.40, d. 7.8	132.1	7.52, d, 7.8	135.0	7.43, d, 7.9	132.4	7.53, d, 7.8	135.0
8	7.95, d, 7.9	126.2	7.99, d, 7.9	126.2	7.92, d, 7.8	126.2	7.99, d, 7.8	126.2	7.96, d, 7.9	126.3	8.00, d, 7.8	126.2
9	-	128.3	-	131.6	-	128.4	-	130.4	-	128.3	-	130.3
10	-	133.5	-	130.3	-	133.6	-	131.5	-	133.3	-	131.2
11	3.83, t, 5.7	44.8	3.83, t, 5.7	44.9	3.40, q, 6.9	43.7	3.39, q, 7.0	43.8	3.98, s	32.3	3.98, s	32.2
12	5.87, m	131.5	5.88, m	131.4	2.90, t, 7.2	33.7	2.90, t, 7.1	33.4	-	88.0	-	88.0
13	5.29, m	118.1	5.29, m	118.2	-	129.9	-	129.9	2.34, m	73.1	2.33, m	73.3
14	-	-	-	-	6.80, d, 8.5	116.0	6.80, d, 8.5	115.7	-	-	-	-
15	-	-	-	-	7.08, d, 8.5	129.8	7.08, d, 8.5	129.8	-	-	-	-
16	-	-	-	-	-	154.8	-	154.6	-	-	-	-
17	-	-	-	-	7.08, d, 8.5	129.8	7.08, d, 8.5	129.8	-	-	-	-
18	-	-	-	-	6.80, d, 8.5	116.0	6.80, d, 8.5	115.7	-	-	-	-
1'	2.76, t, 7.6	36.4	2.73, t, 7.5	35.9	2.74, t, 7.5	36.5	2.72, t, 7.5	35.9	2.75, t, 7.6	36.4	2.74, t, 7.5	35.9
2'	2.33, q, 7.7	29.3	2.32, q, 7.6	29.4	2.33, q, 7.5	29.7	2.32, q, 7.5	29.4	2.34. m	29.3	2.33, m	29.4
3'	5.12, t, 7.2	122.7	5.12, t, 7.2	122.7	5.12, t, 7.2	122.9	5.12, t, 7.1	122.7	5.12, t, 7.1	122.7	5.12, t, 7.1	122.7
4'	-	133.0	-	133.0	-	133.0	-	133.0	-	133.0	-	133.1
5'	1.53, s	17.6	1.52, s	17.7	1.53, s	17.9	1.52, s	17.6	1.53, s	17.7	1.52, s	17.7
6'	1.66, s	25.6	1.67, s	25.6	1.67, s	25.7	1.67, s	25.6	1.67, s	25.6	1.67, s	25.6

NB. C-2 substituted naphthoquinones are presented as isomer A and C-3 substituted ones as isomer B

Solubility is an important aspect to consider when designing new therapeutic agents. Most of the naphthoquinone analogues considered here appear to be significantly lipophilic which could potentially impact on their activity. The next set of molecules was synthesized to improve water solubility of naphthoquinones (**4.24-4.26**). A morpholino functionality was coupled to naphthoquinone **4.10** as indicated in **Scheme 4.9**.

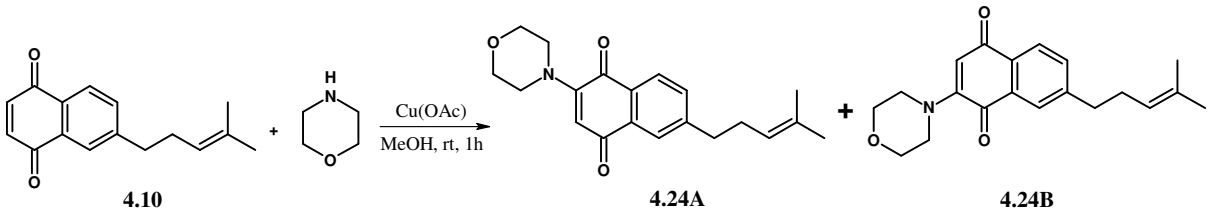

4.10 **4.24A** **4.24B**

Scheme 4.9: Reaction scheme for the preparation of compound **4.24**

For this reaction, $Cu(OAc)_2$ catalyst was used to facilitate the reaction. Naphthoquinone **4.10** was reacted with morpholine in the presence of $Cu(OAc)_2$ at room temperature under atmospheric O_2 to give the morpholine-coupled naphthoquinone **4.24.** The product obtained contained the usual regioisomers of the morpholine added to either the C-2 or C-3 position of the naphthoquinone. The important signals to consider in the ^1H NMR spectra of **4.24** were two sets of methylene protons coupled to each other at δ 3.49 (t, *J* = 4.9 Hz, H-11 and H-14) and δ 3.86 (t, *J* = 4.9 Hz, H-12 and H-13) for isomer **4.24A** and at δ 3.48 (t, *J* = 4.9 Hz, H-11 and H-14) and δ 3.86 (t, *J* = 4.9 Hz, H-12 and H-13) for isomer **4.24B,** indicative of the morpholino moiety. The ^{13}C NMR spectrum showed additional signals at δ 49.2 (C-11, C-14) and δ 66.4 (C-12, C-13) belonging to the morpholino group. Identification of the isomers was also done by analysing H-7 and C-6, ^1H and ^{13}C NMR chemical shifts (**Table 4.10**). HRMS obtained for both isomers of **4.24** showed an adduct ion at 326.1746, consistent with the molecular formula of $C_{20}H_{24}NO_3$+H

Attempts to functionalize the terminal alkene on naphthoquinone **4.10** were conducted, initially by converting the alkene to an epoxide with the use of m-chloroperoxybenzoic acid (mCPBA). in the presence of $NaHCO_3$ in CH_2Cl_2. Stirring was done at room temperature for an hour before quenching the reaction with $Na_2S_2O_3$ (**Scheme 4.10**)

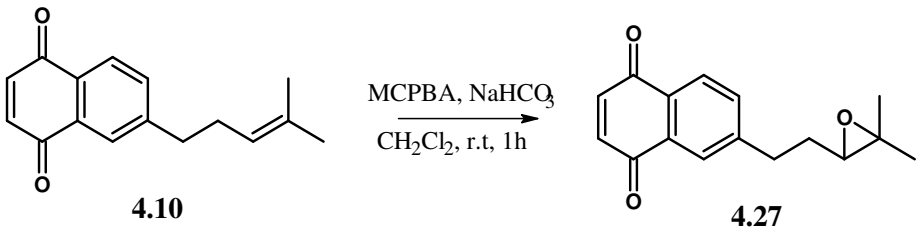

Scheme 4.10: Epoxidation of **4.10**

Compound **4.27** was anticipated to provide an entry to a new series of β amino alcohols (**Scheme 4.11**). Reactions with tyramine and morpholine were attempted by stirring the epoxide **4.27** with the amine at room temperature for 18 hours in a mixture of EtOH and H_2O. Two possible reactions were likely to occur due to the presence of two nucleophilic centres on compound **4.27**. Coupling to the quinone moiety was favoured, probably because of steric hindrance at the epoxide region caused by the two methyl groups.

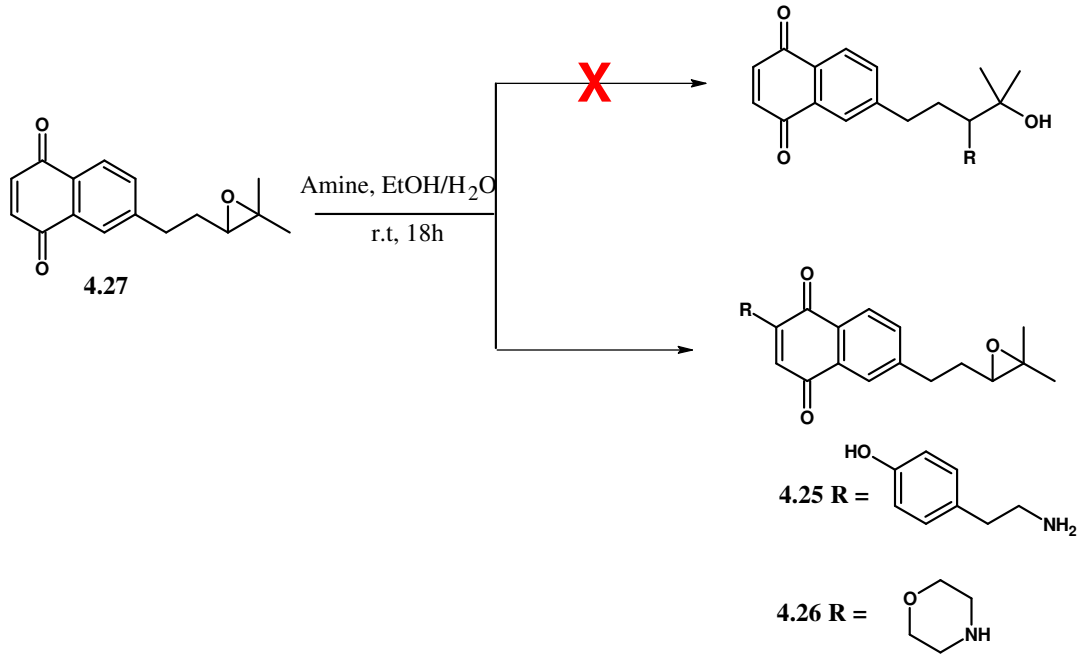

Scheme 4.11: Reaction of amines with naphthoquinone epoxide **4.27**

For the reaction with tyramine, the ^{1}H NMR data obtained showed changes in the region between δ 0.5 – δ 3.5 compared to compound **4.22.** Multiplet signals were observed at δ 1.89 and δ 2.89 corresponding to H-2' and H-1' respectively, and a triplet at δ 2.75 (t, J = 6.3 Hz) belonging to H-3' confirmed by integral values relative to the benzoquinone methine signal. The methyl signals were less deshielded and were noted at δ 1.16 (s, H-5') and δ 1.27 (s, H-6'). From the ^{13}C NMR spectra, C-3' and C-4' were observed at δ 63.5 and δ 58.6 respectively, indicative of an epoxide moiety and absence of an alkene functionality (**Table 4.10**). Further

evidence was acquired *via* mass spectrometry, with the adduct ion noted at 392.1850 corresponding to a molecular formula $C_{24}H_{26}NO_4$+H of compound **4.25.**

For compound **4.26**, the multiplet signals were noticed at δ 1.90 (m, H-1') and δ 2.90 (m, H-2'), and two less deshielded terminal methyl groups at δ 1.17 (s, H-5') and 1.28 (s, H-6'). The ^{13}C NMR spectrum showed a new set of signals at δ 63.6 (C-3') and δ 58.6 (C-4') indicative of an epoxide. Further confirmation of the chemical structure was ascertained by acquiring HRMS data that showed an adduct ion at 342.1697 corresponding to a molecular formula of $C_{20}H_{24}NO_4$+H, compound **4.26.** Identification of isomers was also based on similar trends observed in ^{1}H and ^{13}C NMR spectra for H-7 and C-6 chemical shifts, respectively (**Table 4.10**).

Percentage yields and calculated ratios for the isomers in the mixture after separation by HPLC are shown below in **Table 4.9.** The regioisomers existed in approximately 1:1 ratio.

Table 4.9: Percentage yields and HPLC fractions obtained

Compound	% yield	Ratio of isomers		Retention times (mins)	
		A (%)	**B (%)**	**A**	**B**
4.24	80.4	50.0	50.0	35.4	38.1
4.25	59.8	50.2	49.8	21.5	14.9
4.26	55.7	50.0	50.0	22.0	21.1

Table 4.10: ^{1}H and ^{13}C NMR chemical shifts of compound **4.24 – 4.26**

	4.24A		**4.24B**		**4.25A**		**4.25B**		**4.26A**		**4.26B**	
Carbon no.	δ_H, mult, *J*(Hz)	δ_C	δ_H, mult, *J*(Hz)	δ_C	δ_H, mult, *J*(Hz)	δ_C	δ_H, mult, *J*(Hz)	δ_C	δ_H, mult, *J*(Hz)	δ_C	δ_H, mult, *J*(Hz)	δ_C
1	-	182.7	-	183.9	-	181.4	-	183.0	-	182.6	-	183.7
2	-	153.9	5.98, s	112.2	-	148.0	5.74, s	101.0	-	153.7	5.99, s	112.2
3	5.98, s	111.9	-	153.7	5.74, s	100.7	-	147.7	5.99. s	111.9	-	153.7
4	-	184.1	-	183.2	-	183.2	-	182.0	-	183.9	-	183.0
5	7.85, s	125.5	7.81, s	126.6	7.94, s	126.1	7.86, s	126.0	7.88, s	125.4	7.84, s	126.7
6	-	149.6	-	147.9	-	149.5	-	146.2	-	148.5	-	147.2
7	7.45, d, 7.9	132.8	7.50, d, 7.8	134.2	7.44, d, 7.8	132.2	7.56, d, 7.8	135.0	7.48, d, 7.9	132.9	7.54, d, 7.9	134.3
8	7.90, d, 7.9	127.0	7.94, d, 7.8	125.8	7.95, d, 7.8	126.8	8.02, d, 7.8	126.5	7.94, d, 7.9	127.3	7.97, d, 7.9	126.0
9	-	130.7	-	130.3	-	128.7	-	130.5	-	130.9	-	130.5
10	-	132.2	-	132.6	-	130.5	-	131.8	-	132.4	-	132.8
11	3.49, t, 4.9	49.2	3.48, t, 4.9	49.2	3.38, q, (t), 6.8	43.8	3.39, q (t), 6.8	43.9	3.50, t, 4.8	49.2	3.48, t, 4.7	49.3
12	3.86, t, 4.9	66.4	3.86, t, 4.9	66.4	2.88, t, 7.1	33.4	2.90, t, 7.1	35.5	3.86, t, 4.8	66.5	3.86, t, 4.7	66.6
13	3.86. t, 4.9	66.4	3.86, t, 4.9	66.4	-	129.6	-	129.9	3.86, t, 4.8	66.5	3.86, t, 4.7	66.6
14	3.49, t, 4.9	49.2	3.48, t, 4.9	49.2	6.81, d, 8.4	115.8	6.80, d, 8.4	115.7	3.50, t, 4.8	49.2	3.48, t, 4.7	49.3
15	-	-	-	-	7.07, d, 8.4	129.7	7.08, d, 8.4	129.8	-	-	-	-
16	-	-	-	-	-	154.8	-	154.6	-	-	-	-
17	-	-	-	-	7.07, d, 8.4	129.7	7.08, d, 8.4	129.8	-	-	-	-
18	-	-	-	-	6.81, d, 8.4	115.8	6.80, d, 8.4	115.7	-	-	-	-
1'	2.74, t, 7.5	36.3	2.74, t, 7.6	36.1	2.88, m	32.7	2.89, m	32.7	2.90, m	33.0	2.89, m	32.9
2'	2.33, q, 7.4	29.3	2.33, t, 7.5	29.4	1.89, m	30.1	1.89, m	30.2	1.90, m	30.2	1.90, m	30.3
3'	5.12, t, 7.2	122.3	5.13, t, 7.2	122.7	2.76, t, 6.2	63.5	2.75, t, 6.3	63.5	2.75, t, 6.2	63.7	2.75, t, 6.2	63.6
4'	-	133.0	-	133.0	-	58.7	-	58.6	-	58.6	-	58.6
5'	1.53, s	17.8	1.53, s	17.7	1.16, s	18.6	1.16, s	18.6	1.16, s	18.8	1.17, s	19.1
6'	1.67 s	25.7	1.67, s	25.7	1.28, s	24.7	1.27, s	24.7	1.28, s	24.7	1.29, s	24.6

NB. C-2 substituted naphthoquinones are presented as isomer A and C-3 substituted one as isomer B

4.2.5 Tricyclic naphthoquinones (fourth series)

Tricyclic naphthoquinones constituted the last series of our compounds. Thiazino-naphthoquinone (**4.28**) and a chromene-naphthoquinone hybrid (**4.29**) molecules were synthesized to assess the influence of the thiazino and pyran moieties respectively on cytotoxicity and Hsp90 inhibition. It was anticipated that compound **4.29** would mimic novobiocin binding to the ATP binding site of Hsp90.

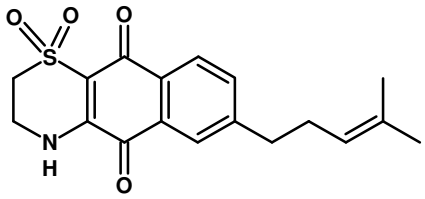

4.28

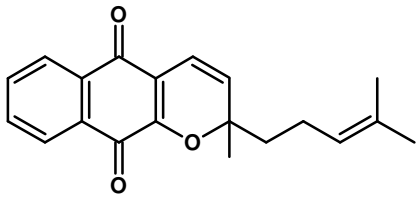

4.29

Synthesis and characterization of compound 4.28

The synthesis of compound **4.28** was carried out by reacting naphthoquinone **4.10** with hypotaurine in a mixture of solvents, (CH_3CN: EtOH: H_2O, 5:5:1) at 70 °C for 2.5 hours (**Scheme 4.12**). Two isomers **4.28A** and **4.28B** were formed but **4.28A** was obtained in greater yield (9:1) and purified by column chromatography. Only NMR data for **4.28A** is presented.

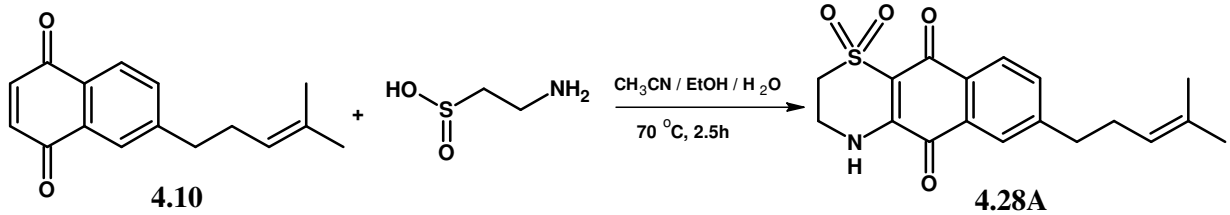

4.10

4.28A

4.28B

Scheme 4.12: Preparation of compound **4.28** from compound **4.10**

In the ^1H NMR spectrum of **4.28**, the important features to note were the disappearance of the benzoquinone methine signal and the appearance of two sets of methylene signals at δ 3.36 (m, H-11) and δ 4.13 (m, H-12). The ^{13}C NMR spectrum indicated two additional methylene signals at δ 49.1 and δ 39.9 and the product was determined to be compound **4.28** (**Table 4.11**)

The correct orientation of the thiazine moiety fused to the naphthoquinone was assigned based on comparison to data published for this compound by Aiello and colleagues (2003).

Table 4.11: ^{1}H and ^{13}C NMR chemical shifts for **4.28**

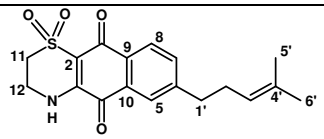

Carbon no.	δ_H, mult, *J*(Hz)	δ_C
1	-	178.6
2	-	113.3
3	-	145.4
4	-	175.7
5	8.01, s	127.2
6	-	152.7
7	7.47, d, 7.8	133.4
8	7.96, d, 7.8	127.1
9	-	127.2
10	-	132.6
11	3.36, m	49.1
12	4.13, m	39.9
1'	2.77, t, 7.5	36.6
2'	2.33, q, 7.3	29.2
3'	5.09, t, 7.1	122.3
4'	-	133.3
5'	1.51, s	17.6
6'	1.66, s	25.7

.

Synthesis and characterization of compound 4.29

Compound **4.29** was synthesized to integrate the naphthoquinone and chromene moieties in one molecule and determine whether a synergistic effect may arise from such a combination. This type of system is present in sargachromenol (**3.3**) that showed the most cytotoxic activity amongst the meroterpenoids isolated from *S. incisifolium*. Compound **4.29** was prepared from a mixture of reagents that included 2 hydroxynaphthoquinone, citral, β-alanine and AcOH, dissolved in C_6H_6 and refluxed for 3 hours at 80- 85 °C (**Scheme 4.13**).

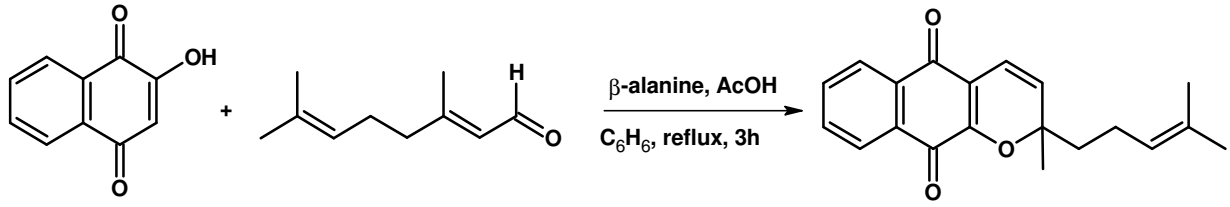

4.29

Scheme 4.13: Reaction scheme demonstrating the synthesis of chromene-naphthoquinone hybrid (**4.29**)

The ^{1}H NMR spectrum (**Figure 4.8**) for compound **4.29** was characterized by four aromatic protons observed at δ 8.06 (dd, *J* = 7.5; *J* = 1.4 Hz, H-11, H-14) and δ 7.67 (m, H-12, H-13) belonging to the benzenoid ring, two methine doublets at δ 5.65 (d, *J* = 10.1 Hz, H-7) and δ 6.68 (d, *J* = 10.1 Hz, H-8) of the pyran moiety, with no benzoquinone methine H-2 or H-3 signal indicating three fused rings. The presence of the two carbonyl groups of the quinone could only be verified on the ^{13}C NMR spectrum (**Figure 4.9**) and appeared at δ 181.8 and δ 179.6 for C-1 and C-4 respectively. The prenyl side chain system had a different signal pattern comprising of multiplet signals at δ 1.93 (m, H-1') and δ 2.11 (m, H-2'), and a less deshielded H-3' proton at 5.03 (t, *J* = 7.1 Hz). Three sets of methyl signals were noticed at δ 1.53 (s, H-5'), δ 1.60 (s, H-6') and δ 1.50 (s, H-7'). The position of the methyl group displayed at δ 1.50 (s, H-7') could be verified by HMBC correlations to H-1'. HMBC correlations of C-6 relative to H-7, H-8 and H-1', H-2' indicated it to be a non-aromatic carbon and had a chemical shift of δ 83.1. All other chemical shifts are presented in **Table 4.12.**

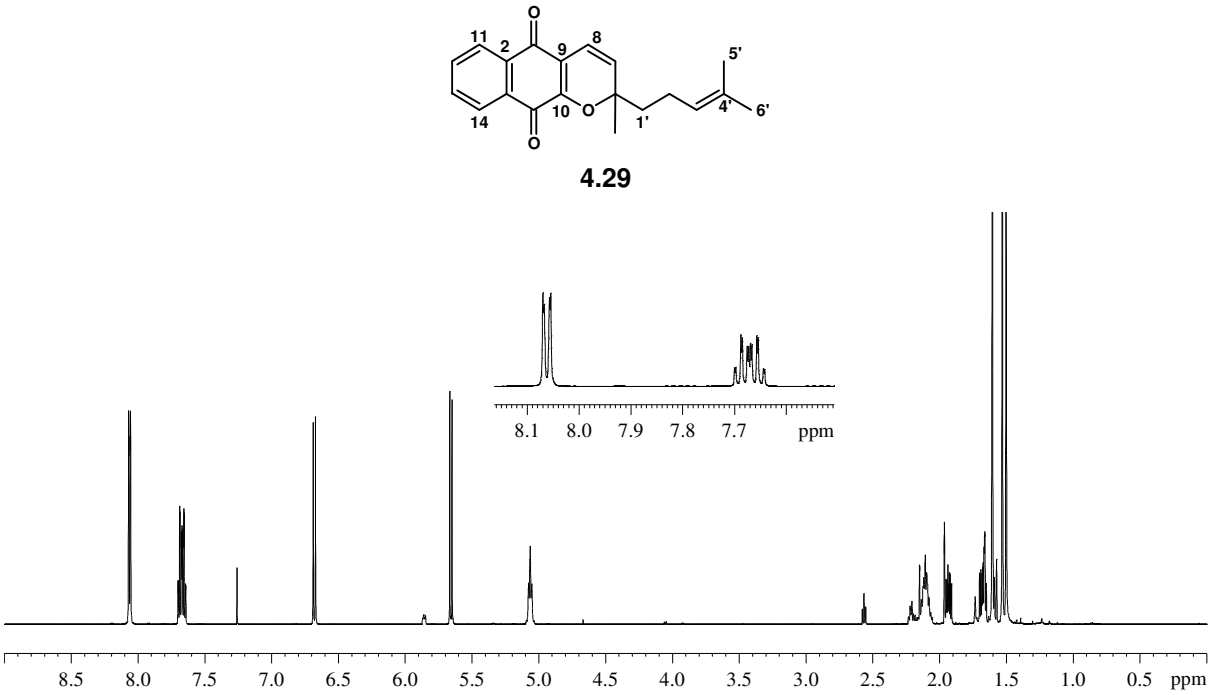

4.29

Figure 4.8: ^{1}H NMR spectrum (600 MHz, $CDCl_3$) of compound **4.29**

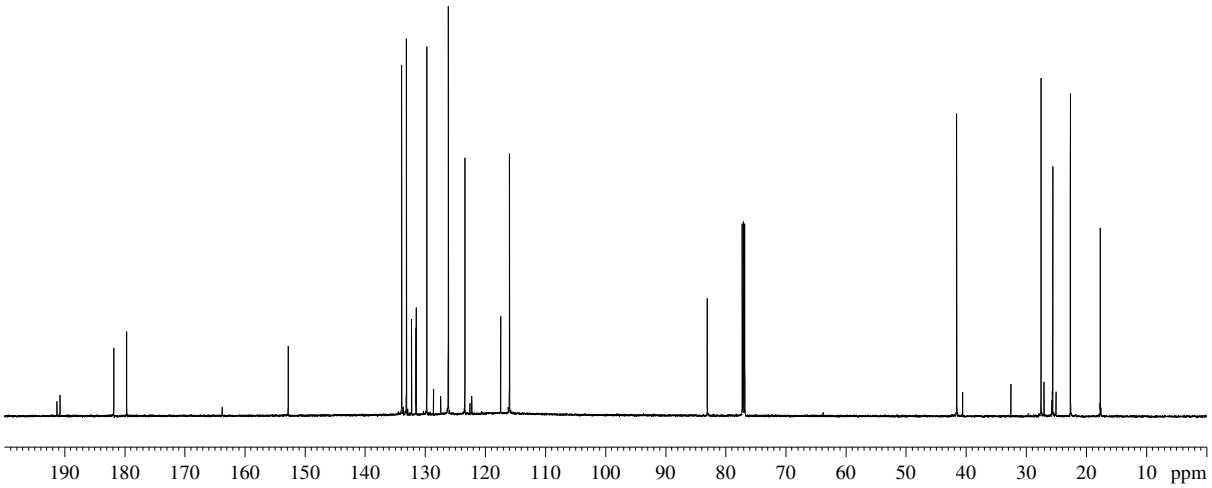

Figure 4.9: ^{13}C NMR spectrum (150 MHz, $CDCl_3$) of compound **4.29**

Table 4.12: ^{1}H and ^{13}C NMR chemical shifts of compound **4.29**

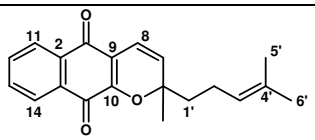

Carbon no.	δ_H, mult, *J*(Hz)	δ_C
1	-	181.8
2	-	131.5
3	-	131.5
4	-	179.6
5	-	-
6	-	83.1
7	5.69, d, 10.1	129.7
8	6.68, d, 10.1	116.0
9	-	117.4
10	-	152.7
11	8.06, dd, 7.5; 1.4	126.1
12	7.67, m	133.9
13	7.67, m	133.1
14	8.06, dd, 7.5; 1.4	126.1
1'	1.93, m	41.2
2'	2.11, m	22.6
3'	5.03, t, 7.1	123.5
4'	-	132.2
5'	1.53, s	17.7
6'	1.60, s	25.8
7'	1.50, s	27.6

4.3 Conclusion

A series of naphthoquinone derivatives were successfully synthesized as a starting point for the design of cytotoxic Hsp90 protein inhibitors. This set of molecules present a new class of compounds that could be used to assess Hsp90 protein binding. Cytotoxicity of the synthesized molecules was determined, together with isolated metabolites discussed in chapter three. Hsp90 inhibition assays were then conducted and the results compared to establish if correlations exist between cytotoxicity and Hsp90 inhibition. The details of these assays are presented in the next chapter.

4.4 EXPERIMENTAL

General experimental:

See chapter three, section 3.4.1

4.4.1 Synthesis of first series of naphthoquinone derivatives

Preparation of naphthoquinone scaffold

REPRESENTATIVE PROCEDURE

*Preparation of 6-(4-methylpent-3-en-1-yl) naphthalene-1, 4-dione (**4.10**)*

A mixture of myrcene (0.500 g; 3.6 mmoles) and benzoquinone (0.190 g; 1.8 mmoles) dissolved in absolute EtOH (10 ml) was placed in a 100 ml round bottomed flask and refluxed for 5 hours at 70 – 80 °C. The reaction mixture was allowed to cool to room temperature before concentrating under vacuum on a rotavap to yield 0.515 g of crude Diels-Alder product (**4.32**) (58.5 % yield).

The crude mixture was used without further purification. It was dissolved in C_6H_6 in a 100 ml round bottomed flask and MnO_2 (1.070 g, 12.3 mmoles) added with stirring. The mixture was heated to 80 – 85 °C and kept under reflux for 4 hours. After cooling to room temperature, the reaction mixture was filtered through celite x 2 and the solvent removed under reduced pressure to yield 0.3157 of crude product **4.10.** The crude product (0.158 g) was purified by column chromatography eluting with Hex/EtOAc 9:1 to produce pure naphthoquinone **4.10** (0.462 g, 96.2 % yield).

The same method was used for the preparation of **4.11-4.13** from the respective benzoquinone derivatives with myrcene. See the supplementary data for details (**Table S1-S2**).

Compound **4.10**

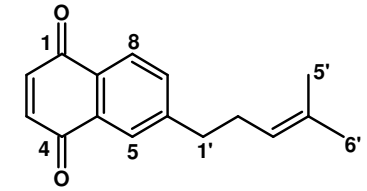

^{1}H NMR ($CDCl_3$): δ 6.93 (s, H-2; H-3), 7.88 (s, H-5), 7.55 (dd, 7.8 Hz; 1.6 Hz, H-7), 7.98 (d, 7.8 Hz, H-8), 2.76 (t, 7.8 Hz, H-1'), 2.34 (q, 7.5 Hz, H-2'), 5.11 (t, 7.1 Hz, H-3'), 1.54 (s, H-5'), 1.66 (s, H-6'). ^{13}C NMR ($CDCl_3$): δ 184.9 (C-1), 138.5 (C-2), 138.7 (C-3), 185.4 (C-4), 126.5 (C-5), 149.4 (C-6), 134.1 (C-7), 126.2 (C-8), 129.9 (C-9), 133.1 (C-10), 36.2 (C-1'), 29.3 (C-2'), 122.5 (C-3'), 131.8 (C-4'), 17.6 (C-5'), 25.6 (C-6') (Miguel del Corral, *et al*., 2002).

Compound **4.11A**

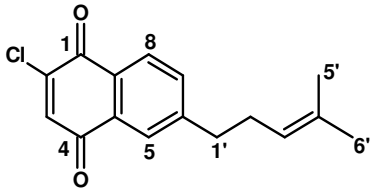

^{1}H NMR ($CDCl_3$): δ 7.19 (s, H-3), 7.89 (s, H-5), 7.56 (d, 7.9 Hz, H-7), 8.07 (d, 7.8 Hz, H-8), 2.78 (t, 7.7 Hz, H-1'), 2.34 (q, 7.6 Hz, H-2'), 5.11 (t, 7.1 Hz, H-3'), 1.52 (s, H-5'), 1.66 (s, H-6'). ^{13}C NMR ($CDCl_3$): δ 177.8 (C-1), 146.4 (C-2), 135.7 (C-3), 183.0 (C-4), 126.6 (C-5), 150.2 (C-6), 134.3 (C-7), 127.7 (C-8), 129.2 (C-9), 133.3 (C-10), 36.2 (C-1'), 29.2 (C-2'), 122.4 (C-3'), 131.7 (C-4'), 17.6 (C-5'), 25.6 (C-6') (Miguel del Corral, *et al.,* 2006)**.**

Compound **4.11B**

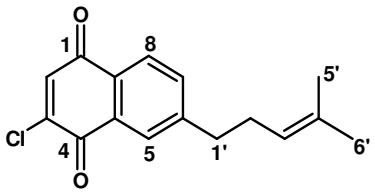

^{1}H NMR ($CDCl_3$): δ 7.18 (s, H-2), 7.97 (s, H-5), 7.57 (d, 7.7 Hz, H-7), 7.99 (d, 7.7 Hz, H-8), 2.78 (t, 7.7 Hz, H-1'), 2.34 (q, 7.4 Hz, H-2'), 5.11 (t, 7.0 Hz, H-3'), 1.52 (s, H-5'), 1.67 (s, H-6'). ^{13}C NMR ($CDCl_3$): δ 182.6 (C-1), 135.9 (C-2), 146.1 (C-3), 178.3 (C-4), 127.4 (C-5), 149.8 (C-6), 134.7 (C-7), 126.8 (C-8), 129.7 (C-9), 133.3 (C-10), 36.1 (C-1'), 29.2 (C-2'), 122.4 (C-3'), 131.2 (C-4'), 17.7 (C-5'), 25.6 (C-6') (Miguel del Corral, *et al.,* 2006)**.**

Compound **4.12A**

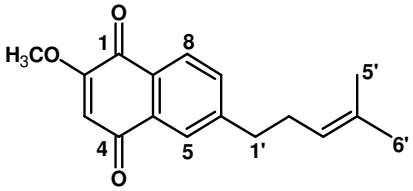

^{1}H NMR ($CDCl_3$): δ 6.14 (s, H-3), 7.89 (s, H-5), 7.51 (d, 7.8 Hz, H-7), 8.03 (d, 7.8 Hz, H-8), 3.89 (s, H-11), 2.76 (t, 7.6 Hz, H-1'), 2.34 (q, 7.4 Hz, H-2'), 5.12 (t, 7.1 Hz, H-3'), 1.53 (s, H-5'), 1.67 (s, H-6'). ^{13}C NMR ($CDCl_3$): δ 180.2 (C-1), 155.3 (C-2), 113.4 (C-3), 183.1 (C-4), 127.1 (C-5), 149.5 (C-6), 136.6 (C-7), 126.7 (C-8), 131.5 (C-9), 133.8 (C-10), 58.8 (C-11), 36.3 (C-1'), 29.4 (C-2'), 122.5 (C-3'), 132.0 (C-4'), 17.6 (C-5'), 25.6 (C-6') (Miguel del Corral, *et al*., 1998).

Compound **4.12B**

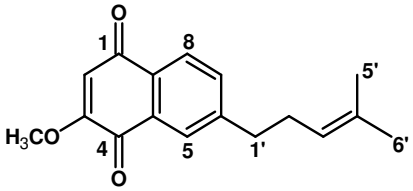

^{1}H NMR ($CDCl_3$): δ 6.13 (s, H-2), 7.93 (s, H-5), 7.53 (d, 7.9 Hz, H-7), 7.98 (d, 7.9 Hz, H-8), 3.89 (s, H-11), 2.75 (t, 7.6 Hz, H-1'), 2.34 (q, 7.6 Hz, H-2'), 5.12 (t, 7.2 Hz, H-3'), 1.52 (s, H-5'), 1.66 (s, H-6'). ^{13}C NMR ($CDCl_3$): δ 182.9 (C-1), 113.2 (C-2), 155.6 (C-3), 181.1 (C-4), 127.9 (C-5), 149.5 (C-6), 135.8 (C-7), 126.8 (C-8), 131.7 (C-9), 132.0 (C-10), 58.9 (C-11), 36.2 (C-1'), 29.5 (C-2'), 122.6 (C-3'), 131.9 (C-4'), 17.7 (C-5'), 25.6 (C-6') (Miguel del Corral, *et al*., 1998).

Compound **4.13A**

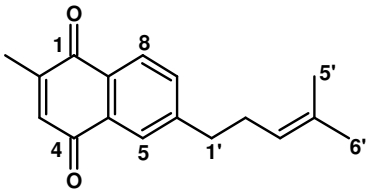

^{1}H NMR ($CDCl_3$): δ 6.80 (s, H-3), 7.86 (s, H-5), 7.52 (dd, 7.9 Hz; 1.7 Hz, H-7), 8.00 (d, 7.9 Hz, H-8), 2.18 (s, H-11), 2.75 (t, 7.5 Hz, H-1'), 2.34 (q, 7.2 Hz, H-2'), 5.12 (t, 7.1 Hz, H-3'), 1.52 (s, H-5'), 1.66 (s, H-6'). ^{13}C NMR ($CDCl_3$): δ 185.5 (C-1), 148.2 (C-2), 133.8 (C-3), 185.6 (C-4), 126.7 (C-5), 149.2 (C-6), 135.5 (C-7), 125.9 (C-8), 130.1 (C-9), 133.1 (C-10), 16.5 (C-

11), 36.2 (C-1'), 29.3 (C-2'), 122.6 (C-3'), 132.2 (C-4'), 17.7 (C-5'), 25.6 (C-6') (Miguel del Corral, *et al*., 1998).

Compound **4.13B**

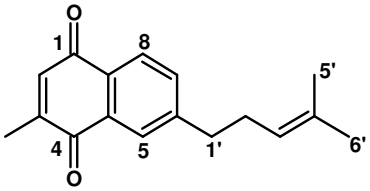

^{1}H NMR ($CDCl_3$): δ 6.80 (s, H-2), 7.90 (s, H-5), 7.52 (dd, 7.8 Hz; 1.65 Hz, H-7), 7.95 (d, 7.8 Hz, H-8), 2.18 (s, H-11), 2.76 (t, 7.6 Hz, H-1'), 2.33 (q, 7.2 Hz, H-2'), 5.12 (t, 7.3 Hz, H-3'), 1.52 (s, H-5'), 1.66 (s, H-6').^{13}C NMR ($CDCl_3$): δ 185.9 (C-1), 133.9 (C-2), 147.9 (C-3), 185.0 (C-4), 126.4 (C-5), 149.0 (C-6), 135.7 (C-7), 126.2 (C-8), 130.2 (C-9), 133.1 (C-10), 16.5 (C-11), 36.2 (C-1'), 29.4 (C-2'), 122.6 (C-3'), 132.0 (C-4'), 17.7 (C-5'), 25.7 (C-6') (Miguel del Corral, *et al*., 1998).

4.4.2 Synthesis of second series of naphthoquinone derivatives

REPRESENTATIVE PROCEDURE

6-(4-methylpent-3-en-1-yl)-2-(phenylamino) naphthalene-1, 4-dione (4.14)

Naphthoquinone (**4.10**) (0.118 g, 0.4 mmoles), H_2O (1 drop) and $Cu(OAc)_2$ (0.008 g, 0.049 mmoles) were dissolved in AcOH (5 ml) in a glass vial. Dissolution was facilitated by warming the mixture on a hot oil bath, after which aniline (0.046 g, 0.4 mmoles) was added and the reaction mixture heated between 60-70 °C for 30 mins under atmospheric O_2. After cooling the reaction mixture to room temperature, the solvent was evaporated, followed by reconstitution of the remaining residue in CH_2Cl_2 (15 ml). The collected CH_2Cl_2 sample was passed through a plug of silica gel (7 g), eluting with approximately 40 ml of CH_2Cl_2 and the solvent evaporated again under reduced pressure on the rotary evaporator to give 0.127 g of a deep red crude product (**4.14**) (96.2 % yield). The same method was used for the preparation of **4.14-4.19** from compound **4.10** and the respective anilines. See the supplementary data for details (**Table S4.3**).

Compound **4.14A**

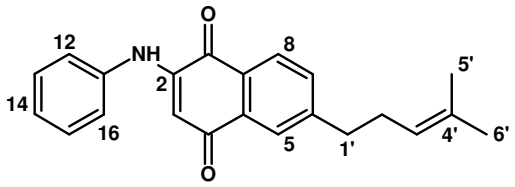

^{1}H NMR ($CDCl_3$): δ 6.40 (s, H-3), 7.92 (s, H-5), 7.46 (dd, 7.6 Hz; 1.5 Hz, H-7), 8.03 (d, 7.6 Hz, H-8), 7.27 (d, 7.9 Hz, H-12), 7.42 (t, 7.6 Hz, H-13), 7.21 (t, 7.4 Hz, H-14), 7.42 (t, 7.6 Hz, H-15), 7.27 (d, 7.9 Hz, H-16), 2.76 (t, 7.6 Hz, H-1'), 2.34 (q, 7.6 Hz, H-2'), 5.13 (t, 7.1 Hz, H-3'), 1.53 (s, H-5'), 1.67 (s, H-6'). ^{13}C NMR ($CDCl_3$): δ 181.8 (C-1), 144.8 (C-2), 103.2 (C-3), 184.4 (C-4), 126.2 (C-5), 150.7 (C-6), 132.5 (C-7), 126.8 (C-8), 128.2 (C-9), 133.2 (C-10), 137.5 (C-11), 122.5 (C-12), 129.6 (C-13), 125.5 (C-14), 129.6 (C-15), 122.5 (C-16), 36.5 (C-1'), 29.3 (C-2'), 122.6 (C-3'), 133.1 (C-4'), 17.7 (C-5'), 25.7 (C-6') (Miguel del Corral, *et al.,* 2005)**.**

Compound **4.14B**

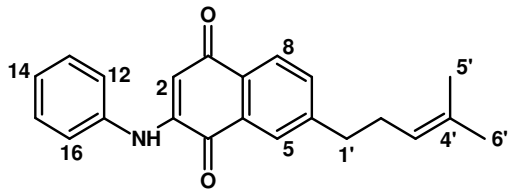

^{1}H NMR ($CDCl_3$): δ 6.39 (s, H-2), 7.93 (s, H-5), 7.56 (dd, 7.9 Hz; 1.8 Hz, H-7), 8.01 (d, 7.8 Hz, H-8), 7.27 (d, 7.7 Hz, H-12), 7.42 (t, 7.6 Hz, H-13), 7.21 (t, 7.5 Hz, H-14), 7.42 (t, 7.6 Hz, H-15), 7.27 (d, 7.7 Hz, H-16), 2.76 (t, 7.6 Hz, H-1'), 2.35 (q, 7.6 Hz, H-2'), 5.14 (t, 7.1 Hz, H-3'), 1.54 (s, H-5'), 1.68 (s, H-6'). ^{13}C NMR ($CDCl_3$): δ 184.3 (C-1), 103.4 (C-2), 144.6 (C-3), 182.5 (C-4), 126.4 (C-5), 147.6 (C-6), 135.0 (C-7), 126.1 (C-8), 131.2 (C-9), 130.4 (C-10), 137.4 (C-11), 122.5 (C-12), 129.7 (C-13), 125.6 (C-14), 129.7 (C-15), 122.5 (C-16), 36.1 (C-1'), 29.4 (C-2'), 122.6 (C-3'), 133.1 (C-4'), 17.6 (C-5'), 25.7 (C-6') (Miguel del Corral, *et al.,* 2005)**.**

Compound **4.15A**

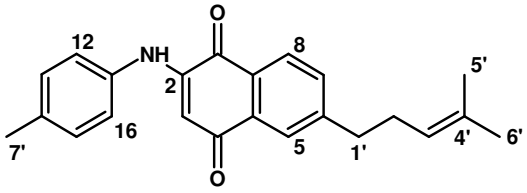

^{1}H NMR ($CDCl_3$): δ 6.33 (s, H-3), 7.92 (s, H-5), 7.45 (d, 7.9 Hz, H-7), 8.02 (d, 7.9 Hz, H-8), 7.21 (d, 8.2 Hz, H-12), 7.16 (d, 8.2 Hz, H-13), 7.16 (d, 8.2 Hz, H-15), 7.21 (d, 8.2 Hz, H-16), 2.76 (t, 7.5 Hz, H-1'), 2.34 (q, 7.5 Hz, H-2'), 5.13 (t, 7.1 Hz, H-3'), 1.54 (s, H-5'), 1.68 (s, H-6'), 2.36 (s, H-7'). ^{13}C NMR ($CDCl_3$): δ 181.9 (C-1), 145.1 (C-2), 102.8 (C-3), 184.3 (C-4), 126.2 (C-5), 150.7 (C-6), 132.4 (C-7), 126.7 (C-8), 133.3 (C-9), 128.3 (C-10), 135.5 (C-11), 130.2 (C-12), 122.7 (C-13), 134.8 (C-14), 122.7 (C-15), 130.2 (C-16), 36.5 (C-1'), 29.4 (C-2'), 122.7 (C-3'), 133.1 (C-4'), 17.7 (C-5'), 25.7 (C-6'), 21.0 (C-7') (Lisboa, *et al*., 2011) (Miguel del Corral, *et al*., 2005).

Compound **4.15B**

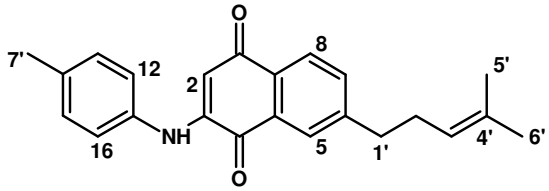

^{1}H NMR ($CDCl_3$): δ 6.32 (s, H-2), 7.92 (s, H-5), 7.55 (d, 7.9 Hz, H-7), 8.00 (d, 7.9 Hz, H-8), 7.21 (d, 8.3 Hz, H-12), 7.16 (d, 8.3 Hz, H-13), 7.16 (d, 8.3 Hz, H-15), 7.21 (d, 8.3 Hz, H-16), 2.76 (t, 7.6 Hz, H-1'), 2.34 (q, 7.4 Hz, H-2'), 5.13 (t, 7.2 Hz, H-3'), 1.53 (s, H-5'), 1.68 (s, H-6'), 2.36 (s, H-7'). ^{13}C NMR ($CDCl_3$): δ 184.1 (C-1), 102.9 (C-2), 144.9 (C-3), 182.5 (C-4), 126.4 (C-5), 147.5 (C-6), 135.1 (C-7), 126.2 (C-8), 131.2 (C-9), 128.8 (C-10), 135.5 (C-11), 130.2 (C-12), 122.6 (C-13), 134.8 (C-14), 122.6 (C-15), 130.2 (C-16), 36.0 (C-1'), 29.4 (C-2'), 122.6 (C-3'), 133.1 (C-4'), 17.7 (C-5'), 25.7 (C-6'), 21.0 (C-7') (Lisboa, *et al*., 2011) (Miguel del Corral, *et al*., 2005).

Compound **4.16A**

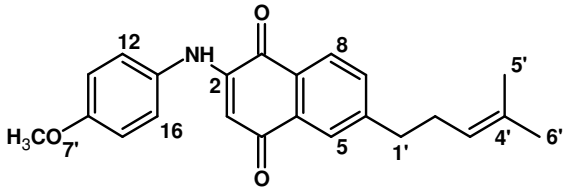

^{1}H NMR ($CDCl_3$): δ 6.20 (s, H-3), 7.92 (s, H-5), 7.44 (d, 7.8 Hz, H-7), 8.01 (d, 7.8 Hz, H-8), 7.19 (d, 8.9 Hz, H-12), 6.94 (d, 8.9 Hz, H-13), 6.94 (d, 8.9 Hz, H-15), 7.19 (d, 8.9 Hz, H-16), 2.76 (t, 7.5 Hz, H-1'), 2.34 (q, 7.6 Hz, H-2'), 5.13 (t, 7.2 Hz, H-3'), 1.54 (s, H-5'), 1.67 (s, H-6'), 3.83 (s, H-7'). ^{13}C NMR ($CDCl_3$): δ 181.9 (C-1), 145.8 (C-2), 102.3 (C-3), 184.1 (C-4), 126.2 (C-5), 150.6 (C-6), 132.3 (C-7), 126.7 (C-8), 133.4 (C-9), 128.3 (C-10), 130.1 (C-11), 124.8 (C-12), 114.9 (C-13), 157.7 (C-14), 114.9 (C-15), 124.8 (C-16), 36.5 (C-1'), 29.4 (C-2'), 122.7 (C-3'), 133.0 (C-4'), 17.6 (C-5'), 25.6 (C-6'), 55.6 (C-7') (Lisboa, *et al*., 2011) (Miguel del Corral, *et al*., 2005).

Compound **4.16B**

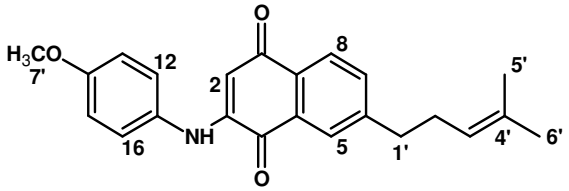

^{1}H NMR ($CDCl_3$): δ 6.19 (s, H-2), 7.92 (s, H-5), 7.55 (d, 7.8 Hz, H-7), 7.99 (d, 7.8 Hz, H-8), 7.20 (d, 8.9 Hz, H-12), 6.94 (d, 8.9 Hz, H-13), 6.94 (d, 8.9 Hz, H-15), 7.20 (d, 8.9 Hz, H-16), 2.76 (t, 7.5 Hz, H-1'), 2.35 (q, 7.6 Hz, H-2'), 5.14 (t, 7.2 Hz, H-3'), 1.54 (s, H-5'), 1.68 (s, H-6'), 3.83 (s, H-7'). ^{13}C NMR ($CDCl_3$): δ 183.9 (C-1), 102.7 (C-2), 145.6 (C-3), 182.4 (C-4), 126.3 (C-5), 147.4 (C-6), 135.0 (C-7), 126.2 (C-8), 131.3 (C-9), 130.3 (C-10), 130.1 (C-11), 124.7 (C-12), 114.8 (C-13), 157.7 (C-14), 114.8 (C-15), 124.7 (C-16), 36.0 (C-1'), 29.4 (C-2'), 122.7 (C-3'), 133.1 (C-4'), 17.7 (C-5'), 25.7 (C-6'), 55.6 (C-7') (Lisboa, *et al*., 2011) (Miguel del Corral, *et al*., 2005).

Compound **4.17A**

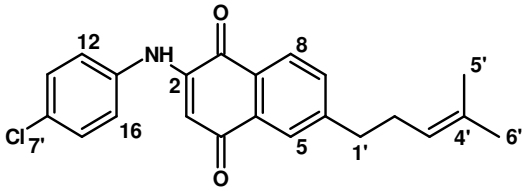

^{1}H NMR ($CDCl_3$): δ 6.33 (s, H-3), 7.92 (s, H-5), 7.47 (d, 7.8 Hz, H-7), 8.03 (d, 7.9 Hz, H-8), 7.21 (d, 8.8 Hz, H-12), 7.33 (d, 8.8 Hz, H-13), 7.33 (d, 8.8 Hz, H-15), 7.21 (d, 8.8 Hz, H-16), 2.77 (t, 7.5 Hz, H-1'), 2.35 (q, 7.5 Hz, H-2'), 5.13 (t, 7.2 Hz, H-3'), 1.54 (s, H-5'), 1.67 (s, H-6'). ^{13}C NMR ($CDCl_3$): δ 183.2 (C-1), 144.5 (C-2), 103.5 (C-3), 184.3 (C-4), 126.2 (C-5), 150.9 (C-6), 132.6 (C-7), 126.8 (C-8), 133.2 (C-9), 128.2 (C-10), 130.1 (C-11), 123.7 (C-12), 129.8 (C-13), 136.1 (C-14), 129.8 (C-15), 123.7 (C-16), 36.5 (C-1'), 29.4 (C-2'), 122.6 (C-3'), 133.0 (C-4'), 17.6 (C-5'), 25.7 (C-6') HRESIMS: *m/z*: 366.1248 $[M+H]^+$, $C_{22}H_{20}ClNO_2$, calculated: 366.1260; FTIR: 3315.41, 2924.32, 1677.28, 1606.12, and 1566.34 cm^{-1}.

Compound **4.17B**

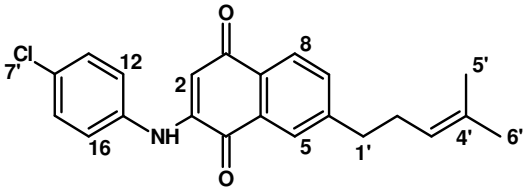

^{1}H NMR ($CDCl_3$): δ 6.33 (s, H-2), 7.92 (s, H-5), 7.56 (d, 7.9 Hz, H-7), 8.00 (d, 7.8 Hz, H-8), 7.22 (d, 8.7 Hz, H-12), 7.38 (d, 8.7 Hz, H-13), 7.38 (d, 8.7 Hz, H-15), 7.22 (d, 8.7 Hz, H-16), 2.76 (t, 7.5 Hz, H-1'), 2.34 (q, 7.5 Hz, H-2'), 5.13 (t, 7.1 Hz, H-3'), 1.53 (s, H-5'), 1.68 (s, H-6'). ^{13}C NMR ($CDCl_3$): δ 184.1 (C-1), 103.7 (C-2), 144.3 (C-3), 182.1 (C-4), 126.5 (C-5), 147.7 (C-6), 135.2 (C-7), 126.3 (C-8), 131.0 (C-9), 130.7 (C-10), 130.1 (C-11), 123.7 (C-12), 129.8 (C-13), 136.1 (C-14), 129.8 (C-15), 123.7 (C-16), 36.0 (C-1'), 29.4 (C-2'), 122.6 (C-3'), 133.2 (C-4'), 17.6 (C-5'), 25.7 (C-6'), HRESIMS: *m/z*: 366.1249 $[M+H]^+$, $C_{22}H_{20}ClNO_2$, calculated: 366.1260; FTIR: 3315.41, 2924.32, 1677.28, 1606.12, and 1566.34 cm^{-1}.

Compound **4.18A**

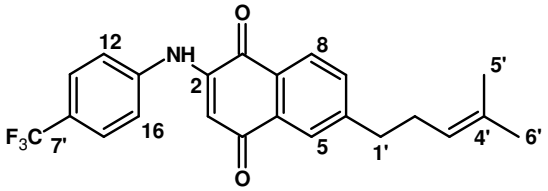

^{1}H NMR ($CDCl_3$): δ 6.50 (s, H-3), 7.93 (s, H-5), 7.49 (d, 7.9 Hz, H-7), 8.04 (d, 7.9 Hz, H-8), 7.38 (d, 8.5 Hz, H-12), 7.67 (d, 8.5 Hz, H-13), 7.67 (d, 8.5 Hz, H-15), 7.38 (d, 8.5 Hz, H-16), 2.77 (t, 7.5 Hz, H-1'), 2.35 (q, 7.5 Hz, H-2'), 5.13 (t, 7.1 Hz, H-3'), 1.53 (s, H-5'), 1.67 (s, H-6'). ^{13}C NMR ($CDCl_3$): δ 181.4 (C-1), 143.7 (C-2), 104.7 (C-3), 184.4 (C-4), 126.3 (C-5), 151.0 (C-6), 132.9 (C-7), 126.6 (C-8), 133.2 (C-9), 128.1 (C-10), 140.7 (C-11), 126.9 (C-12), 121.5 (C-13), 141.0 (C-14), 121.5 (C-15), 126.9 (C-16), 36.5 (C-1'), 29.3 (C-2'), 122.6 (C-3'), 132.8 (C-4'), 17.6 (C-5'), 25.7 (C-6'), 124.7 (C-7') HRESIMS: *m/z*: 400.1512 $[M+H]^+$, $C_{23}H_{20}F_3NO_2$, calculated: 400.1524; FTIR: 3309.86, 2923.15, 2853.84, 1736.26, 1672.20, 1604.86 and 1588.08 cm^{-1}.

Compound **4.18B**

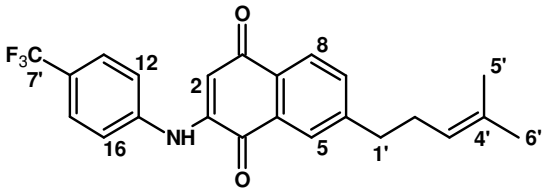

^{1}H NMR ($CDCl_3$): δ 6.50 (s, H-2), 7.94 (s, H-5), 7.58 (d, 7.9 Hz, H-7), 8.01 (d, 7.9 Hz, H-8), 7.38 (d, 8.4 Hz, H-12), 7.67 (d, 8.5 Hz, H-13), 7.7 (d, 8.5 Hz, H-15), 7.38 (d, 8.4 Hz, H-16), 2.77 (t, 7.5 Hz, H-1'), 2.35 (q, 7.5 Hz, H-2'), 5.13 (t, 7.2 Hz, H-3'), 1.53 (s, H-5'), 1.67 (s, H-6'). ^{13}C NMR ($CDCl_3$): δ 184.2 (C-1), 104.9 (C-2), 143.5 (C-3), 182.0 (C-4), 126.3 (C-5), 148.0 (C-6), 135.4 (C-7), 126.4 (C-8), 130.8 (C-9), 130.1 (C-10), 140.7 (C-11), 126.9 (C-12), 121.5 (C-13), 141.0 (C-14), 121.5 (C-15), 126.9 (C-16), 36.0 (C-1'), 29.4 (C-2'), 122.6 (C-3'), 133.8 (C-4'), 17.6 (C-5'), 25.7 (C-6'), 124.7 (C-7') HRESIMS: *m/z*: 400.1509 $[M+H]^+$, $C_{23}H_{20}F_3NO_2$, calculated: 400.1524; FTIR: 3309.86, 2923.15, 2853.84, 1736.26, 1672.20, 1604.86 and 1588.08 cm^{-1}.

Compound **4.19A**

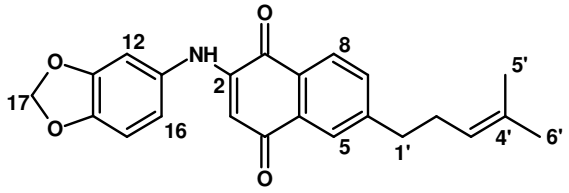

^{1}H NMR ($CDCl_3$): δ 6.21 (s, H-3), 7.91 (d, 1.7 Hz, H-5), 7.45 (dd, 7.8; 1.8 Hz, H-7), 8.01 (d, 7.8 Hz, H-8), 6.77 (d, 2.2 Hz, H-12), 6.83 (d, 8.2 Hz, H-15), 6.71 (dd, 8.2; 2.2 Hz, H-16), 6.01 (s, H-17), 2.76 (t, 7.5 Hz, H-1'), 2.34 (q, 7.5 Hz, H-2'), 5.13 (t, 7.2 Hz, H-3'), 1.53 (s, H-5'), 1.67 (s, H-6'). ^{13}C NMR ($CDCl_3$): δ 181.8 (C-1), 133.3 (C-2), 101.7 (C-3), 184.1 (C-4), 126.2 (C-5), 150.6 (C-6), 132.6 (C-7), 126.7 (C-8), 131.3 (C-9), 128.8 (C-10), 148.5 (C-11), 104.9 (C-12), 145.6 (C-13), 145.7 (C-14), 108.5 (C-15), 116.9 (C-16), 101,7 (C-17), 36.5 (C-1'), 29.3 (C-2'), 122.7 (C-3'), 133.1 (C-4'), 17.7 (C-5'), 25.6 (C-6') HRESIMS: *m/z*: 376.1537 $[M+H]^+$, $C_{23}H_{21}NO_4$, calculated: 376.1548; FTIR: 3321.78, 2969.75, 2913.94, 1738.11, 1670.63 and 1628.45 cm^{-1}.

Compound **4.19B**

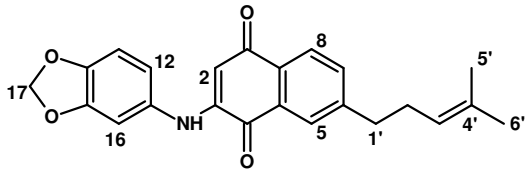

^{1}H NMR ($CDCl_3$): δ 6.20 (s, H-2), 7.91 (d, 1.7 Hz, H-5), 7.55 (dd, 7.9; 1.8 Hz, H-7), 7.99 (d, 7.9 Hz, H-8), 6.78 (d, 2.2 Hz, H-12), 6.83 (d, 8.2 Hz, H-15), 6.72 (dd, 8.3; 2.1 Hz, H-16), 6.01 (s, H-17), 2.76 (t, 7.5 Hz, H-1'), 2.35 (q, 7.5 Hz, H-2'), 5.13 (t, 7.2 Hz, H-3'), 1.54 (s, H-5'), 1.68 (s, H-6'). ^{13}C NMR ($CDCl_3$): δ 184.0 (C-1), 102.7 (C-2), 131.2 (C-3), 182.3 (C-4), 126.3 (C-5), 148.4 (C-6), 135.0 (C-7), 126.2 (C-8), 131.3 (C-9), 130.3 (C-10), 145.5 (C-11), 104.8 (C-12), 147.5 (C-13), 147.7 (C-14), 108.6 (C-15), 116.1 (C-16), 101,5 (C-17), 36.0 (C-1'), 29.4 (C-2'), 122.7 (C-3'), 133.1 (C-4'), 17.7 (C-5'), 25.6 (C-6') HRESIMS: *m/z*: 376.1534 $[M+H]^+$, $C_{23}H_{21}NO_4$, calculated: 376.1548; FTIR: 3321.78, 2969.75, 2913.94, 1738.11, 1670.63 and 1628.45 cm^{-1}.

4.4.3 Synthesis of third series of naphthoquinone derivatives

REPRESENTATIVE PROCEDURE

6-(4-methylpent-3-en-1-yl)-2-(prop-2-en-1-ylamino)naphthalene-1,4-dione (4.20)

To a dissolved sample of naphthoquinone **4.10** (0.120 g, 0.5 mmoles) in MeOH (5 ml) in a glass vial, was added allylamine (0.028 g, 0.5 mmoles) and the reaction mixture stirred at room temperature for 48 hours under atmospheric O_2. The solvent was removed under reduced pressure on a rotavap and the crude product obtained (0.106 g, 71.8 % yield) purified by column chromatography using Hex/EtOAc 8:2 to give a mixture of regioisomers. The same method was used for the preparation of **4.21-4.23** from compound **4.10**. See the supplementary data for details (**Table S4.4**).

Compound **4.20A**

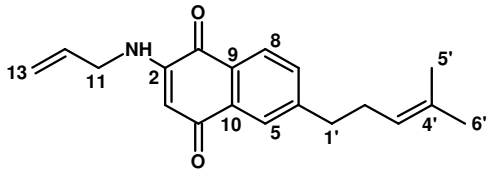

^{1}H NMR ($CDCl_3$): δ 5.71 (s, H-3), 7.91 (s, H-5), 7.41 (d, 7.9 Hz, H-7), 7.95 (d, 7.9 Hz, H-8), 3.83 (t, 5.7 Hz, H-11), 5.87 (m, H-12), 5.29 (m, H-13), 2.76 (t, 7.6 Hz, H-1'), 2.33 (q, 7.7 Hz, H-2'), 5.12 (t, 7.2 Hz, H-3'), 1.53 (s, H-5'), 1.66 (s, H-6'). ^{13}C NMR ($CDCl_3$): δ 181.6 (C-1), 148.0 (C-2), 101.3 (C-3), 183.4 (C-4), 126.5 (C-5), 150.5 (C-6), 132.1 (C-7), 126.2 (C-8), 128.3 (C-9), 133.5 (C-10), 44.8 (C-11), 131.5 (C-12), 118.1 (C-13), 36.4 (C-1'), 29.3 (C-2'), 122.7 (C-3'), 133.0 (C-4'), 17.6 (C-5'), 25.6 (C-6'), HRESIMS: *m/z*: 296.1638 $[M+H]^+$, $C_{19}H_{21}NO_2$, calculated: 296.1650; FTIR: 3380.08, 2925.76, 1736.64, 1673.66 and 1608.06 cm^{-1}.

Compound **4.20B**

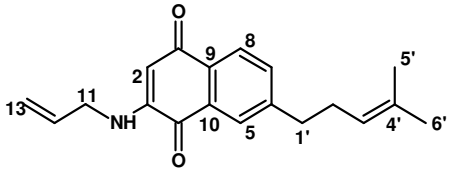

^{1}H NMR ($CDCl_3$): δ 5.70 (s, H-2), 7.86 (s, H-5), 7.52 (d, 7.9 Hz, H-7), 7.99 (d, 7.9 Hz, H-8), 3.83 (t, 5.7 Hz, H-11), 5.88 (m, H-12), 5.29 (m, H-13), 2.73 (t, 7.5 Hz, H-1'), 2.33 (q, 7.6 Hz, H-2'), 5.12 (t, 7.2 Hz, H-3'), 1.52 (s, H-5'), 1.67 (s, H-6'). ^{13}C NMR ($CDCl_3$): δ 183.3 (C-1), 101.4 (C-2), 147.7 (C-3), 182.1 (C-4), 126.3 (C-5), 147.1 (C-6), 135.0 (C-7), 126.2 (C-8), 131.6.3 (C-9), 130.3 (C-10), 44.9 (C-11), 131.4 (C-12), 118.2 (C-13), 35.9 (C-1'), 29.4 (C-2'), 122.7 (C-3'), 133.0 (C-4'), 17.7 (C-5'), 25.6 (C-6') HRESIMS: *m/z*: 296.1642 $[M+H]^+$, $C_{19}H_{21}NO_2$, calculated: 296.1650; FTIR: 3380.08, 2925.76, 1736.64, 1673.66 and 1608.06 cm^{-1}.

Compound **4.22A**

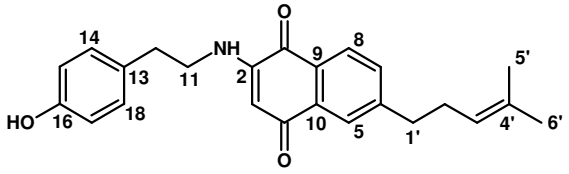

^{1}H NMR ($CDCl_3$): δ 5.74 (s, H-3), 7.93 (s, H-5), 7.40 (d, 7.8 Hz, H-7), 7.92 (d, 7.8 Hz, H-8), 3.40 (q, 6.9 Hz, H-11), 2.90 (t, 7.2 Hz, H-12), 6.80 (d, 8.5, Hz, H-14), 7.08 (d, 8.5 Hz, H-15), 7.08 (d, 8.5 Hz, H-17), 6.80 (d, 8.5 Hz, H-18), 2.74 (t, 7.5 Hz, H-1'), 2.33 (q, 7.5 Hz, H-2'), 5.12 (t, 7.2 Hz, H-3'), 1.53 (s, H-5'), 1.67 (s, H-6'). ^{13}C NMR ($CDCl_3$): δ 181.5 (C-1), 147.9 (C-2), 101.1 (C-3), 183.4 (C-4), 126.5 (C-5), 150.6 (C-6), 132.1 (C-7), 126.2 (C-8), 128.4 (C-9), 133.6 (C-10), 43.7 (C-11), 33.7 (C-12), 129.9 (C-13), 116.0 (C-14), 129.8 (C-15), 154.8 (C-16), 129.8 (C-17), 116.0 (C-18), 36.5 (C-1'), 29.7 (C-2'), 122.9 (C-3'), 133.0 (C-4'), 17.9 (C-5'), 25.7 (C-6') HRESIMS: *m/z*: 376.1903 $[M+H]^+$, $C_{24}H_{25}NO_3$, calculated: 376.1919; FTIR: 3353.55, 2922.73, 2853.68, 1677.19 and 1558.48 cm^{-1}.

Compound **4.22B**

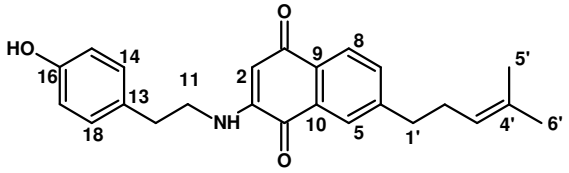

^{1}H NMR ($CDCl_3$): δ 5.73 (s, H-2), 7.83 (s, H-5), 7.52 (d, 7.8 Hz, H-7), 7.99 (d, 7.8 Hz, H-8), 3.39 (q, 7.0 Hz, H-11), 2.90 (t, 7.1 Hz, H-12), 6.80 (d, 8.5, Hz, H-14), 7.08 (d, 8.5 Hz, H-15), 7.08 (d, 8.5 Hz, H-17), 6.80 (d, 8.5 Hz, H-18), 2.72 (t, 7.5 Hz, H-1'), 2.32 (q, 7.5 Hz, H-2'), 5.12 (t, 7.1 Hz, H-3'), 1.52 (s, H-5'), 1.67 (s, H-6'). ^{13}C NMR ($CDCl_3$): δ 183.2 (C-1), 100.8 (C-2), 147.7 (C-3), 182.1 (C-4), 126.3 (C-5), 147.1 (C-6), 135.0 (C-7), 126.2 (C-8), 130.4 (C-9), 131.5 (C-10), 43.8 (C-11), 33.4 (C-12), 129.9 (C-13), 115.7 (C-14), 129.8 (C-15), 154.6 (C-16), 129.8 (C-17), 115.7 (C-18), 35.9 (C-1'), 29.4 (C-2'), 122.7 (C-3'), 133.0 (C-4'), 17.6 (C-5'), 25.6 (C-6') HRESIMS: *m/z*: 376.1906 $[M+H]^+$, $C_{24}H_{25}NO_3$, calculated: 376.1919; FTIR: 3353.55, 2922.73, 2853.68, 1677.19 and 1558.48 cm^{-1}.

Compound **4.23A**

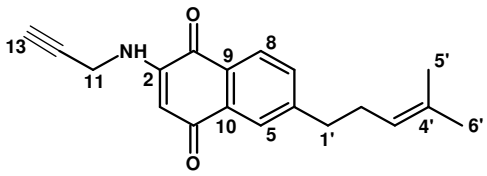

^{1}H NMR ($CDCl_3$): δ 5.81 (s, H-3), 7.92 (s, H-5), 7.43 (d, 7.9 Hz, H-7), 7.96 (d, 7.9 Hz, H-8), 3.98 (s, H-11), 2.34 (m, H-13), 2.75 (t, 7.6 Hz, H-1'), 2.34 (m, H-2'), 5.12 (t, 7.1 Hz, H-3'), 1.53 (s, H-5'), 1.67 (s, H-6'). ^{13}C NMR ($CDCl_3$): δ 181.3 (C-1), 147.1 (C-2), 102.4 (C-3), 183.5 (C-4), 126.5 (C-5), 150.8 (C-6), 132.4 (C-7), 126.3 (C-8), 128.3 (C-9), 133.3 (C-10), 32.3 (C-11), 88.0 (C-12), 73.1 (C-13), 36.4 (C-1'), 29.3 (C-2'), 122.7 (C-3'), 133.0 (C-4'), 17.7 (C-5'), 25.6 (C-6') HRESIMS: *m/z*: 294.1490 $[M+H]^+$, $C_{19}H_{19}NO_2$, calculated: 294.1493; FTIR: 3377.96, 3215.60, 2924.82, 1669.05 and 1629.36 cm^{-1}.

Compound **4.23B**

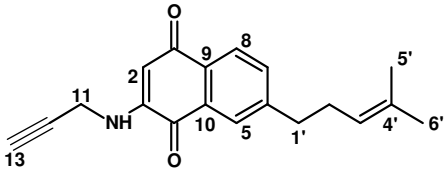

^{1}H NMR ($CDCl_3$): δ 5.80 (s, H-2), 7.86 (s, H-5), 7.53 (d, 7.8 Hz, H-7), 8.00 (d, 7.8 Hz, H-8), 3.98 (s, H-11), 2.33 (m, H-13), 2.74 (t, 7.5 Hz, H-1'), 2.33 (m, H-2'), 5.12 (t, 7.1 Hz, H-3'), 1.52 (s, H-5'), 1.67 (s, H-6'). ^{13}C NMR ($CDCl_3$): δ 183.3 (C-1), 102.5 (C-2), 147.4 (C-3), 181.8 (C-4), 126.4 (C-5), 147.0 (C-6), 135.0 (C-7), 126.2 (C-8), 130.3 (C-9), 131.2 (C-10), 32.2 (C-11), 88.0 (C-12), 73.3 (C-13), 35.9 (C-1'), 29.4 (C-2'), 122.7 (C-3'), 133.1 (C-4'), 17.7 (C-5'), 25.6 (C-6') HRESIMS: *m/z*: 294.1484 $[M+H]^+$, $C_{19}H_{19}NO_2$, calculated: 294.1493; FTIR: 3377.96, 3215.60, 2924.82, 1669.05 and 1629.36 cm^{-1}.

6-(4-methylpent-3-en-1-yl)-2/3-(morpholin-4-yl)naphthalene-1,4-dione (4.24)

A mixture of morpholine (0.116 g, 1.3 mmoles), $Cu(OAc)_2$ (0.080 g, 0.4 mmoles) and H_2O (2 drops) was dissolved in MeOH (3 ml) facilitated by warming on a heated oil bath. The naphthoquinone **4.10** (0.107 g, 0.4 mmoles) dissolved on the side in MeOH (2 ml) was then added to the mixture with vigorous stirring, and the stirring continued for an hour at room temperature under atmospheric O_2. After 1 hour, the solvent was evaporated under reduced pressure and the residue remaining dissolved in Et_2O (5 ml) and 4 % H_2SO_4 (5 ml). The organic layer was collected and the aqueous mixture further extracted using CH_2Cl_2 (3 x 15 ml). Pooled layers were dried over anhydrous Mg_2SO_4 and the organic solvent evaporated to yield 0.104 g (80.4 % yield) of a mixture of Regioisomers.

Compound **4.24A**

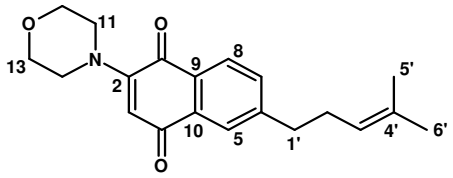

^{1}H NMR ($CDCl_3$): δ 5.98 (s, H-3), 7.85 (s, H-5), 7.45 (d, 7.9 Hz, H-7), 7.90 (d, 7.9 Hz, H-8), 3.49 (t, 4.9 Hz, H-11), 3.86 (t, 4.9 Hz, H-12), 3.86 (t, 4.9 Hz, H-13), 3.49 (t, 4.9 Hz, H-14), 2.74 (t, 7.5 Hz, H-1'), 2.33 (q, 7.4 Hz, H-2'), 5.12 (t, 7.2 Hz, H-3'), 1.53 (s, H-5'), 1.67 (s, H-6'). ^{13}C NMR ($CDCl_3$): δ 182.7 (C-1), 153.9 (C-2), 111.9 (C-3), 184.1 (C-4), 125.5 (C-5), 149.6 (C-6), 132.8 (C-7), 127.0 (C-8), 130.7 (C-9), 132.2 (C-10), 49.2 (C-11), 66.4 (C-12), 66.4 (C-13), 49.2 (C-14), 36.3 (C-1'), 29.3 (C-2'), 122.3 (C-3'), 133.0 (C-4'), 17.8 (C-5'), 25.7 (C-6') HRESIMS: *m/z*: 326.1746 $[M+H]^+$, $C_{20}H_{23}NO_3$, calculated: 326.1755; FTIR: 2964.12, 2922.40.60, 2856.01, 1672.21 and 1632.54 cm^{-1}.

Compound **4.24B**

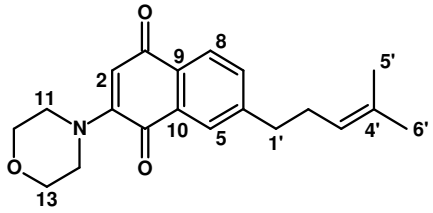

^{1}H NMR ($CDCl_3$): δ 5.98 (s, H-2), 7.81 (s, H-5), 7.50 (d, 7.9 Hz, H-7), 7.94 (d, 7.9 Hz, H-8), 3.48 (t, 4.9 Hz, H-11), 3.86 (t, 4.9 Hz, H-12), 3.86 (t, 4.9 Hz, H-13), 3.48 (t, 4.9 Hz, H-14), 2.74 (t, 7.6 Hz, H-1'), 2.33 (q, 7.5 Hz, H-2'), 5.13 (t, 7.2 Hz, H-3'), 1.53 (s, H-5'), 1.67 (s, H-6'). ^{13}C NMR ($CDCl_3$): δ 183.9 (C-1), 112.2 (C-2), 153.7 (C-3), 183.2 (C-4), 126.6 (C-5), 147.9 (C-6), 134.3 (C-7), 125.8 (C-8), 130.3 (C-9), 132.6 (C-10), 49.2 (C-11), 66.4 (C-12), 66.4 (C-13), 49.2 (C-14), 36.1 (C-1'), 29.4 (C-2'), 122.7 (C-3'), 133.0 (C-4'), 17.7 (C-5'), 25.7 (C-6') HRESIMS: *m/z*: 326.1746 $[M+H]^+$, $C_{20}H_{23}NO_3$, calculated: 326.1755; FTIR: 2964.12, 2922.40.60, 2856.01, 1672.21 and 1632.54 cm^{-1}.

6-(2-(3,3-dimethyloxiran-2-yl)ethyl)-2-(4-hydroxyphenethylamino)naphthalene-1,4-dione (4.25)

A sample of naphthoquinone **4.10** (0.250 g, 1.0 mmoles) was dissolved in anhydrous CH_2Cl_2 (25 ml), and to it added $NaHCO_3$ (0.874 g, 10.0 mmoles) with vigorous stirring for 1 min. m-chloroperoxybenzoic acid (mCPBA) (0.897 g, 5.0 mmoles) was added afterwards to the reaction mixture and stirring continued for an hour at room temperature. The reaction was quenched by addition of 10% $Na_2S_2O_3$ (30 ml) and CH_2Cl_2 (20 ml), followed by collection of the organic layer which was dried over anhydrous Na_2SO_4. The solvent was evaporated off and the crude product (**4.27**) obtained (0.233 g, 91.3 % yield) used in the following reaction with no further purification. A reaction mixture of the epoxide **4.27** (0.110 g, 0.4 mmoles) and tyramine (0.077 g, 0.5 mmoles) dissolved in EtOH/H_2O (10 ml, 1:1 mixture) was stirred at room temperature for 18 hours. During the work up, H_2O (10 ml) and Et_2O (10 ml) were added and the organic layer collected. The aqueous layer was further extracted using Et_2O (2 x 25 ml) and the pooled organic layers dried over anhydrous Na_2SO_4. The solvent was then removed under pressure on a rotary evaporator to yield 0.094 g (59.8 % yield) of compound **4.25.** Compound **4.26** was prepared from **4.27** using the same method and details are the supplementary section.

Compound **4.25A**

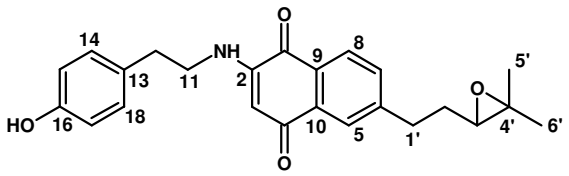

^{1}H NMR ($CDCl_3$): δ 5.74 (s, H-3), 7.94 (s, H-5), 7.44 (d, 7.8 Hz, H-7), 7.95 (d, 7.8 Hz, H-8), 3.38 (q, (t), 6.8 Hz, H-11), 2.88 (t, 7.1 Hz, H-12), 6.81 (d, 8.4 Hz, H-14), 7.07 (d, 8.4 Hz, H-15), 7.07 (d, 8.4 Hz, H-17), 6.81 (d, 8.4 Hz, H-18), 2.88 (m, H-1'), 1.89 (m, H-2'), 2.76 (t, 6.22 Hz, H-3'), 1.16 (s, H-5'), 1.28 (s, H-6'). ^{13}C NMR ($CDCl_3$): δ 181.4 (C-1), 148.0 (C-2), 100.7 (C-3), 183.2 (C-4), 126.1 (C-5), 149.5 (C-6), 132.2 (C-7), 126.8 (C-8), 128.7 (C-9), 130.5 (C-10), 43.8 (C-11), 33.4 (C-12), 129.6 (C-13), 115.8 (C-14), 129.7 (C-15), 154.8 (C-16), 129.7 (C-17), 115.8 (C-18), 32.7 (C-1'), 30.1 (C-2'), 63.5 (C-3'), 58.7 (C-4'), 18.6 (C-5'), 24.7 (C-6') HRESIMS: *m/z*: 392.1843 $[M+H]^+$, $C_{24}H_{25}NO_4$, calculated: 392.1861; FTIR: 3358.95, 2926.80, 1676.77 and 1557.80 cm^{-1}.

Compound **4.25B**

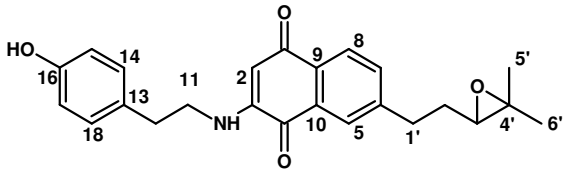

^{1}H NMR ($CDCl_3$): δ 5.74 (s, H-2), 7.86 (s, H-5), 7.56 (d, 7.8 Hz, H-7), 8.02 (d, 7.8 Hz, H-8), 3.39 (q, (t), 6.8 Hz, H-11), 2.90 (t, 7.1 Hz, H-12), 6.80 (d, 8.4 Hz, H-14), 7.08 (d, 8.4 Hz, H-15), 7.08 (d, 8.4 Hz, H-17), 6.80 (d, 8.4 Hz, H-18), 2.89 (m, H-1'), 1.89 (m, H-2'), 2.75 (t, 6.30 Hz, H-3'), 1.16 (s, H-5'), 1.27 (s, H-6'). ^{13}C NMR ($CDCl_3$): δ 183.0 (C-1), 101.0 (C-2), 147.7 (C-3), 182.0 (C-4), 126.0 (C-5), 146.2 (C-6), 135.0 (C-7), 126.5 (C-8), 130.5 (C-9), 131.8 (C-10), 43.9 (C-11), 35.5 (C-12), 129.9 (C-13), 115.7 (C-14), 129.8 (C-15), 154.6 (C-16), 129.8 (C-17), 115.7 (C-18), 32.7 (C-1'), 30.2 (C-2'), 63.5 (C-3'), 58.6 (C-4'), 18.6 (C-5'), 24.7 (C-6'), HRESIMS: *m/z*: 392.1850 $[M+H]^+$, $C_{24}H_{25}NO_4$, calculated: 392.1861; FTIR: 3358.95, 2926.80, 1676.77 and 1557.80 cm^{-1}.

Compound **4.26A**

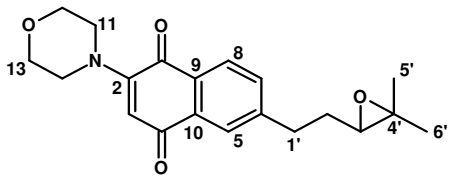

^{1}H NMR ($CDCl_3$): δ 5.99 (s, H-3), 7.88 (s, H-5), 7.48 (d, 7.9 Hz, H-7), 7.94 (d, 7.9 Hz, H-8), 3.50 (t, 4.8 Hz, H-11), 3.86 (t, 4.8 Hz, H-12), 3.86 (t, 4.8 Hz, H-13), 3.50 (t, 4.8 Hz, H-14), 2.90 (m, H-1'), 1.90 (m, H-2'), 2.75 (t, 6.2 Hz, H-3'), 1.16 (s, H-5'), 1.28 (s, H-6'). ^{13}C NMR ($CDCl_3$): δ 182.6 (C-1), 153.7 (C-2), 111.9 (C-3), 183.9 (C-4), 125.4 (C-5), 148.5 (C-6), 132.9 (C-7), 127.3 (C-8), 130.9 (C-9), 132.4 (C-10), 49.2 (C-11), 66.5 (C-12), 66.5 (C-13), 49.2 (C-14), 33.0 (C-1'), 30.2 (C-2'), 63.7 (C-3'), 58.6 (C-4'), 18.8 (C-5'), 24.7 (C-6') HRESIMS: *m/z*: 342.1699 $[M+H]^+$, $C_{20}H_{23}NO_4$, calculated: 342.1705; FTIR: 2925.98, 1736.12, 1672.30 and 1630.33 cm^{-1}.

Compound **4.26B**

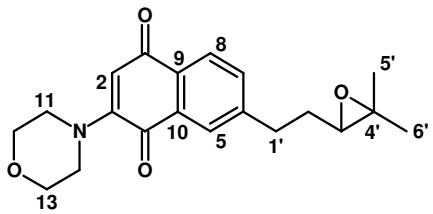

^{1}H NMR ($CDCl_3$): δ 5.99 (s, H-2), 7.84 (s, H-5), 7.54 (d, 7.9 Hz, H-7), 7.97 (d, 7.9 Hz, H-8), 3.48 (t, 4.7 Hz, H-11), 3.86 (t, 4.7 Hz, H-12), 3.86 (t, 4.5 Hz, H-13), 3.48 (t, 4.7 Hz, H-14), 2.89 (m, H-1'), 1.90 (m, H-2'), 2.75 (t, 6.22 Hz, H-3'), 1.17 (s, H-5'), 1.29 (s, H-6'). ^{13}C NMR ($CDCl_3$): δ 183.7 (C-1), 112.2 (C-2), 153.7 (C-3), 183.0 (C-4), 126.7 (C-5), 147.2 (C-6), 134.3 (C-7), 126.0 (C-8), 130.5 (C-9), 132.8 (C-10), 49.3 (C-11), 66.6 (C-12), 66.6 (C-13), 49.3 (C-14), 32.9 (C-1'), 30.3 (C-2'), 63.6 (C-3'), 58.6 (C-4'), 19.1 (C-5'), 24.6 (C-6') HRESIMS: *m/z*: 342.1697 $[M+H]^+$, $C_{20}H_{23}NO_4$, calculated: 342.1705; FTIR: 2925.98, 1736.12, 1672.30 and 1630.33 cm^{-1}.

4.4.4 Synthesis of fourth series of naphthoquinone derivatives

8-(4-methylpent-3-en-1-yl)-3,4-dihydro-2H-naphtho[2,3-b][1,4]thiazine-5,10-dione 1,1-dioxide (4.28)

Hypotaurine (0.033 g, 0.3 mmoles in 1 ml H_2O) was added in portions to a pre-dissolved naphthoquinone **4.10** (0.050 g, 0.2 mmoles) in CH_3CN/EtOH (10 ml, 1:1) maintained at a temperature of 70 °C. The reaction mixture was allowed to reflux at 70 °C for 2.5 hours, after which it was cooled to room temperature and the solvent evaporated. The remaining residue was reconstituted in H_2O (20 ml) and extracted using EtOAc (3 x 25 ml). The pooled EtOAc fractions were washed twice with H_2O (2 x 20 ml) and dried over anhydrous Na_2SO_4. The solvent was then removed under reduced pressure to give 0.047 g (68.3 % yield) of crude product which was purified by column chromatography (Hex/EtOAc 25:75).

Compound **4.28**

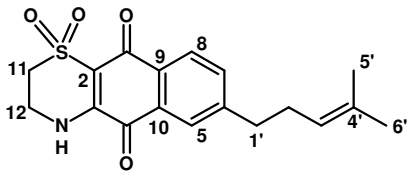

^{1}H NMR ($CDCl_3$): δ 8.01 (s, H-5), 7.47 (d, 7.8 Hz, H-7), 7.96 (d, 7.9 Hz, H-8), 3.36 (m, H-11), 4.13 (m, H-12), 2.77 (t, 7.5 Hz, H-1'), 2.33 (q, 7.3 Hz, H-2'), 5.09 (t, 7.1 Hz, H-3'), 1.51 (s, H-5'), 1.66 (s, H-6'). Anal. ($C_{18}H_{19}NO_4S$). ^{13}C NMR ($CDCl_3$): δ 178.6 (C-1), 113.3 (C-2), 145.4 (C-3), 175.7 (C-4), 127.2 (C-5), 152.7 (C-6), 133.4 (C-7), 127.1 (C-8), 127.2 (C-9), 132.6 (C-10), 49.1 (C-11), 39.9 (C-12), 36.6 (C-1'), 29.2 (C-2'), 122.3 (C-3'), 133.3 (C-4'), 17.6 (C-5'), 25.7 (C-6') (Aiello, *et al*., 2003)**.**

2-methyl-2-(4-methylpent-3-en-1-yl)-2H-benzo[g]chromene-5, 10-dione (4.29)

A mixture of reagents, 2-hydroxynaphthoquinone (1.470 g, 8.44 mmoles), citral (0.479 g, 2.8 mmoles), β-alanine (0.038 g, 0.4 mmoles) and AcOH (0.2 ml) was dissolved in C_6H_6 (100 ml) in a 250 ml round bottomed flask and refluxed at 80-85 °C for 3 hours. The reaction mixture was then cooled to room temperature and the solvent evaporated off under vacuum. The resulting crude was passed through a plug of silica gel eluting in step-gradient fashion, initially with 9:1 (Hex/EtOAc), 50:50 (Hex/EtOAc and 100 % MeOH. 50:50 (Hex/EtOAc) fraction yield compound **4.30** (2.076 g, 79.8 % yield) in its pure form.

Compound **4.29**

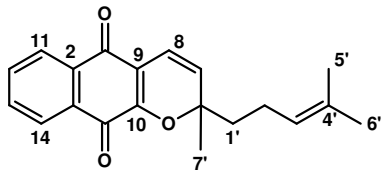

^{1}H NMR ($CDCl_3$): δ 5.69 (d, 10.1 Hz, H-7), 6.68 (d, 10.1 Hz, H-8), 8.06 (dd, 7.5; 1.4 Hz, H-11), 7.67 (m, H-12), 7.67 (m. H-13), 8.06 (dd, 7.5; 1.4 Hz, H-14), 1.93 (m, H-1'), 2.11 (m, H-2'), 5.03 (t, 7.1 Hz, H-3'), 1.53 (s, H-5'), 1.60 (s, H-6'), 1.50 (s, H-7'). ^{13}C NMR ($CDCl_3$): δ 181.3 (C-1), 131.5 (C-2), 131.5 (C-3), 179.6 (C-4), 83.1 (C-6), 129.7 (C-7), 116.0 (C-8), 117.4 (C-9), 152.7 (C-10), 126.1 (C-11), 133.9 (C-12), 133.1 (C-13), 126.1 (C-14), 41.2 (C-1'), 22.6 (C-2'), 123.5 (C-3'), 132.2 (C-4'), 17.6 (C-5'), 25.8 (C-6'), 27.6 (C-7') (Jung, *et al*., 2010).

References

Achari, B., Bandyopadhyay, S., Basu, K., & Pakrashi, S. (1985). Studies on indian medicinal plants, part LXXIX : synthesis proves the structure of aristolindiqu inone. *Tetrahedron, 41*, 107-110.

Aiello, A., Fattorusso, E., Luciano, P., Menna, M., Esposito, G., Iuvone, T., & Pala, D. (2003). Conicaquinones A and B, two novel cytotoxic terpene quinones from the mediterranean ascidian Aplidium conicum. *European Journal of Organic Chemistry, 2003, 898-900.*

Castro, F., Mariani, D., Panek, A., Eleutherio, E., & Pereira, M. (2008). Cytotoxicity mechanism of two naphthoquinones (menadione and plumbagin) in Saccharomyces cerevisiae. *PLoS ONE, 3*, 1-6.

Chung, Y., Yoo, J., Park, S., Kim, B., Chen, X., Zhan, C., & Cho, H. (2007). Dependence of antitumor activity on the electrophilicity of 2-substituted 1,4-naphthoquinone derivatives. *Bulletin of the Korean Chemical Society, 28*, 691-694.

Criddle, D., Gillies, S., Baumgartner-Wilson, H., Jaffar, M., Chinje, E., Passmore, S., Chvanov, M., Barrow, S., Gerasimenko, O.V., Tepikin, A.V., Sutton, R., & Petersen, O. (2006). Menadione-induced reactive oxygen species generation via redox cycling promotes apoptosis of murine pancreatic acinar cells. *The Journal of Biological Chemistry, 281*, 40485–40492.

Dinkova-Kostova, A., & Talalay, P. (2000). Persuasive evidence that quinone reductase type 1 (DT diaphorase) protects cells against the toxicity of electrophiles and reactive forms of oxygen. *Free Radical Biology and Medicine, 29*, 231-240.

Dubowchik, G., Mosure, K., Knipe, J., & Firestone, R. (1998). Cathepsin B-sensitive dipeptide prodrugs. 2. Models of anticancer drugs paclitaxel (Taxol®), mitomycin C and doxorubicin. *Bioorganic & Medicinal Chemistry Letters, 8*, 3347–3352.

Jung, E., Park, B., & Lee, Y. (2010). Environmentally benign, one-pot synthesis of pyrans by domino Knoevenagel/6p-electrocyclization in water and application to natural products. *Green Chemistry, 12*, 2003-2011.

Lee, J., Yeon, J., Kim, H., Roh, W., Chae, J., Park, H., & Kim, D. (2012). The natural anticancer agent plumbagin induces potent cytotoxicity in MCF-7 human breast cancer cells by inhibiting a PI-5 Kinase for ROS generation. *PLoS ONE, 7*, 1-10.

Lisboa, C., Santos, V., Vaz, B., de Lucas, N., Eberlin, M., & Garden, S. (2011). C-H functionalization of 1, 4 naphthoquinone by oxidative coupling with anilines in the presence of a catalytic quantity of copper (II) acetate. *Journal of Organic Chemistry, 76*, 5264–5273.

Miguel del Corral, J., Castro, M., Gordaliza, M., Martin, M., Gualberto, S., Gamito, A., Cuevas, C., & Feliciano, A. (2005). Synthesis and cytotoxicity of new aminoterpenylquinones. *Bioorganic & Medicinal Chemistry, 13*, 631–644.

Miguel del Corral, J., Castro, M., Oliveira, A., Gualberto, S., Cuevas, C., & San Feliciano, A. (2006). New cytotoxic furoquinones obtained from terpenyl- 1, 4-naphthoquinones and 1,4-anthracenediones. *Bioorganic & Medicinal Chemistry, 14*, 7231–7240.

Miguel del Corral, J., Castro, M., Gordaliza, M., Martin, M., Oliveira, A., Gualberto, S., García-Grávalos, M.D,. & San Feliciano, A. (2002). Synthesis and biological evaluation of cytotoxic 6(7)-alkyl-2-hydroxy-1, 4-naphthoquinones. *Archiv der Pharmazie - Pharmaceutical and Medicinal Chemistry, 335*, 427–437.

Miguel del Corral, J., Gordaliza, M., Castroa, M., Mar Mahiquesa, M., San Feliciano, A., & Garcia-Gravalos, M. (1998). Further antineoplastic terpenylquinones and terpenylhydroquinones. *Bioorganic & Medicinal Chemistry, 6*, 31-41.

Paulsen, M., & Ljungman, M. (2005). The natural toxin juglone causes degradation of p53 and induces rapid H2AX phosphorylation and cell death in human fibroblasts. *Toxicology and Applied Pharmacology, 209*, 1-9.

Pierpont, C. (2001). Unique properties of transition metal quinone complexes of the MQ3 Series. *Coordination Chemistry Reviews*, 219–221, 415-433.

Rahmoun, N., Atmani, Z., Benabdallah, M., Boucherit, K., Villemin, D., & Braham, N. (2013). Antimicrobial activities of the henna extract and some synthetic naphthoquinones derivatives. *American Journal of Medical and Biological Research,, 1*, 16-22.

Ramirez, O., Motta-Mena, L., Cordova, A., & Garza, K. (2014). A small library of synthetic di-dubstituted 1, 4-naphthoquinones induces ROS-mediated cell death in murine fibroblasts. *PLOS ONE , 9*, 1-9.

Ryu, C. K., Kang, H. Y., Yi, Y. J., Shin, K. H., & Lee, B. (2000). Synthesis and antifungal activities of 5/6-arylamino-4,7-dioxobenzothiazoles. *Bioorganic & Medicinal Chemistry Letters, 10*, 1589-1591.

Sagar, S., Kaur, M., Minneman, K., & Bajic, V. (2010). Anti-cancer activities of diospyrin, its derivatives and analogues. *European Journal of Medicinal Chemistry, 45*, 3519-3530.

Seung, S., Lee, J., Lee, M., Park, J., & Chung, J. (1998). The relative importance of oxidative stress versus arylation in the mechanism of quinone-induced cytotoxicity to platelets. *Chemico-Biological Interactions, 113*, 133–144.

Sibi, M., Dankwardt, J., & Snieckus, V. (1986). Anionic aromatic ring annelation of o-allyl benzamides. Regiospecific synthesis of naphthols and naphthoquinones. *The Journal of Organic Chemistry, 51*, 271-273.

Ting, C., Hsu, C., Hsu, H., Su, J., Chen, T., Tarn, W., Kuo, Y., Whang-Peng, J., Liu, L., & Hwang, J. (2003). Isodiospyrin as a novel human DNA topoisomerase I inhibitor. *Biochemical Pharmacology, 66*, 1981–1991.

Witayakran, S., & Ragauskas, A. (2007). One-pot synthesis of 1, 4-naphthoquinones and related structures with laccase. *Green Chemistry, 9*, 475–480.

CHAPTER FIVE

Biological activity of truncated prenylated naphthoquinones

Abstract

Cytotoxicity and client protein degradation assays were conducted on selected natural products and synthesized truncated prenylated naphthoquinones. The synthesized analogues showed improved cytotoxicity compared to the natural products, and also demonstrated moderate activity for Hsp90 inhibition. Arylamino-naphthoquinones (**4.14-4.19**) were the most cytotoxic derivatives, whilst SQA (**2.47**) showed the most potency as an Hsp90 protein inhibitor. Binding to Hsp90 protein was somehow different compared to geldanamycin's (**2.28**) interaction with the chaperone, as no Hsp70 induction was noticed with both SQA (**2.47**) and selected naphthoquinone derivatives, which could potentially mean binding to the C-terminus of Hsp90 protein. The assays are described in more detail in this chapter.

5.1 Introduction

In vitro assays were conducted to determine cytotoxic properties of the synthesized truncated prenylated naphthoquinones (**4.10-4.29**) and natural products (**2.47, 3.1-3.3**, **3.5** and **3.6-3.11**). Client protein degradation assays were also done as a measure for Hsp90 inhibition. Our main goal was to develop cytotoxic compounds that inhibit Hsp90 function as a potential class of anticancer compounds.

5.1.1 Cytotoxicity assays

Cytotoxicity studies with cell culture systems provide useful information during the screening of substances with potential anticancer properties. Several indicators are used to determine the toxic effect of compounds on cancer cells. The most readily observed effect of cytotoxicity is morphological changes in the cells, which can be done microscopically. Other indicators include altered cell growth/cell reproduction measured by cell count, and determination of cell death by use of vital dyes and cell proliferation reagents to measure cell viability (Gerets, *et al*., 2009). A number of approaches have been developed to rapidly evaluate the cytotoxic activity of test substances (Liu, *et al*., 1997). Accepted methods used to quantify cell viability in cell-based assays include lactate dehydrogenase (LDH) release assays, trypan blue exclusion, and 3-(4, 5-dimethylthiazol-2-yl)-2, 5-diphenyl tetrazolium bromide (MTT) reduction assays (Kim, *et al*., 2009).

5.1.1.1 3-(4, 5-dimethylthiazol-2-yl)-2, 5-diphenyl tetrazolium bromide (MTT) reduction assays

This assay measures the conversion of a yellow tetrazolium salt, MTT (**5.1**), into purple formazan crystals (**5.2**) by redox activity of metabolically active cells (Vistica, *et al*., 1991) (**Scheme 5.1**). The MTT (**5.1**) reagent is absorbed *via* endocytosis and reduction occurs in active cellular mitochondria (Burdon, *et al*., 1993). Reduction to formazan (**5.2**) is effected by intracellular NAD(P)H oxidoreductases enzymes (Berridge, *et al*., 2005) and the formazan (**5.2**) dye formed is quantified by absorbance at 550 nm and 650 nm using a scanning multi-well spectrophotometer (ELISA plate reader). Cell viability is proportional to the increase in formazan product (**5.2**) formed. Conversely, a decrease in MTT (**5.1**) reduction can be used as a marker for cell damage/death.

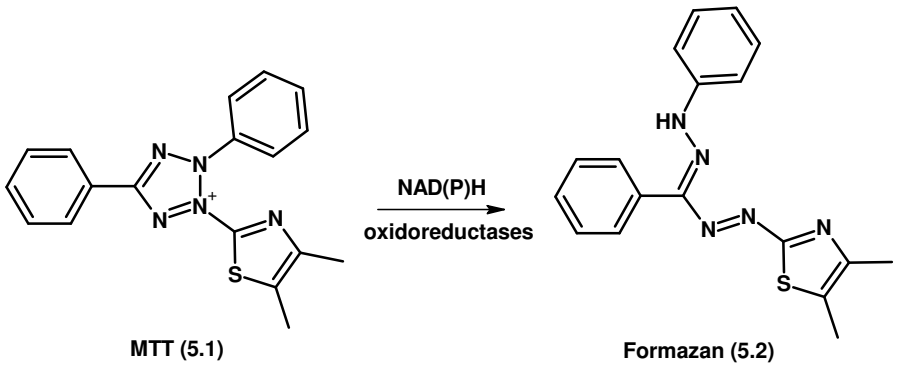

Scheme 5.1: Reduction of MTT (**5.1**) to a formazan (**5.2**) salt by viable cells

Various different tetrazolium dyes can be used for colorimetric assays. A common alternative to MTT (**5.1**) involves the use of disodium mono (4-(3-(-iodophenyl)-2-(4-nitrophenyl)-2H-tetrazol-3-ium-5-yl) benzene-1, 3-disulfonate (WST-1), as a cell proliferation reagent. It is also a tetrazolium salt and works on similar principles as MTT (**5.1**), namely that it is reduced to formazan dye by active cellular mitochondria, which indicates cell viability (Ngamwongsatit, *et al*., 2008). The WST-1 formazan product is detected by absorbance at 440 nm and a decrease in WST-1 reduction signifies cell damage or death.

Mammalian cell culture is an important component of research in understanding disease profiles and possible treatments especially in the cancer field. The majority of breast cancer research is conducted using established breast cancer cell lines as *in-vitro* models and these include cell lines such as the MCF7 and MDA-MB-231 breast adenocarcinoma and Hs578T breast carcinoma (Burdall, *et al*., 2003). Immortalised cell lines are relatively easy to handle, easy to replace from frozen stocks in case of contamination and have the ability to grow to infinite quantities when cultured. However they are susceptible to genotypic and phenotypic changes when continuously cultured. Despite some disadvantages, cell cultures are still commonly used for cancer research. For this study, we used the Hs578T breast carcinoma (triple negative) and its properties are briefly discussed below.

5.1.1.2 Hs578T breast carcinoma

Hs578T breast carcinoma belongs to a rare subset of cancer known as metaplastic breast cancers. Morphology of the tumour comprises of adenocarcinoma cells that co-exist with an admixture of spindle cell, squamous, chondroid or bone-forming neoplastic cells. (Schwartz, *et al*., 2013). Under the NCI guidelines, Hs578T breast carcinoma cells are categorized as a triple negative form of breast cancer and are extremely difficult to treat (Chavez, *et al*., 2010). Their growth is not influenced by the hormones oestrogen and progesterone nor by the presence of human epidermal growth factor receptors 2 (HER 2), therefore cannot be treated by hormonal therapy such as tamoxifen or HER 2 receptor blockers like Herceptin (Otvos, *et al*., 2011). Since this form of cancer is difficult to treat, the Hs578T breast carcinoma cell line is a good choice to use in cytotoxic studies for novel anticancer compounds.

5.1.2 Client protein degradation assays

Several *in vitro* assays have been developed to assess Hsp90 inhibition by monitoring concentrations of oncogenic client proteins before and after exposure of the chaperone to suspected inhibitors (Jhaveri, *et al*., 2012). While it is possible to obtain a direct measure of Hsp90 activity by assessing ATPase activity, the low *in vitro* ATPase activity of human Hsp90 means that these assays are technically challenging. In addition, ATPase activity is only relevant for Hsp90 inhibitors that bind to the N-terminal ATPase domain. The routine and accepted assays for inhibition of Hsp90 depend on assessment of the levels of proteins associated and regulated by its action. As previously indicated, Hsp90 inhibition leads to ubiquitination of client proteins prior to proteasomal degradation (Zuehlke and Johnson, 2010). Several canonical client proteins such as CDK4, Raf-1 and c-KIT are reduced in concentration in the presence of Hsp90 inhibitors. Hsp70 induction can also be used as a marker for inhibition of Hsp90 function, and is used in several cancer models to assess Hsp90 activity (Jhaveri, *et al*., 2012).

5.1.3 Aim of study

The aim of the study was to determine the cytotoxicity of the synthesized analogues (**4.10-4.29**) in comparison to the natural compounds SQA (**2.47**) and SNQA (**3.5**), and to assess Hsp90 function in the presence of selected naphthoquinones by monitoring client protein concentrations. The rationale for the synthesis of these analogues was to develop a series of cytotoxic molecules that have Hsp90 inhibition properties, and we also aimed to determine if any correlation exists between cytotoxicity and Hsp90 inhibition.

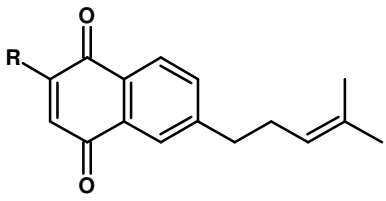

4.10 R = H

4.11 R = Cl

4.12 R = OCH_3

4.13 R = CH_3

4.14 R = 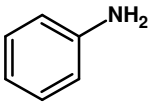

4.15 R = 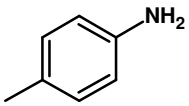

4.16 R = 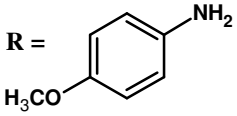

4.17 R = 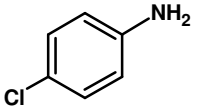

4.18 R = 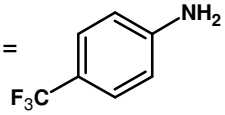

4.19 R = 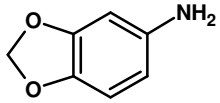

4.20 R = 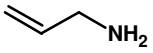

4.21 R = 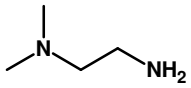

4.22 R = 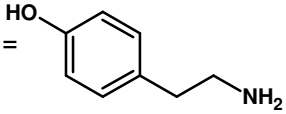

4.23 R = 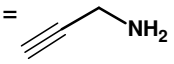

4.24 R = 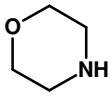

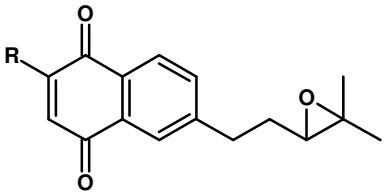

4.25 R = 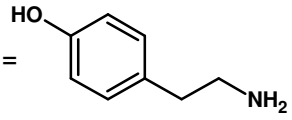

4.26 R = 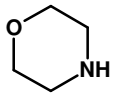

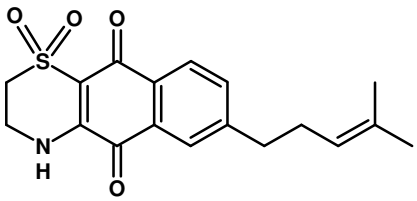

4.28

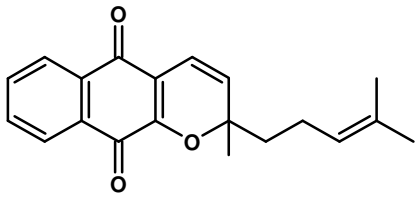

4.29

NB: i) Chemical structures have been redrawn for convenience ii) Only C-2 substituted naphthoquinones are displayed but both isomers were tested for biological activity

5.2 Results and discussion

5.2.1 Cytotoxicity of natural product quinones

The reported *in vitro* assays were conducted by Dr Adrienne L. Edkins and Dr Jo Anne de Mare of the Biomedical Biotechnology Research Unit (BioBRU) at Rhodes University, South Africa. Cytotoxicity assays were conducted in triplicate against MDA-MB-231 cell line for the meroterpenoids (de la Mare, *et al*., 2012) and against Hs578T cell line for lapachol (**3.6**) and its related compounds. Both cell lines are classified as triple negative forms of cancer and are difficult to treat. The results obtained are shown in **Table 5.1**.

Table 5.1: Cytotoxicity of natural product quinones

Sample	MDA-MB-231 IC_{50} (µM)	Hs578T IC_{50} (µM)
3.1	70.0	-
2.47	658.0	-
3.2	69.0	-
3.3	56.0	-
3.4	-	-
3.5	2140.0	-
3.6	-	38.4
3.7	-	13.0
3.8	-	1.2
3.9	-	4.2
3.10	-	2.1
3.11	-	15.1

The meroterpenoids (**2.47, 3.1-3.4 and 3.5**) isolated from *S. incisifolium* displayed moderate cytotoxic properties. The transition from the hydroquinone - quinone - naphthoquinone in compounds **3.1**, **2.47** and **3.5** showed a decrease in activity. Compound **3.3**, containing a chromene moiety exhibited the highest potency of the meroterpenoid series (IC_{50} = 56.0 µM) while sarganaphthoquinoic acid (**3.5**) was in essence non-toxic. Interestingly, lapachol and its derivatives (**3.6-3.11**) showed enhanced cytotoxicity, with values as low as 1.2 µM for compound **3.8**. Given the data above, the challenge was to improve on the cytotoxicity of SQA (**2.47**) while maintaining its ability to inhibit Hsp90 function. Attention was given to a prenylated naphthoquinone series because of the increased cytotoxicity of lapachol

naphthoquinones and the reported Hsp90 inhibition potential of acetamide and benzamide naphthoquinone analogues (Hadden, *et al*., 2009).

5.2.2 Cytotoxicity of truncated prenylated naphthoquinones

The first series of naphthoquinones contained H, Cl, CH_3 and CH_3O at the 2- or 3- position. These compounds closely resemble sarganaphthoquinoic acid (**3.5**), the lead structure for this series. Naphthoquinones (**4.10-4.13**) were evaluated in a three point assay against Hs578T breast cancer carcinoma (triple negative), with taxol as the control. An MTT assay was used to determine percentage cell survival after 96 hours, and percentage cell survival results obtained at 10 µM are displayed in **Table 5.2.** Percentage cell survival results at 1 µM and 100 µM are shown in the supplementary section **(Figures S5.1-S5.8)**

Table 5.2: Percentage cell survival at 10 µM concentrations

Sample	Breast carcinoma Hs578T (Percentage survival at 10 µM concentration)
4.10	10.3
4.11A	54.3
4.11B	66.9
4.12A	63.9
4.12B	56.3
4.13A	57.8
4.13B	24.3

Estimated IC_{50} values for compounds in this series suggested either similar or improved cytotoxicity when compared to the natural products. This is remarkable especially when one compares naphthoquinone **4.13A** to sarganaphthoquinoic acid (**3.5**) (IC_{50} = 2140.0 µM). The main difference between these two compounds is the shortened prenylated chain in **4.13A**. The unsubstituted naphthoquinone, **4.10**, was more cytotoxic than the substituted compounds **4.11-4.13.** A possible explanation could be its increased likelihood to undergo redox cycling and an increased susceptibility to nucleophilic attack by biological nucleophiles.

Cytotoxicity of aryl and alkyl amino-substituted naphthoquinone derivatives **4.14-4.29** is shown in **Table 5.3**. Assays were also conducted against the Hs578T breast cancer carcinoma (triple negative) at a concentration range between 0.005 to 50 µM. The assays were done in triplicate for an incubation period of 96 hours and analysed by MTT assay.

Table 5.3: Cytotoxicity of aryl and alkyl amino-substituted naphthoquinone derivatives against Hs578T breast cancer carcinoma (triple negative)

Sample	Breast carcinoma Hs578T IC_{50} values (µM)
4.10	9.6
Arylamino analogues	
4.14A	2.3
4.14B	4.3
4.15A	0.3
4.15B	0.6
4.16A	0.3
4.16B	1.8
4.17A	4.9
4.17B	2.7
4.18A	> 50
4.18B	0.8
4.19A	0.9
4.19B	0.9
Alkylamino analogues	
4.20A	7.6
4.20B	> 50
4.21	2.6
4.22A	> 50
4.22B	15.6
4.23A	8.6
4.23B	> 50
4.24A	> 50
4.24B	> 50
4.25A	> 50
4.25B	> 50
4.26A	> 50
4.26B	> 50
Tricyclic analogues	
4.28	8.4
4.29	10.7
Natural Product: sargaquinoic acid	
2.47	> 50

Substitution with arylamino moieties for compounds **4.14-4.19** resulted in an increase in cytotoxicity, with some IC_{50} values falling within the nanomolar range. No clear trends could be observed from this group although activity seemed to be enhanced by electron donating groups in the *para*-position of the aniline moiety. Compounds **4.15** and **4.16** that had $-CH_3$ and $-OCH_3$ groups respectively on the *para*-position of the aniline moiety were the most active with IC_{50} values as low as 0.3 μM. Oxygenated substituents e.g. **4.19** also showed enhanced cytotoxic properties. Differences in cytotoxic activity between regioisomers was relatively small indicating that C-2 or C-3 substitution does not necessarily influence cytotoxic behaviour except for compounds **4.18A** and **4.18B**.

With regards to alkylamino-naphthoquinones (**4.20-4.26**), our preliminary results showed that they were less potent than the arylamino substituted compounds (**4.14-4.19**). The most active compound amongst the alkylamino-naphthoquinones was **4.21** with an IC_{50} value of 2.6 μM. Introduction of an aryl moiety in exchange of the tertiary amine in **4.21**, to prepare **4.22** resulted in a less potent molecule. A terminal amino-moiety might be influential in increasing cytotoxic activity of these naphthoquinones.

Attempts to increase the water solubility of naphthoquinones by attaching a morpholino functionality resulted in less cytotoxic compounds (**4.24** and **4.26**). Their IC_{50} values were undetermined since the cut off activity in our studies was 50 μM. Any manipulation of the prenyl side chain also resulted in less potent molecules. Introduction of an epoxide functionality rendered the naphthoquinones **4.25** and **4.26** inactive which was surprising given that epoxides are reactive species that are more likely to interact with macromolecules in a biological system.

Tricyclic prenylated naphthoquinones **4.28** and **4.29** were more active than the parent natural product but comparable to the unsubstituted naphthoquinone **4.10**. The recorded IC_{50} values were 8.4 μM and 10.7 μM for compounds **4.28** and **4.29** respectively, whilst for compound **4.10**, it was 9.6 μM.

According to these preliminary results, substitution with arylamines at the C-2 or C-3 position of the quinone increases potency of naphthoquinones as cytotoxic agents, approximately 700 times and 2000 times more compared to natural compounds **2.47** and **3.5**, respectively. Questions may arise with regards to how redox potential is affected by such substitution but it is probable that a new mode of action is at play with arylamino substituted naphthoquinones. Improved cytotoxicity values from the synthesized derivatives were encouraging, and with the

goal of developing cytototoxic Hsp90 inhibitiors, *in vitro* assays to assess the ability of naphthoquinones to inhibit Hsp90 protein and its functions were advocated for. Client protein degradation assays were conducted as a measure for Hsp90 function. It was however not possible to screen all synthesized derivatives in these studies due to limited protein availability, and a selected few were chosen.

5.2.3 Selected naphthoquinones for client protein degradations assays

Compounds for client protein degradation assays were chosen based on the cytotoxicity data discussed. The obtained cytotoxic results enabled compounds to be categorized into three groups i.e. active (IC_{50} value: nanomolar range), less active (IC_{50} value: 1-50 µM) and inactive (IC_{50} value: > 50 µM) compounds. One or two compounds from each of these groups were selected i.e. **4.16A**, **4.28**, **4.29**, **2.47** and **4.20A**. Compound **4.16A** was the most active naphthoquinone with an IC_{50} value of 0.3 µM. Compounds **4.28** and **4.29** were less active with IC_{50} values of 8.4 µM and 10.7 µM respectively, whilst **2.47** had an undetermined IC_{50} value greater than 50 µM. Compound **4.20A** had an interesting allylamine moiety observed on 17-AAG (**2.29**) and was included in the study. The effect of these compounds was compared to treatment with an equivalent level of the known N-terminal Hsp90 inhibitor, geldanamycin (**2.28**). The selection was done as indicated so as to assess Hsp90 inhibition properties across the board, from cytotoxic to non-cytotoxic molecules.

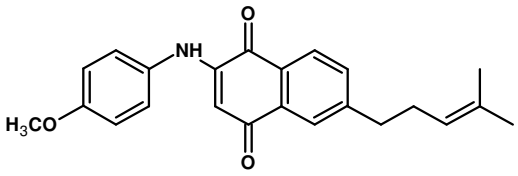

4.16A

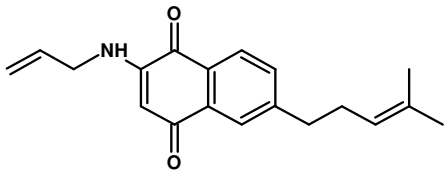

4.20A

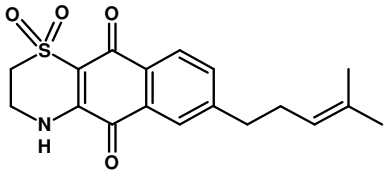

4.28

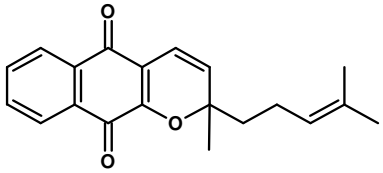

4.29

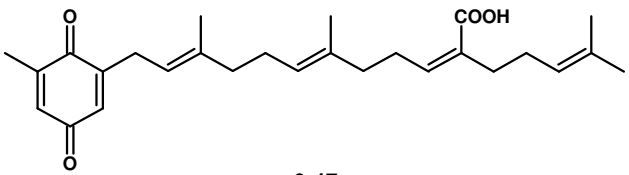

2.47

5.2.4 Client protein degradation assays results

The discussed assays were conducted by Dr Adrienne L. Edkins and Dr Jo Anne de Mare of the Biomedical Biotechnology Research Unit (BioBRU) at Rhodes University, South Africa. Hs578T breast cancer cells were treated with 1 µM concentrations of compounds **4.16A, 4.20A, 4.28, 4.29** and **2.47** for 16 hours. Equal cell numbers were probed for the levels of CDK4, Hsp70 and Histone H3 (loading control for total protein). A densitometry graph was plotted from data obtained from the Western blot. The signal of either CDK4 or Hsp70 was normalised to the loading control by dividing the densitometry of CDK4 or Hsp70 by the densitometry of the Histone H3 band in the respective lanes (**Figure 5.1**).

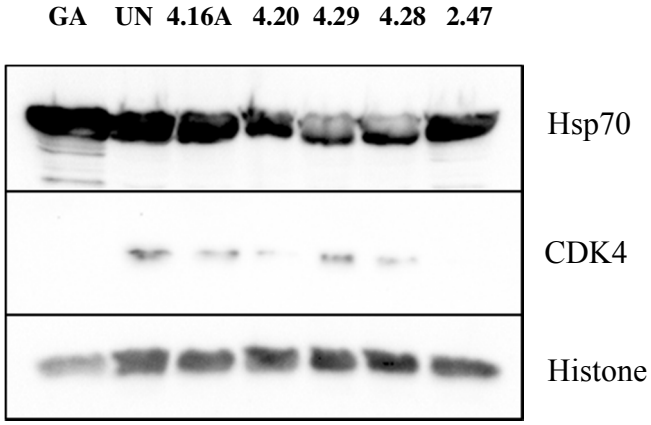

Figure 5.1: Western Blot indicating bands for Hsp70, CDK4 and histone

All signals were normalised to the untreated that was assigned a value of 1 with the rest being relative to this value. The results obtained are shown in the **Figure 5.2** below:

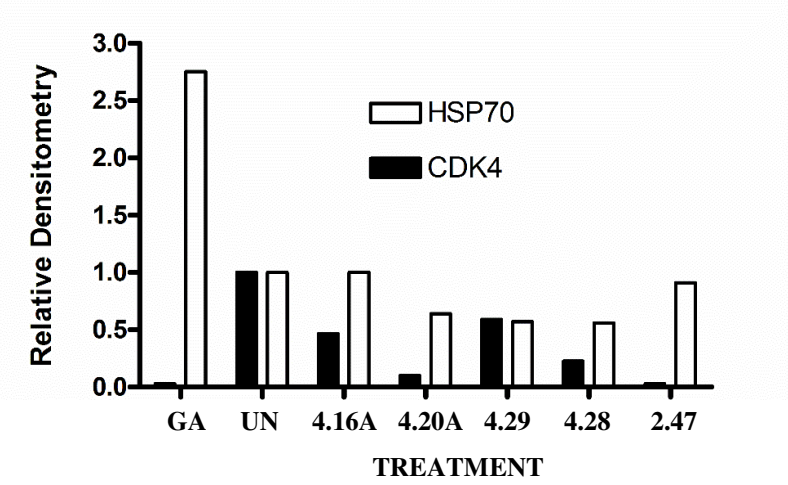

Figure 5.2: A densitometry graph showing levels of Hsp70 and CDK4 in the presence of selected inhibitors

The positive control used was geldanamycin (**2.28**) which gave the anticipated increase in Hsp70 levels (relative to the untreated) and decrease in CDK4 levels (relative to the untreated). Increase in Hsp70 levels is consistent with published reports for N-terminal inhibitors and has been established to be a source of Hsp90 drug resistance and failed cancer therapies with this target (Piper and Millson, 2011). N-terminal domain inhibitors result in the formation of active heat shock transcription factor 1 (HSF 1) that induces a heat shock response and increases cellular levels of pro-survival chaperones like Hsp27 and Hsp70 (Bagatell, *et al*., 2000). These chaperones inhibit cytochrome c and TNF-mediated cell death as part of their pro-survival core functions with enhanced ability to evade apoptosis (McCollum, *et al*., 2006; Powers, *et al*., 2008). Silencing of Hsp70 expression has been shown to promote proteasome-dependant degradation of Hsp90 client proteins. In other human cancer cell lines, G1 cell cycle arrest occurs, together with extensive tumour specific apoptosis (Powers, *et al*., 2008). This setback is common in other classes of compounds e.g. purines and resorcinol derivatives (McCollum, *et al*., 2008).

The set of compounds tested showed moderate Hsp90 inhibition by reducing levels of CDK4, but interestingly showed no increase in Hsp70 concentrations. Compound **2.47** displayed inhibition comparable to that of geldanamycin (**2.28**) with regards to CDK4 reduction. Of the naphthoquinones, **4.20A** was the most potent Hsp90 inhibitor, with **4.29** showing the least potency. No correlation between cytotoxicity and Hsp90 inhibition could be made. Interestingly, **2.47** was deemed non-toxic but demonstrated the most potential as an Hsp90 inhibitor in this assay. Unfortunately, sarganaphthoquinoic acid (**3.5**) could not be assessed in the same assay. The most cytotoxic compounds from the naphthoquinones, **4.16A,** and the less active cytotoxic compounds **4.28** and **4.29,** all exhibited average Hsp90 inhibition. **4.20A** included on the basis of it having the allylamine moiety found on 17 AAG (**2.29**) was the second most potent Hsp90 inhibitor after compound **2.47**. Although there was no correlation between cytotoxicity and Hsp90 inhibition, the positive results obtained indicated the possibility of developing a molecule that possesses both cytotoxic and Hsp90 inhibition properties.

Lack of Hsp70 induction by these molecules is favourable and most likely lessens the chances of drug resistance development. Lack of Hsp70 induction also suggests C-terminal binding on Hsp90 that promotes client protein degradation without activation of HSF1 function; hence no increase in Hsp70 or Hsp27 concentrations occurs (Shelton, *et al*., 2009). Research has been shifting in designing inhibitors that bind to this C terminal pocket in preference to the N-

terminal domain. One such inhibitor being researched on is KU135 (Shelton, *et al*., 2009). Other studies are focusing on blocking the effects of HSF1 though such a route has its own draw backs of compromising normal tissue functioning (de Billy, *et al*., 2009). Combination therapy with N-terminal inhibitors is also being considered to reduce drug resistance (Piper and Millson, 2011).

5.3 Conclusion

Further studies to determine N- or C- terminal binding of naphthoquinones were conducted using Saturation Transfer Difference (STD) NMR and molecular docking studies. We aimed to deduce whether our series of naphthoquinones bind to the C-terminal domain, or bind to both with a higher affinity for the C-terminus. Was it also possible that they were binding to the N-terminal domain with no increase in Hsp70 concentrations? All these questions were attempted to be answered in the next chapter that deals with interactions of the naphthoquinones with the Hsp90 protein's active sites.

5.4 Experimental

5.4.1 Cell culture

Hs578T breast cancer cells were cultured in Dulbecco's Modified Eagle Medium (DMEM) (Gibco) supplemented with 10 % (v/v) heat inactivated fetal bovine serum (FBS), 100 U/ml penicillin, 100 µg/ml streptomycin and 2.5 µg/ml amphotericin (Lonza) in T75 culture flasks (Corning). The flasks were incubated at 10 % CO_2, 37 ºC until cell confluency was observed under the microscope. The cells were then harvested by aspirating the media from the flask, washing the cells with a phosphate buffered saline solution (PBS) and adding 0.5 ml of trypsin/ethylenediaminetetra acetic acid (EDTA) (Gibco) to facilitate dislodging of adherent cells. The trypsinized flask was incubated at 10 % CO_2, 37 ºC for 5-7 minutes for the cells to be lifted. Once cells had been dislodged, trypsin was quenched by addition of 10 ml of DMEM supplemented with FCS. The cells were transferred to a 15 ml centrifuge tube and centrifuged (Eppendorf centrifuge 5804R instrument) at 2000 rpm for 2 minutes, and resuspended in 10 ml of growth medium. A cell count was then carried out using a haemocytometer and volumes adjusted so as to obtain a cell density of 1.2 x 10^5 (120 000) cells per ml.

5.4.2 Cytotoxicity assay

Hs578T breast cancer cells were seeded in 96 well microplates at a concentration of 6000 cells per well (i.e. 50 µl of 1.2 x 10^5 cells/ml cell suspension was added to each well), and the plates were incubated overnight at 37ºC, 10 % CO_2. Concentrations between a range of 0.005 to 50 µM were chosen. Sample analogues were first dissolved in sterile DMSO (Sigma). The assay was validated by including paclitaxel as a positive control on each 96 well microplate, at concentrations ranging from 50 nM to 10 µM. Duplicate wells were left blank with only cells and media with no dosing, and another set dosed with DMSO only. These acted as negative controls of the assay. Dosed plates were then incubated at 37 ºC, 10% CO_2 for 96 h. Cytotoxicity testing for the individual analogues was carried out in duplicate.

A qualitative analysis of the cells was done by viewing respective wells under a microscope after 96 h. The morphology and density of cells were noted as additional indicators of cytotoxicity. Quantitative analysis was done using a Cell Proliferation Kit 1 (MTT) (Roche) whereby 10 µl of MTT cell proliferation reagent was added to each well, followed by an incubation period of 4 hours at 37 ºC and 10% CO_2. A 100 µl volume of solubilization solution was added to all the wells and overnight incubation done at 37 ºC and 10 % CO_2. The colour

change from yellow to purple for each well was measured using a multi-well spectrophotometer (PowerWave) set at dual wavelengths, 550 nm and 650 nm. The average absorbance for each analogue at different concentrations was calculated and wells with cells and media only, assigned a 100% cell survival. Percentage survival of cells at each concentration for all the analogues was calculated relative to the DMEM control. The calculation of the IC_{50} value (which represents the concentration of compound resulting in 50% growth inhibition) was determined by taking the $\log_{10}$ of the concentrations and plotting percentage survival against $\log_{10}$ concentration, to which a trendline was added and IC_{50} values calculated using the equation of the line $y = mx + c$.

5.4.3 Client protein degradation assay

Hs578T breast cancer cells were cultured in Dulbecco's modified Eagle's Medium (DMEM) supplemented with 5 % (v/v) foetal calf serum (FCS), 2 mM glutamine and 100 U/mL penicillin-streptomycin-amphotericin. Hs578T cells were seeded on to tissue culture plastic and allowed to adhere overnight prior to treatment with 1 μM concentrations of compounds **4.16A, 4.20A, 4.28, 4.29** and **2.47** or vehicle control (DMSO) for 16 hours. Cells were harvested by trypsinisation, counted using a haemocytometer and resuspended to the same cell density in SDS-PAGE lysis buffer (250 mM Tris-HCl, pH 6.8, 10% w/v SDS, 30% v/v glycerol, 5% v/v β-mercaptoethanol, 0.02% w/v bromophenol blue) and boiled for 5 minutes. Total protein from equal cell numbers were resolved by SDS-PAGE according to the protocol of Laemmli (1970). The proteins were separated by electrophoresis for 1 hour and 30 minutes at 100 V in 1 x SDS running buffer (0.25 mM Tris, 192 mM glycine, 1% w/v SDS) using a 12% (v/v) resolving gel (1.5 M Tris-HCl, pH 8.8), and a 4% (v/v) stacking gel (0.5 M Tris-HCl, pH 6.8). Proteins were subsequently transferred on to nitrocellulose, and the levels of CDK4, Hsp70 and Histone H3 (loading control for total protein) determined by Western blot analysis with chemiluminescent detection according to the protocol of Towbin (1979). The chemiluminescent patterns were captured electronically and the densitometry of the bands detected using ImageJ. A densitometry graph was plotted from data obtained from the Western blot, whereby the signal of either CDK4 or Hsp70 was normalised to the loading control by dividing the densitometry of CDK4 or Hsp70 by the densitometry of the Histone H3 band in the respective lanes"

References

Bagatell, R., Paine-Murrieta, G., Taylor, C., Pulcini, E., Akinaga, S., & Whitesell, L. (2000). Induction of a heat shock factor 1-dependent stress response and cytotoxic activity of Hsp90-binding agents. *Clinical Cancer Research, 6*, 3312–3318.

Berridge, M., Herst, P., & Tan, A. (2005). Tetrazolium dyes as tools in cell biology: new insights into their cellular reduction. *Biotechnology Anuual Review, 11*, 127-152.

Burdall, S., Hanby, A., Lansdown, M., & Speirs, V. (2003). Breast cancer cell lines: friend or foe? *Breast Cancer Research, 5*, 89-95.

Burdon, R., Gill, V., & Rice-Evans, C. (1993). Reduction of a tetrazolium salt and superoxide generation in human tumor cells (HeLa). *Free Radical Research Community, 18*, 369-380.

Chavez, K., Garimella, S., & Lipkowitz, S. (2010). Triple negative breast cancer cell lines: one tool in the search for better treatment of triple negative breast cancer. *Breast Disease*, *32*, 35–48.

de Billy, E., Powers, M., Smith, J., & Workman, P. (2009). Drugging the heat shock factor 1 pathway: exploitation of the critical cancer cell dependence on the guardian of the proteome. *Cell Cycle, 8*, 3806–3808.

de la Mare, J., Lawson, J., Chiwakata, M., Beukes, D., Edkins, A., & Blatch, G. (2012). Quinones and halogenated monoterpenes of algal origin show anti-proliferative effects against breast cancer cells in vitro. *Investigational New Drugs, 30*, 2187-2200.

Gerets, H., Hanon, E., Cornet, M., Dhalluin, S., Depelchin, O., Canning, M., & Atienzar, F. (2009). Selection of cytotoxicity markers for the screening of new chemical entities in a pharmaceutical context. A preliminary study using a multiplexing approach. *Toxicology in Vitro, 23*, 319-332.

Hadden, M., Hill, S., Davenport, J., Matts, R., & Blagg, B. (2009). Synthesis and evaluation of Hsp90 inhibitors that contain the 1, 4- naphthoquinone scaffold. *Bioorganic and Medicinal Chemistry, 17*, 634–640

Jhaveri, K., Taldone, T., Modi, S., & Chiosis, G. (2012). Advances in the clinical development of heat shock protein 90 (Hsp90) inhibitors in cancers. *Biochimica et Biophysica Acta*, *1823*, 742–755.

Kim, H., Yoon, S., Lee, T., & Jeong, D. (2009). Discriminative cytotoxicity assessment based on various cellular damages. *Toxicology Letters, 184*, 13-17.

Liu, Y., Peterson, D., Kimura, H., & Schubert, D. (1997). Mechanism of cellular 3-(4,5-dimethylthiazol-2-yl)-2,5-diphenyltetrazolium bromide (MTT) reduction. *Journal of Neurochemistry*, *69*, 581-593.

McCollum, A., Lukasiewicz, K., Teneyck, C., Lingle, W., Toft, D., & Erlichman, C. (2008). Cisplatin abrogates the geldanamycin-induced heat shock response. *Molecular Cancer Therapeutics, 7*, 3256–3264.

McCollum, A., Teneyck, C., Sauer, B., Toft, D., & Erlichman, C. (2006). Up-regulation of heat shock protein 27 induces resistance to 17-allylamino-demethoxygeldanamycin through a glutathione-mediated mechanism. *Cancer Research, 66*, 10967–10975.

Miguel del Corral, J., Castro, M., Gordaliza, M., Martin, M., Gualberto, S., Gamito, A.,Cuevas, C., & Feliciano, A. (2005). Synthesis and cytotoxicity of new aminoterpenylquinones. *Bioorganic & Medicinal Chemistry, 13*, 631–644.

Ngamwongsatit, P., Banada, P., Panbangred, W., & Bhunia, A. (2008). WST-1-based cell cytotoxicity assay as a substitute for MTT-based assay for rapid detection of toxigenic Bacillus species using CHO cell line. *Journal of Microbiology Methods, 73*, 211-215.

Otvos, L., Kovalszky, I., Riolfi, M., Ferla, R., Olah, J., Sztodola, A., Nama, K., Molino, A., Piubello, Q., Wade, J.D., & Surmacz, E. (2011). Efficacy of a leptin receptor antagonist peptide in a mouse model of triple-negative breast cancer. *European Journal of Cancer, 47*, 1578-1584.

Piper, P., & Millson, S. (2011). Mechanisms of resistance to Hsp90 inhibitor drugs: a complex mosaic emerges. *Pharmaceuticals, 4*, 1400-1422.

Powers, M., Clarke, P., & Workman, P. (2008). Dual targeting of Hsc70 and Hsp72 inhibits Hsp90 function and induces tumor-specific apoptosis. *Cancer Cell, 14*, 250–262.

Ratasuk, N., & Nanny, M. (2007). Characterization and quantification of reversible redox sites in humic substances. *Environmental Science and Technology, 41*, 7844–7850.

Schwartz, T., Mogal, H., Papageorgiou, C., Veerapong, J., & Hsueh, E. (2013). Metaplastic breast cancer: histologic characteristics,prognostic factors and systemic treatment strategies. *Experimental Hematology & Oncology, 2*, 1-6.

Shelton, S., Shawgo, M., Matthews, S., Lu, Y., Donnelly, A., Szabla, K., Tanol, M., Vielhauer, G., Rajewski, R., Matts, R., Blagg, B., & Robertson, J. (2009). KU135, a novel novobiocin-derived C-terminal inhibitor of the 90-kDa heat shock protein, exerts potent antiproliferative effects in human leukemic cells. *Molecular Pharmacology, 76*, 1314–1322.

Vistica, D., Skehan, P., Scudiero, D., Monks, A., Pittman, A., & Boyd, M. (1991). Tetrazolium-based assays for cellular viability: a critical examination of selected parameters affecting formazan production. *Cancer Research, 51*, 2515-2520.

Zuehlke, A., & Johnson, J. (2010). Hsp90 and co-chaperones twist the functions of diverse client proteins. *Biopolymers*, *93*, 211–217.

CHAPTER SIX

Molecular modelling and STD NMR studies

Abstract

Binding interactions of selected naphthoquinone derivatives with Hsp90 protein were assessed using molecular docking and saturation transfer difference (STD) NMR techniques. Molecular docking results indicated N-terminal binding with aryl amino-naphthoquinones (**4.14-4.19**) having binding energies comparable to ATP. However STD NMR results were inconclusive, and no binding was observed on both the N- and C- terminal ends, probably due to weak binding and poor water solubility of the selected compounds. This chapter describes the two techniques separately and the results obtained for each technique.

6.1 Introduction

In chapter five, we provided indirect evidence for Hsp90 inhibition by the synthesized naphthoquinones. In this chapter we explored additional studies to assess the direct interaction of naphthoquinones with Hsp90 protein, and to determine whether binding occurs at the N- or C- terminal domain. Molecular docking studies were advocated for but are insufficient as "stand alone" experiments to deduce accurate conclusions about actual binding interactions. Saturation Transfer Difference (STD) NMR studies were attempted to complement results that were obtained from docking studies. The two techniques are described in detail in this chapter.

6.1.1 Molecular docking

Geldanamycin (**2.28**) was the first natural product isolated from *Streptomyces hygroscopicus* that exhibited Hsp90 inhibition properties (He, *et al*., 2006; Neckers and Workman, 2012). It comprises of a benzoquinone moiety bridged by an aliphatic chain as shown in chapter two (section 2.3.2). Naphthoquinones possess a similar benzoquinone moiety fused to a benzenoid ring that could potentially fit the ATP binding site at the N-terminus of Hsp90. Reports have previously been published suggesting that 1, 4-naphthoquinones possibly bind to the C-terminal domain of Hsp90 (Hadden, *et al*., 2009), but conflicting results were obtained in studies involving the effect of lapachol on modulation of subcellular localisation and expression levels of Hsp90, Hsp70, Hop, HSF1 and selected Hsp90 client proteins (pSTAT3, STAT3 and AKT) in the MDA-MB-231 breast cancer cell line. The results suggested that binding of this naphthoquinone based natural product occurs at the N-terminus of Hsp90 (Moyo, 2013). We therefore undertook *in silico* docking studies in order to investigate the possibility of our series of naphthoquinones binding to the N-terminus of Hsp90. Unfortunately, a comparative *in silico* assessment of binding to the C-terminus of Hsp90 was not possible *via* our method since a co-crystal structure of the C-terminus of Hsp90 with a ligand is not yet available. It should be noted that published reports of naphthoquinones which show potential Hsp90 inhibition have structural features related to lapachol (**3.6**) (Hadden, *et al*., 2009). Our class of compounds contained a short prenyl chain system on the benzenoid ring offering a new set of compounds that could possibly act as Hsp90 inhibitors.

In silico assessment of small molecules against drug targets is a powerful tool in drug discovery, as a method of large scale screening as well as optimizing ligand drug interactions through a rational design approach (Trott and Olson, 2010). This technique has proven to be a cost effective method of accurately screening libraries of molecules (Bailey and Brown, 2001),

which the pharmaceutical industry increasingly relies upon (Stark and Powers, 2012). Interactions between small molecules and their respective binding sites on a given receptor can be visualized and characterized at an atomic level following two basic concepts centred at predictions of the ligand conformation and assessment of binding affinities *via* sampling algorithms and scoring functions respectively (McConkey, *et al*., 2001).

6.1.2 Sampling algorithm

Docking studies aim to give an accurate prediction of interactions between ligands and receptors. However one critical limitation is associated with this technique. Docking studies represent the receptor as a rigid structure determined by NMR spectroscopy, X-ray crystallography or homology modelling. It does not take into consideration changes in receptor conformations that occur when in solution and during binding with a ligand (Yuriev, *et al*., 2011). Docking simulation methods give details of the ligand-receptor complex. They allow flexibility in the ligand to explore conformations that can fit a particular active site (Morris, *et al*., 1998). AutoDock Vina now takes into consideration a limited degree of flexibility on selected regions of the receptor. A set number of amino acids can be selected and modelled separately to allow conformational changes to occur during ligand binding (Trott and Olson, 2010). It should be noted that such a selection is mainly determined by assessing the conformation of a receptor with its bound ligand that was present during the receptor's structural determination. Ligands screened against this conformation may be over or underestimated, depending on results that will be obtained in *in vitro* assays.

With regards to ligand flexibility, it is virtually impossible to predict all possible conformations a ligand can assume in the active site, hence the use of sampling algorithms. AutoDock Vina makes use of a Lamarckian genetic algorithm to perform adaptive global—local searches of optimal ligand binding (Morris, *et al*., 1998; Trott and Olson, 2010). A set of values which describe translation, orientation and conformation of a ligand in relation to its receptor represents the ligands 'genotype' (Morris, *et al*., 1998). Genetic algorithms randomly assign these values to a ligand in order to generate a diverse population of conformations for the ligand. The algorithm allows for these possible conformations to evolve over several generations through cross over between parent conformations and random mutations of the genotype in order to generate off spring which will be more or less fit for their environment than their parents. Fitness, in this context is assessed by total interaction energy between the

ligand and receptor. Less fit individuals will not be allowed to produce further generations and therefore less optimal interactions will be lost.

The Lamarckian element of the genetic algorithm consists of an inverse mapping function whereby conformational information gleaned from local minima searches can be mapped back onto the genotype therefore producing a non-random mutation to the genotype (**Figure 6.1**). It ensures that a local search around a specific state will have an influence on future generations which may encounter similar local minima (Morris, *et al*., 1998; Wiley, *et al*., 2006).

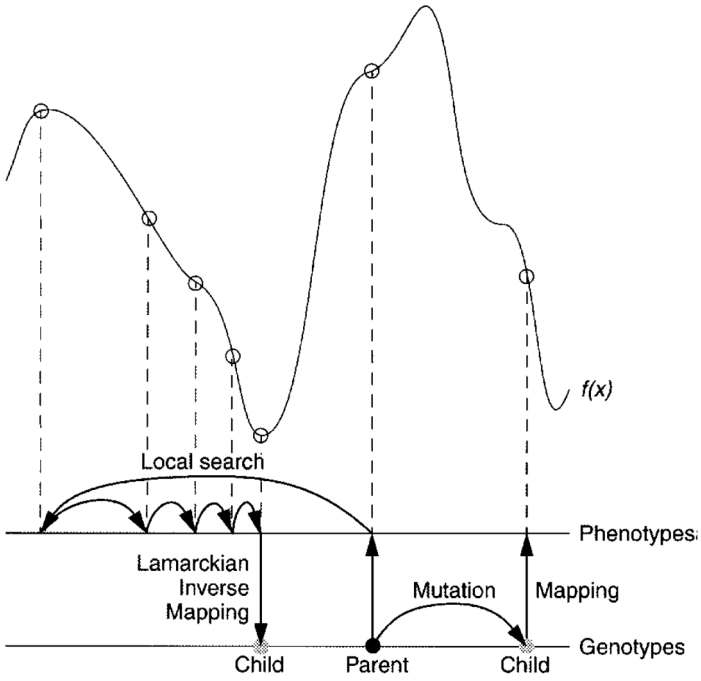

Figure 6.1: Illustration of the difference between Darwinian (right) and Lamarckian search (left) with the fitness function depicted $f(x)$ (Morris, *et al*., 1998).

6.1.3 Scoring function

The scoring functions focus on the binding affinities between the ligand and the receptor, which can be divided into three groups that take into consideration different interactions between the ligand and receptor. The classical force-field based scoring function focuses on binding energies that are as a result of non-bonded (electrostatic and van der Waals forces) interactions, with some extensions to hydrogen bonding and solvation. (Kollman, 1993). The empirical scoring function gives final binding energies as a sum of hydrogen bonding, ionic interaction, hydrophobic effect and binding entropy (Bohm, 1998) whilst the knowledge-based scoring function makes use of interatomic contact frequencies and distances between the ligand and

protein (Muegge and Martin, 1999). All these aspects have been integrated in computational softwares like Autodock Vina (Trott and Olson, 2010) that was used for this study.

6.1.4 Aim of study

As previously highlighted, geldanamycin (**2.28**) contains a benzoquinone system that is thought to be essential for Hsp90 protein inhibition *via* binding to the ATP binding site of the N-terminal domain (Neckers and Workman, 2012). Inhibition of ATPase activity of Hsp90 affects all six hallmarks of cancer making it an ideal target for drug design and development (Miyata, *et al*., 2013). Our series of truncated sarganaphthoquinoic acid derivatives consists of a similar quinone moiety fused to a benzenoid ring (naphthoquinone), which sparked our interest in investigating their interactions with Hsp90 protein. In the previous chapter, we discussed the cytotoxicity of the synthesized naphthoquinones which on some occasions displayed IC_{50} values in the nanomolar range, which may be accredited to their ability to take part in redox reactions according to literature (Castro, *et al*., 2008). The ability to inhibit Hsp90 protein activity will be an added advantage to this class of molecules. It would suggest several modes of action for quinone systems, which is advantageous in preventing drug resistance from cancer cells. Our aims and objectives were therefore to

- To determine whether any of our naphthoquinones had the potential to interact with the ATP binding site of Hsp90 by way of molecular docking.
- Assess docking conformations and binding affinities in comparison to those of ATP and geldanamycin (**2.28**) with Hsp90 protein.

6.2 Results and discussion

6.2.1 Docking software

The molecular docking studies discussed in this chapter were conducted using Autodock Vina (Trott and Olson, 2010). Discovery Studio 4.0 visualizer (Accelrys Software Inc., Discovery Studio Modeling Environment, Release 4.0, San Diego: Accelrys Software Inc., 2013) was used to process all results obtained and to visualize the docking conformations and orientations.

6.2.2 Preparation of Hsp90 protein and ligand for docking

One protomer of Hsp90 protein bound with ATP in the N-terminal domain (PDB accession number 1AM1) was obtained from the RCSB Protein Data Bank as a PDB text file. The original ligand and additional water molecules were removed from the protein, leaving the ATP binding site vacant for docking and the protein in its *apo* form (**Figure 6.2**)

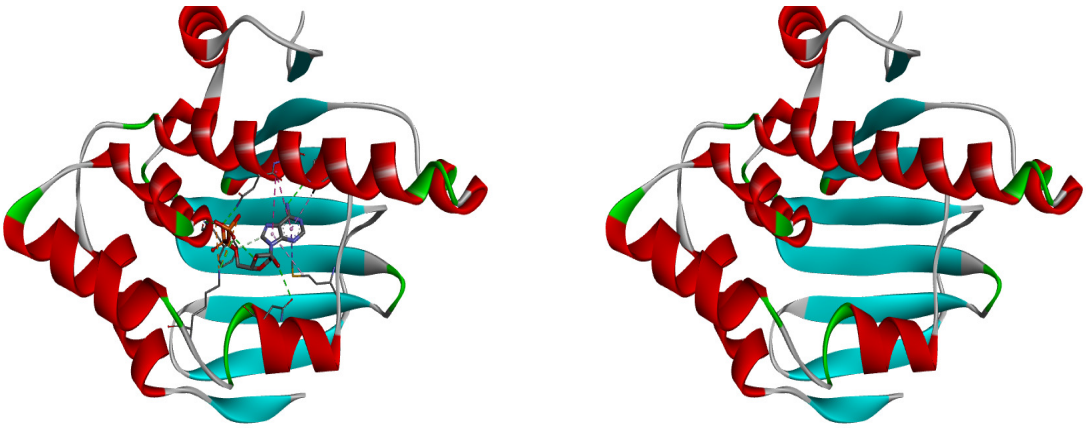

Figure 6.2: Hsp90 protein bound with ATP (left) and in its *apo* form (right)

Preparation of the *apo* protein using AutoDock tools involved merging all non-polar hydrogens followed by the addition of polar ones. Atoms were assigned by Autodock 4 typing rules while electrostatic charges were computed as Gasteiger charges. The original ligand found in PDB 1AM1 (ATP) was prepared for docking using AutoDock tools, whereby Gasteiger charges were added, 8 non-polar hydrogens merged and 5 aromatic carbons and 9 rotatable bonds were detected. ATP docking experiments were conducted as a means to validate the method and parameters set, and will be discussed briefly in the next section. All additional ligands reported in this chapter were prepared for docking using the same method.

6.2.3 Validation: Interactions and binding affinities

Initial experiments involved docking ATP into its active site as a means of validating and optimizing the parameters set for docking studies. A 'search space area' for ligand docking was constrained to a box of 30 Å in each of the three spacial dimensions, centered on a coordinate randomly chosen in the known ATP binding site. The docking of ATP was done two times, with the aim of obtaining similar docking conformations and binding energies for validation to pass. Autodock Vina gives an output consisting of several active conformations that are ranked according to their binding energies. The first run was conducted with an exhaustiveness of 32 to adequately search the binding site, and the second one done at an exhaustiveness of 8. The highest ranking conformations were identical in both runs (**Figure 6.3**) suggesting that an exhaustiveness of 8 was adequate for the docking studies of our compounds.

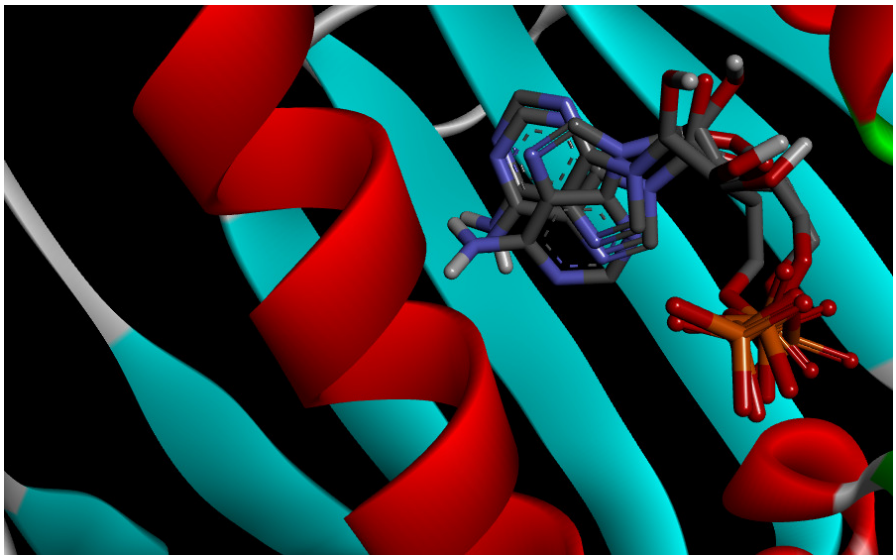

Figure 6.3: Illustration of similar docking conformations of ATP in the N-terminal domain of Hsp90 in validation experiments

The binding energies obtained were also similar for all conformations as displayed in **Table 6.1**.

Table 6:1 Binding energies for ATP docking studies on Hsp90 Protein

ATP docking experiment	Exhaustiveness	Binding Energy (kcal/mol)
1	32	−7.6
2	8	−7.3

It was noticed that ATP interacts with seven amino acids in its active site and has a network of six hydrogen bonds with ASN37, ASP79, LYS98, GLY123 and PHE124. The overall type of interactions involved are shown in **Figure 6.4**

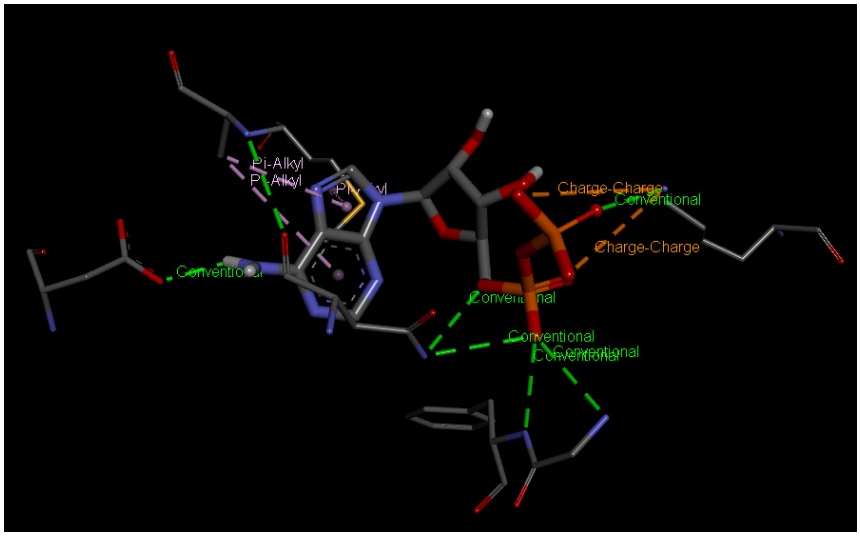

Figure 6.4: ATP interactions within the active site of Hsp90

It should be noted that other bond-bond interactions i.e., Pi-alkyl interactions, charge-charge interactions, amide-pi stacked interactions etc. contribute to the binding energies that result, in addition to the hydrogen bonds that are mainly considered, and care should be taken in the interpretation of results obtained not to ignore these interactions.

Confirmation of similar docking conformations and binding energies indicated that the set parameters were accurate and reproducible. The method set was deemed validated and suitable for docking studies discussed in the next sections. Only hydrogen bonding interactions are reported within this chapter, and other bond-bond interactions between the ligand and the active site are highlighted in the supplementary section.

6.2.4 First series of naphthoquinone analogues

We had hypothesized that naphthoquinones bind to Hsp90 in a similar way to geldanamycin (**2.28**), therefore it was included in the study. Nine active conformations were detected with an exhaustiveness of 8. The best docked conformation was selected based on the docking energy, visual examination of how close in orientation it is to the ATP results obtained and the hydrogen bond network around the ligand.

As expected ATP displayed the best binding energy of −7.6 kcal/mol, followed by geldanamycin (**2.28**). The naphthoquinones all exhibited encouraging binding energies ranging

between –6.4 and –7.1 kcal/mol. Compound **4.11B** displayed the best binding energy to Hsp90 (–7.1 kcal/mol) in addition to having the highest number interactions with amino acids within the active site. It also showed two hydrogen bonding interactions of the carbonyl functionalities on the quinone moiety to ASN37 and THR171. Its regioisomer **4.11A** however indicated the worst binding energy of -6.4 kcal/mole, with no hydrogen bonding occurring. Overall, C-2 or C-3 substitution had no influence on the binding affinity of this series to Hsp90 except in the case of compounds **4.11A** and **4.11B**. These results are displayed in **Table 6.2**.

Docking orientations of all naphthoquinones within the active site were similar. When overlaid, the naphthoquinone component of the docked ligands occupied a similar region to the purine moiety of ATP, with the prenyl side chain of the ligands occupying similar regions to the sugar moiety and triphosphate chain of ATP (**Figure 6.5A**). Further analysis of the docking conformations indicated deep grove docking for ATP and naphthoquinones, while for geldanamycin (**2.28**), half of the molecule only gets embedded into the active site (**Figure 6.5B**). This could be attributed to the size of the molecule, but nonetheless demonstrated better binding with more hydrogen bonding interactions than most of the naphthoquinones

A **B**

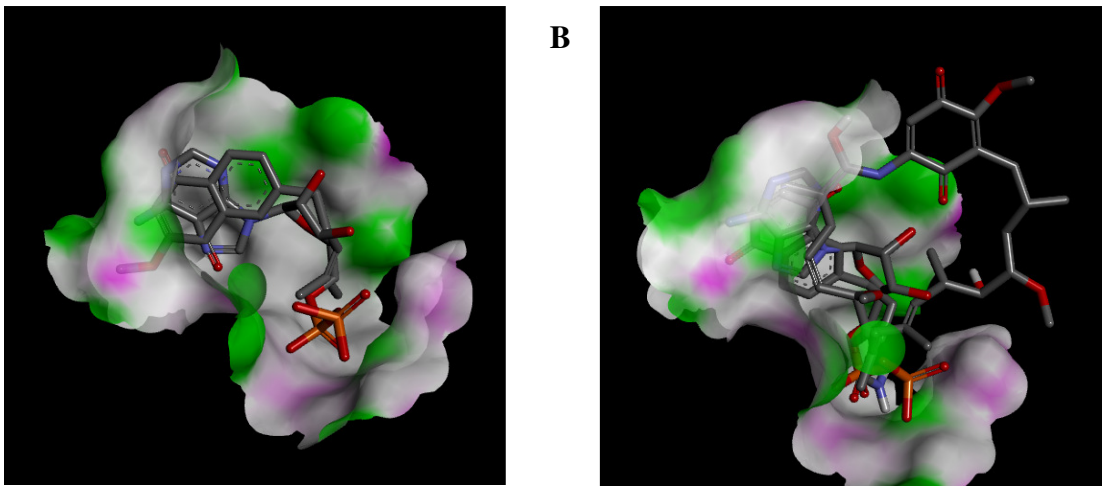

Figure 6.5: A. Compound **4.11B** and ATP docked in the same active site of Hsp90 **B.** Compound **4.10,** geldanamycin (**2.28**) and ATP docked in the same active site of Hsp90

Table 6.2: Binding energies of first series of naphthoquinones in comparison to ATP and Geldanamycin (**2.28**)

Compound	Structure	Binding energies kcal/mol	Number of hydrogen bonds	Number of amino acids in interactions
ATP	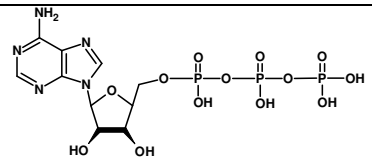	−7.6	6	10
Geldanamycin 2.28	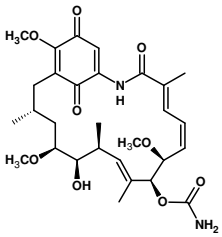	−7.1	4	11
4.7	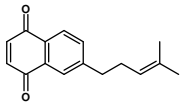	−6.8	0	7
4.9A	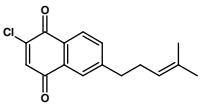	−6.8	1	8
4.9B	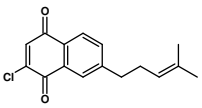	−6.8	1	5
4.11A	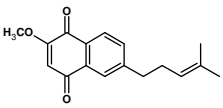	−6.4	0	9
4.11B	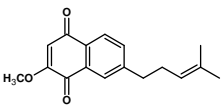	−7.1	2	10
4.13A	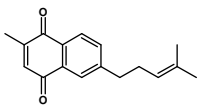	−7.0	1	8
4.13B	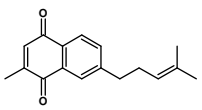	−6.7	1	6

6.2.5 Second series of naphthoquinone analogues (arylamino naphthoquinones)

The second series of analogues that comprised of aniline coupled naphthoquinones was docked in the same way as described above. The binding energies obtained are shown in **Table 6.3**

Table 6.3: Binding energies of aryl amino naphthoquinones in comparison to ATP and Geldanamycin (**2.28**)

Compound	Structure	Binding energies kcal/mol	Number of hydrogen bonds	Number of amino acids in interactions
ATP	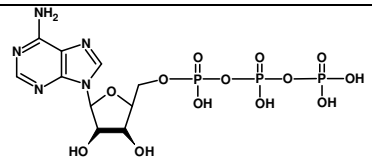	−7.6	6	10
Geldanamycin 2.28	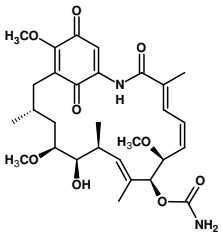	−7.1	4	11
4.14A	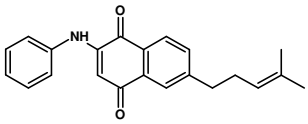	−7.5	2	5
4.14B	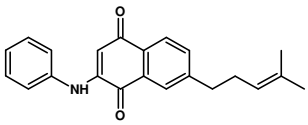	−7.5	2	4
4.15A	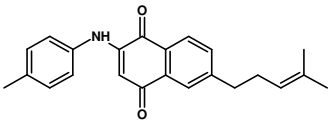	−7.7	2	5
4.15B	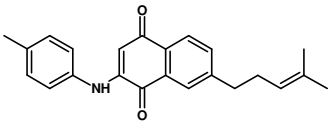	−7.6	2	5
4.16A	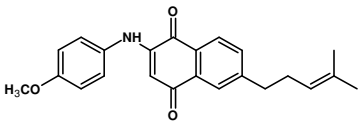	−7.6	2	6
4.16B	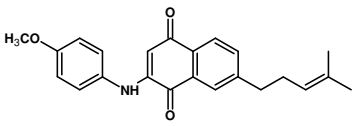	−7.7	3	7

Compound	Structure	Binding energies kcal/mol	Number of hydrogen bonds	Number of amino acids in interactions
4.17A	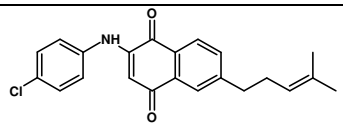	−7.6	2	5
4.17B	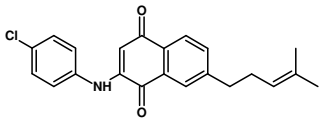	−7.6	2	5
4.18A	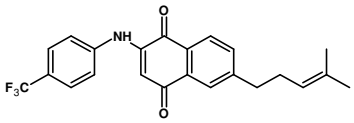	−7.3	2	7
4.18B	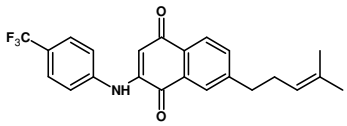	−8.1	4	9
4.19A	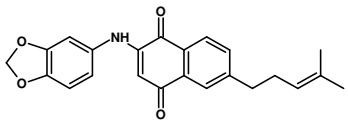	−7.4	4	9
4.19B	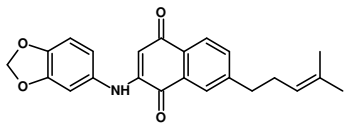	−8.2	3	6

Addition of the arylamino moiety improved binding energies of the naphthoquinones (**4.14-4.19**) to Hsp90 to values above −7.0 kcal/mol. However more active conformations were predicted from docking. The reported results were based on visual assessments of a conformation that matched that of ATP and of results that showed a root mean square distance (rmsd) of 2 or less Å. Whilst other molecules had an average number of two hydrogen bonds, enhanced binding was observed in compounds **4.18B** and **4.19B** with four and three hydrogen bonds respectively. It demonstrated the importance of having hydrogen bond centres offered by H bond acceptors on CF_3 and methylenedioxy moieties. The general trend observed was that C-2 substituted arylamino-naphthoquinones interacted *via* hydrogen bonding using the C-4 ketone on the quinone with GLY123 and PHE124, whilst C-3 substituted arylamino - naphthoquinones interacted with ASN37 and GLY121 *via* C-4 ketone and the –NH linker moiety used for coupling amines to naphthoquinones. This is displayed in **Figure 6.6** using **4.14 A** and **4.14B** as examples.

A **B**

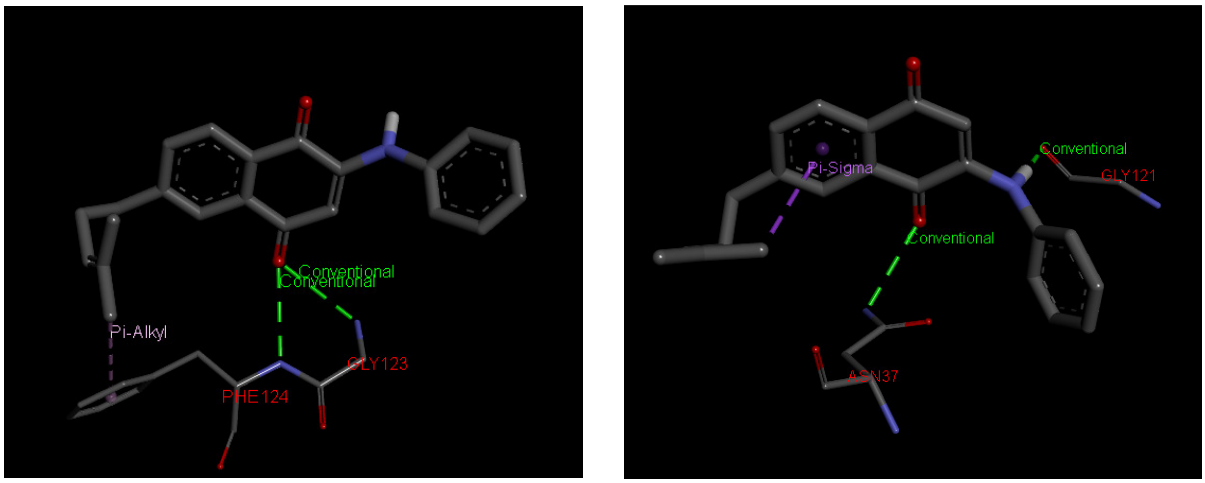

Figure 6.6: **A.** C-2 substituted-naphthoquinone **4.14A** interaction with GLY123 and PHE124 *via* hydrogen bonding **B.** C-3 substituted-naphthoquinone **4.14B** interaction with ASN37 and GLY121*via* hydrogen bonding

The most active conformation assumed with aryl amino naphthoquinones was in a reverse orientation to that observed with the first series of naphthoquinones. The prenyl side chain was embedded into the active site together with the purine nucleoside moiety of ATP, whilst the naphthoquinone functionality orientated with the phosphate groups and aniline component orientated out of the active site.

Introduction of aryl amino moieties influenced the binding behaviour of these molecules. It resulted in molecules possessing comparable binding energies to ATP, with some exhibiting higher binding affinities for Hsp90. An investigation into substituting aryl amino- moieties with alkyl amines was conducted.

6.2.6 Third series of naphthoquinone analogues (alkyl amino naphthoquinones)

The same parameters and preparation protocols were adapted, and docking was conducted as indicated in the first two series of naphthoquinones. The binding energies obtained are shown in **Table 6.4**

Table 6.4: Binding energies of alkyl amino naphthoquinones in comparison to ATP and Geldanamycin (**2.28**)

Compound	Structure	Binding energies kcal/mol	Number of hydrogen bonds	Number of amino acids in interactions
ATP	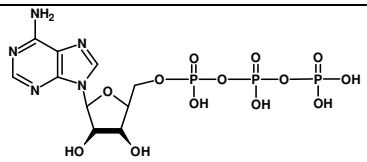	−7.6	6	10
Geldanamycin 2.28	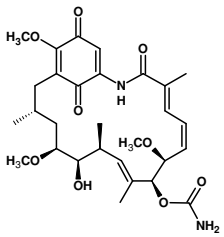	−7.1	4	11
4.20A	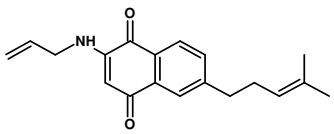	−7.3	2	5
4.20B	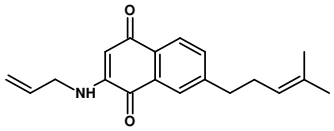	−7.7	0	6
4.21A	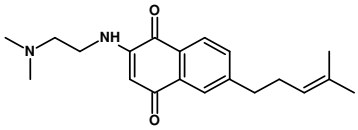	−6.4	2	5
4.21B	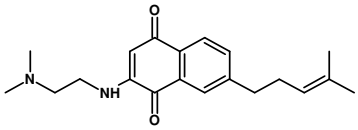	−6.6	1	6
4.22A	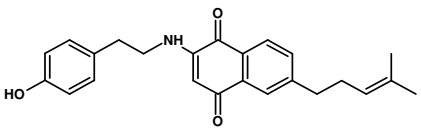	−7.8	3	7
4.22B	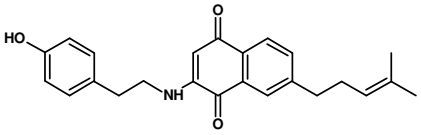	−7.2	3	9

Compound	Structure	Binding energies kcal/mol	Number of hydrogen bonds	Number of amino acids in interactions
4.23A	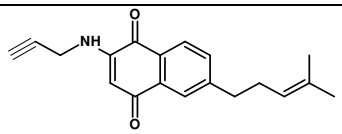	−7.3	2	6
4.23B	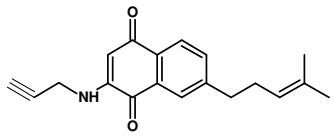	−7.2	1	8
4.24A	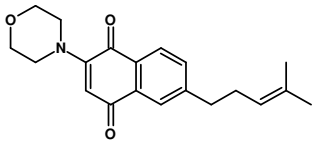	−7.1	0	4
4.24B	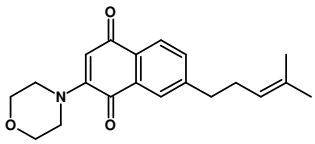	−6.8	2	8
4.25A	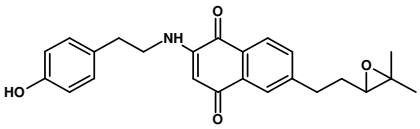	−7.1	4	11
4.25B	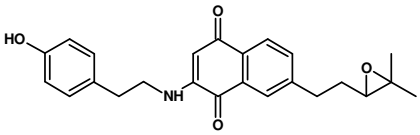	−7.3	3	8
4.26A	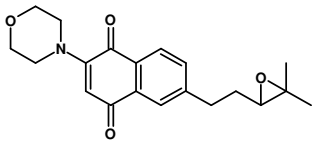	−6.7	3	3
4.26B	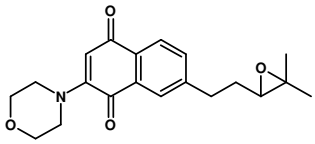	−7.3	0	5

Introduction of alkyl amines in exchange for aryl amines to the core structure slightly lowered the binding affinity of the naphthoquinones to the active site of Hsp90. The best binding energy was observed for compound **4.22A,** with two hydrogen bond interactions between the phenolic OH with GLU33 and SER36, and a third observed between the ketone moiety of the quinone and ASN37. Epoxide containing molecules (**4.25-4.26**) had more hydrogen bond interactions within the active site, however their binding affinity was not enhanced to a greater level. Introduction of a morpholino moiety (**4.24**) also did not enhance binding. The conformation which the ligand assumes within the active site is essential in assuring that functional groups on the ligand and relevant amino acids that can potentially interact with each other are in close proximity within the active site during binding.

Compounds **4.20** and **4.21** had allylamine and *N*, *N*-dimethylethane-1, 2-diamine moieties at C-2 or C-3 positions that mimicked 17-AAG (**2.29**) and 17 DMAG (**2.30**) respectively. **4.20** displayed a better binding energy than **4.21**, which showed the worst binding energy within this series. It is possible that the presence of a terminal tertiary amine in **4.21** is not favourable for binding to the active site.

With regards to the docking conformation, there was no uniform direction from this series of compounds. Compounds **4.20** and **4.23** orientated in a similar way to the first series of compounds, the naphthoquinone moiety occupying the same region as the purine nucleoside of ATP and the prenyl side chain overlaying the sugar and phosphate groups. The rest of the molecules had the prenyl system embedded into the active site, with the naphthoquinone moiety and C-2 or C-3 substituted groups overlaying the sugar and phosphate groups. The docked orientations are available in the supplementary data.

6.2.7 Fourth series of analogues

The effect of having a thiazino- moiety or chromene-hybrid system was also investigated for Hsp90 inhibition. The natural product sargaquinoic acid (**2.47**), sarganaphthoquinonic (**3.5**) and lapachol (**3.6**) were also included for comparison purposes to the synthesized derivatives. Docking experiments were conducted as above and the binding energies obtained are displayed in **Table 6.5**

Table 6.5: Binding energies of tricyclic naphthoquinones in comparison to ATP and Geldanamycin (**2.28**)

Compound	Structure	Binding energies kcal/mol	Number of hydrogen bonds	Number of amino acids in interactions
ATP	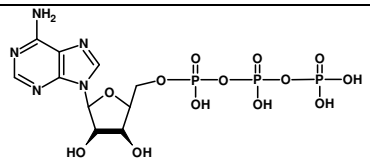	−7.6	6	10
Geldanamycin 2.28	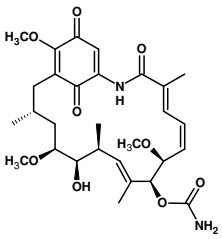	−7.1	4	11
4.28	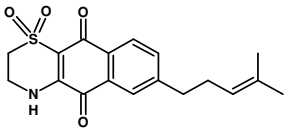	−7.9	0	6
4.29	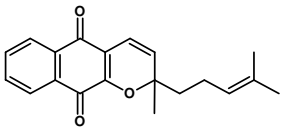	−7.6	1	7
3.6	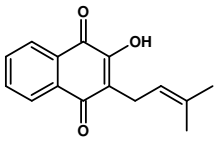	−7.0	1	6
2.47	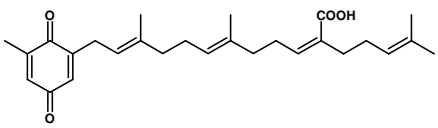	−6.7	3	5
3.5	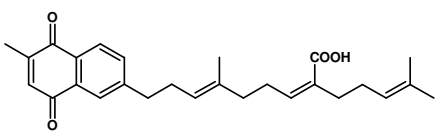	−7.2	1	7

Thiazino-naphthoquinone (**4.28**) and the chromene-naphthoquinone hybrid (**4.29**) also had comparable binding energies to ATP but lacked extensive hydrogen bond networks. Compound **4.29** only had 1 hydrogen bond of the carbonyl to ASN37, with **4.28** having none. This further indicates the importance of other bond-bond interactions that take place within the binding pocket. The two compounds occupied similar regions of the active site and interacted with almost similar numbers of amino acids. Compounds **2.47, 3.5** and **3.6** displayed lesser binding affinities compared to **4.28** and **4.29. 2.47,** however had an established hydrogen bond system with ASN37, GLY123 and PHE124 and displayed a folding conformation to fit within the active site (**Figure 6.7A**). Compound **3.11** also exhibited a similar folding conformation to **2.47** and occupied the same space (**Figure 6.7B**).

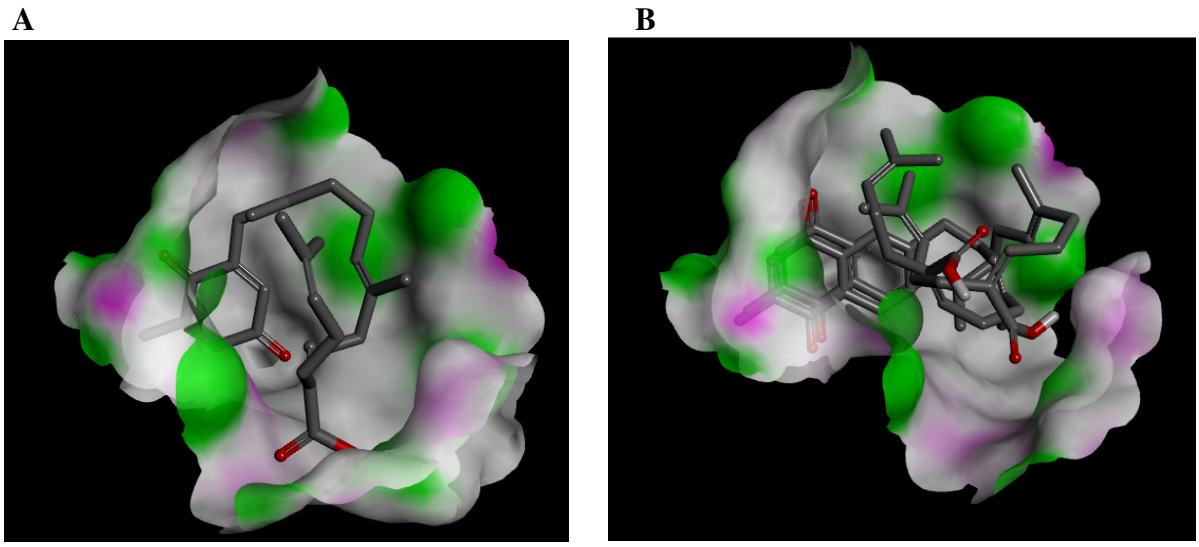

Figure 6.7: A. Sargaquinoic acid (**2.47**) folding to fit within the N-terminal active site of Hsp90 **B**. Folding conformations of **2.47** and **3.5** within the N-terminal active site of Hsp90

Compounds **2.47** and **3.5** had docking orientations similar to the first series of naphthoquinones. The long prenyl chain system however folds on itself, whereas in the first series of naphthoquinones, the chain is shorter and just fits into the active site. Their binding energies were also comparable to those of the first series of compounds, with **2.47** slightly lower. This indicated that the prenyl side chain could be shortened with no influence on the biological activity of these molecules.

These preliminary results indicated that naphthoquinone derivatives possibly bind to the N-terminus of Hsp90 protein. Substitution with aryl amino compounds on the quinone moiety of the naphthoquinone is favoured for better binding and results obtained were comparable to those of ATP. No significant differences were apparent with regards to binding energies

between regioisomers. C-2 or C-3 substitution could not be ascertained as important in conformations assumed by the ligands during the study.

From the docking studies, compounds **4.15A, 4.16B, 4.18B, 4.19B, 4.22A** and **4.28** showed binding affinities slightly better than ATP and presented themselves as potential Hsp90 inhibitors. However it should be noted that molecular docking is a virtual screening tool, which solely depends on estimations and predictions. Definitive conclusions relating to a particular compound and its activity cannot be drawn with certainty unless further studies are conducted.

The results shown are contradictory to those obtained in client protein degradation assays that seemed to suggest C-terminal binding rather than N-terminal binding to Hsp90 due to lack of Hsp70 induction. However, one short-fall with this technique in assessing Hsp90 inhibition is that there is no crystal structure for the C-terminal domain for comparable docking studies to be done. The question still remained unanswered as to the active site to which naphthoquinones bind. Saturation transfer difference (STD) NMR studies that focus on interactions on both binding domains of Hsp90 were attempted.

6.3 Saturation transfer difference (NMR) studies

Molecular interactions between small ligands and relevant biological macromolecules can be studied using Nuclear Magnetic Resonance (NMR) (Lepre, *et al.*, 2004). Saturation Transfer Difference (STD) NMR has become a useful tool in characterizing ligand-receptor complexes in solution, and has been useful in identifying lead structures and ligand moieties that are essential for binding as part of rational drug-discovery process. It makes use of reduced protein/receptor concentrations and can be applied on large molecular weight proteins, giving this technique advantages over other NMR techniques (Mayer and Meyer, 1999).

6.3.1 Principles of STD NMR

STD NMR experiments make use of nuclear Overhauser effects in observing ligand resonance signals that are in contact with the receptor (Viegas, *et al*, 2011). As the name suggests, STD takes into account the difference between the *on-resonance* and *off-resonance* spectra. It involves subtracting signal intensities of the *on resonance* spectrum denoted $I_{SAT,}$ from signal intensities of the *off resonance* spectrum $I_{O,}$ to obtain a difference spectrum I_{STD}, that is represented by the following formula

$$I_{STD} = I_O - I_{SAT}$$

The *on-resonance* experiment encompasses selective saturation by irradiating a region of the spectrum that contains only resonances of the receptor, normally between −1 ppm and 0 ppm where majority of methyl resonances for folded proteins appear. The *off resonance* is set at an irradiation frequency that is far from any ligand or protein signal e.g. 40 ppm. In the difference spectrum, only ligand signals that would have received saturation transfer *via* spin diffusion from the receptor are displayed (Kalk and Berendsen, 1984). Saturation is propagated from the selected receptor protons to other receptor protons *via* intramolecular ^{1}H-^{1}H cross relaxation pathways, and *via* ^{1}H-^{1}H cross relaxation and chemical exchange mechanisms at the ligand-receptor interface to bound molecules. Dissociated molecules carry the saturation state back into solution whilst fresh unsaturated ligands exchange on and off the receptor site. Saturation energy is maintained by application of irradiation energy which results in an increase in saturated free ligands in solution.

Other molecules that do not bind to the receptor and might be present in the sample will not receive saturation transfer, hence the difference spectrum will not show any signals. The *on resonance* and *off resonance* signals will be of the same intensity. This is demonstrated in

Figure 6.8 that indicates the differences in I_O, I_{SAT} and I_{STD} spectra of the ligand and non-ligand entities.

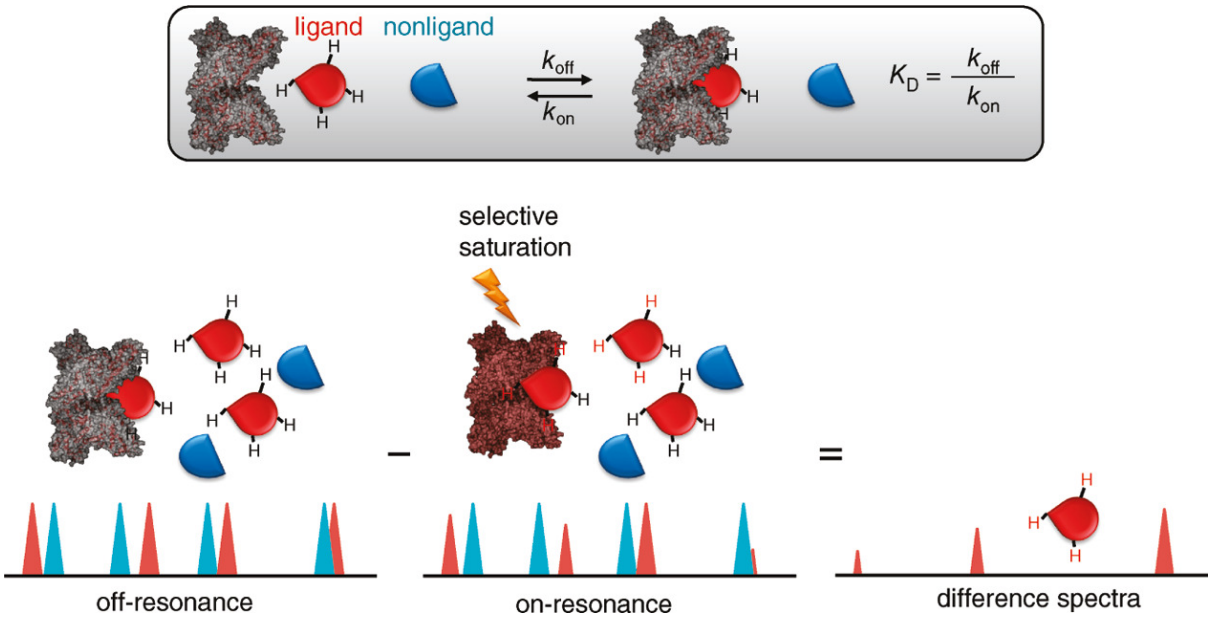

Figure 6.8: A schematic representation of the STD-NMR experiment. The exchange between free and bound ligand allows intermolecular transfer of magnetization from the receptor to the bound small molecule (Viegas, *et al*, 2011).

For the bound ligand, hydrogens that are ≤ 5 Å in proximity to the protein interface receive saturation transfer and appear in the difference spectrum. The closer the hydrogen to the receptor/protein, the greater the intensity of the signal observed due to efficient saturation transfer (Viegas, *et al*, 2011). It should also be noted that only signals of the ligand appear on the spectrum. The receptor resonances are normally not visible due to the concentrations used, and lessen the complexity of the spectra obtained. However a $T_{1\rho}$ filter can be used to remove disturbing protein signals prior to detection, otherwise a simple 1D ^{1}H spectrum of the bound ligands is obtained.

6.3.2 Limitations of STD NMR studies

Several aspects have been identified that affect the quality of results obtained from STD NMR experiments. Sensitivity is a big factor for this technique. It is highly dependent on ligand concentrations that are normally in excess (between 10-100 fold), such that the probability of molecules in solution that receive saturation is increased. However high ligand concentrations in relation to the protein may also result in non-specific ligand binding, causing interference with the obtained STD spectrum. An optimal ligand concentration has to be decided upon or additional experiments are done to negate the effect of non-specific binding (Viegas, *et al*., 2011).

Saturation times set on the instrument are important to allow transfer of saturation from the receptor to more than one ligand molecule in the solution. Long saturation times of up to three seconds are usually suggested, thereby increasing signal intensities observed on the STD spectrum. This compensates for the minute concentrations of the protein used during the experiments, and are a critical factor in these studies that can compromise the quality of results obtained (Viegas, *et al*., 2011; Yan, *et al*, 2003).

The STD NMR methods also fall short in analysing high affinity ligands. Saturation is not transferred to the solution effectively due to the longer periods spend by the ligand bound to the receptor. At the same time, probability of weaker ligands being in the active site during irradiation is very low, resulting in weak STD signals. It therefore suggests that this technique is depended on the receptor in question and the value of K_D for a particular ligand which should fall within the range of $10^{-8} < K_D < 10^{-3}$ M for the STD experiment to be successful (Ji, *et al*., 2009).

Despite these limitations, STD NMR is still being used extensively in the analysis of ligand-protein complexes in solution (Haselhorst, *et al*., 2009). Care should be taken in setting the parameters and optimizing the experiment to suit the study at hand. For our work, we employed this technique to obtain preliminary results for Hsp90 binding at N- and C- terminal domains.

6.3.3 Aim of study

The client protein degradation assay results (section 5.3) showed a lack of Hsp70 activation. This was suggestive of C-terminal binding of naphthoquinones to Hsp90. However, molecular docking results also indicated potential N-terminal binding for these compounds. Such conflicting results led us to decide on an alternative technique that could allow us to visualize and characterize interactions of naphthoquinones with both N- and C-terminal domains of Hsp90. Saturation transfer difference (STD) NMR seemed to be the most appropriate technique to employ as it is quick, easy to do and does not require characterization of the protein's binding site for it only focuses on signals of the ligand. Therefore the main aim of this section was to perform STD NMR studies on selected naphthoquinones on both N- and C- terminal domains to determine the actual site for naphthoquinone binding.

6.3.4 N- and C-terminal domains of Hsp90

The Hsp90 N- and C-terminal domains used were expressed and purified by Dr Adrienne L. Edkins and Lorraine Mutsvunguma of the Biomedical Biotechnology Research Unit (BioBru) at Rhodes University, South Africa. The protein was expressed and tagged to glutathione *S*-transferase (GST), whose DNA sequence is frequently integrated into expression vectors for the production of recombinant proteins. GST is normally incorporated due to its stable folding conformation and highly soluble nature, which promotes solubility of the recombinant protein and greater protein expression compared to expression without the tag (Harper and Speicher, 2001).

The GST tag also allows purification of the protein based on the ability of GST to bind to its substrate, glutathione (GSH). Reduced GSH is immobilized on a solid support such as cross-linked beaded agarose, and such enzyme-substrate reactions ensure that pure GST tagged proteins are isolated from other non-bonded components. The pure tagged protein is recovered by addition of excess reduced GSH that competitively dislodges the GST tagged protein from the solid support and is then eluted from the affinity column. The GST tag can be removed after the purification step if need be, by use of protease enzymes provided a cleavage site had been included between the GST and protein in the DNA design of the vector (Harper and Speicher, 2011). For this study, GST (used as a control) and the GST-tagged Hsp90 fusion proteins were purified by GST batch purification and a Coomassie stained SDS-PAGE showing the respective domains of Hsp90 protein (**Figure 6.9**).

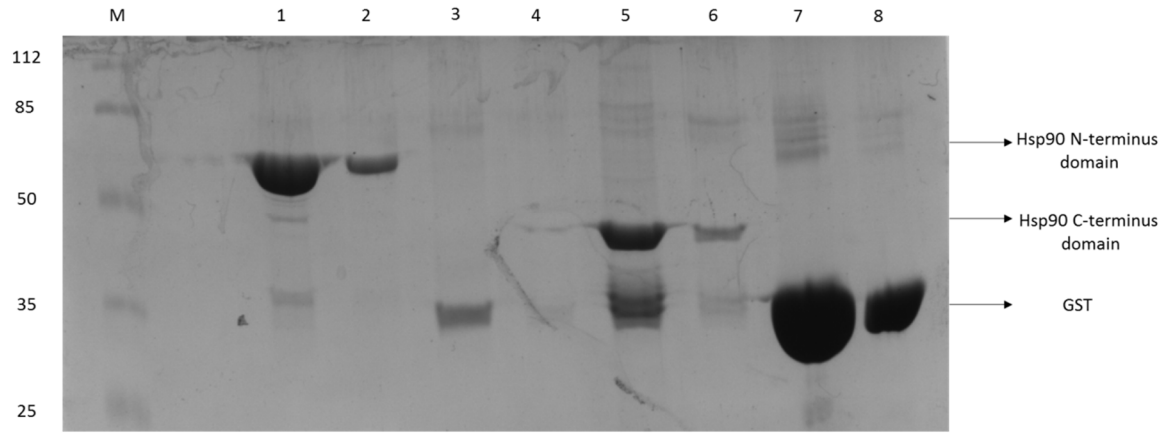

Figure 6.9: GST-tagged Hsp90 N, M and C domains.

Coomassie stained SDS-PAGE showing the purification of GST and GST-Hsp90 fusion proteins after GSH affinity chromatography using a batch purification protocol. Lane M: Molecular weight marker with sizes indicated as kDA, Lane 1-2: GST-Hsp90N elution fractions, Hsp90 N-terminal domain fused to an N-terminal GST tag, Lane 3-4: GST-Hsp90M elution fractions, Hsp90 M domain fused to an N-terminal GST tag, Lane 5-6: GST-Hsp90C elution fractions, Hsp90 C-terminus fused to an N-terminal GST tag, Lane 7-8: GST protein elution fractions.

6.3.5 Selected naphthoquinones

Due to limited amounts of protein, we could only analyse a small selection of compounds. Compounds **2.47, 4.16A, 4.20A, 4.28** and **4.29** used for the client protein degradation assays were also selected for use in the STD NMR studies. This was done such that comparisons could be made between the various techniques reported in this thesis for the assessment of Hsp90 inhibition i.e. molecular docking, client protein degradation assays and STD NMR studies.

6.3.6 Standardization of the STD experimental conditions

An STD assay using bovine serum albumin (BSA) with *L*-tryptophan and glucose was carried out to validate and optimize the STD parameters. *L*-tryptophan is a known ligand of BSA whereas glucose, a non-ligand was added as a negative control. Solutions of BSA (8.4×10^{-5} M), *L*-tryptophan (7.75×10^{-3} M) and D-glucose (5.32×10^{-2} M) were made in 50 mM Tris/HCl buffer (pH 7.3). A total volume sample of 500 µL was prepared in an NMR tube containing 25 µL of D_2O, 240 µL of BSA, 120 µL of Tris/HCl buffer, 130 µL of *L*-tryptophan and 19 µL of glucose such that the final assay solution constituted 40 µM BSA, 2 mM *L*-tryptophan and 2 mM glucose in Tris/HCl buffer. The STD NMR experiment was run on a 500 MHz Bruker NMR spectrometer using water suppression at 4.7 ppm, with the on-resonance pulse train set

to 422 Hz and the off resonance pulse train set to 20 000 Hz ppm with phase cycling. The pre-saturation Gaussian pulse was applied for 2 ms and 16 scans were run.

The STD-NMR spectrum obtained for the mixture of BSA, *L*-tryptophan, and glucose is depicted in **Figure 6.10**. The reference spectrum (**A**) for the mixture under study displayed signals of the two ligands whilst in (**B**), only strong STD signals from *L*-tryptophan were noticeable. The absence of STD signals from glucose is in accordance with the fact that glucose does not bind to BSA, whilst *L*-tryptophan is an active ligand of the protein. The validation was therefore successful and set parameters on the instrument were used in the STD experiments conducted with selected naphthoquinones and Hsp90 N- and C-terminal domains.

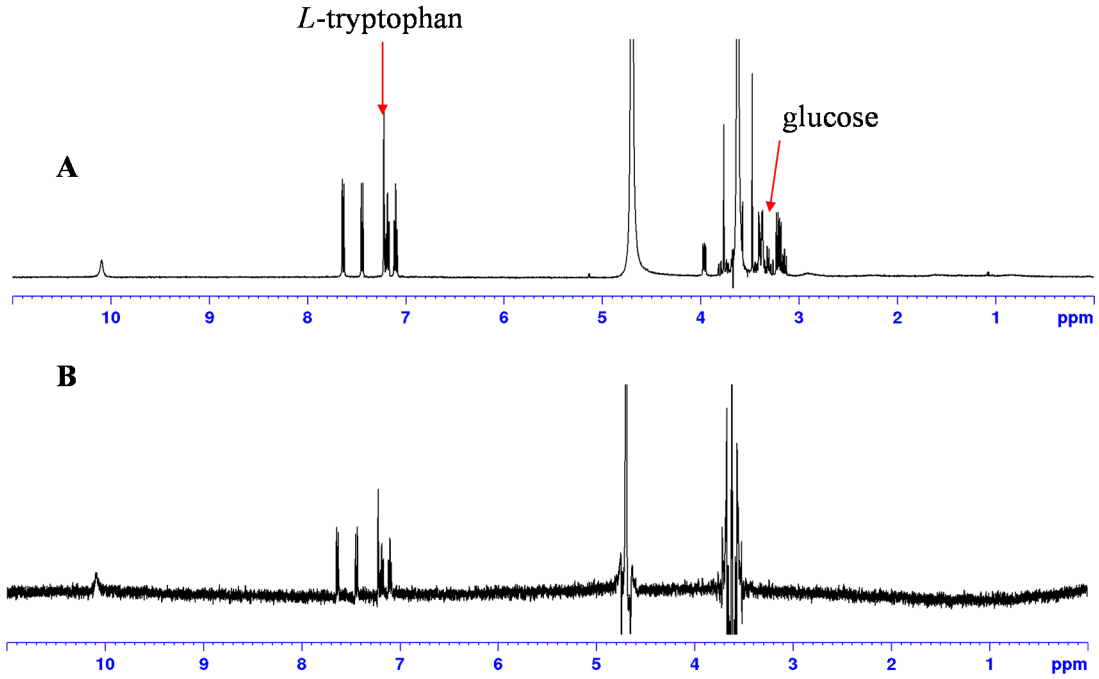

1.

Figure 6.10: The STD-NMR validation experiment: (**A**) reference ^{1}H spectrum for the mixture of BSA, *L*- tryptophan and glucose and (**B**) corresponding STD-NMR spectrum.

6.3.7 Results and discussion

The STD NMR experiments with Hsp90 N- and C- terminal domains were initially conducted using novobiocin (**2.41**), a known C-terminal inhibitor. According to our knowledge, this was the "first" STD NMR study of novobiocin (**2.41**) and the C-terminal domain of Hsp90.

Novobiocin (**2.41**) binds to the C-terminus of Hsp90, and as expected saturation transfer was observed to the bound ligand in the STD NMR spectrum (**Figure 6.11).** The fairly visible signals of the chromene moiety on novobiocin (**2.41**) suggested that the chromene system was

in close proximity to the C-terminal receptor interface during binding, hence received more saturation. Results for the N-terminal binding of Hsp90 by novobiocin (**2.41**) showed a very weak interaction (**Figure 6.12**). A positive result with novobiocin (**2.41**) and the C-terminus confirmed the appropriateness of the set parameters on the NMR instrument, and also confirmed the integrity of the protein being used.

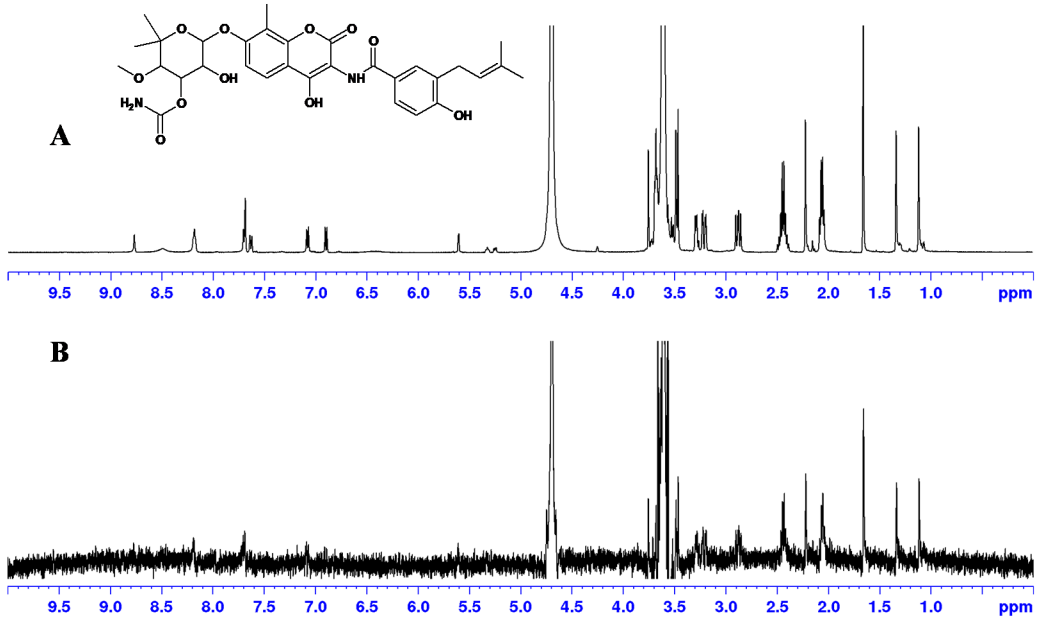

Figure 6.11: (**A**) reference ^{1}H spectrum for the mixture of C-terminal domain of Hsp90 and novobiocin (**2.41**) (**B**) corresponding STD-NMR spectrum

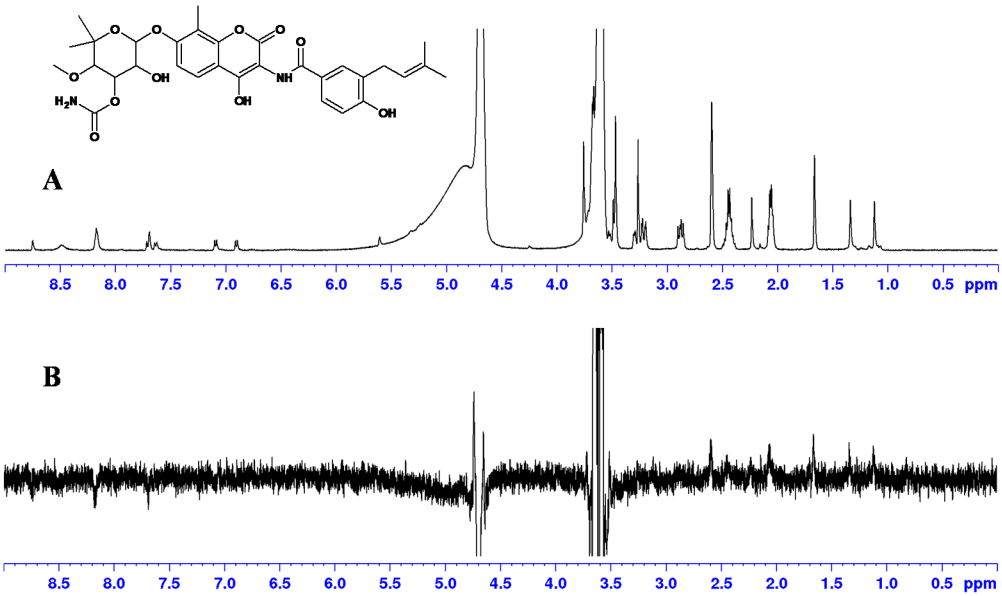

Figure 6.12: (**A**) reference ^{1}H spectrum of the N-terminal domain of Hsp90 and novobiocin **(2.41)** (**B**) corresponding STD-NMR spectrum

6.3.7.1 Attempted STD NMR studies of selected naphthoquinones

The selected naphthoquinones were insoluble in the 50 mM Tris/HCl buffer solution, therefore stock solutions of the individual compounds were first prepared in deuterated DMSO, and dilutions made accordingly to required concentrations in NMR tubes. The set NMR parameters used for the experiments with novobiocin were employed for the selected set of naphthoquinone derivatives. The reference ^{1}H NMR spectra and the corresponding STD NMR spectra obtained for compounds **4.20A, 4.28** and **2.47** and the C-terminus are shown in **Figures 6.13 - 6.15.**

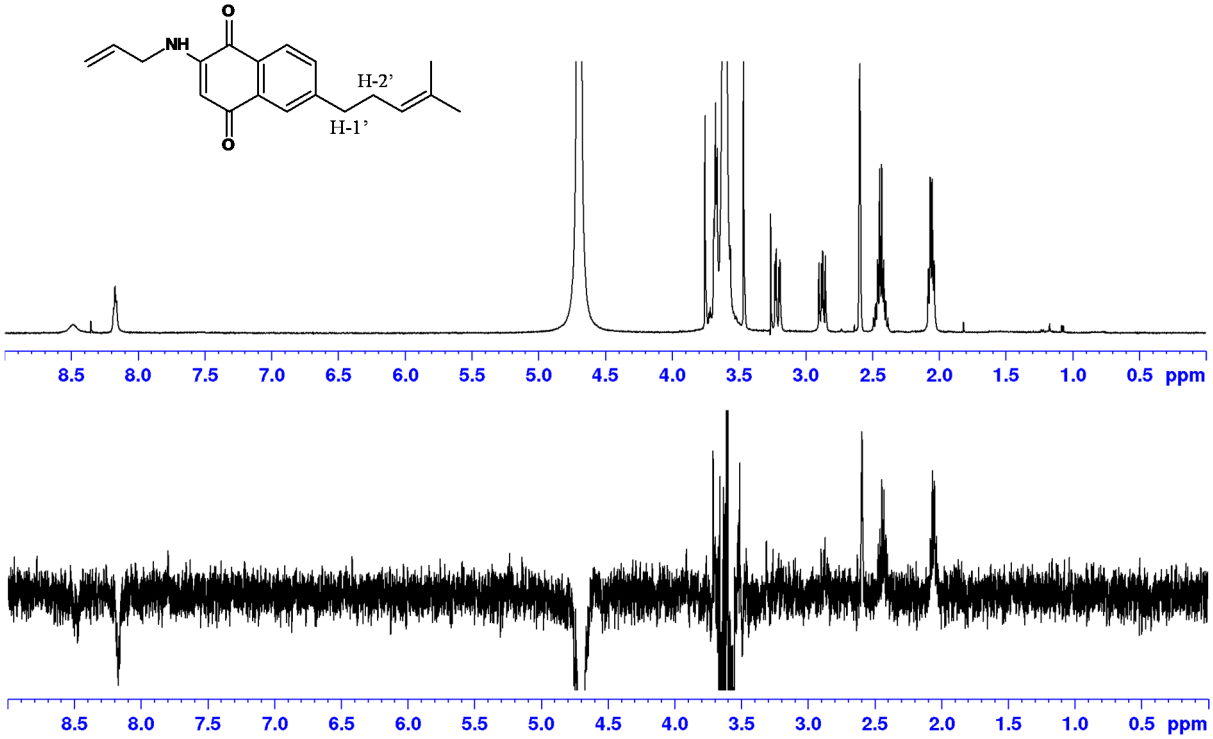

Figure 6.13: (**A**) reference ^{1}H spectrum for the mixture of C-terminal domain of Hsp90 and **4.20A** (**B**) corresponding STD-NMR spectrum

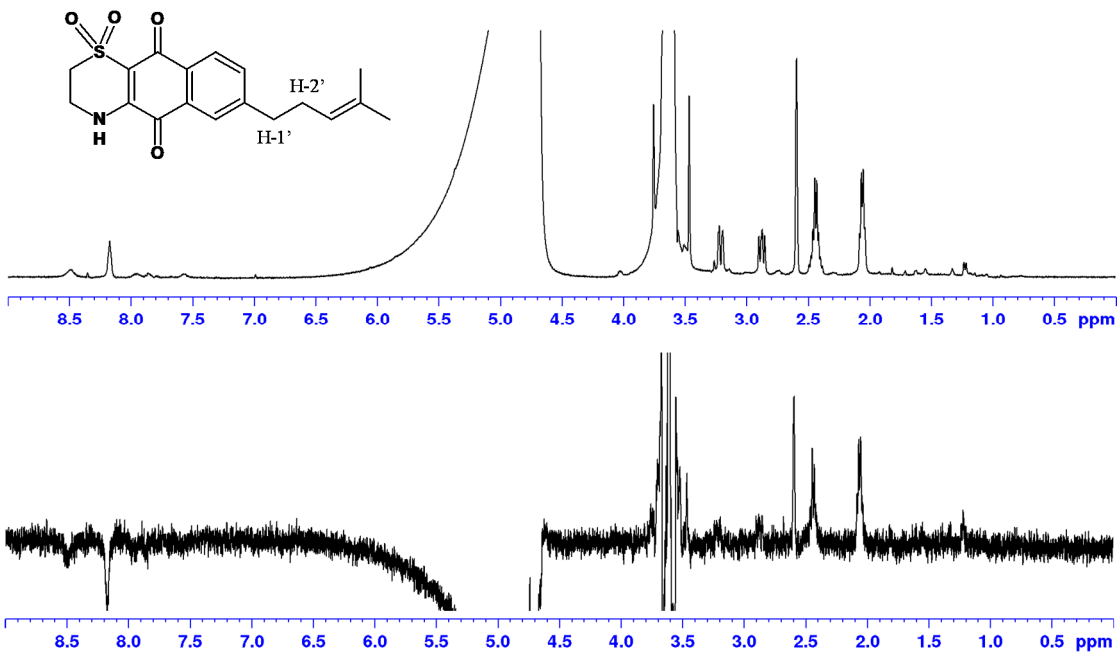

Figure 6.14: (**A**) reference ^{1}H spectrum of the C-terminal domain of Hsp90 and **4.28** (**B**) corresponding STD-NMR spectrum

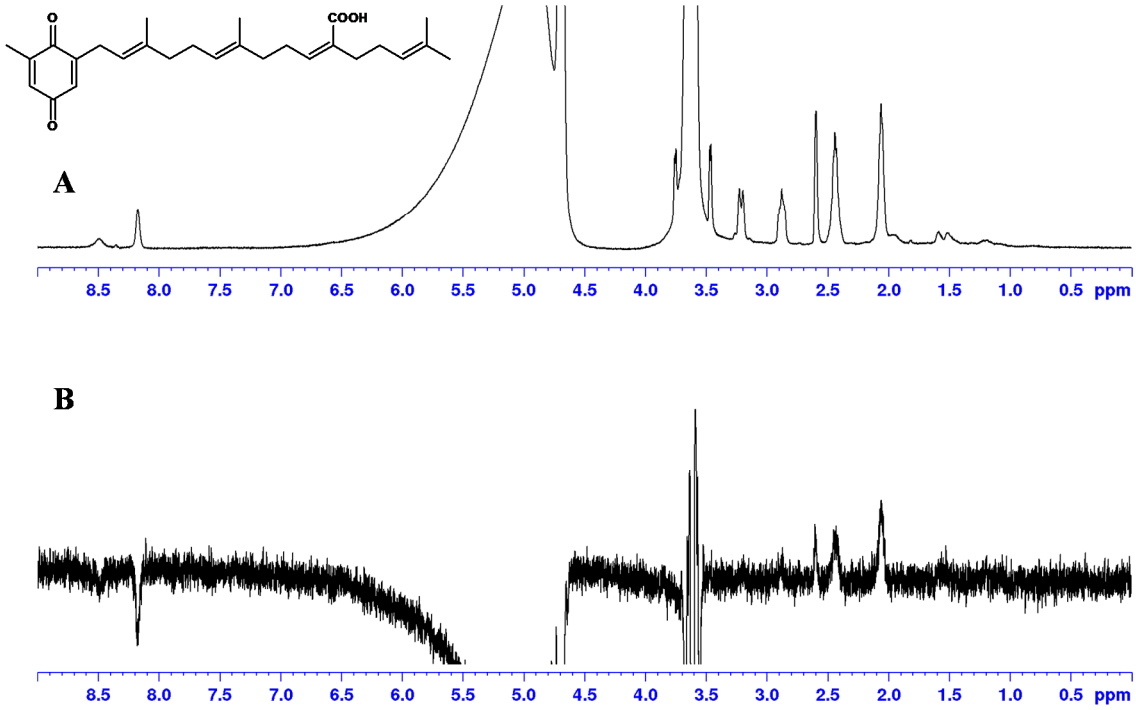

Figure 6.15: (**A**) reference ^{1}H spectrum of the C-terminal domain of Hsp90 and **2.47** (**B**) corresponding STD-NMR spectrum

Resonance signals of the synthesized naphthoquinones were absent from all the NMR spectra obtained. The signals observed at δ 2.0, δ 2.45, δ 2.85 and δ 3.25 were present in each and every spectrum, possibly indicating the presence of an impurity in the tested samples**.** After careful analysis, the signals noticed belonged to glutathione introduced during the protein's purification. The same results were observed in the STD NMR experiments conducted of the test compounds and the N-terminus. Resonances due to the synthesized compounds could also not be observed as shown in **Figures 6.16 – 6.18**.

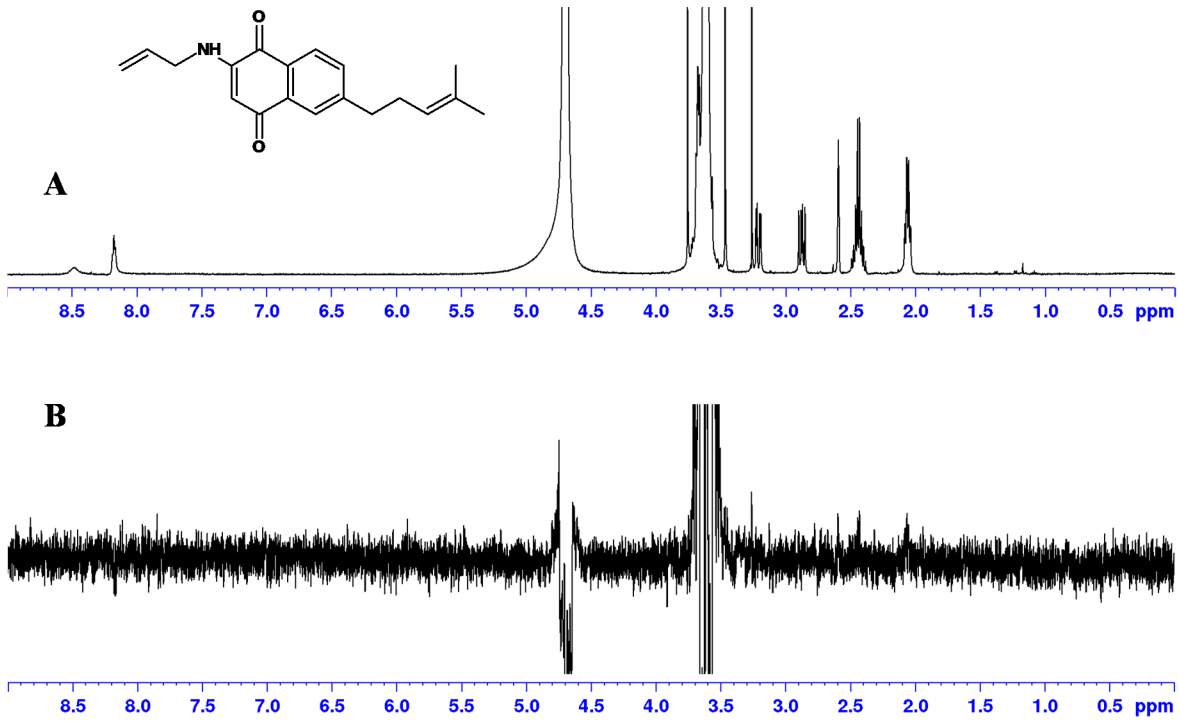

Figure 6.16: (**A**) reference ^{1}H spectrum of the N-terminal domain of Hsp90 and **4.20A** (**B**) corresponding STD-NMR spectrum

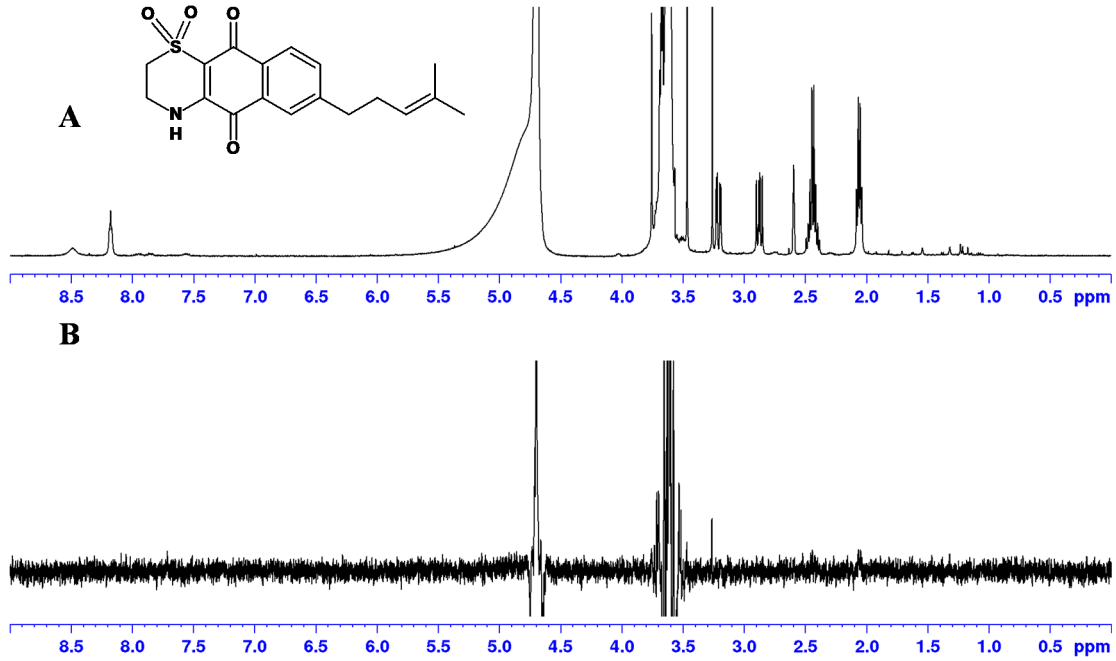

Figure 6.17: (**A**) reference ^{1}H spectrum of the N-terminal domain of Hsp90 and **4.28** (**B**) corresponding STD-NMR spectrum

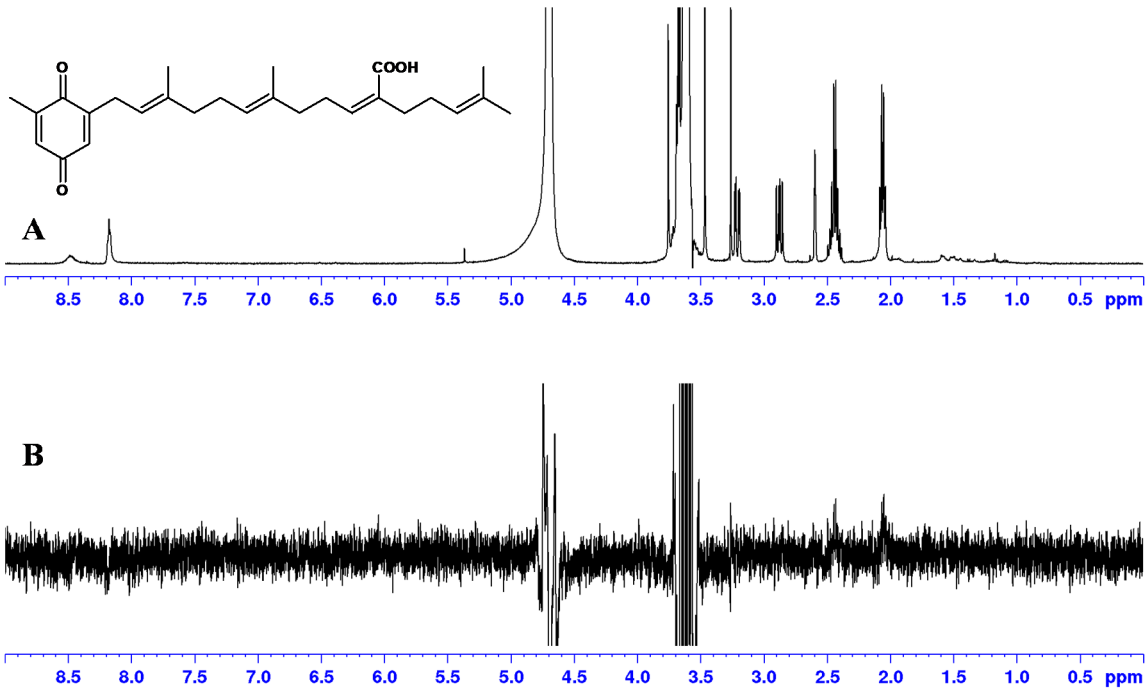

Figure 6.18: (**A**) reference ^{1}H spectrum of the N-terminal domain of Hsp90 and **2.47** (**B**) corresponding STD-NMR spectrum.

Lack of STD NMR signals corresponding to the test compounds indicated no saturation transfer at the receptor-ligand interface. The NMR parameters set on the spectrometer had been validated using BSA / *L*-tryptophan, and novobiocin / C-terminus experiments. The possibility of inaccurate STD NMR parameters used in conducting experiments with the naphthoquinones was therefore ruled out. The ligand: protein ratio of 60:1 used for the selected synthesized compounds and Hsp90 was similar to that used for novobiocin and the C-terminus. Lack of resonance signals on the STD NMR spectra could also not be attributed to incorrect ligand: protein ratios during the runs. One of two reasons might have been responsible for the lack of resonance signals on the STD NMR spectra, i.e. weak binding of the ligands to the N- or C-termini of Hsp90 or poor water solubility of the naphthoquinone derivatives in the test solution.

Weak binding to the relevant active site results in a lesser than optimum time required for the ligand to be in contact with the receptor to receive saturation, hence the STD signals obtained are either weak or non-existent. As indicated previously, the value of K_D for a particular ligand should fall within the range of $10^{-8} < K_D < 10^{-3}$ M for the STD experiment to be successful (Ji, *et al*., 2009). We hypothesize that the synthesized naphthoquinones might have been out of this range, hence the lack of STD NMR resonances corresponding to the tested compounds. However this aspect requires further investigation.

With regards to solubility, the initial attempts to dissolve the naphthoquinones in the 50 mM Tris/HCl buffer were unsuccessful. DMSO was added to aid the solubility of the compounds in the buffer before the STD NMR experiments were conducted. However absolute dissolution could not be guaranteed as a limited volume of DMSO constituting to 3 % of the total volume of solvent in the NMR tube could not be exceeded. Poor water solubility could have compromised interaction between the ligand and the protein which resulted in no ligand binding being observed.

Further STD studies are required to investigate molecular interactions between naphthoquinones and Hsp90 N- and C-terminal domains. Client protein degradations assays indicated some form of inhibition of the protein, which we are confident occurs. An increase in both ligand and protein concentrations can be attempted to increase the sensitive of the technique, and more scans can be used during the runs to observe any weak binding interactions that might occur. Unfortunately the presented STD NMR data was inconclusive, and posted questions regarding N- terminal or C-terminal binding by naphthoquinones could not be answered in this regard.

The STD NMR spectra for **4.16A** and **4.29** are presented in the supplementary data and also showed negative results as indicated for the other tested compounds (**Figures S6.81, S6.83, S6.85** and **S6.88**).

6.4 Conclusion

The STD NMR results obtained showed ligand binding to neither the N-terminus nor C-terminus of Hsp90, a result which did not support the data from the client protein degradation assays. We propose lack of solubility of naphthoquinones in the test solution or weak binding interactions between the naphthoquinones and Hsp90 as possible reasons why negative results were obtained with this technique. However, little is known with regards to Hsp90 and STD NMR experiments and this serves as a platform on which experiments can be conducted to assess binding to Hsp90 domains, especially at the C-terminal domain that has a co-crystal structure that still has to be resolved. Molecular docking studies had indicated that naphthoquinones could potentially bind to the N-terminal domain, however computational methods are based on estimations and predictions which in some cases can give misleading results. In light of these preliminary results, the new series of naphthoquinone derivatives that was synthesized inhibit Hsp90 function, but conclusions could not be drawn as to which active site they bind to, either the N- terminus or C-terminus.

6.5 Experimental

6.5.1 *In silico* Hsp90 inhibition assay

6.5.1.1 Ligand preparation for docking

Structures of all ligands described in this chapter were sketched in Discovery Studio Visualizer 4.0 with the hydrogens missing, which were later added and geometry of all bonds corrected before saving as pdb files. The pdb files were reopened in AutoDock Vina and addition of gasteiger charges was carried out. All non-polar hydrogens were merged and TORSDOF set. The individual files were then saved as PDBQT files that were used for docking experiments.

6.5.1.2 Hsp90 Protein Preparation for Docking

The X-ray crystal structure of the N-terminal domain of Hsp90 protein (PDB code: 1AM1) was obtained from the Protein Data Bank. The water molecules and ATP ligand were stripped off prior to saving it as an *apo* protein in PDB format. Preparation of the *apo* protein using AutoDock tools involved merging all non-polar hydrogens with the addition of polar ones. A total gasteiger charge of -9.9969 was added and an AD4 type assigned to all atoms before saving it as a PDBQT file that was used for docking experiments.

6.5.1.3 Docking Experiments

The 'search space' in the coordinate system of the receptor was chosen. The experimental bound ligand structure was used and coordinates were selected that were 30 Å larger for each dimension i.e. x, y, z from the selected centre point. The centre coordinates chosen that included the target site for binding were 15.253, -1.123, -4.212 for x, y, z respectively. Dockings were conducted twice for comparison, firstly with an exhaustiveness of 32 and then an exhaustiveness of 8. A Lamarckian genetic algorithm was employed for the docking simulation in AutoDock vina and default genetic algorithm parameters were used.

The docked conformations were visualized in Discovery Studio Visualizer 4.0. The docked conformers were assessed based on binding energies, hydrogen bond networks and other bond-bond interactions, and visual assessment of the orientation of the conformers at the active site of the enzyme.

6.5.2 Expression and purification of N- and C- terminal domains of Hsp90

6.5.2.1 Plasmids

Recombinant GST was expressed from the pGEX-4T1 plasmid, while recombinant GST-tagged Hsp90 domains were expressed from plasmids GST-Hsp90 N(9-236) (Addgene plasmid #22481), GST-Hsp90 M(272-617) (Addgene plasmid #22482) and GST-Hsp90 C(626-732) (Addgene plasmid #22483) kindly provided by William Sessa.

6.5.2.2 Plasmid expression and protein purification

XL Blue 1 E. coli cells were transfected with different GST-tagged Hsp90 domain plasmids indicated above, after which protein expression was induced for 3 hours with 1 mM IPTG. Post expression, cell were harvested by centrifugation at 4 °C for 10 minutes at 6000 x *g* and the pellet resuspended in Phosphate buffered saline (PBS) containing lysozyme and phenylmethylsulfonyl fluoride (PMSF) at a final concentration of 1 mg/ml and 1 mM, respectively and stored at -80°C. The lysates were thawed on ice, followed by 10 rounds of sonication for 30 seconds with 15 second cooling periods in between. Lysate clarification was done by centrifuging at 10000 x *g* for 30 minutes at 4 °C. The clarified lysates were added to pre-washed Protino® Glutathione Agarose resin (Thermo Scientific, USA) and the mixture incubated for 30 minutes at room temperature with gentle shaking. The mixture was centrifuged at 500 x *g* for 5 minutes. The supernatant was decanted, and the resin washed three times with 10 bead volumes of PBS. Each wash step was followed by centrifugation at 500 x *g* for 5 minutes. After the wash steps, 1 bead volume of GST elution buffer (50 mM Tris pH 8, 10 mM glutathione) was added to the agarose resin and incubated with gentle shaking at room temperature for 10 minutes, followed by centrifugation at 500 x *g* for 5 minutes. The elution step was repeated twice, with the resulting supernatant transferred to new Eppendorf tubes. Four aliquots of each for the N terminus, C-terminus and GST control were prepared at a concentration of 1.05 mg/ml, 1.14 mg/ml and 7 mg/ml respectively and kept at -80 °C until use. Success of the purification protocol was evaluated by SDS-PAGE and Coomassie blue staining.

6.5.3 STD NMR studies

6.5.3.1 STD NMR studies of novobiocin and the C-terminus of Hsp90

Novobiocin (2.5 x 10^{-7} moles)(**2.41**) was dissolved in a Tris/HCl 50 mM buffer and transferred to the NMR tube such that its final concentration was 0.5 mM in a total NMR volume of 500 µL. The C-terminal protein was thawed and a sample (4.2 x 10^{-8} moles) transferred to the same NMR tube with novobiocin (**2.41**) with the aim of having a final protein concentration of 9 µM in a 500 µL volume of sample, and a protein to ligand ratio of approximately 1:60. 25 µL D_2O was added, with the deficit volume covered by the Tris/HCl buffer to a total volume of 500 µL.

6.5.3.2 STD NMR studies of naphthoquinones and the N- and C- termini of Hsp90

Weighed samples (1-2 mg) of test compounds (**2.47, 4.16A, 4.20A, 4.28** and **4.29**) were dissolved in pre-calculated volumes of deuterated DMSO that resulted in 15 µL of the individual stock solutions containing 2.5 x 10^{-7} moles of the ligand. Each aliquot of the protein contained 0.1 mg of the N- or C-terminal domain in 100 µL of Tris/HCl buffer, of which half the volume was used for each sample preparation which was equivalent to 4.2 x 10^{-8} moles of the C-terminus and 2 x 10^{-9} moles of the N-terminus. For the C-terminal domain sample preparations, 15 µL of ligand stock solution, 50 µL of C-terminal domain solution, 25 µL of D_2O and 410 µL of Tris/HCl 50 mM buffer were constituted in the NMR tube for the STD NMR experiments. For the N-terminal domain sample preparations, 7.2 µL of ligand stock solution, 50 µL of N-terminal domain solution, 25 µL of D_2O and 417.8 µL of Tris/HCl 50 mM buffer were constituted in the NMR tube for the STD NMR experiments.

6.5.3.3 STD NMR parameters: As set in the standardization experiment.

The STD NMR experiments were run on a 500 MHz Bruker NMR spectrometer using water suppression at 4.7 ppm, with the on-resonance pulse train set to 422 Hz and the off resonance pulse train set to 20 000 Hz ppm with phase cycling. The pre-saturation Gaussian pulse was applied 2 ms and 16 scans were run.

References

Bohm, H. (1998). Prediction of binding constants of protein ligands: a fast method for the prioritization of hits obtained from de novo design or 3D database search programs. *Journal of Computer-Aided Molecular Design, 12*, 309–323.

Accelrys Software Inc., Discovery Studio Modeling Environment, Release 4.0, San Diego: Accelrys Software Inc. (2013). Retrieved from http://accelrys.com/products/discovery-studio/index.html

Bailey, D., & Brown, D. (2001). High-throughput chemistry and structure-based design: survival of the smartest. *Drug Discovery Today, 6*, 57-59.

Castro, F., Mariani, D., Panek, A., Eleutherio, E., & Pereira, M. (2008). Cytotoxicity mechanism of two naphthoquinones (menadione and plumbagin) in Saccharomyces cerevisiae. *PLoS ONE, 3*, 1-6.

Frydman, J. (2001). Folding of newly translated proteins in vivo: the role of molecular chaperones. *Annual Review of Biochemistry, 70*, 603–647.

Hadden, M., Hill, S., Davenport, J., Matts, R., & Blagg, B. (2009). Synthesis and evaluation of Hsp90 inhibitors that contain the 1, 4- naphthoquinone scaffold. *Bioorganic and Medicinal Chemistry, 17*, 634–640.

Harper, S., & Speicher, D. (2001). Expression and purification of GST fusion proteins. In *Current Protocols in Molecular Biology* (Chapter 6, Unit 6.6).

Harper, S., & Speicher, D. (2011). Purification of proteins fused to glutathione S-tranferase. *Methods in Molecular Biology, 681*, 259–280.

Haselhorst, T., Lamerz, A., & I. M. (2009). Saturation transfer difference NMR spectroscopy as a technique to investigate protein-carbohydrate interactions in solution. *Methods in Molecular Biology*, 375-386.

He, W., Wu, L., Gao, Q., Du, Y., & Wang, Y. (2006). Identification of AHBA biosynthetic genes related to geldanamycin biosynthesis in Streptomyces hygroscopicus 17997. *Current Microbiology, 52*, 197-203.

Ji, Z., Yao, Z., & Liu, M. (2009). Saturation transfer difference nuclear magnetic resonance study on the specific binding of ligand to protein. *Analytical Biochemistry, 385*(2), 380-382.

Kalk, A., & Berendsen, H. J. (1984). Proton magnetic relaxation and spin diffusion in proteins. *Journal of Magnetic Resonance, 24*, 343-366.

Kollman, P. (1993). Free energy calculations: applications to chemical and biochemical phenomena. *Chemical Reviews, 93*, 2395–2417.

Lepre, C. A., Moore, J. M., & Peng, J. W. (2004). Theory and applications of NMR-Based screening in pharmaceutical research. *Chemical Reviews, 104*, 3641–3675.

Mayer, M., & Meyer, B. (1999). Characterization of ligand binding by saturation transfer difference NMR spectroscopy. *Angewandte Chemie-International Edition, 38*, 1784-1788.

McConkey, B., Sobolev, V., & Edelman, M. (2001). The performance of current methods in ligand-protein docking. *Current Science, 83*, 845–855.

Miyata, Y., Nakamoto, H., & Neckers, L. (2013). The therapeutic target Hsp90 and cancer hallmarks. *Current Pharmaceutical Design, 19*, 347-365.

Morris, G., Goodsell, D., Halliday, R., Heuy, R., Hart, W., Belew, R., & Olson, A. (1998). Automated docking using a Lamarckian genetic algorithm and an empirical binding free energy function. *Journal of Computational Chemistry, 19*, 1639-1662.

Morris, G., Goodsell, D., Huey, R., & Olson, J. (1996). Distributed automated docking of flexible ligands to proteins: parallel applications of AutoDock 2.4. *Journal of Computer-Aided Molecular Design*, *10*, 293-304.

Moyo, B. (2013). *The screening and characterisation of compounds for modulators of Heat shock protein (Hsp90) in a breast cancer cell model.* (Phd) Rhodes University.

Muegge, I., & Martin , Y. (1999). A general and fast scoring function for protein-ligand interactions: a simplified potential approach. *Journal of Medicinal Chemistry, 42*, 791–804.

Neckers, L., & Workman, P. (2012). Hsp90 Molecular chaperone inhibitors: are we there yet? *Clinical Cancer Research, 18*, 64-76.

Stark, J., & Powers, R. (2012). Application of NMR and molecular docking in structure-based drug discovery. *Topics in Current Chemistry, 326*, 1-34.

Trott, O., & Olson, A. (2010). AutoDock Vina: improving the speed and accuracy of docking with a new scoring function, efficient optimization and multithreading. *Journal of Computational Chemistry, 31*, 455–461.

Viegas, A., Manso, J., Nobrega, F., & Cabrita, E. (2011). Saturation-Transfer Difference (STD) NMR: a simple and fast method for ligand screening and characterization of protein binding. *Journal of Chemical Education, 88*, 990–994.

Wiley, E. A., Macdonald, M., Lambropoulos, A., Harriman, D. J., & Deslongchamps, G. (2006). LGA-Dock/EM-Dock — Exploring Lamarckian genetic algorithms and energy-based local search for ligand–receptor docking. *Canadian Journal of Chemistry, 84*, 384–391.

Yan, J. L., Kline, A. D., Mo, H. P., Shapiro, M. J., & Zartler, E. R. (2003). The effect of relaxation on the epitope mapping by saturation transfer difference NMR. *Journal of Magnetic Resonance, 163*, 270-276.

Yuriev, E., Agostino, M., & Ramsland, P. A. (2011). Challenges and advances in computational docking: 2009 in review . *Journal of Molecular Recognition, 24*, 149–164.

CHAPTER SEVEN

Conclusion

All results obtained for cytotoxicity and Hsp90 inhibition assays/experiments were pooled together in this chapter and conclusions drawn to determine if our set goal was achieved. From the preliminary results obtained, cytotoxicity of naphthoquinones was successfully enhanced into the nanomolar range. A degree of Hsp90 inhibition was imparted by introduction of alkylamines and a thiazino-moiety on the naphthoquinone. Overall, moderately cytotoxic Hsp90 inhibitors were synthesized that could serve as lead compounds for further development.

It was previously shown that sargaquinoic acid (**2.47**) inhibited Hsp90 function. However, this compound exhibited relatively weak cytotoxic activity against a MDA-MB-231 breast cancer cell line. The recent discovery of naphthoquinone derivatives as Hsp90 inhibitors (Hadden, *et al*., 2009) encouraged us to explore the potential of prenylated naphthoquinones as Hsp90 inhibitors.

The main goal of the study was therefore to develop cytotoxic Hsp90 inhibitors, inspired by chemical structures of sargaquinoic acid (**2.47**), sarganaphthoquinoic acid (**3.5**) and lapachol (**3.6**). Isolated metabolites from *S. incisifolium* demonstrated weak cytotoxic activities with IC_{50} values of 658.0 µM and 2140.0 µM against a MDA-MB-231 breast cancer cell line for compounds **2.47** and **3.5** respectively. The naphthoquinone, lapachol (**3.6**) showed much better activity against Hs578T breast cancer carcinoma (triple negative) with an IC_{50} value of 2.1 µM.

The synthesized naphthoquinones showed improved cytotoxic properties, especially the aryl amino-naphthoquinones (**4.14-4.19**). Compounds **4.15** and **4.16** were the most potent with average IC_{50} values of 0.5 µM and 1.1 µM, respectively against Hs578T breast cancer carcinoma (triple negative). No significant differences were noticed between the isomers in terms of their biological activity except for compound **4.18**. It was deduced that for cytotoxic enhancement of naphthoquinones, aryl amino-moieties gave the best results.

Hsp90 inhibition was assessed using *in vitro* and *in silico* methods. *In vitro* assessment of the naphthoquinones was conducted *via* client protein degradation assays in which moderate Hsp90 inhibition by test compounds was observed. In this study, not all compounds could be tested, therefore selection was done based on the cytotoxicity results obtained. Compounds **2.47, 4.16A, 4.20A, 4.28** and **4.29** were selected and **2.47** displayed the most potency as an Hsp90 inhibitor, followed by **4.20A**. The allylamine moiety on **4.20A** that is also observed on 17-AAG (**2.29**) seemed influential in Hsp90 binding. Compounds **4.16A, 4.28** and **4.29** were less potent, with **4.29** being the least amongst the group. With all these compounds, no Hsp70 induction was noticed as was with the case with geldanamyin (**2.28**) that was used as a control. It led us to postulate that most likely Hsp90 binding was occurring at the C-terminus. This conclusion was made on the basis of novobiocin (**2.41**) having a similar effect of not inducing an increase in Hsp70 concentrations in client protein degradation assays. Perhaps two controls should have been used that represented both N- and C- terminal domains of Hsp90. Several deductions could be made from the client protein degradation assay results that needed clarification and included;

i) naphthoquinones possibly binding to the C-terminal domain of Hsp90
ii) naphthoquinones binding to both domains but with a higher affinity for the C-terminal end
iii) naphthoquinones binding to the N-terminus but with no Hsp70 induction.

We had hypothesized that this series of naphthoquinones might bind to the N-terminus since functionalities of geldanamycin (**2.28**) and its analogues (**2.29-2.30**) were incorporated onto the naphthoquinone scaffold. We therefore assessed possible binding to the N-terminus using molecular docking studies.

Analysis of possible binding to the N-terminus of Hsp90 was conducted using AutoDock Vina. All synthesized derivatives (**4.10-4.31**), **2.47, 3.5** and **3.6** were docked and comparable binding energies to ATP were noticed from arylamino-naphthoquinones (**4.14-4.19**) and **4.20B.** According to the results obtained, it seemed to suggest that the N-terminal domain of Hsp90 is the binding site for naphthoquinones especially with binding energies that were comparable to ATP. Unfortunately, the co-crystal structure of the C-terminal end has not been resolved yet, therefore comparable docking studies on the C-terminus could not be conducted. Interaction on the C-terminal end could only be assessed by STD NMR studies.

The STD NMR experiments were conducted on both N- and C-terminal domains of Hsp90. Novobiocin (**2.41**) was used as a control and to our knowledge such a study involving STD NMR experiments of novobiocin and the C-terminal domain of Hsp90 had not be done. This gave some preliminary exciting results that indicated binding of novobiocin to the C-terminus *via* its chromene type system. Similar compounds used in the client protein degradation assays were also used for the STD NMR experiments. However no binding interactions could be observed on both N- and C- termini all the NMR spectra obtained, which could be attributed to limited sensitivity of the technique. Meaningful conclusions could not be drawn from the STD NMR experiments.

In summary we successfully developed a new set of moderately active compounds with cytotoxic and Hsp90 inhibition properties. The best candidates from amongst the series of naphthoquinones prepared were compounds **4.20** and **4.28**. These two derivatives can serve as lead compounds for further development in the treatment of cancer.

Further structural modifications can be conducted on the naphthoquinone scaffold to enhance cytotoxicity and Hsp90 inhibition properties. Of interest will be to convert this class of compounds into molecular probes that can be used in *in vivo* studies. From our series, we

managed to synthesize compound **4.23** that contains an alkyne functionality. A deeper understanding into the mechanism of action of naphthoquinones can be probed *via* fluorescent probe synthesis using click chemistry reactions with compound **4.23,** or by attaching biotin in an effort to pull out proteins to which naphthoquinones bind to in cancer cells. Naphthoquinones are a promising class of compounds that can be probed further as lead compounds in drug designing and development for treatment of cancer.

Synthesis and Biological Evaluation of Truncated Sarganaphthoquinoic Acid Derivatives as Hsp90 Inhibitors

A Thesis Submitted in Fulfillment of the Requirements

for the Degree of

DOCTOR OF PHILOSOPHY (PHARMACY)

of

RHODES UNIVERSITY

By

Maynard T. Chiwakata

February 2015

CHAPTER THREE

Supplementary data

Isolation and characterization of selected natural products

The selected natural product quinones presented in chapter three are known compounds, and have been published in literature. The ^{13}C NMR spectra for these compounds that were not shown in the thesis are displayed in this section.

LIST OF FIGURES

S. incisifolium metabolites

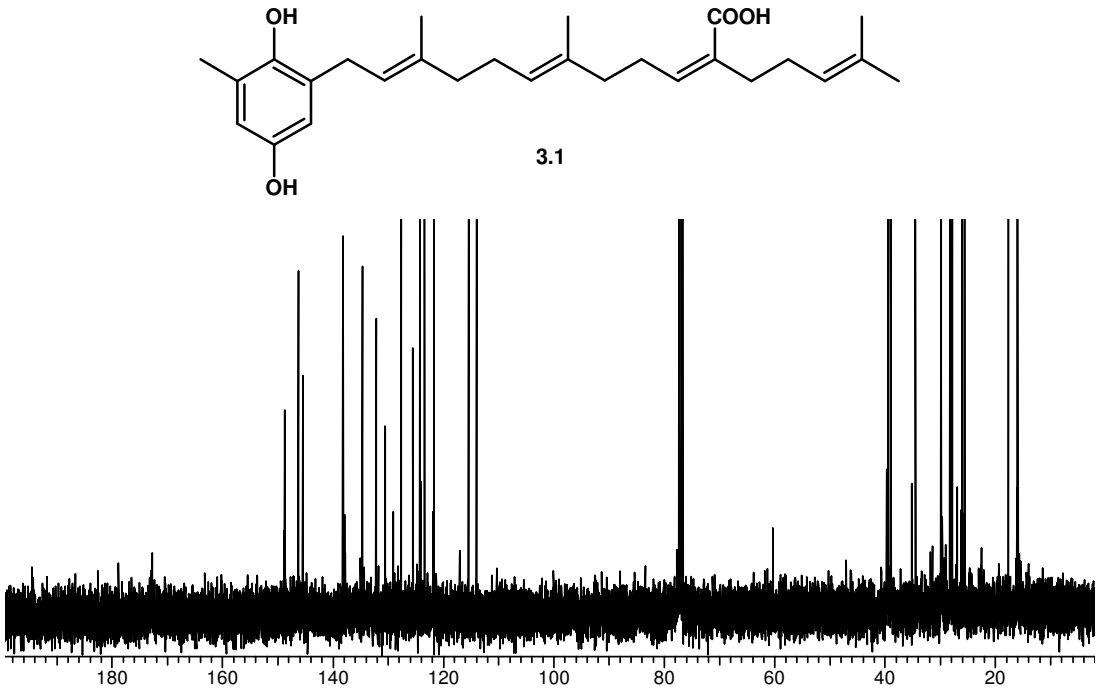

Figure S3.1: ^{13}C NMR spectrum (150 MHz, $CDCl_3$) of compound **3.1**

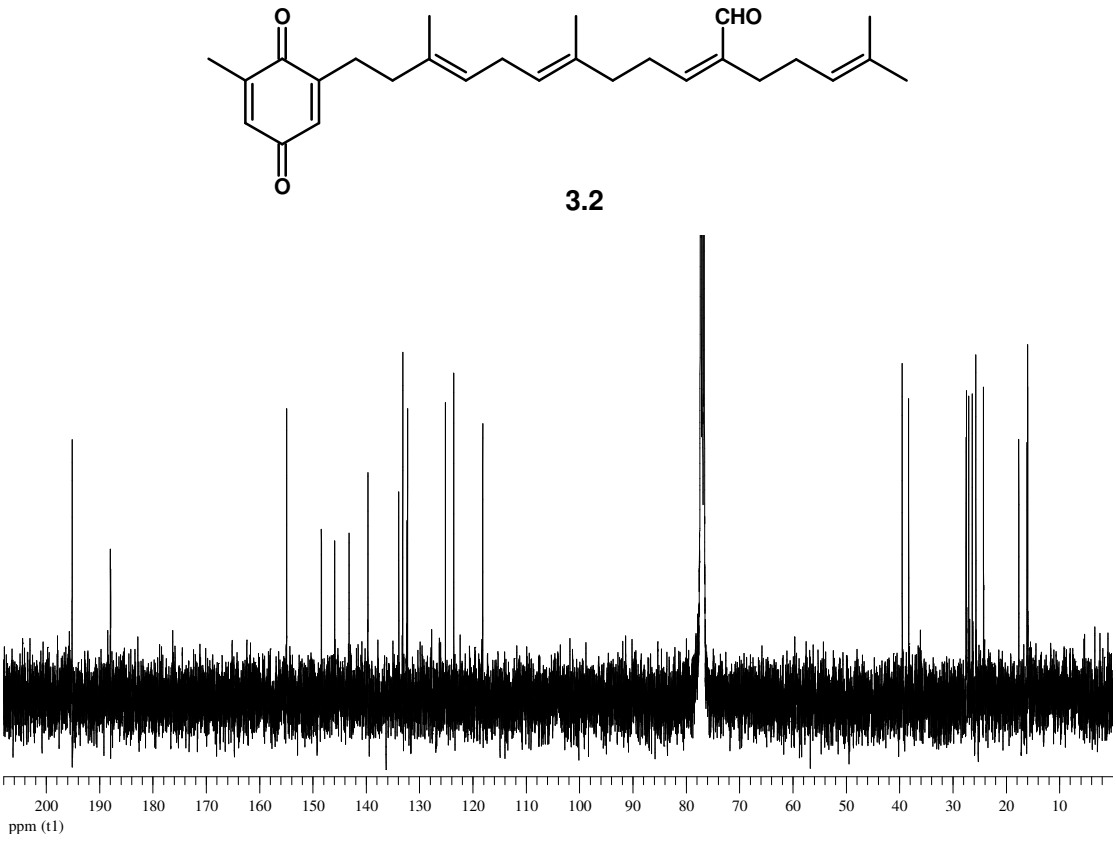

Figure S3.2: ^{13}C NMR spectrum (150 MHz, $CDCl_3$) of compound **3.2**

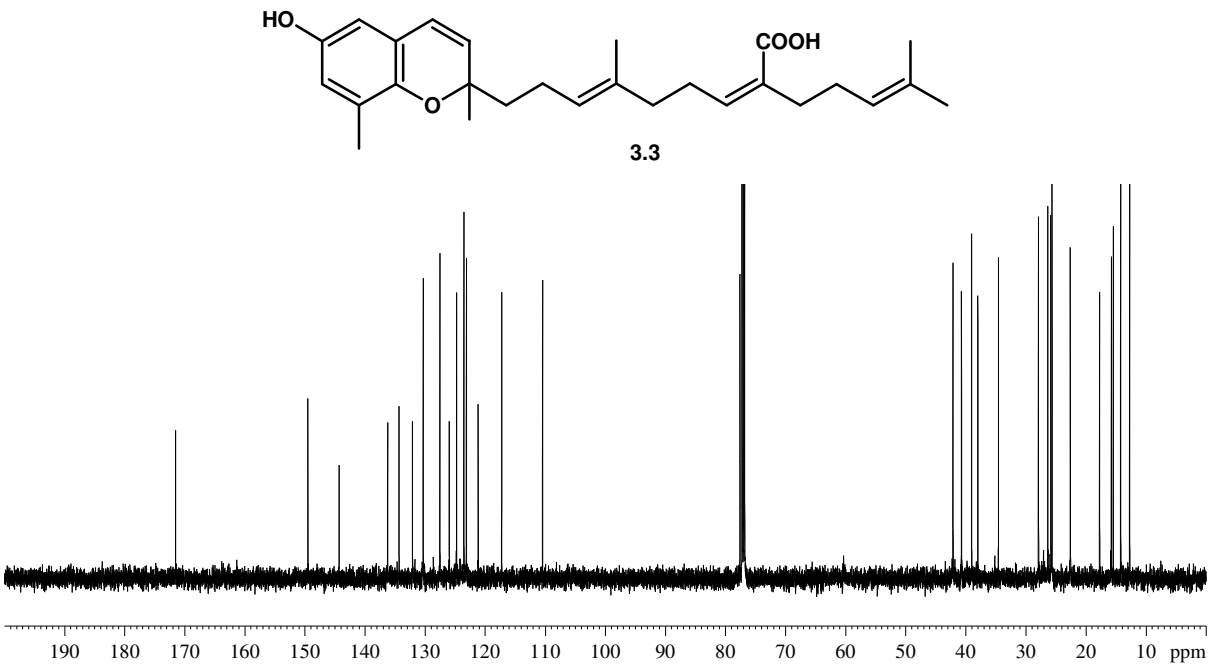

Figure S3.3: ^{13}C NMR spectrum (150 MHz, $CDCl_3$) of compound **3.3**

Lapachol and related compounds

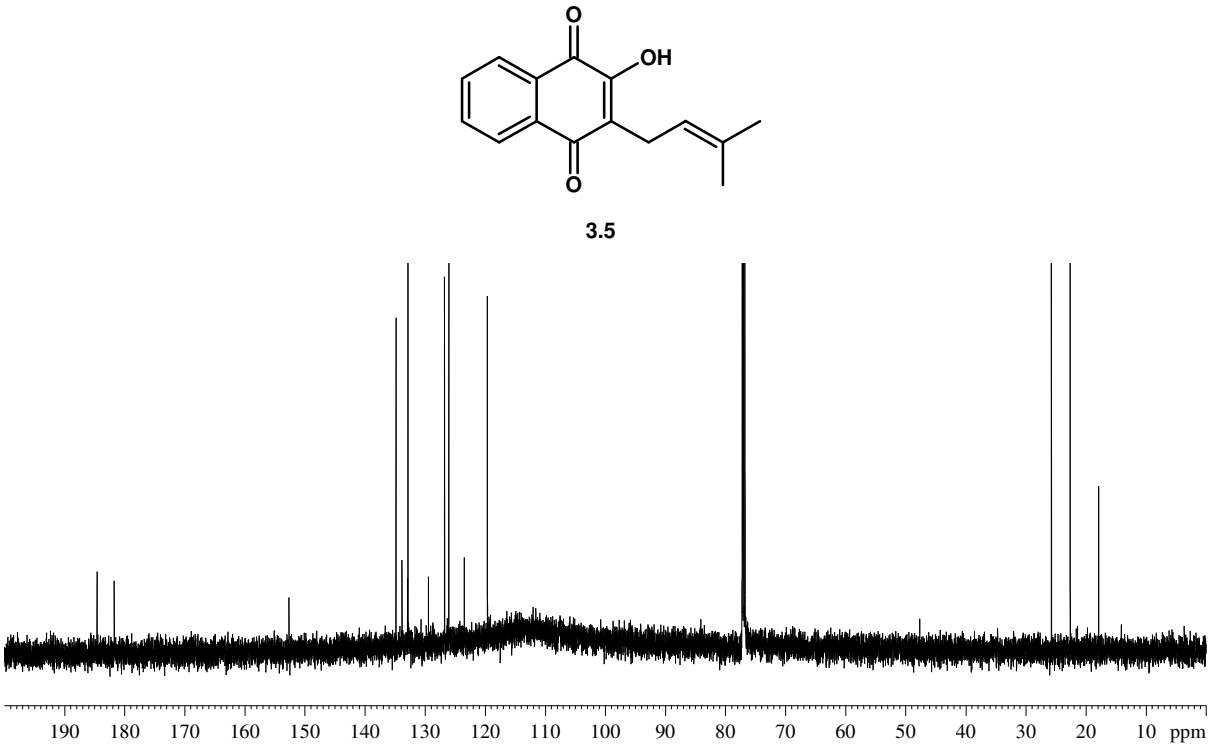

Figure S3.4: ^{13}C NMR spectrum (150 MHz, $CDCl_3$) of compound **3.6**

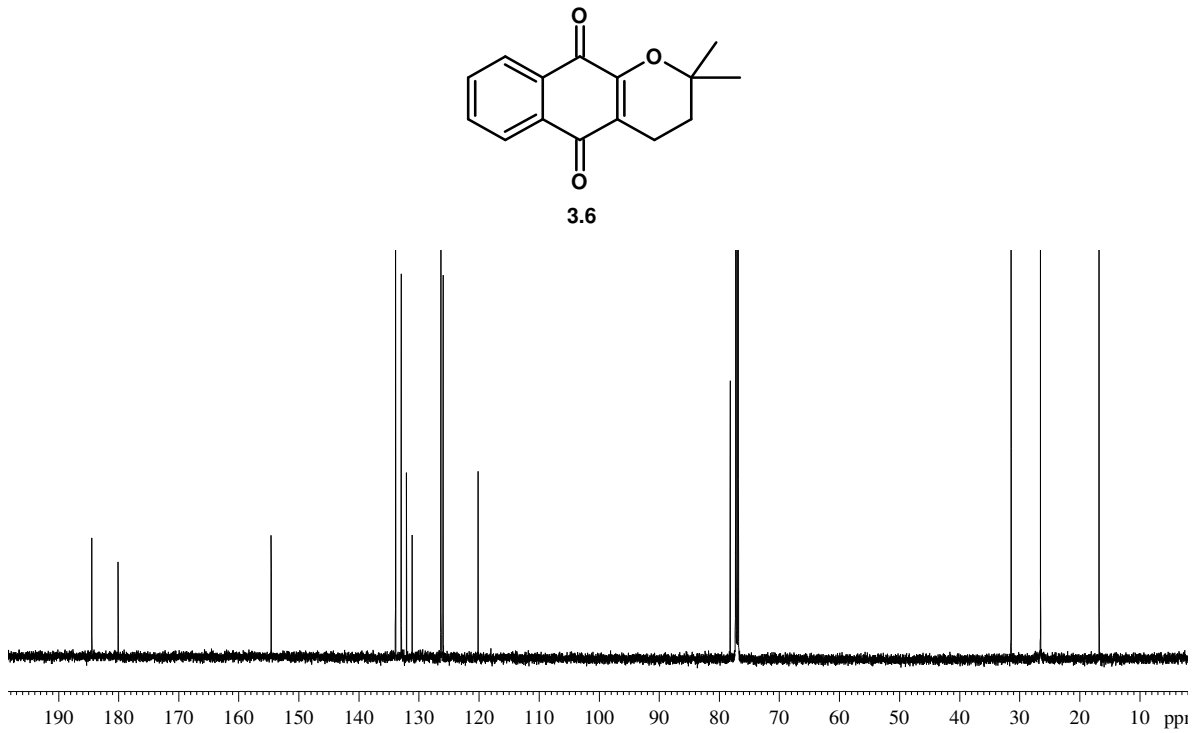

Figure S3.5: ^{13}C NMR spectrum (150 MHz, $CDCl_3$) of compound **3.7**

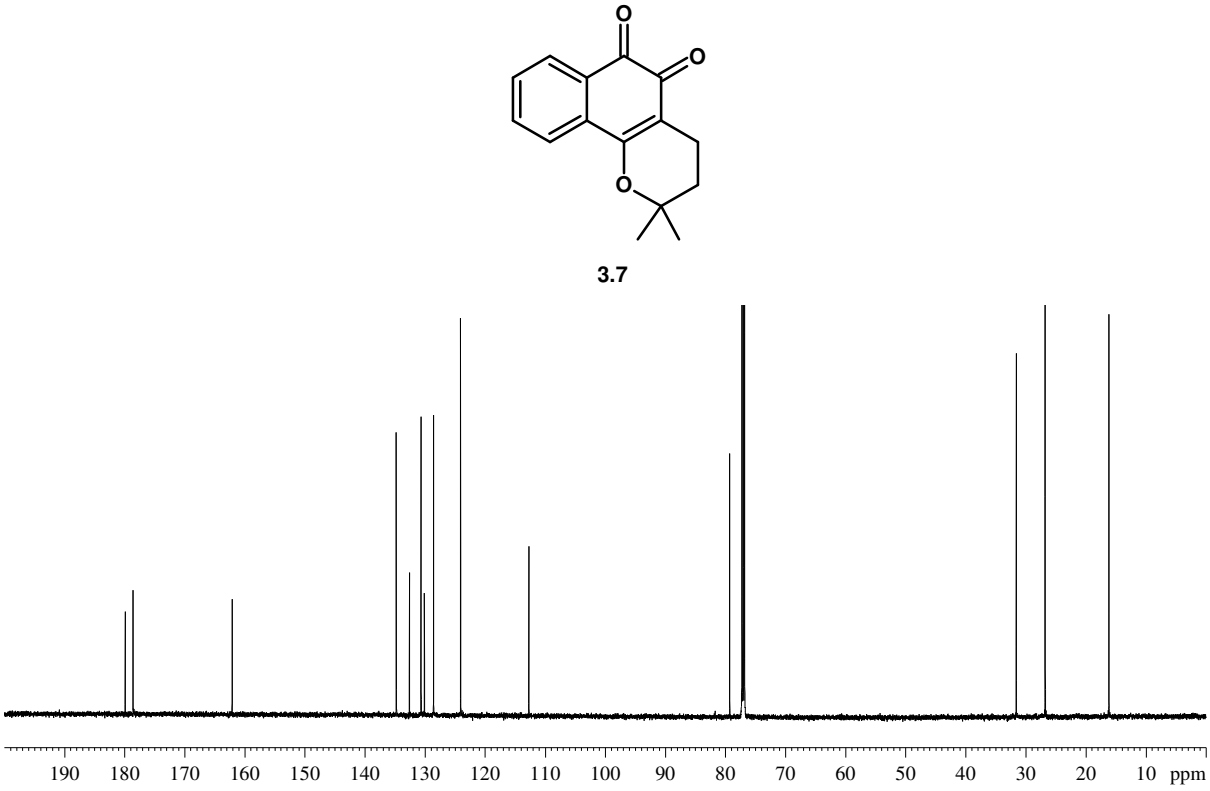

Figure S3.6: ^{13}C NMR spectrum (150 MHz, $CDCl_3$) of compound **3.8**

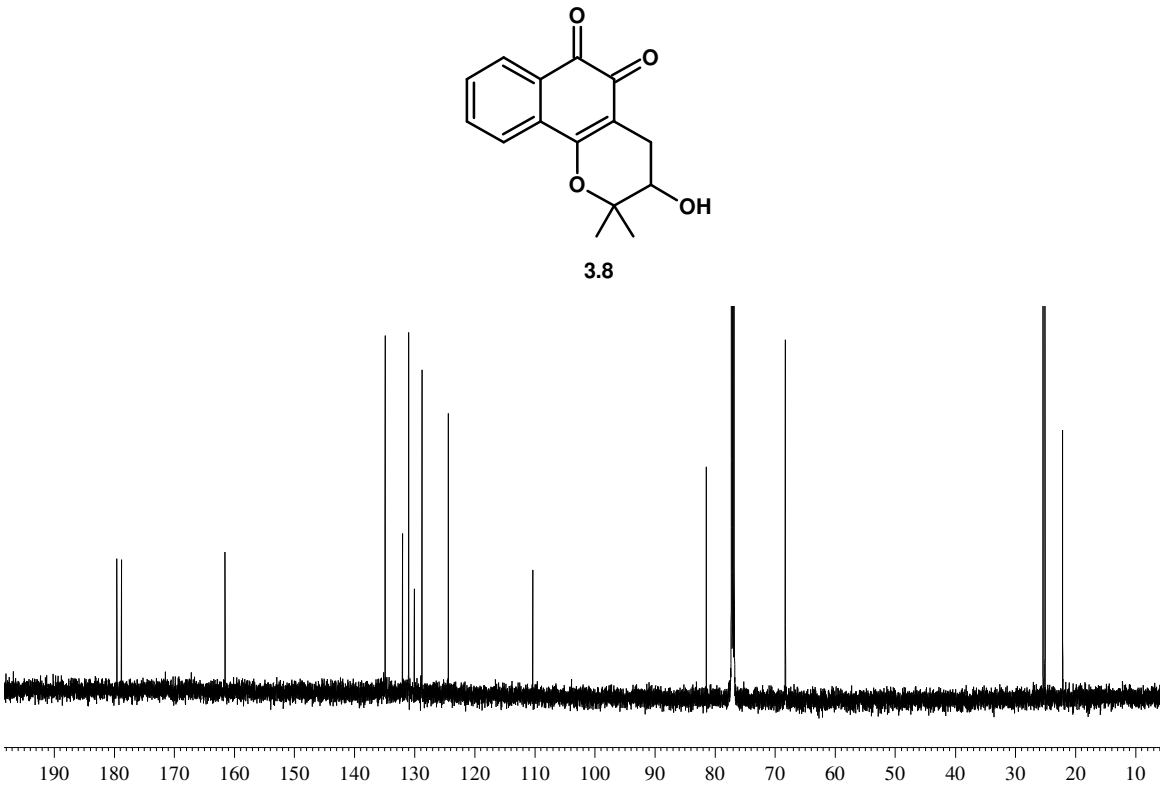

Figure S3.7: ^{13}C NMR spectrum (150 MHz, $CDCl_3$) of compound **3.9**

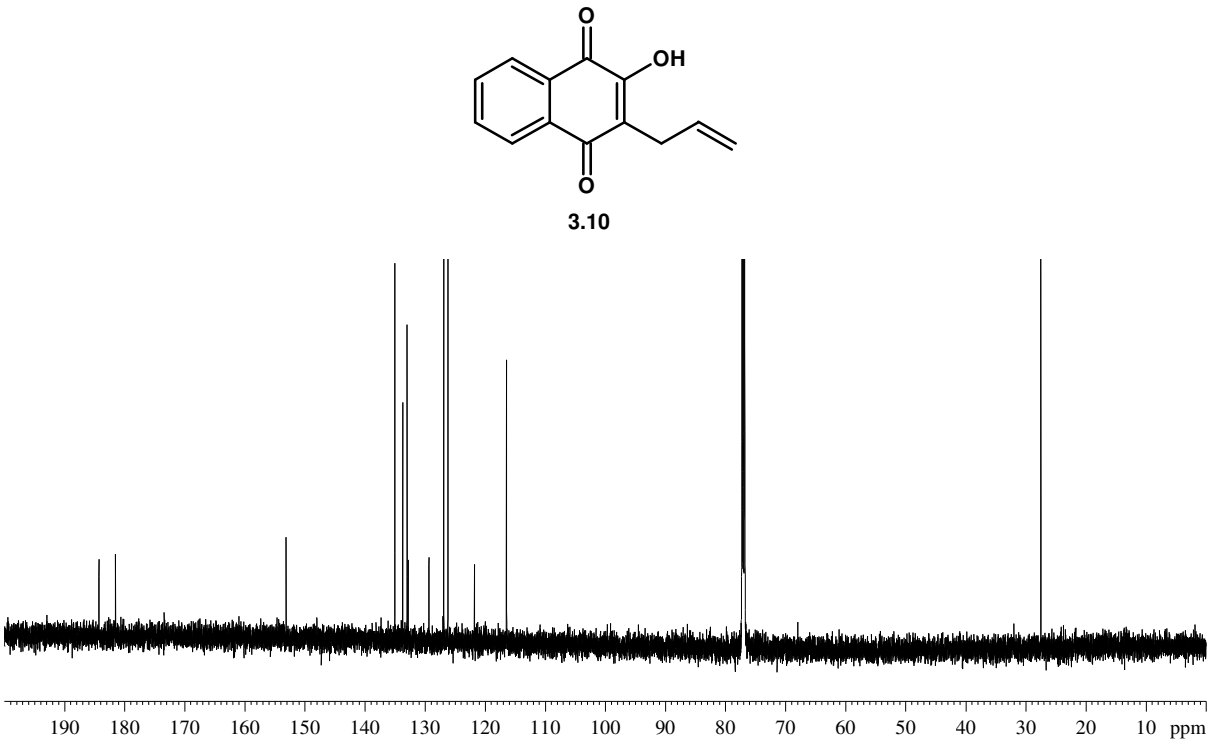

Figure S3.8: ^{13}C NMR spectrum (150 MHz, $CDCl_3$) of compound **3.11**

CHAPTER FOUR

Supplementary data

Synthesis of truncated sarganaphthoquinonic acid (SNQA) derivatives

The characterization of synthesized naphthoquinones involved use of 1D and 2D NMR spectroscopy, Infra-red and high resolution mass spectroscopy (HRMS). The relevant data that was not included in the body of the thesis is shown in this section, including chromatograms obtained during separation of the different isomers *via* normal phase HPLC.

LIST OF FIGURES

First series of naphthoquinones

Second series of naphthoquinones

Figure S4.13: ^{1}H NMR spectrum (600 MHz, $CDCl_3$) of compound **4.14A**

Figure S4.14: ^{13}C NMR spectrum (150 MHz, $CDCl_3$) of compound **4.14A**

Figure S4.15: HMBC correlations of compound **4.14A**

Figure S4.16: ^{1}H NMR spectrum (600 MHz, $CDCl_3$) of compound **4.14B**

Figure S4.17: ^{13}C NMR spectrum (150 MHz, $CDCl_3$) of compound **4.14B**

Figure S4.18: HPLC chromatogram showing the retention times for the two isomers: **4.14A**: 23.8 min and **4.14B**: 26.8 min

Figure S4.19: ^{1}H NMR spectrum (600 MHz, $CDCl_3$) of compound **4.15A**

Figure S4.20: ^{13}C NMR spectrum (150 MHz, $CDCl_3$) of compound **4.15A**

Figure S4.21: ^{1}H NMR spectrum (600 MHz, $CDCl_3$) of compound **4.15B**

Figure S4.22: ^{13}C NMR spectrum (150 MHz, $CDCl_3$) of compound **4.15B**

Figure S4.23: HPLC chromatogram showing the retention times for the two isomers: **4.15A**: 23.5 min and **4.15B**: 27.1 min

Figure S4.24: ^{1}H NMR spectrum (600 MHz, $CDCl_3$) of compound **4.16A**

Figure S4.25: ^{13}C NMR spectrum (150 MHz, $CDCl_3$) of compound **4.16A**

Figure S4.26: ^{1}H NMR spectrum (600 MHz, $CDCl_3$) of compound **4.16B**

Figure S4.27: ^{13}C NMR spectrum (150 MHz, $CDCl_3$) of compound **4.16B**

Figure S4.28: HPLC chromatogram showing the retention times for the two isomers: **4.16A**: 22.3 min and **4.16B**: 25.3 min

Figure S4.29: ^{1}H NMR spectrum (600 MHz, $CDCl_3$) of compound **4.17A**

Figure S4.30: ^{1}H NMR spectrum (150 MHz, $CDCl_3$) of compound **4.17A**

Figure S4.31: ^{1}H NMR spectrum (600 MHz, $CDCl_3$) of compound **4.17B**

Figure S4.32: ^{13}C NMR spectrum (150 MHz, $CDCl_3$) of compound **4.17B**

Figure S4.33: HPLC chromatogram showing the retention times for the two isomers: **4.17A**: 23.5 min and **4.17B**: 23.9 min

Figure S4.34: HRMS of compound **4.17A**

Figure S4.35: HRMS of compound **4.17B**

Figure S4.36: IR spectrum of compound **4.17**

Figure S4.37: ^{1}H NMR spectrum (600 MHz, $CDCl_3$) of compound **4.18A**

Figure S4.38: ^{1}H NMR spectrum (600 MHz, $CDCl_3$) of compound **4.18B**

Figure S4.39: ^{13}C NMR spectrum (150 MHz, $CDCl_3$) of compound **4.18B**

Figure S4.40: HPLC chromatogram showing the retention times for the two isomers: **4.18A**: 21.0 min and **4.18B**: 23.4 min

Figure S4.41: HRMS of compound **4.18A**

Figure S4.42: HRMS of compound **4.18B**

Figure S4.43: IR spectrum of compound **4.18B**

Figure S4.44: ^{1}H NMR spectrum (600 MHz, $CDCl_3$) of compound **4.19A**

Figure S4.45: ^{13}C NMR spectrum (150 MHz, $CDCl_3$) of compound **4.19A**

Figure S4.46: COSY NMR spectrum of compound **4.19A**

Figure S4.47: HSQC NMR spectrum of compound **4.19A**

Figure S4.48: HMBC NMR spectrum of compound **4.19A**

Figure S4.49: HRMS of compound **4.19A**

Figure S4.50: ^{1}H NMR spectrum (600 MHz, $CDCl_3$) of compound **4.19B**

Figure S4.51: ^{13}C NMR spectrum (150 MHz, $CDCl_3$) of compound **4.19B**

Figure S4.52: COSY NMR spectrum of compound **4.19B**

Figure S4.53: HMBC NMR spectrum of compound **4.19B**

Figure S4.54: HSQC NMR spectrum of compound **4.19B**

Figure S4.55: HRMS of compound **4.19B**

Figure S4.56: IR spectrum of compound **4.19B**

Figure S4.57: HPLC chromatogram showing the retention times for the two isomers: **4.19A**: 19.6 min and **4.19B**: 21.3 min

Third series of naphthoquinones

Figure S4.58: ^{1}H NMR spectra (600 MHz, $CDCl_3$) of alkylamino-naphthoquinone **4.20** illustrating the mixture of isomers before and after normal phase HPLC

Figure S4.59: ^{1}H NMR spectra (600 MHz, $CDCl_3$) of alkylamino-naphthoquinone **4.20** showing differences between the isomers in the aromatic region

Figure S4.60: ^{13}C NMR spectrum (150 MHz, $CDCl_3$) of compound **4.20A**

Figure S4.61: COSY NMR spectrum of compound **4.20A**

Figure S4.62: HMBC NMR spectrum of compound **4.20A**

Figure S4.63: HSQC NMR spectrum of compound **4.20A**

Figure S4.64: HRMS spectrum of compound **4.20A**

Figure S4.65: ^{13}C NMR spectrum (150 MHz, $CDCl_3$) of compound **4.20B**

Figure S4.66: COSY NMR spectrum of compound **4.20B**

Figure S4.67: HSQC NMR spectrum of compound **4.20B**

Figure S4.68: HMBC NMR spectrum of compound **4.20B**

Figure S4.69: HRMS of compound **4.20B**

Figure S4.70: HPLC chromatogram showing the retention times for the two isomers: **4.20A**: 24.0 min and **4.20B**: 27.2 min

Figure S4.71: IR spectrum of compound **4.20B**

Figure S4.72: COSY NMR spectrum of compound **4.21** mixture

Figure S4.73: DEPT135 NMR spectrum of compound **4.21** mixture

Figure S4.74: HRMS of compound **4.21** mixture

Figure S4.75: IR spectrum of compound **4.21** mixture

Figure: S4.76: Stacked ^{1}H NMR spectra (600 MHz, $CDCl_3$) of alkyl amino-naphthoquinone **4.22** illustrating the mixture of isomers before and after HPLC

Figure: S4.77: ^{1}H NMR spectra (600 MHz, $CDCl_3$) of alkyl amino-naphthoquinone **4.22** showing differences between the isomers in the aromatic region

Figure S4.78: ^{13}C NMR spectrum (150 MHz, $CDCl_3$) of compound **4.22A**

Figure S4.79: COSY NMR spectrum of compound **4.22A**

Figure S4.80: HSQC NMR spectrum of compound **4.22A**

Figure S4.81: HRMS of compound **4.22A**

Figure S4.82: ^{13}C NMR spectrum (150 MHz, $CDCl_3$) of compound **4.22B**

Figure S4.83: COSY NMR spectrum of compound **4.22B**

Figure S4.84: HRMS of compound **4.22B**

Figure S4.85: HPLC chromatogram showing the retention times for the two isomers: **4.22A**: 19.3 min and **4.22B**: 21.6 min

Figure S4.86: IR spectrum of compound **4.22**

Figure: S4.87: ^{1}H NMR spectra (600 MHz, $CDCl_3$) of alkylamino-naphthoquinone **4.23** illustrating the mixture of isomers before and after HPLC

Figure: S4.88: ^{1}H NMR spectra (600 MHz, $CDCl_3$) of alkylamino-naphthoquinone **4.23** showing differences between the isomers in the aromatic region

Figure S4.89: ^{13}C NMR spectrum (150 MHz, $CDCl_3$) of compound **4.23A**

Figure S4.90: COSY NMR spectrum of compound **4.23A**

Figure S4.91: HMBC NMR spectrum of compound **4.23A**

Figure S4.92: HSQC NMR spectrum of compound **4.23A**

Figure S4.93: HRMS of compound **4.23A**

Figure S4.94: ^{13}C NMR spectrum (150 MHz, $CDCl_3$) of compound **4.23B**

Figure S4.95: COSY NMR spectrum of compound **4.23B**

Figure S4.96: HRMS of compound **4.23B**

Figure S4.97: HPLC chromatogram showing the retention times for the two isomers: **4.23A**: 25.7 min and **4.23B**: 28.1 min

Figure S4.98: IR spectrum of compound **4.23**

Figure: S4.99: ^{1}H NMR spectra (600 MHz, $CDCl_3$) of alkylamino-naphthoquinone **4.24** illustrating the mixture of isomers before and after HPLC

Figure: S4.100: ^{1}H NMR spectra (600 MHz, $CDCl_3$) of alkylamino-naphthoquinone **4.24** showing differences between the isomers in the aromatic region

Figure S4.101: ^{13}C NMR spectrum (150 MHz, $CDCl_3$) of compound **4.24A**

Figure S4.102: COSY NMR spectrum of compound **4.24A**

Figure S4.103: HMBC NMR spectrum of compound **4.24A**

Figure S4.104: HSQC NMR spectrum of compound **4.24A**

Figure S4.105: HRMS of compound **4.24A**

Figure S4.106: ^{13}C NMR spectrum (150 MHz, $CDCl_3$) of compound **4.24B**

Figure S4.107: HMBC NMR spectrum of compound **4.24B**

Figure S4.108: HSQC NMR spectrum of compound **4.24B**

Figure S4.109: HRMS of compound **4.24B**

Figure S4.110: HPLC chromatogram showing the retention times for the two isomers: **4.24A**: 38.1 min and **4.24B**: 35.4 min

Figure S4.111: IR spectrum of compound **4.24**

Figure S4.112: ^{1}H NMR spectra (600 MHz, $CDCl_3$) of alkylamino-naphthoquinone **4.25** illustrating the mixture of isomers before and after HPLC

Figure S4.113: ^{1}H NMR spectra (600 MHz, $CDCl_3$) of alkylamino-naphthoquinone **4.25** showing differences between the isomers in the aromatic region

Figure S4.114: ^{13}C NMR spectrum (150 MHz, $CDCl_3$) of compound **4.25A**

Figure S4.115: HMBC NMR spectrum of compound **4.25A**

Figure S4.116: HSQC NMR spectrum of compound **4.25A**

Figure S4.117: COSY NMR spectrum of compound **4.25A**

Figure S4.118: HRMS of compound **4.25A**

Figure S4.119: ^{13}C NMR spectrum (150 MHz, $CDCl_3$) of compound **4.25B**

Figure S4.120: HMBC NMR spectrum of compound **4.25B**

Figure S4.121: HSQC NMR spectrum of compound **4.25B**

Figure S4.122: COSY NMR spectrum of compound **4.25B**

Figure S4.123: HRMS of compound **4.25B**

Figure S4.124: HPLC chromatogram showing the retention times for the two isomers: **4.25A**: 14.9 min and **4.25B**: 21.5 min

Figure S4.125: IR spectrum of compound **4.25**

Figure S4.126: ^{1}H NMR spectra (600 MHz, $CDCl_3$) of alkylamino-naphthoquinone **4.26** illustrating the mixture of isomers before and after HPLC

Figure S4.127: ^{1}H NMR spectra (600 MHz, $CDCl_3$) alkylamino-naphthoquinone **4.26** showing differences between the isomers in the aromatic region

Figure S4.128: ^{13}C NMR spectrum (150 MHz, $CDCl_3$) of compound **4.26A**

Figure S4.129: HMBC spectrum of compound **4.26A**

Figure S4.130: HSQC spectrum of compound **4.26A**

Figure S4.131: COSY spectrum of compound **4.26A**

Figure S4.132: HRMS of compound **4.26A**

Figure S4.133: ^{13}C NMR spectrum (150 MHz, $CDCl_3$) of compound **4.26B**

Figure S4.134: HMBC spectrum of compound **4.26B**

Figure S4.135: HSQC spectrum of compound **4.26B**

Figure S4.136: COSY spectrum of compound **4.26B**

Figure S4.137: HRMS spectrum of compound **4.26B**

Figure S4.138: HPLC chromatogram showing the retention times for the two isomers: **4.26A**: 22.0 min and **4.26B**: 21.5 min

Figure S4.139: IR spectrum of compound **4.26**

Table S4.1: Preparation of Diels-Alder products from selected benzoquinones

Table S4.2: Aromatization of Diels-Alder products to the naphthoquinone

Table S4.3: Oxidative coupling of naphthoquinone **4.10** with *para*-substituted anilines

Table S4.4: Coupling of alkyl amines with naphthoquinone **4.10**

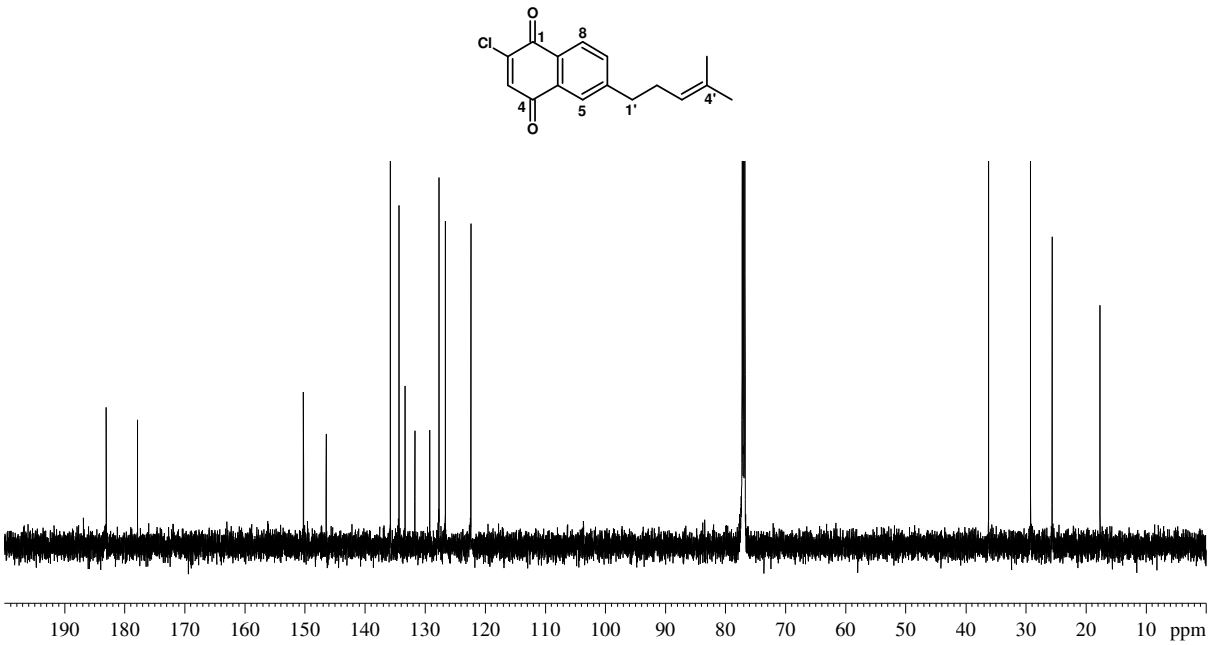

Figure S4.1: ^{13}C NMR spectrum (150 MHz, $CDCl_3$) of compound **4.11A**

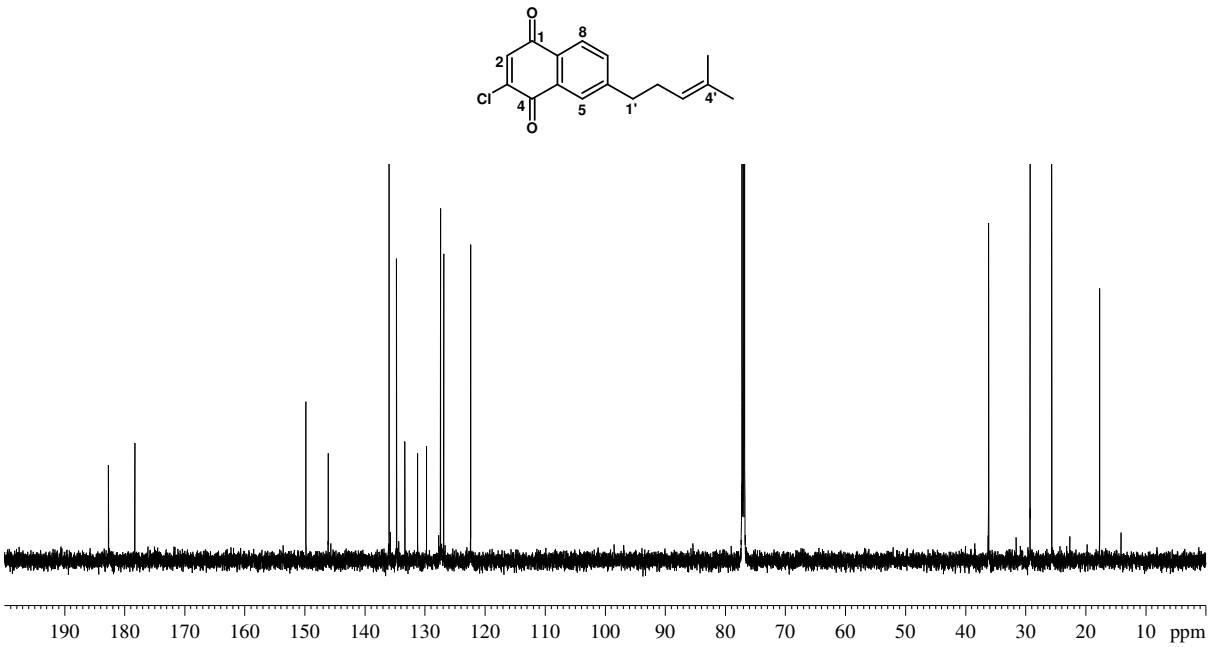

Figure S4.2: ^{13}C NMR spectrum (150 MHz, $CDCl_3$) of compound **4.11B**

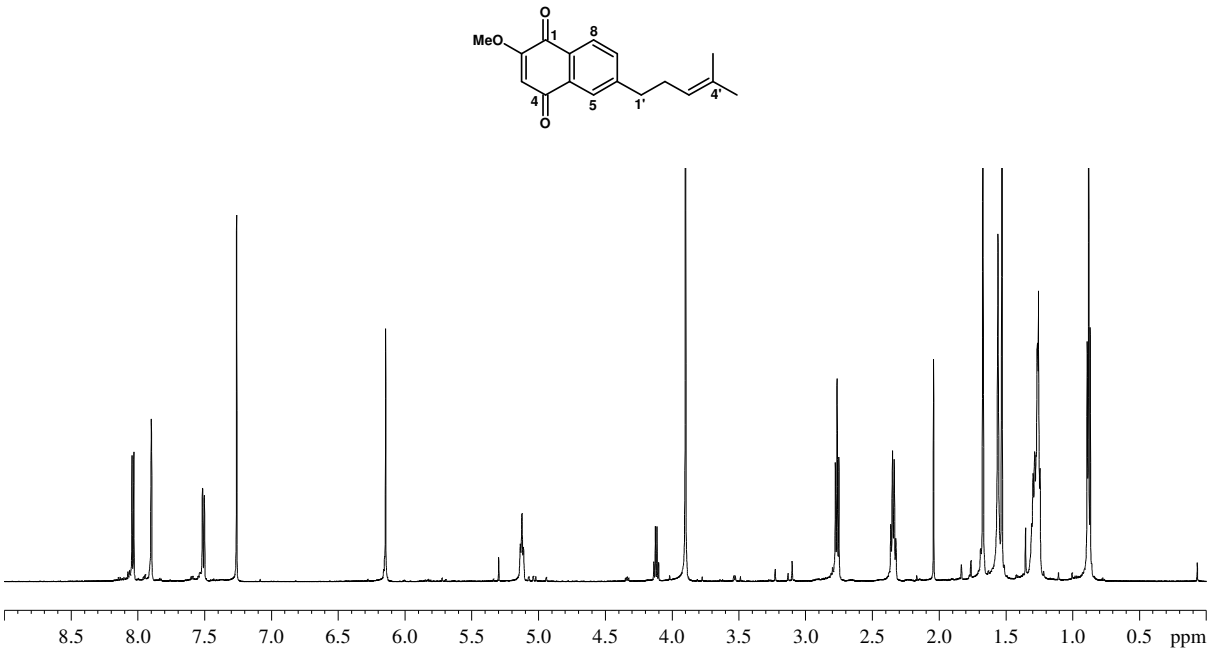

Figure S4.3: ^{1}H NMR spectrum (600 MHz, $CDCl_3$) of compound **4.12A**

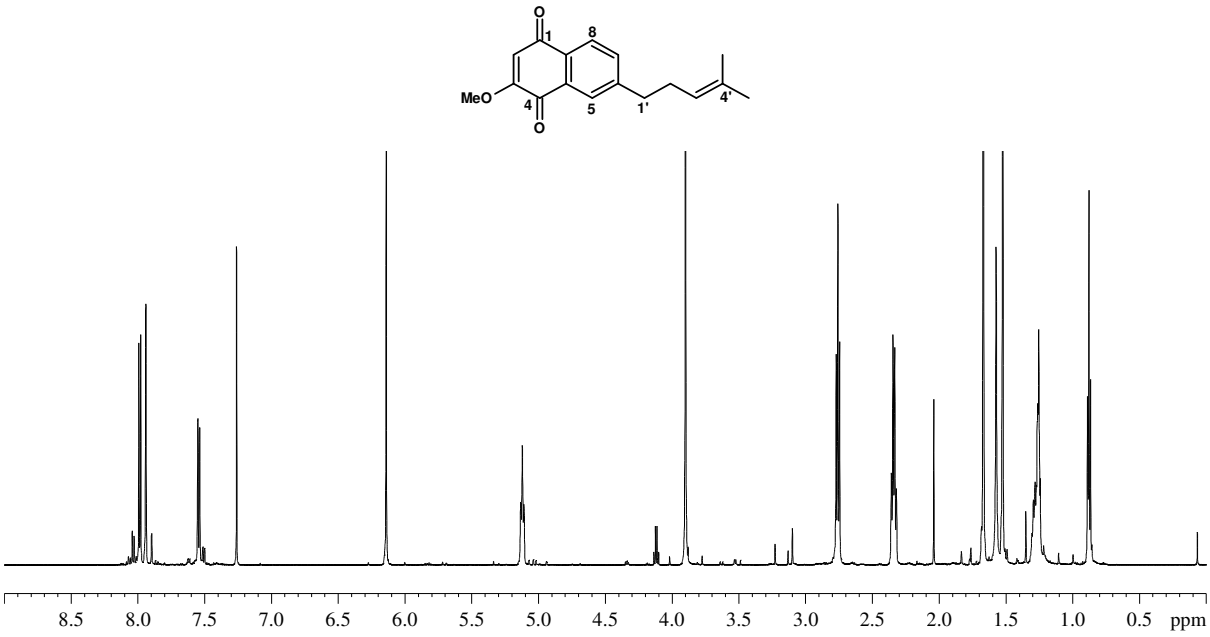

Figure S4.4: ^{1}H NMR spectrum (600 MHz, $CDCl_3$) of compound **4.12B**

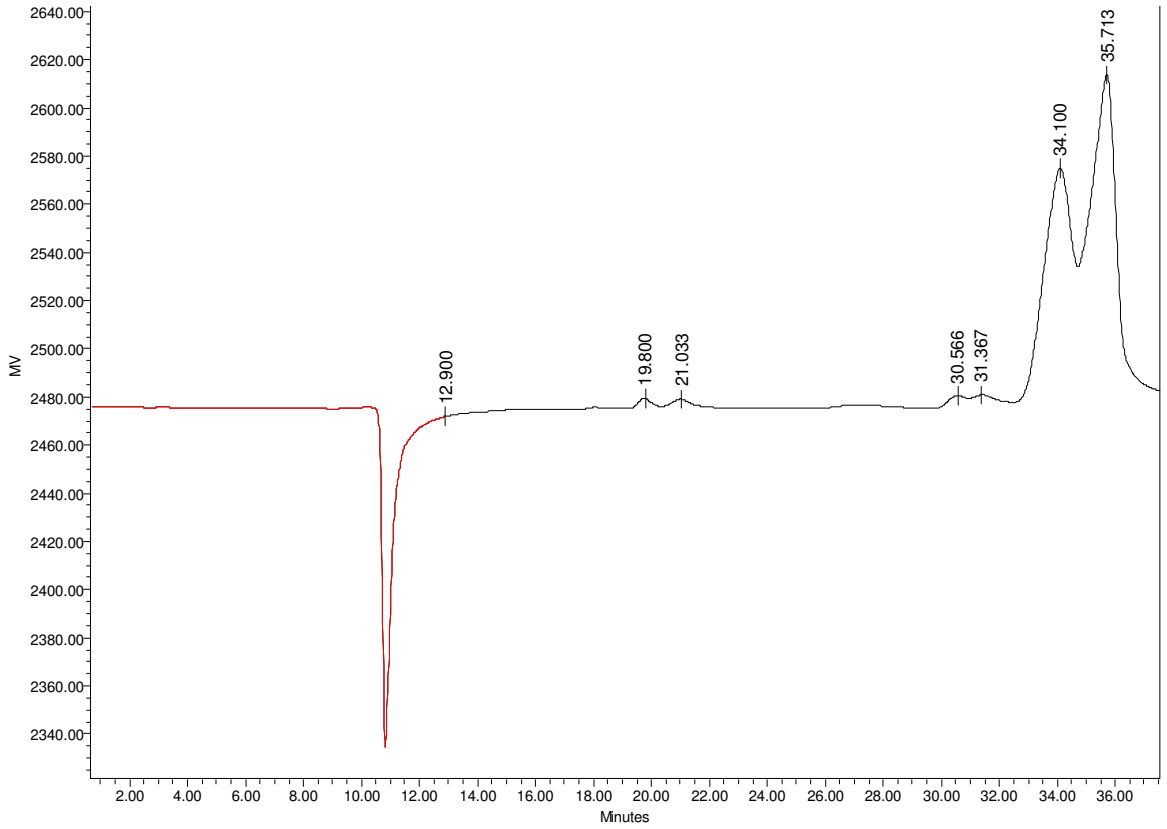

Figure S4.5: HPLC chromatogram showing the retention times for the two isomers: **4.12A**: 34.1 min and **4.12B**: 35.7 min

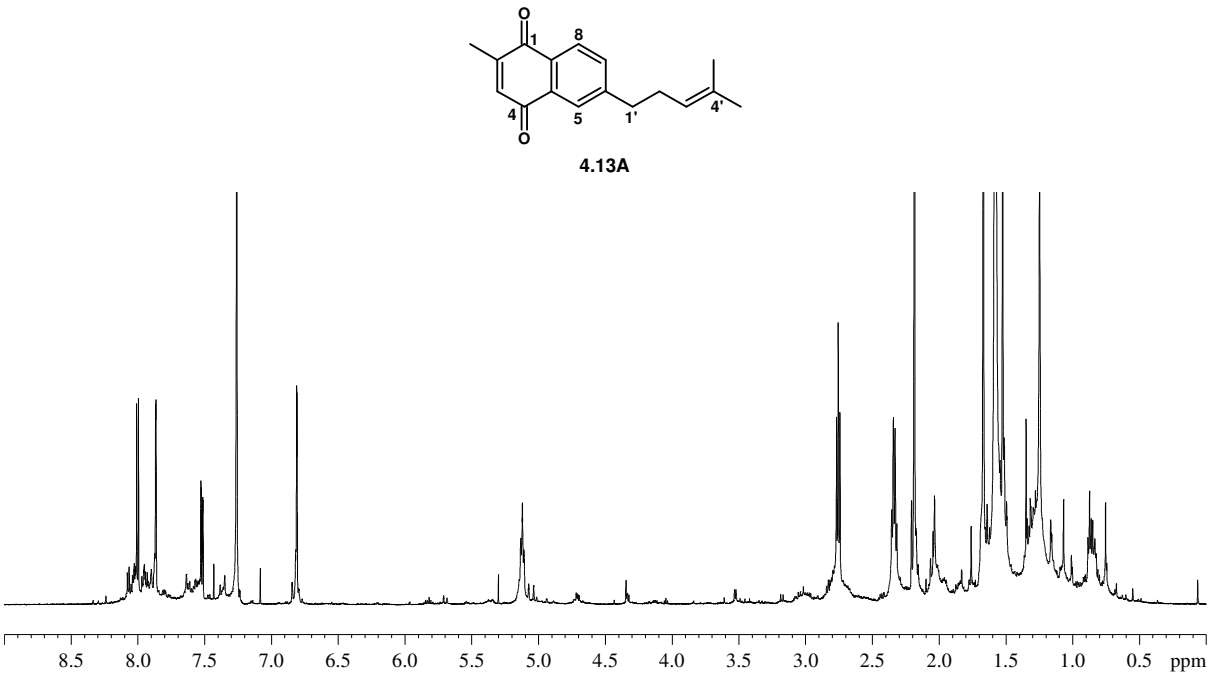

Figure S4.6: ^{1}H NMR spectrum (600 MHz, $CDCl_3$) of compound **4.13A**

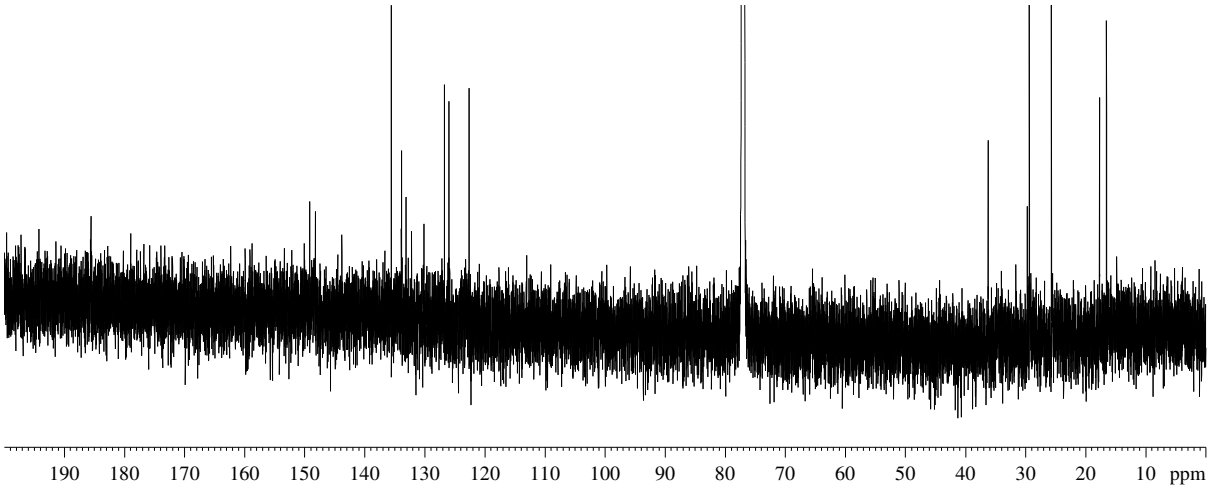

Figure S4.7: ^{13}C NMR spectrum (150 MHz, $CDCl_3$) of compound **4.13A**

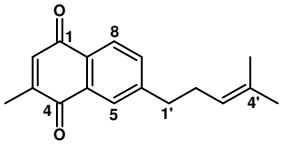

4.13B

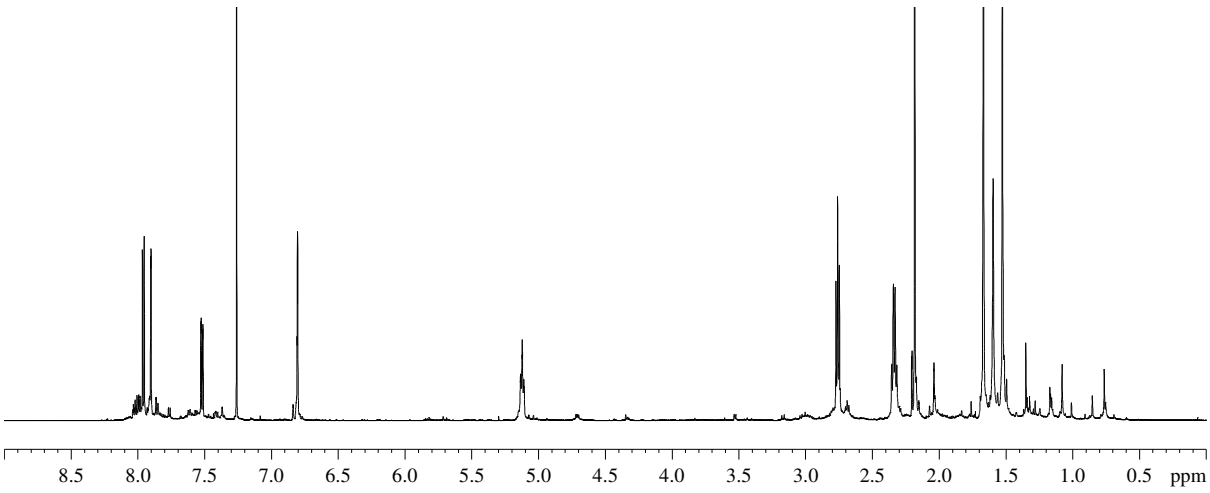

Figure S4.8: ^{1}H NMR spectrum (600 MHz, $CDCl_3$) of compound **4.13B**

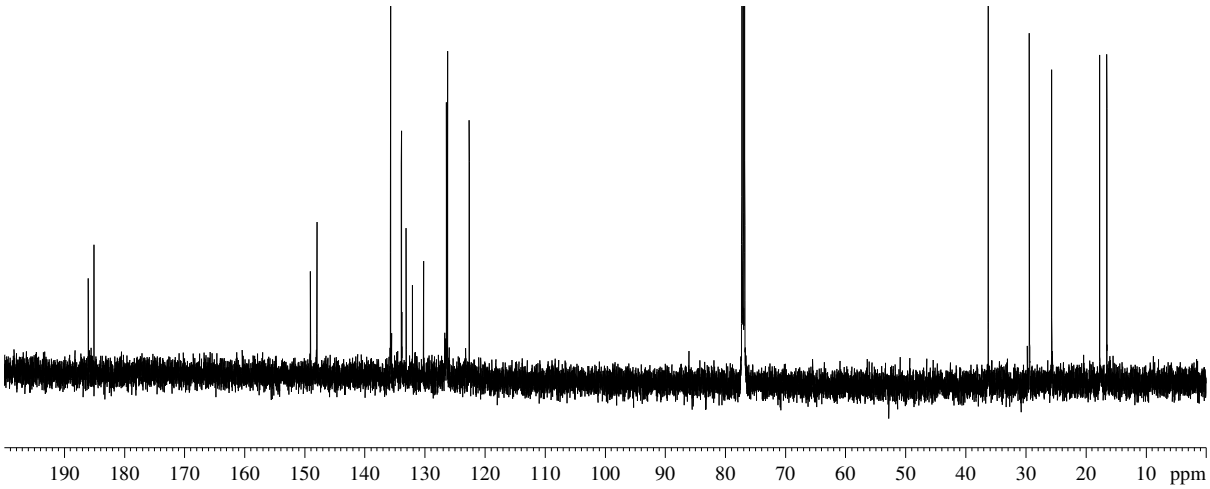

Figure S4.9: ^{13}C NMR spectrum (150 MHz, $CDCl_3$) of compound **4.13B**

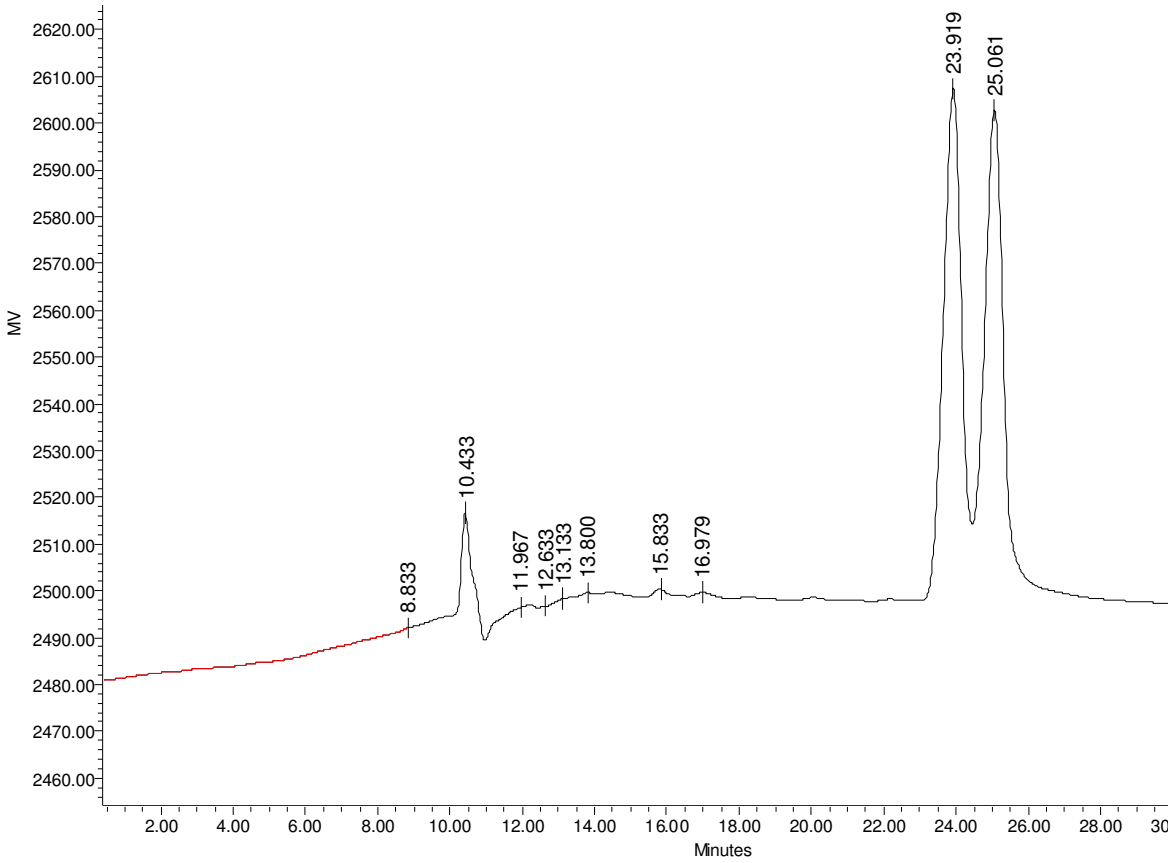

Figure S4.10: HPLC chromatogram showing the retention times for the two isomers: **4.13A**: 23.9 min and **4.13B**: 25.0 min

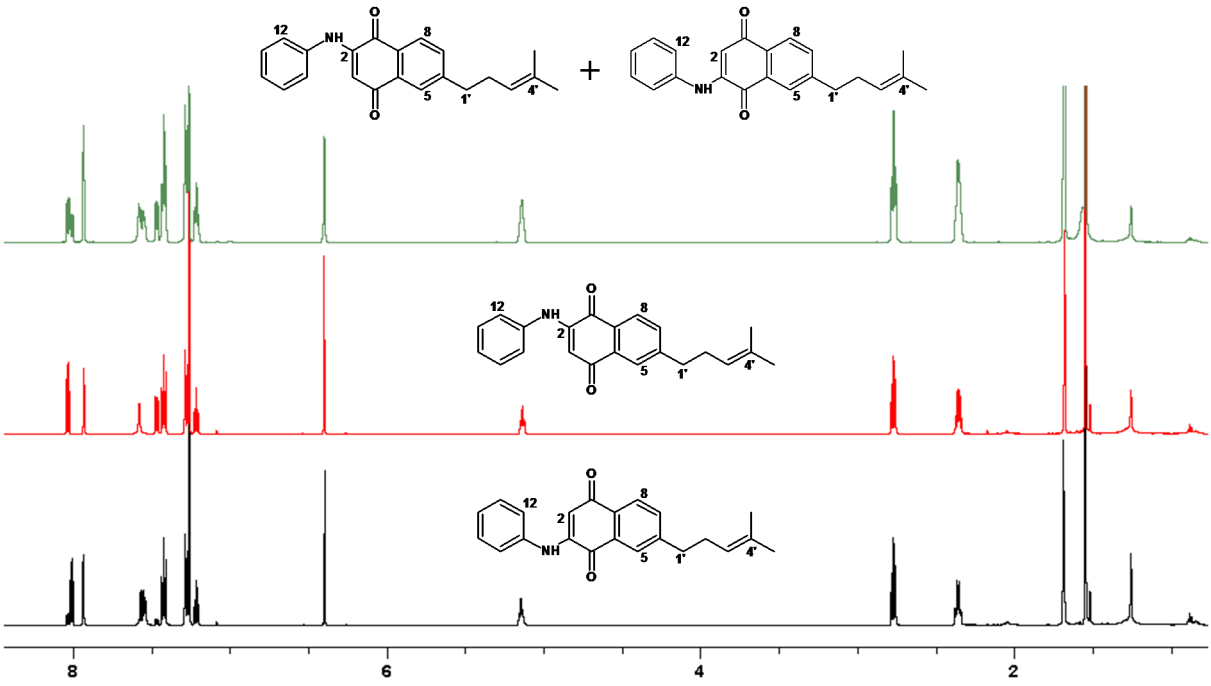

Figure S4.11: ^{1}H NMR spectra (600 MHz, $CDCl_3$) of compound **4.14** as a mixture and of the individual isomers after separation by normal phase HPLC.

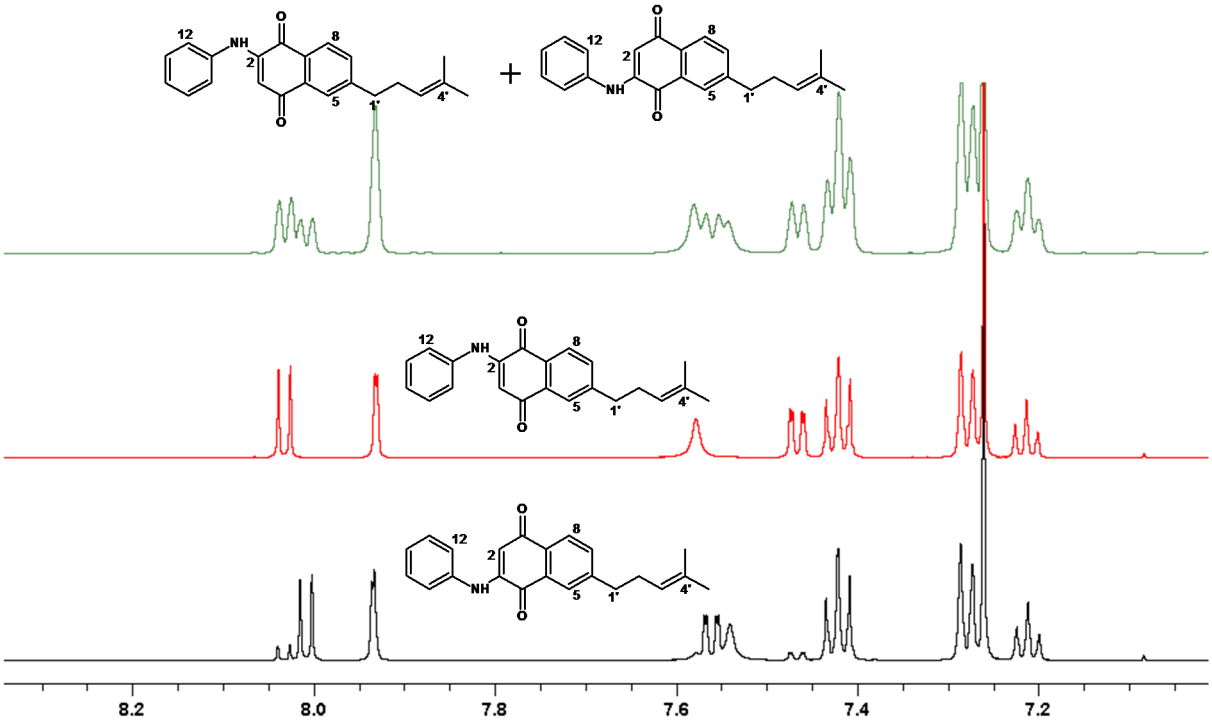

Figure S4.12: ^{1}H NMR spectra (600 MHz, $CDCl_3$) of compound **4.14** showing the splitting of aromatic protons.

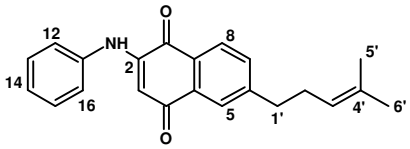

4.14A

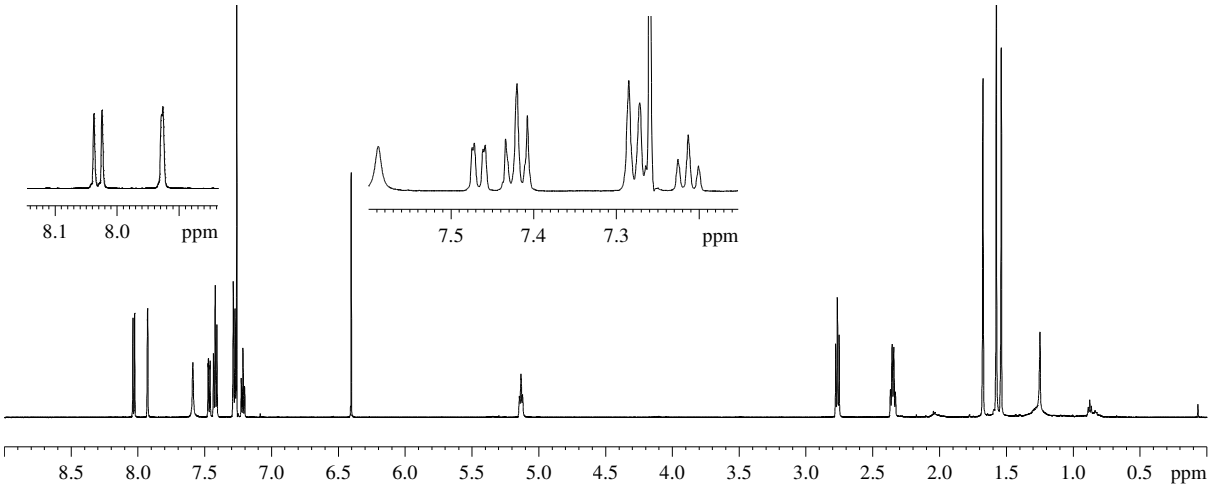

Figure S4.13: ^{1}H NMR spectrum (600 MHz, $CDCl_3$) of compound **4.14A**

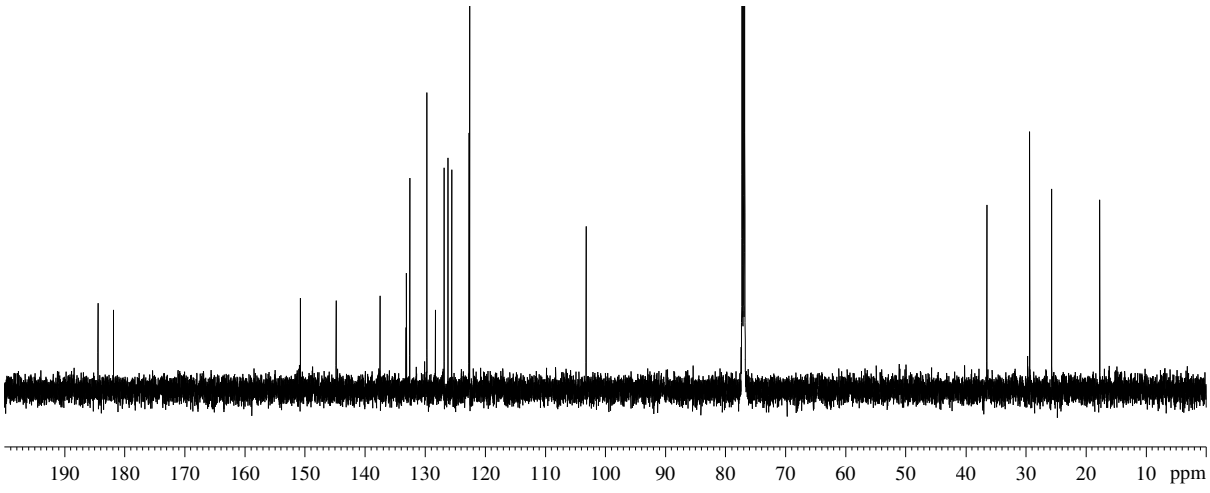

Figure S4.14: ^{13}C NMR spectrum (150 MHz, $CDCl_3$) of compound **4.14A**

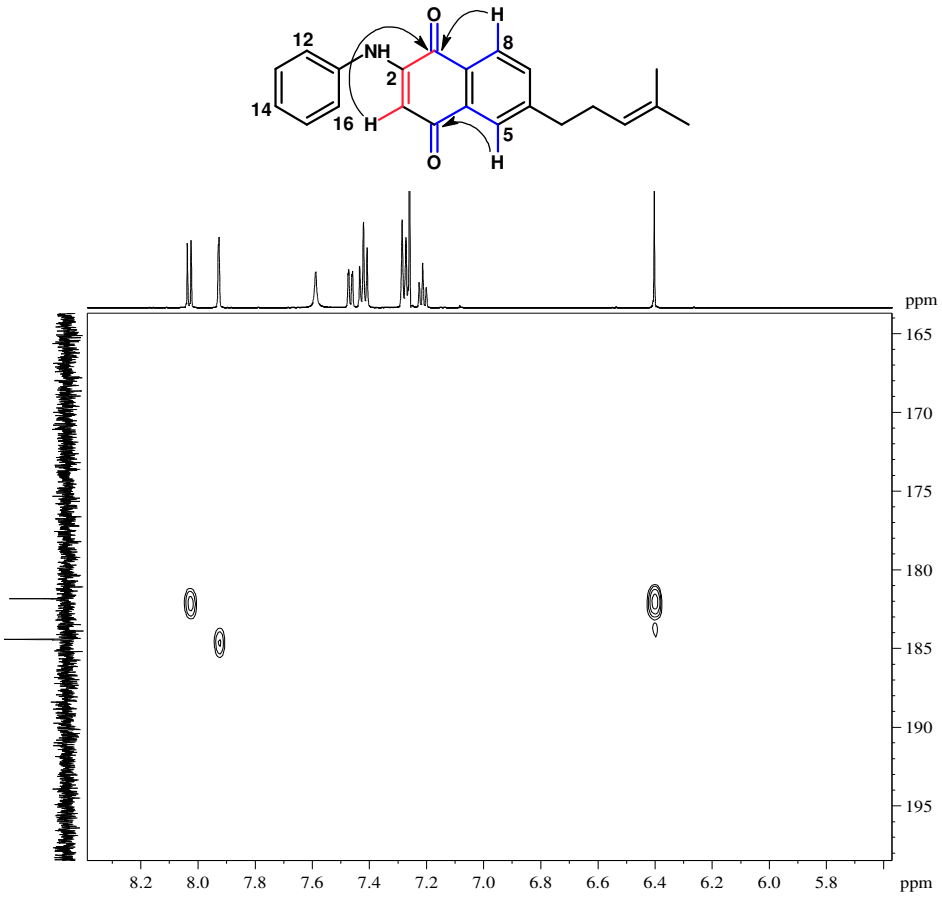

Figure S4.15: HMBC correlations of compound **4.14A**

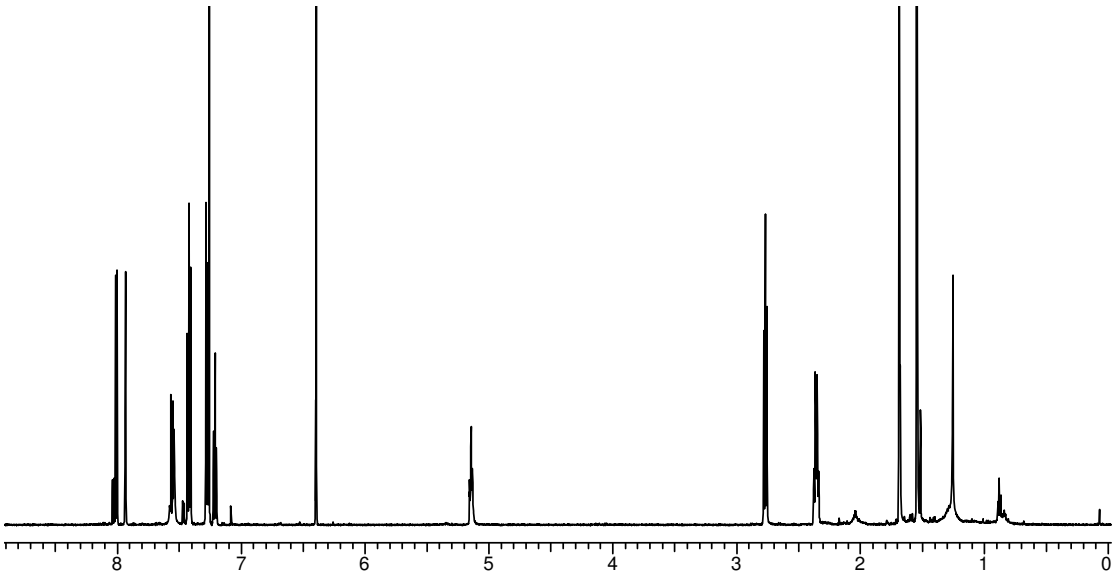

Figure S4.16: ^{1}H NMR spectrum (600 MHz, $CDCl_3$) of compound **4.14B**

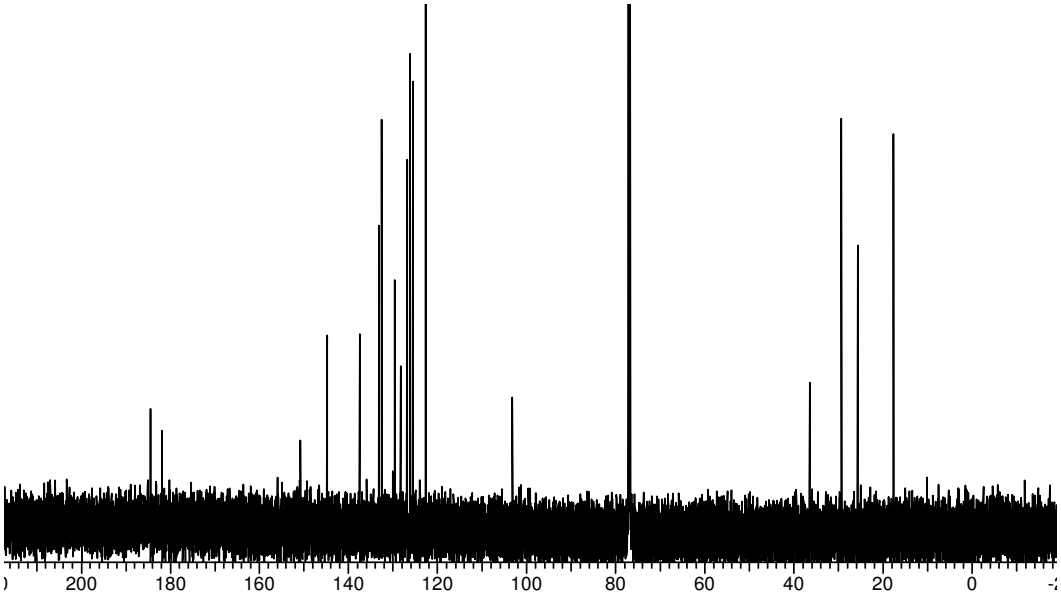

Figure S4.17: ^{13}C NMR spectrum (150 MHz, $CDCl_3$) of compound **4.14B**

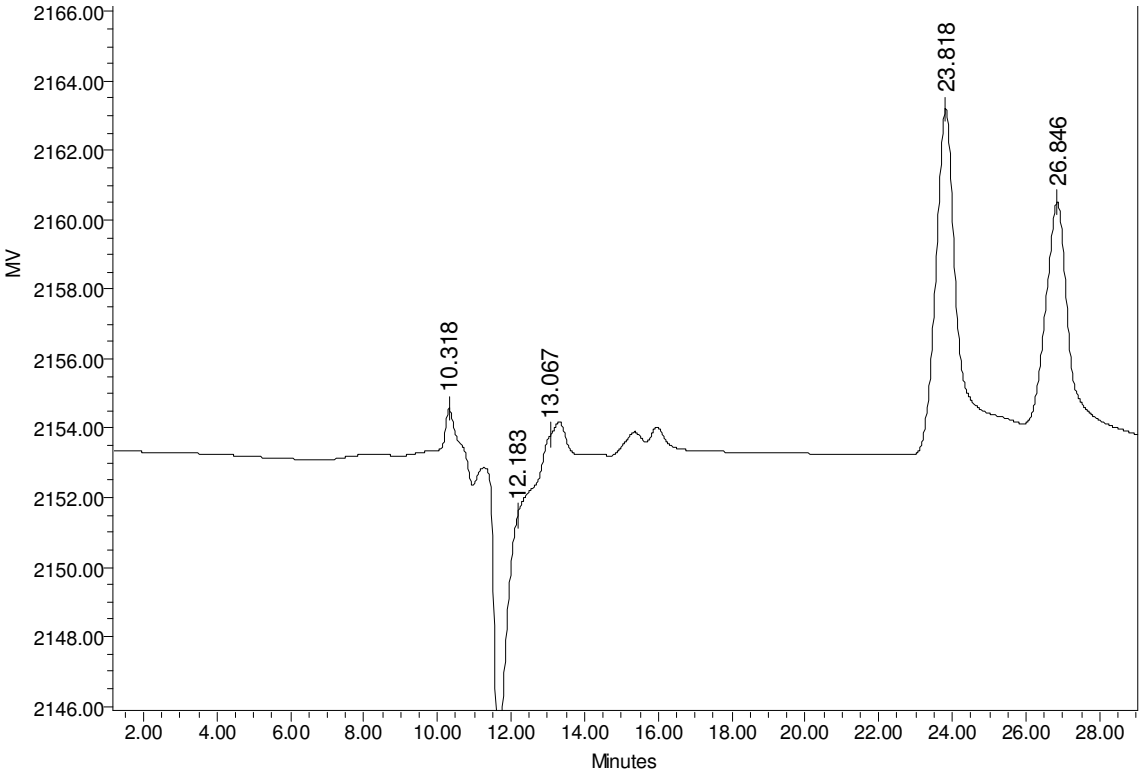

Figure S4.18: HPLC chromatogram showing the retention times for the two isomers: **4.14A**: 23.8 min and **4.14B**: 26.8 min

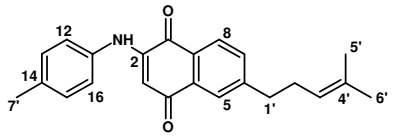

4.15A

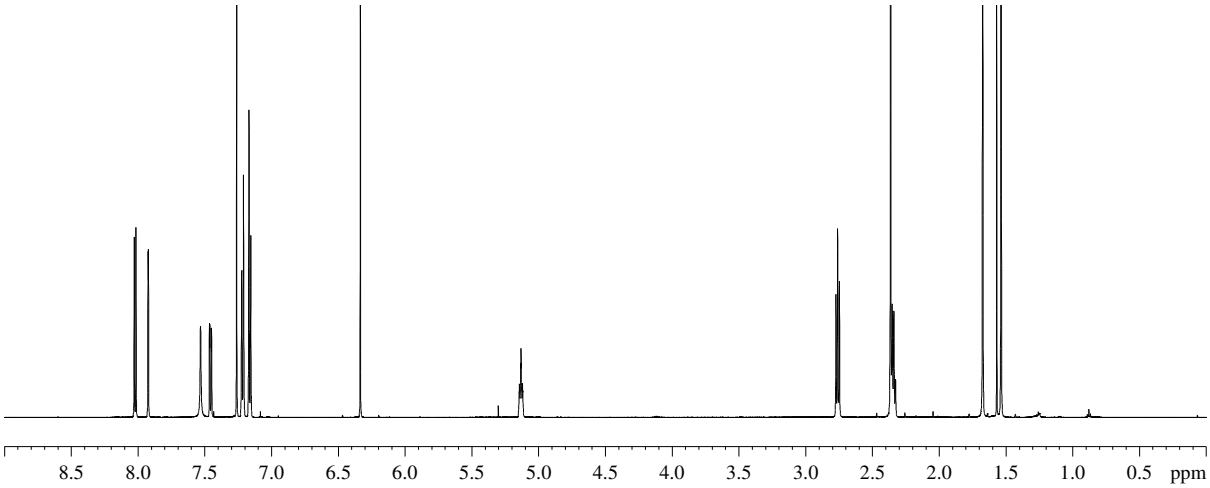

Figure S4.19: ^{1}H NMR spectrum (600 MHz, $CDCl_3$) of compound **4.15A**

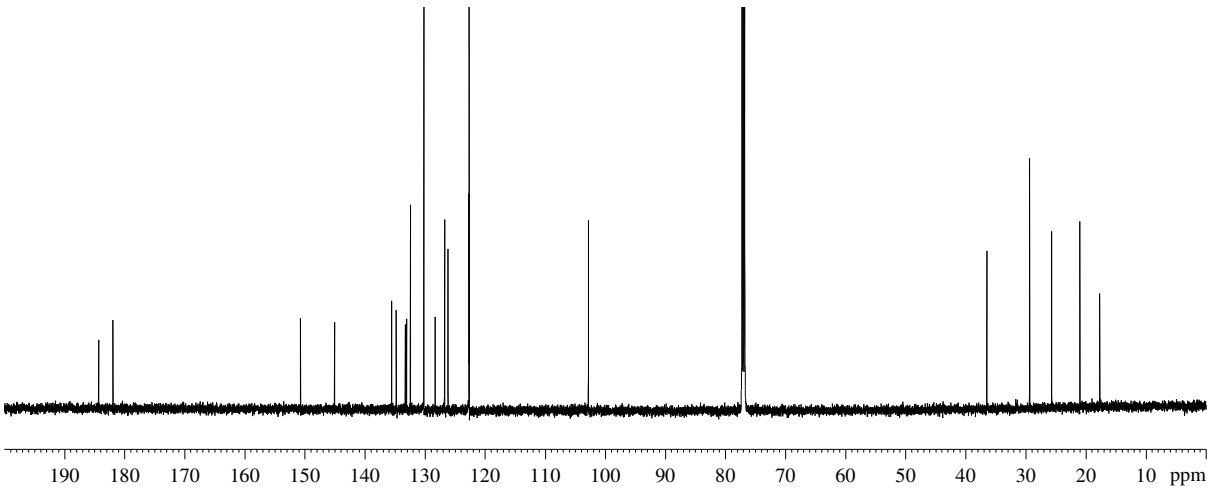

Figure S4.20: ^{13}C NMR spectrum (150 MHz, $CDCl_3$) of compound **4.15A**

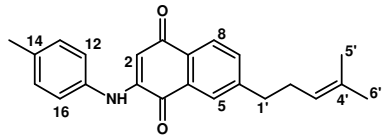

4.15B

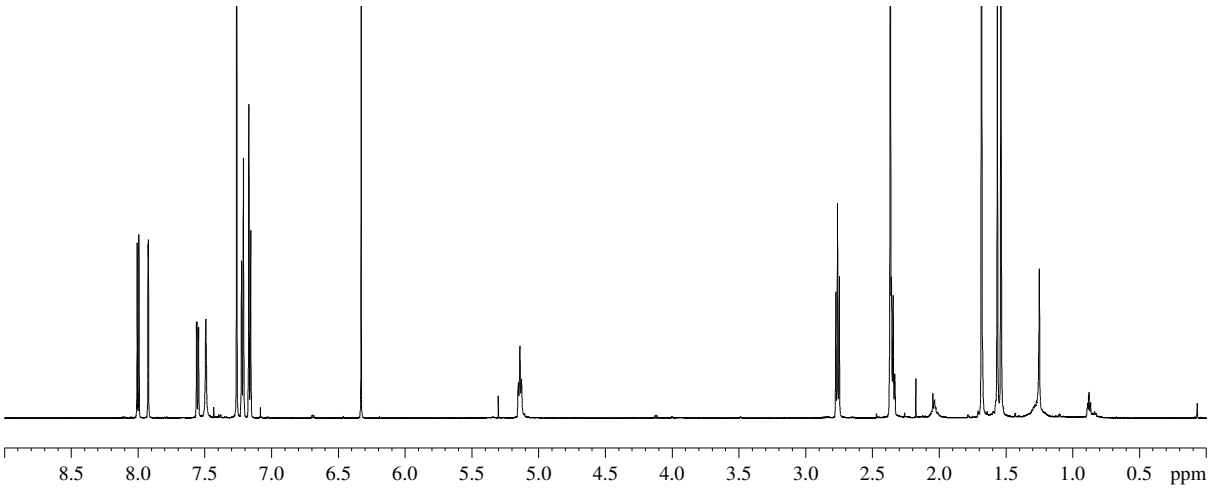

Figure S4.21: ^{1}H NMR spectrum (600 MHz, $CDCl_3$) of compound **4.15B**

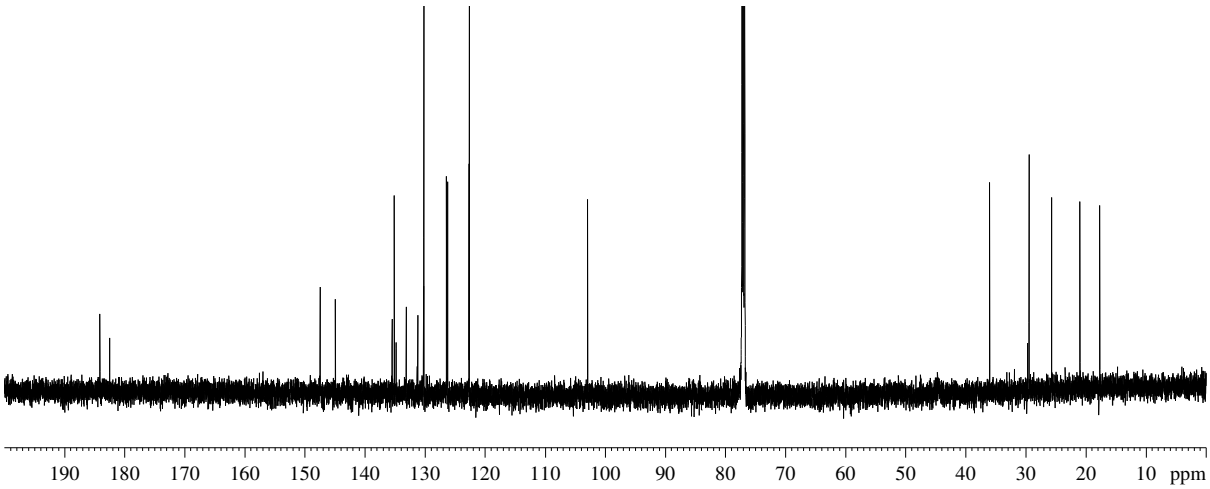

Figure S4.22: ^{13}C NMR spectrum (150 MHz, $CDCl_3$) of compound **4.15B**

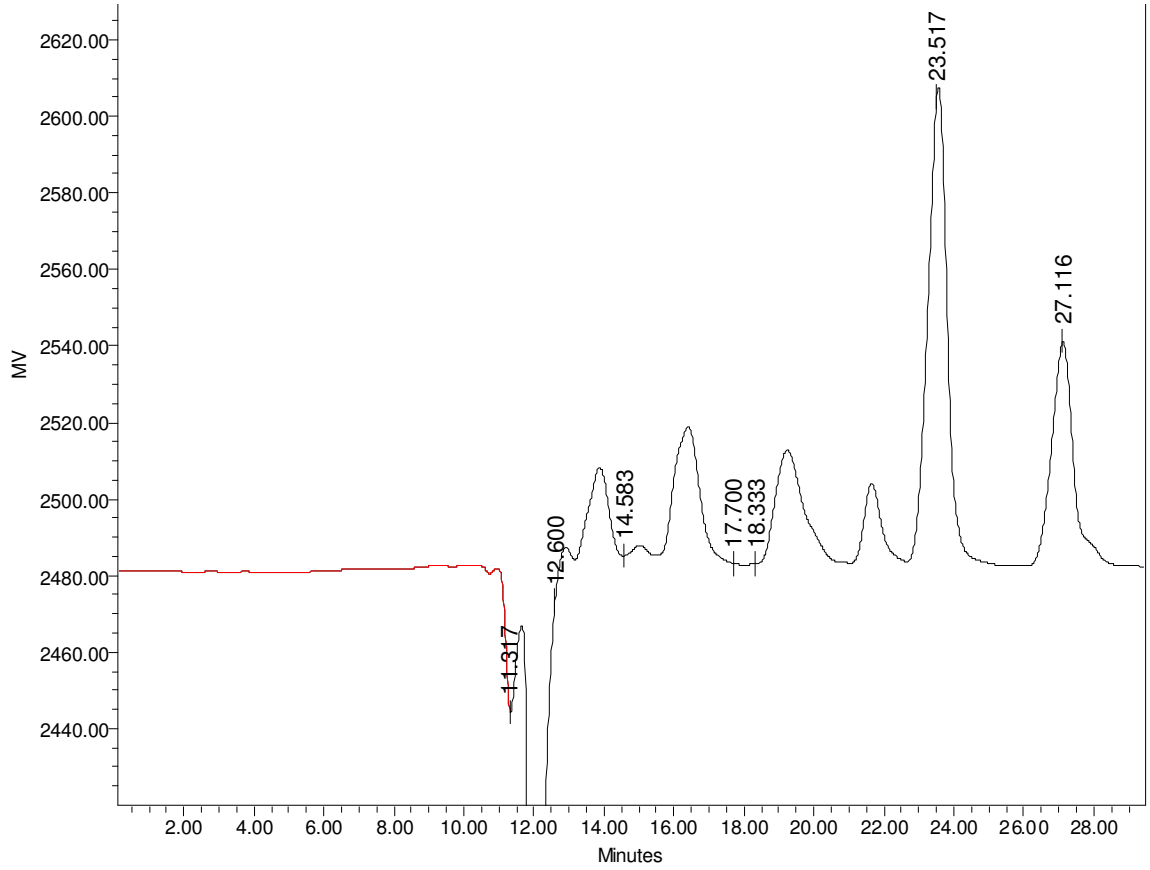

Figure S4.23: HPLC chromatogram showing the retention times for the two isomers: **4.15A**: 23.5 min and **4.15B**: 27.1 min

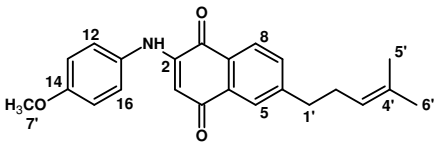

4.16A

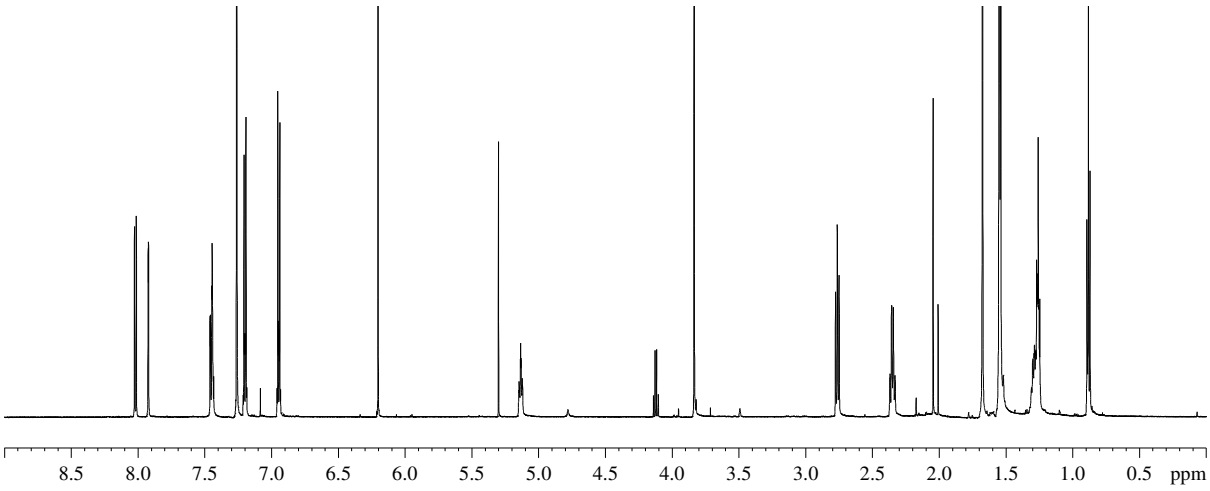

Figure S4.24: ^{1}H NMR spectrum (600 MHz, $CDCl_3$) of compound **4.16A**

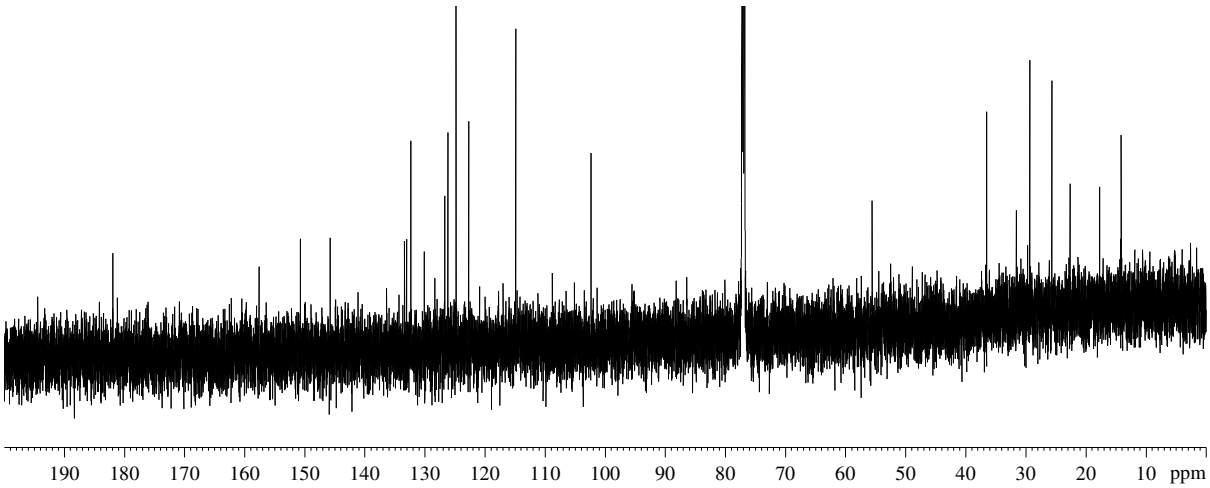

Figure S4.25: ^{13}C NMR spectrum (150 MHz, $CDCl_3$) of compound **4.16A**

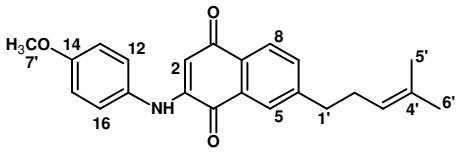

4.16B

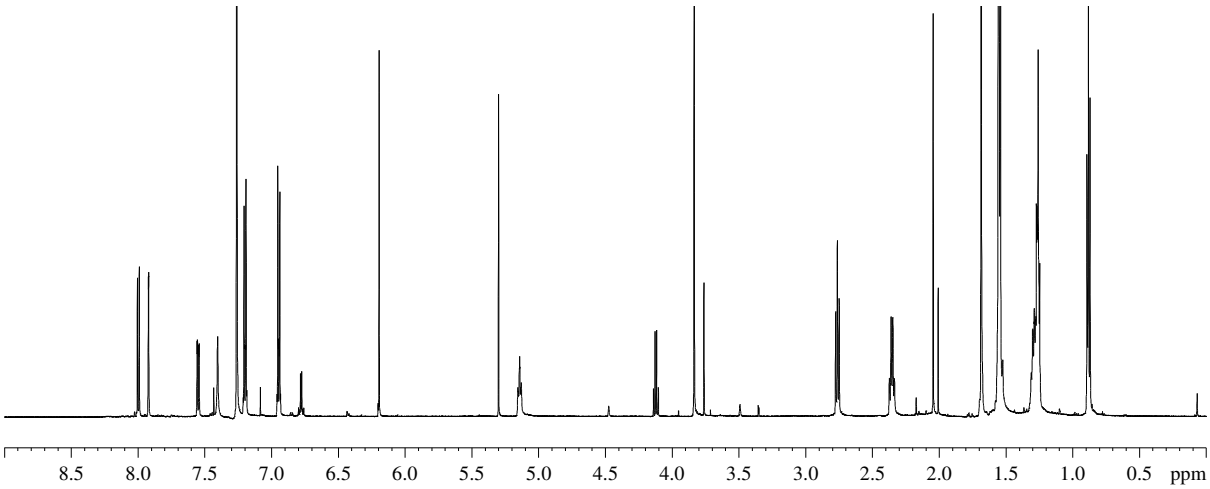

Figure S4.26: ^{1}H NMR spectrum (600 MHz, $CDCl_3$) of compound **4.16B**

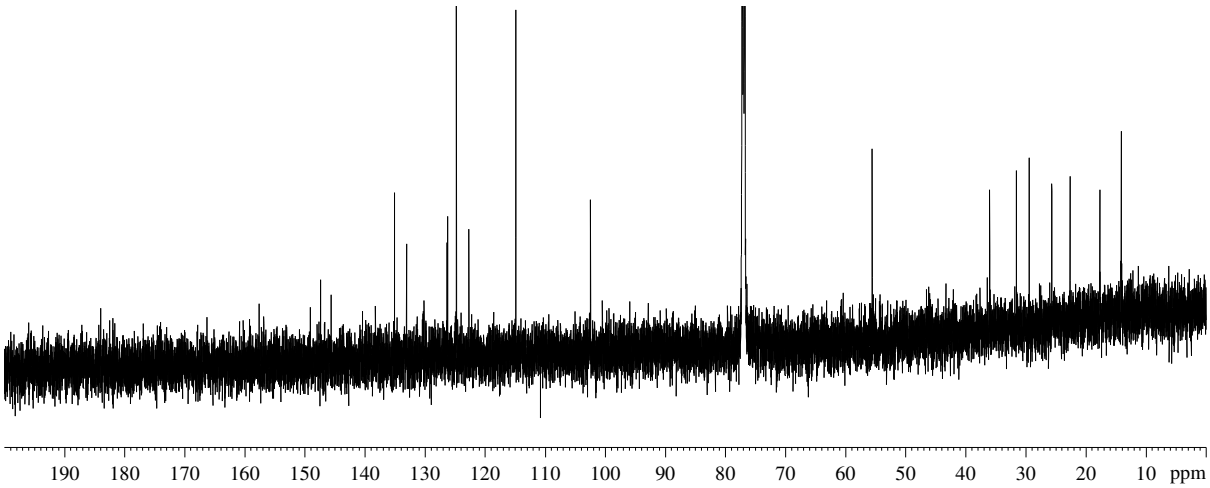

Figure S4.27: ^{13}C NMR spectrum (150 MHz, $CDCl_3$) of compound **4.16B**

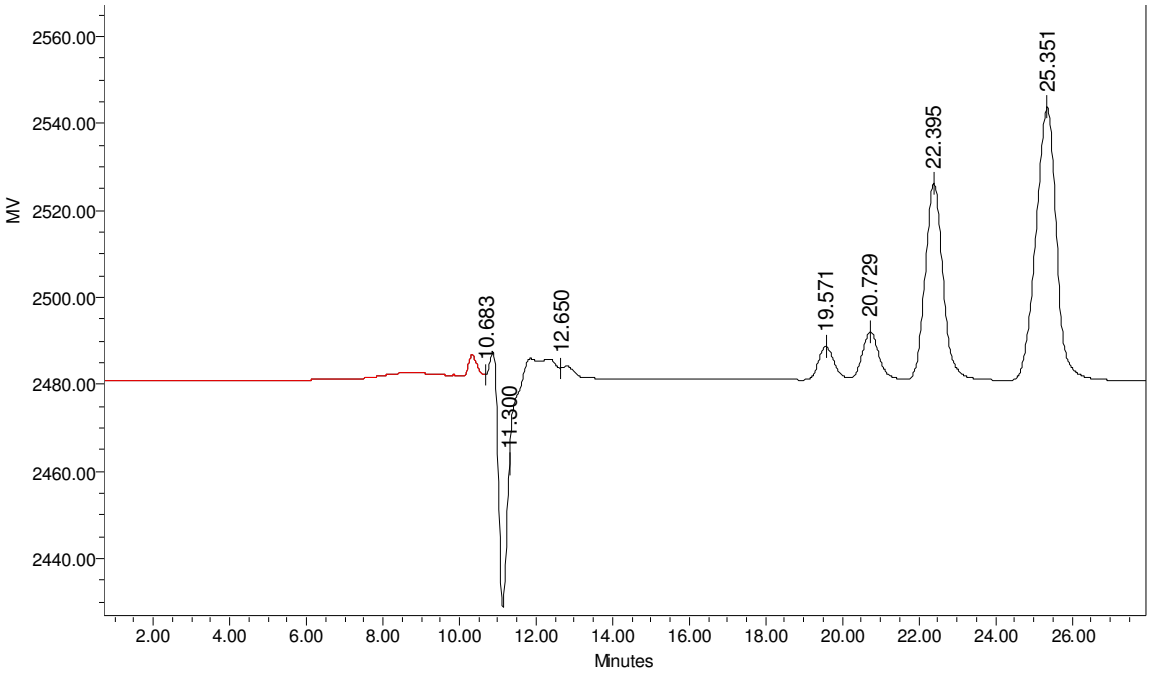

Figure S4.28: HPLC chromatogram showing the retention times for the two isomers: **4.16A**: 22.3 min and **4.16B**: 25.3 min

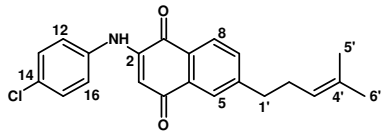

4.17A

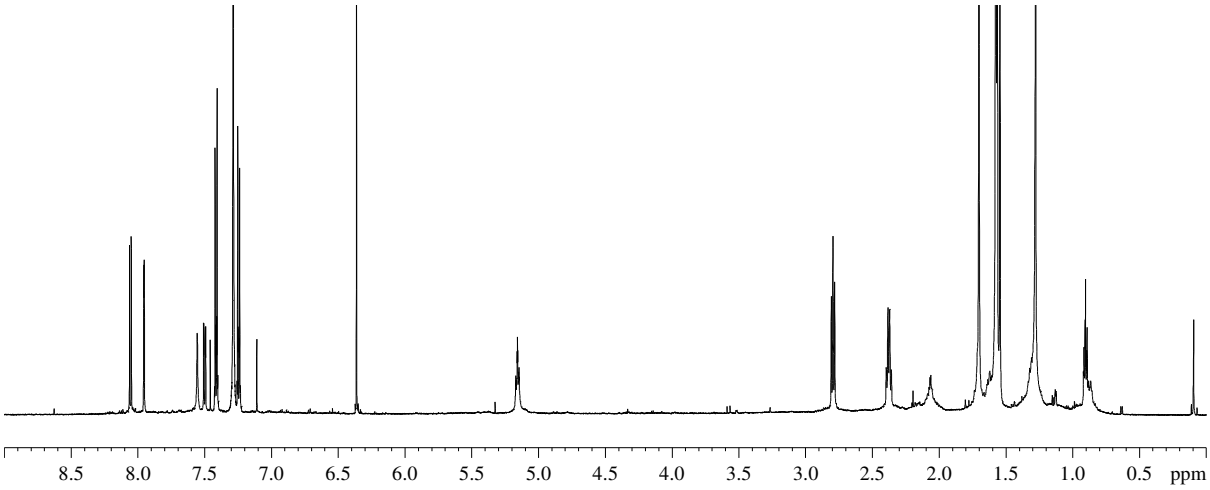

Figure S4.29: ^{1}H NMR spectrum (600 MHz, $CDCl_3$) of compound **4.17A**

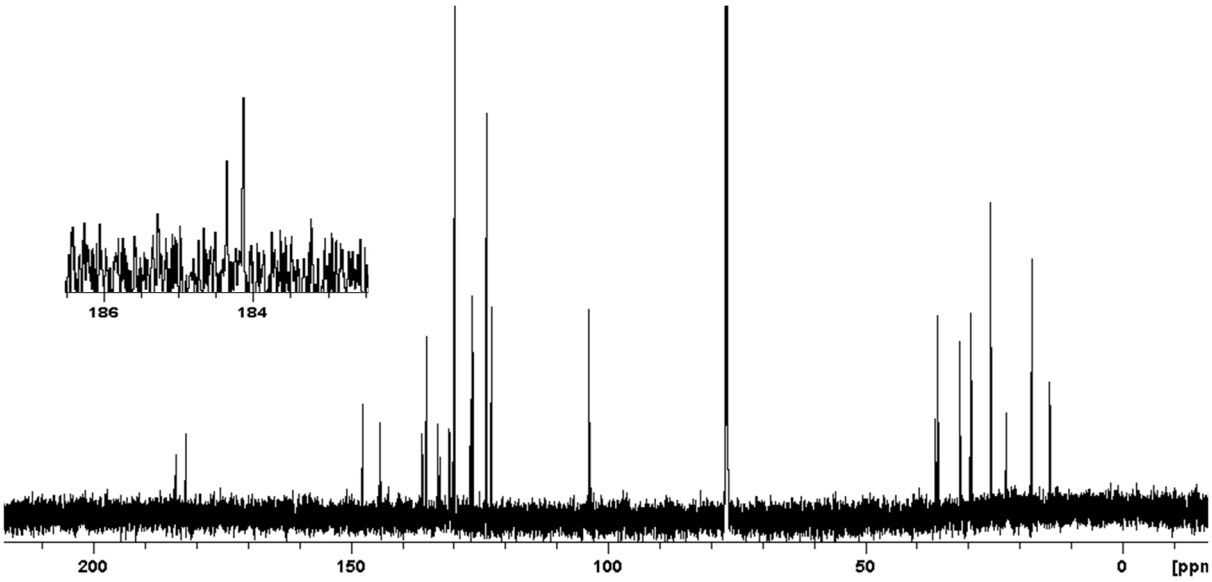

Figure S4.30: ^{1}H NMR spectrum (150 MHz, $CDCl_3$) of compound **4.17A**

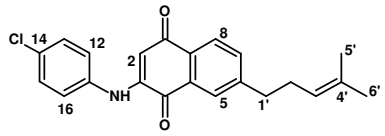

4.17B

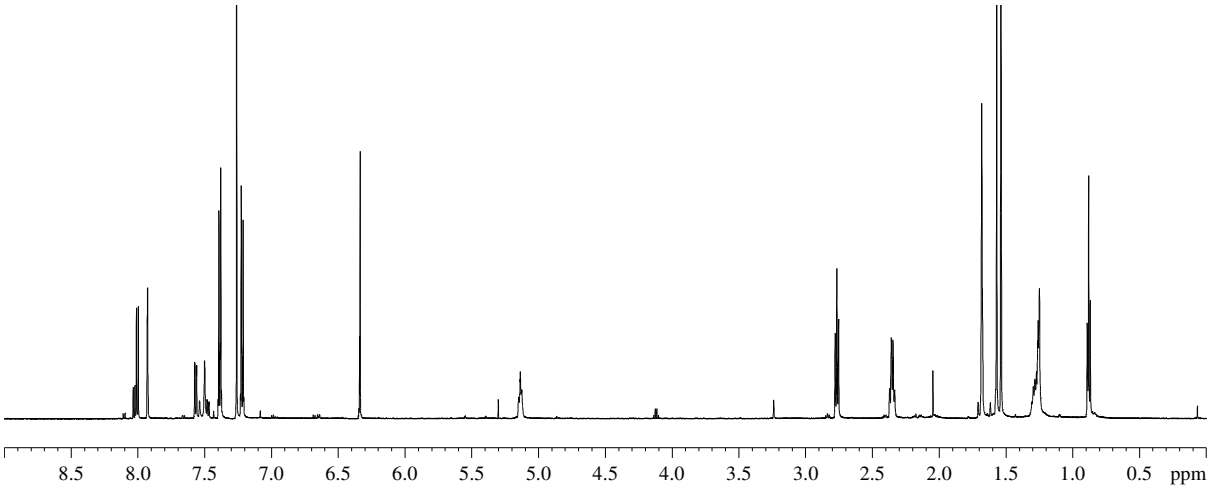

Figure S4.31: ^{1}H NMR spectrum (600 MHz, $CDCl_3$) of compound **4.17B**

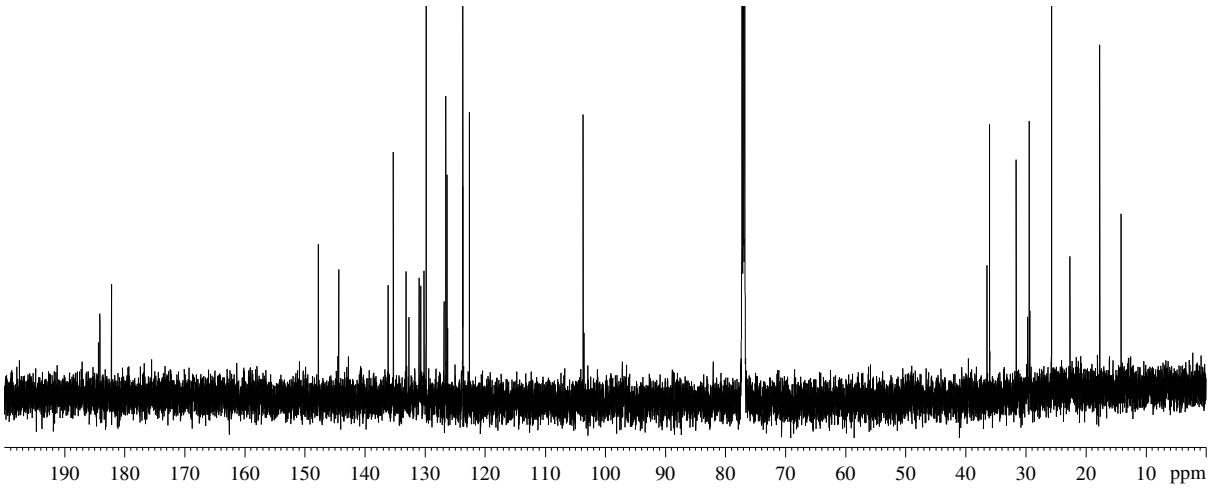

Figure S4.32: ^{13}C NMR spectrum (150 MHz, $CDCl_3$) of compound **4.17B**

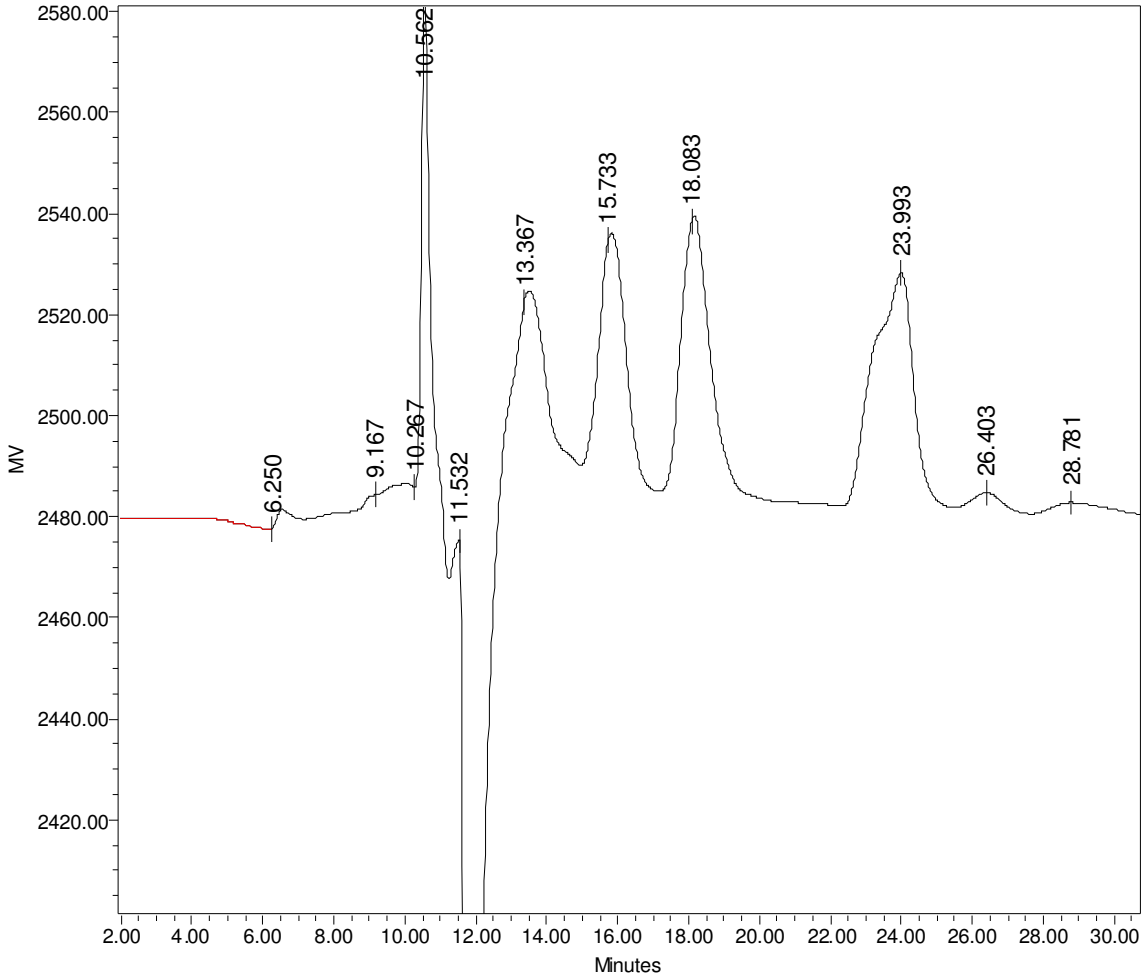

Figure S4.33: HPLC chromatogram showing the retention times for the two isomers: **4.17A**: 23.5 min and **4.17B**: 23.9 min

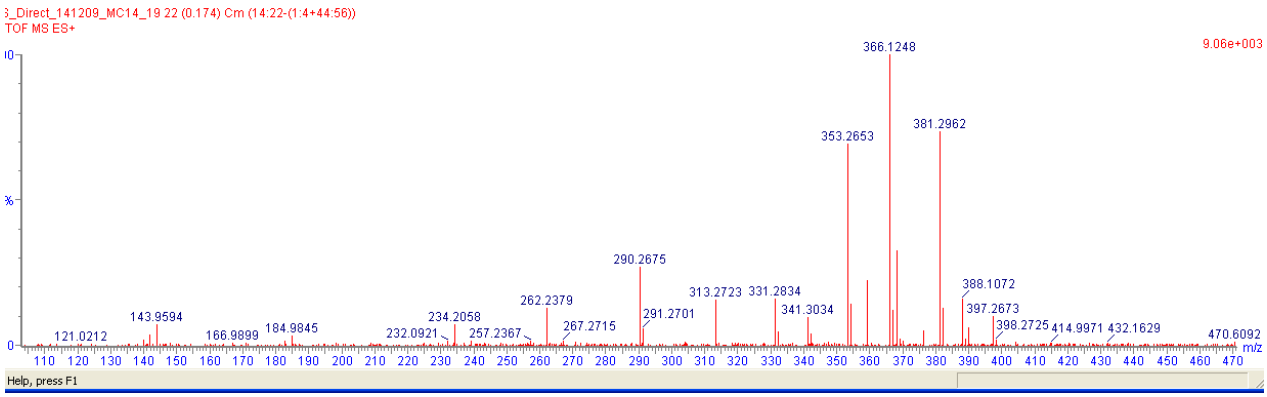

Figure S4.34: HRMS of compound **4.17A**

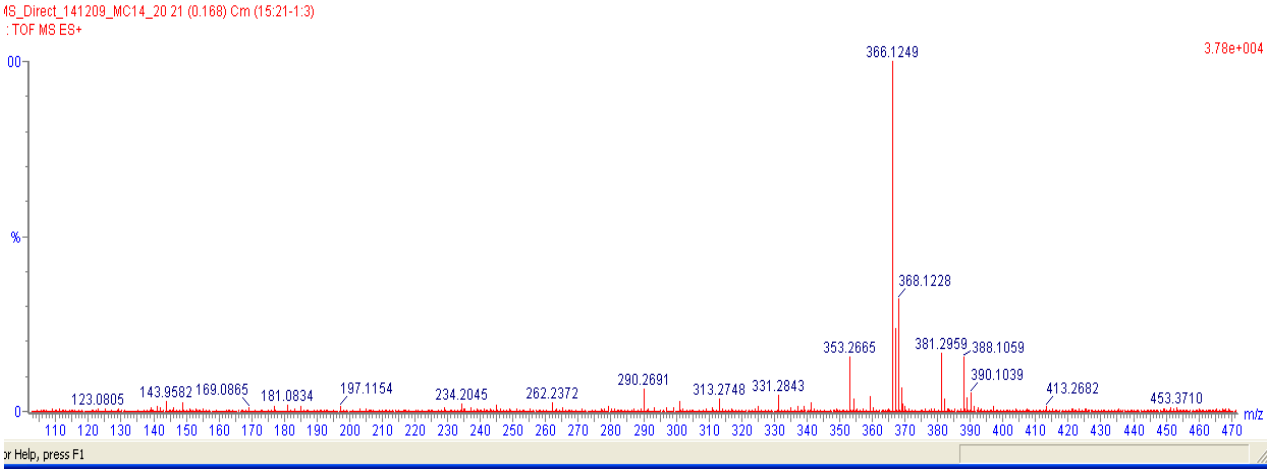

Figure S4.35: HRMS of compound **4.17B**

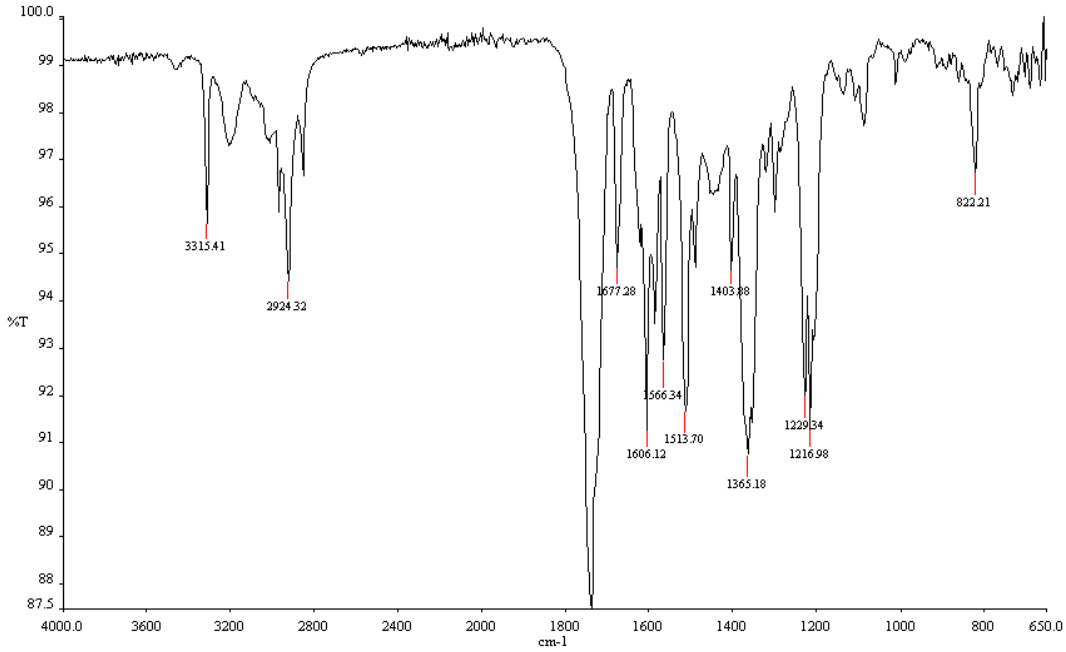

Figure S4.36: IR spectrum of compound **4.17**

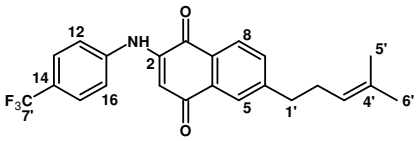

4.18A

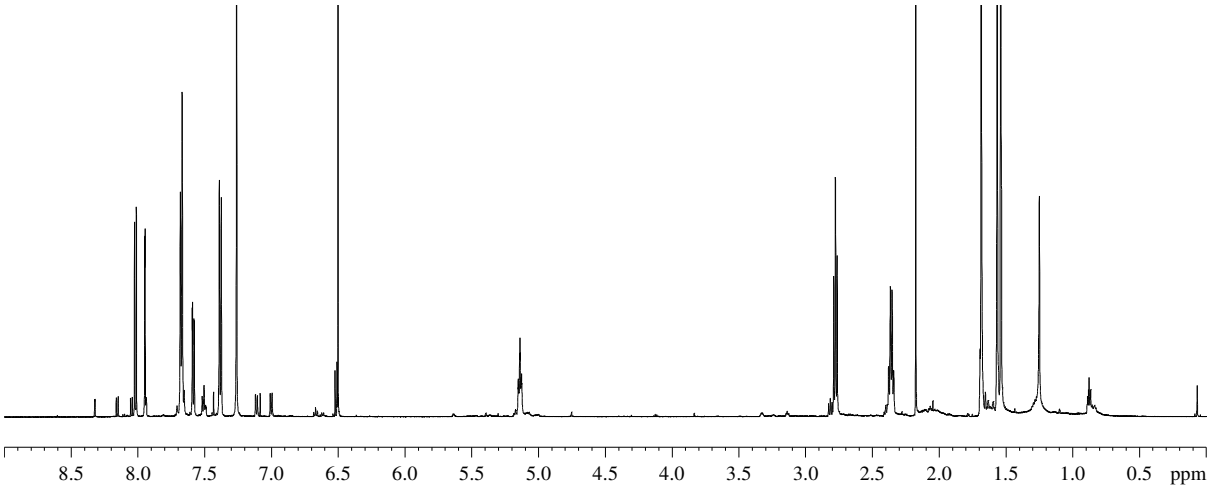

Figure S4.37: ^{1}H NMR spectrum (600 MHz, $CDCl_3$) of compound **4.18A**

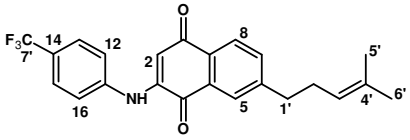

4.18B

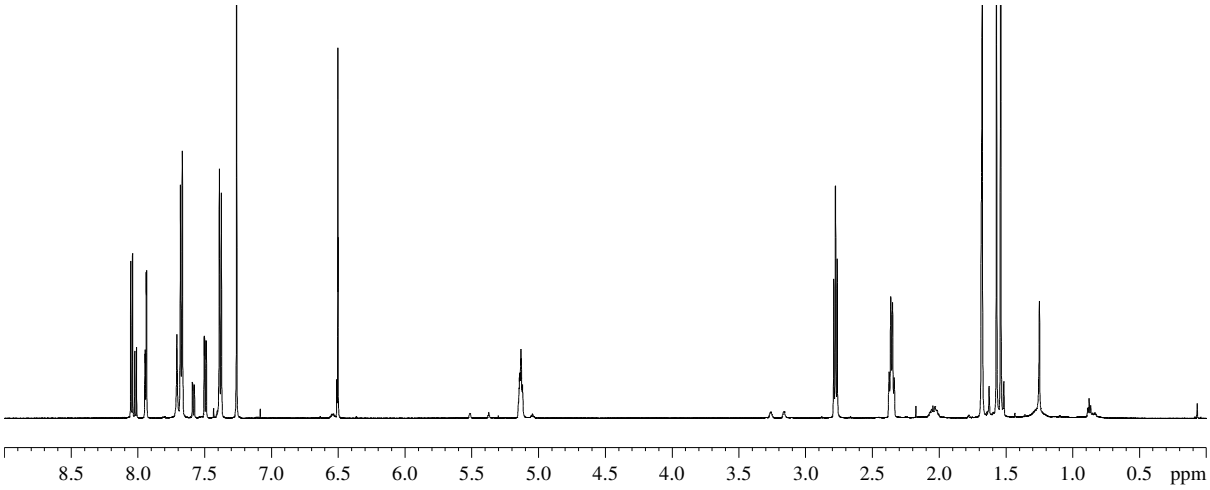

Figure S4.38: ^{1}H NMR spectrum (600 MHz, $CDCl_3$) of compound **4.18B**

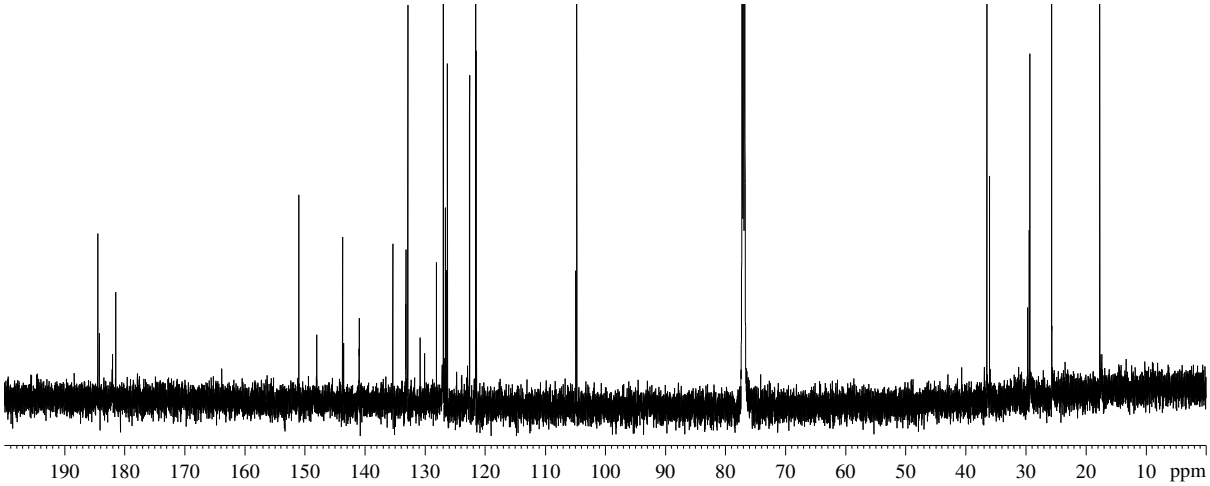

Figure S4.39: ^{13}C NMR spectrum (150 MHz, $CDCl_3$) of compound **4.18B**

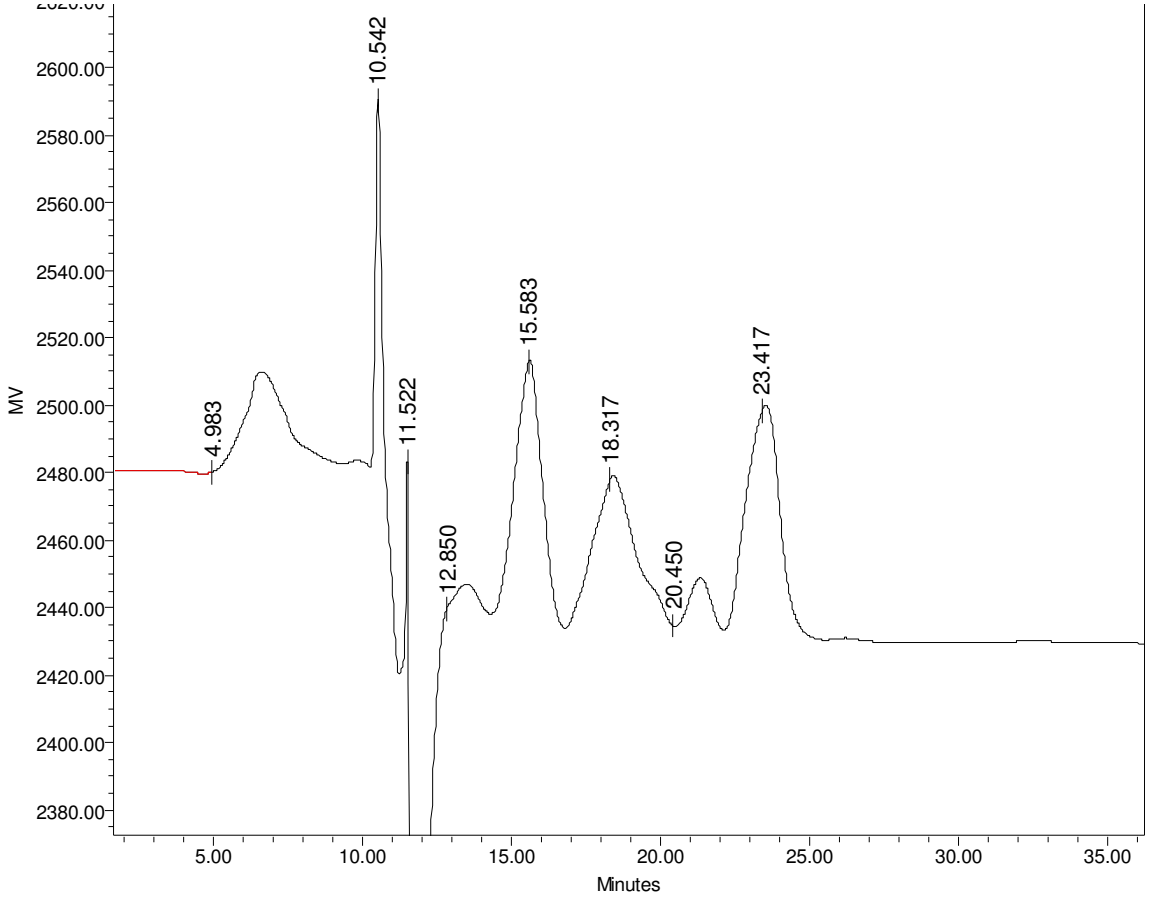

Figure S4.40: HPLC chromatogram showing the retention times for the two isomers: **4.18A**: 21.0 min and **4.18B**: 23.4 min

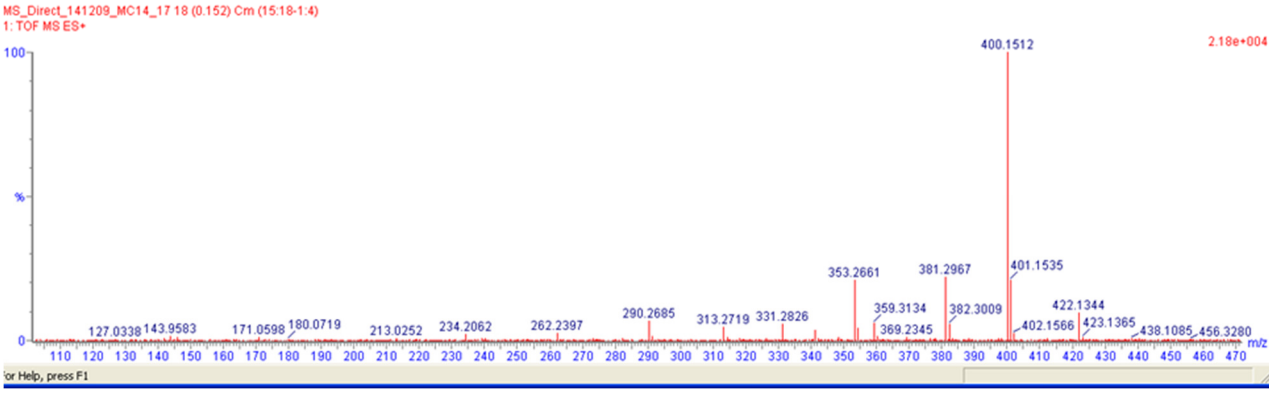

Figure S4.41: HRMS of compound **4.18A**

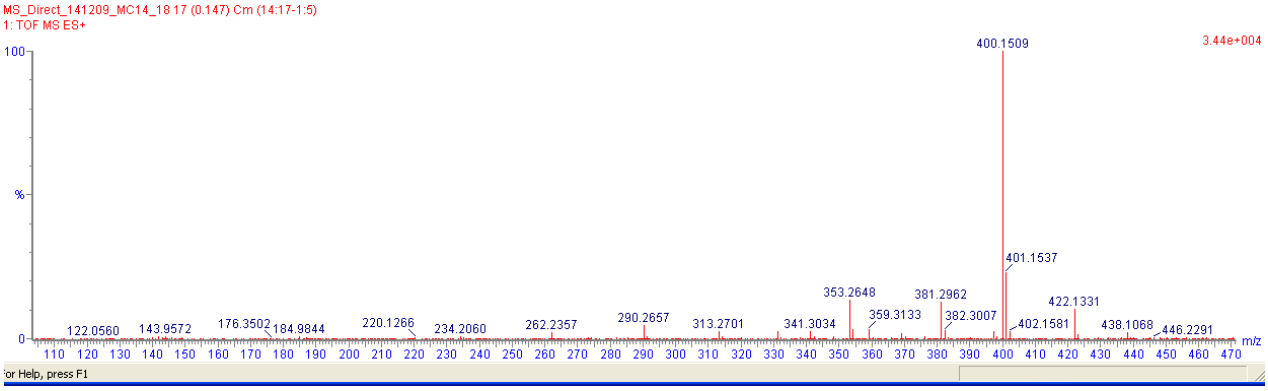

Figure S4.42: HRMS of compound **4.18B**

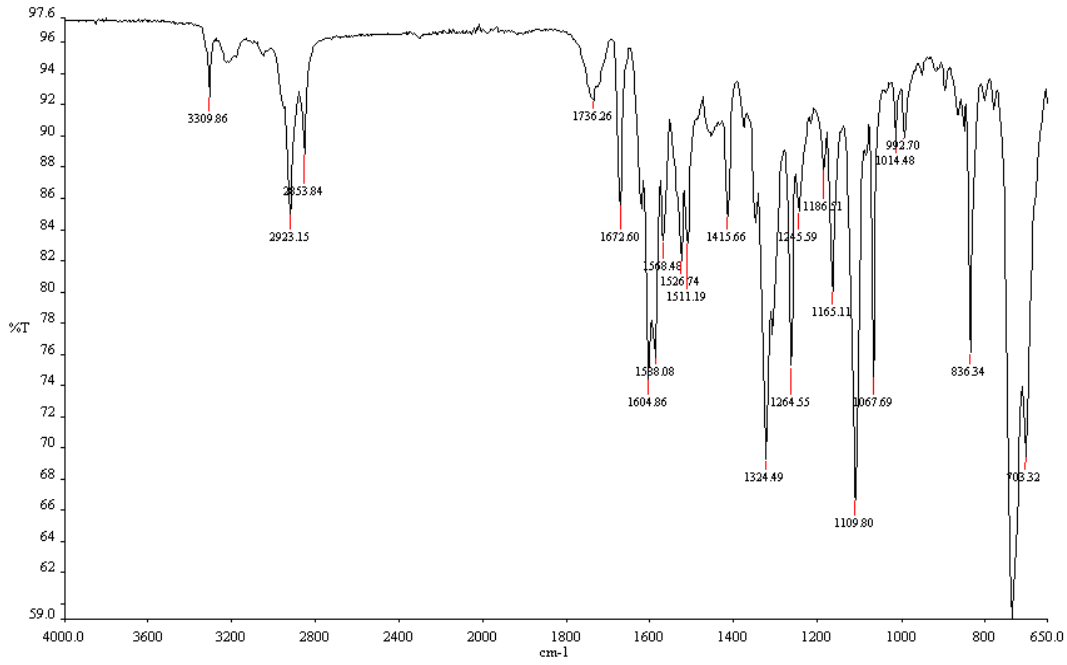

Figure S4.43: IR spectrum of compound **4.18B**

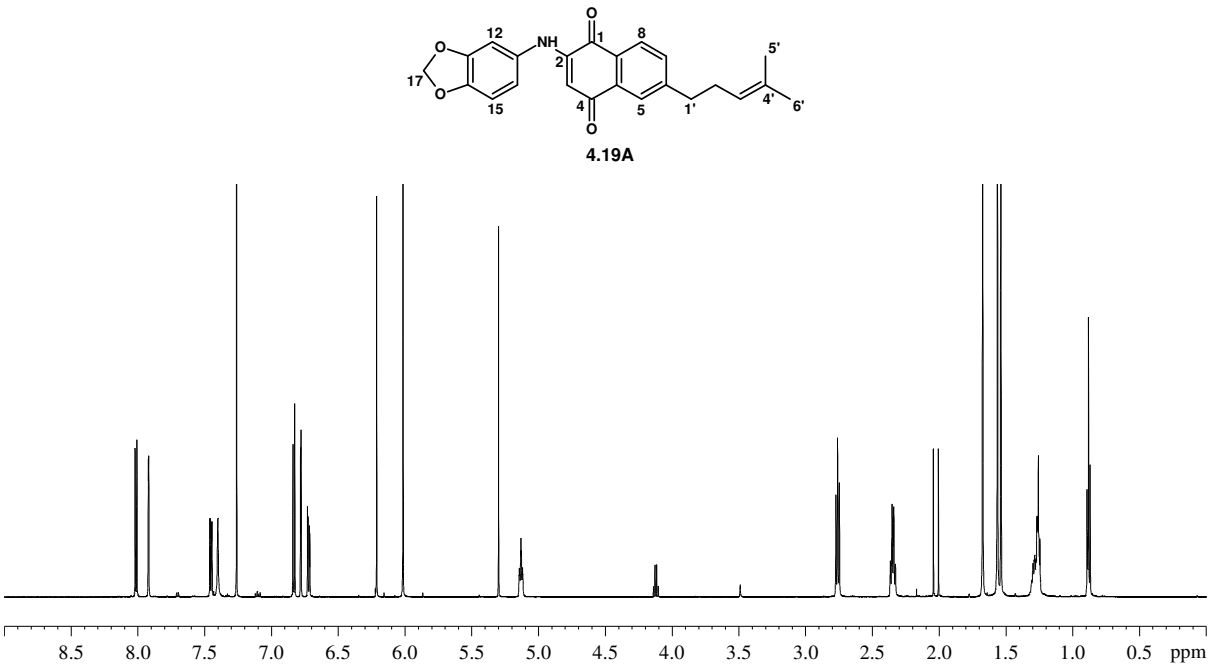

Figure S4.44: ^{1}H NMR spectrum (600 MHz, $CDCl_3$) of compound **4.19A**

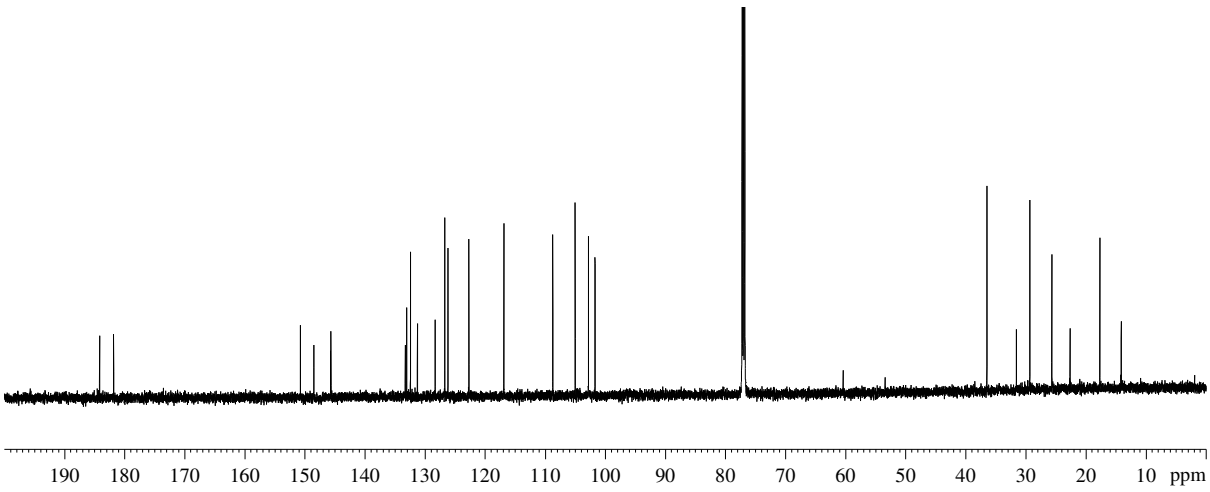

Figure S4.45: ^{13}C NMR spectrum (150 MHz, $CDCl_3$) of compound **4.19A**

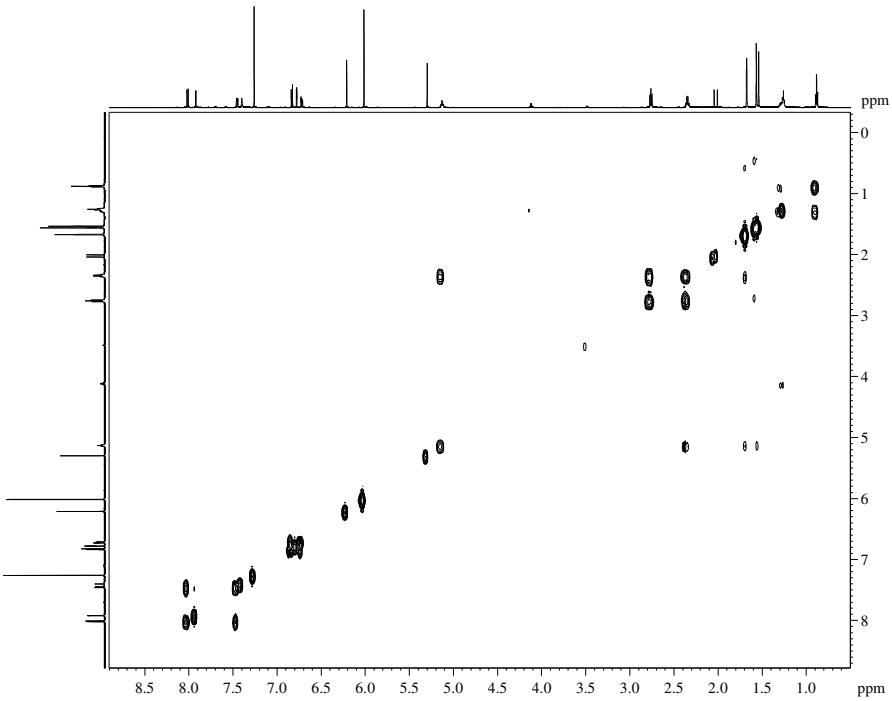

Figure S4.46: COSY NMR spectrum of compound **4.19A**

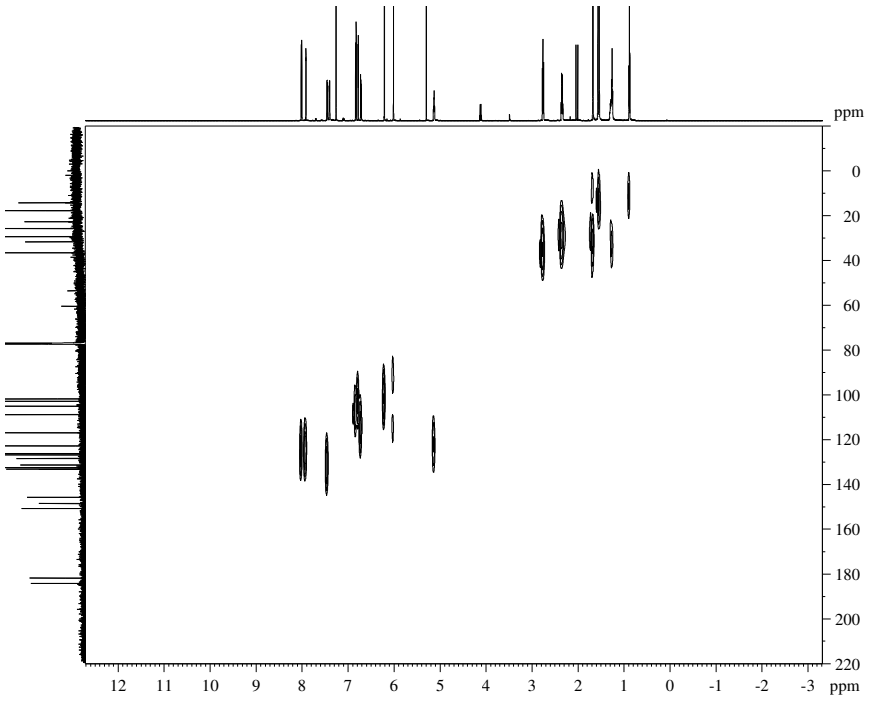

Figure S4.47: HSQC NMR spectrum of compound **4.19A**

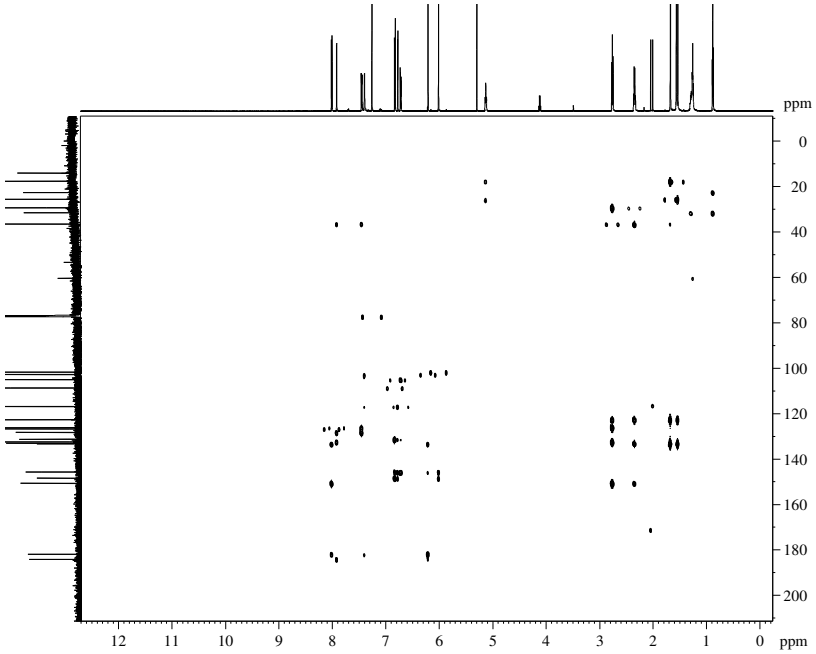

Figure S4.48: HMBC NMR spectrum of compound **4.19A**

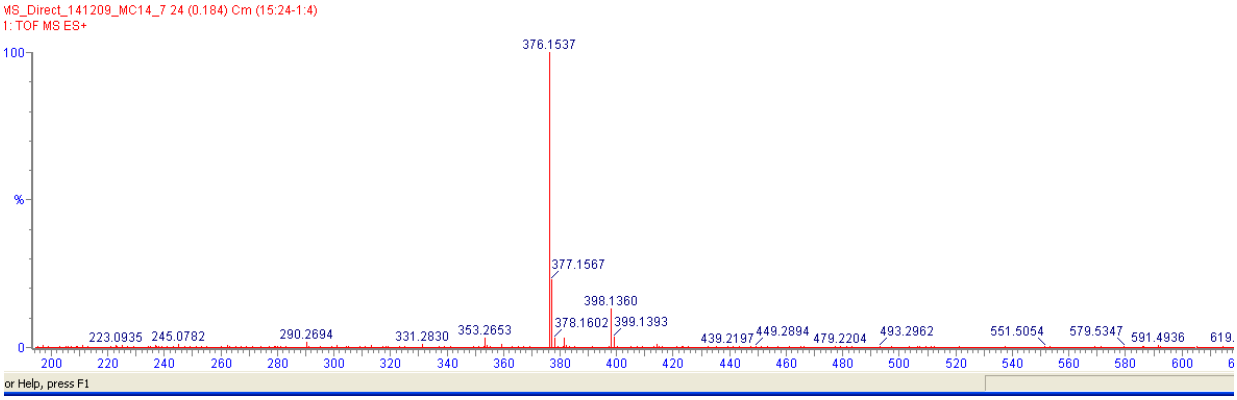

Figure S4.49: HRMS of compound **4.19A**

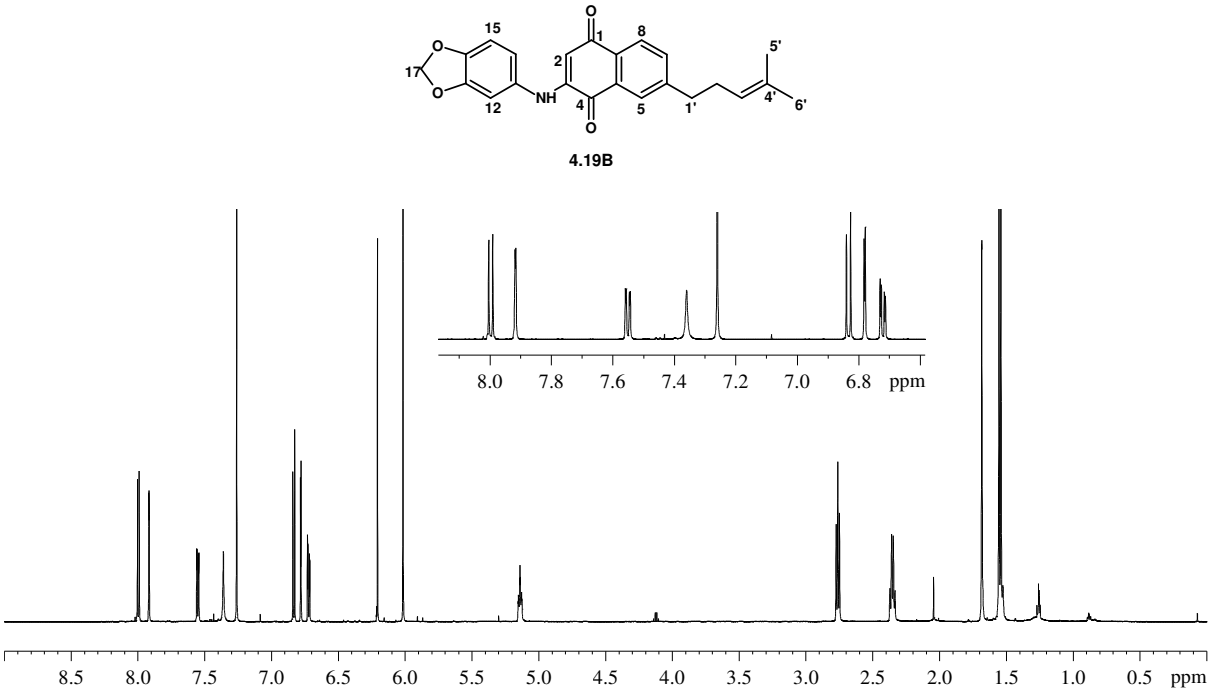

Figure S4.50: ^{1}H NMR spectrum (600 MHz, $CDCl_3$) of compound **4.19B**

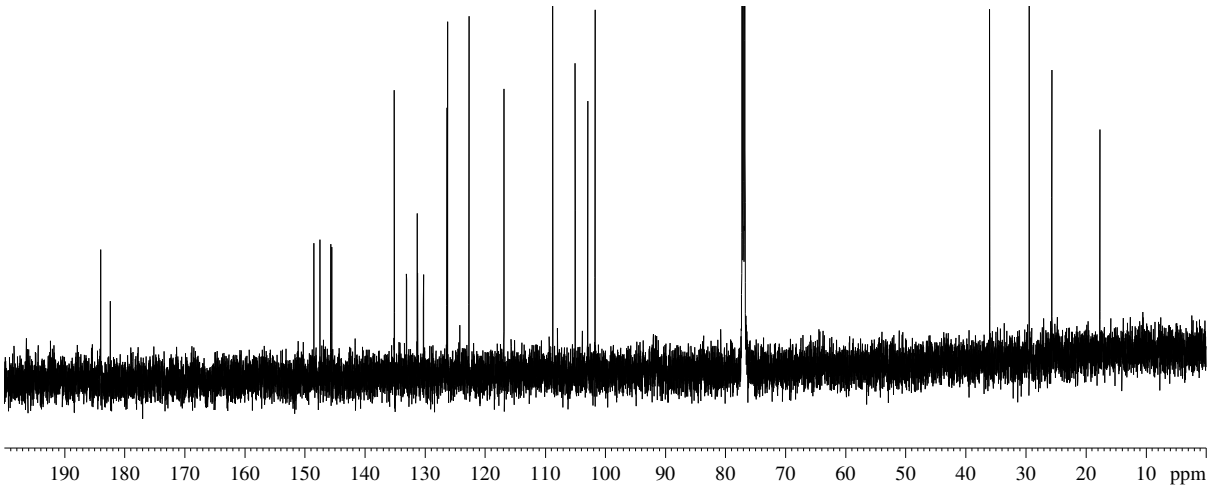

Figure S4.51: ^{13}C NMR spectrum (150 MHz, $CDCl_3$) of compound **4.19B**

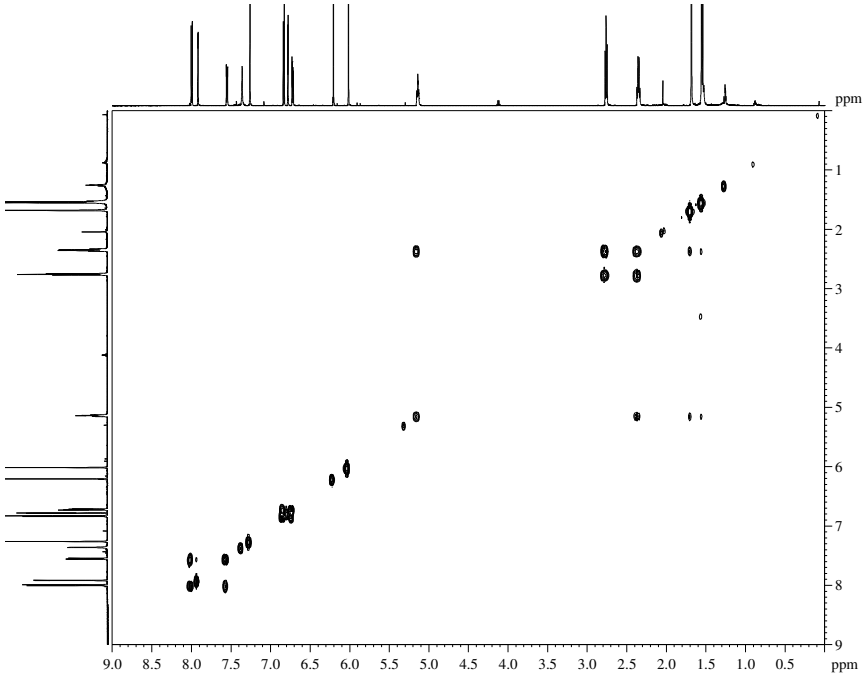

Figure S4.52: COSY NMR spectrum of compound **4.19B**

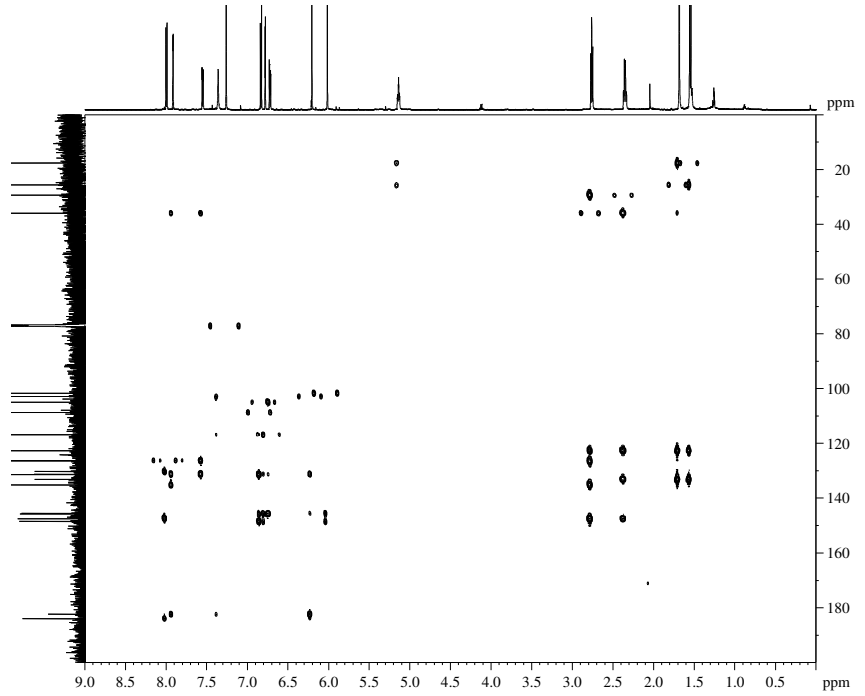

Figure S4.53: HMBC NMR spectrum of compound **4.19B**

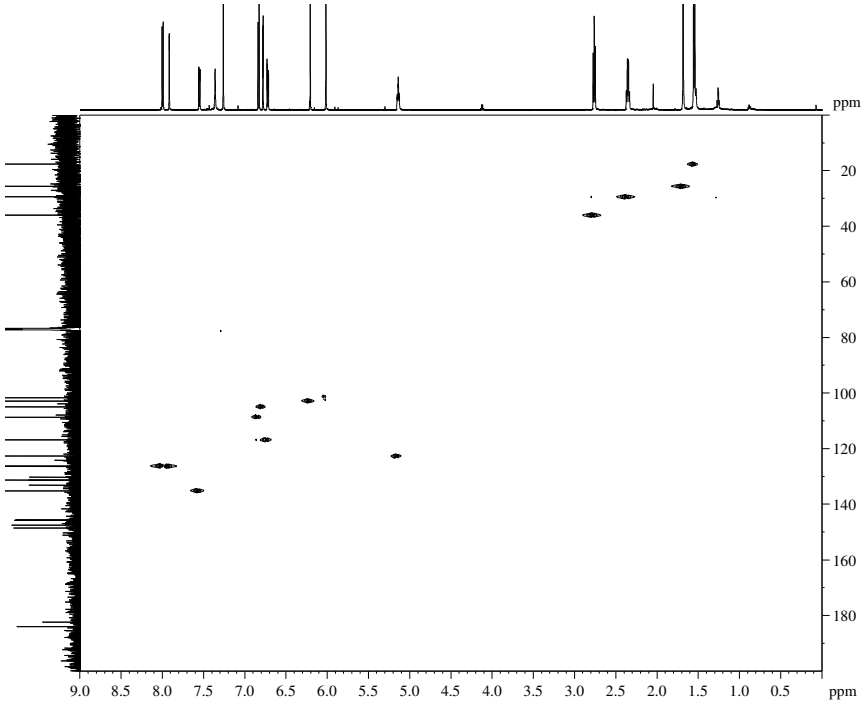

Figure S4.54: HSQC NMR spectrum of compound **4.19B**

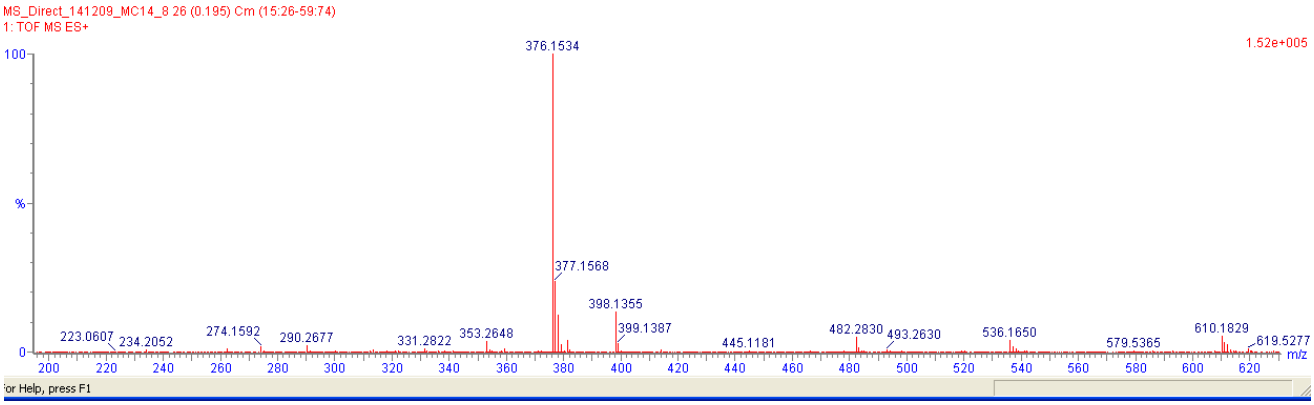

Figure S4.55: HRMS of compound **4.19B**

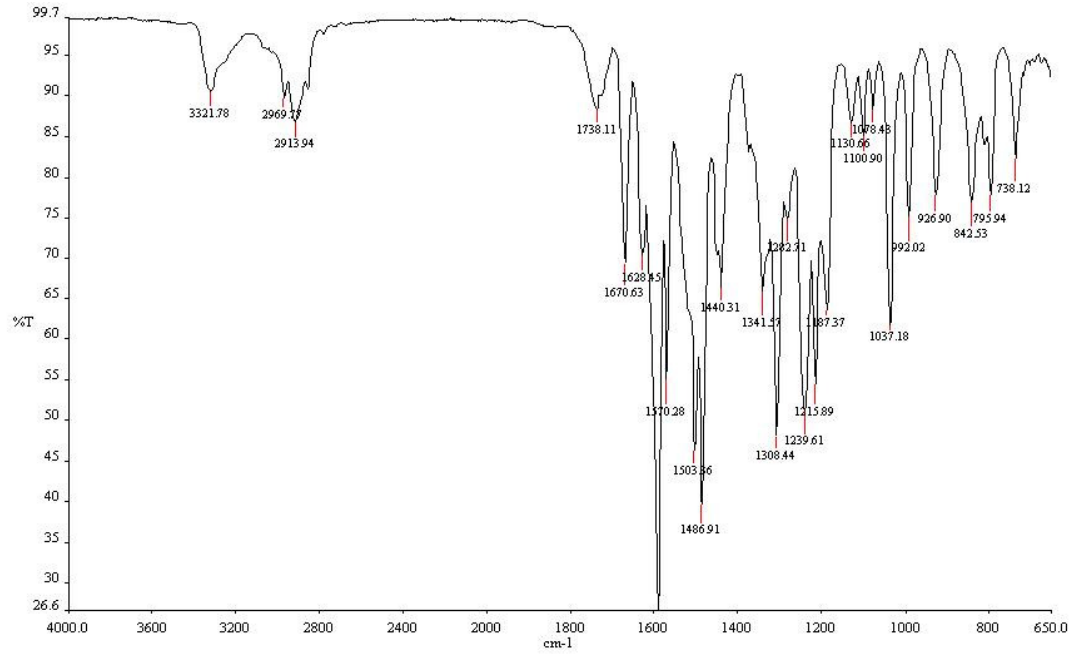

Figure S4.56: IR spectrum of compound **4.19B**

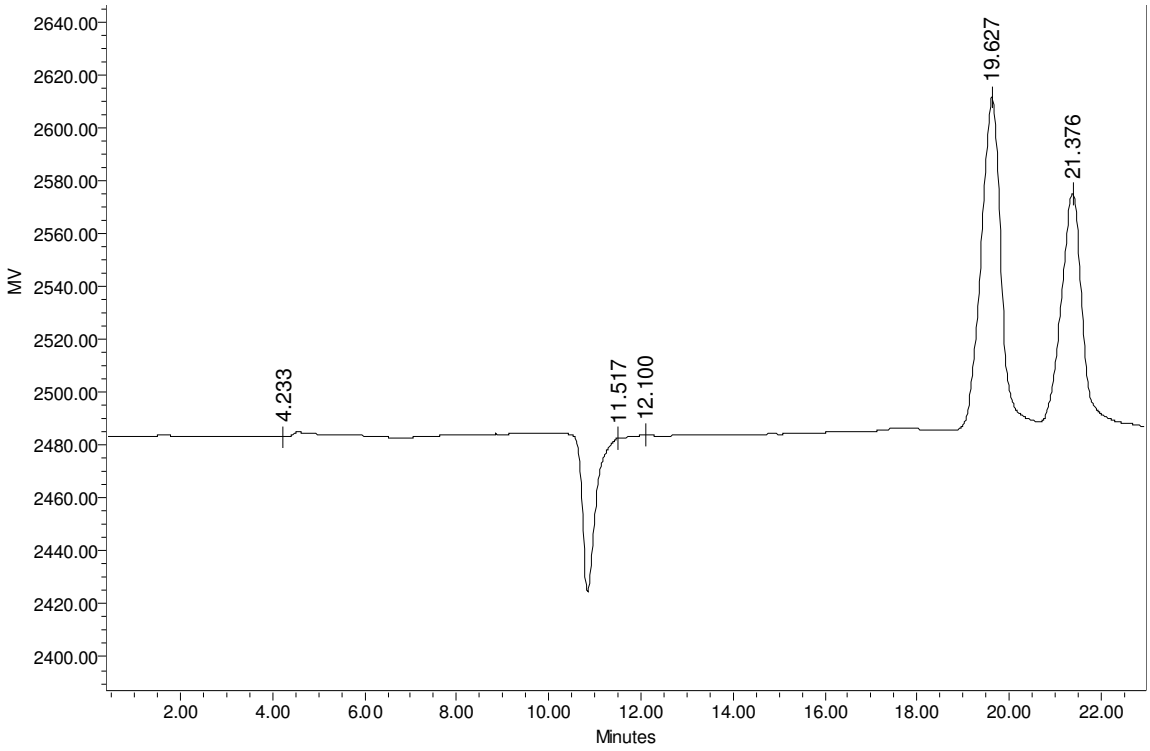

Figure S4.57: HPLC chromatogram showing the retention times for the two isomers: **4.19A**: 19.6 min and **4.19B**: 21.3 min

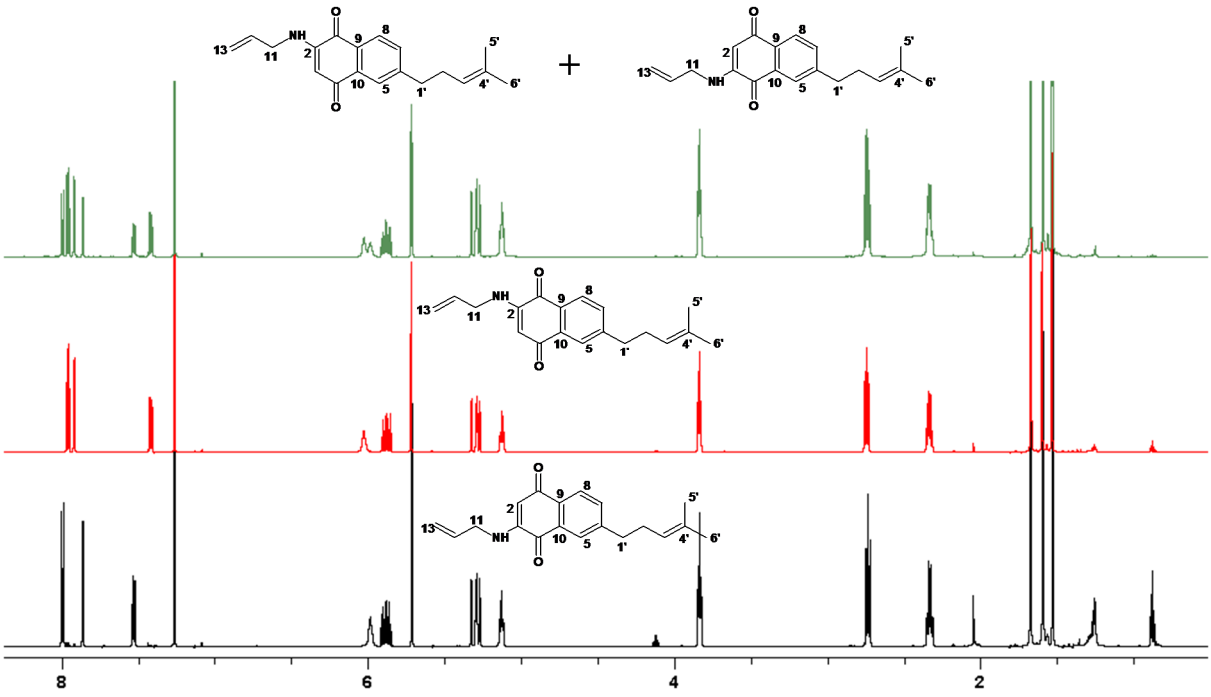

Figure S4.58: ^{1}H NMR spectra (600 MHz, $CDCl_3$) of alkylamino-naphthoquinone **4.20** illustrating the mixture of isomers before and after normal phase HPLC.

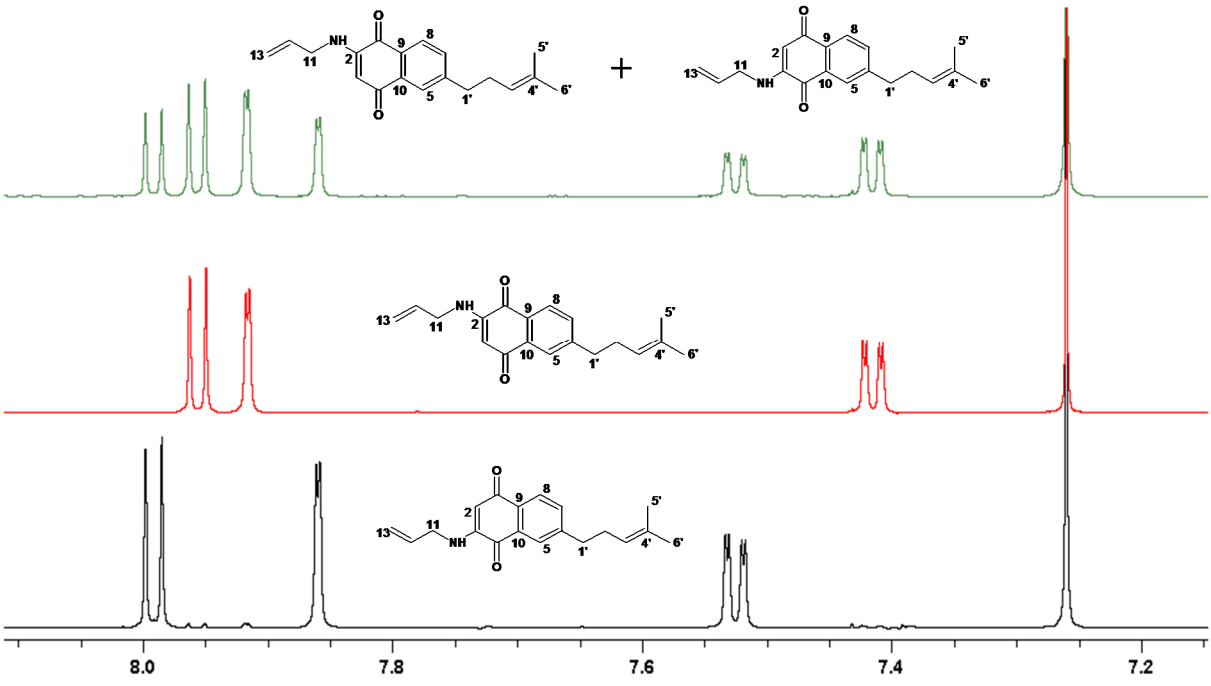

Figure S4.59: ^{1}H NMR spectra (600 MHz, $CDCl_3$) of alkylamino-naphthoquinone **4.20** showing differences between the isomers in the aromatic region

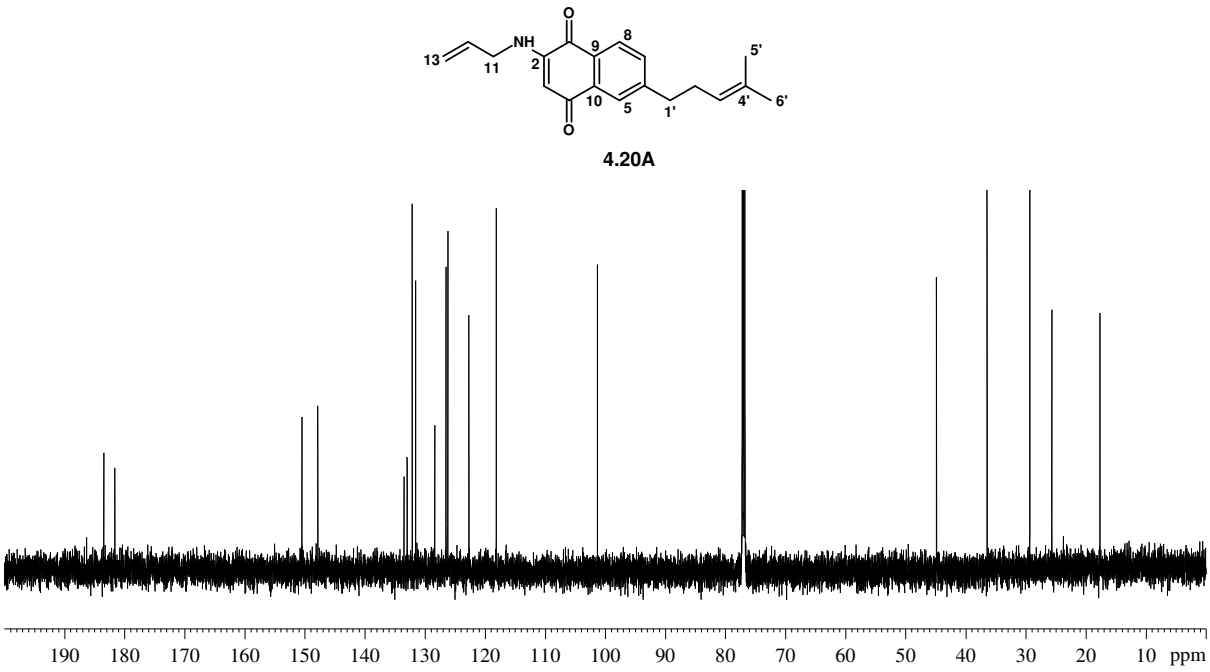

Figure S4.60: ^{13}C NMR spectrum (150 MHz, $CDCl_3$) of compound **4.20A**

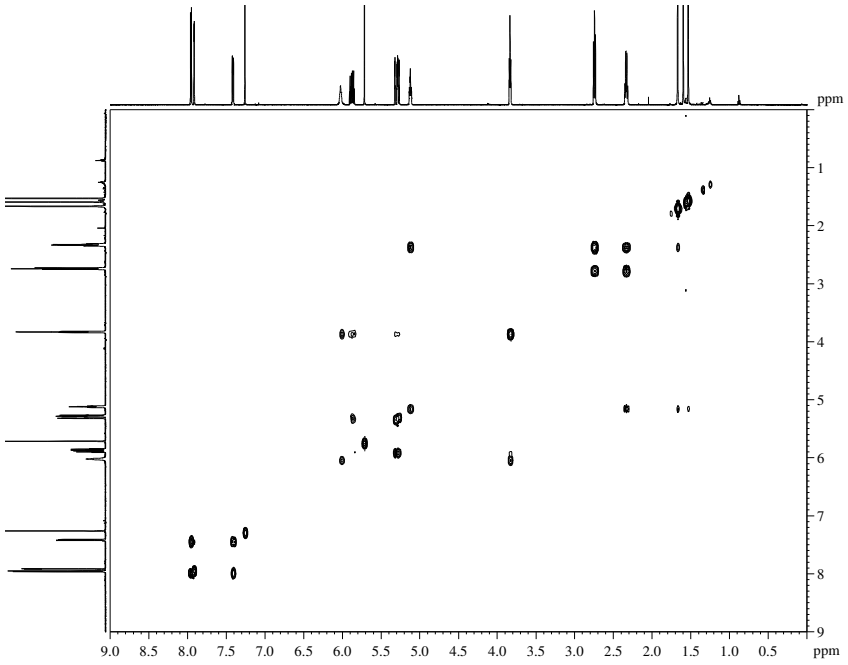

Figure S4.61: COSY NMR spectrum of compound **4.20A**

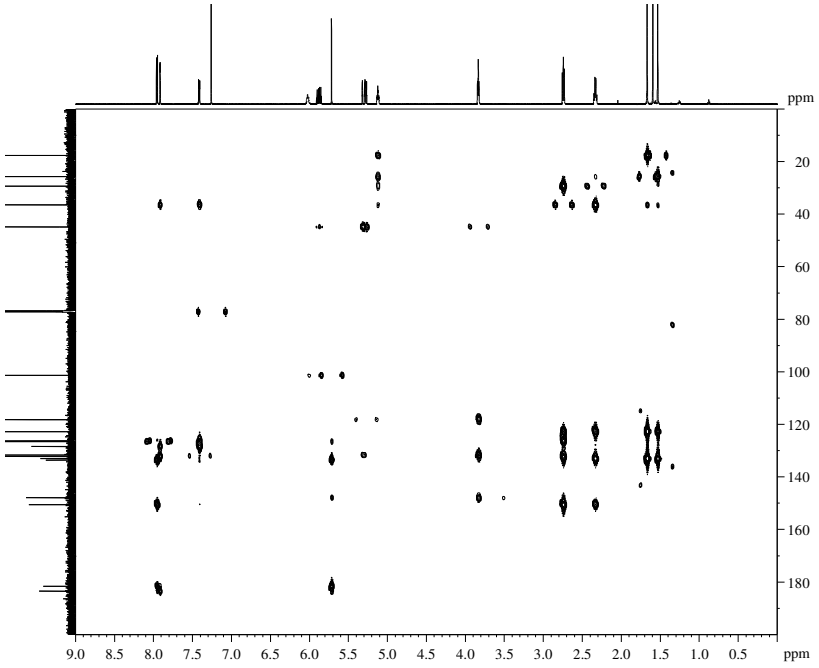

Figure S4.62: HMBC NMR spectrum of compound **4.20A**

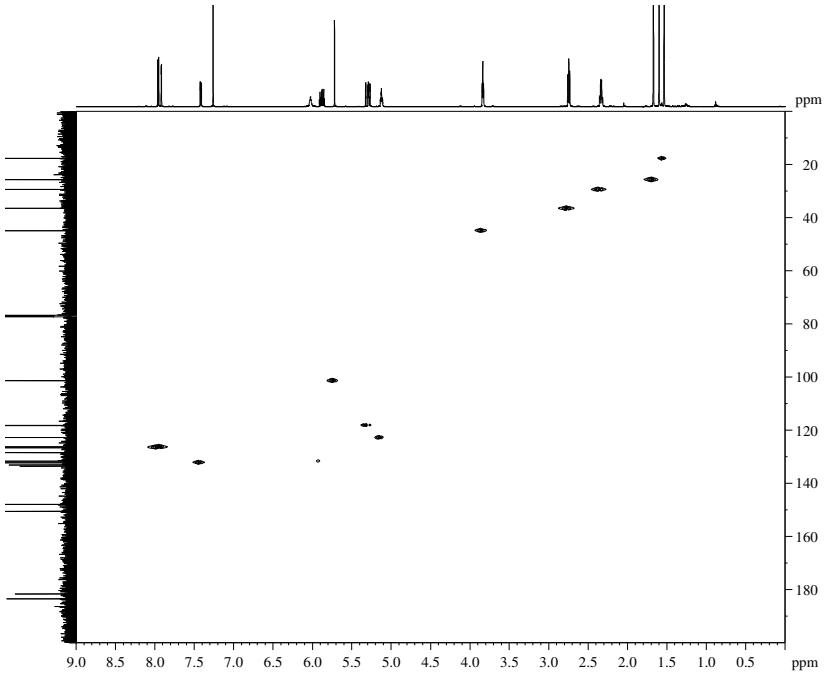

Figure S4.63: HSQC NMR spectrum of compound **4.20A**

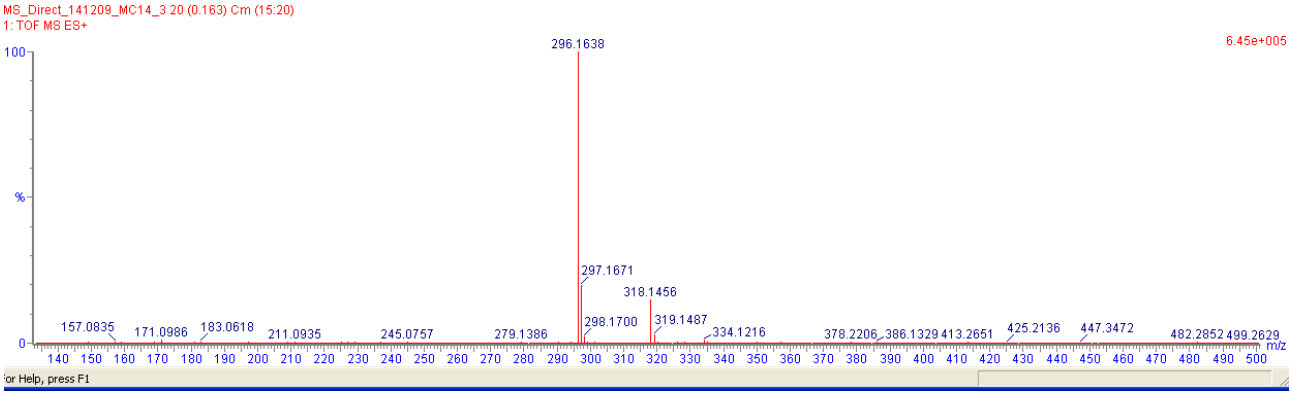

Figure S4.64: HRMS spectrum of compound **4.20A**

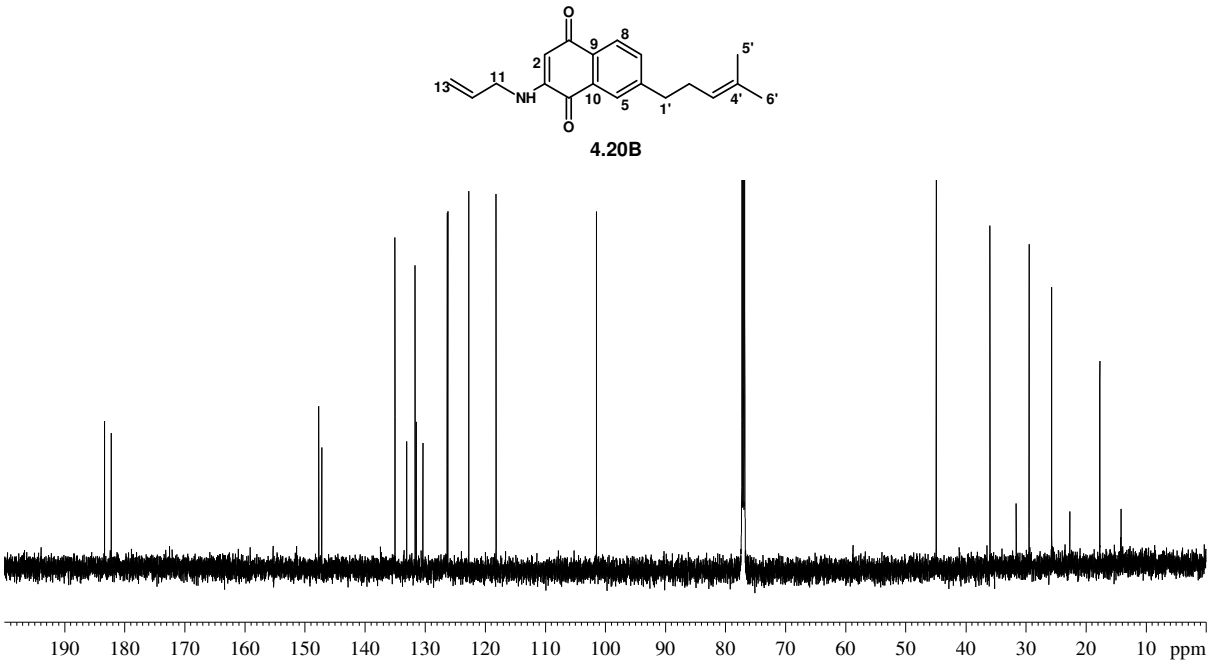

Figure S4.65: ^{13}C NMR spectrum (150 MHz, $CDCl_3$) of compound **4.20B**

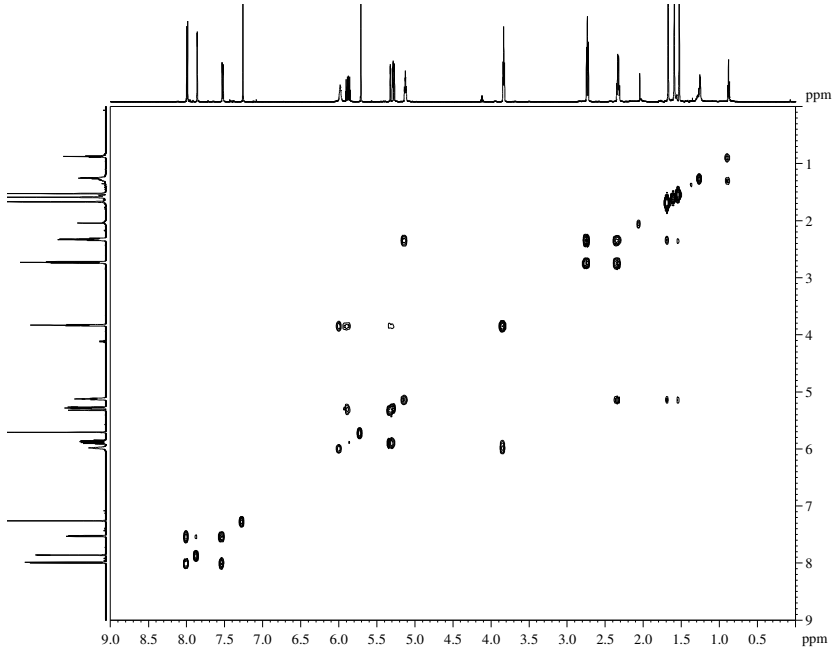

Figure S4.66: COSY NMR spectrum of compound **4.20B**

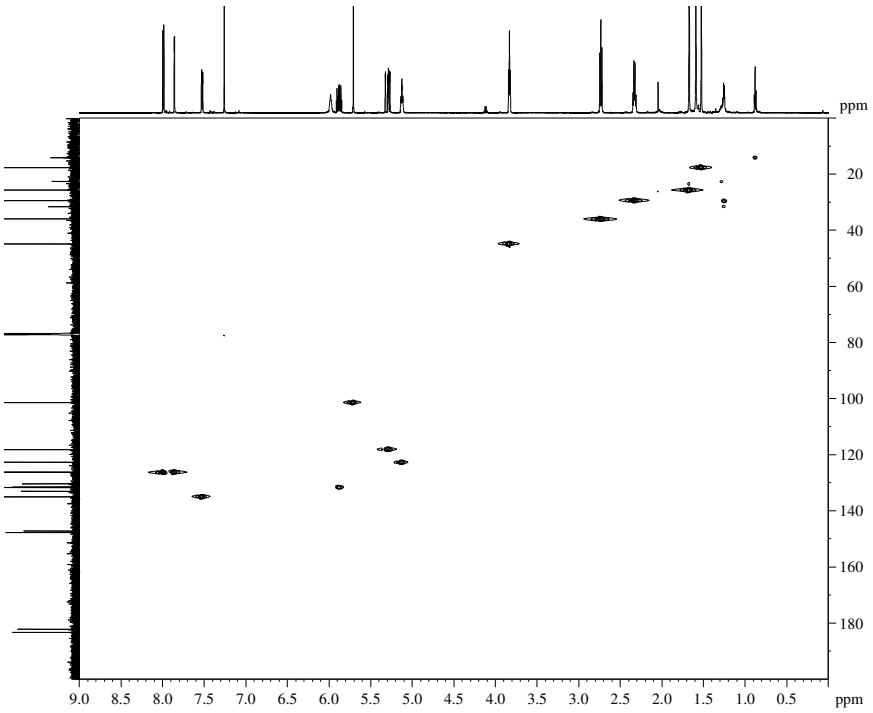

Figure S4.67: HSQC NMR spectrum of compound **4.20B**

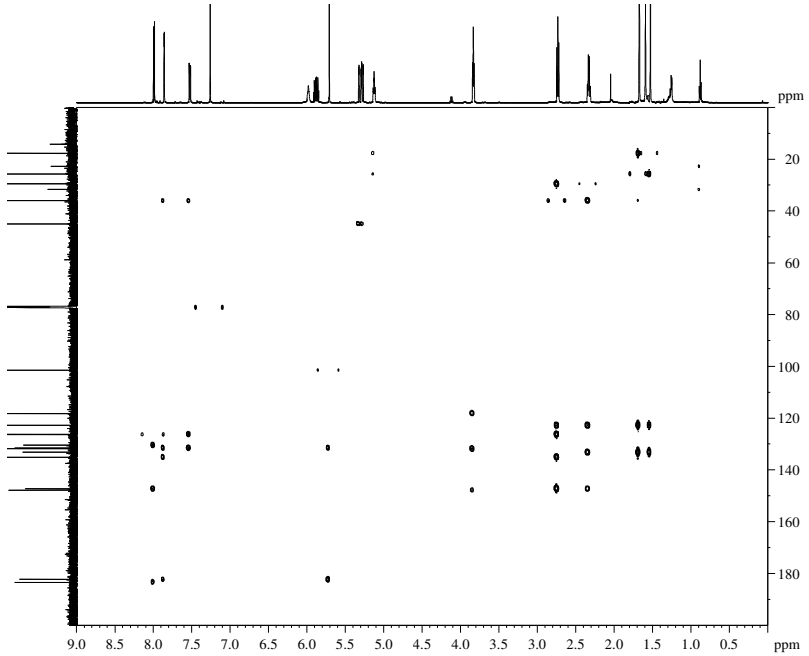

Figure S4.68: HMBC NMR spectrum of compound **4.20B**

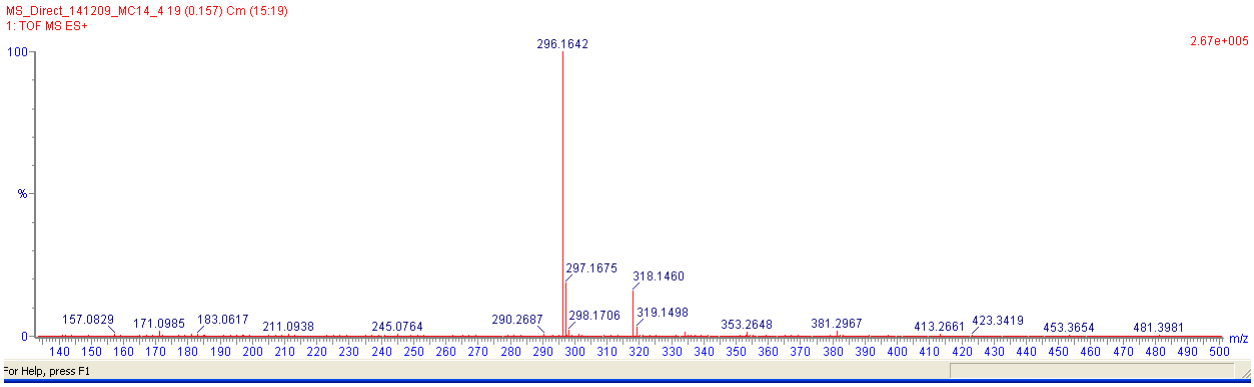

Figure S4.69: HRMS of compound **4.20B**

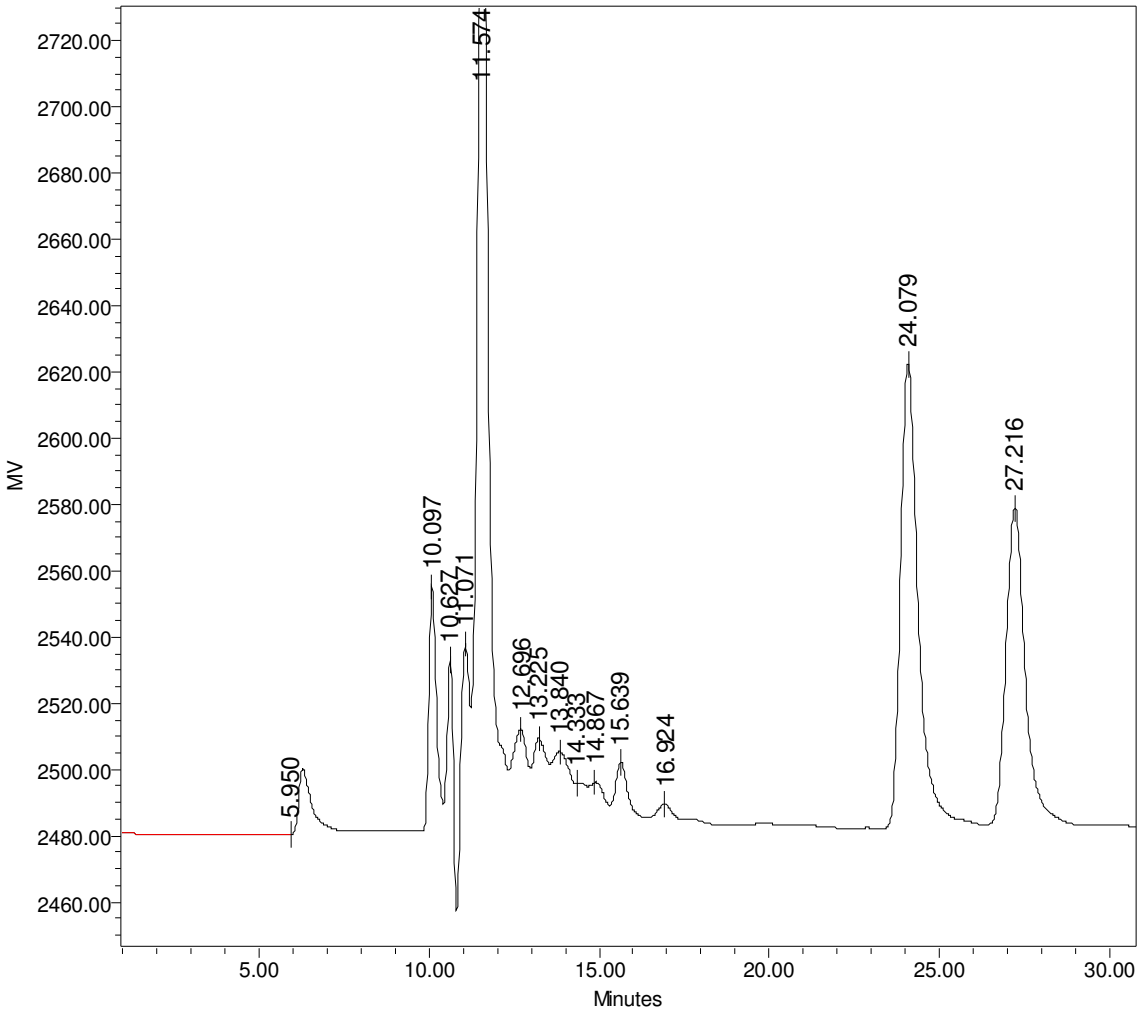

Figure S4.70: HPLC chromatogram showing the retention times for the two isomers: **4.20A**: 24.0 min and **4.20B**: 27.2 min

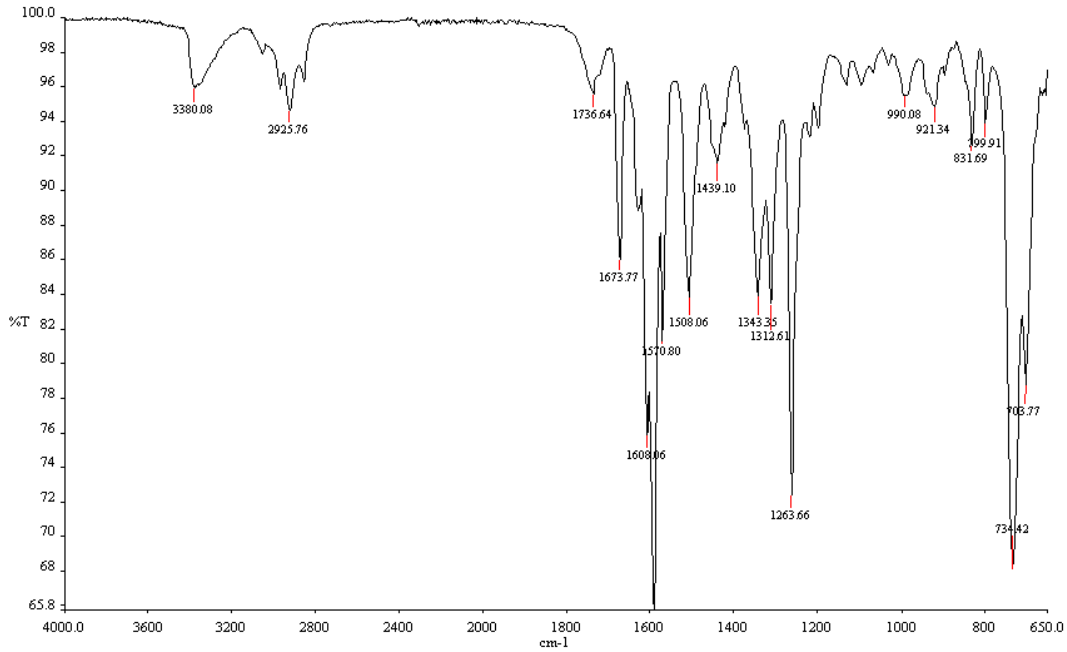

Figure S4.71: IR spectrum of compound **4.20B**

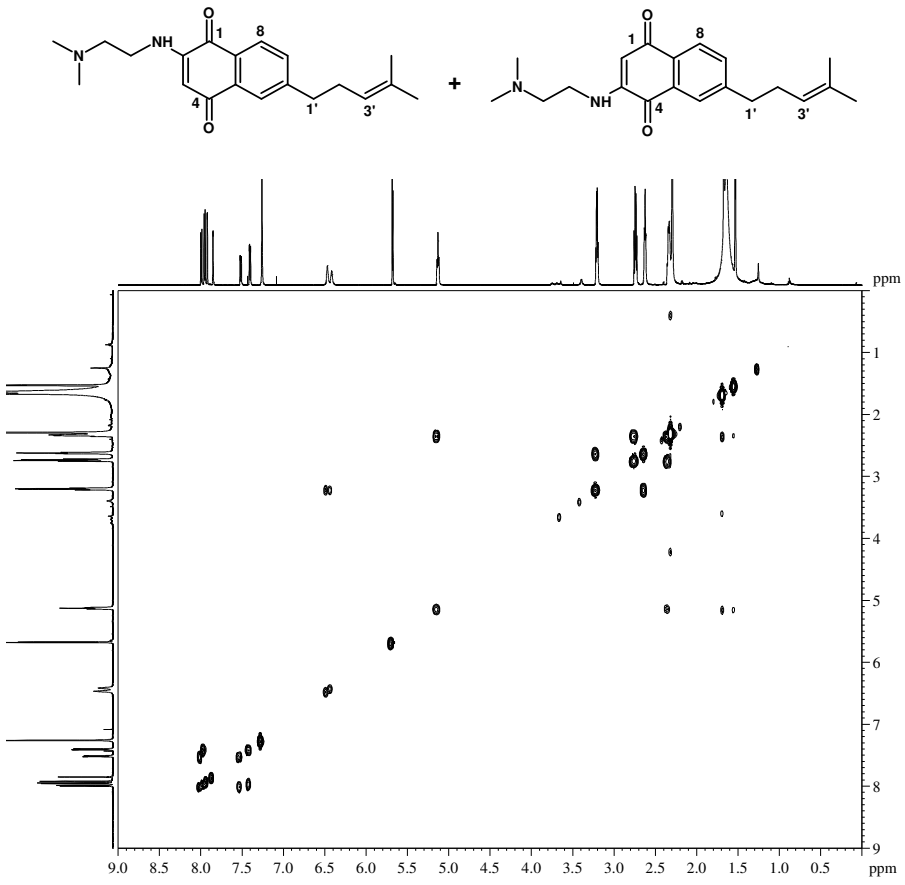

Figure S4.72: COSY NMR spectrum of compound **4.21** mixture

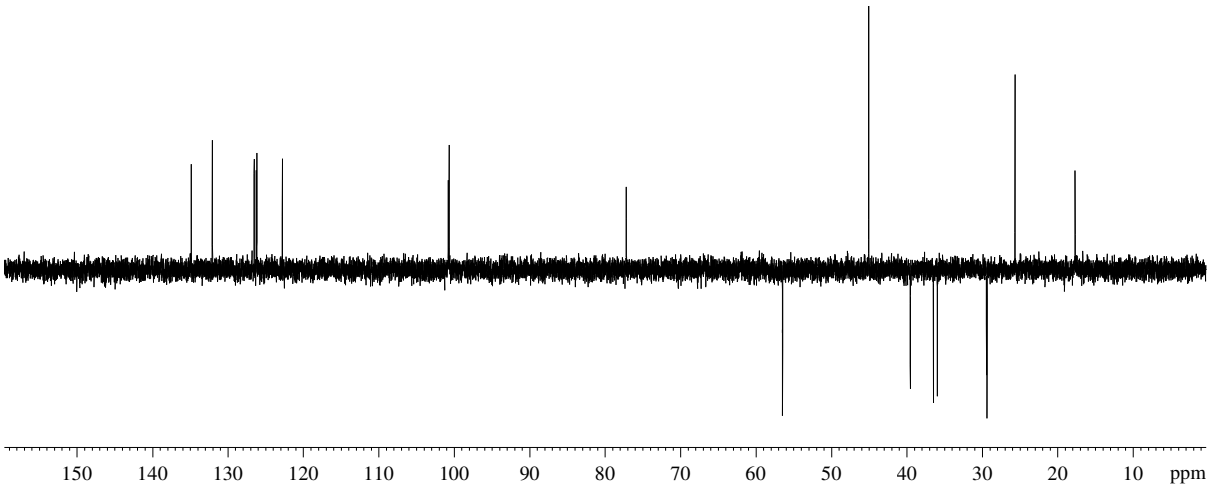

Figure S4.73: DEPT135 NMR spectrum of compound **4.21** mixture

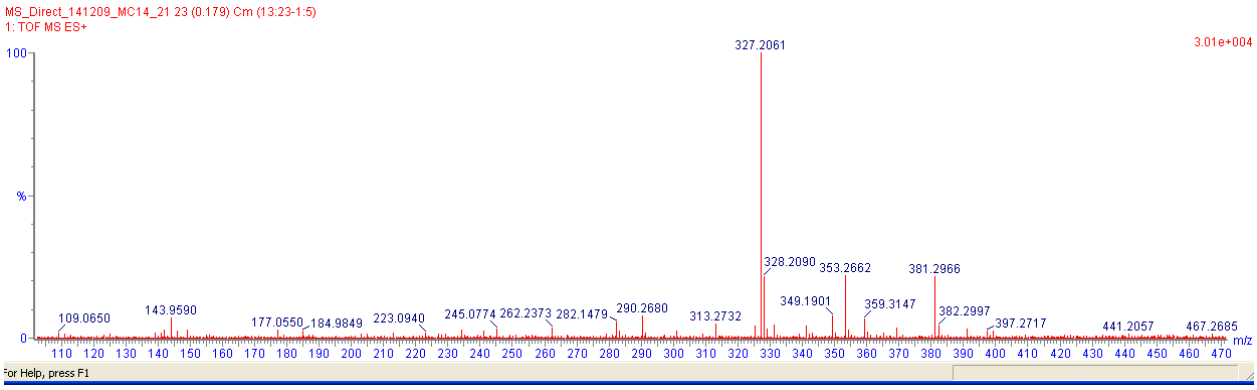

Figure S4.74: HRMS of compound **4.21** mixture

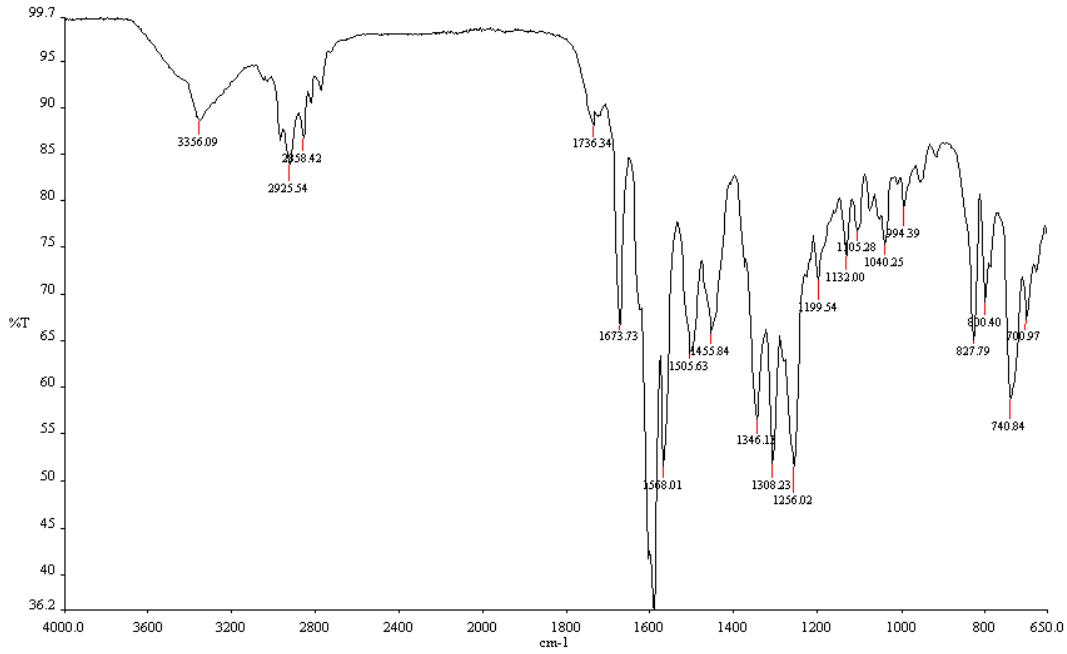

Figure S4.75: IR spectrum of compound **4.21** mixture

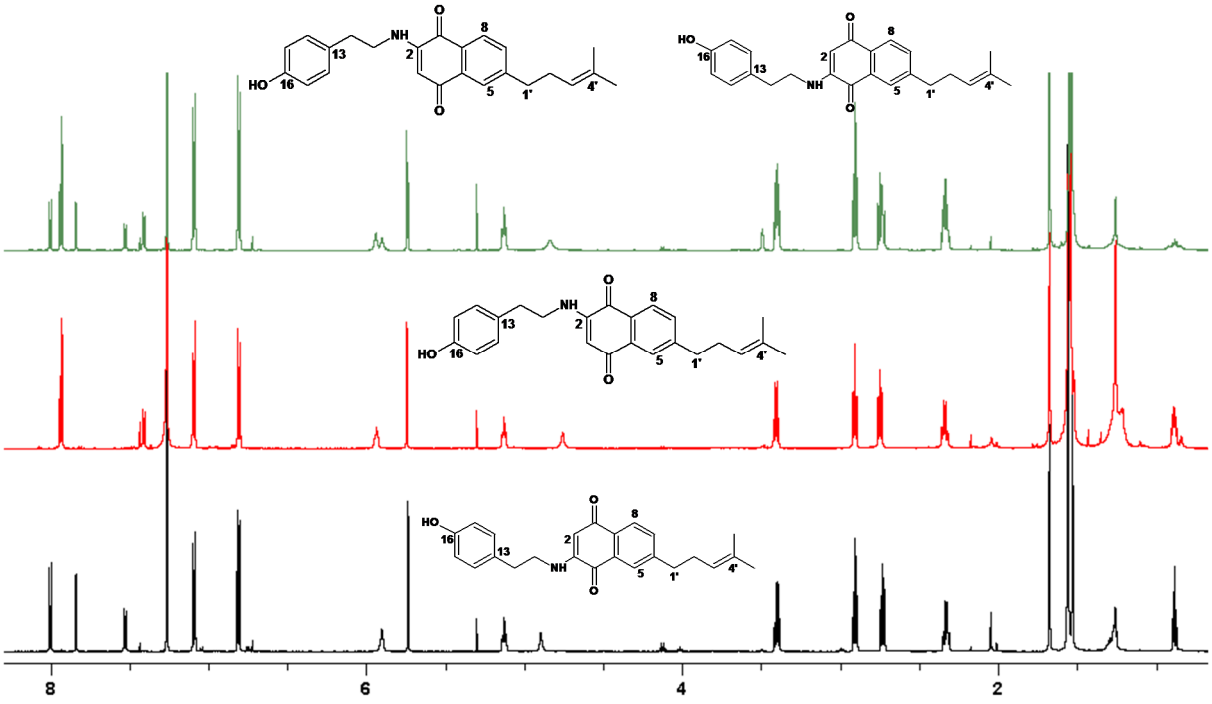

Figure: S4.76: Stacked ^{1}H NMR spectra (600 MHz, $CDCl_3$) of alkylamino-naphthoquinone **4.22** illustrating the mixture of isomers before and after HPLC

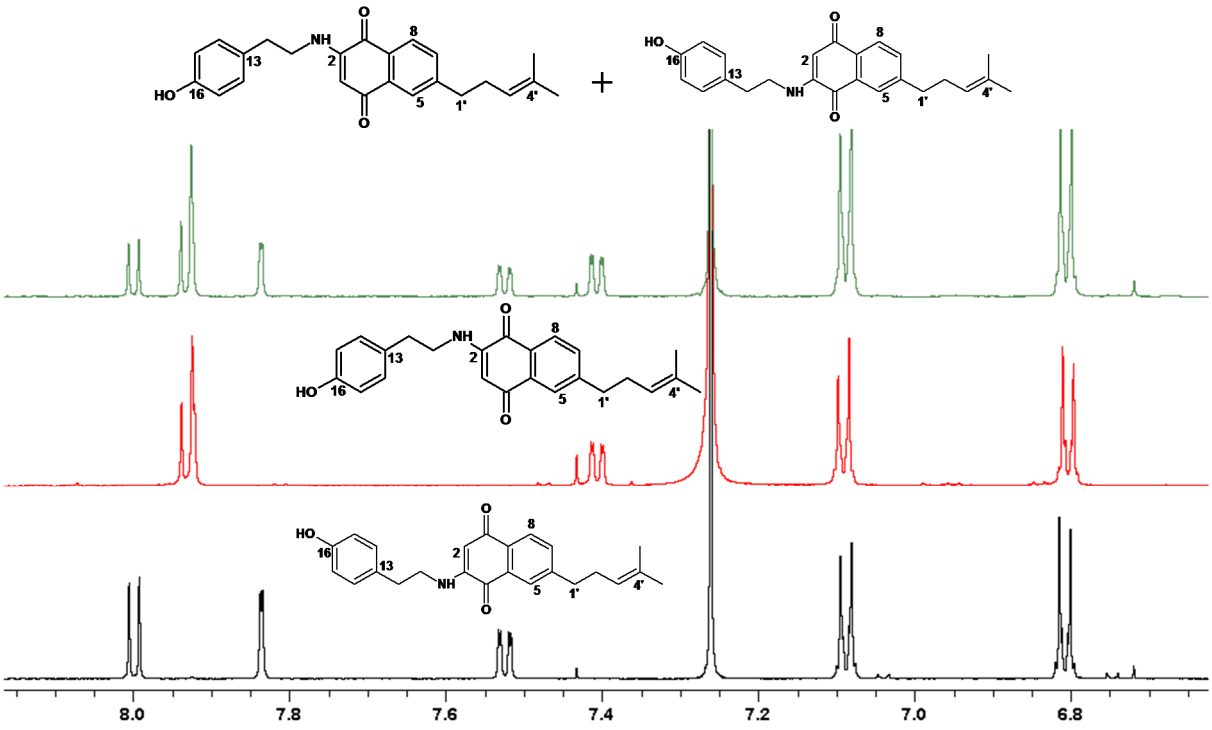

Figure: S4.77: ^{1}H NMR spectra (600 MHz, $CDCl_3$) of alkylamino-naphthoquinone **4.22** showing differences between the isomers in the aromatic region

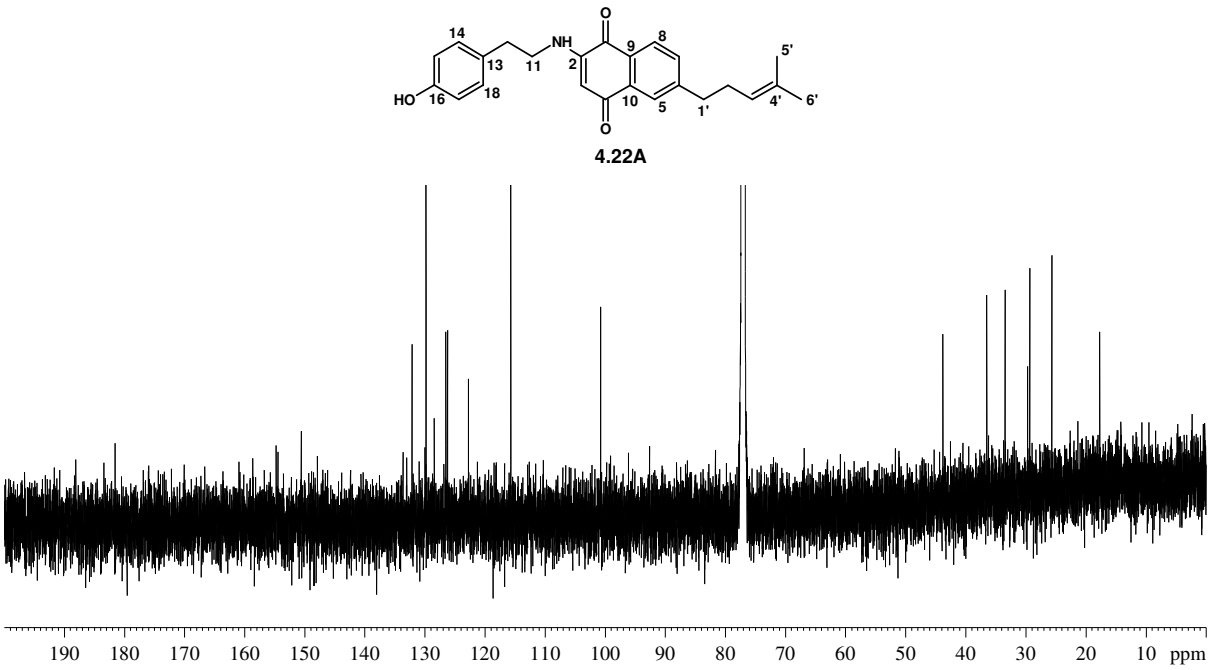

Figure S4.78: ^{13}C NMR spectrum (150 MHz, $CDCl_3$) of compound **4.22A**

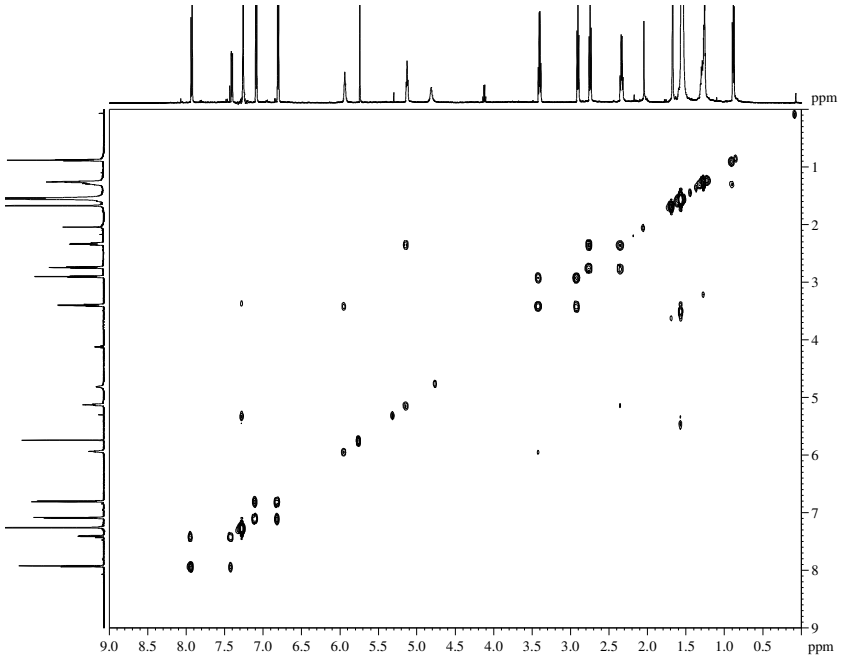

Figure S4.79: COSY NMR spectrum of compound **4.22A**

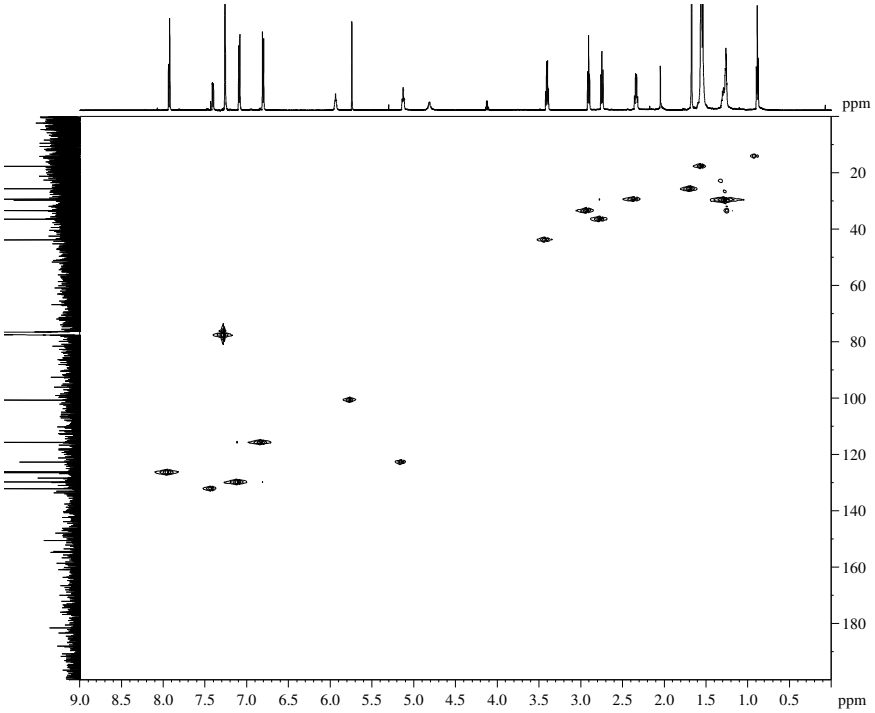

Figure S4.80: HSQC NMR spectrum of compound **4.22A**

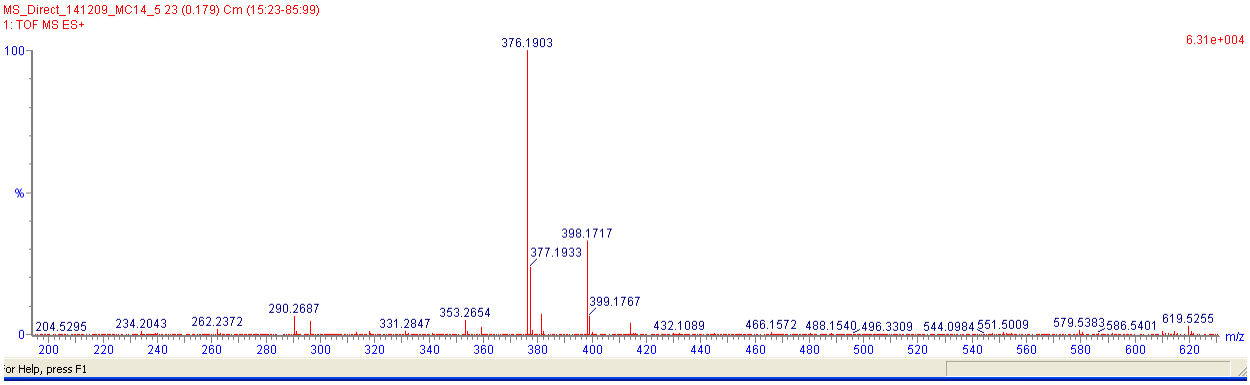

Figure S4.81: HRMS of compound **4.22A**

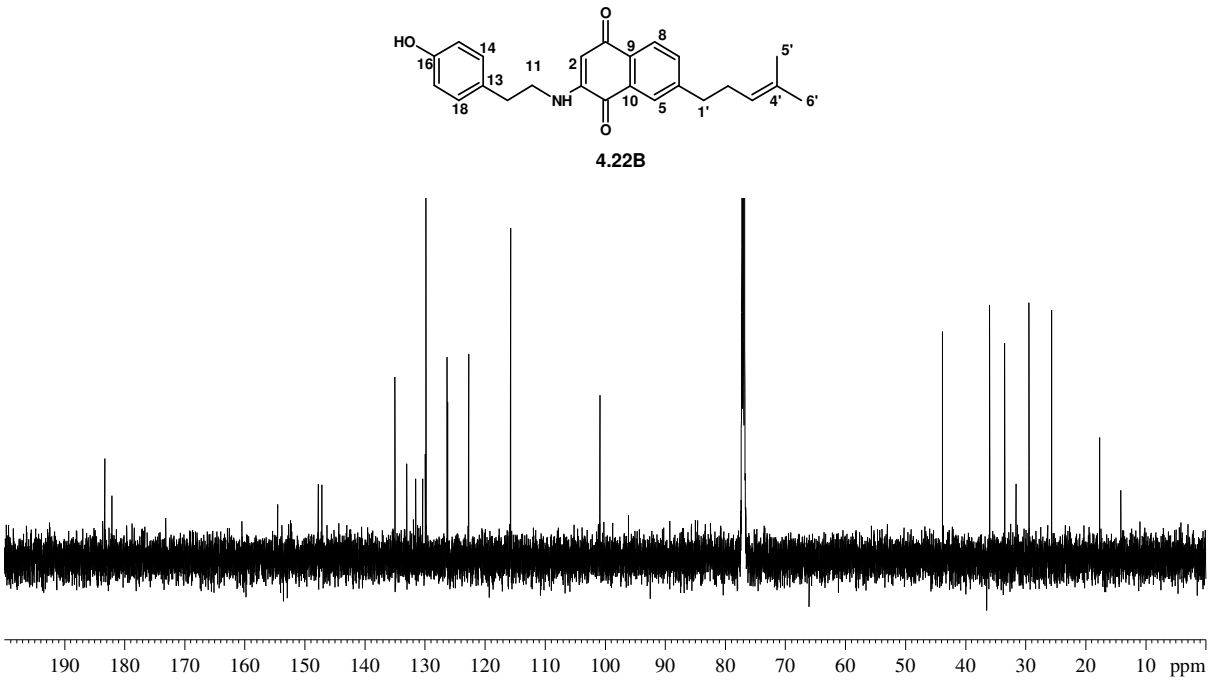

Figure S4.82: ^{13}C NMR spectrum (150 MHz, $CDCl_3$) of compound **4.22B**

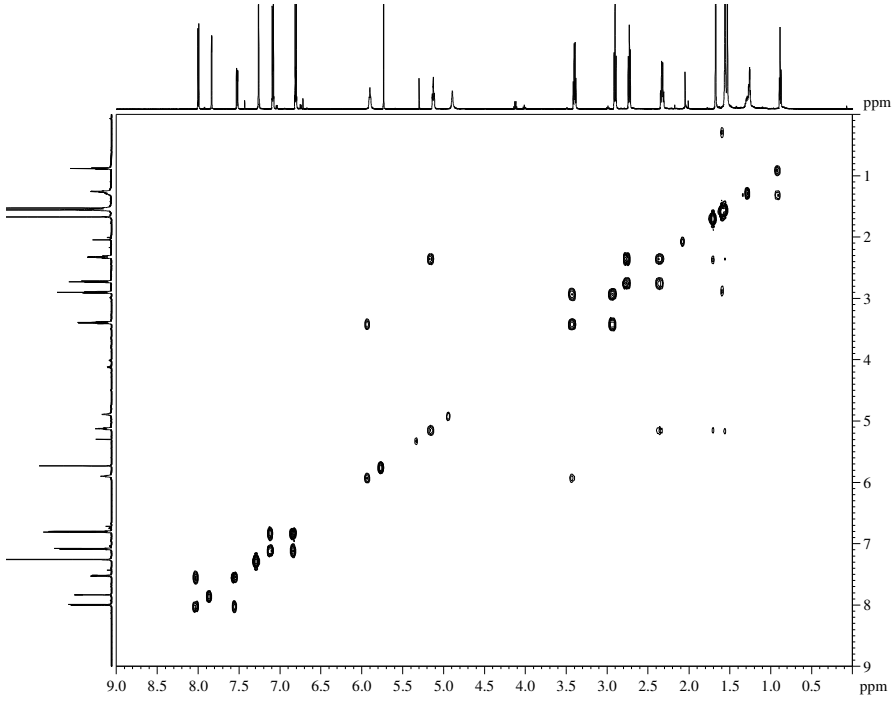

Figure S4.83: COSY NMR spectrum of compound **4.22B**

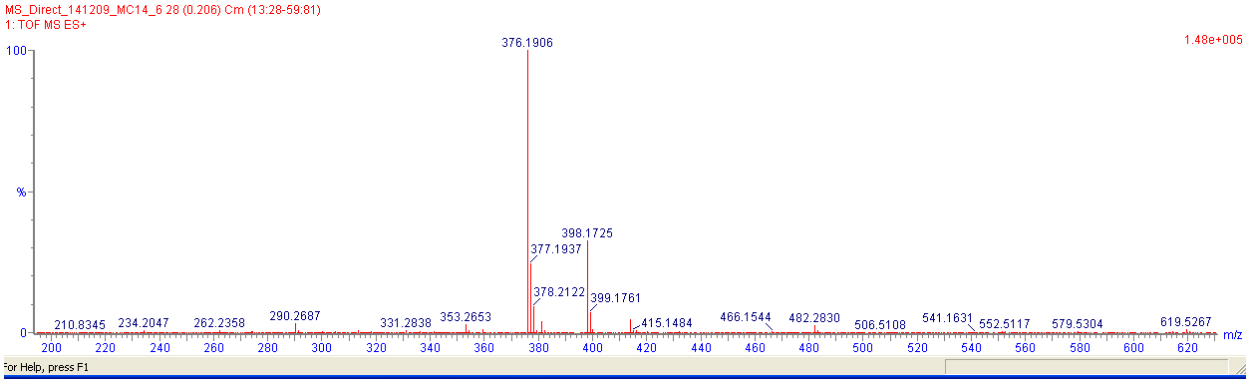

Figure S4.84: HRMS of compound **4.22B**

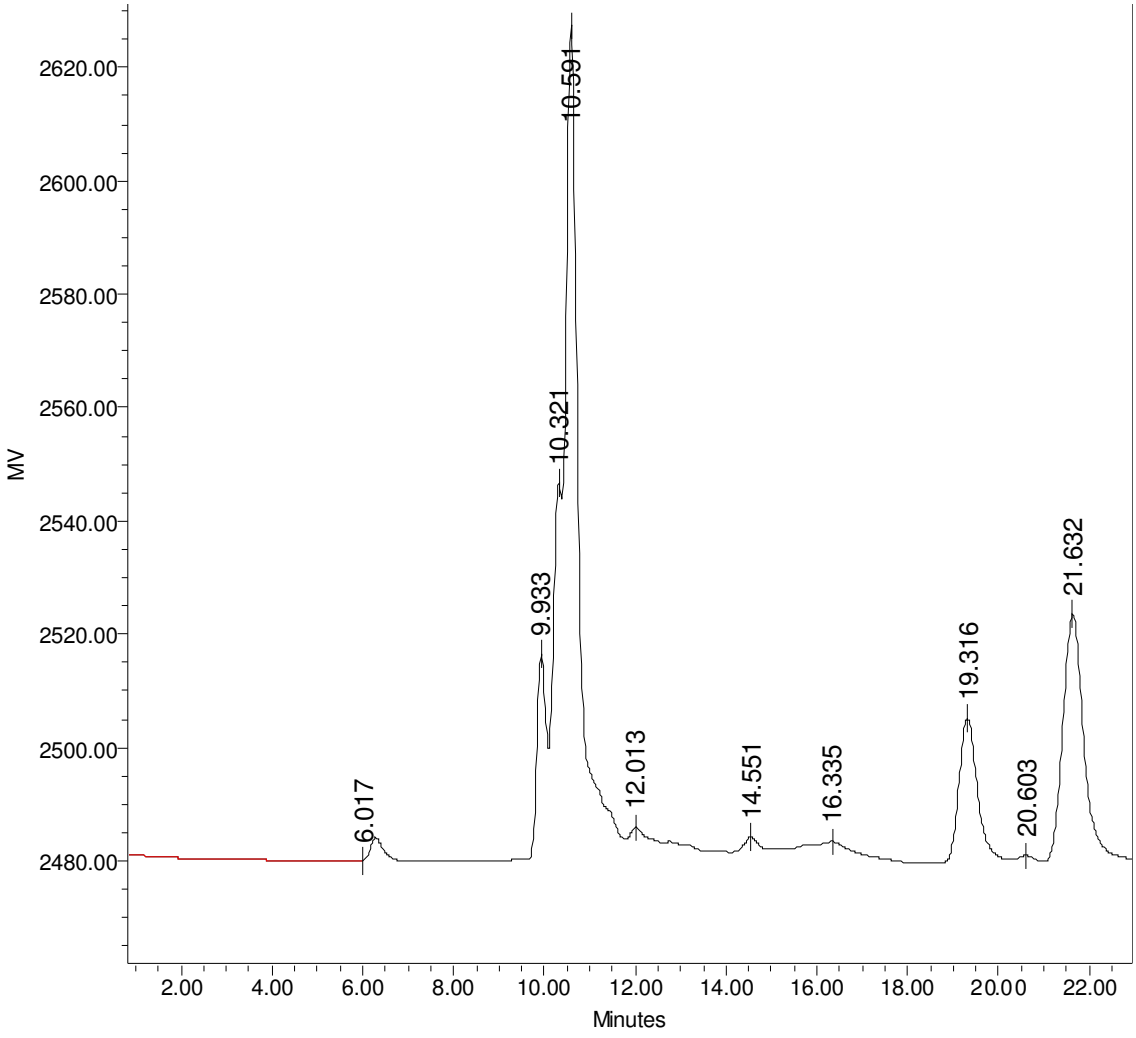

Figure S4.85: HPLC chromatogram showing the retention times for the two isomers: **4.22A**: 19.3 min and **4.22B**: 21.6 min

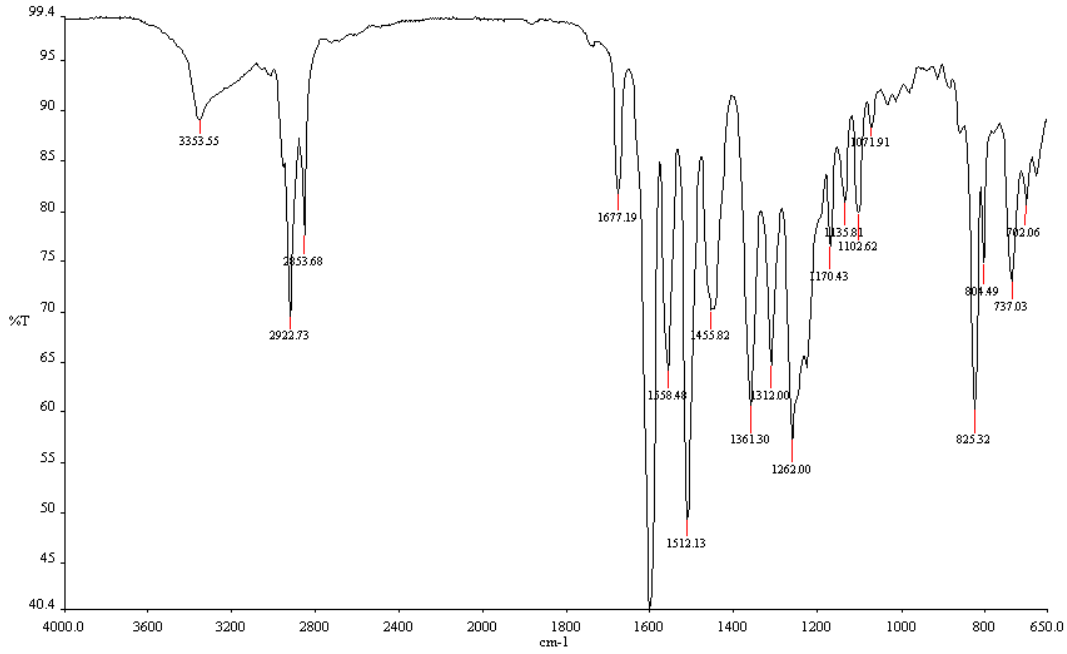

Figure S4.86: IR spectrum of compound **4.22**

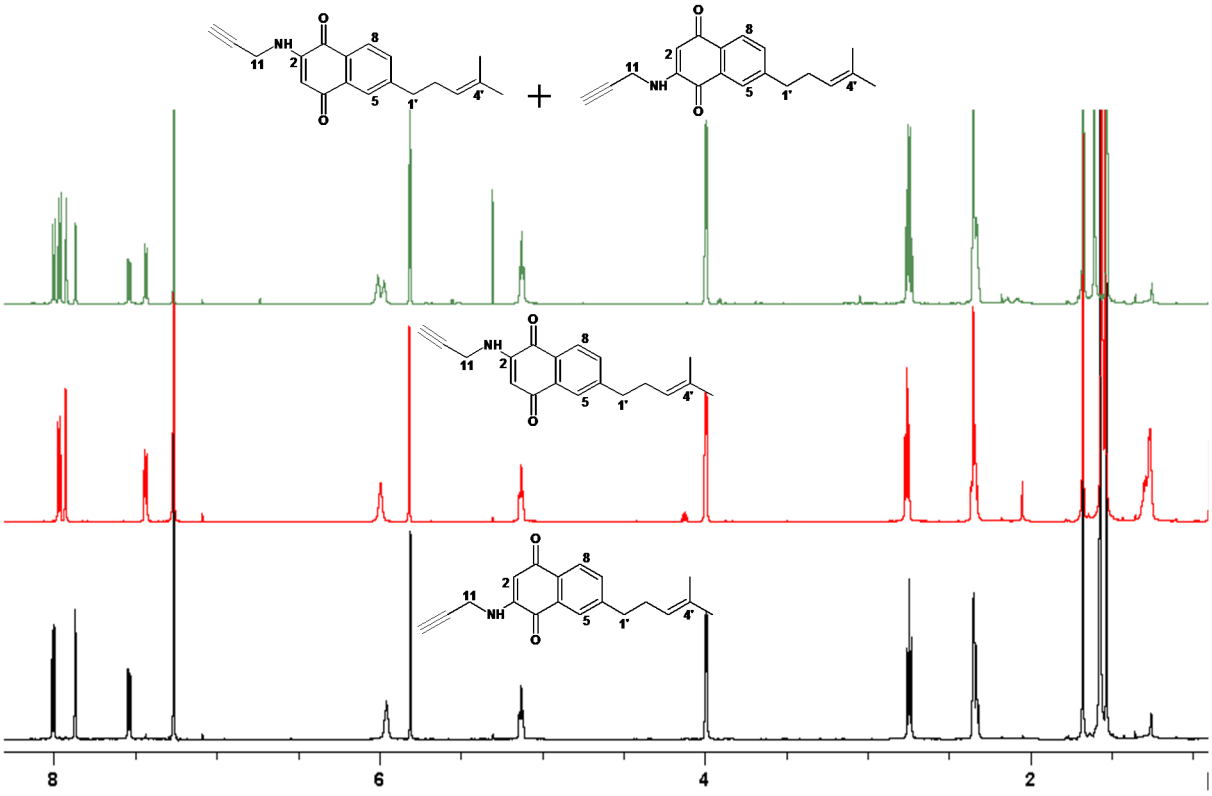

Figure: S4.87: ^{1}H NMR spectra (600 MHz, $CDCl_3$) of alkylamino-naphthoquinone **4.23** illustrating the mixture of isomers before and after HPLC

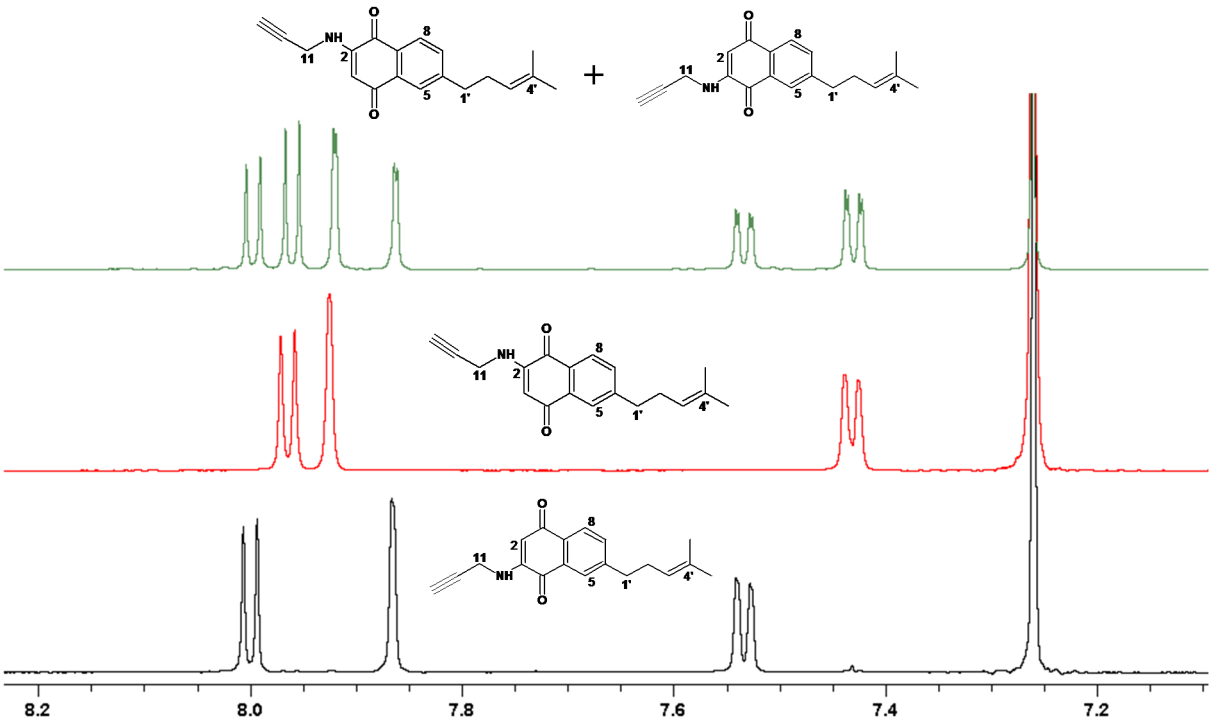

Figure: S4.88: ^{1}H NMR spectra (600 MHz, $CDCl_3$) of alkylamino-naphthoquinone **4.23** showing differences between the isomers in the aromatic region

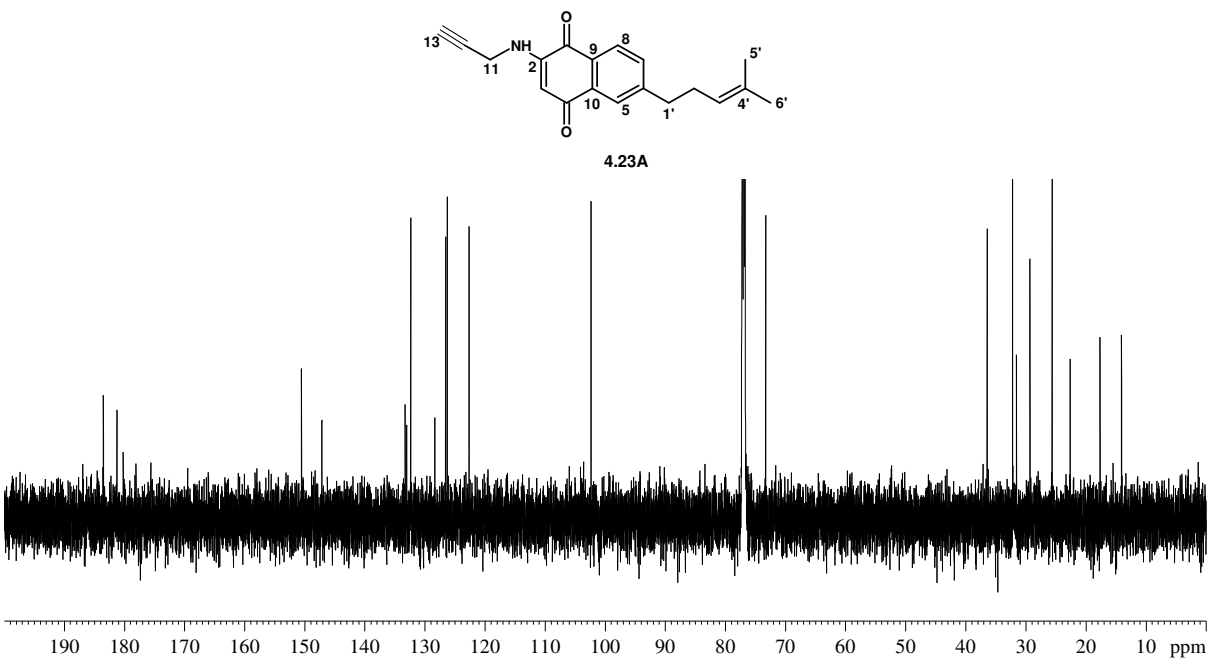

Figure S4.89: ^{13}C NMR spectrum (150 MHz, $CDCl_3$) of compound **4.23A**

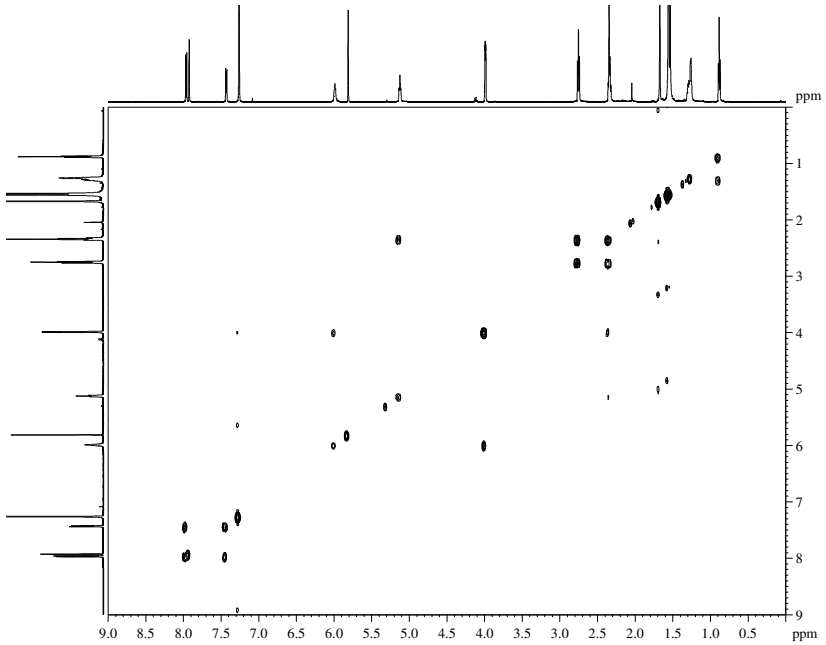

Figure S4.90: COSY NMR spectrum of compound **4.23A**

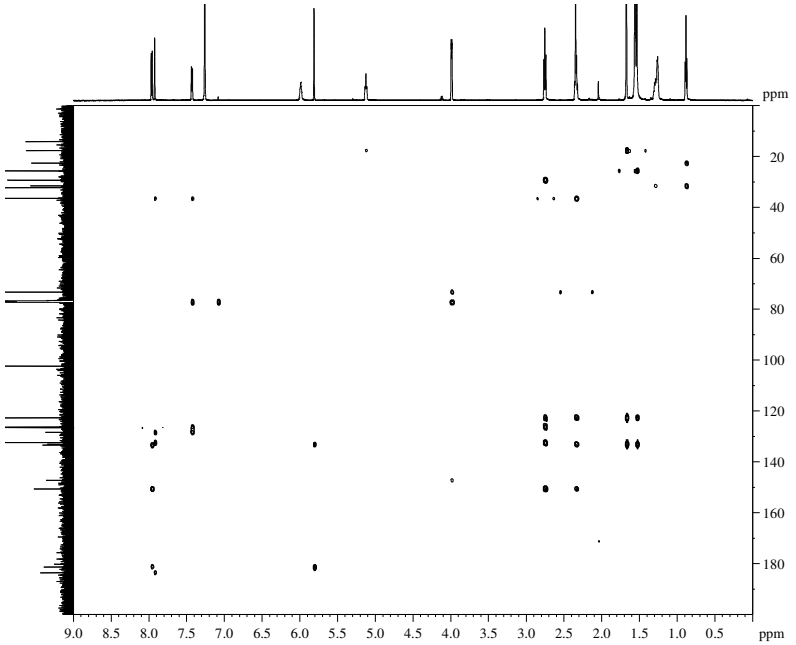

Figure S4.91: HMBC NMR spectrum of compound **4.23A**

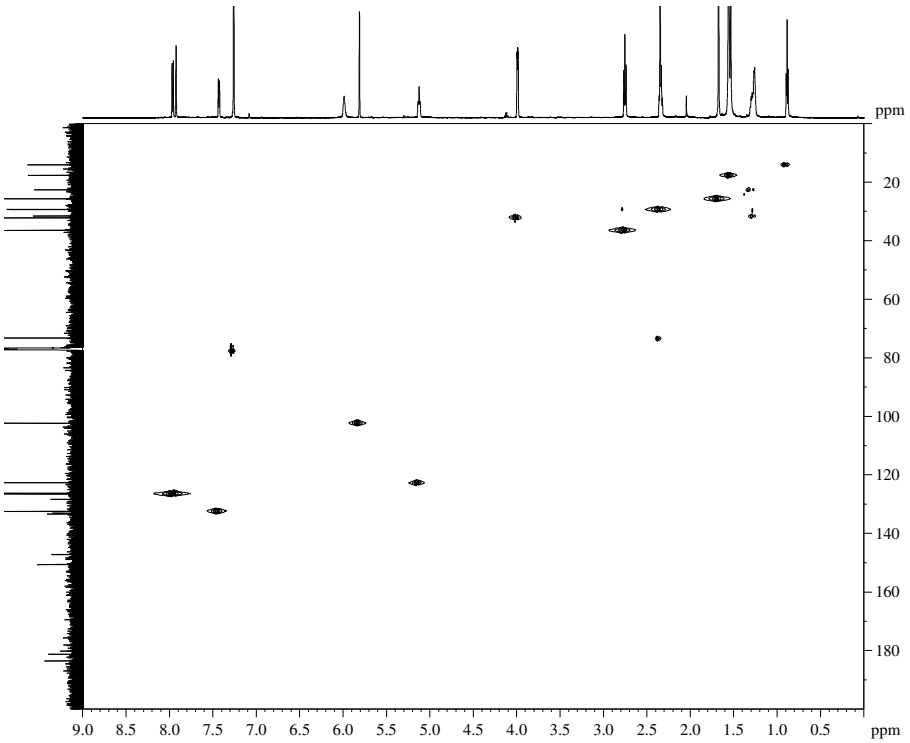

Figure S4.92: HSQC NMR spectrum of compound **4.23A**

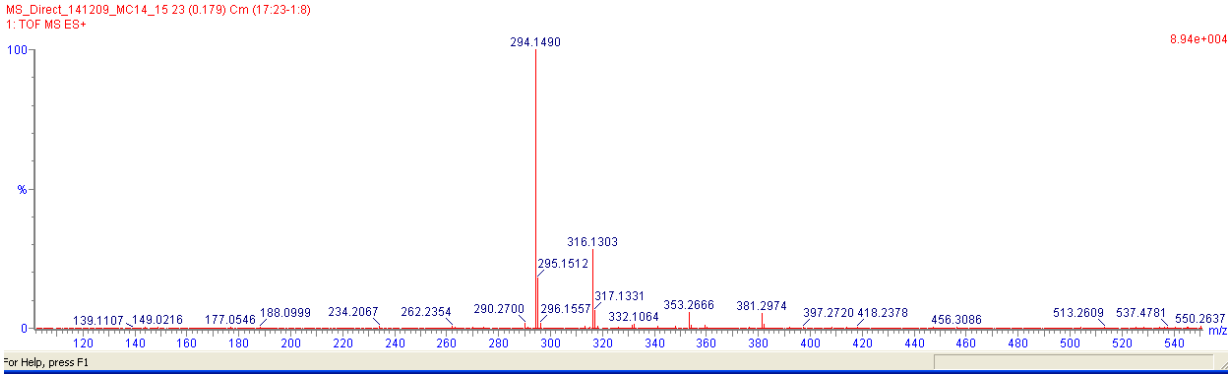

Figure S4.93: HRMS of compound **4.23A**

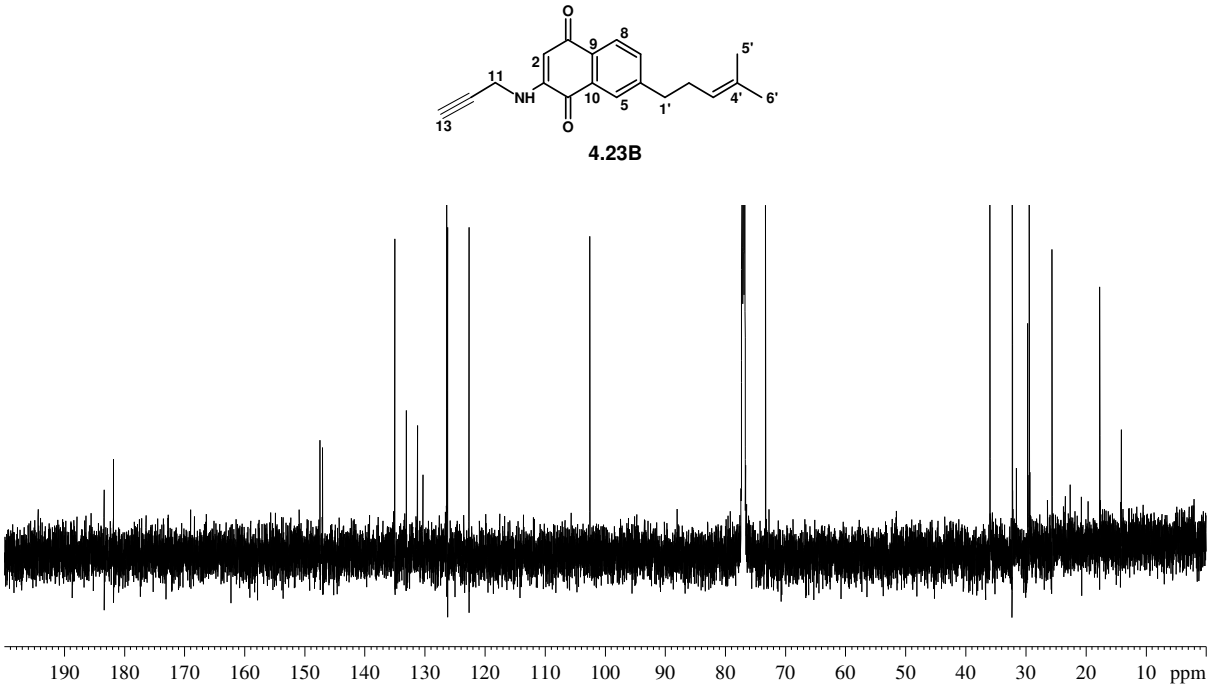

Figure S4.94: ^{13}C NMR spectrum (150 MHz, $CDCl_3$) of compound **4.23B**

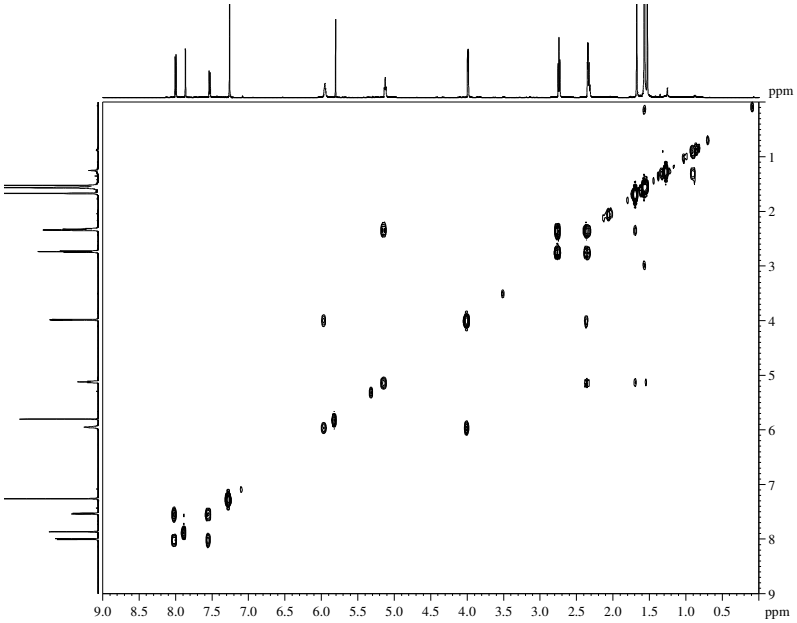

Figure S4.95: COSY NMR spectrum of compound **4.23B**

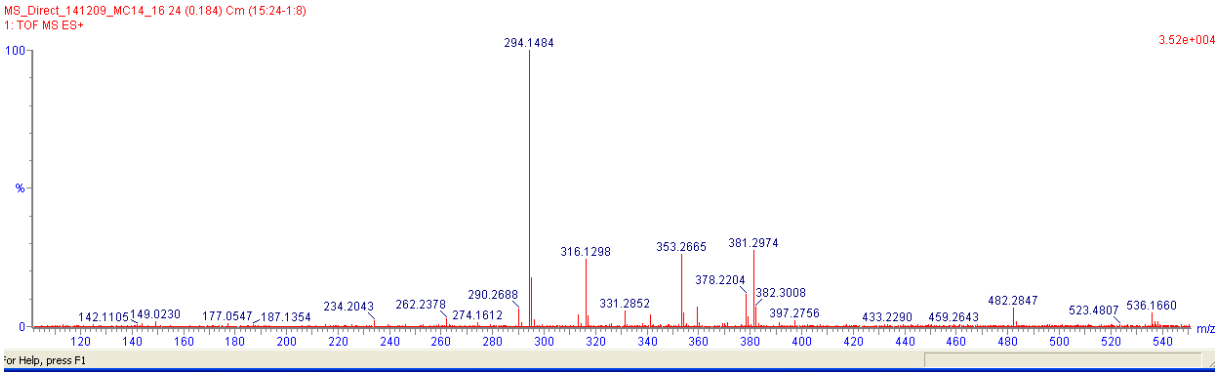

Figure S4.96: HRMS of compound **4.23B**

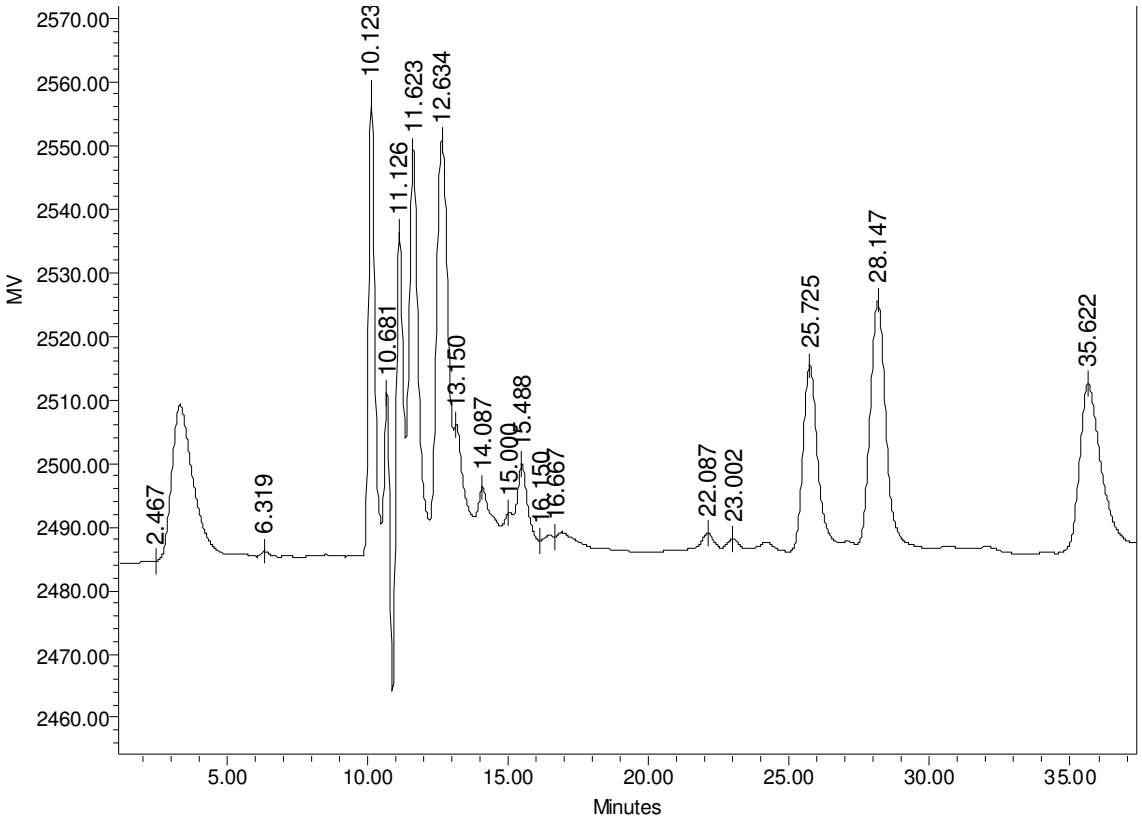

Figure S4.97: HPLC chromatogram showing the retention times for the two isomers: **4.23A**: 25.7 min and **4.23B**: 28.1 min

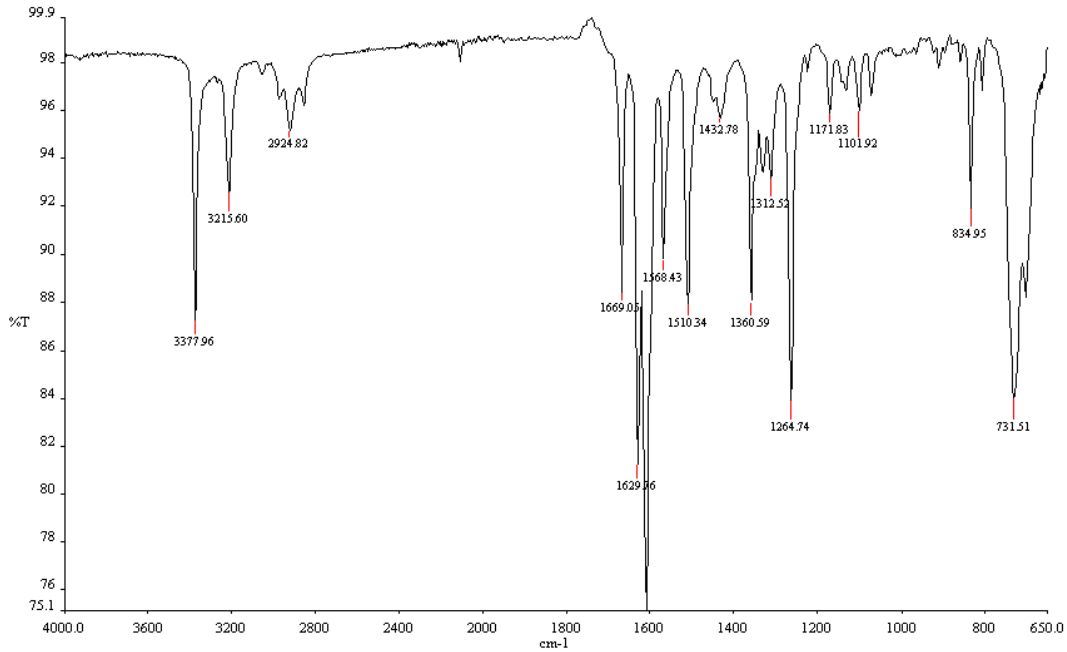

Figure S4.98: IR spectrum of compound **4.23**

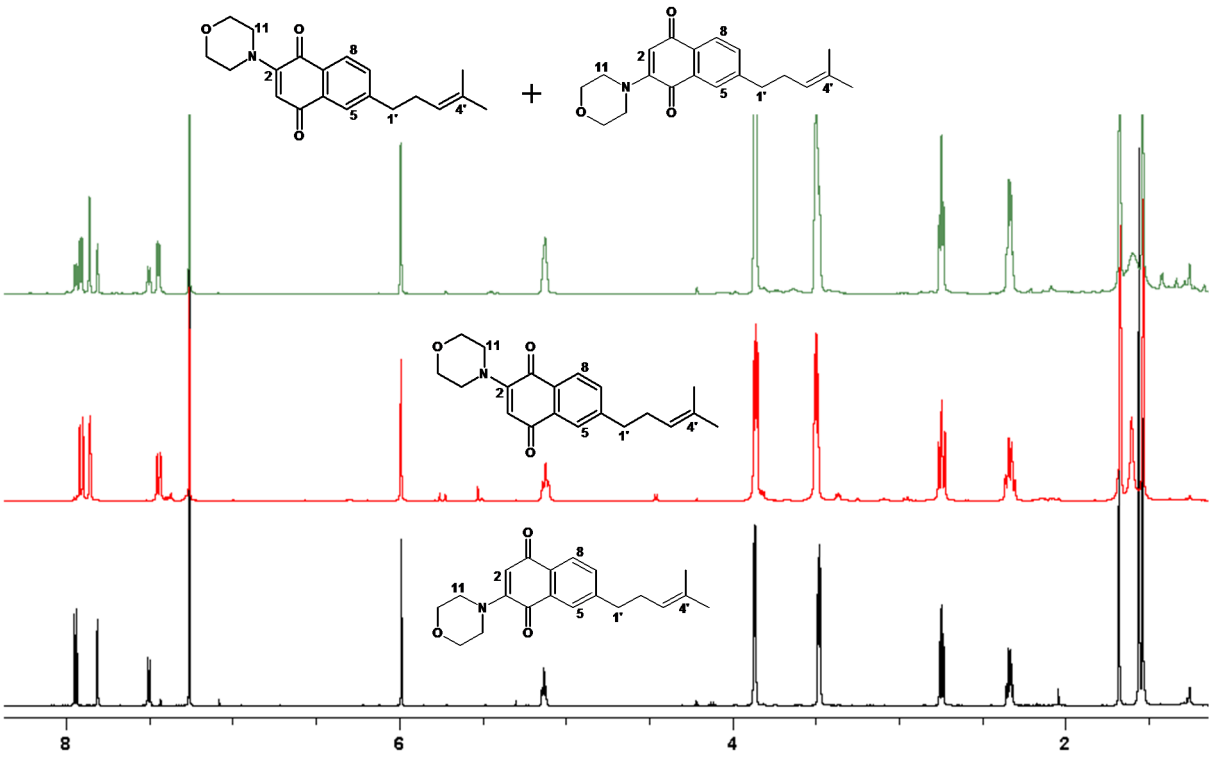

Figure: S4.99: ^{1}H NMR spectra (600 MHz, $CDCl_3$) of alkylamino-naphthoquinone **4.24** illustrating the mixture of isomers before and after HPLC

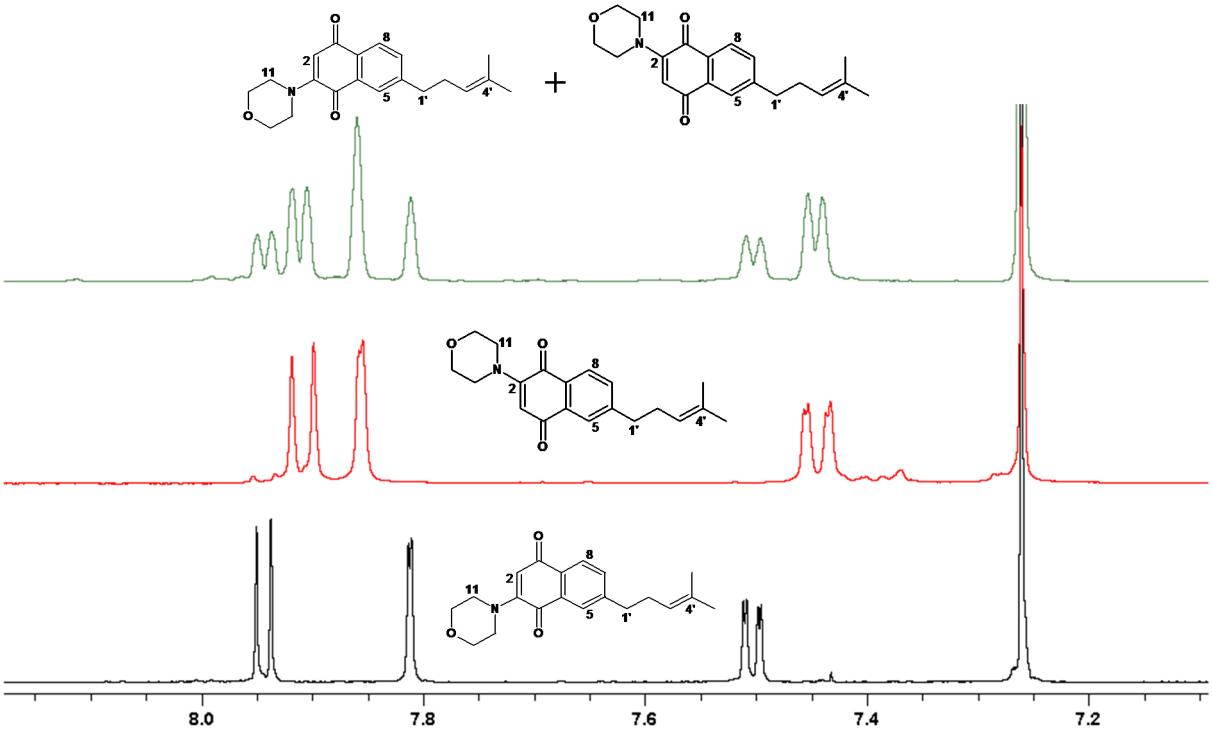

Figure: S4.100: ^{1}H NMR spectra (600 MHz, $CDCl_3$) of alkylamino-naphthoquinone **4.24** showing differences between the isomers in the aromatic region

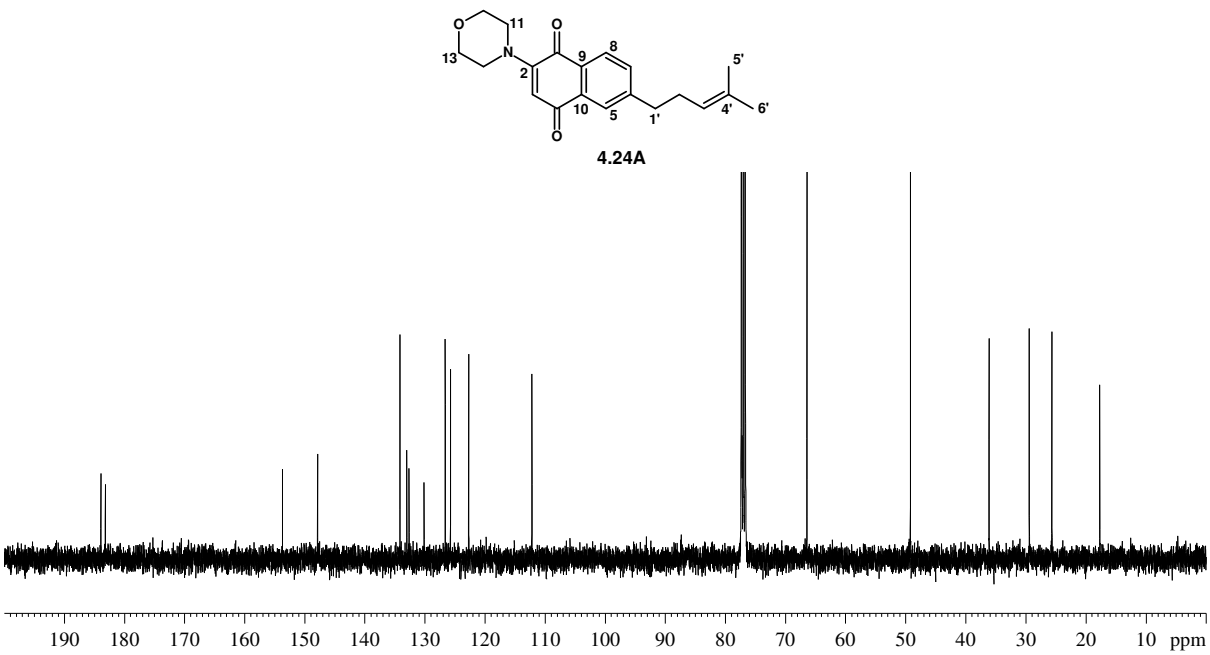

Figure S4.101: ^{13}C NMR spectrum (150 MHz, $CDCl_3$) of compound **4.24A**

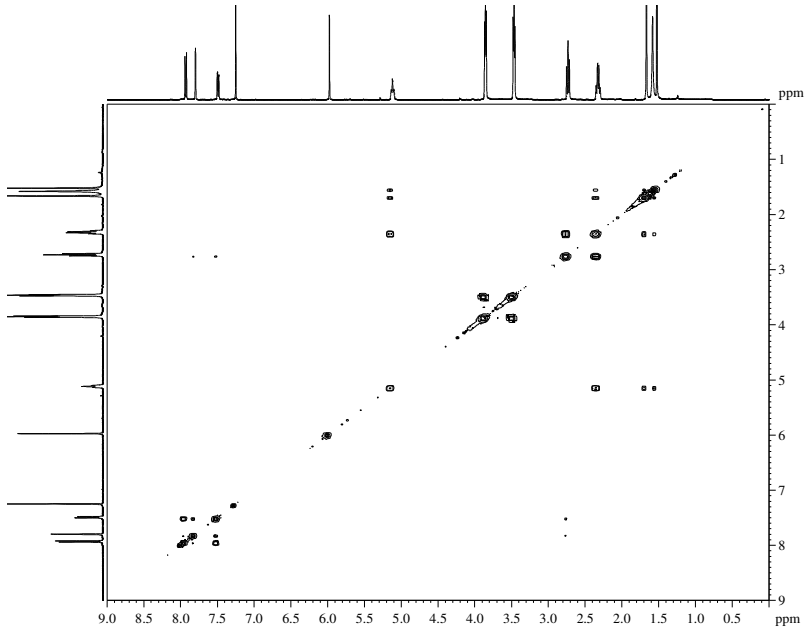

Figure S4.102: COSY NMR spectrum of compound **4.24A**

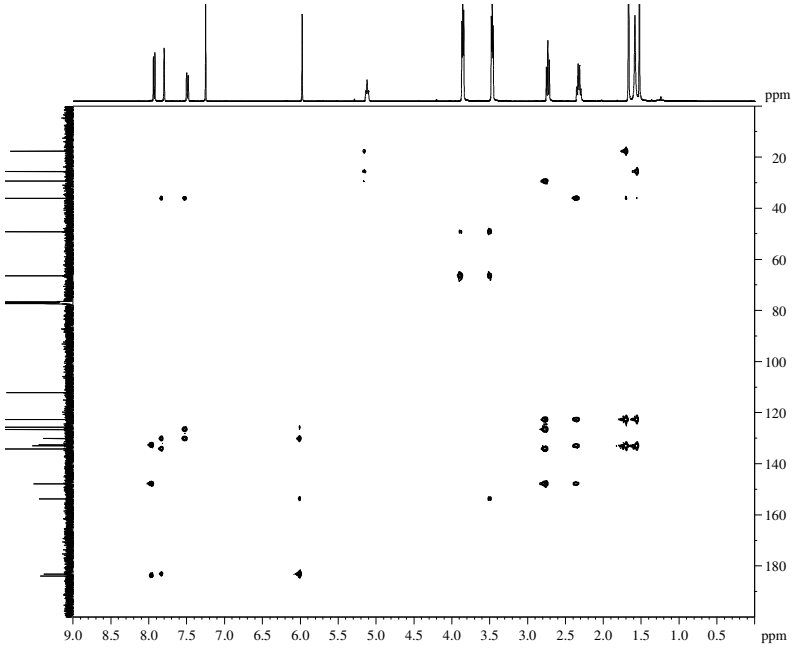

Figure S4.103: HMBC NMR spectrum of compound **4.24A**

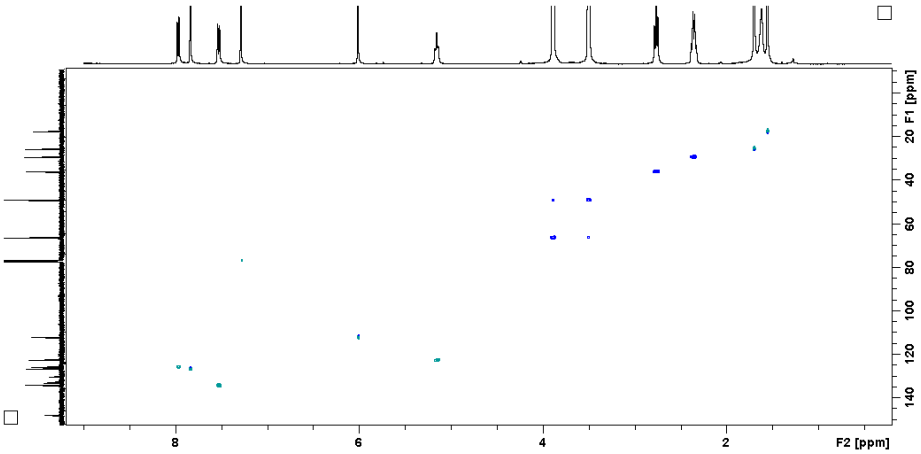

Figure S4.104: HSQC NMR spectrum of compound **4.24A**

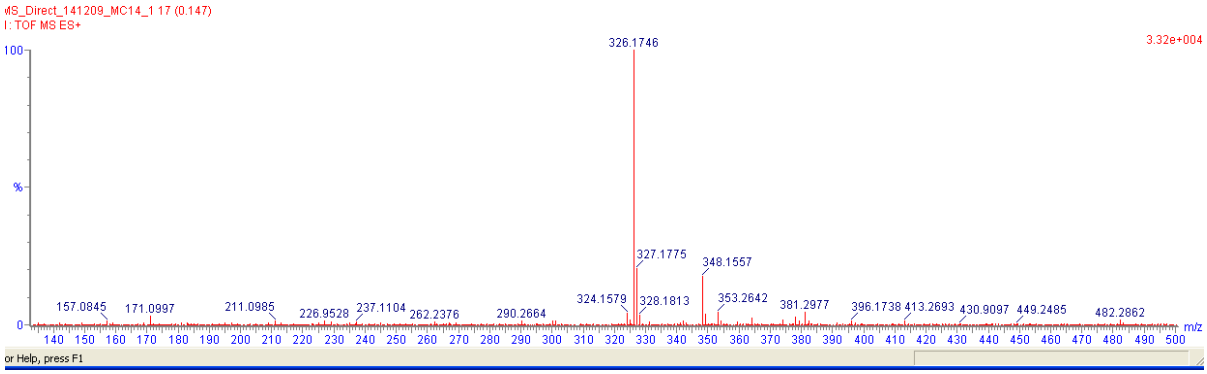

Figure S4.105: HRMS of compound **4.24A**

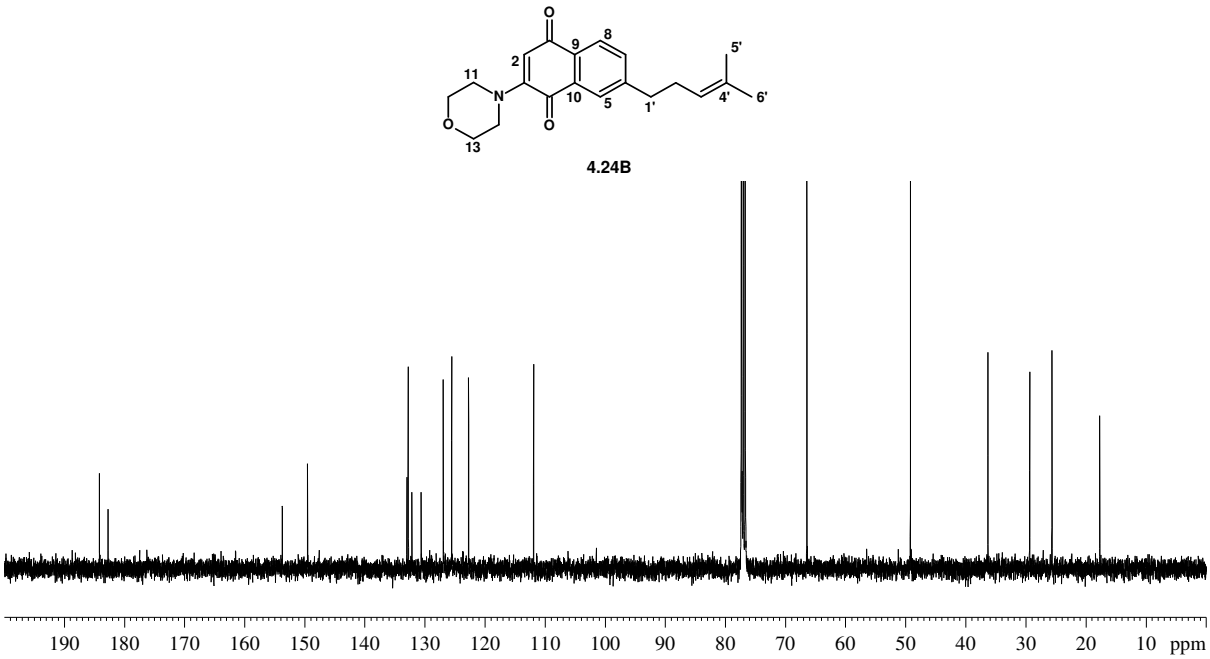

Figure S4.106: ^{13}C NMR spectrum (150 MHz, $CDCl_3$) of compound **4.24B**

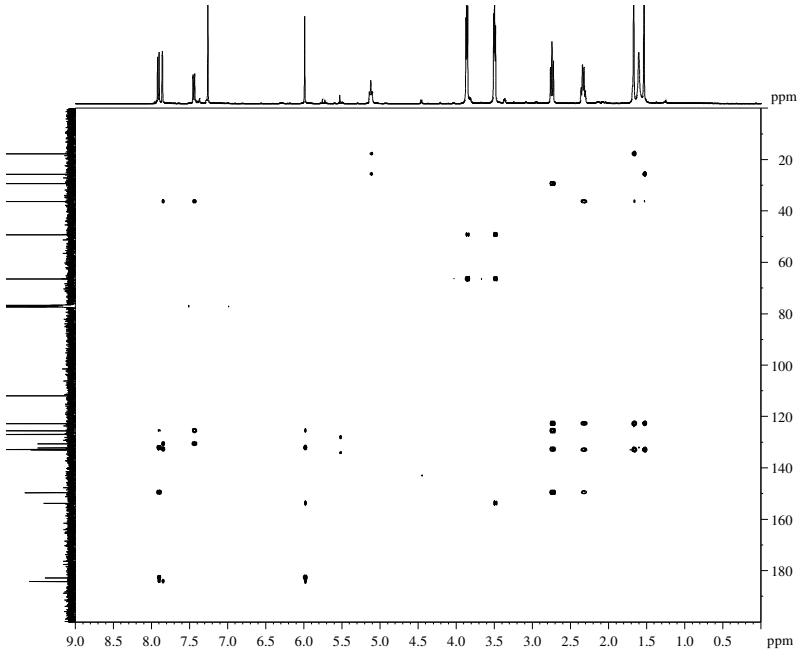

Figure S4.107: HMBC NMR spectrum of compound **4.24B**

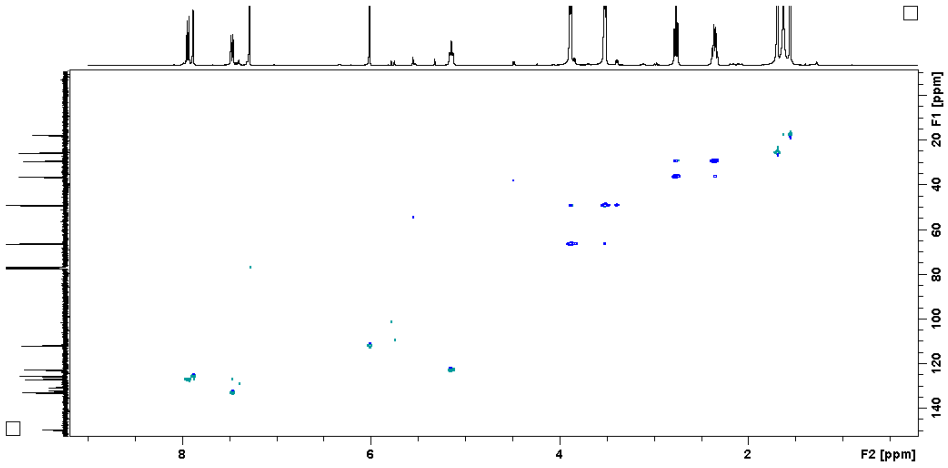

Figure S4.108: HSQC NMR spectrum of compound **4.24B**

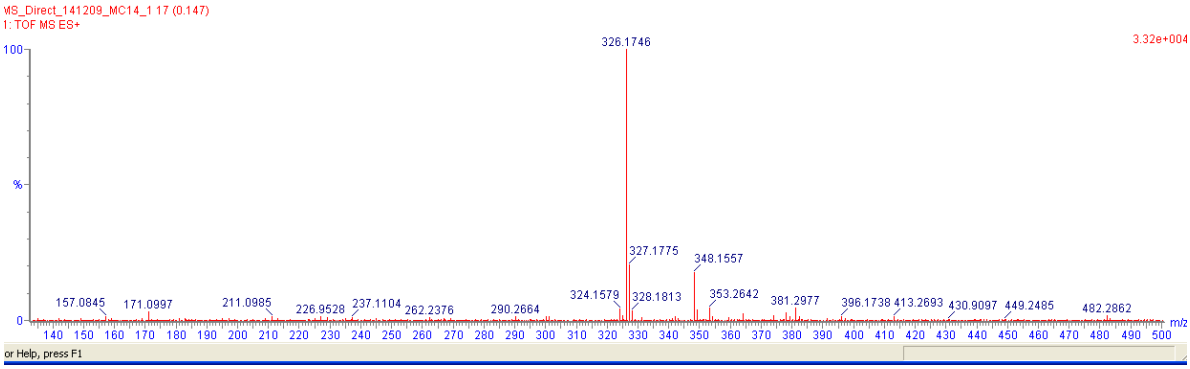

Figure S4.109: HRMS of compound **4.24B**

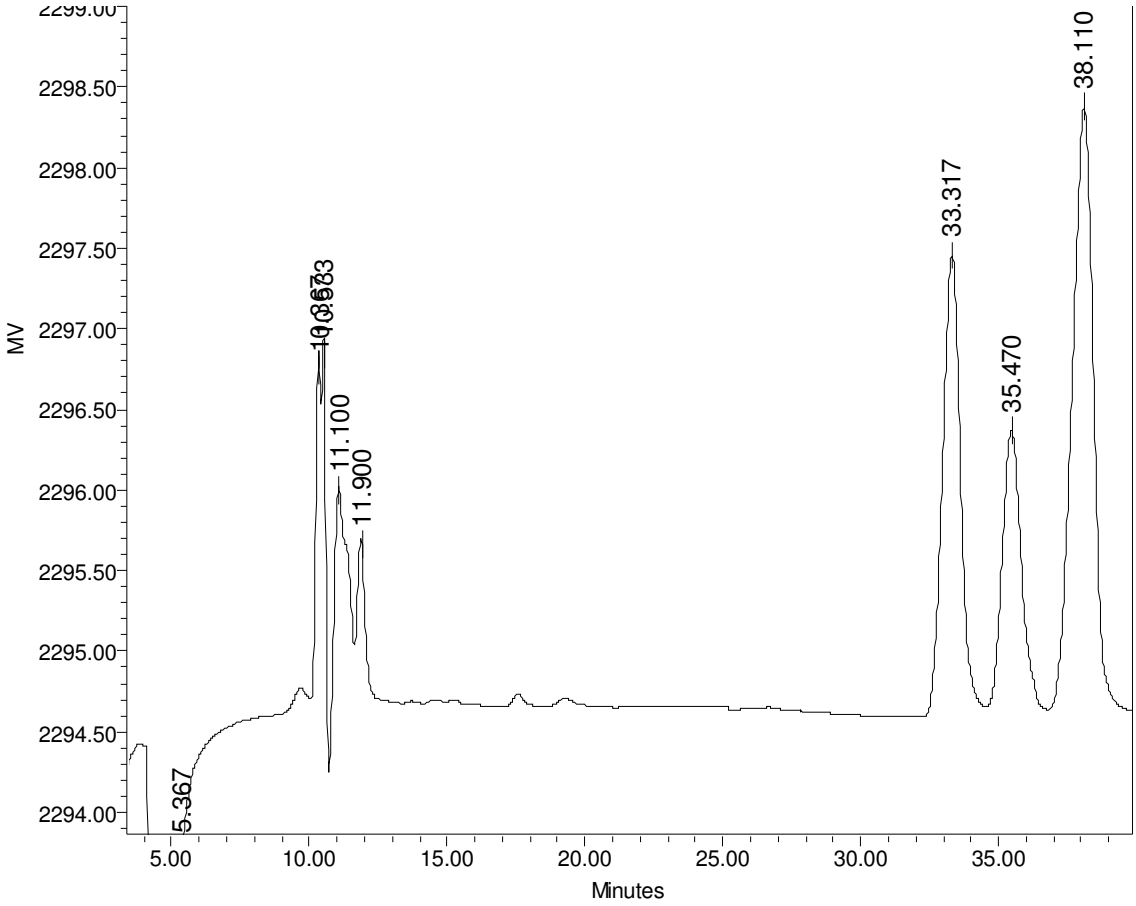

Figure S4.110: HPLC chromatogram showing the retention times for the two isomers: **4.24A**: 38.1 min and **4.24B**: 35.4 min

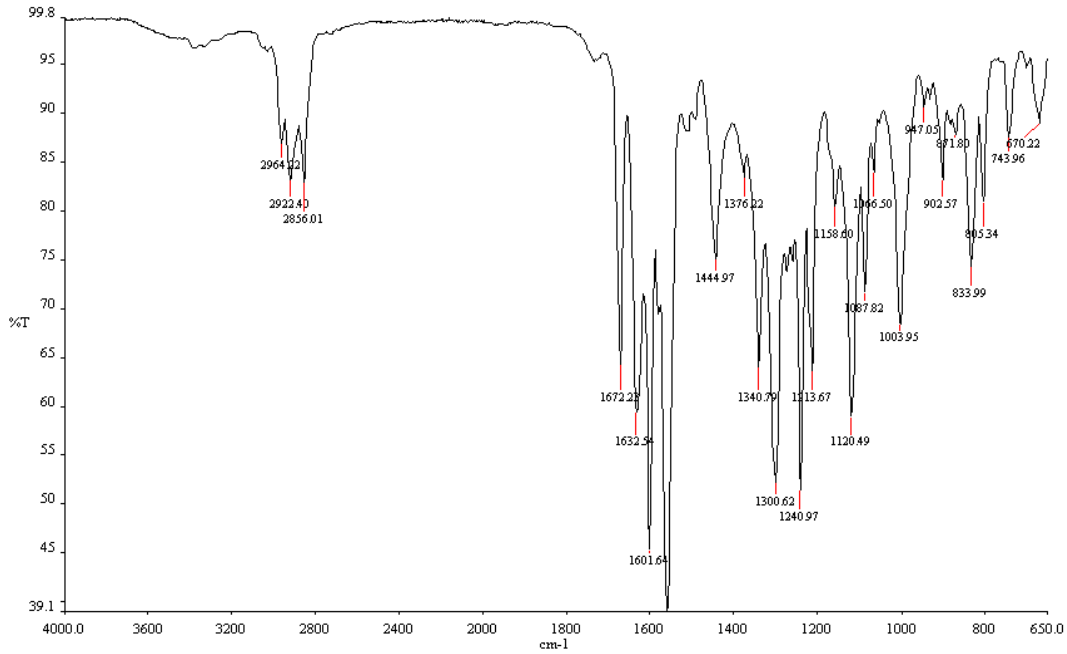

Figure S4.111: IR spectrum of compound **4.24**

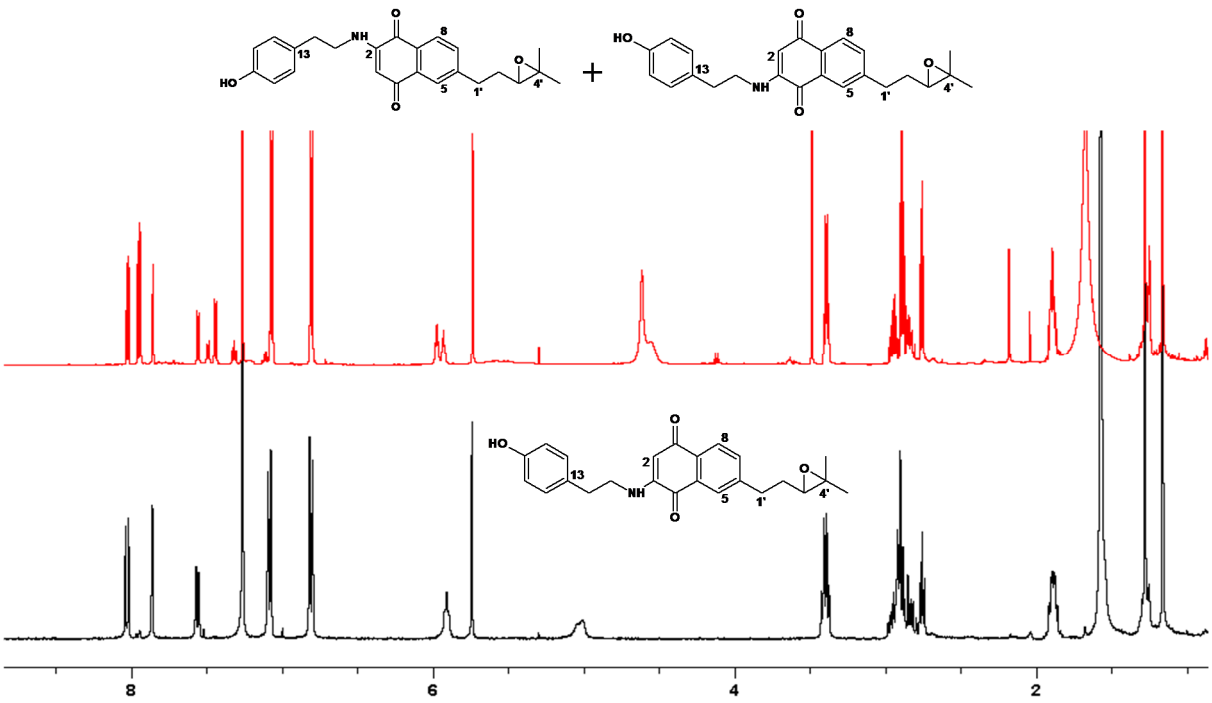

Figure S4.112: ^{1}H NMR spectra (600 MHz, $CDCl_3$) of alkylamino-naphthoquinone **4.25** illustrating the mixture of isomers before and after HPLC

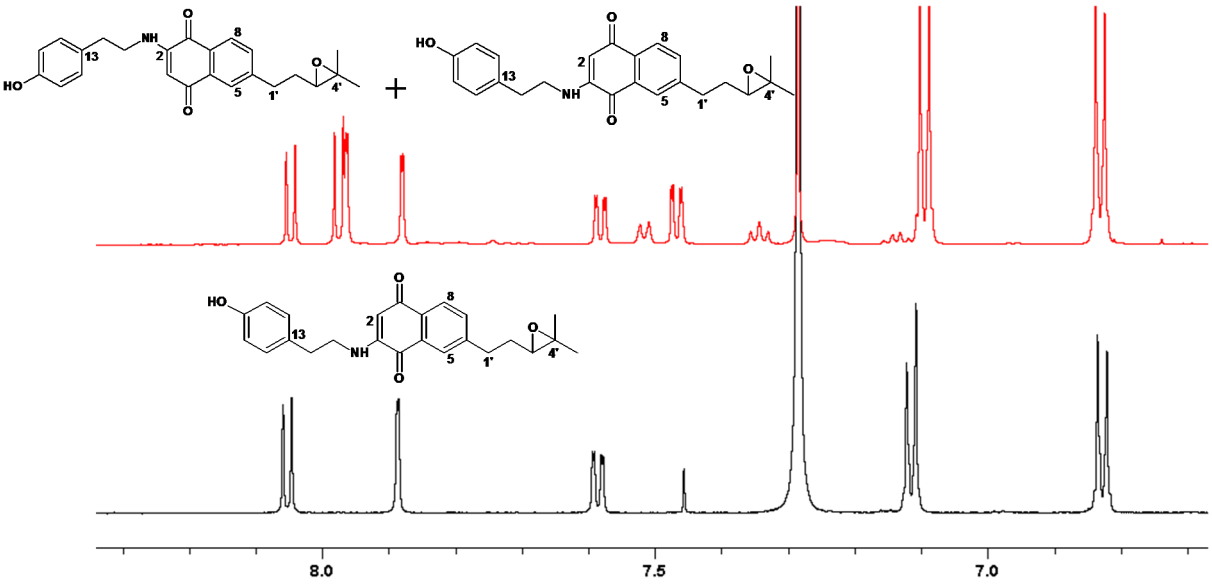

Figure S4.113: ^{1}H NMR spectra (600 MHz, $CDCl_3$) of alkylamino-naphthoquinone **4.25** showing differences between the isomers in the aromatic region

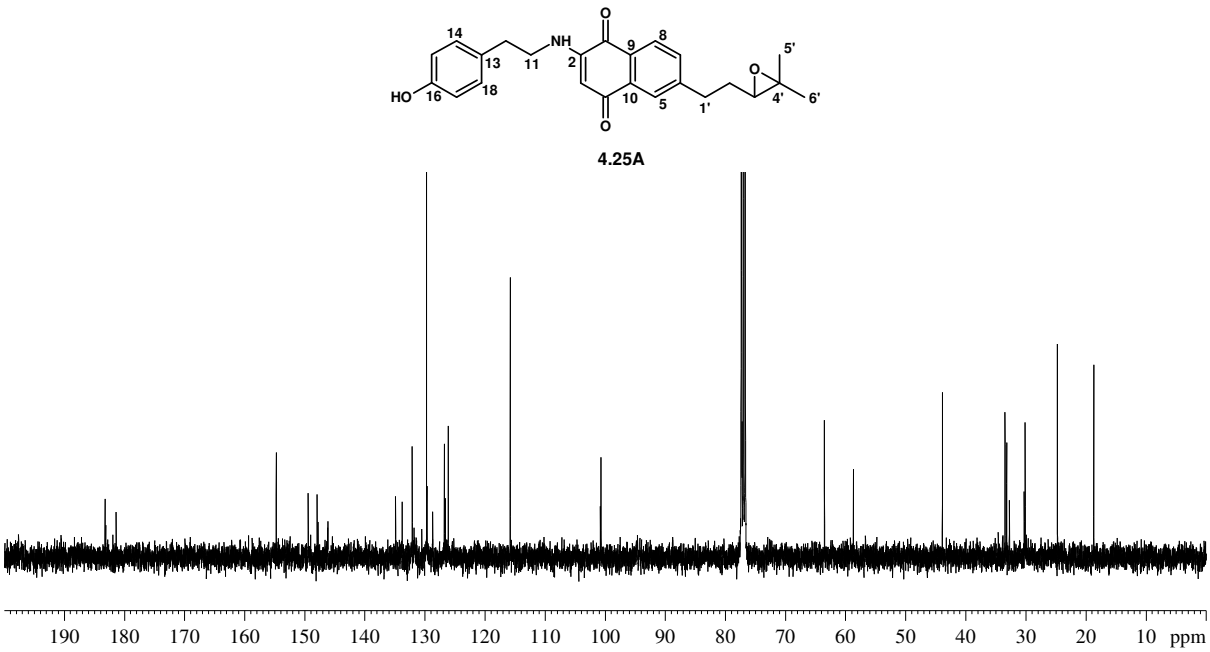

Figure S4.114: ^{13}C NMR spectrum (150 MHz, $CDCl_3$) of compound **4.25A**

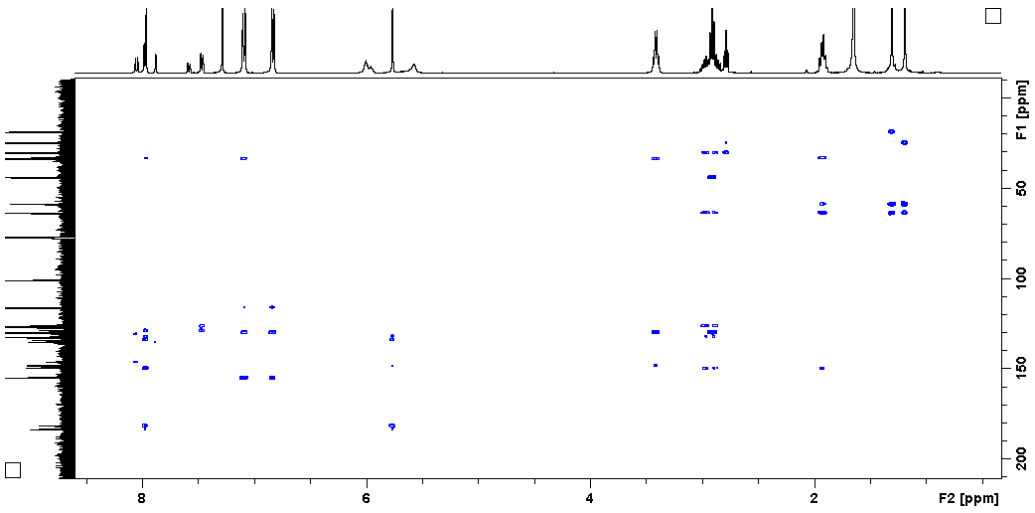

Figure S4.115: HMBC NMR spectrum of compound **4.25A**

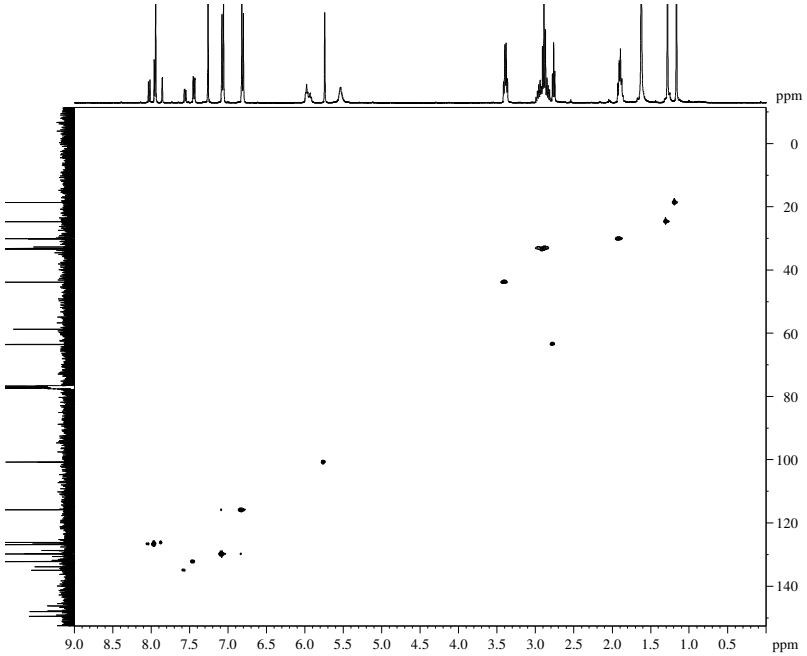

Figure S4.116: HSQC NMR spectrum of compound **4.25A**

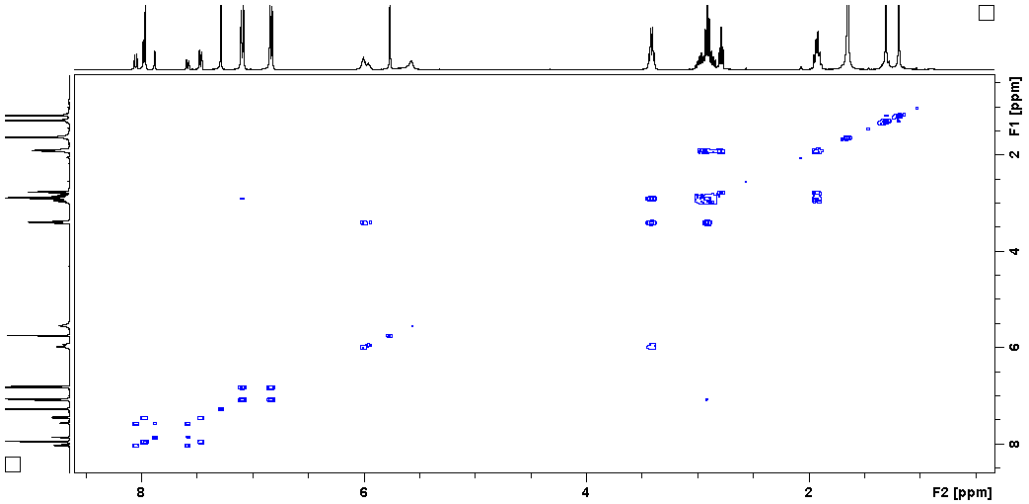

Figure S4.117: COSY NMR spectrum of compound **4.25A**

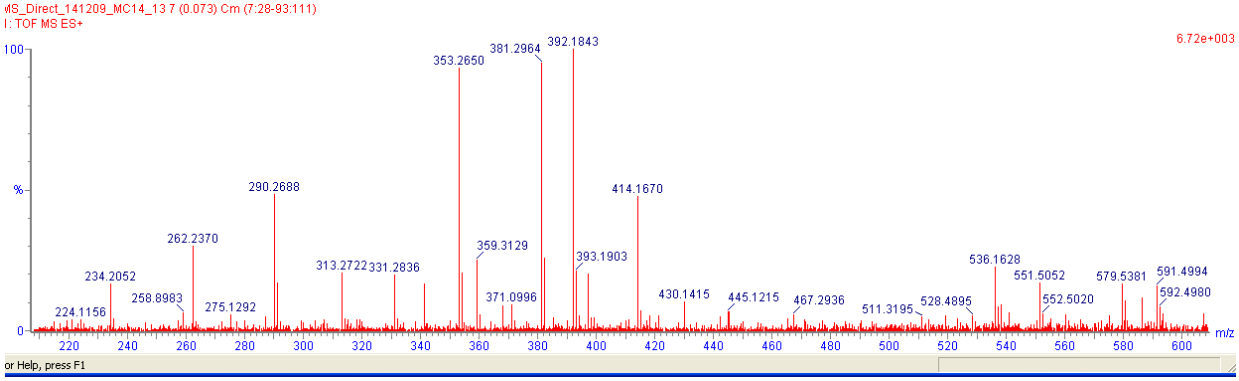

Figure S4.118: HRMS of compound **4.25A**

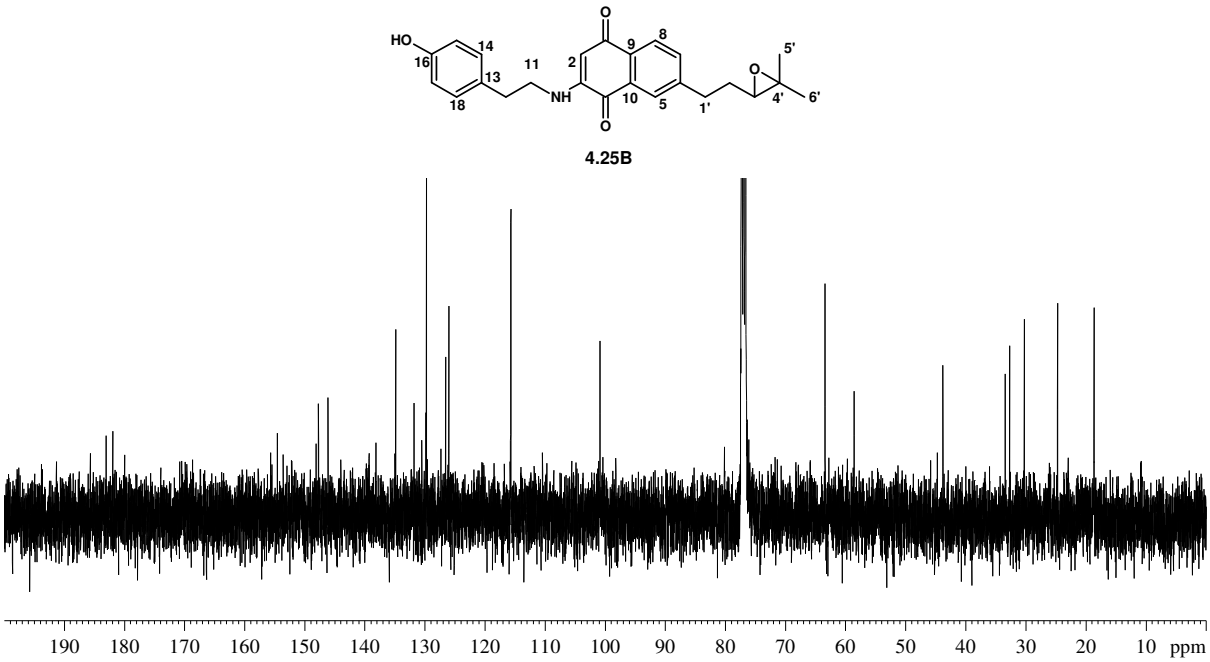

Figure S4.119: ^{13}C NMR spectrum (150 MHz, $CDCl_3$) of compound **4.25B**

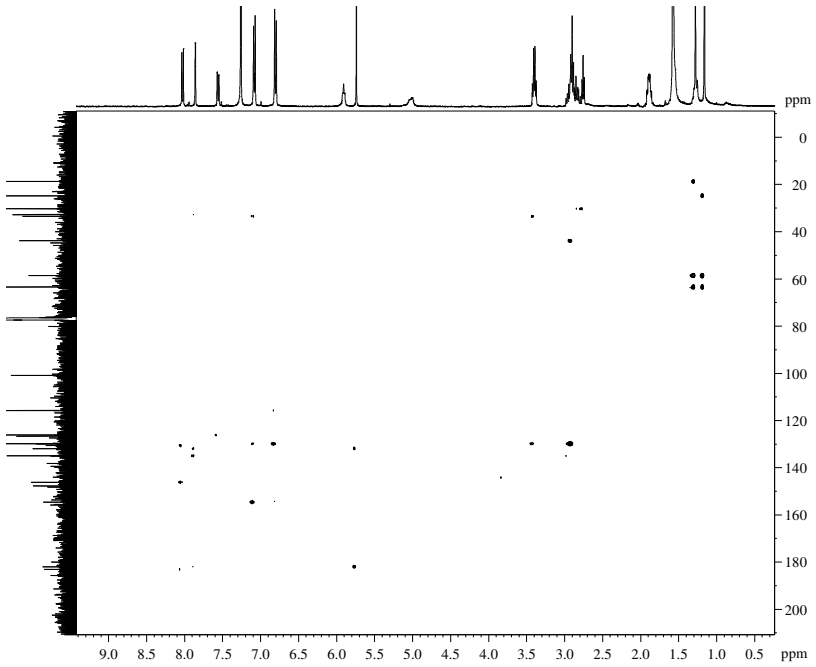

Figure S4.120: HMBC NMR spectrum of compound **4.25B**

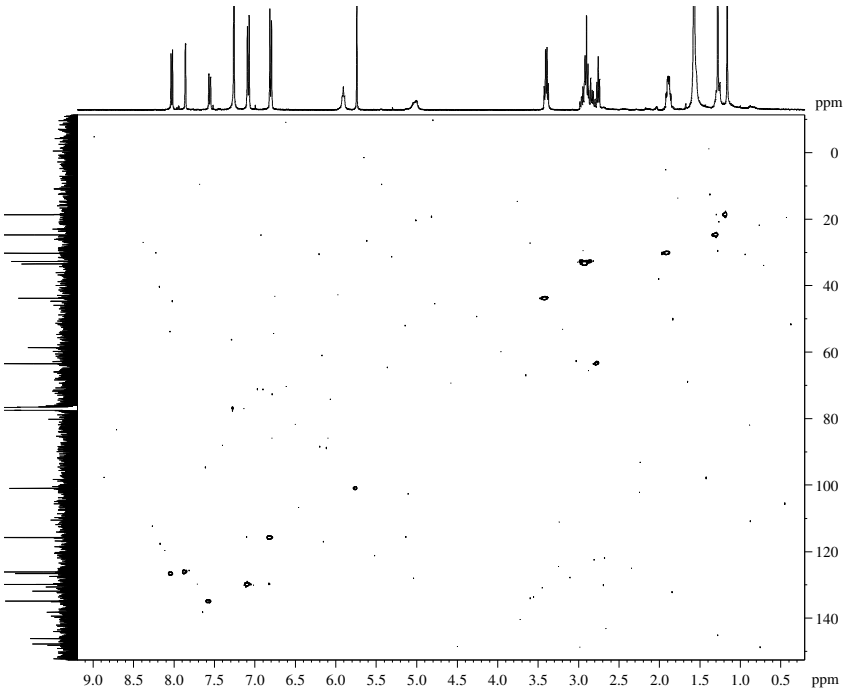

Figure S4.121: HSQC NMR spectrum of compound **4.25B**

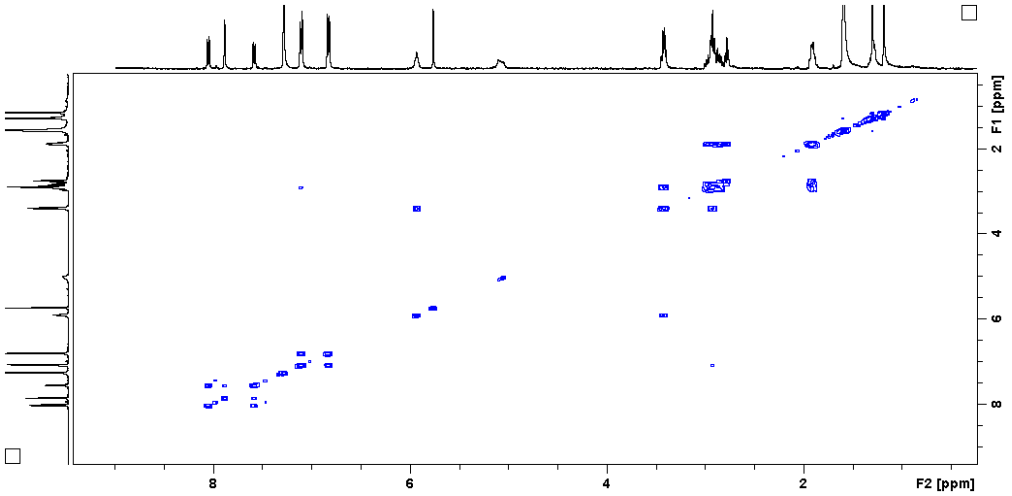

Figure S4.122: COSY NMR spectrum of compound **4.25B**

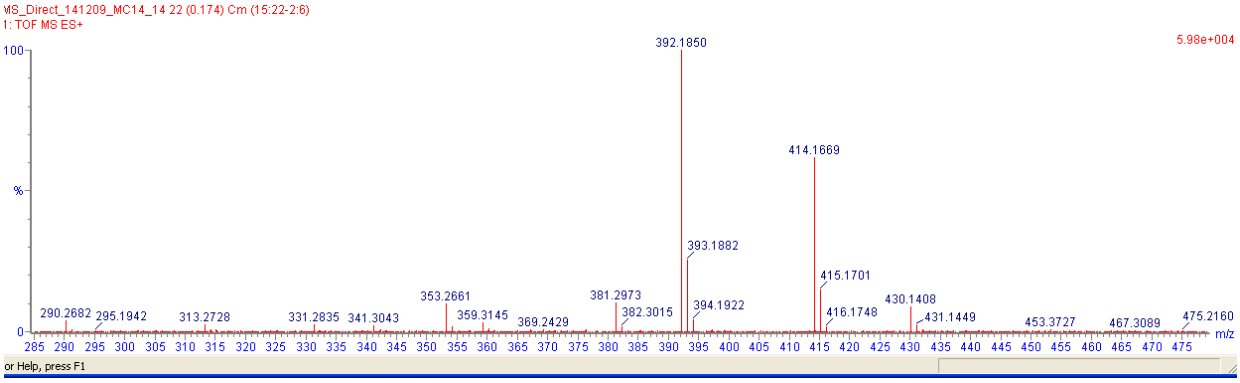

Figure S4.123: HRMS of compound **4.25B**

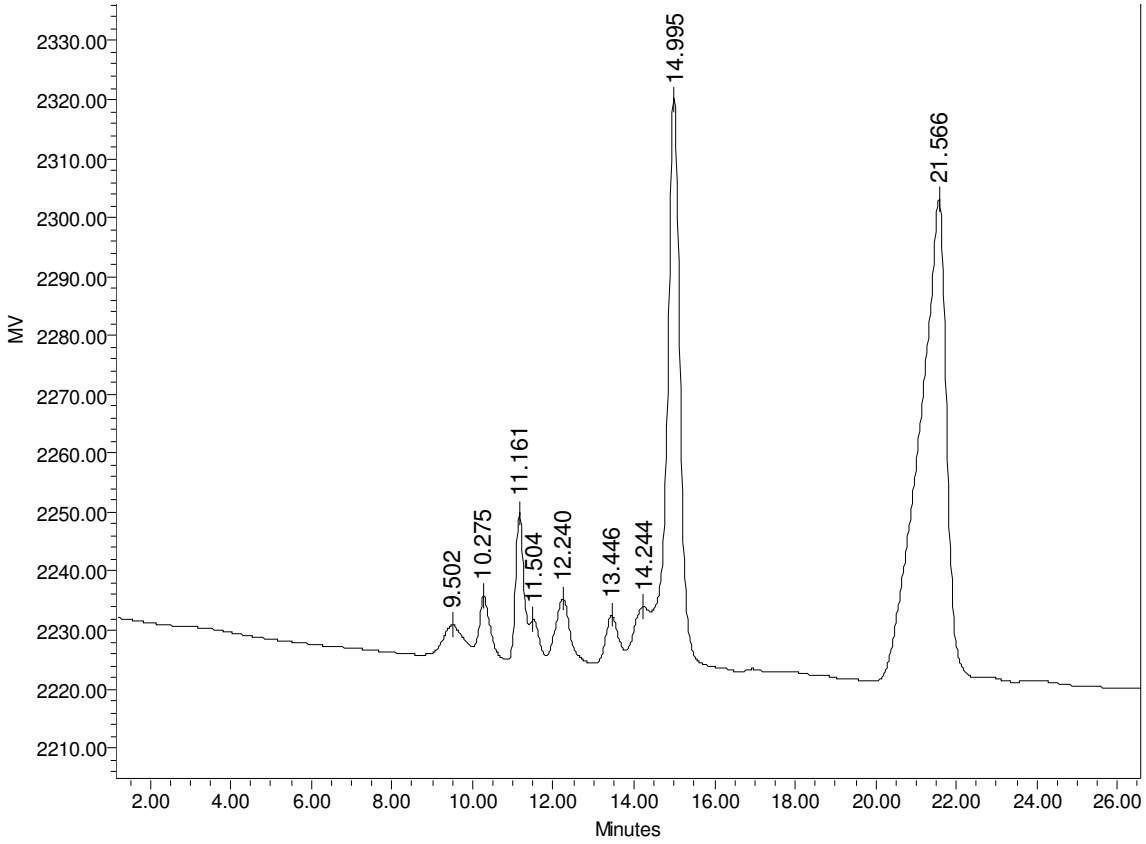

Figure S4.124: HPLC chromatogram showing the retention times for the two isomers: **4.25A**: 14.9 min and **4.25B**: 21.5 min

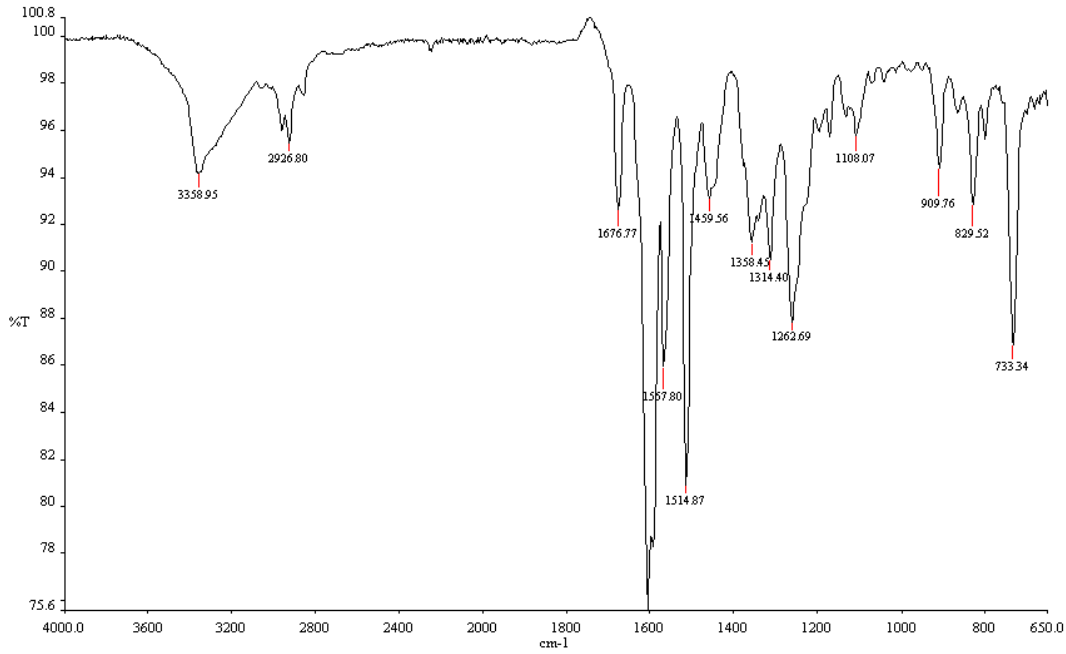

Figure S4.125: IR spectrum of compound **4.25**

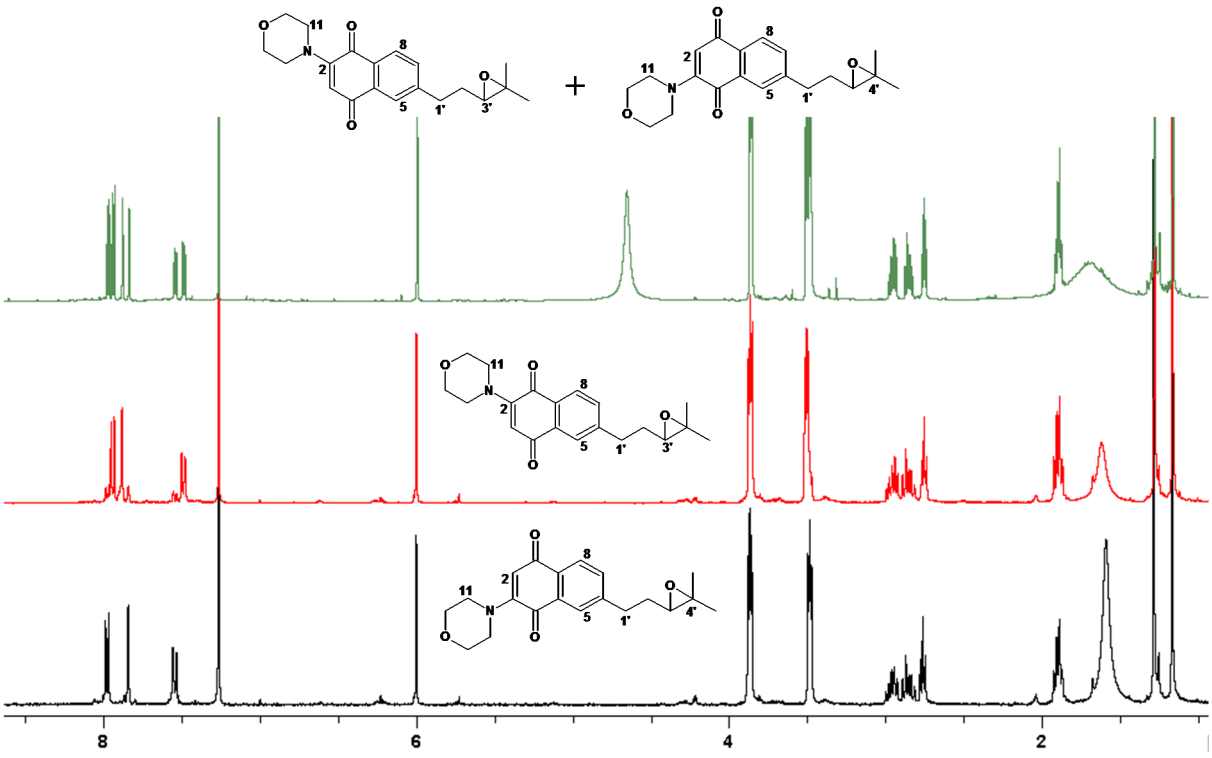

Figure S4.126: ^{1}H NMR spectra (600 MHz, $CDCl_3$) of alkylamino-naphthoquinone **4.26** illustrating the mixture of isomers before and after HPLC

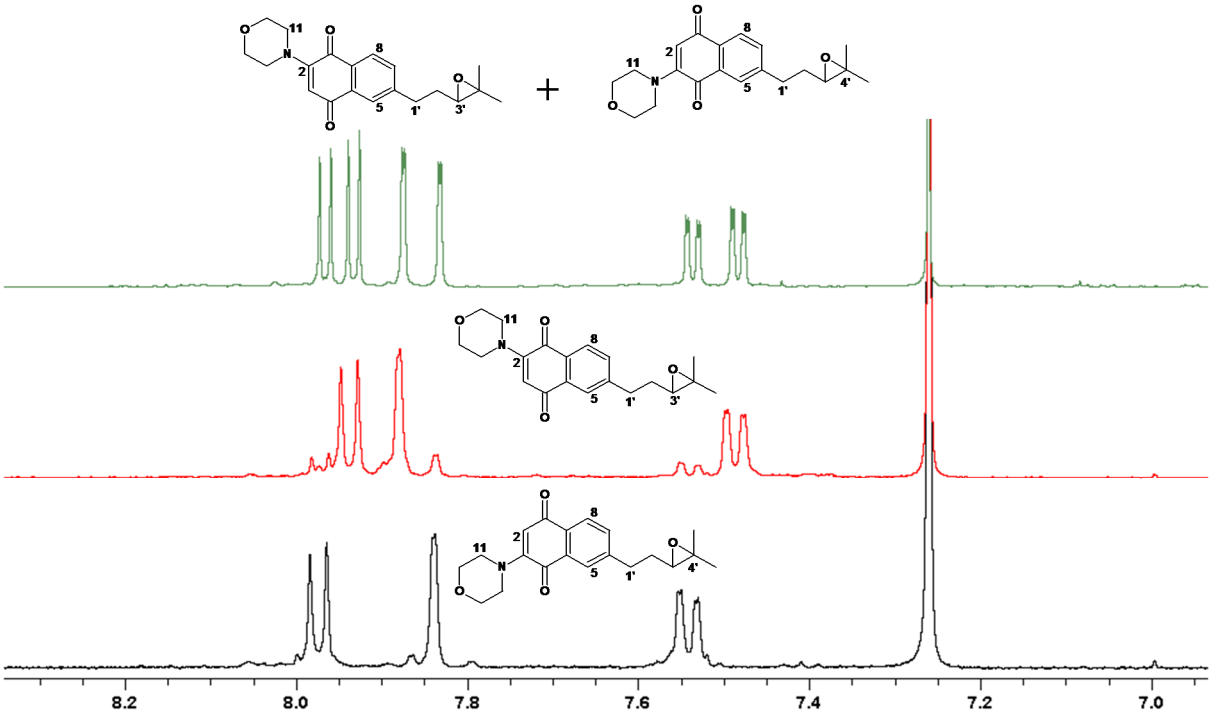

Figure S4.127: ^{1}H NMR spectra (600 MHz, $CDCl_3$) of alkylamino-naphthoquinone **4.26** showing differences between the isomers in the aromatic region

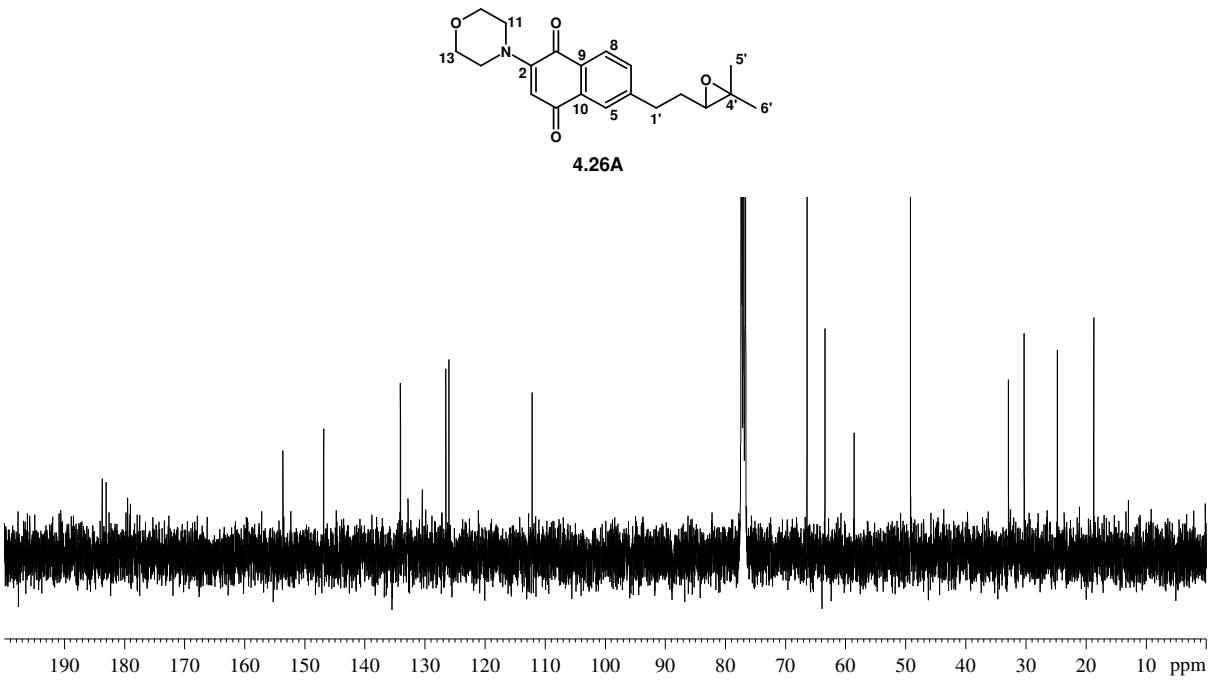

Figure S4.128: ^{13}C NMR spectrum (150 MHz, $CDCl_3$) of compound **4.26A**

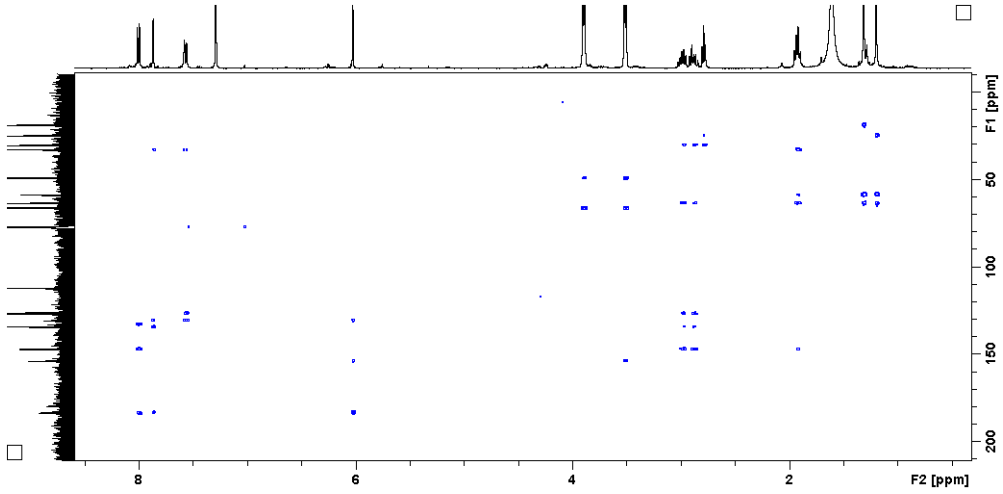

Figure S4.129: HMBC spectrum of compound **4.26A**

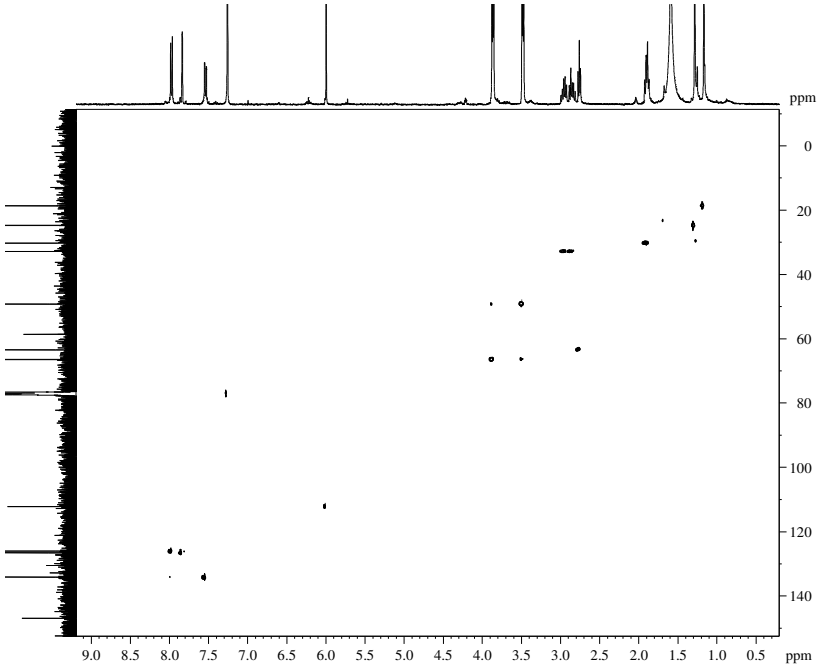

Figure S4.130: HSQC spectrum of compound **4.26A**

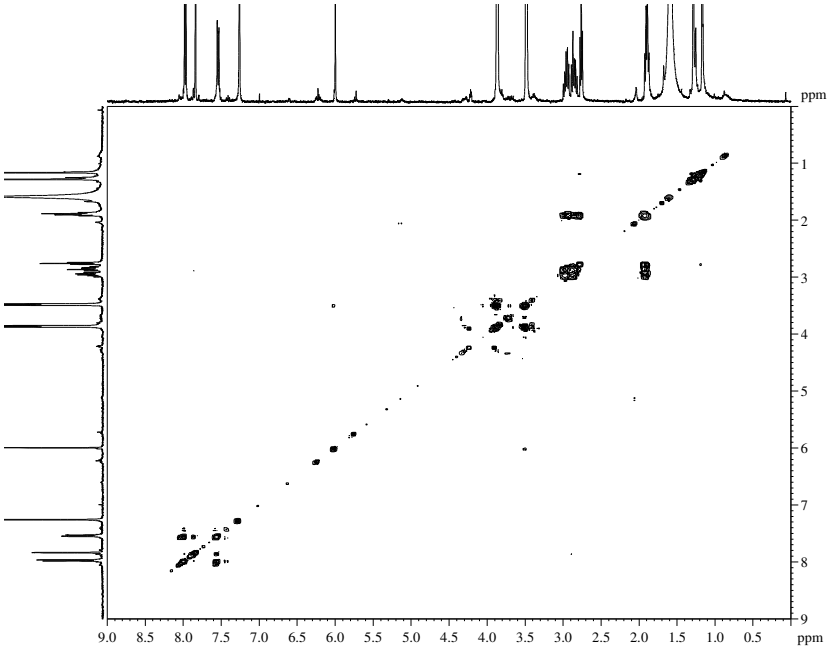

Figure S4.131: COSY spectrum of compound **4.26A**

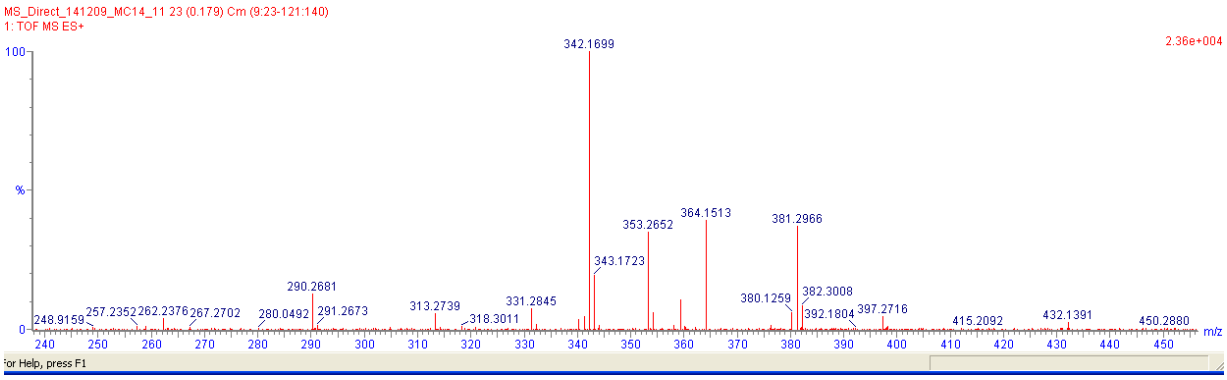

Figure S4.132: HRMS of compound **4.26A**

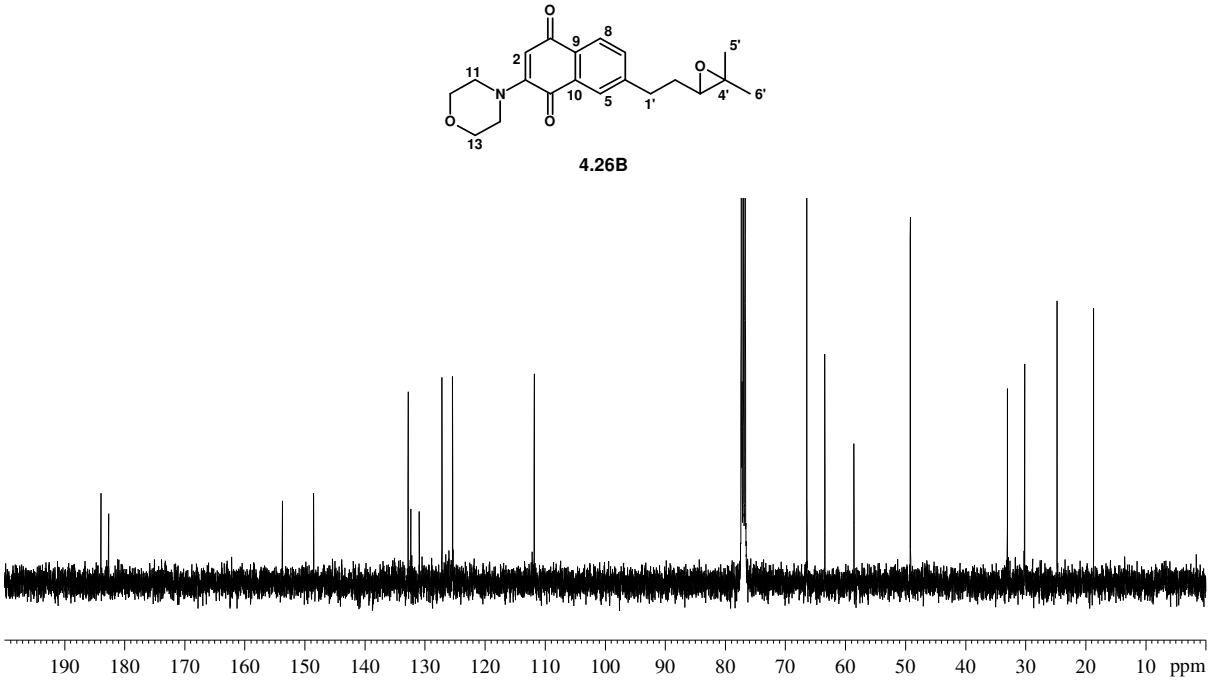

Figure S4.133: ^{13}C NMR spectrum (150 MHz, $CDCl_3$) of compound **4.26B**

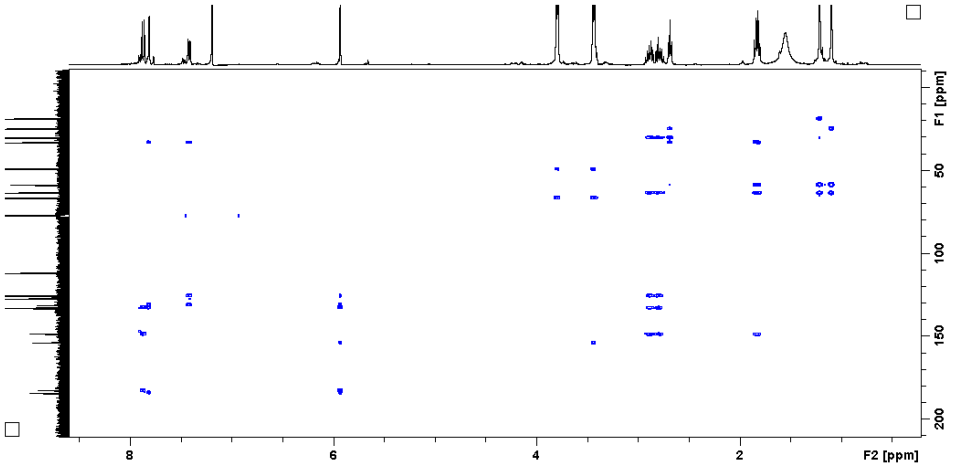

Figure S4.134: HMBC spectrum of compound **4.26B**

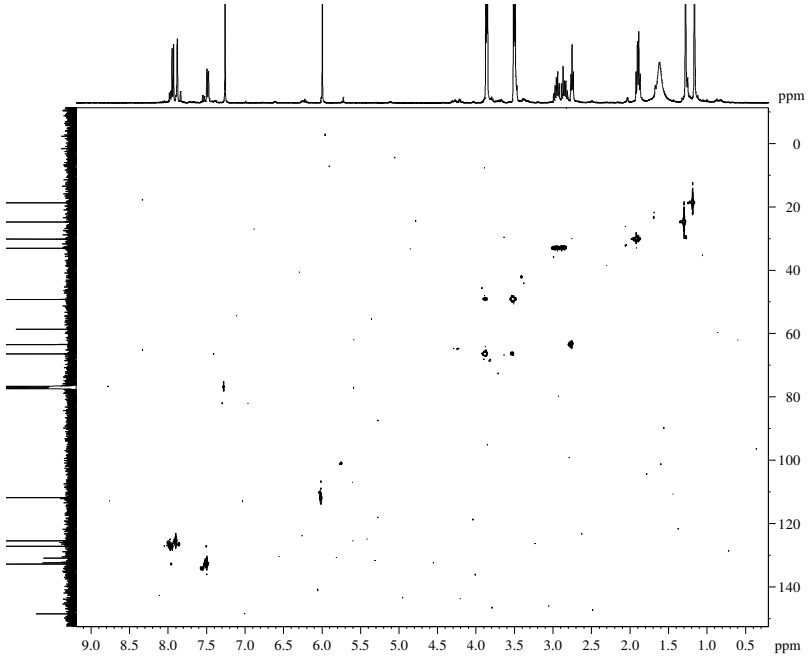

Figure S4.135: HSQC spectrum of compound **4.26B**

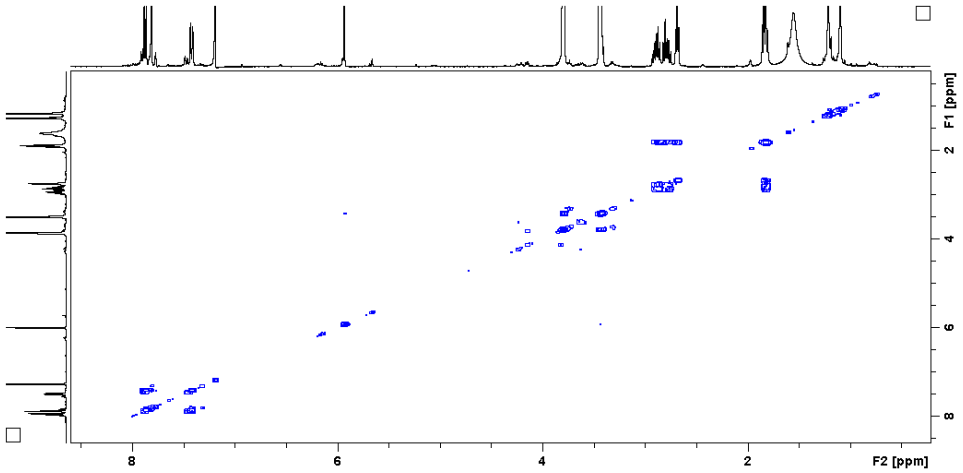

Figure S4.136: COSY spectrum of compound **4.26B**

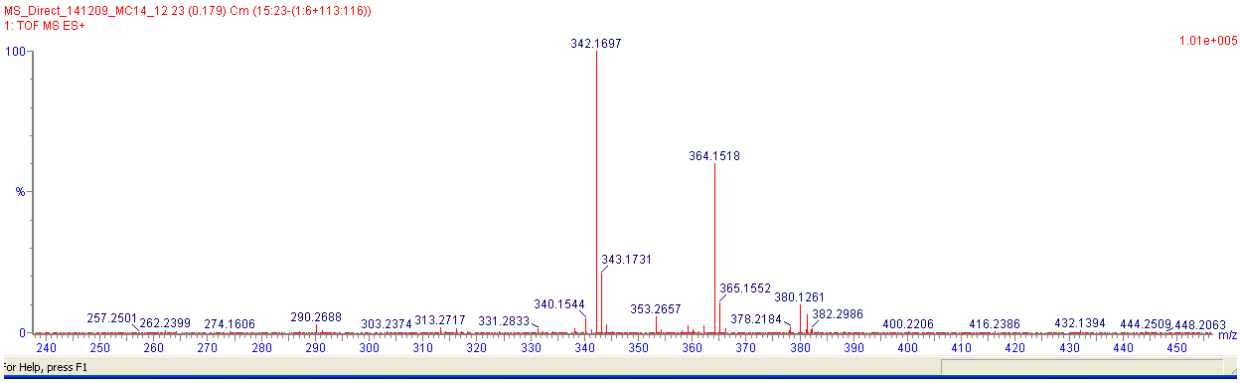

Figure S4.137: HRMS spectrum of compound **4.26B**

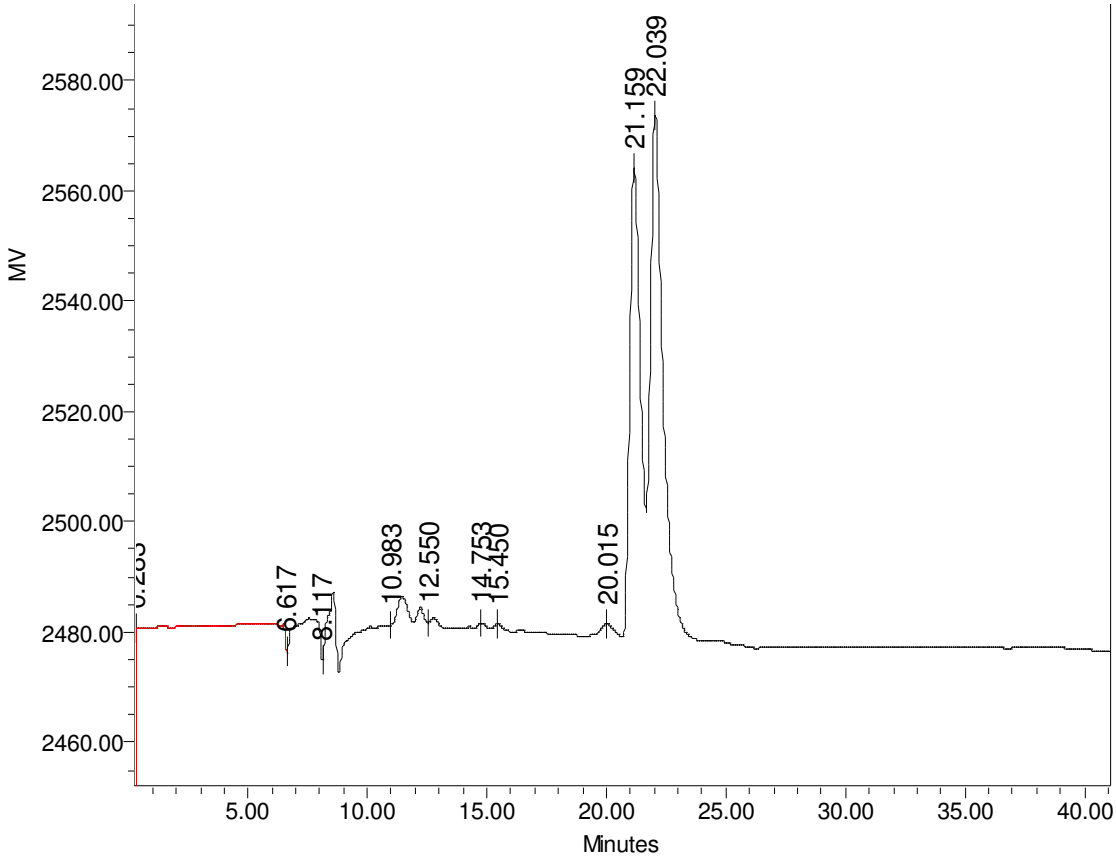

Figure S4.138: HPLC chromatogram showing the retention times for the two isomers: **4.26A**: 22.0 min and **4.26B**: 21.5 min

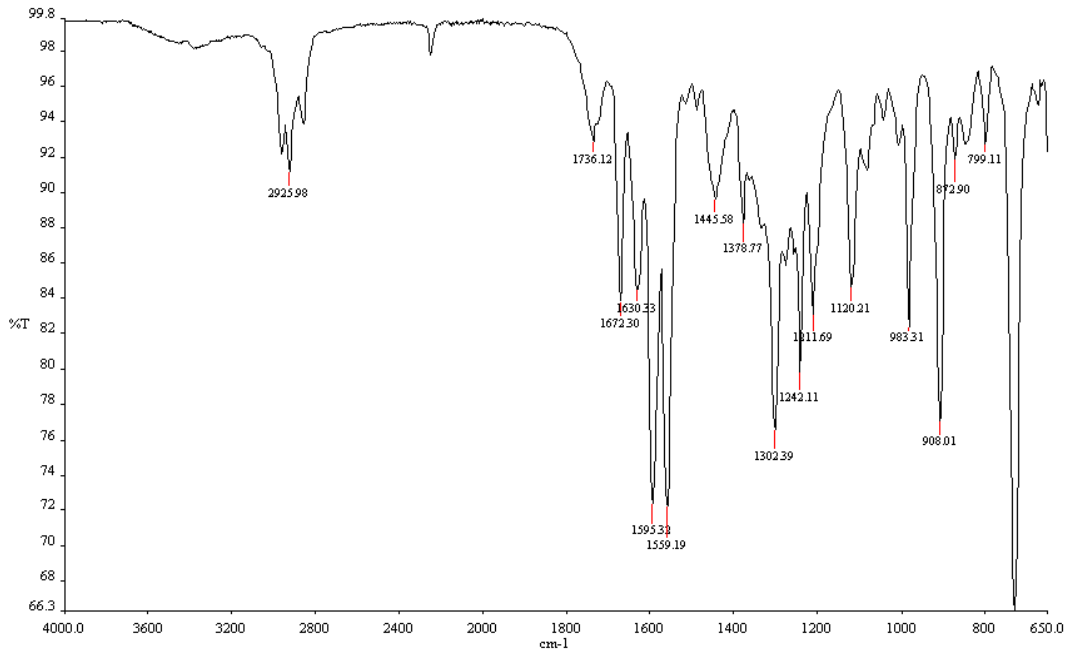

Figure S4.139: IR spectrum of compound **4.26**

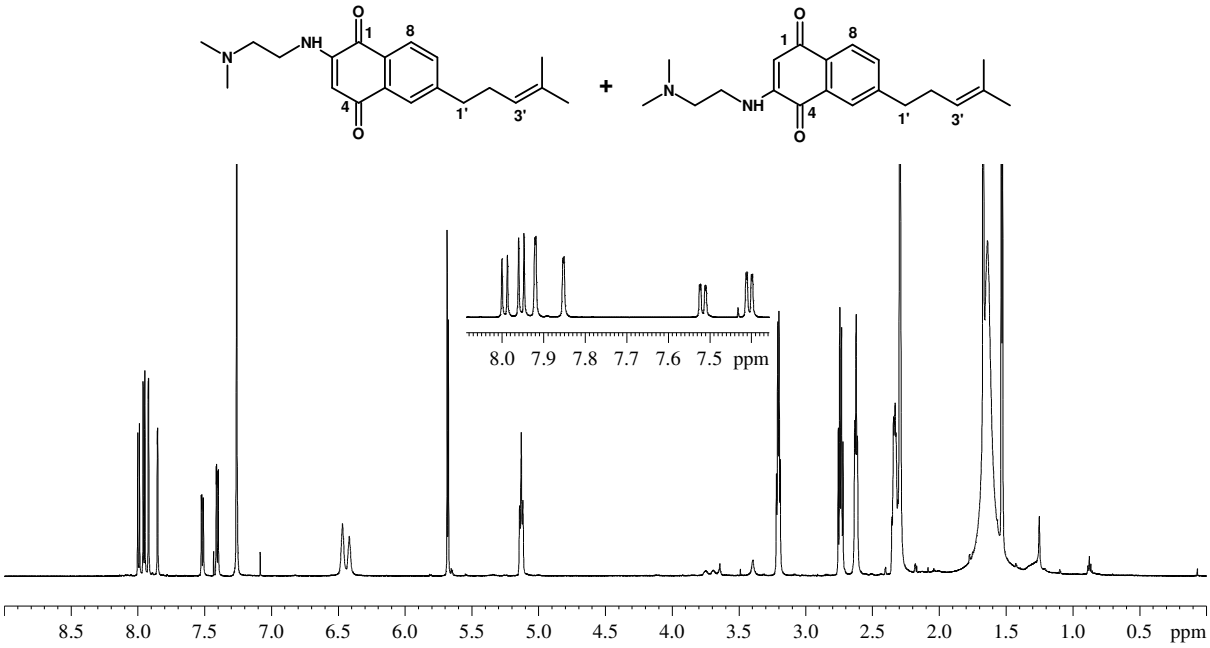

Figure S4.140: ^{1}H NMR spectrum ($CDCl_3$, 600 MHz) of a mixture of isomers **4.21A** and **4.21B**

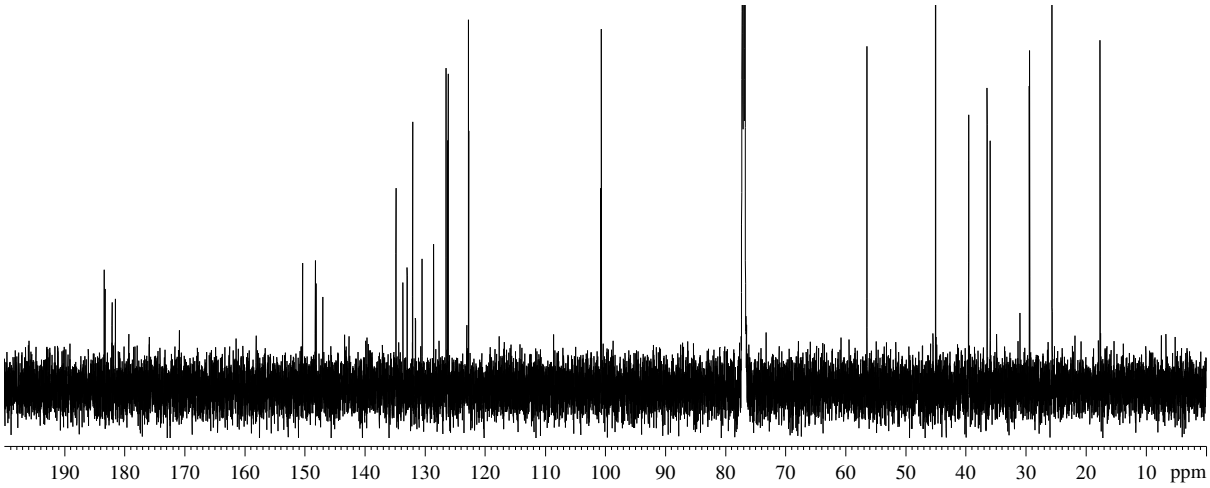

Figure S4.141: ^{13}C NMR spectrum ($CDCl_3$, 150 MHz) of a mixture of isomers **4.21A** and **4.21B**

Table S4.1: Preparation of Diels-Alder products from selected benzoquinones

	Quinone	Myrcene	EtOH	Mass/Weight of product	% yield
2-chloro-benzoquinone	0.500 g, 3.5 mmoles	0.955 g, 7.0 mmoles	10 ml	0.840 g	86.1
2-methoxy-benzoquinone	0.500 g, 3.6 mmoles	0.963 g, 7.2 mmoles	20 ml	0.568 g	57.5
2-methyl-benzoquinone	0.224 g, 1.8 mmoles	0.500 g, 3.6 mmol	20 ml	0.350 g	75.2

Table S4.2: Aromatization of Diels-Alder products to the naphthoquinone

	Diels-Alder Product	MnO_2	C_6H_6	Product	Mass/Weight of product	% yield
2-Cl	0.200 g, 0.7 mmoles	0.374 g, 4.3 mmoles	10 ml	**4.11**	0. 160g	83.3
2-OCH_3	0.200 g, 0.7 mmoles	0.380 g, 4.3 mmoles	10 ml	**4.12**	0. 160g	84.6
2-CH_3	0.100 g, 0.3 mmoles	0.201 g, 2.3 mmoles	10 ml	**4.13**	0. 075 g	98.4

Table S4.3: Oxidative coupling of naphthoquinone **4.10** with *para*-substituted anilines

p-substituent	Aniline	**4.7**	$Cu(OAc)_2$	Product	Mass/Weight	% yield
-CH_3-aniline	0.0499 g, 0.4 mmoles	0.112 g, 0.4 mmoles	0.010 g, 0.04 mmoles	**4.15**	0.109 g	79.5
-OCH_3-aniline	0.0568 g, 0.4 mmoles	0.111 g, 0.4 mmoles	0.010 g, 0.04 mmoles	**4.16**	0.129	89.3
-Cl-aniline	0.059 g, 0.4 mmoles	0.112 g, 0.4 mmoles	0.010 g, 0.04 mmoles	**4.17**	0.123	84.3
-CF_3-aniline	0.078 g, 0.4 mmoles	0.117 g, 0.4 mmoles	0.010 g, 0.04 mmoles	**4.18**	0.115	72.1
methylenedioxy aniline	0.057 g, 0.4 mmoles	0.100 g, 0.4 mmoles	0.010 g, 0.04 mmoles	**4.19**	0.122	81.9

Table S4.4: Coupling of alkyl amines with naphthoquinone **4.10**

	Amine mmol)	**4.7**	Product	Mass/Weight	% yield
N, N dimethylethyleneamine	0.036 g, 0.4 mmoles	0.100 g, 0.4 mmoles	**4.21**	0.0912	69.9
tyramine	0.057 g, 0.4 mmoles	0.100 g, 0.4 mmoles	**4.22**	0.107	71.7
propargylamine HCl	0.038 g, 0.4 mmoles	0.100 g, 0.4 mmoles	**4.23**	0.086	73.5

6-[2-(3,3-dimethyloxiran-2-yl)ethyl]-2-(morpholin-4-yl)naphthalene-1,4-dione (4.26)

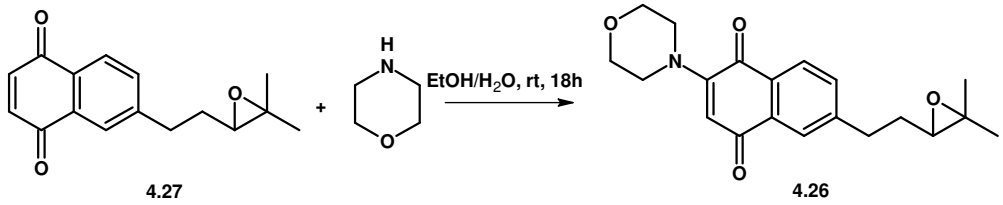

4.27 4.26

A similar method used for the preparation of **4.25** was used to synthesize **4.26.** Morpholine (0.044 g, 0.4 mmoles) was reacted with **4.27** (0.102 g, 0.4 mmoles) in EtOH/H_2O (10 ml, 1:1 mixture) with stirring at room temperature for 18 hours to yield 0.076 g (55.7 % yield) of **4.26**.

CHAPTER FIVE

Supplementary data

Biological activity of truncated prenylated naphthoquinones

Cytotoxicity data for the first series of naphthoquinones was conducted using as a three point assay. IC_{50} values were not determined, instead percentage survival of cancer cells was calculated at 1 µM, 10 µM and 100 µM concentrations of the compounds (**4.10-4.13**) used. The calculated percentage survival rates are presented in this section as bar and line graphs.

LIST OF FIGURES

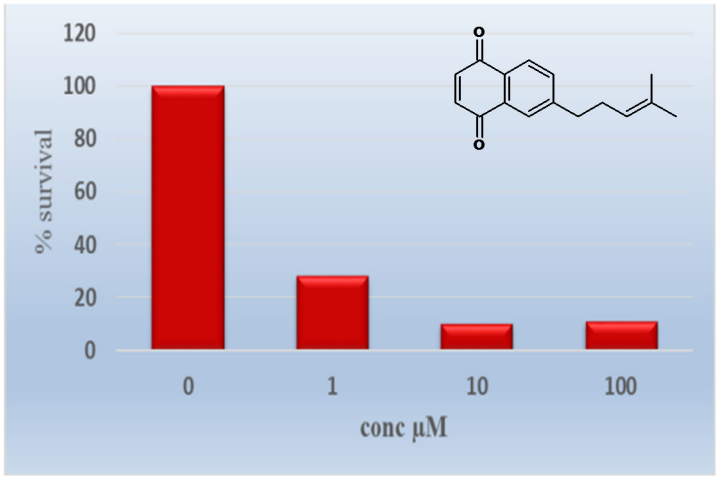

Figure S5.1: Bar graph representation of percentage survival of cancer cells at 1 µM, 10 µM and 100 µM concentrations of compound **4.10**

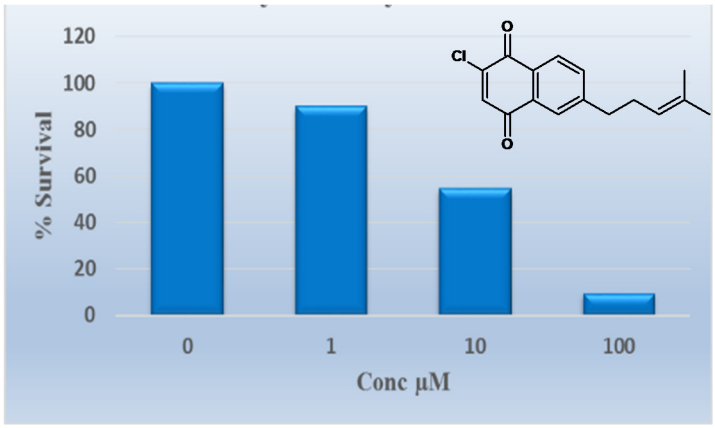

Figure S5.2: Bar graph representation of percentage survival of cancer cells at 1 µM, 10 µM and 100 µM concentrations of compound **4.11A**

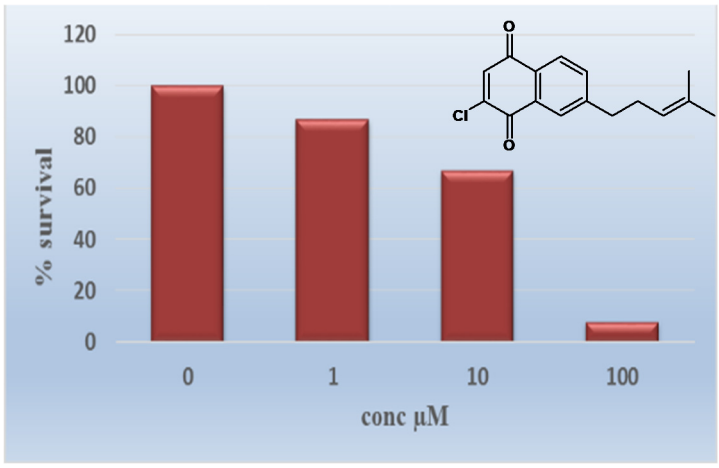

Figure S5.3: Bar graph representation of percentage survival of cancer cells at 1 µM, 10 µM and 100 µM concentrations of compound **4.11B**

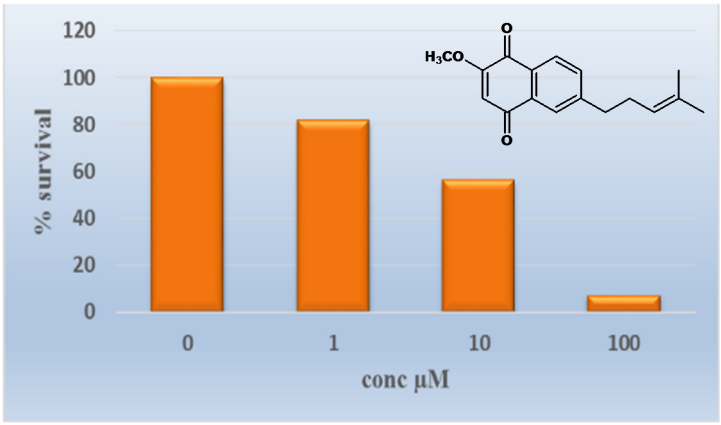

Figure S5.4: Bar graph representation of percentage survival of cancer cells at 1 µM, 10 µM and 100 µM concentrations of compound **4.12A**

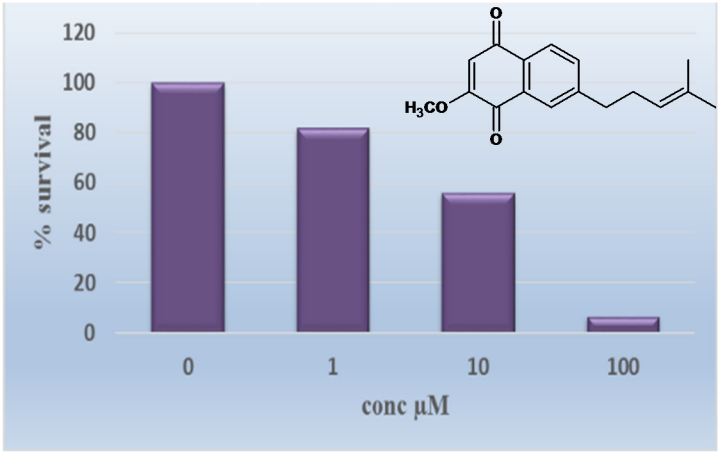

Figure S5.5: Bar graph representation of percentage survival of cancer cells at 1 µM, 10 µM and 100 µM concentrations of compound **4.12B**

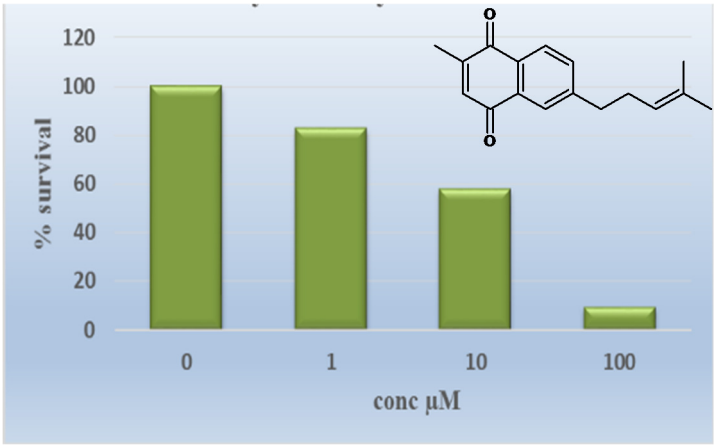

Figure S5.6: Bar graph representation of percentage survival of cancer cells at 1 µM, 10 µM and 100 µM concentrations of compound **4.13A**

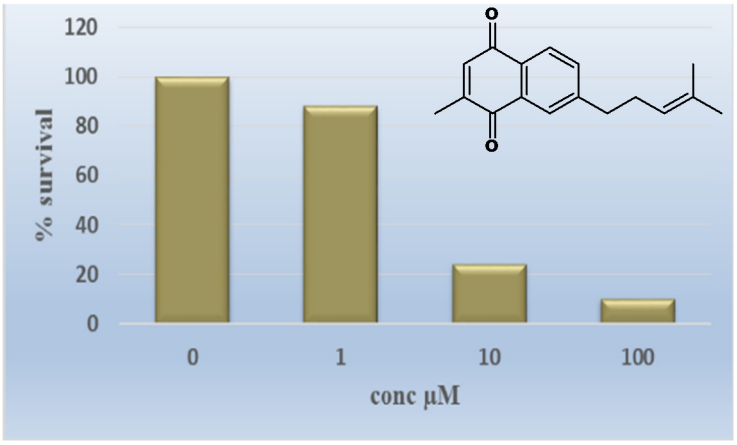

Figure S5.7: Bar graph representation of percentage survival of cancer cells at 1 µM, 10 µM and 100 µM concentrations of compound **4.13B**

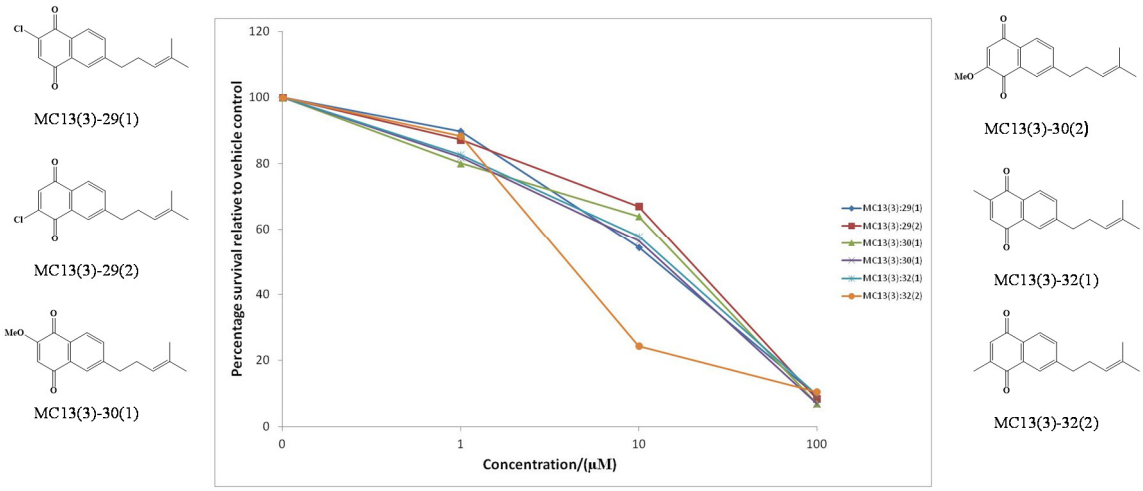

Figure S5.8: A line graph presentation of the first series of naphthoquinones, showing trends

NB: The book codes displayed in the graph correspond to the compound numbers displayed below

- MC13(3)-29(1) – **4.11A**
- MC13(3)-29(2) – **4.11B**
- MC13(3)-30(1) – **4.12A**
- MC13(3)-30(2) – **4.12B**
- MC13(3)-32(1) – **4.13A**
- MC13(3)-32(2) – **4.13B**

CHAPTER SIX

Supplementary data

Molecular modelling and STD NMR studies

All molecular docking conformations of the synthesized truncated naphthoquinones (**4.10-4.31**), SQA (**2.47**), lapachol (**3.5**) and SNQA (**3.11**) are presented in this chapter. The different bond interactions within the N-terminal ATP binding site of Hsp90 are also included. Known Hsp90 inhibitor e.g. geldanamycin (**2.28**) was also docked a control and for comparison purposes with our set of compounds.

The different STD NMR spectra obtained for the selected naphthoquinones **4.16A, 4.20A, 4.28, 4.29** and **2.47** are shown, for both N- and C- terminal domains.

LIST OF FIGURES

Figure S6.70: ATP and **4.28** docked in the same active site of the N-terminal domain

Figure S6.71: Bond-bond interactions of **4.29** with the N-terminal ATP binding site of Hsp90

Figure S6.72: ATP and **4.29** docked in the same active site of the N-terminal domain

Figure S6.73: Bond-bond interactions of **2.47** with the N-terminal ATP binding site of Hsp90

Figure S6.74: ATP and **2.47** docked in the same active site of the N-terminal domain

Figure S6.75: Bond-bond interactions of **3.11** with the N-terminal ATP binding site of Hsp90

Figure S6.76: ATP and **3.11** docked in the same active site of the N-terminal domain

Figure S6.77: 2.47 and **3.11** docked in the same N-terminal domain of Hsp90

Figure S6.78: Bond-bond interactions of **3.5** with the N-terminal ATP binding site of Hsp90

Figure S6.79: ATP and **3.5** docked in the same active site of the N-terminal domain

Figure S6.80: (**A**) reference ^{1}H spectrum of the C-terminal domain of Hsp90 and **2.47** (**B**) corresponding STD-NMR spectrum

Figure S6.81: (**A**) reference ^{1}H spectrum of the C-terminal domain of Hsp90 and **4.16A** (**B**) corresponding STD-NMR spectrum

Figure S6.82: (**A**) reference ^{1}H spectrum of the C-terminal domain of Hsp90 and **4.28** (**B**) corresponding STD-NMR spectrum

Figure S6.83: (**A**) reference ^{1}H spectrum of the C-terminal domain of Hsp90 and **4.29** (**B**) corresponding STD-NMR spectrum

Figure S6.84: (**A**) reference ^{1}H spectrum of the N-terminal domain of Hsp90 and novobiocin **(2.41)** (**B**) corresponding STD-NMR spectrum

Figure S6.85: (**A**) reference ^{1}H spectrum of the N-terminal domain of Hsp90 and **4.16A** (**B**) corresponding STD-NMR spectrum

Figure S6.86: (**A**) reference ^{1}H spectrum of the N-terminal domain of Hsp90 and **4.20A** (**B**) corresponding STD-NMR spectrum

Figure S6.87: (**A**) reference ^{1}H spectrum of the N-terminal domain of Hsp90 and **4.28** (**B**) corresponding STD-NMR spectrum

Figure S6.88: (**A**) reference ^{1}H spectrum of the N-terminal domain of Hsp90 and **4.29** (**B**) corresponding STD-NMR spectrum

Figure S6.89: (**A**) reference ^{1}H spectrum of the N-terminal domain of Hsp90 and **2.47** (**B**) corresponding STD-NMR spectrum

Molecular Docking

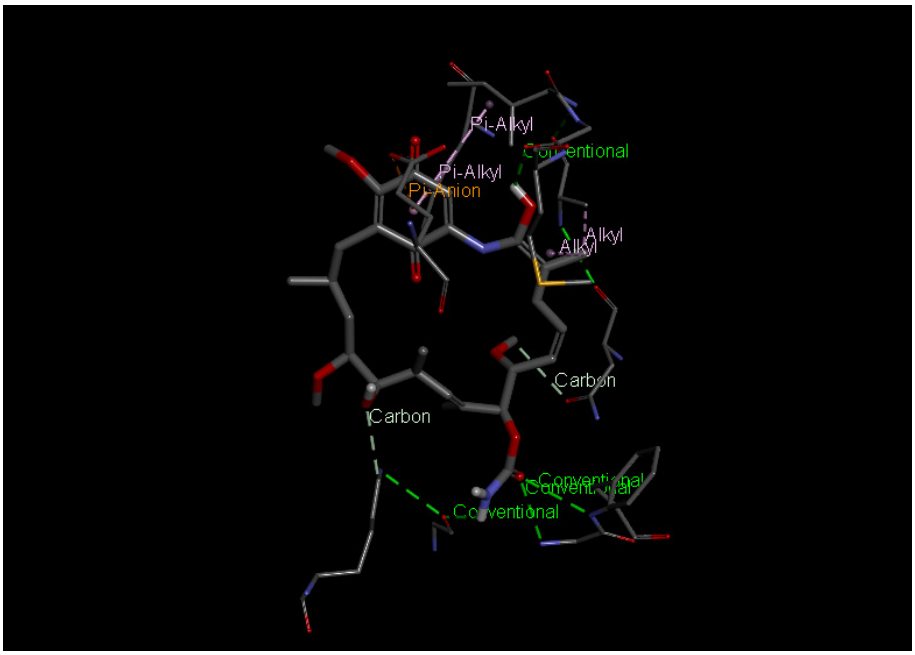

Figure S6.1: Geldanamycin (**2.28**) bond interactions with the N-terminal ATP binding site of Hsp90

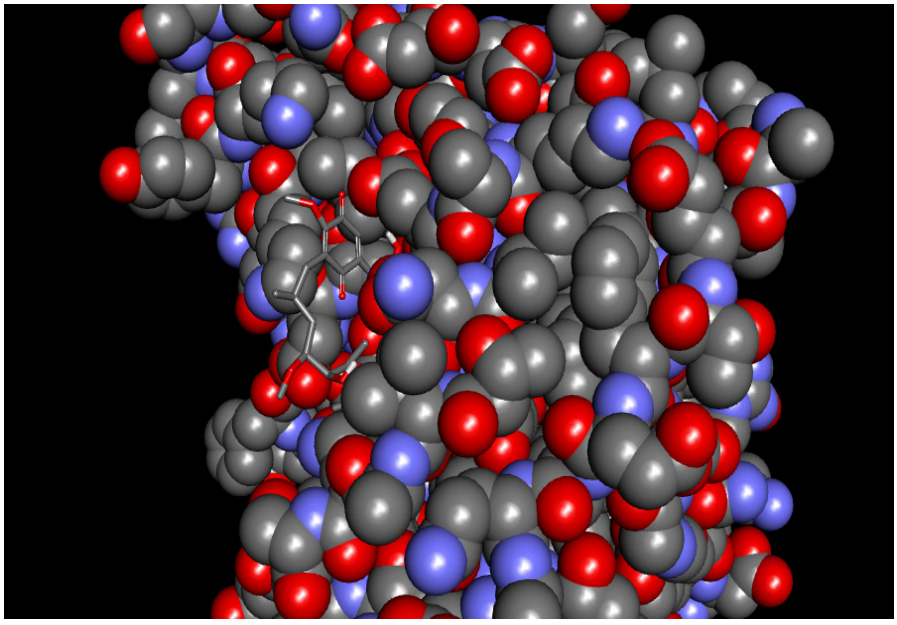

Figure S6.2: Ball and stick presentation of geldanamycin (**2.28**) showing its orientation within the active site. The quinone system sticks out of the binding site.

First series of naphthoquinone analogues

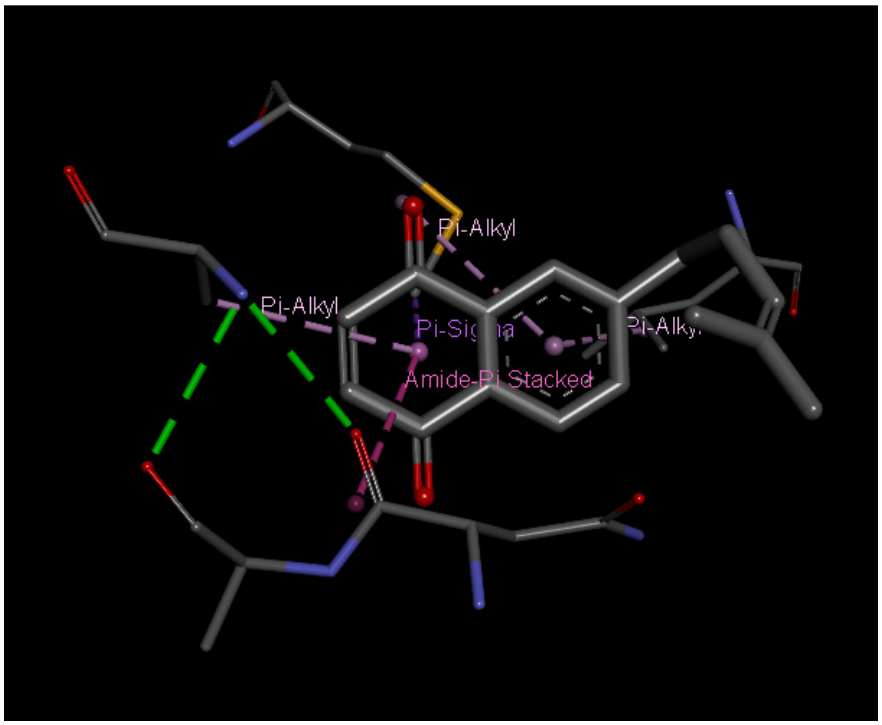

Figure S6.3: Bond-bond interactions of **4.10** with the N-terminal ATP binding site of Hsp90

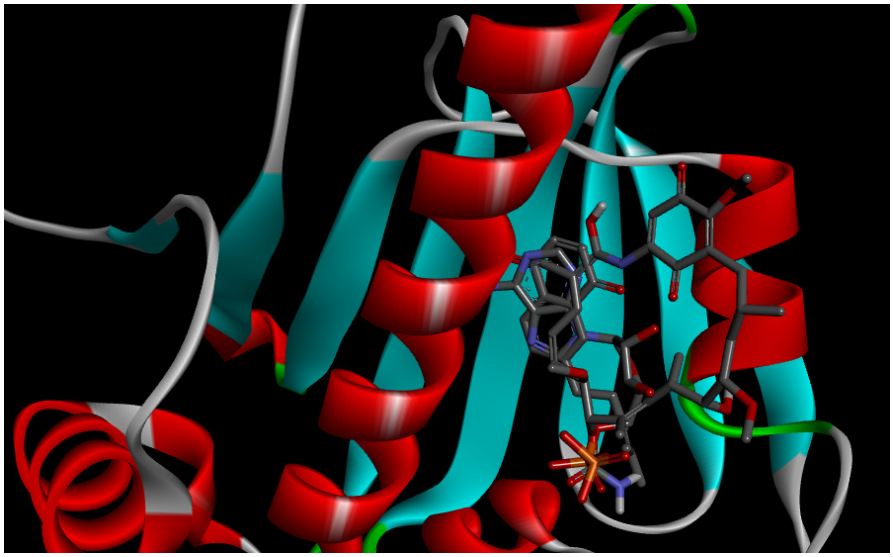

Figure S6.4: Docking conformations of ATP, geldanamycin (**2.28**) and **4.10** in the same active site of N-terminal domain.

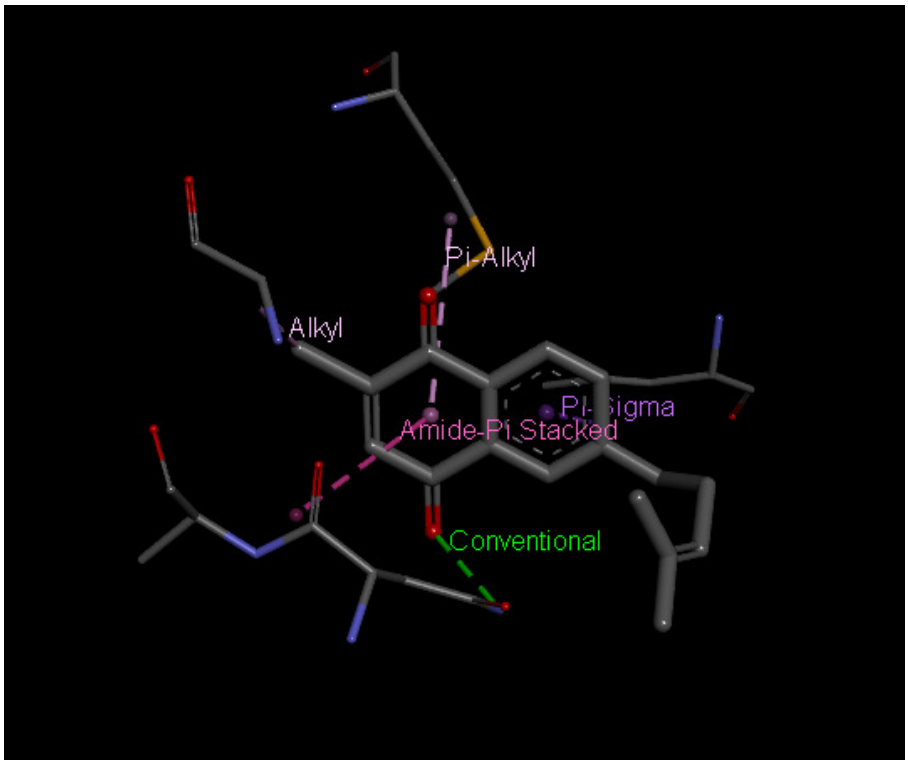

Figure S6.5: Bond-bond interactions of **4.11A** with the N-terminal ATP binding site of Hsp90

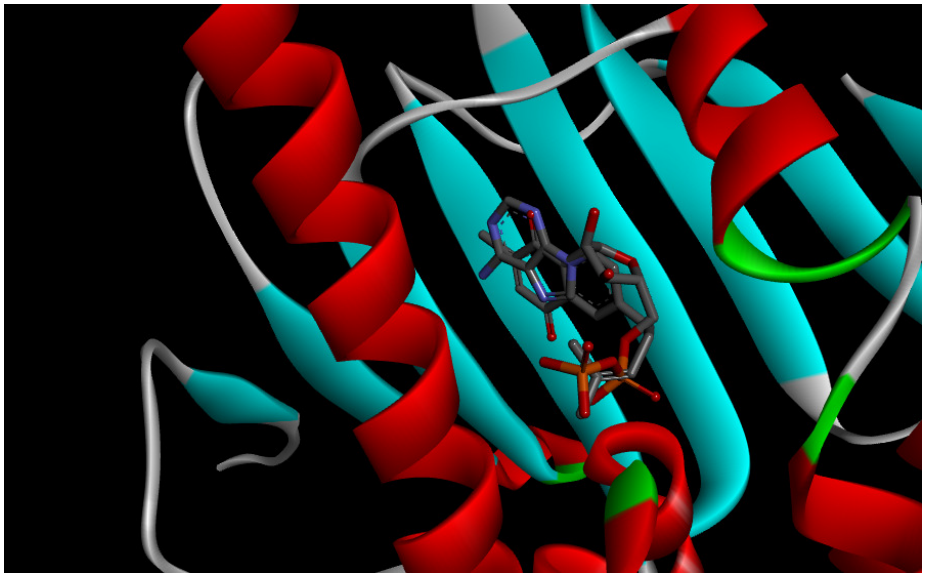

Figure S6.6: ATP and **4.11A** docked in the same active site of the N-terminal domain

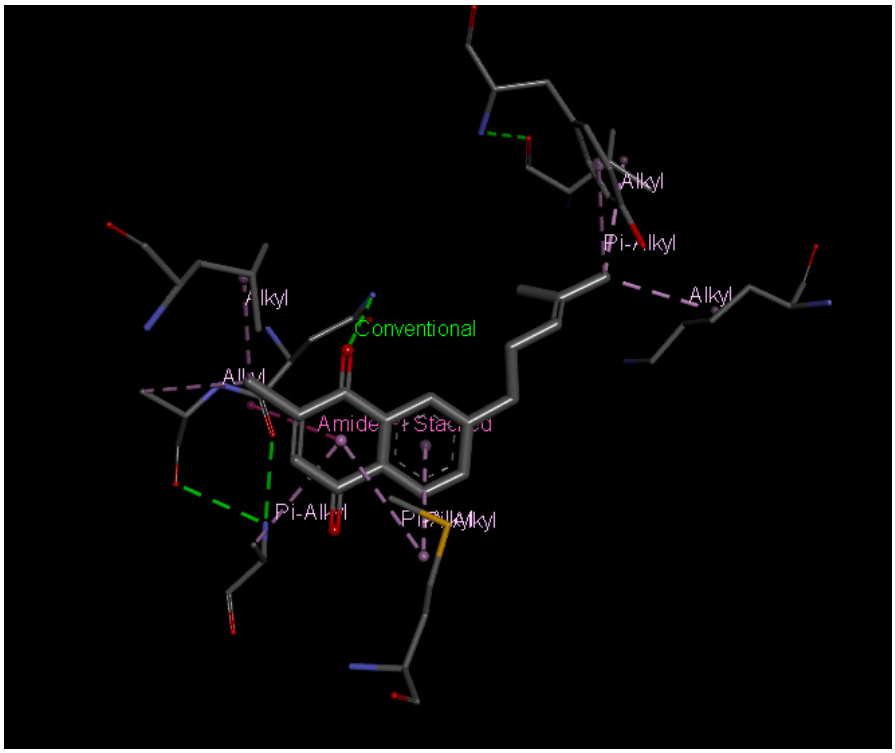

Figure S6.7: Bond-bond interactions of **4.11B** with the N-terminal ATP binding site of Hsp90

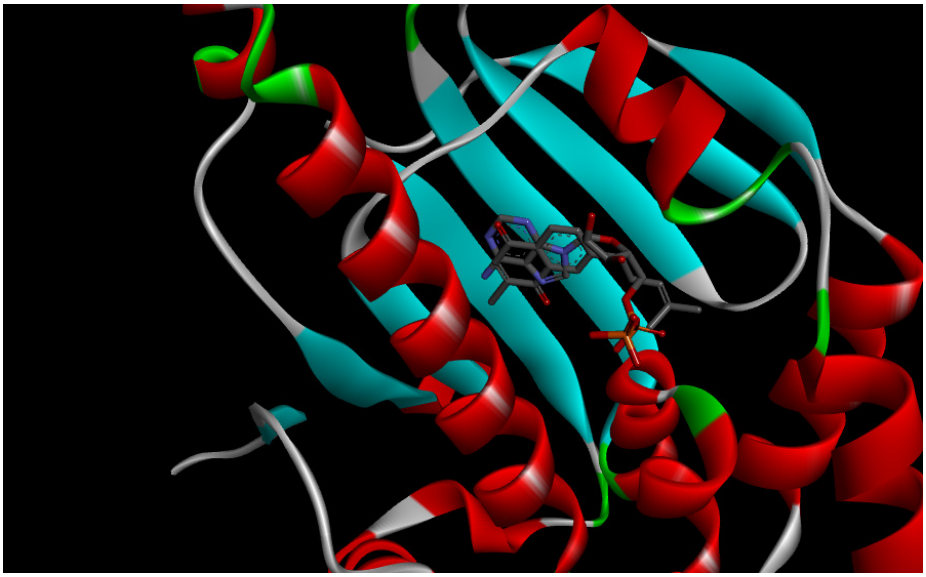

Figure S6.8: ATP and **4.11B** docked in the same active site of the N-terminal domain

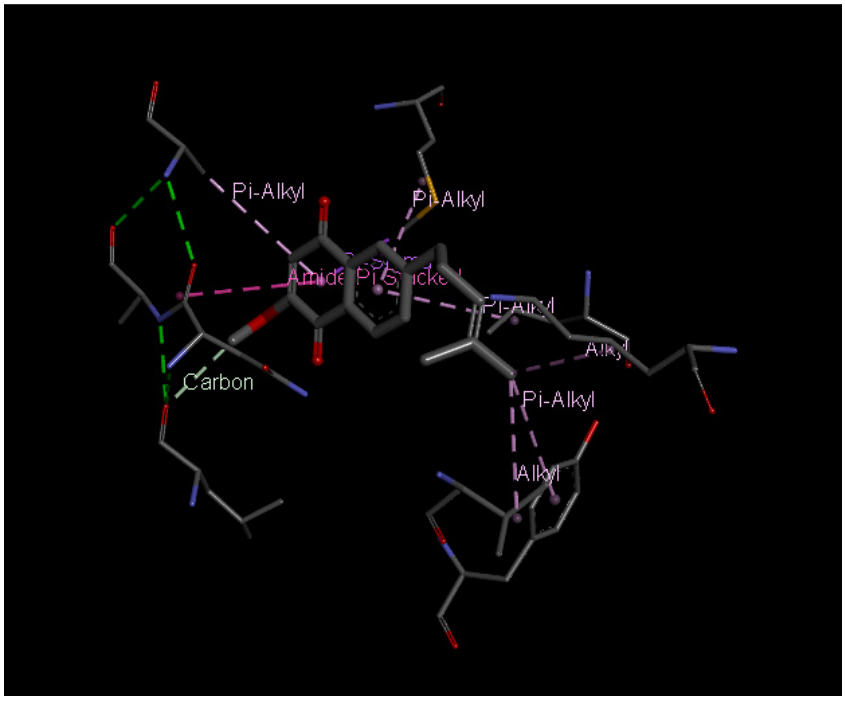

Figure S6.9: Bond-bond interactions of **4.12A** with the N-terminal ATP binding site of Hsp90

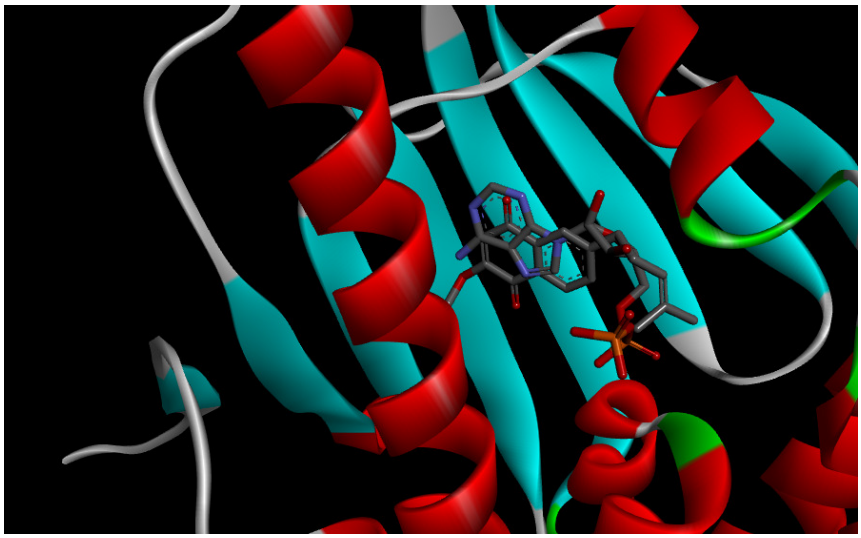

Figure S6.10: ATP and **4.12A** docked in the same active site of the N-terminal domain

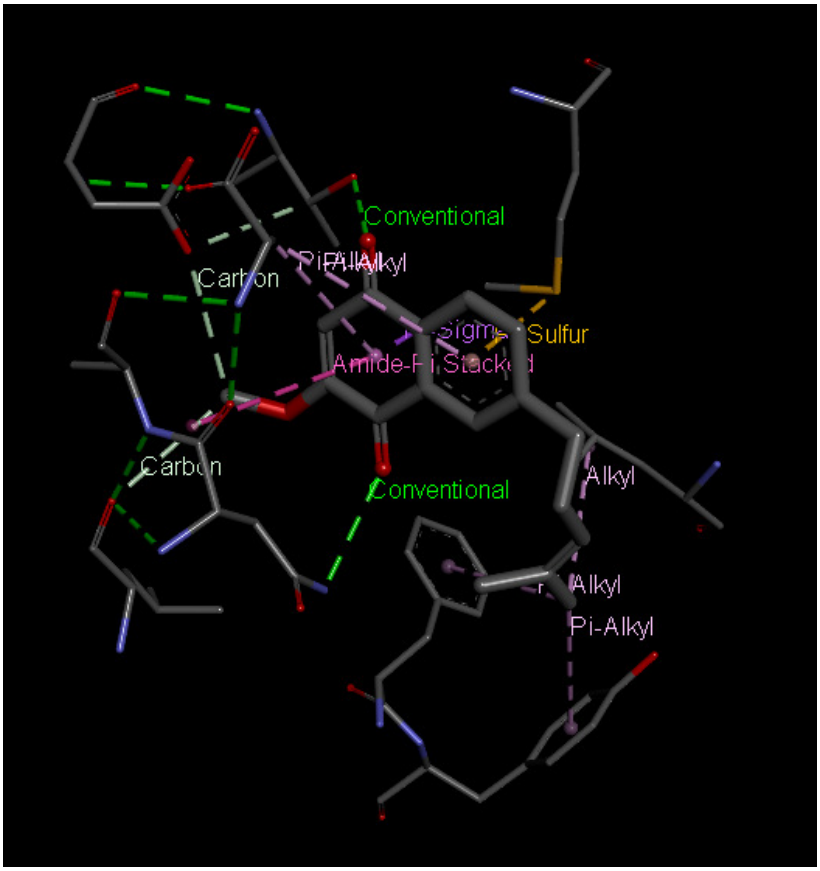

Figure S6.11: Bond-bond interactions of **4.12B** with the N-terminal ATP binding site of Hsp90

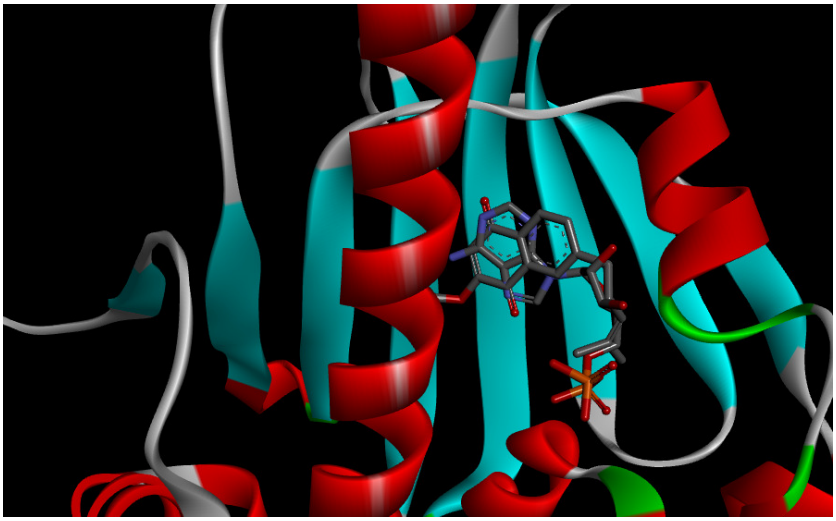

Figure S6.12: ATP and **4.12B** docked in the same active site of the N-terminal domain

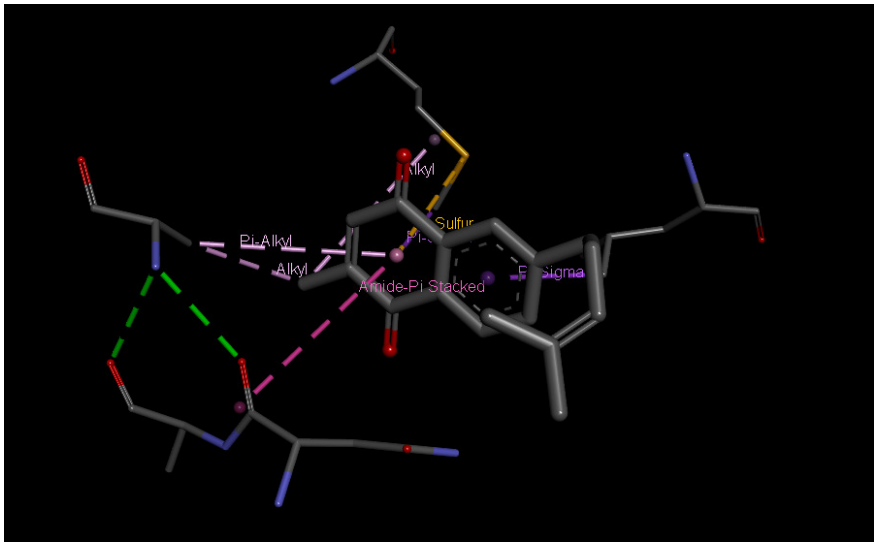

Figure S6.13: Bond-bond interactions of **4.13A** with the N-terminal ATP binding site of Hsp90

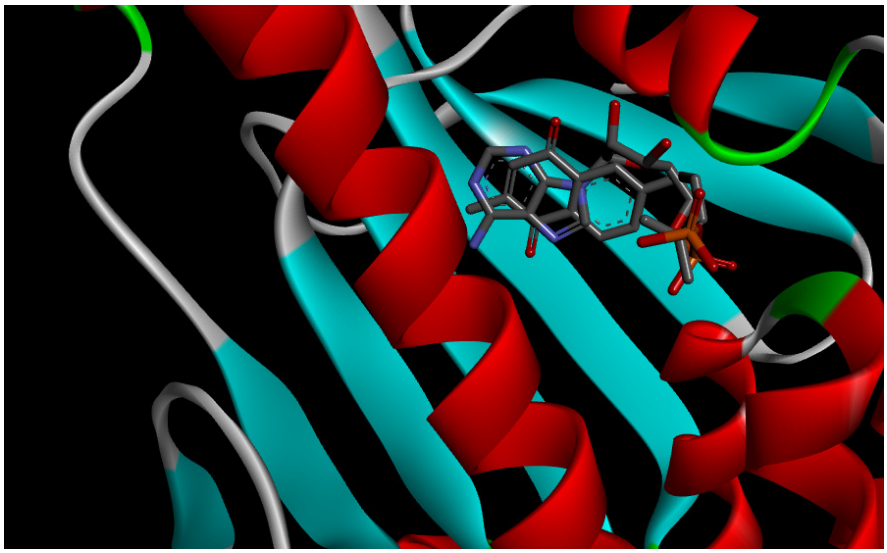

Figure S6.14: ATP and **4.13A** docked in the same active site of the N-terminal domain

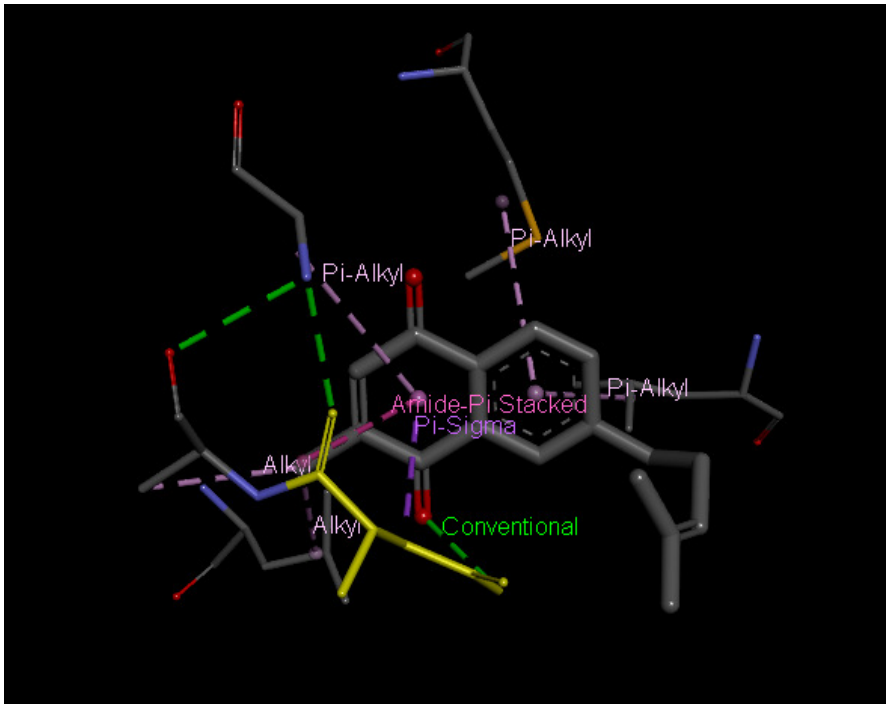

Figure S6.15: Bond-bond interactions of **4.13B** with the N-terminal ATP binding site of Hsp90

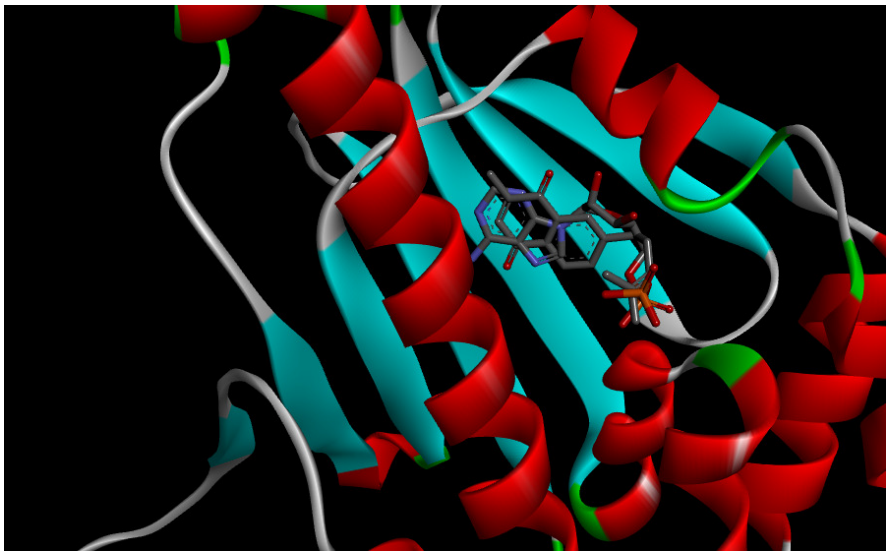

Figure S6.16: ATP and **4.13B** docked in the same active site of the N-terminal domain

Second series of naphthoquinone analogues

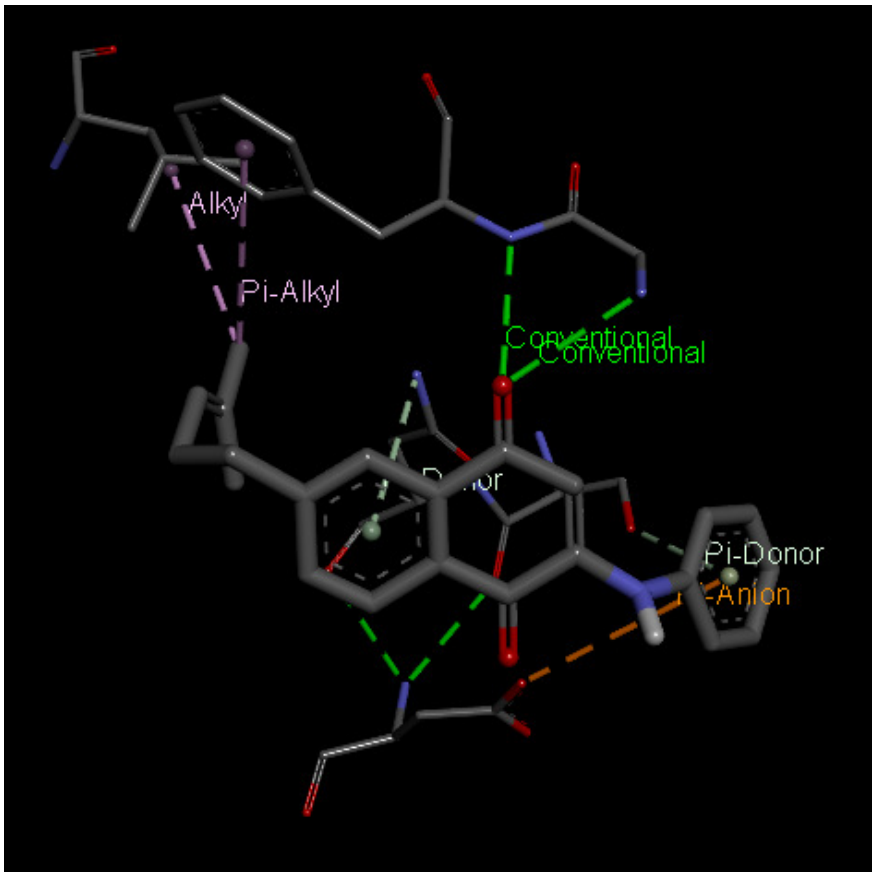

Figure S6.17: Bond-bond interactions of **4.14A** with the N-terminal ATP binding site of Hsp90

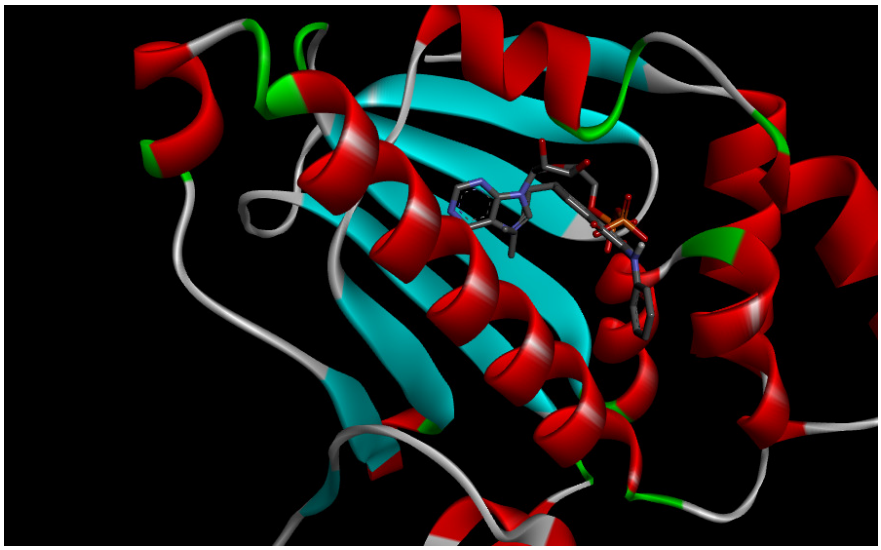

Figure S6.18: ATP and **4.14A** docked in the same active site of the N-terminal domain

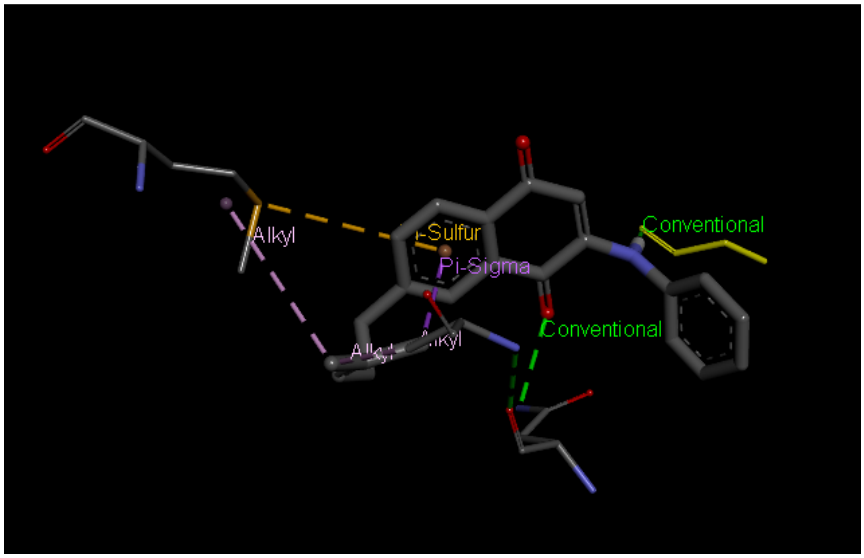

Figure S6.19: Bond-bond interactions of **4.14B** with the N-terminal ATP binding site of Hsp90

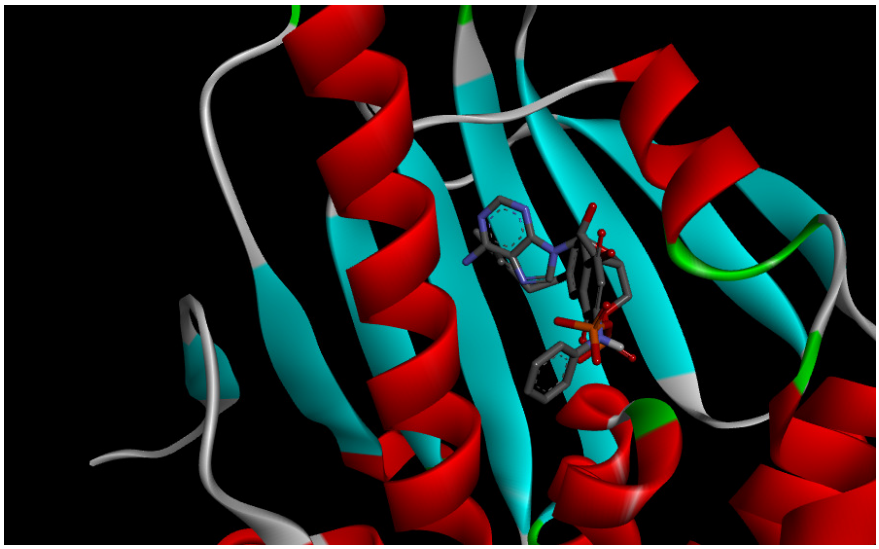

Figure S6.20: ATP and **4.14B** docked in the same active site of the N-terminal domain

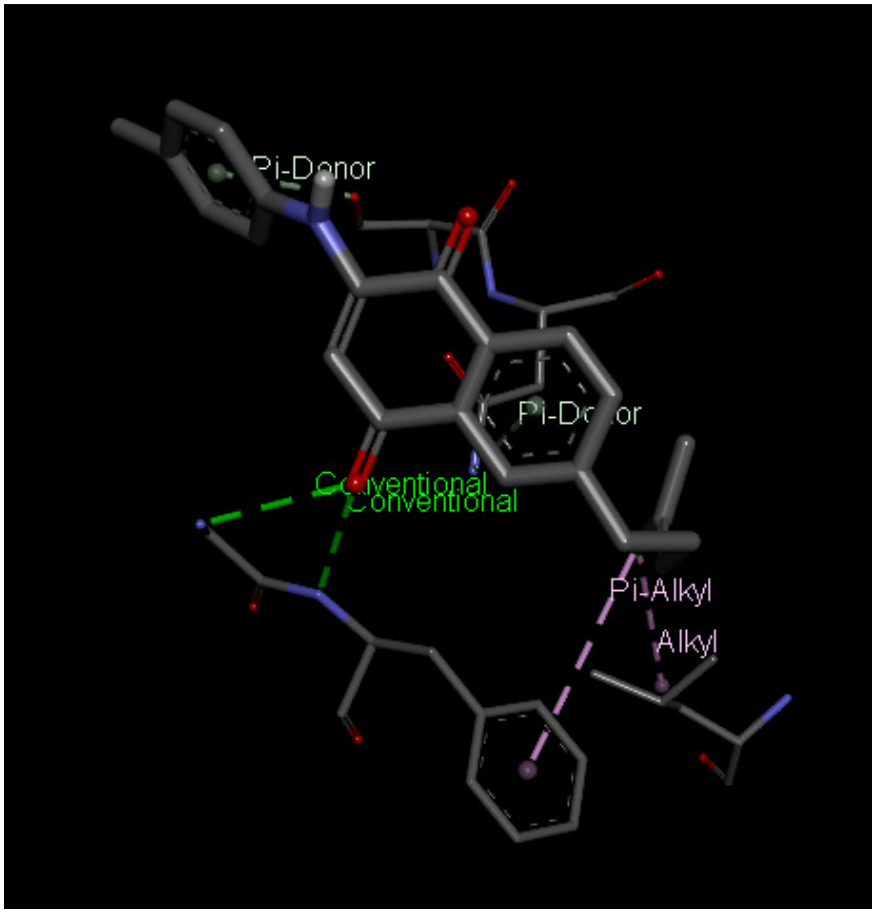

Figure S6.21: Bond-bond interactions of **4.15A** with the N-terminal ATP binding site of Hsp90

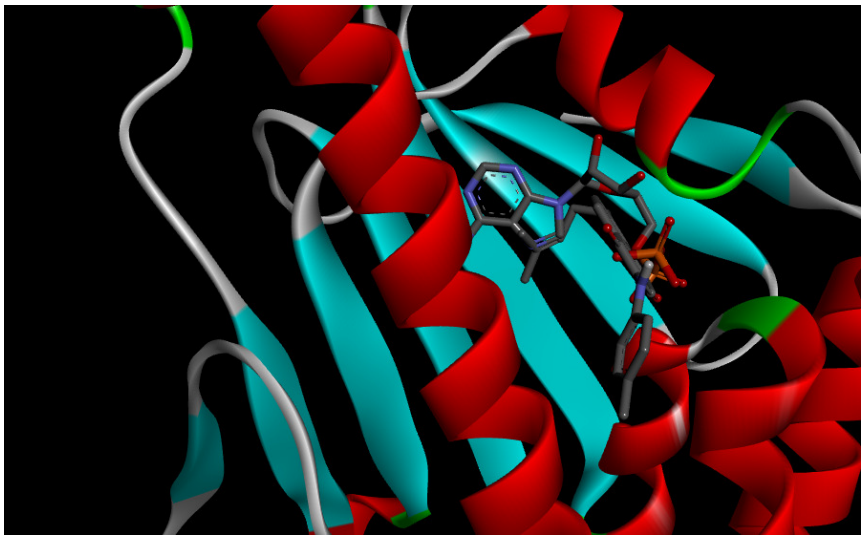

Figure S6.22: ATP and **4.15A** docked in the same active site of the N-terminal domain

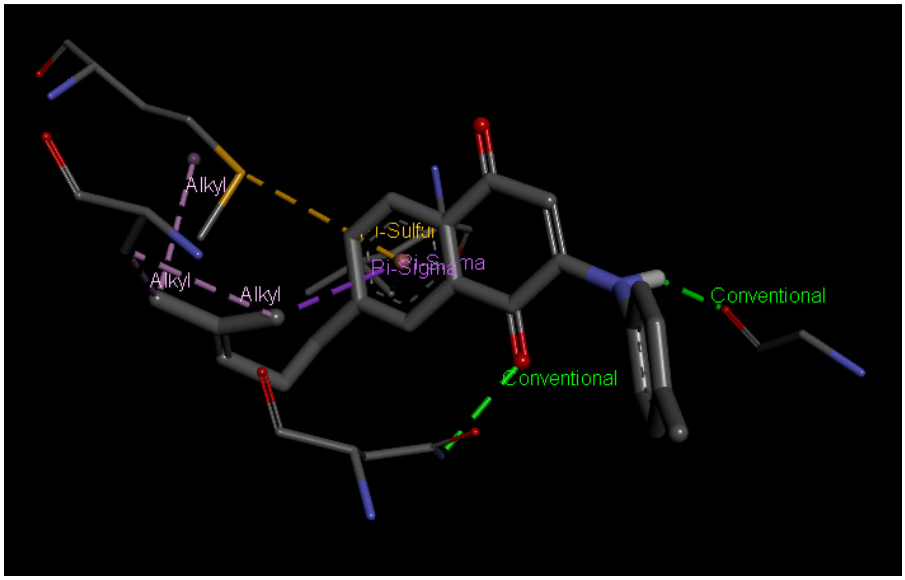

Figure S6.23: Bond-bond interactions of **4.15B** with the N-terminal ATP binding site of Hsp90

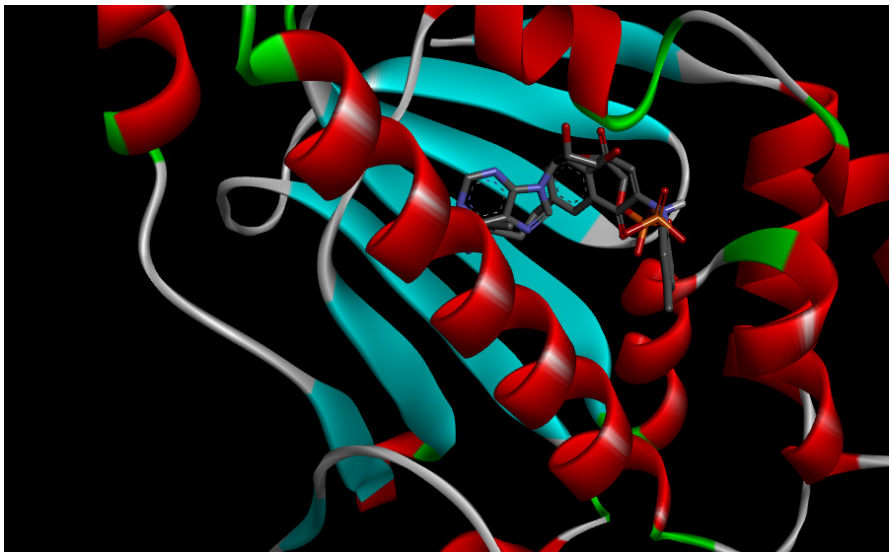

Figure S6.24: ATP and **4.15B** docked in the same active site of the N-terminal domain

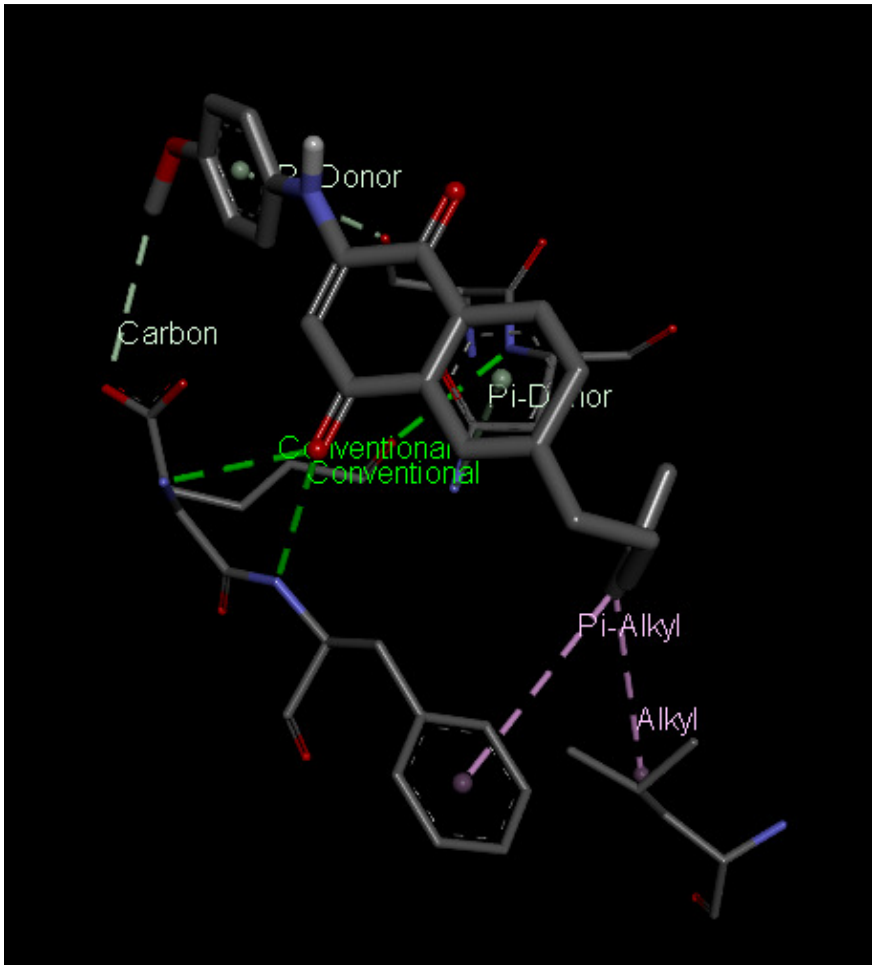

Figure S6.25: Bond-bond interactions of **4.16A** with the N-terminal ATP binding site of Hsp90

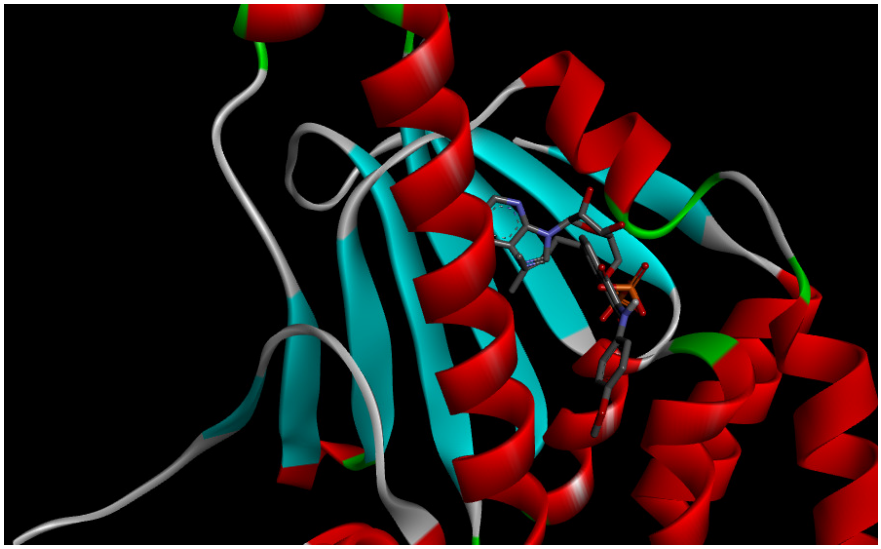

Figure S6.26: ATP and **4.16A** docked in the same active site of the N-terminal domain

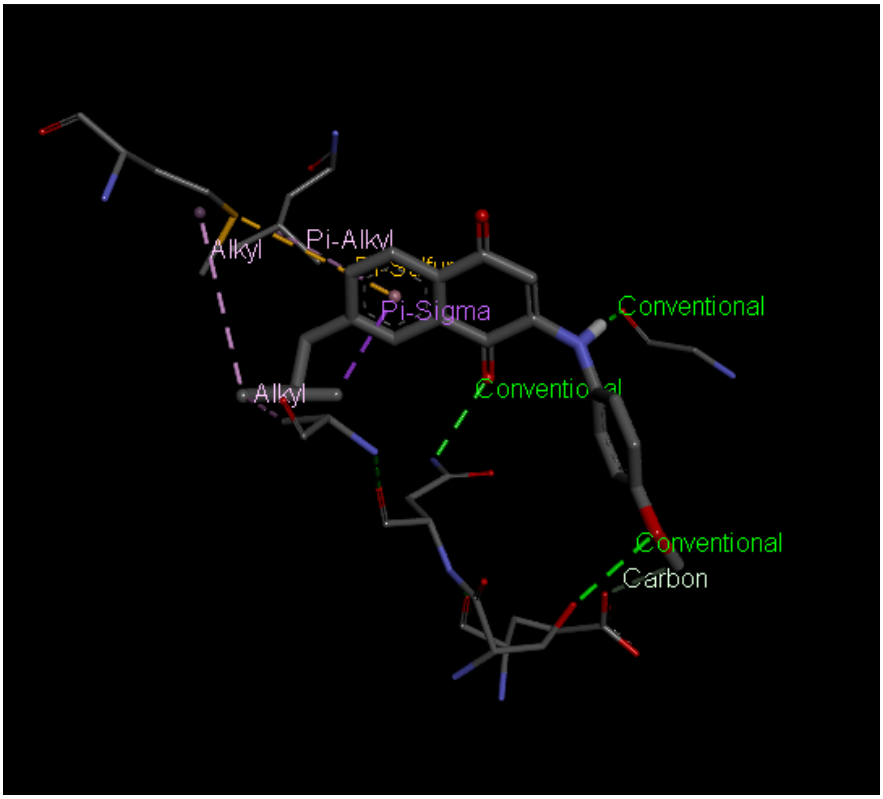

Figure S6.27: Bond-bond interactions of **4.16B** with the N-terminal ATP binding site of Hsp90

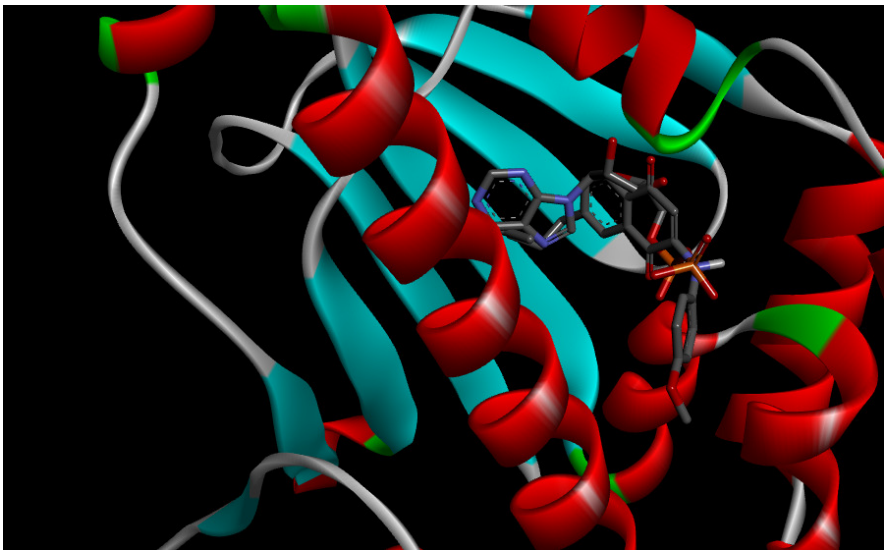

Figure S6.28: ATP and **4.16B** docked in the same active site of the N-terminal domain

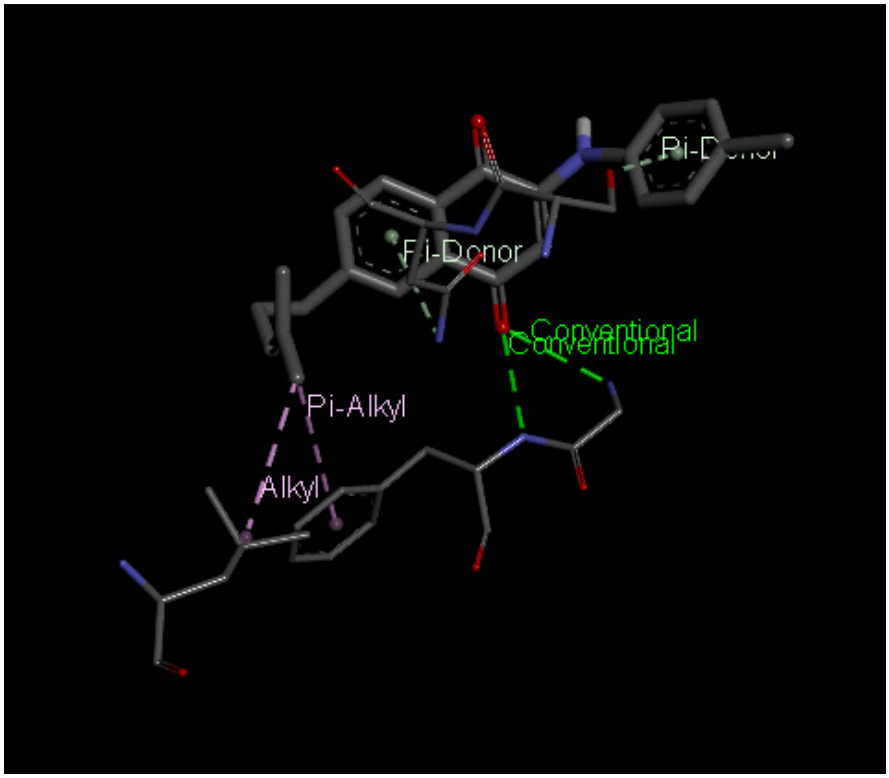

Figure S6.29: Bond-bond interactions of **4.17A** with the N-terminal ATP binding site of Hsp90

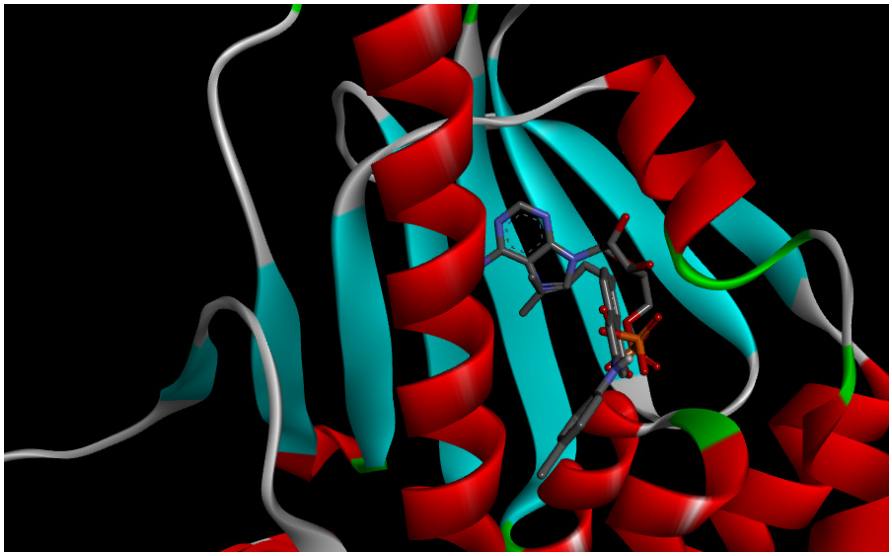

Figure S6.30: ATP and **4.17A** docked in the same active site of the N-terminal domain

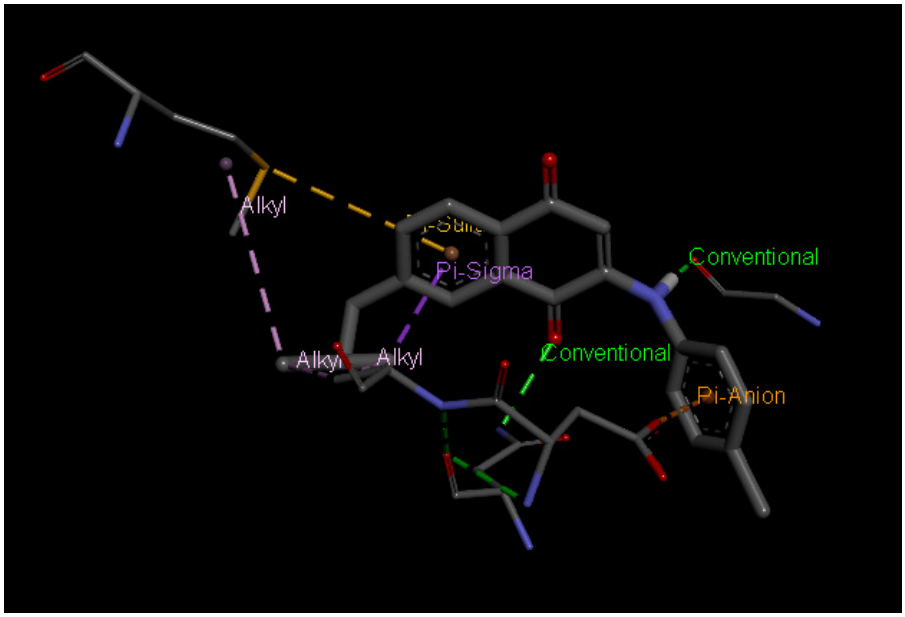

Figure S6.31: Bond-bond interactions of **4.17B** with the N-terminal ATP binding site of Hsp90

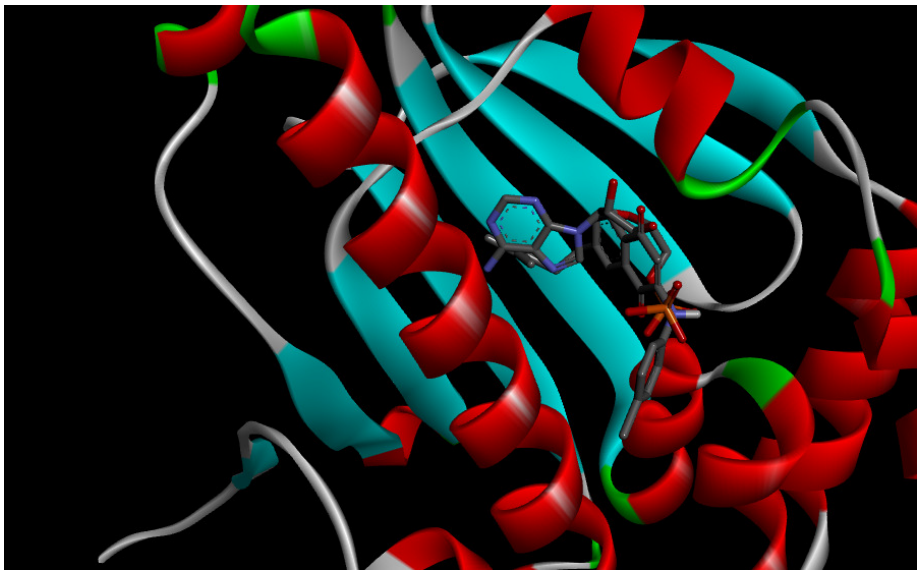

Figure S6.32: ATP and **4.17B** docked in the same active site of the N-terminal domain

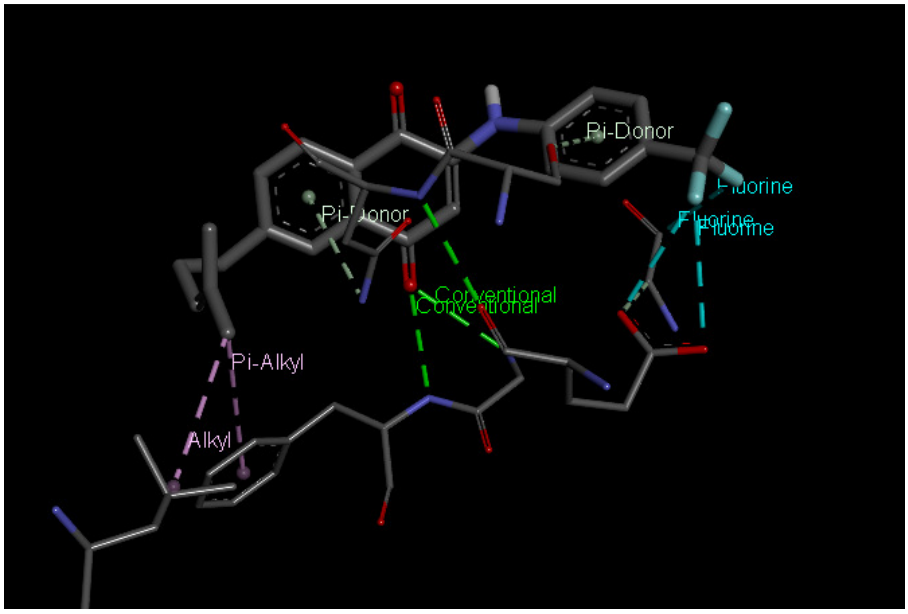

Figure S6.33: Bond-bond interactions of **4.18A** with the N-terminal ATP binding site of Hsp90

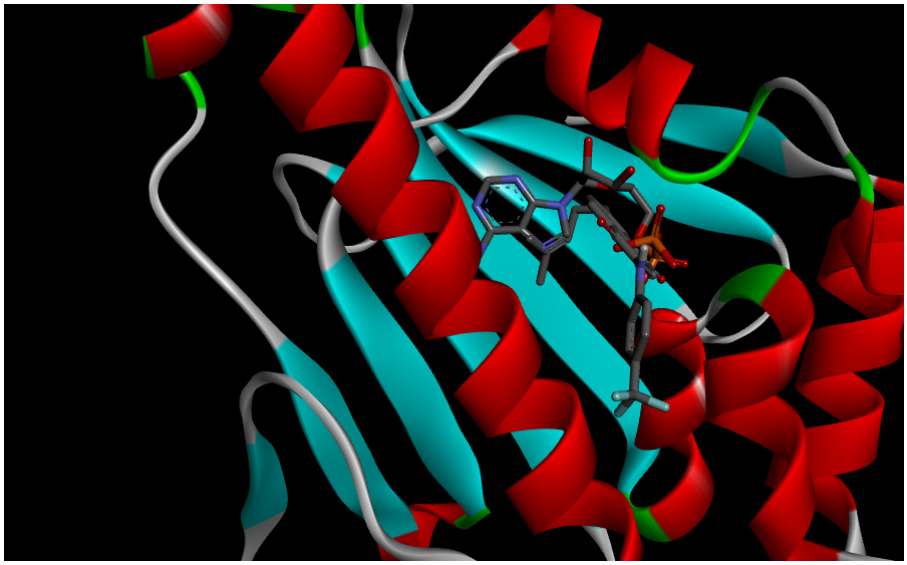

Figure S6.34: ATP and **4.18A** docked in the same active site of the N-terminal domain

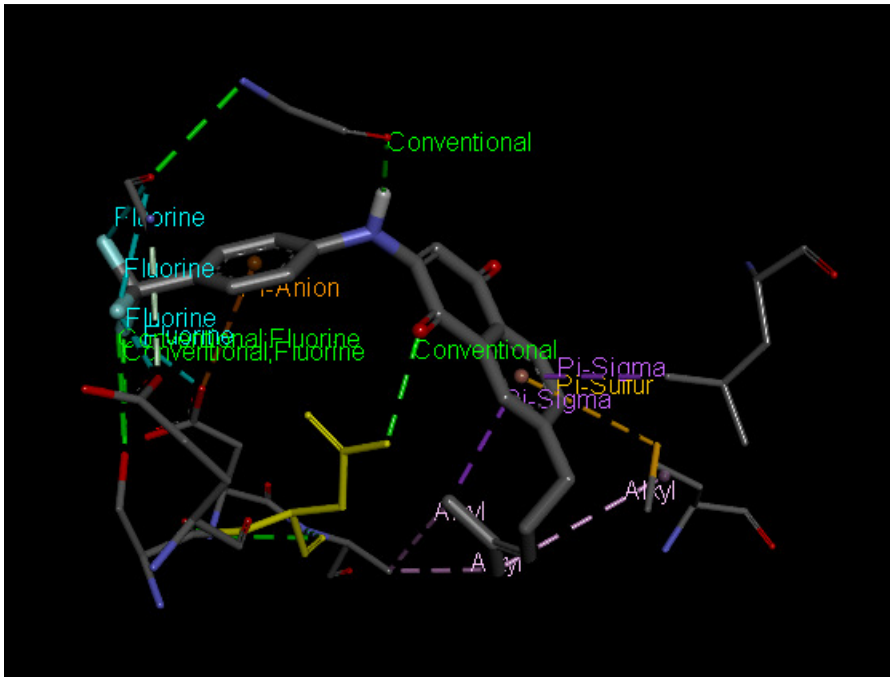

Figure S6.35: Bond-bond interactions of **4.18B** with the N-terminal ATP binding site of Hsp90

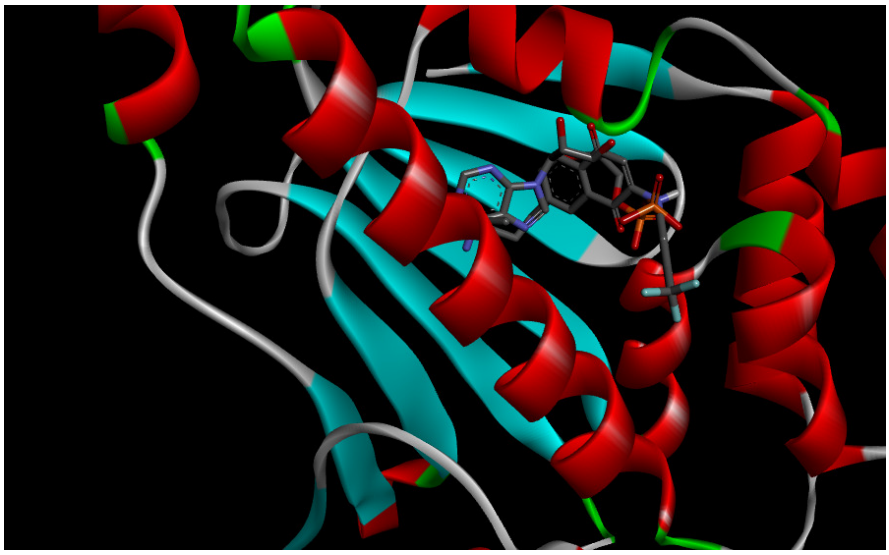

Figure S6.36: ATP and **4.18B** docked in the same active site of the N-terminal domain

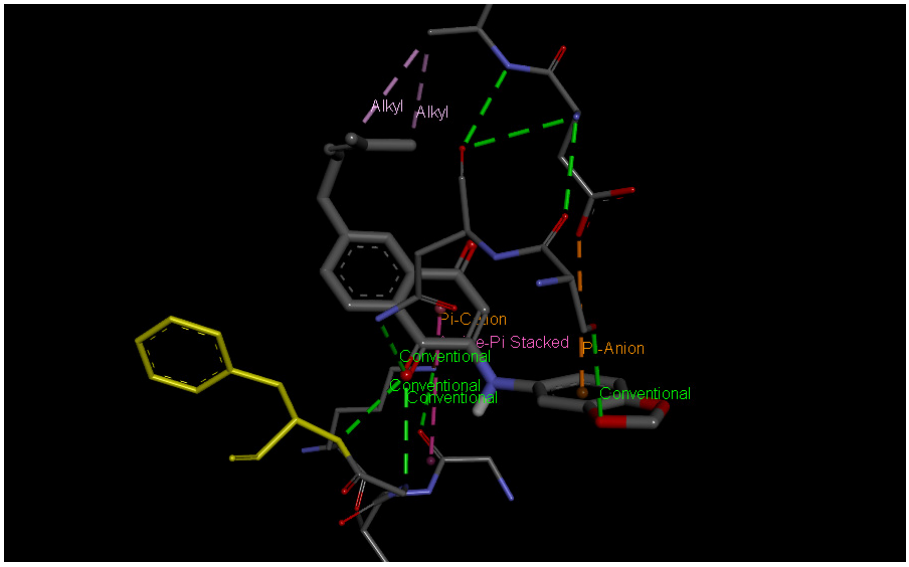

Figure S6.37: Bond-bond interactions of **4.19A** with the N-terminal ATP binding site of Hsp90

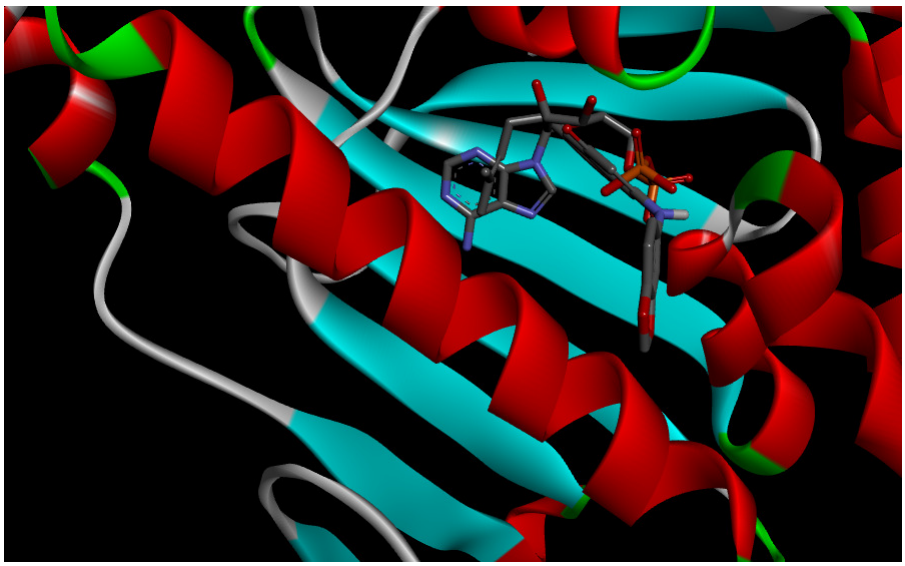

Figure S6.38: ATP and **4.19A** docked in the same active site of the N-terminal domain

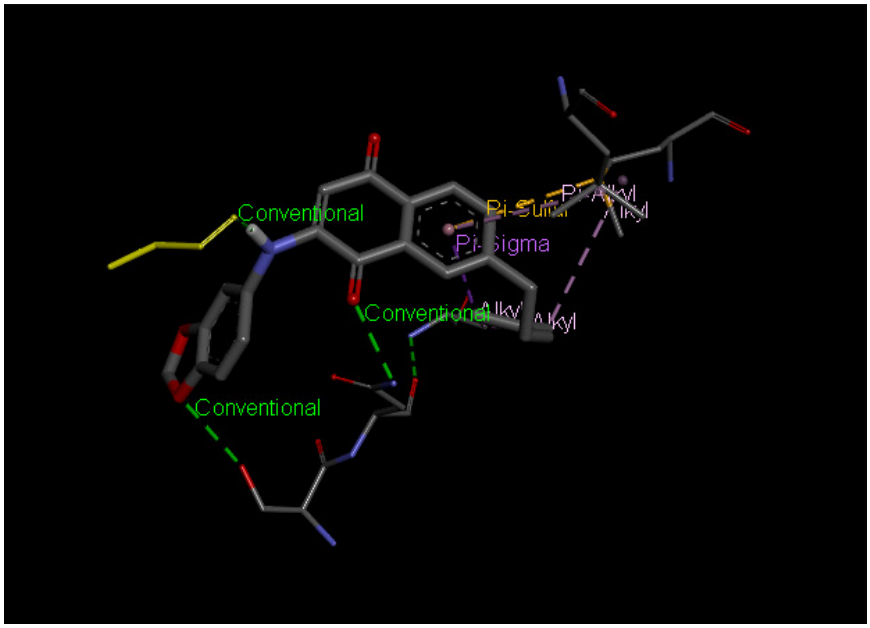

Figure S6.39: Bond-bond interactions of **4.19B** with the N-terminal ATP binding site of Hsp90

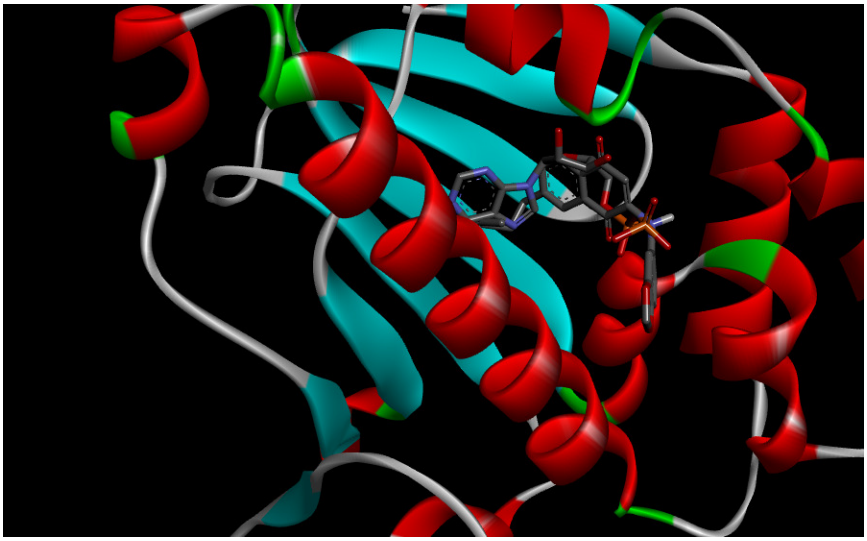

Figure S6.40: ATP and **4.19B** docked in the same active site of the N-terminal domain

Third series of naphthoquinone analogues

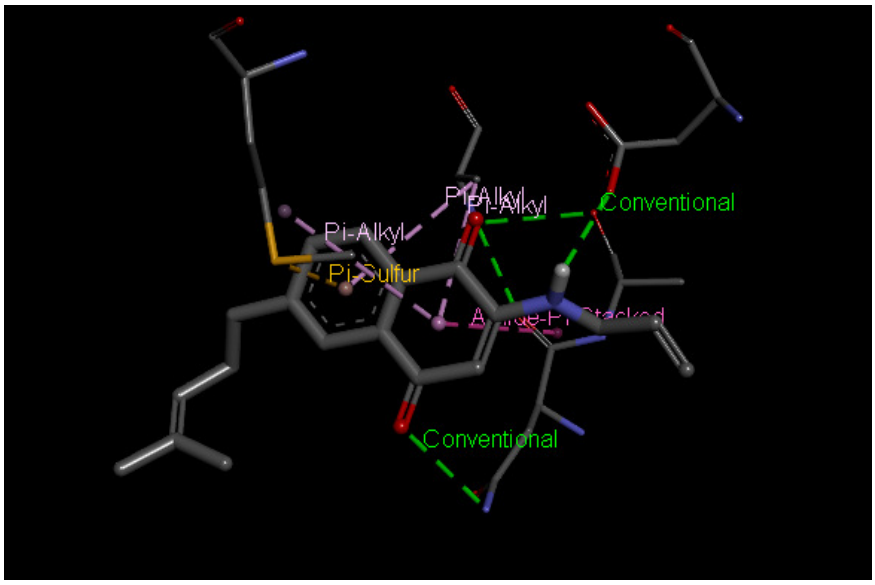

Figure S6.41: Bond-bond interactions of **4.20A** with the N-terminal ATP binding site of Hsp90

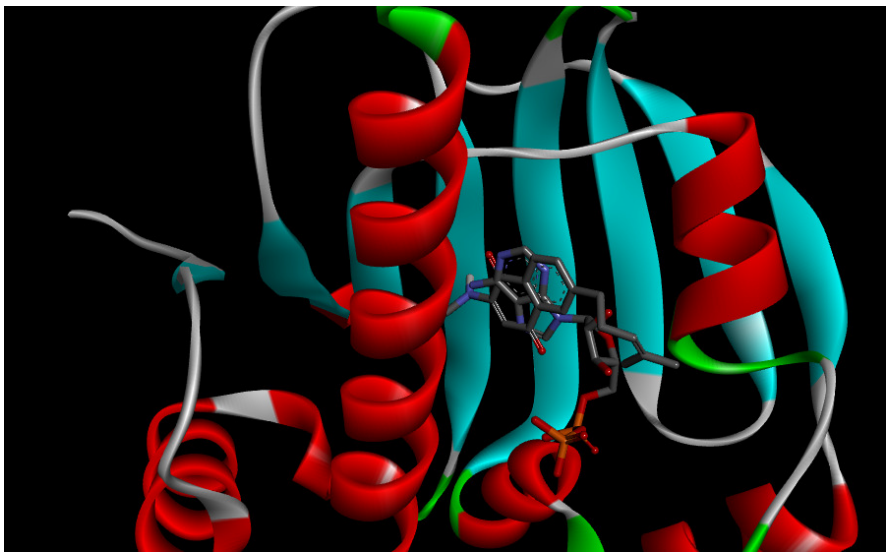

Figure S6.42: ATP and **4.20A** docked in the same active site of the N-terminal domain

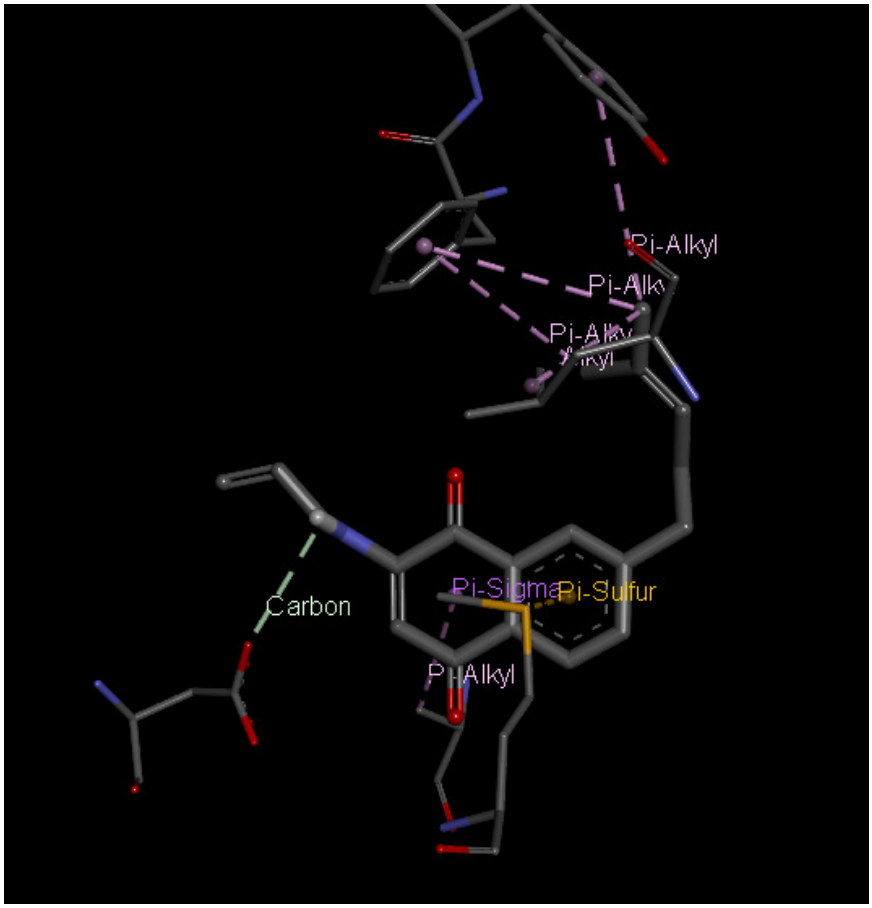

Figure S6.43: Bond-bond interactions of **4.20B** with the N-terminal ATP binding site of Hsp90

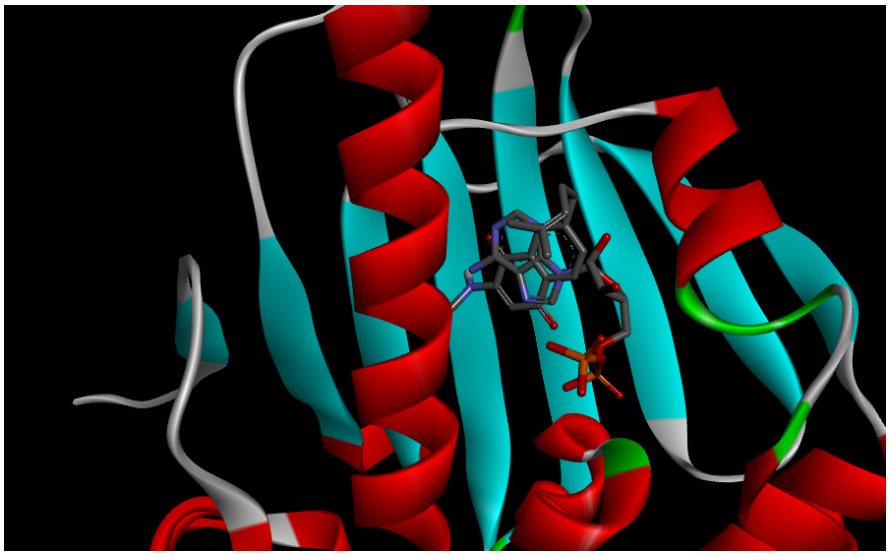

Figure S6.44: ATP and **4.20B** docked in the same active site of the N-terminal domain

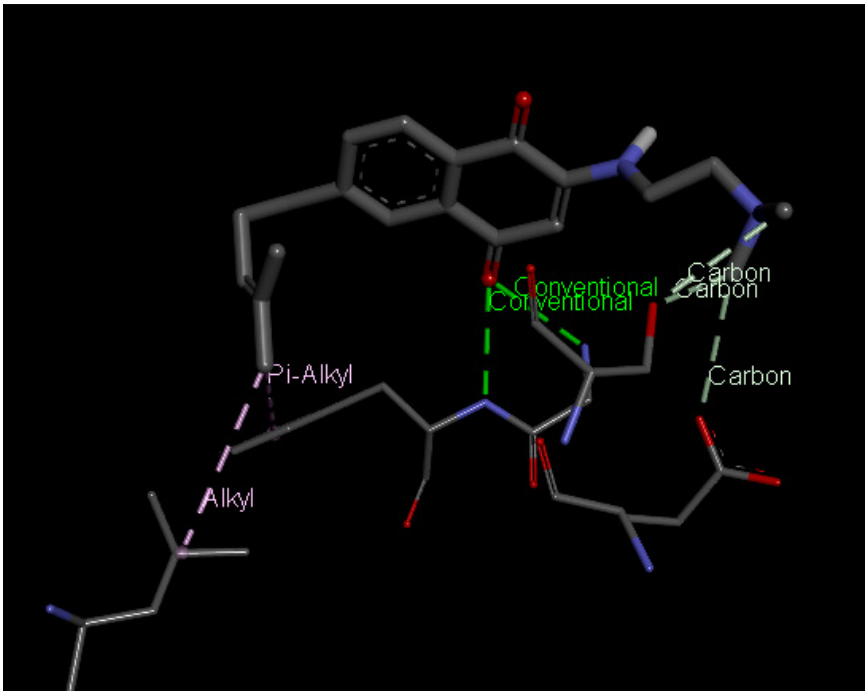

Figure S6.45: Bond-bond interactions of **4.21A** with the N-terminal ATP binding site of Hsp90

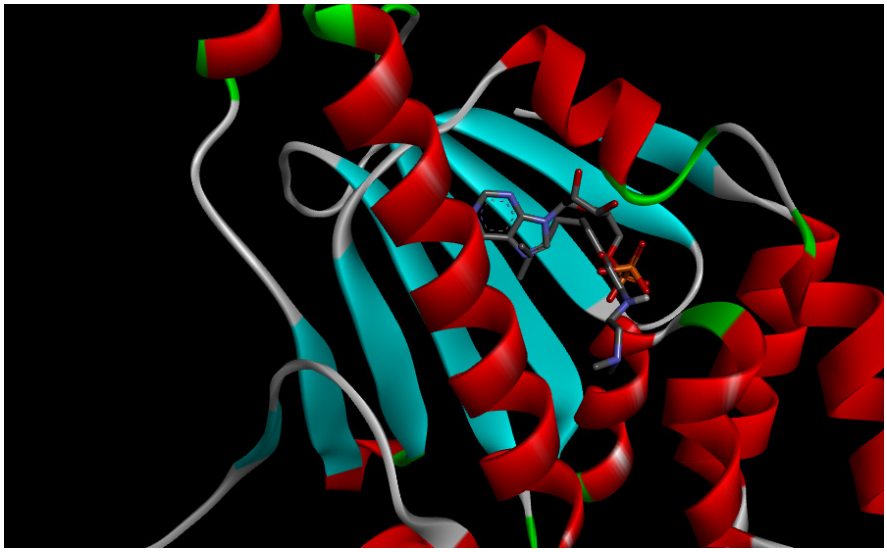

Figure S6.46: ATP and **4.21A** docked in the same active site of the N-terminal domain

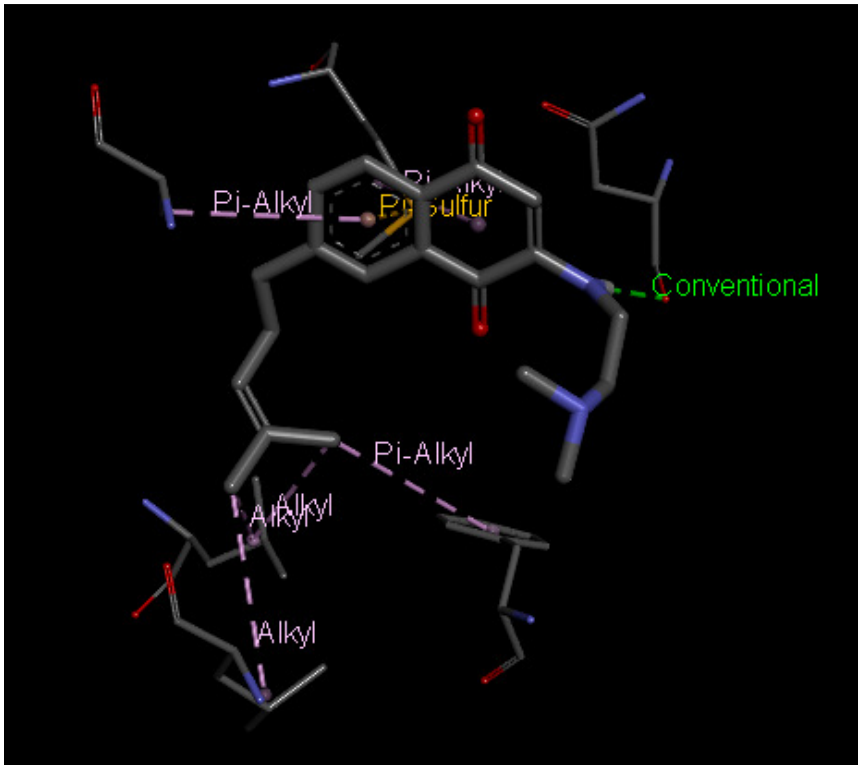

Figure S6.47: Bond-bond interactions of **4.21B** with the N-terminal ATP binding site of Hsp90

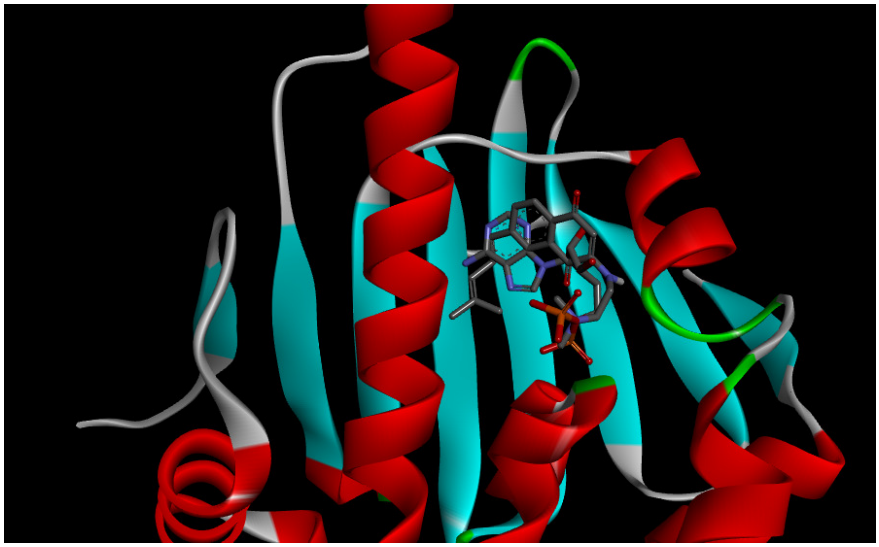

Figure S6.48: ATP and **4.21B** docked in the same active site of the N-terminal domain

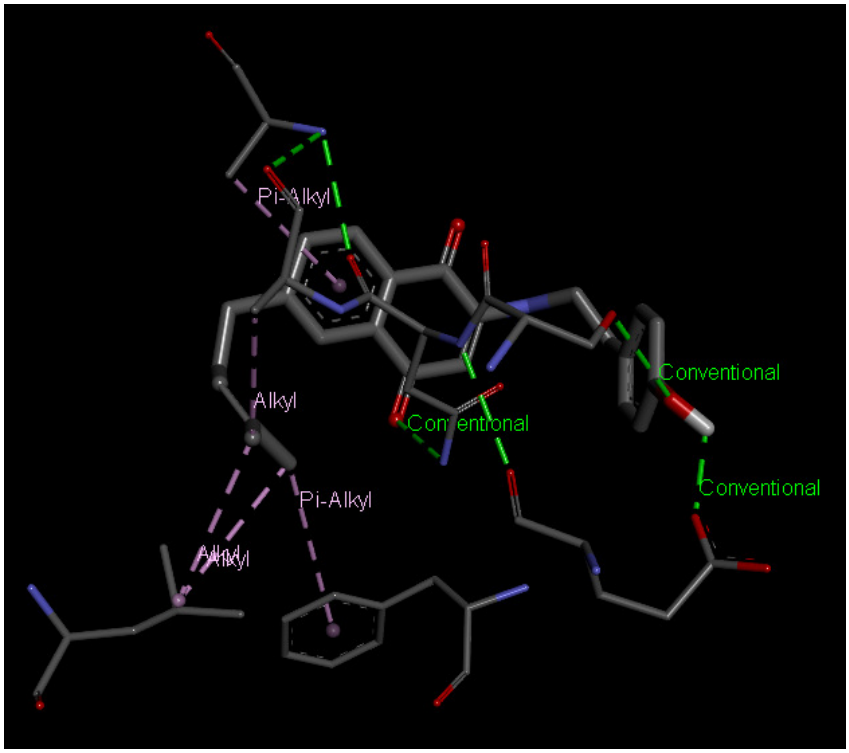

Figure S6.49: Bond-bond interactions of **4.22A** with the N-terminal ATP binding site of Hsp90

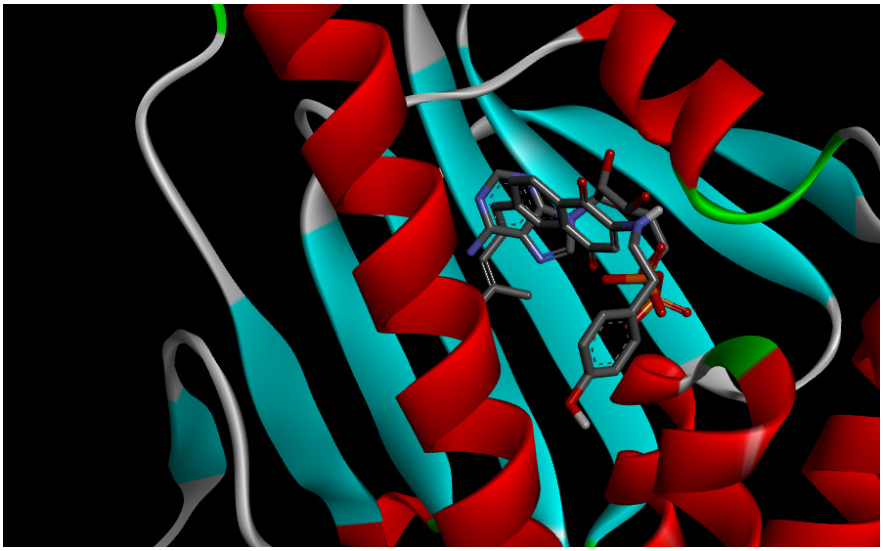

Figure S6.50: ATP and **4.22A** docked in the same active site of the N-terminal domain

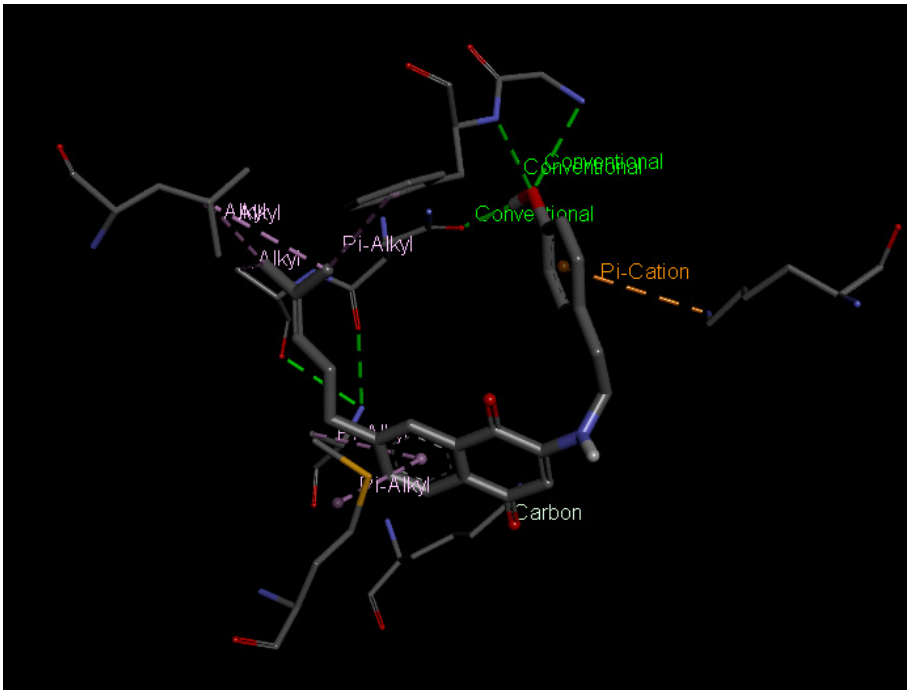

Figure S6.51: Bond-bond interactions of **4.22B** with the N-terminal ATP binding site of Hsp90

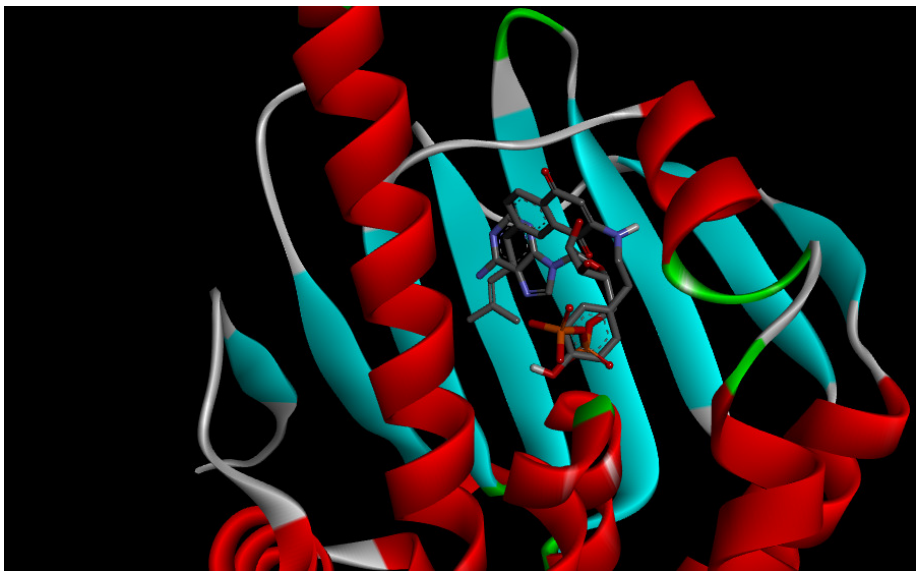

Figure S6.52: ATP and **4.22B** docked in the same active site of the N-terminal domain

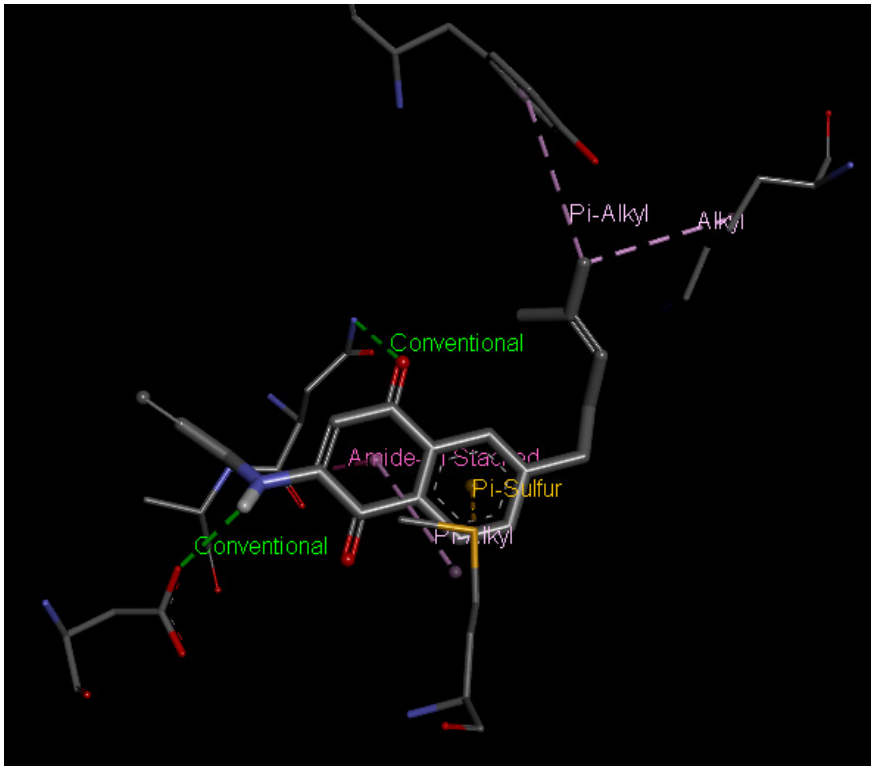

Figure S6.53: Bond-bond interactions of **4.23A** with the N-terminal ATP binding site of Hsp90

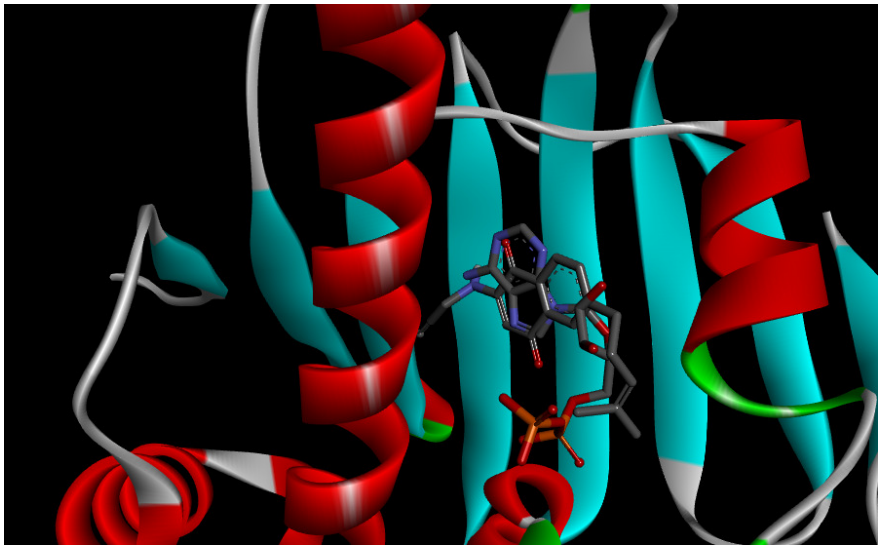

Figure S6.54: ATP and **4.23A** docked in the same active site of the N-terminal domain

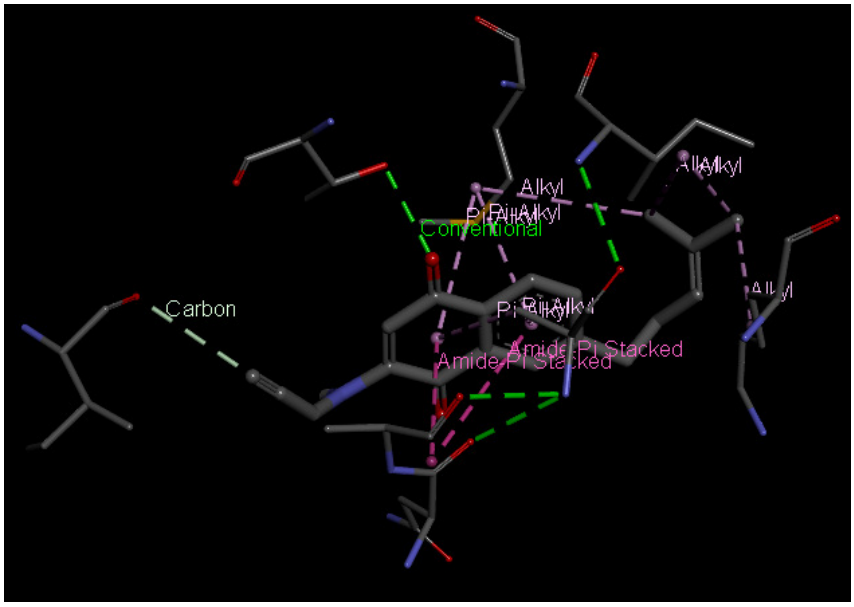

Figure S6.55: Bond-bond interactions of **4.23B** with the N-terminal ATP binding site of Hsp90

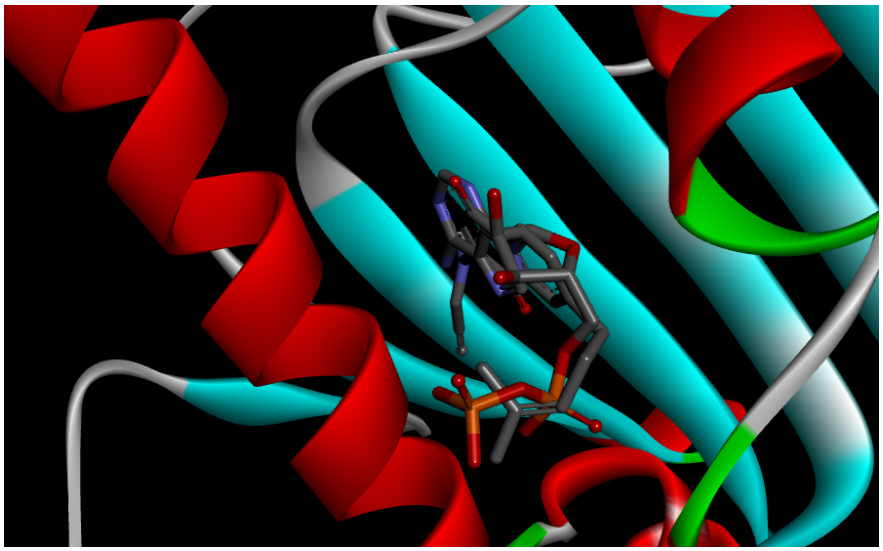

Figure S6.56: ATP and **4.23B** docked in the same active site of the N-terminal domain

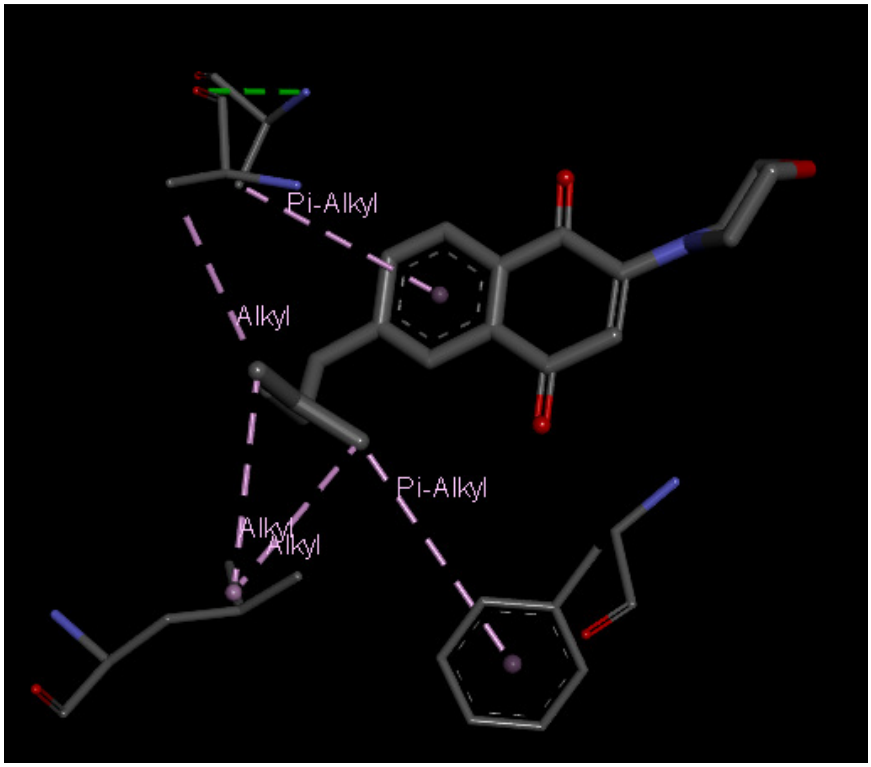

Figure S6.57: Bond-bond interactions of **4.24A** with the N-terminal ATP binding site of Hsp90

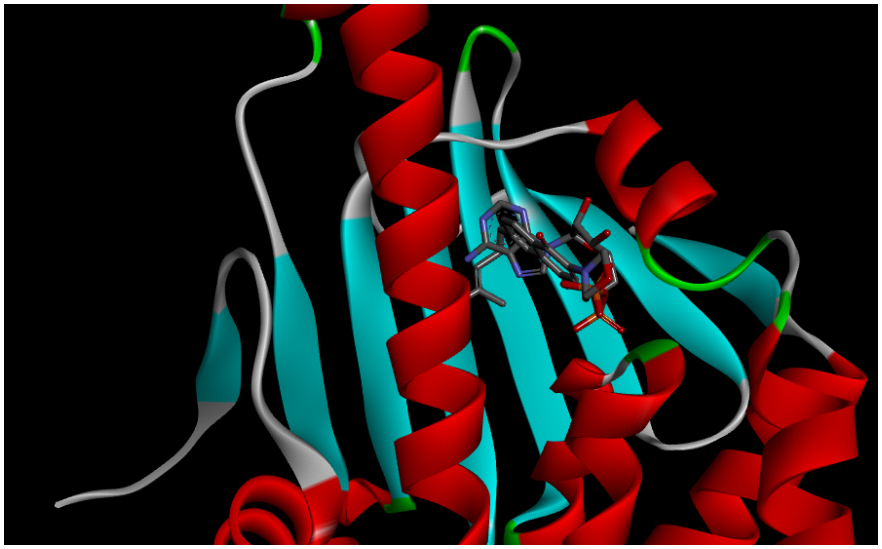

Figure S6.58: ATP and **4.24A** docked in the same active site of the N-terminal domain

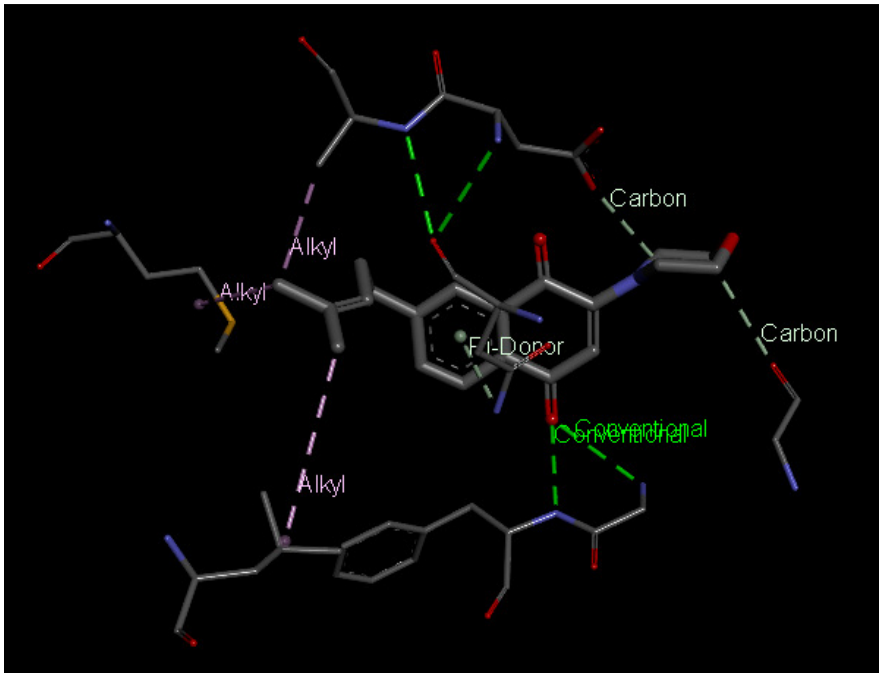

Figure S6.59: Bond-bond interactions of **4.24B** with the N-terminal ATP binding site of Hsp90

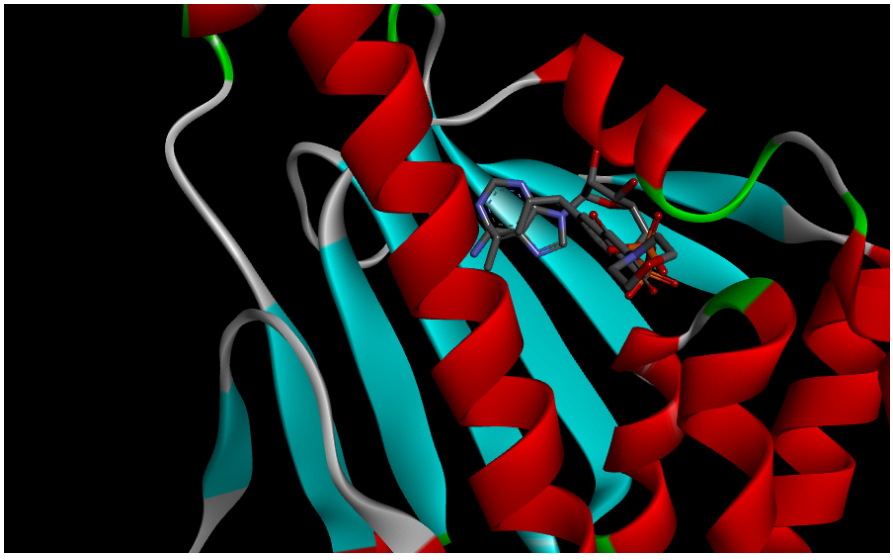

Figure S6.60: ATP and **4.24B** docked in the same active site of the N-terminal domain

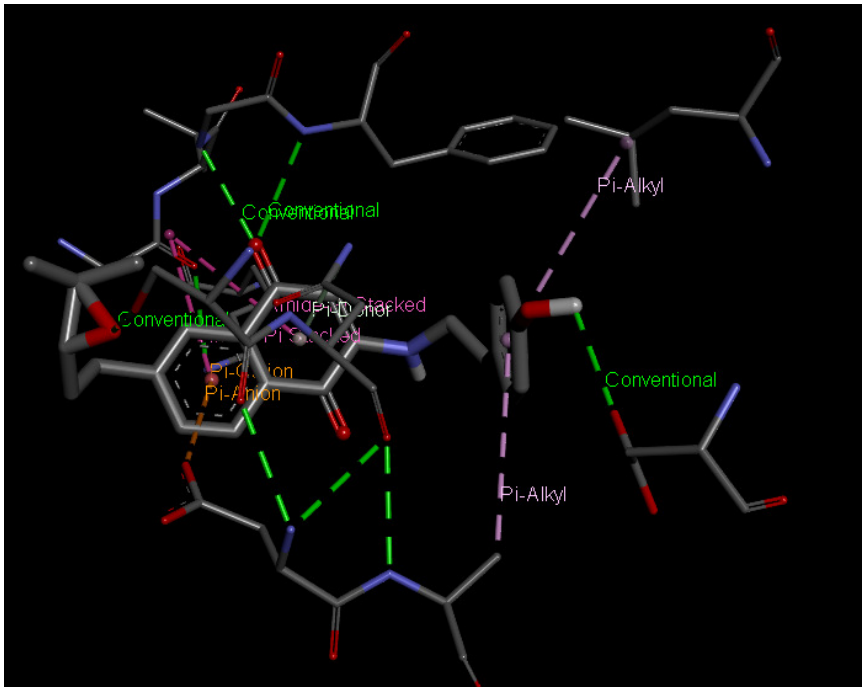

Figure S6.61: Bond-bond interactions of **4.25A** with the N-terminal ATP binding site of Hsp90

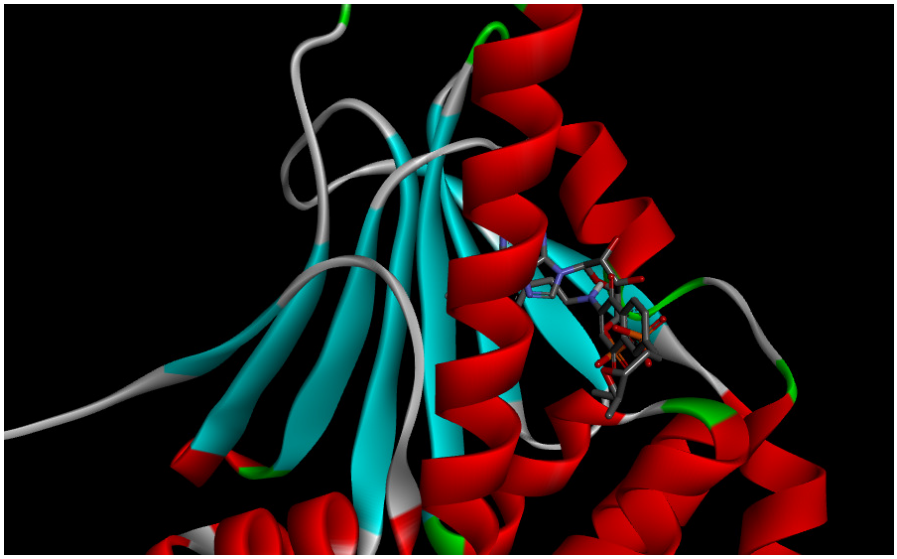

Figure S6.62: ATP and **4.25A** docked in the same active site of the N-terminal domain

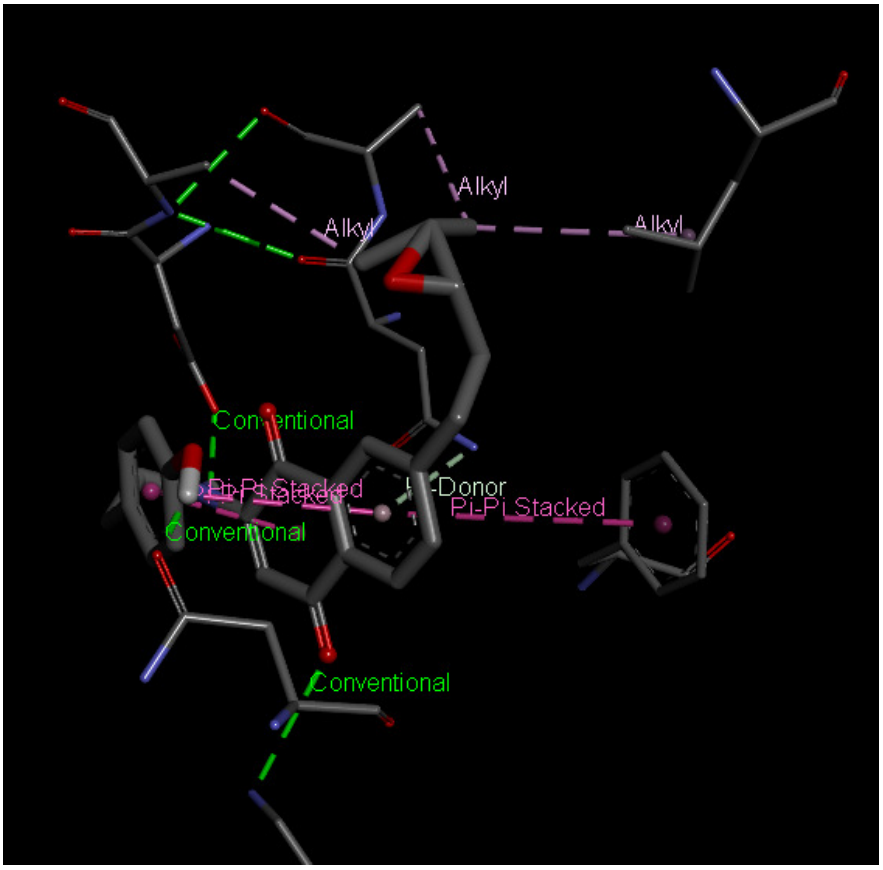

Figure S6.63: Bond-bond interactions of **4.25B** with the N-terminal ATP binding site of Hsp90

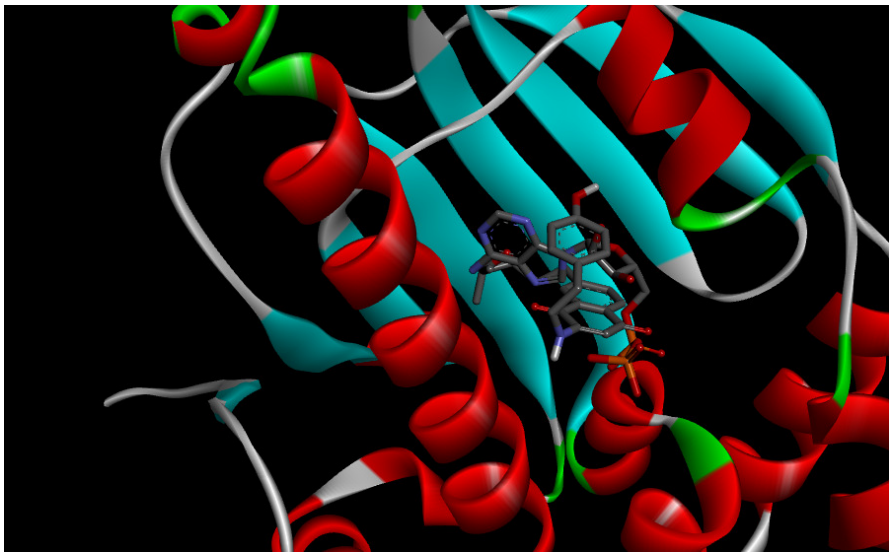

Figure S6.64: ATP and **4.25B** docked in the same active site of the N-terminal domain

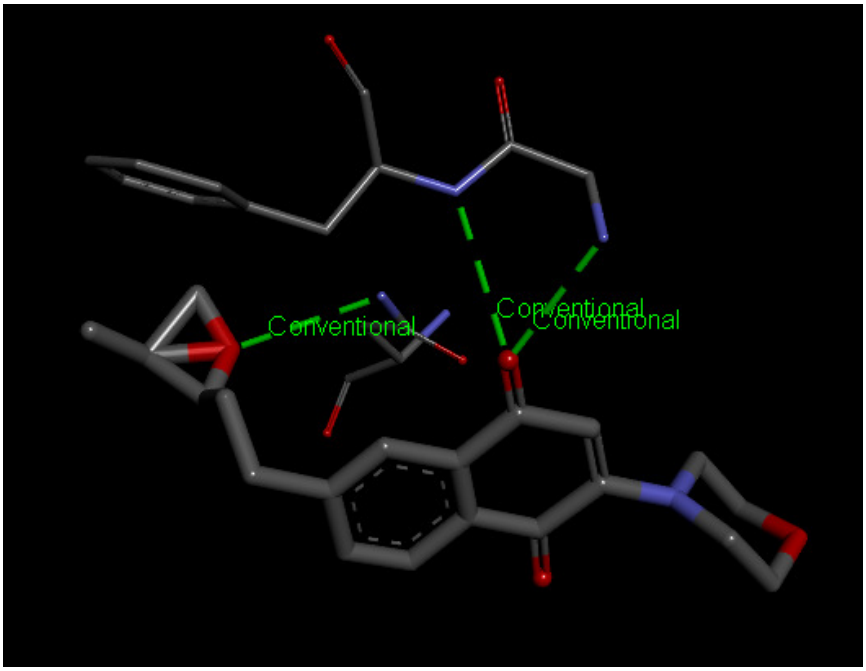

Figure S6.65: Bond-bond interactions of **4.26A** with the N-terminal ATP binding site of Hsp90

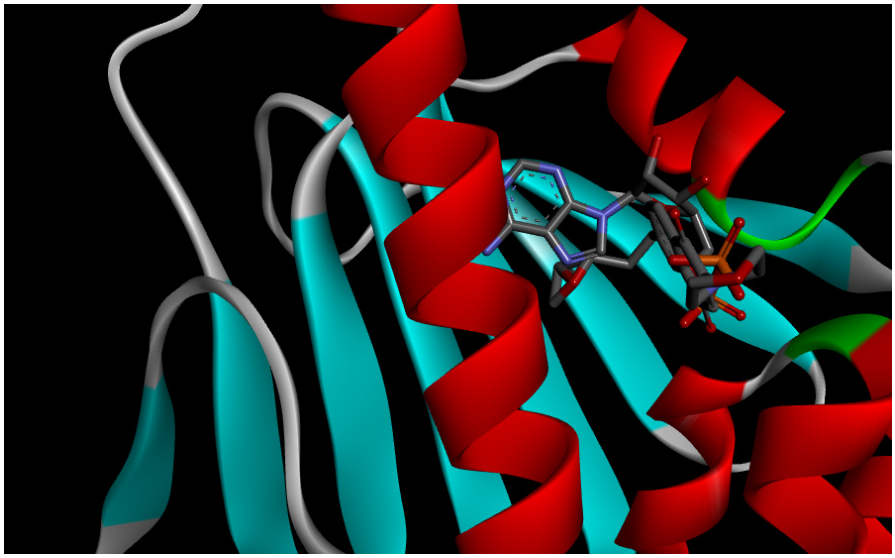

Figure S6.66: ATP and **4.26A** docked in the same active site of the N-terminal domain

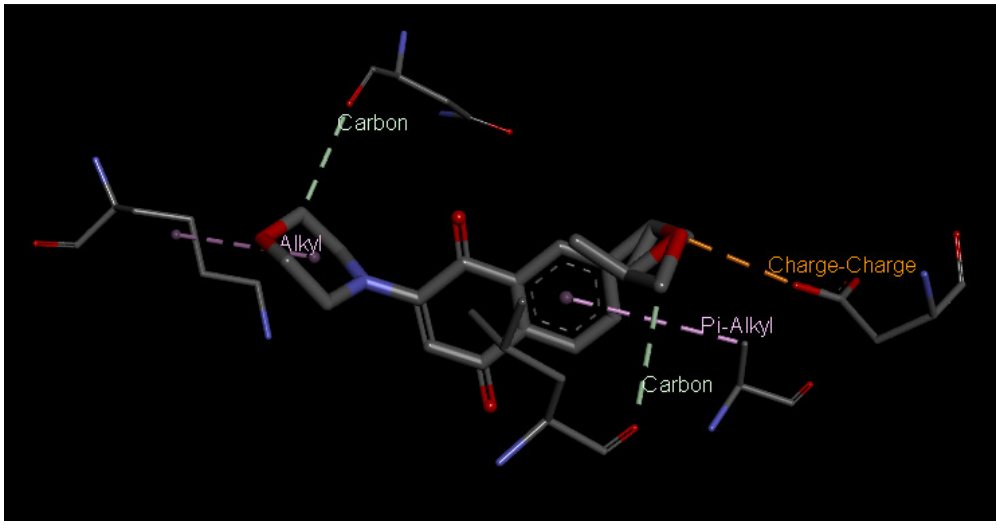

Figure S6.67: Bond-bond interactions of **4.26B** with the N-terminal ATP binding site of Hsp90

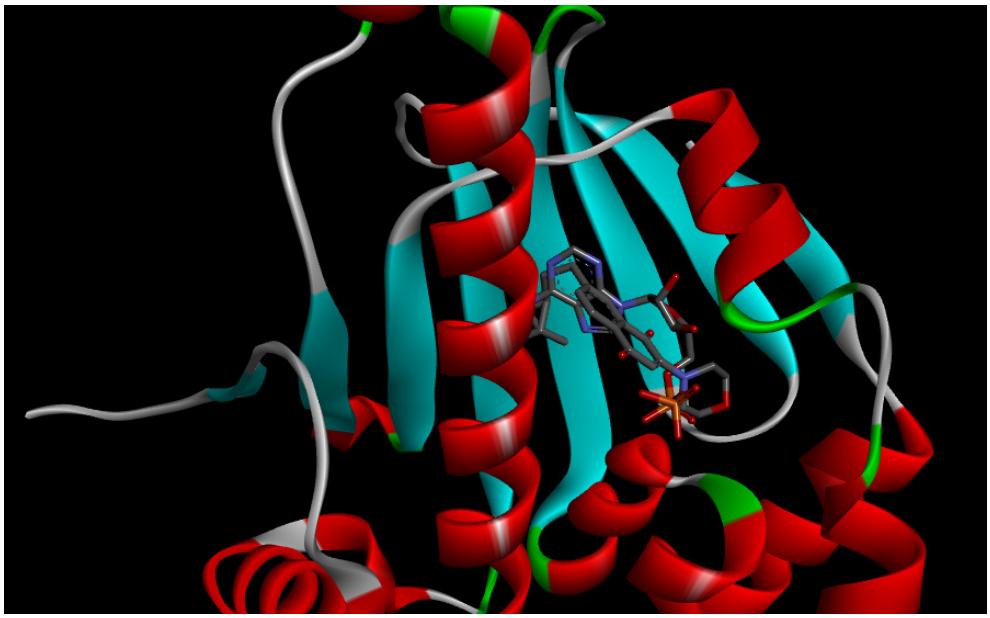

Figure S6.68: ATP and **4.26B** docked in the same active site of the N-terminal domain

Fourth series of naphthoquinone analogues

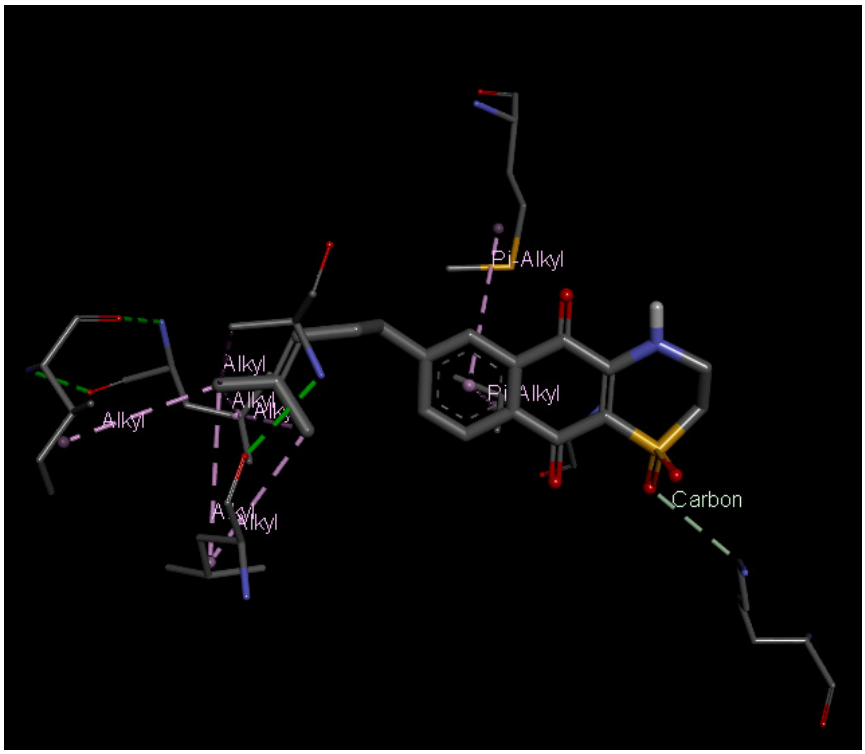

Figure S6.69: Bond-bond interactions of **4.28** with the N-terminal ATP binding site of Hsp90

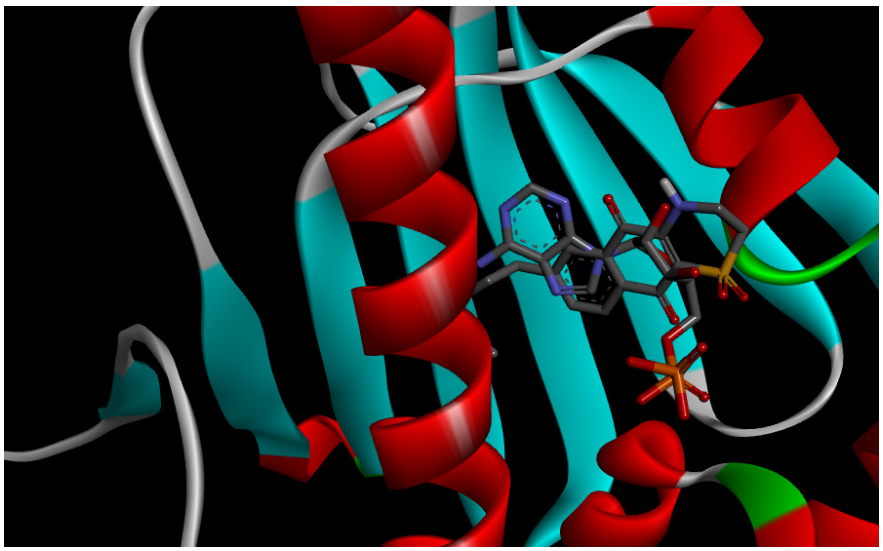

Figure S6.70: ATP and **4.28** docked in the same active site of the N-terminal domain

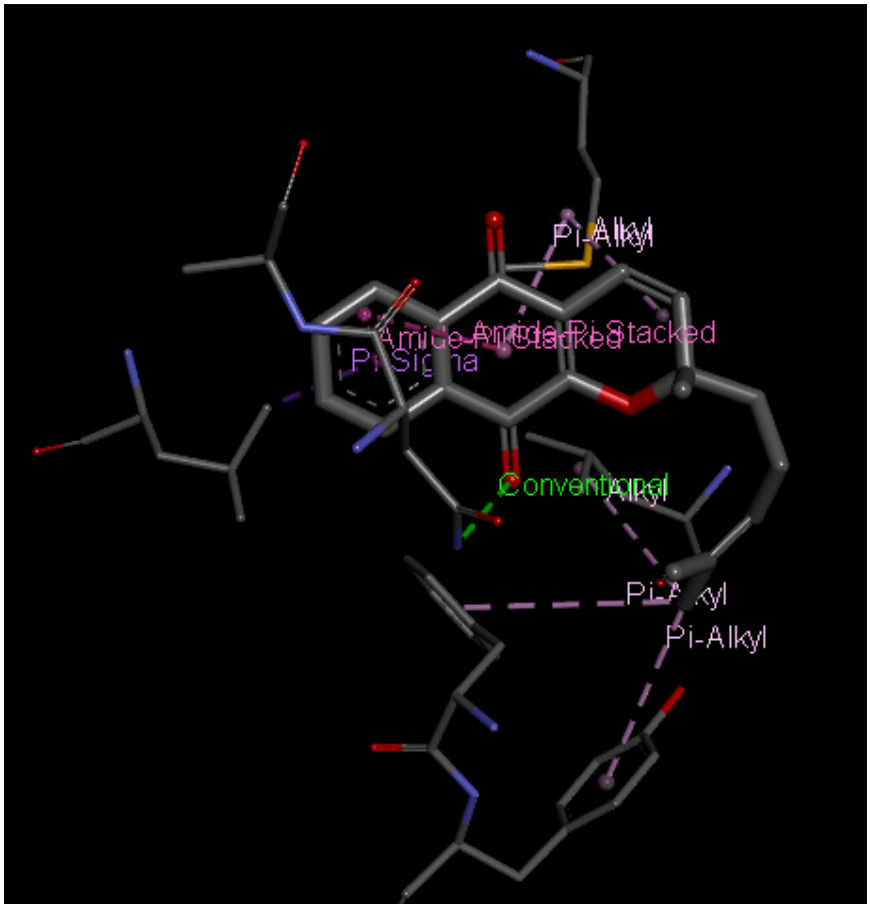

Figure S6.71: Bond-bond interactions of **4.29** with the N-terminal ATP binding site of Hsp90

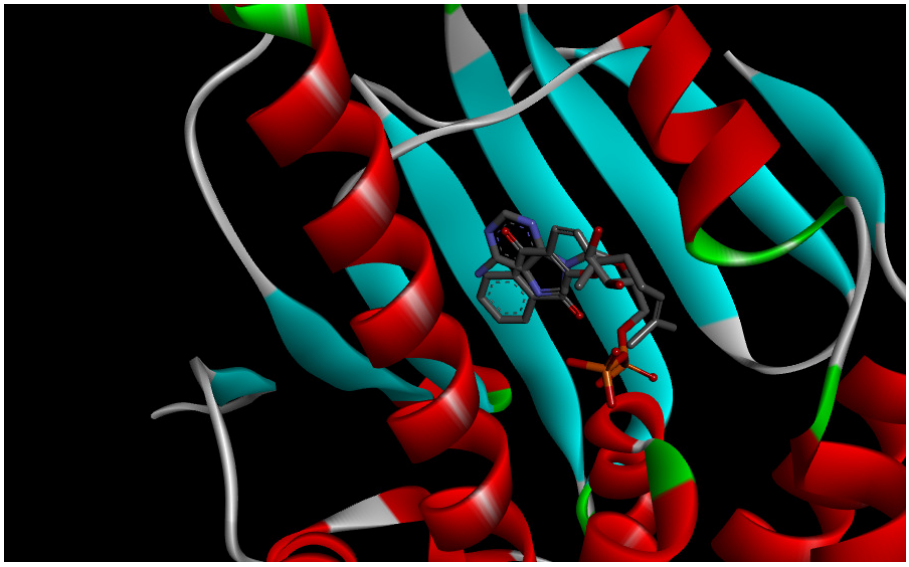

Figure S6.72: ATP and **4.29** docked in the same active site of the N-terminal domain

Natural Products

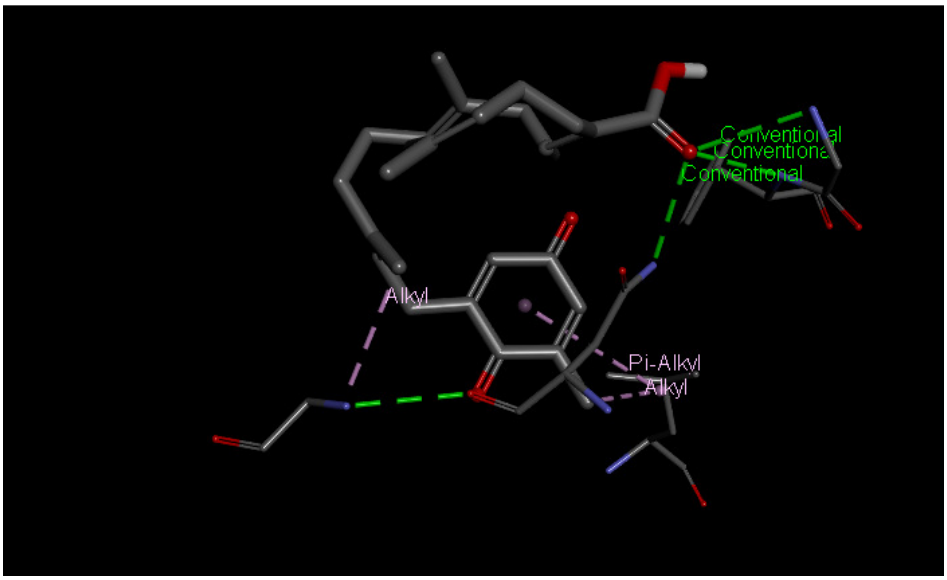

Figure S6.73: Bond-bond interactions of **2.47** with the N-terminal ATP binding site of Hsp90

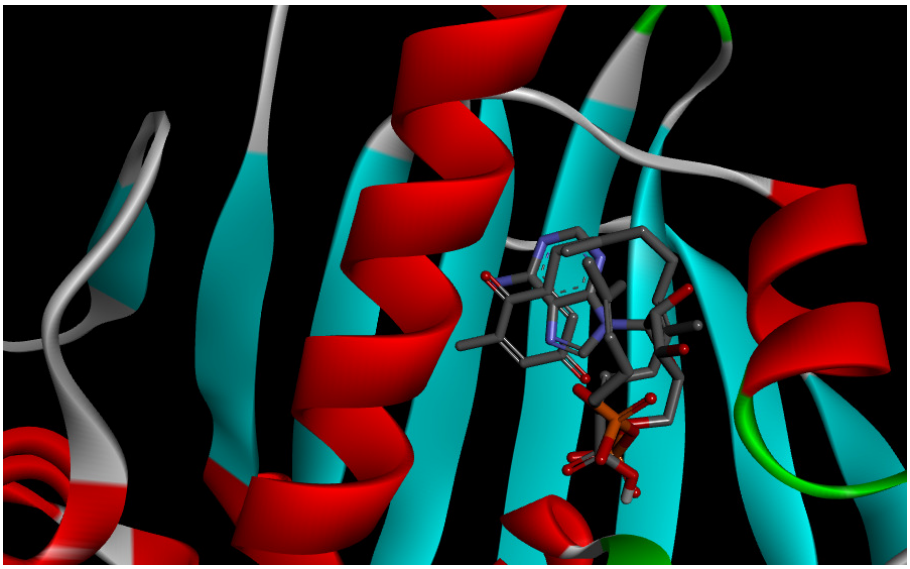

Figure S6.74: ATP and **2.47** docked in the same active site of the N-terminal domain

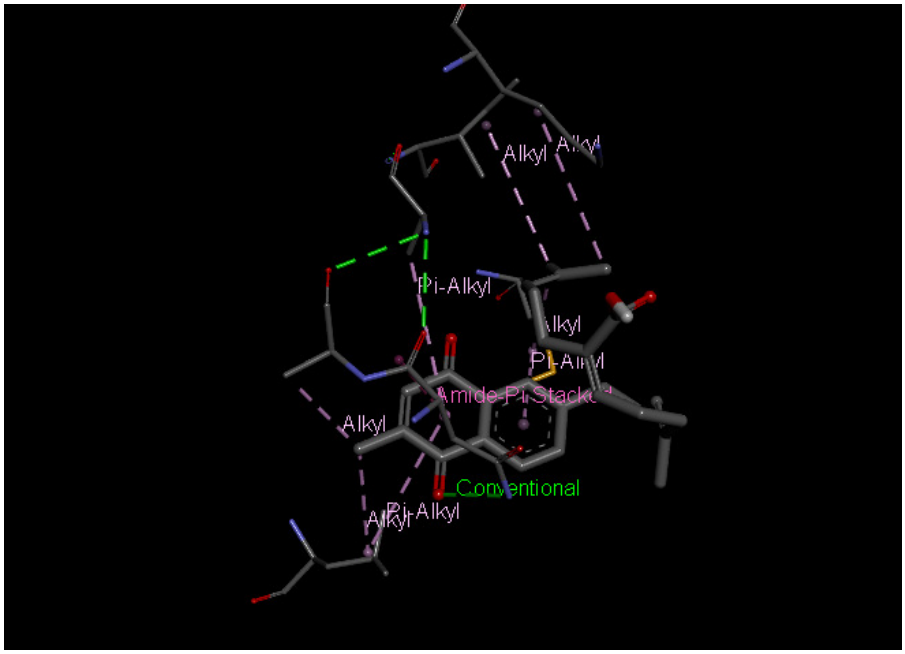

Figure S6.75: Bond-bond interactions of **3.11** with the N-terminal ATP binding site of Hsp90

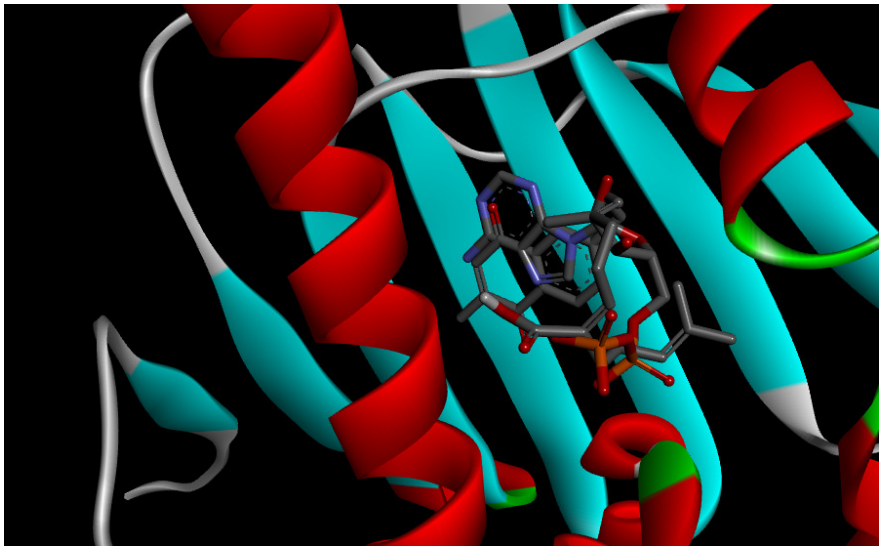

Figure S6.76: ATP and **3.11** docked in the same active site of the N-terminal domain

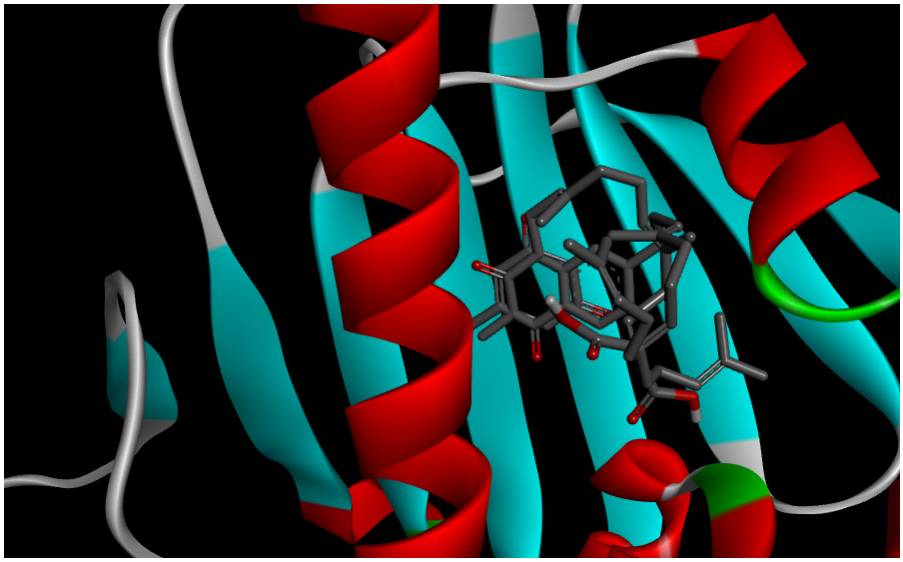

Figure S6.77: **2.47** and **3.11** docked in the same N-terminal domain of Hsp90

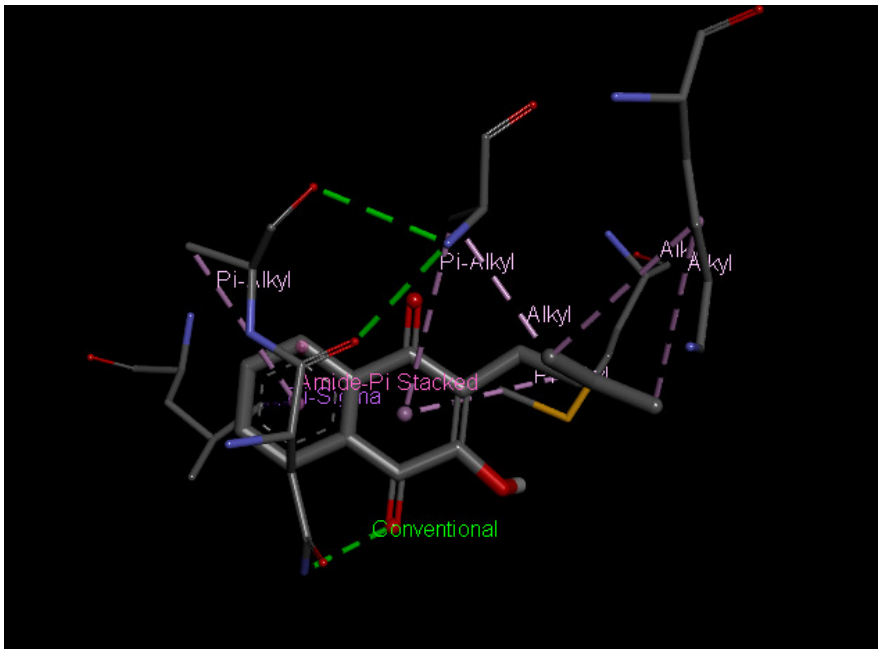

Figure S6.78: Bond-bond interactions of **3.5** with the N-terminal ATP binding site of Hsp90

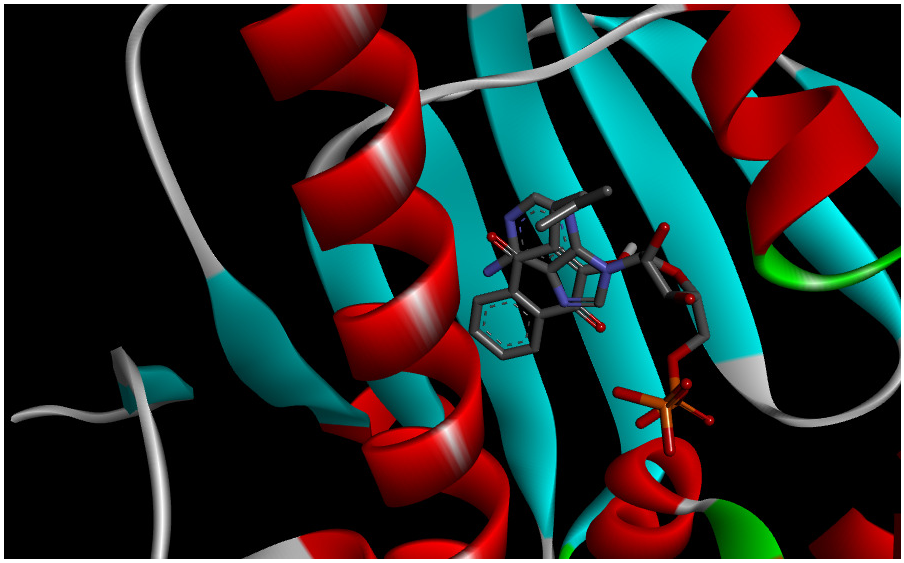

Figure S6.79: ATP and **3.5** docked in the same active site of the N-terminal domain

Saturation Transfer Difference NMR spectra

STD NMR spectra for the C-terminal experiments

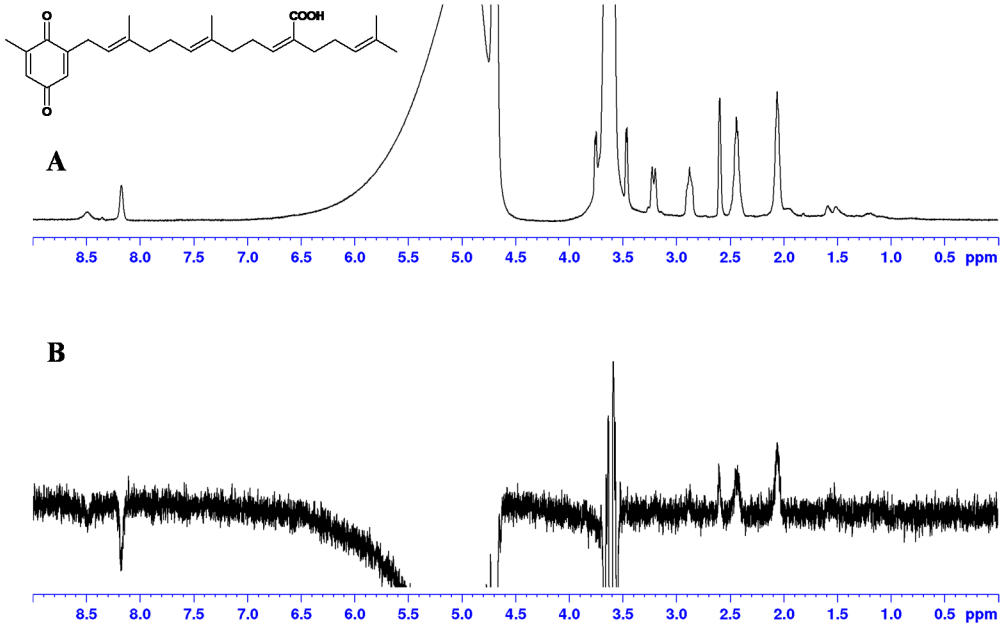

Figure S6.80: (**A**) reference ^{1}H spectrum of the C-terminal domain of Hsp90 and **2.47** (**B**) corresponding STD-NMR spectrum

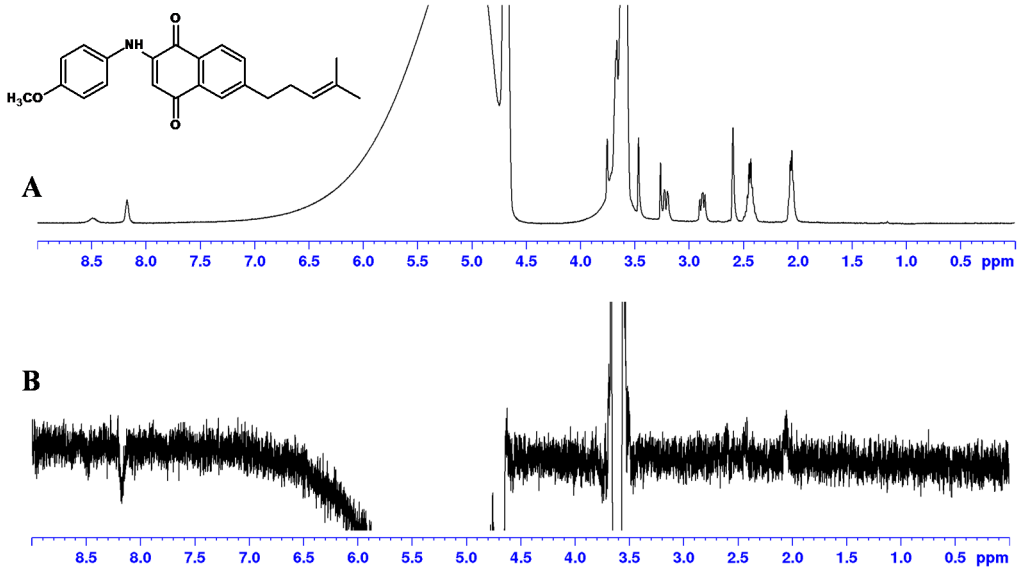

Figure S6.81: (**A**) reference ^{1}H spectrum of the C-terminal domain of Hsp90 and **4.16A** (**B**) corresponding STD-NMR spectrum

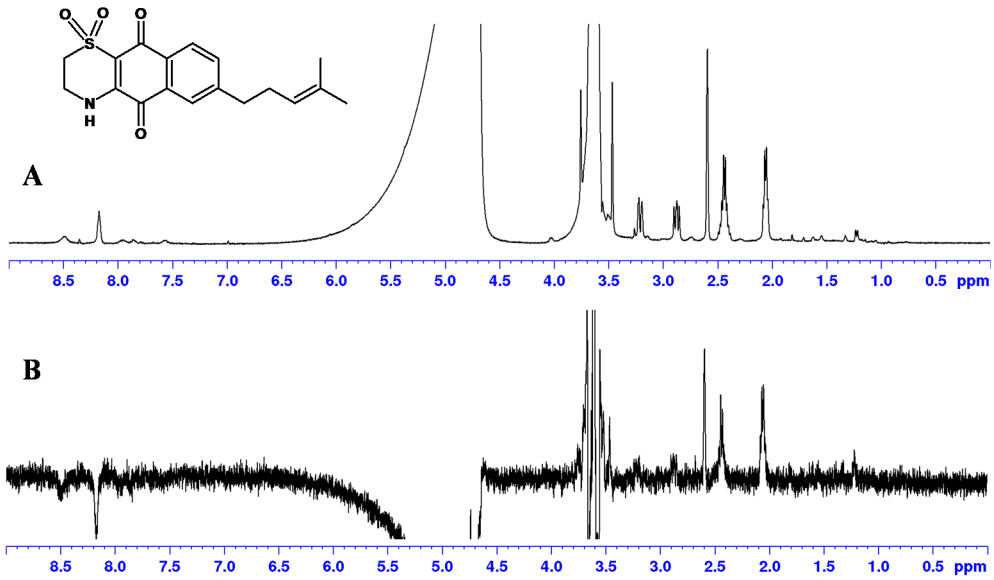

Figure S6.82: (**A**) reference ^{1}H spectrum of the C-terminal domain of Hsp90 and **4.28** (**B**) corresponding STD-NMR spectrum

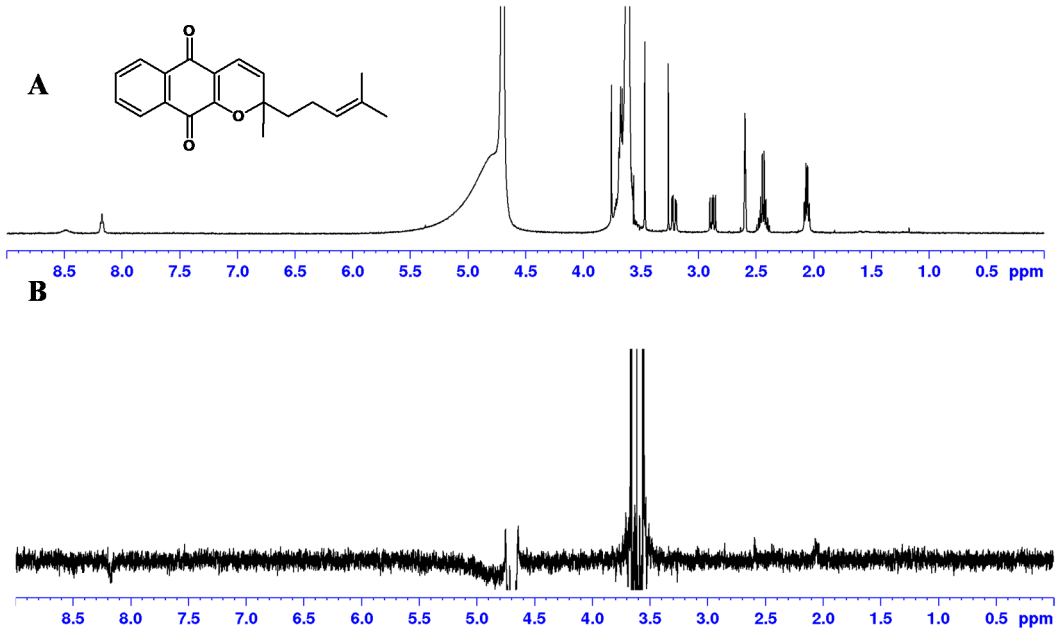

Figure S6.83: (**A**) reference ^{1}H spectrum of the C-terminal domain of Hsp90 and **4.29** (**B**) corresponding STD-NMR spectrum

STD NMR spectra for the N-terminal experiments

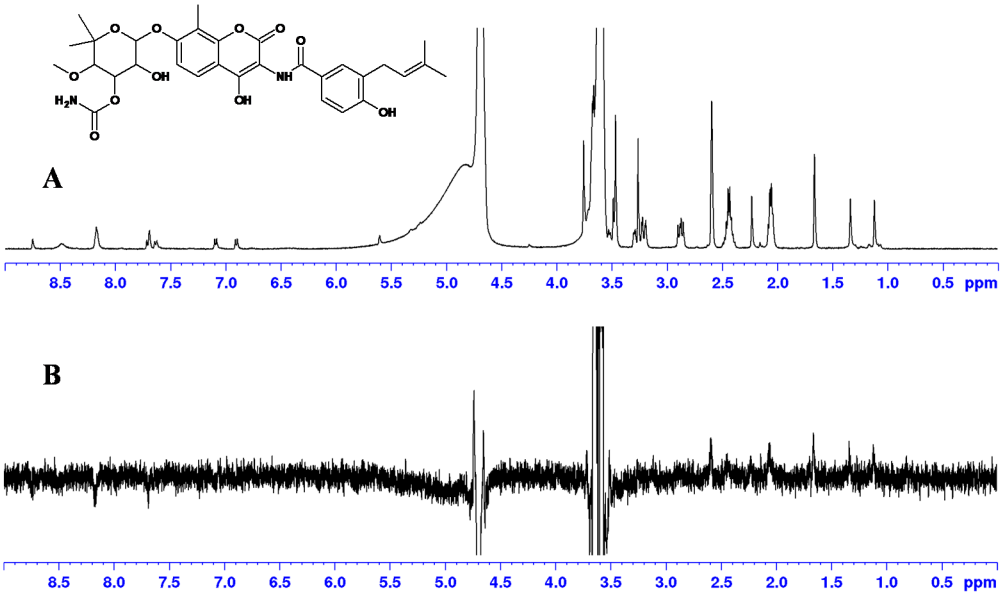

Figure S6.84: (**A**) reference ^{1}H spectrum of the N-terminal domain of Hsp90 and novobiocin **(2.41)** (**B**) corresponding STD-NMR spectrum

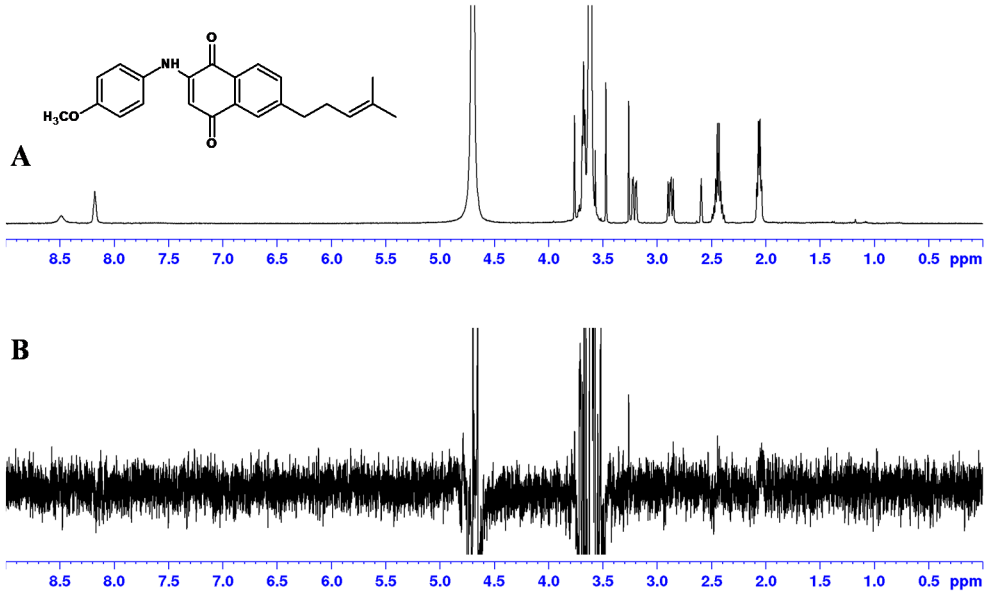

Figure S6.85: (**A**) reference ^{1}H spectrum of the N-terminal domain of Hsp90 and **4.16A** (**B**) corresponding STD-NMR spectrum

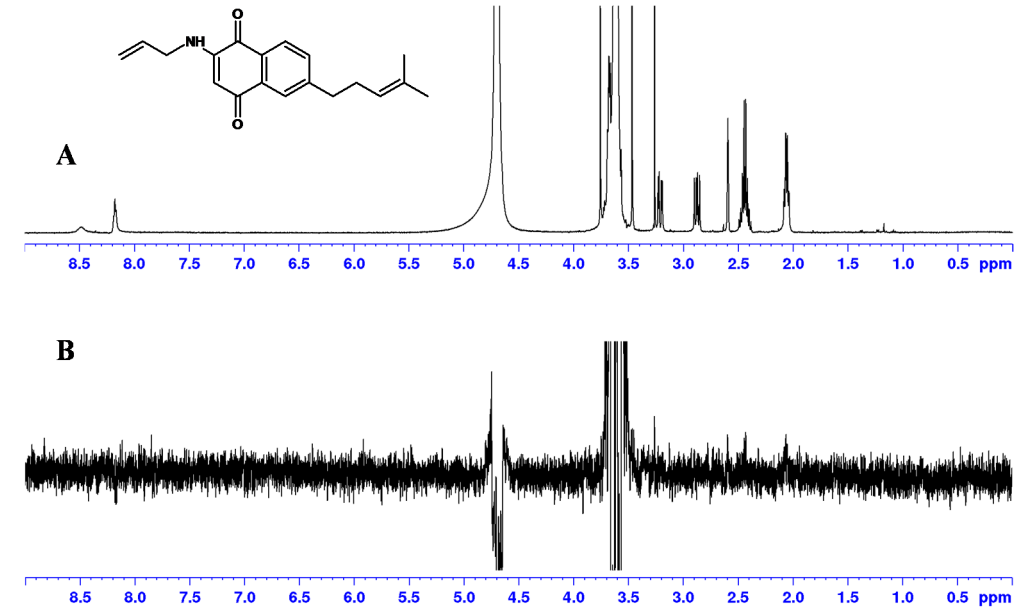

Figure S6.86: (**A**) reference ^{1}H spectrum of the N-terminal domain of Hsp90 and **4.20A** (**B**) corresponding STD-NMR spectrum

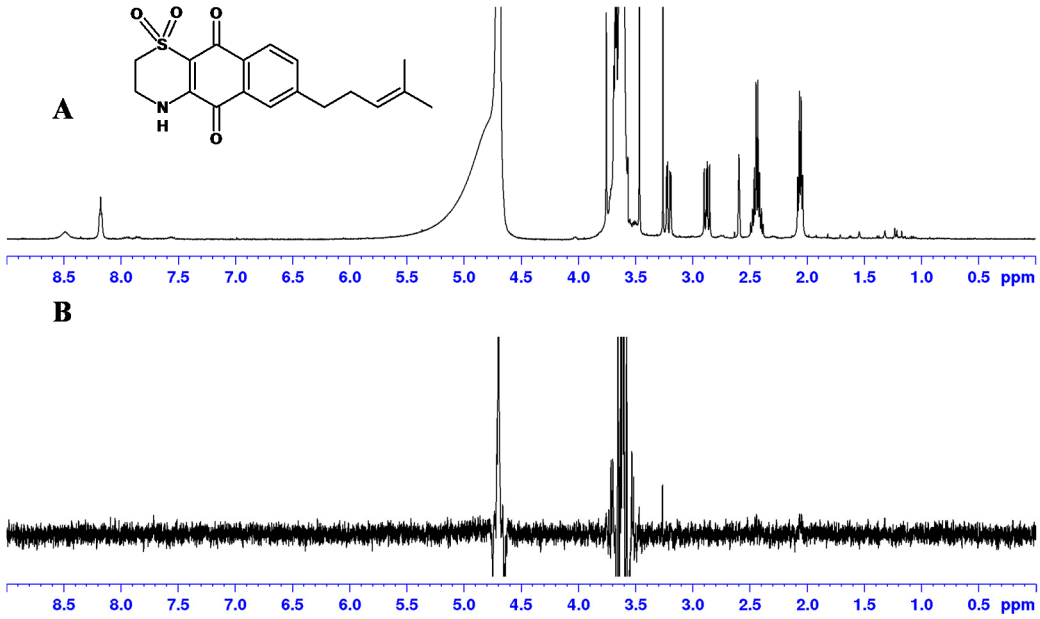

Figure S6.87: (**A**) reference ^{1}H spectrum of the N-terminal domain of Hsp90 and **4.28** (**B**) corresponding STD-NMR spectrum

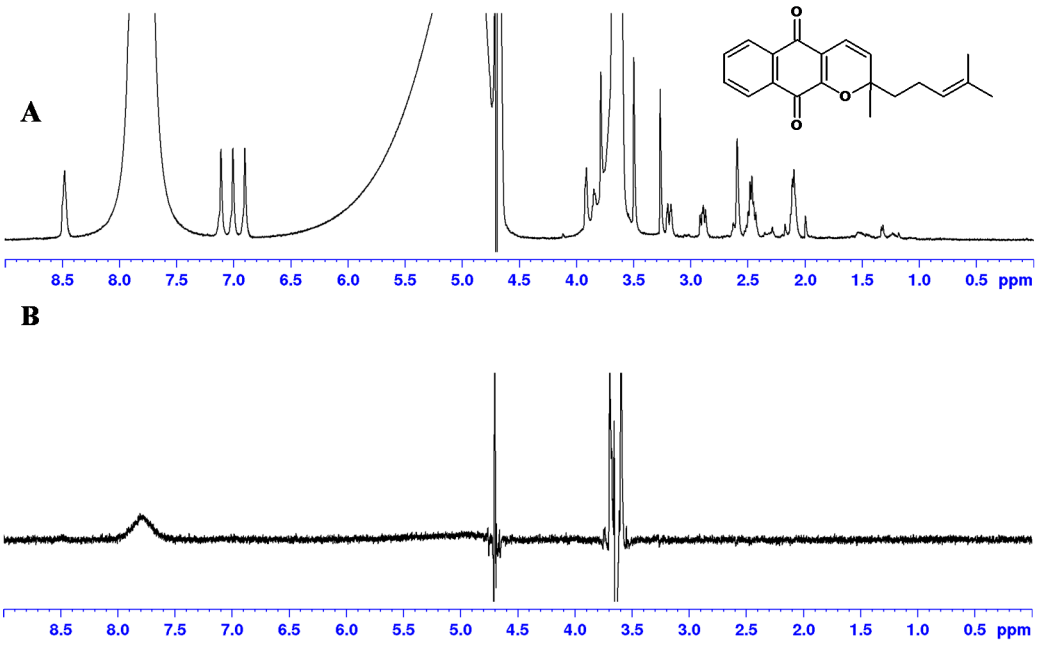

Figure S6.88: (**A**) reference ^{1}H spectrum of the N-terminal domain of Hsp90 and **4.29** (**B**) corresponding STD-NMR spectrum

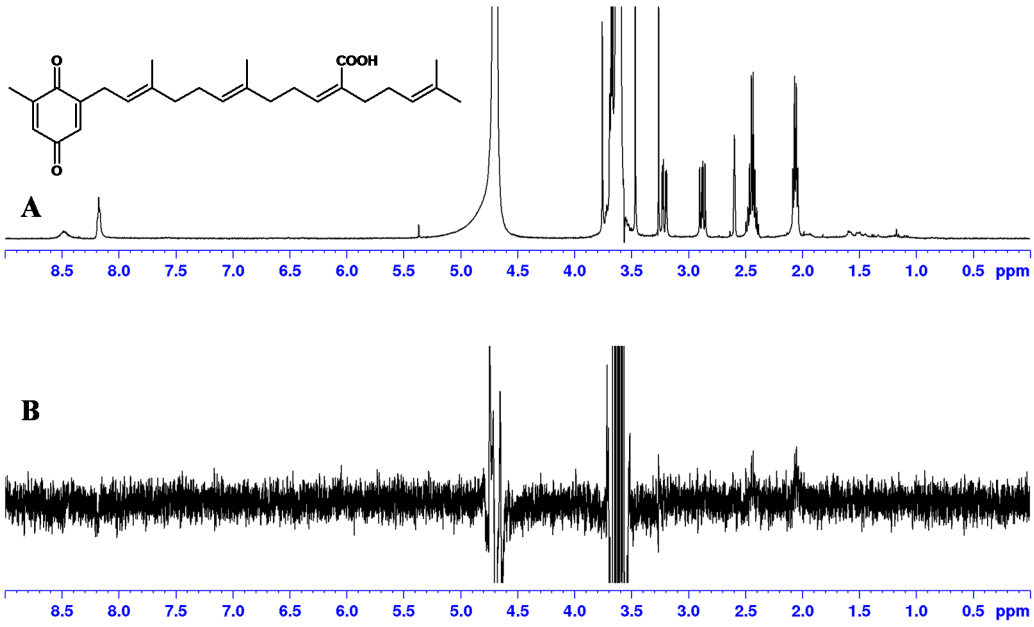

Figure S6.89: (**A**) reference ^{1}H spectrum of the N-terminal domain of Hsp90 and **2.47** (**B**) corresponding STD-NMR spectrum